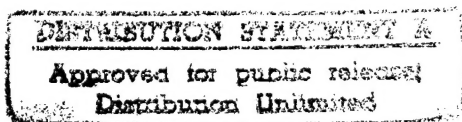
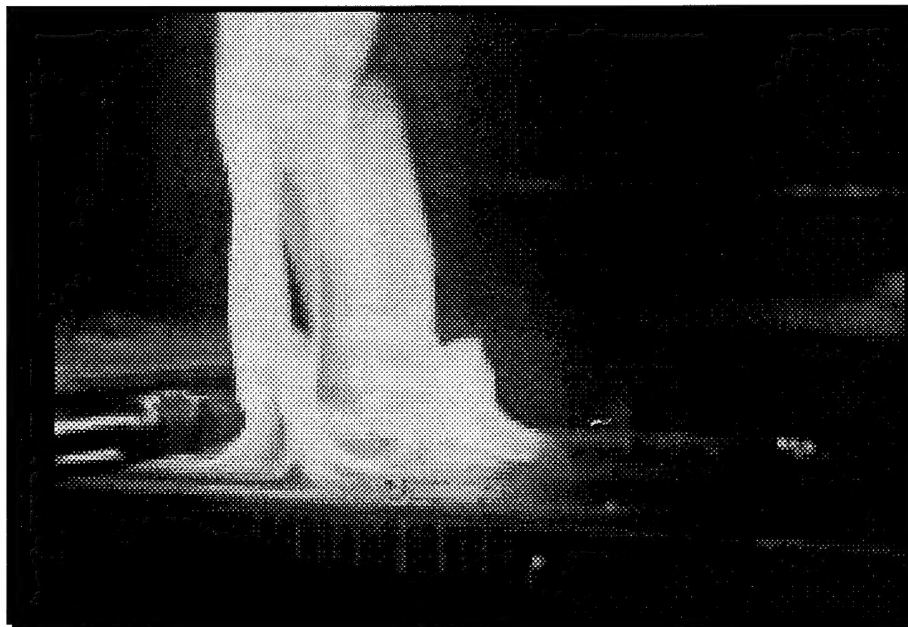


# FINAL REPORT

## HORIZONTAL FLAME SPREAD ON SHIP COMPARTMENT SURFACES



for the

**NAVAL RESEARCH LABORATORY**

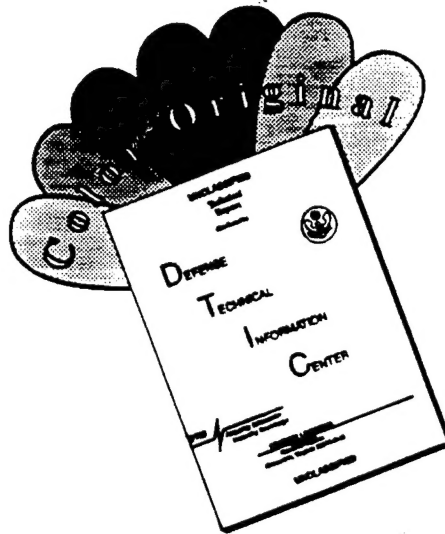
by

**Dr. Vahid Motevalli**  
**Mechanical Engineering Department**  
**Worcester Polytechnic Institute**

19960411 037

THIS DOCUMENT IS UNCLASSIFIED

# DISCLAIMER NOTICE



THIS DOCUMENT IS BEST QUALITY AVAILABLE. THE COPY FURNISHED TO DTIC CONTAINED A SIGNIFICANT NUMBER OF COLOR PAGES WHICH DO NOT REPRODUCE LEGIBLY ON BLACK AND WHITE MICROFICHE.





## **FINAL REPORT**

**Grant N00014-91-J-2023**

# **HORIZONTAL FLAME SPREAD ON SHIP COMPARTMENT SURFACES**

**Yonggang Chen and Vahid Motevalli**  
**Mechanical Engineering Department**  
**Worcester Polytechnic Institute**

**Michael Delichatsios**  
**Factory Mutual Research**  
**Corporation**

**Submitted to**

**NAVAL RESEARCH LABORATORY**

**Dr. Patricia Tatem**  
**Scientific Officer**

**Submitted by:**

  
**Dr. Vahid Motevalli, Principal Investigator**

# EXECUTIVE SUMMARY

This is the final report submitted to the Naval Research Laboratory which contains the results and conclusions of research performed under grant #N00014-91-J-2023 between September of 1991 to June of 1995. This effort benefited from close collaboration between the primary institution, Worcester Polytechnic Institute, and the Factory Mutual Research Corporation as a subcontractor. A Ph.D. student was employed full-time during 91-94 period and another graduate student and a number of undergraduate students participated in the effort.

This research resulted in the development of a computer model for prediction of Horizontal Flame Spread on Compartment Surfaces (HFSCS) complemented by a Combustion Model. The HFSCS was developed to predict flame spread on real material (whose properties are not always known or well-defined). The intent of the work was to provide the Navy with a validated and practical numerical model that can be used either as an stand alone for material flame spread characterization or ideally be incorporated into a compartment fire model, such as C-FAST developed by NIST.

The research program can be described by the following key components:

1. Development of the core of the HFSCS for charring and non-charring material by relying on a pragmatic integral model. This model requires key material flammability properties and char thermal properties applied to a transient integral heat transfer model with surface reradiation. The need for known properties was minimized through careful theoretical analysis.
2. Development and validation of a methodology to obtain the key properties referred to in (1) using a numerical model and measurements from a standard Cone Calorimeter test method (ASTM 1354) with (or without) additional measurements.
3. In order for HFSCS to be applicable to real material and be practical (i.e. executed on a Unix Workstation as well as a PC and in a short time) one could not attempt to solve a complex 2 or 3 dimensional heat transfer problem (including radiation) with combustion, surface kinetics and pyrolysis. We opted for using the surface temperature to track the flame front position (i.e. when the surface temperature reached the pyrolysis temperature we assumed the flame front to have reached that point) and thus being able to rely on a thermal model which uses key experimental results. The analysis of the problem revealed that the flame heat fluxes need to be characterized, especially the gas-phase convective flux at the leading edge. We identified the maximum flux,  $\dot{q}_g$ , and the characteristic thermal length,  $\delta_g$ , to be the key parameters. These two parameters

account for the complex heat transfer, finite chemistry and, flow dynamics at the flame leading edge as well as the ambient conditions. Thus, we developed a methodology to obtain these two parameters using flame spread data obtained from a constant speed flame spread experiment.

4. We developed a Constant Speed Horizontal Flame Spread (CSHFS) experiment to both evaluate the HFSCS predictions and construct a methodology to determine the two key parameters,  $\dot{q}_g$  and  $\delta_g$ , described in (3).

5. An integral combustion model was developed and validated. This model was first examined for a jet flame (to obtain some confidence) and then applied to a pool fire configuration. The combustion model determines the flame height, major species yield, flame temperature and velocity distribution and most importantly (for the HFSCS) the radiation distribution per unit height of the flame. This radiation distribution can be used to calculate the flame radiative flux ahead of the flame front as well as to the fuel burning surface. The latter with the developed pyrolysis model can be used to calculate the mass pyrolysis rate and thus the heat release rate. However, calculating the flame radiation surface to the burning surface is not trivial as the soot absorption needs to be accounted for. It is also possible to use the flame temperature distribution with species and soot concentration predictions to calculate radiation fluxes using ray-tracing. The combustion model provides the important coupling needed between the flame spread model and the increasing burning area as the flame spreads. We found the model to be numerically intensive, unless the centerline flame velocity calculation could be avoided by using an empirical relationship. The combustion model uses state relationship for species concentrations that need to be obtained for these real burning material. This is an area of major future research. However, one can use empirical results and data to execute HFSCS without coupling to the combustion model. At this time, this coupling has not been implemented because of the numerical intensity of the combustion model, lack of data for state relationships for real surfaces and difficulties in modelling the radiative heat flux feed-back to the burning surface.

The HFSCS has been validated using a constant speed flame spread experiments that simulated a radiating flame by an external radiant panel. The flame spread model developed here has the following major segments:

- 1) An integral heat-up and pyrolysis model, which has been previously developed and validated both analytically and experimentally for charring and non-charring material, as the core component of the horizontal flame spread model. The flame spread model has been tested for sudden increase in heat flux which is representative of gas-phase convective heat flux and a new formulation has been used to accomplish this.

The integral heat-up model uses as its input, the material flammability properties

(e.g.  $k$ ,  $\rho$ ,  $c$ ,  $L$ ) and heat fluxes at the fuel surface, to determine surface temperature rise ahead of the flame front from which the flame front location can be determined.

- 2) A combustion and radiation model has been developed and validated through limited experimental data.

The combustion model uses a direct correlation of the fluctuation of a conserved scalar and state relationship for species concentration. The soot formation is simulated for an optically thin flame using the smoke-point heat release.

The constant speed flame spread experiment was designed to provide measurement of forward gas-phase convective heat flux which is an essential mechanism for creeping flame spread. In this experiment, the flame and pyrolysis fronts were stationary as the fuel bed was moved at a constant speed by a slide towards the flame. Surface and gas temperatures as well as heat flux histories were measured at three stations over samples of PMMA and particle board as they approached the stationary pyrolysis front in turn. An exponential decay type gas-phase convective heat flux profile (maximum:  $\dot{q}_g$  and length scale:  $\delta_g$ ) has been derived from the experiment. The results are: for particle board,  $\dot{q}_g \approx 30 \text{ kW/m}^2$  and  $\delta_g \approx 1 \text{ mm}$ ; for PMMA,  $\dot{q}_g \approx 70 \text{ kW/m}^2$  and  $\delta_g \approx 1.4 \text{ mm}$ . The uncertainty of these results from a representative case is about 14%.

The horizontal flame spread code has been assembled including burning and radiation from the spreading fire. The numerical model was validated by comparison predicted flame spread rates and surface temperatures with measurements from several experiments which included effects of external and flame radiative heat fluxes. Good agreements between the numerical predictions and the experimental data were obtained.

The theoretical details of the models, subroutines and analysis are contained in Appendixes A-F. The computer code for the HFSCS and the combustion model are provided on magnetic disk. A listing of the HFSCS and the combustion model along with their input and description of the input are included in Appendix (G-J). Extensive presentation of the data and results are included in the Appendixes L and M.

This work has resulted in a number of refereed publications and other presentations during 1991-1995 which are listed here for completeness. Additional paper(s) have and will be submitted for publication.

### **Publications**

Chen, Y., Delichatsios, M.A. and Motevalli, V., "Material Pyrolysis Properties, Part II: Methodology for the Derivation of Solid Pyrolysis Properties of Charring Materials", Comb. Sci. and Tech., Vol. 104, pp. 401-425, 1995.

Delichatsios, M.A., Chen, Y., Motevalli, V. and Tatem, P., "Flame Radiation Distribution from Fires", Fire Safety Science - Proc. of the Fourth Int'l Symposium, Ed. T. Kashiwagi, International Assoc. of Fire Safety Sci., pp. 149-160, June 1994.

Chen, Y., Delichatsios, M.A. and Motevalli, V., "Material Pyrolysis Properties, Part I: An Integral Model for One-Dimensional Transient Pyrolysis of Charring Materials", Comb. Sci. and Technology, 88, 5-6, p. 309, 1993.

Motevalli, V., Chen, Y. and Delichatsios, M.A., "A Numerical Solution for Turbulent Jet Diffusion Flames Using an Integral Model", Proc. of the Int'l Congress on Computational Methods in Engineering, pp. 239-246, Shiraz, Iran, May 3-6, 1993.

Motevalli, V., Chen, Y., Gallagher, G. and Shepard, D., "Measurement of Horizontal Flame Spread on Charring and non-Charring Material using the LIFT apparatus", 1st Int'l Conf. on Fire and Materials, pp. 23-32, Washington D.C., September 24-25, 1992.

**In Chemical and Physical Processes in Combustion, Proceedings of the Eastern States Section. of the Combustion Institute.**

- Chen, Y., Motevalli, V., Delichatsios, M.A. and Tatem, P., "Horizontal Flame Spread: Determination of Gas Phase Convective Heat Flux Using Constant Speed Horizontal Flame Spread Experiment", pp. 203-206, Oct. 16-18, 1995.
- Delichatsios, M.A., Chen, Y. and Motevalli, V., "A Numerical Simulation of Lateral and Horizontal Flame Spread Rates and Comparison with Semi-Empirical Relations", pp. 373-376, Dec. 5-7, 1994.
- Chen, Y., Motevalli, V., Delichatsios, M.A. and Tatem, P., "Validation of Horizontal Flame Spread Model for Horizontal Surfaces", pp. 377-380, Dec. 5-7, 1994.
- Chen, Y., Motevalli, V. and Delichatsios, M.A., "Modelling of Scaler Fluctuations in Turbulent Buoyant Jet Flow and Comparison with Experimental Data", pp. 97-100, Oct. 1993.
- Chen, Y., Motevalli, V. and Delichatsios, M.A., "An Integral Turbulent Radiation and Combustion Model for Diffusion Flames", pp. 51-55, March 1993, New Orleans.
- Chen, Y., Motevalli, V. and Delichatsios, M.A., "Development of an Integral Model for Prediction of Flame Spread on Horizontal Surfaces", pp. 626-630, March 1993, New Orleans.
- Delichatsios, M.A., Chen, Y. and Motevalli, V., "Flame Spread on Charring Materials: Numerical Predictions of Experimental Results", pp. 100.1-100.4, Ithaca, NY, Oct. 1991.

**NIST Annual Conference on Fire Research**

- Motevalli, V., Chen, Y., Delichatsios, M.A. and Tatem, P., "Characterization of Horizontal Flame Spread on Charring Surfaces", NISTIR 5499, pp. 153-154, Oct. 17-20, 1994.
- Chen, Y., Motevalli, V. and Delichatsios, M.A., "An Integral Combustion Model for Buoyant Diffusion Flames", pp. 31-32, Oct. 18-20, 1993.
- Motevalli, V., Chen, Y. and Delichatsios, M.A., "Development of an Integral Model for Prediction of Flame Spread on Horizontal Shipboard Surfaces", pp. 9-10, MD, Oct. 13-16, 1992.

## **ACKNOWLEDGEMENT**

The funding provided for this research by the Naval Research Laboratory, under grant #N00014-91-J-2023, and guidance of Dr. Patricia Tatem, the Scientific Officer, is greatly appreciated.

We also would like to acknowledge the support of the two institutions, Worcester Polytechnic Institute and the Factory Mutual Research Corporation, which enabled us to perform this research.

The CMEE department of the George Washington University is also acknowledged for providing space and computer facility for the sabbatical and post-sabbatical periods of PI's work away from WPI when the report completion and some of the analysis took place.

# TABLE OF CONTENTS

Executive Summary.....	i
Acknowledgment .....	v
List of Figures.....	viii
Nomenclature.....	xii
 Chapter 1     Introduction and Background.....	 1
Chapter 2     Previous Work and Literature Review .....	5
2.1     An Overview of Horizontal Flame Spread Research.....	5
2.1.1     Theoretical Work.....	5
2.1.2     Experimental Work.....	6
2.2     Combustion and Radiation in Fires .....	9
 Chapter 3     Physics of Opposed-Flow Horizontal Flame Spread, Description of the Horizontal Flame Spread Model and Comparison with An Analytical Solution .....	 11
3.1     Physics of Horizontal Flame Spread.....	11
A. Heat-up and Pyrolysis Model.....	13
B. Combustion Model .....	14
C. Heat Flux Model.....	15
D. Constant Speed Horizontal Flame Spread Experiment.....	15
3.2     Description of the Horizontal Flame Spread Model.....	16
3.3     Locating the Flame (Pyrolysis) Front).....	17
3.4     Surface Temperature Calculations Using Two Solid Temperature Profiles.....	21
3.5     Sensitivity Analysis of the Horizontal Flame Spread Model.....	22
3.6     Comparison with an Analytical Solution .....	26
 Chapter 4     Description of Combustion Model and Comparison with Experimental Data.....	 34
4.1     Introduction .....	34
4.2     Model Description and Energy Balance .....	35
4.3     Structure of the Computer Code.....	39
4.4     Comparison of Prediction with Experiments .....	42

Chapter 5	Description of Constant Horizontal Flame Spread (CSHFS) Experiment .....	49
Chapter 6	Experimental Results and Comparison of Simulation of Horizontal Flame Spread Model .....	57
6.1	Experimental approach and procedure .....	57
6.2	Analysis of Experimental Data .....	58
6.3	Examination of the Flammability Properties of PMMA Sheets and Particle Boards Used in the Experiments .....	62
6.4	Estimation of Gas-Phase Conductive Heat Flux .....	63
6.5	Energy Balance at the Flame Leading Edge for Horizontal Flame Spread; A New Interpretation of Experimental Data .....	70
6.6	Numerical Simulation of Flame Spread and Comparison with the Experimental Data .....	76
6.7	Limitations of the Horizontal Flame Spread Model .....	77
6.8	Char Depth Measurements and Additional Discussions .....	83
Chapter 7	Conclusions and Future Work .....	88
References	.....	90
Appendix A	An Integral Model for Prediction of Radiation and Combustion of Turbulent Diffusion Flames	
Appendix B	Scalar Fluctuations in Turbulent Buoyant Jet Flow and Comparison with Experimental Data	
Appendix C	Application of the Combustion Model to Pool Fire	
Appendix D	Analytical Solution for Constant Horizontal Flame Spread Velocity	
Appendix E	Justification for the Gas-Phase Conductive Heat Flux Profile Being the Same as Surface Temperature History	
Appendix F	Algorithm of Heat-up Calculation for Sudden Jump (Drop) in Heat Fluxes at the Surface	
Appendix G	The Input for the Horizontal Flame Spread Model	
Appendix H	The HFSCS Computer Program Listing	
Appendix I	The Input for the Combustion Model	
Appendix J	The Combustion Model Computer Program Listing	
Appendix K	Description of Execution of the Program and Output	
Appendix L	Complete Set of Plots of Experimental Measurements of Temperature and Fluxes, Data Sheets and External Flux Profile. Plots are results after significant processing of the raw data.	
Appendix M	Tables of Char Depth Measurements	



## List of Figures

1-1	The mechanism of horizontal flame spread .....	2
3-1	Components of opposed flow horizontal flame spread.....	12
3-2	A schematic diagram of horizontal flame spread .....	13
3-3	A flowchart and interconnections of the horizontal flame spread on compartment surfaces. ....	20
3-4	Sensitivity analysis of the horizontal flame spread model-different nodal spacings and $\Delta t=1$ seconds.....	23
3-5	Sensitivity analysis of the horizontal flame spread model-different time steps and $\Delta x=4$ mm.....	24
3-6	Sensitivity analysis of the horizontal flame spread model-different heat flux profiles, $\Delta x=1$ mm and $\Delta t=1$ seconds .....	25
3-7	Comparison between numerical solutions of the horizontal flame spread model and an analytical solution with surface reradiation and $\dot{q}_e=5$ kW/m <sup>2</sup> .....	28
3-8	Comparison between numerical solutions of the horizontal flame spread model and an analytical solution with surface reradiation and $\dot{q}_e=0$ kW/m <sup>2</sup> . C is a coefficient accounting for reradiation loss .....	30
3-9	Comparison between numerical solutions of the horizontal flame spread model and an analytical solution with surface reradiation and $\dot{q}_e=10$ kW/m <sup>2</sup> .....	30
3-10	Comparison between numerical solutions of the horizontal flame spread model and an analytical solution with surface reradiation and $\dot{q}_e=20$ kW/m <sup>2</sup> .....	31
3-11	Comparison between numerical solutions of the horizontal flame spread model and an analytical solution with <u>no</u> surface reradiation and $\dot{q}_e=0$ kW/m <sup>2</sup> .....	31
3-12	Comparison between numerical solutions of the horizontal flame spread model and an analytical solution with <u>no</u> surface reradiation and $\dot{q}_e=10$ kW/m <sup>2</sup> .....	32

3-13	Comparison between numerical solutions of the horizontal flame spread model and an analytical solution with <u>no</u> surface reradiation and $\dot{q}_e'' = 5 \text{ kW/m}^2$	32
3-14	Comparison between numerical solutions of the horizontal flame spread model and an analytical solution with <u>no</u> surface reradiation and $\dot{q}_e'' = 5 \text{ kW/m}^2$	33
4-1	A schematic diagram of the integral combustion model	35
4-2	Subroutines and interconnections of the integral combustion model	41
4-3	Chemical heat release rate normalized by the total heat release rate versus distance from the nozzle exit, normalized by twice the length, $L_{0.5}$ , over which half of the combustion has been completed	42
4-4a	Radiation fraction at a given height plotted versus the height normalized by twice the length, $L_{0.5}$ , over which half of the combustion has been completed	42
4-4b	Radiation distribution per unit height versus normalized distance from the nozzle exit (cf. Figure 4-4a). The experimental data are from Tamanini (1982)	43
4-4c	Same data as in Figure 4-4b, except that the radiation per unit height is normalized by its maximum value. The experimental data are from Tamanini (1982)	43
4-5	Reduction of laminar flamelet temperature with height owing to radiation losses for the use of Figure 4-3	44
4-6a	Prediction of radiation fraction versus height for propylene turbulent jet flame. No experiments are available except for the total radiation fraction	44
4-6b	Radiation distribution per unit height versus height for a propylene turbulent jet flame	45
4-6c	Reduction of laminar flamelet temperature vs. height owing to radiation loss for the case of Figure 4-6b	46
4-7	CO production rate vs. scaled height from the flame for a propane jet flame	47
4-8a	Chemical heat release rate versus distance from the base of a propane pool fire 0.38 m in diameter	47
4-8b	Radiation fraction at a given height plotted versus the height from the base of a propane pool fire 0.38 m in diameter	48
5-1	Schematic of the horizontal flame spread experiment	50

5-2	External heat flux from the radiant panel-a decaying profile when $x > 400$ mm. Ordinate is the ratio between heat fluxes at a location and 425 mm.....	50
5-3	Long view of the flame spread apparatus.....	53
5-4	Early stage of flame spread .....	53
5-5	Flame spread after the slide has moved for about 15 cm .....	54
5-6	Same as Figure 5-5, but for different test.....	54
5-7	Flame spread at the middle stage of the experiment .....	55
5-8	Side view of the flame spread experiment.....	55
5-9	The slide stops, the experiment finishes.....	56
5-10	The PMMA samples after experiments (6.35 mm (1/4") thick) .....	56
6-1	Temperature histories of a particle board test, external heat flux level: $20 \text{ kW/m}^2$ .....	59
6-2	Total heat flux histories of a particle board test, external heat flux level: $20 \text{ kW/m}^2$ .....	59
6-3	Net flame (radiation+gas phase conduction) heat flux for a particle board test shown in Figures 6-1 and 6-2 .....	61
6-4	Comparison of surface temperature histories for a particle board test. This comparison is used to check the values of material properties ( $k$ , $\rho$ , $c$ ) .....	62
6-5	The detailed surface temperature histories during the jump period for a particle board test.....	65
6-6	A diagram of heat fluxes at the flame leading edge .....	72
6-7	Comparison of predicted and measured flame spread for a particle board experiment. External heat flux level: $10 \text{ kW/m}^2$ .....	77
6-8	Comparison of predicted and measured flame spread for a particle board experiment. External heat flux level: $20 \text{ kW/m}^2$ .....	78
6-9	Comparison of predicted and measured flame spread for a particle board experiment. External heat flux level: $30 \text{ kW/m}^2$ .....	78

6-10	Comparison of predicted and measured flame spread for a 19 mm thick PMMA sample experiment. External heat flux level: 10 kW/m <sup>2</sup> .....	79
6-11	Comparison of predicted and measured flame spread for a 19 mm thick PMMA sample experiment. External heat flux level: 20 kW/m <sup>2</sup> .....	79
6-12	Comparison of predicted and measured flame spread for a 19 mm thick PMMA sample experiment. External heat flux level: 30 kW/m <sup>2</sup> .....	80
6-13	Comparison of predicted and measured flame spread for a 6.35 mm thick PMMA sample experiment. External heat flux level: 10 kW/m <sup>2</sup> .....	80
6-14	Comparison of predicted and measured flame spread for a 6.35 mm thick PMMA sample experiment. External heat flux level: 20 kW/m <sup>2</sup> .....	81
6-15	Comparison of predicted and measured flame spread for a 6.35 mm thick PMMA sample experiment. External heat flux level: 30 kW/m <sup>2</sup> .....	81
6-16	Detailed comparison of surface temperature at the second measuring station during the sudden increase period with the model prediction for the particle board test. External heat flux level: 20 kW/m <sup>2</sup> .....	82
6-17	Detailed comparison of surface temperature at the first measuring station during the sudden increase period with the model prediction for the 19 mm thick PMMA. External heat flux level: 20 kW/m <sup>2</sup> .....	82
6-18	Char depth measurements along the particle board specimens exposed to 3 different external flux conditions. Three tests for each condition.....	83
6-19	Normalized char depth along the specimen for 3 externally imposed conditions, constant flame spread experiments .....	84
6-20	IR Image, PMMA Test, 19 mm thick, 10 kW/m <sup>2</sup> .....	86
6-21	IR Image, PMMA Test, 19 mm thick, 10 kW/m <sup>2</sup> .....	86
6-22	IR Image, Surface temperature contour map of Figure 6-21, PMMA, 19 mm thick, 10 kW/m <sup>2</sup> .....	87
6-23	Surface temperature profile of Fig. 6-21 along the designated line .....	87

## Nomenclatures

- $A$ = the magnitude of exponential type heat flux ( $\text{kW/m}^2$ )
- $c$ = specific heat ( $\text{J/kg.K}$ )
- $C$ = a coefficient used to account for surface reradiation loss
- $D_a$ = Damkoler number (the ratio of a characteristic chemical reaction rate to a characteristic convective or diffusive transport rate)
- $h$ = enthalpy ( $\text{kW/kg}$ )
- $k$ = thermal conductivity ( $\text{W/m.K}$ )
- $k_{sx}$ = thermal conductivity along x-direction ( $\text{W/m.K}$ )
- $k_{sy}$ = thermal conductivity along y-direction ( $\text{W/m.K}$ )
- $L$ = heat of pyrolysis ( $\text{J/kg}$ )
- $L_{0.5}$ = a length over which half of the combustion has been completed
- $L_e$ = Lewis number (Ratio of thermal diffusivity to mass diffusivity)
- $\ell_f$ = flame length (m)
- $\dot{m}''$ = mass pyrolysis rate ( $\text{kg/m}^2 \cdot \text{s}$ )
- $n$ = number of nodes along the fuel surface
- $P(\xi, \gamma)$ =Probability Density Function (pdf)
- $\dot{Q}_{ch}$ = heat release rate (kW)
- $\dot{Q}_R$ = total radiation loss (kW)
- $\dot{Q}_{sp}$ = laminar smoke-point heat release rate (kW)
- $\dot{Q}_{th}$ = total heat release rate (kW)

$\dot{q}_1''$	imposed heat flux (kW/m <sup>2</sup> )
$\dot{q}_1''$	heat flux before a sudden jump (kW/m <sup>2</sup> )
$\dot{q}_2''$	heat flux behind flame front or heat flux after a sudden jump (kW/m <sup>2</sup> )
$\dot{q}_c''$	convective heat loss/gain from the fuel surface (kW/m <sup>2</sup> )
$\dot{q}_{\text{conv}}''$	flame gas phase conductive (convective) heat flux, kW/m <sup>2</sup>
$\dot{q}_{\text{ext}}''$	external heat flux to the fuel surface (kW/m <sup>2</sup> )
$\dot{q}_g''$	the magnitude of flame gas-phase conductive heat flux (kW/m <sup>2</sup> )
$\dot{q}_R''$	flame radiation loss per unit flame height (kW/m)
$\dot{q}_{r0}''$	the magnitude of flame radiative heat flux (kW/m <sup>2</sup> )
$\dot{q}_{\text{rad}}''$	radiative heat flux from the flame to the fuel surface (kW/m <sup>2</sup> )
$\dot{q}_{\text{rer}}''$	reradiation loss from the fuel surface (kW/m <sup>2</sup> )
$\dot{q}_t''$	total heat flux from the flame (kW/m <sup>2</sup> )
$t$	time (seconds)
$t_p$	time to pyrolysis (seconds)
$T_0$	ambient temperature (K)
$T_{\text{ad}}$	adiabatic temperature
$T_{\text{ext}}$	surface temperature rise owing to external and flame radiation heat fluxes
$T_L$	laminar flamelet temperature (K)
$T_s$	surface temperature of the fuel (K)
$T_p$	fuel pyrolysis temperature (K)
$u$	velocity (m/s)
$V_s, V$	flame spread speed (m/s)

- $x$ = distance along the fuel surface (m)
- $x_p$ = flame/pyrolysis front location (m)
- $Y_s$ = soot concentration (kg/kg)
- $z$ = distance along the normal direction of the fuel surface or height from the flame base (m)

## Greek Letters

- $\alpha$ = thermal diffusivity ( $\text{m}^2/\text{s}$ ) or reduction fraction from adiabatic temperature due to radiation loss
- $\alpha_s$ = thermal diffusivity of the solid ( $\text{m}^2/\text{s}$ )
- $\Delta t$ = time step (seconds)
- $\Delta x$ = mesh size (m)
- $\delta$ = the length scale of heat flux profile (m)
- $\delta_g$ = the length scale of the gas-phase conductive heat flux (m)
- $\delta_H$ = horizontal thermal length (m)
- $\delta_r$ = the length scale of the flame radiative heat flux (m)
- $\epsilon, \epsilon_s$ = emissivity of the fuel surface
- $\theta$ = temperature of the fuel relevant to initial temperature ( $=T-T_0$ ) (K)
- $\theta_p$ = pyrolysis temperature of the fuel relevant to initial temperature ( $=T_p-T_0$ ) (K)
- $\tau_1, \tau_2$ = time spans of the jump periods for first and second station surface

temperature measurements (seconds)

$\chi_R =$  flame radiation fraction

$\xi =$  a conserved scalar

$\bar{\xi} =$  mean value of the conserved scalar

$\rho =$  density ( $\text{kg/m}^3$ )

$\sigma =$  Stefan-Boltzmann constant ( $5.67 \times 10^{-11} \text{ kW/K}^4 \cdot \text{m}^2$ )

$\psi, \psi_t =$  stream function and entrainment rate respectively



## Chapter 1 Introduction and Background

Significant progress has been made in enclosure fire modeling over the last decade. Several zone models have been developed (e.g. CFAST (Jones, 1990), BRI2 (Tanaka, 1983)). Though these fire models generally predict the environment generated from fires (i.e. temperature and velocity of fire induced flow) and transport of fire products, they rely on empirical correlations or experimental data for heat release rates which are inputs to such models because predictive capability of fire spread and fire growth is limited. The use of heat release rates from specific test (e.g. furniture calorimeter) in the fire models to simulate fire growth histories in real fire scenarios having various compartment geometries and ambient conditions makes it (using prescribed heat release rates) questionable.

One would argue that a robust model should be able to account for ambient conditions (e.g. heat flux from the environment), predict fire spread and growth and heat release rate for an arbitrary material (charring and non-charring), and for an arbitrary burning scenario (upward, downward, horizontal flame spread, etc.). Such a flame spread model should also have the capability of estimating products from the burning of pyrolysis gases (CO, CO<sub>2</sub>, etc). The ability to predict fire growth and consequently smoke transport together with appropriate engineering methods can potentially lead to improved ship designs and fire control/fighting strategies.

Upward (vertical) flame spread have been studied extensively and several numerical simulation models have been developed (Delichatsios, M.M. et al, 1990; 1991; Mitler, 1990). These upward flame spread models can match the needs of current compartment fire models. The focus in this research is opposed flow horizontal flame spread although a lot of work has been done in this area. Numerical models of horizontal flame spread are either too complex to use (di Blasi, 1987, Chen, 1990) because their models require large computational time and assume kinetics for gas and solid phases or are not general enough (Atreya, 1984, Quintiere, 1981). The latter approaches have merits for practical usage since they do not require large computational time as the former. In fact, most widely used method to quantify horizontal (lateral) flame spread is described in ASTM 1354 (Quintiere, 1981; Quintiere et al., 1984). This method is not general because 1) it is suitable for thermally thick material, but not valid for thermally thin and intermediate materials, 2) it can be used for ambient conditions, but not apply to other environmental conditions. It is the goal of this project to develop a generalized model that uses material thermal properties which can be obtained from small scale experiment for predicting horizontal flame spread.

Horizontal flame spread is a complex problem and requires modeling of a number of phenomena (Atreya, 1984), namely 1), heat transfer inside the fuel including pyrolysis of the fuel, 2), combustion of the pyrolyzing gases and heat transfer from the flame to the fuel surface (radiative and convective). In light of this, several numerical models are needed to simulate horizontal flame spread:

1. A model for prediction of material pyrolysis during flaming combustion for both charring and non-charring materials.
2. A combustion model that couples the pyrolysis with burning in the gas phase.
3. A model for the preheating of the unburned material prior to flame spread. This preheating must be modeled using a complete heat transfer treatment that includes all three modes of heat transfer: conduction, convection and radiation, including surface reradiation.
4. A model that quantifies gas phase conductive heat flux profile using experimental data obtained from a constant speed horizontal flame spread (CSHFS) experiment. This profile would take into consideration of ambient flow condition.

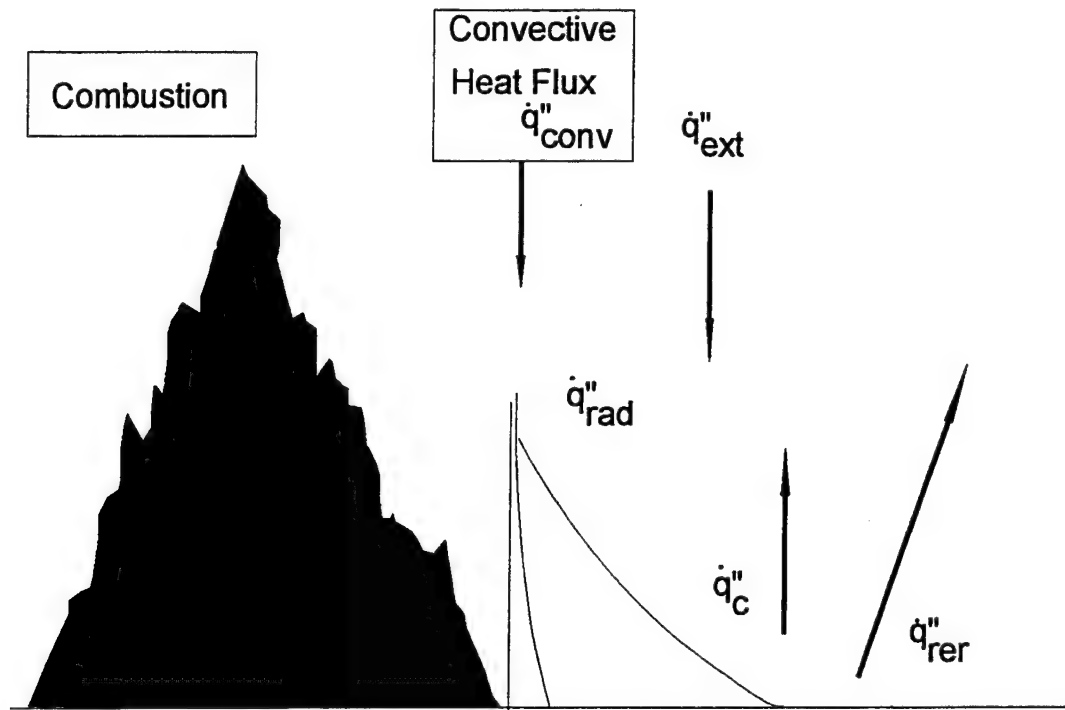


**Figure 1-1** The mechanism of horizontal flame spread

Flame spread occurs when the fuel surface is heated to ignition or pyrolysis temperature. Therefore, surface temperature histories have to be evaluated. In order to do that, heat fluxes at the fuel surface have to be determined. There are a number of heat fluxes involved in heating the fuel surface ahead of flame front (see Figure 1-1): 1) external heat flux(es),  $\dot{q}''_{ext}$  that comes from other sources (such as hot ceiling layers) and other flames, 2) radiative heat flux from the flame to the fuel surface,  $\dot{q}''_{rad}$ , 3) natural convection loss from the fuel surface,  $\dot{q}''_c$ , 4) surface reradiation loss,  $\dot{q}''_{rer}$ , and 5) close to the flame front, there is an additional heat flux from the flame to the fuel surface,  $\dot{q}''_{conv}$ , which is called gas-phase convective (conductive) heat flux.

A discussion of each heat flux and its status concerning current work is followed in the next paragraphs.

1. A integral heat-up and pyrolysis model, that uses material flammability properties and heat fluxes at the fuel surface described above has been developed and validated both analytically and experimentally (Chen et al., 1991, 1993a). This model calculates fuel surface temperature and pyrolysis rate histories by including convective heat loss and surface reradiation,  $\dot{q}_c''$  and  $\dot{q}_{rer}''$ . Natural convection loss is treated using an empirical model for natural convection over a horizontal plate which can be found in the literature readily. The surface reradiation loss can be simply determined as:

$$\dot{q}_{rer}'' = \epsilon \sigma (T_s^4 - T_0^4) \quad (1-1)$$

where  $\epsilon$  is surface emissivity and  $\sigma$  is Stefan-Boltzmann constant,  $T_s$  and  $T_0$  are the surface and ambient temperatures respectively. The integral heat-up model was developed earlier (Chen et al., 1991, 1993a) and was not in the scope of the current work and it will not be discussed further here. This model, has been incorporated into a comprehensive horizontal flame spread model in current work. This incorporation requires the use of the heat-up and pyrolysis model in discrete, time dependent manner. To accomplish this, the heat-up model had to be able to account for the sudden increase in the heat flux at the flame front and transition to the pyrolysis model.

2. The external heat flux(es) towards the fuel surface,  $\dot{q}_{ext}''$ , can be evaluated from a compartment fire model or measurements and it is not the concern here. The model developed in this work simply uses it as an input.
3. The radiative heat flux from the flame to the fuel surface,  $\dot{q}_{rad}''$ , can be determined by a combustion, radiation and heat flux model. A combustion and radiation model has been developed in this work and part of it has been published (Chen et al., 1993, Delichatsios et al., 1994). This model uses the pyrolysis rate determined by the pyrolysis model as its input to estimate combustion of the pyrolysis gases and radiation distribution along the flame length.
4. Another important component of horizontal flame spread is forward gas-phase conduction (convection),  $\dot{q}_{conv}''$  from the flame to the fuel surface. Because of the complex flow involved near the flame front, this heat flux is difficult to simulate or measure. Therefore, a quasi-steady horizontal flame spread experiment has been designed and conducted to determine this gas-phase conductive heat flux.

A comprehensive model, that incorporates all these components, has been developed in this research. Numerical results have been compared with experimental data from several tests and good agreement is observed. The model has been documented and has output that can be readily incorporated into compartment fire models such as C-FAST (Jones, 1990).

This model has been structured such that its' future incorporation into C-FAST would be possible with relative ease.

In this report, a literature review of opposed flow horizontal flame spread research and efforts to model diffusion flames (including fires) and their radiation are presented in Chapter 2. The physics, numerical model as well as comparison between the numerical model and an analytical solution is discussed in Chapter 3. Chapter 4 describes formulation, coding and validation of an integral combustion model. A description of the Constant Speed Horizontal Flame Spread (CSHFS) experiment is included in Chapter 5. Chapter 6 contains: 1) analysis of temperature and heat flux measurement, 2) derivation of gas phase conductive heat flux, and 3) comparison of numerical results with the CSHFS experiments. Finally, the concluding remarks and future work is presented in Chapter 7. A number of appendixes to this report contain the details of the combustion mode, analytical solution for a constant horizontal flame spread velocity, details of the interpretation of the experimental results, numerical schemes to account for sudden flux changes (incident on the fuel surface), detailed comparison of numerical and experimental data, supporting data and the computer code.

## Chapter 2 Previous Work and Literature Review

### 2.1 AN OVERVIEW OF HORIZONTAL FLAME SPREAD RESEARCH

Modes of flame spread can be characterized by flame spreading over the surface of a combustible material in a gaseous oxidizer that flows (either naturally induced or forced) in a direction opposite or concurrent to that of the flame propagation direction (Fernandez-Pello, 1984). Opposed flame spread includes horizontal, downward and lateral flame spread while concurrent mode of flame spread includes wind-assisted and upward flame spreads. This review work is limited to opposed flow flame spread.

#### 2.1.1 Theoretical Work

Modern work in horizontal flame spread started with the work of de Ris (1969) where previous references on flame spread are cited. He pointed out that Emmons (1965) discussed the general subject of fire spread and Tarifa and Torralbo (1967) solved solid phase conduction equations with heat flux from gas phase to solid surface as boundary conditions. de Ris (1969) investigated flame spread over solid fuels in a uniform flow of velocity,  $U$ , in the direction opposite the flame spread. He assumed infinite Damkoler number,  $Da$  (the ratio of a characteristic chemical reaction rate to a characteristic convective or diffusive transport rate), constant thermodynamic and transport properties, and equal diffusivities of thermal energy, fuel, and oxidant (i.e. Lewis number ( $Le$ ) of unity). He derived analytical solutions for flame spread both for thermally thin (approximate analytical solution) and thermally thick (exact analytical solution) conditions. Delichatsios (1986) also derived an exact analytical solution of creeping flame spread over a thermally thin solid. Other analytical solutions become also available (Wichman and Williams, 1983 ).

Wichman and Williams (1983) assume that the flame-sheet is located at the fuel surface, consider non-unity Lewis number and solve coupled gas and solid phase equations. A very interesting result is obtained: for Lewis number unity the analysis produces the same flame spread formula as that obtained by de Ris (1969). They accurately pointed out that de Ris (1969), by linearizing the boundary conditions for the fuel concentration at the surface, actually forces the flame-sheet to be located at the fuel surface.

Frey and T'ien (1979) developed a comprehensive model of opposed flow flame spread. The analysis uses the Oseen approximation (constant flow velocity) and includes a) an Arrhenius type chemical kinetics in the gas phase, b) transient heating and c) Arrhenius pyrolysis kinetics. Their numerical solutions predict gas temperature and species concentration profiles as well as the existence of a quenching layer near the fuel surface in the region of the inception of the flame. Another interesting aspect of this model is that it is

capable of predicting the conditions (flow velocity, pressure, oxygen concentration) for which flame spread stops.

Other full numerical solutions are also available. Chen (1990) solved two-dimensional Navier-Stokes momentum, energy and species equations with one-step overall chemical reaction and second-order, finite-rate Arrhenius kinetics in gas phase. The solid phase is thermally thin and the analysis consists of an energy balance coupled with the heat flux from the gas phase and a mass balance including Arrhenius pyrolysis kinetics. The results show that flame spread speed decreases as the opposed flow velocity is increased. His model can predict flame blowoff limit but experimental validation is not complete. Other interesting phenomena observed from his analysis are: ahead of the flame front, a flow recirculation zone is found for every case of computation and the flame has both premixed and diffusion characteristics. Di Blasi et al. (1987, 1989) numerically simulated opposed flow flame spread over thin paper (charring material). Their numerical results were compared with experimental data and good agreement was observed. Bhattacharjee and Altenkirch (1990) numerically solved opposed flow flame spread over thin solid in a microgravity environment. Specifically, they solved gas-phase radiation using three simple parameters (a Planck mean absorption coefficient, the fraction of total emission directed towards the surface and a shape function that represents the distribution of gas to surface radiation). At low opposing flow velocities, the radiation effects become significant. Flame spread decreases with decreasing opposed flow velocity. This phenomenon was observed in drop-tower experiments. Recently, West et al. (1994) numerically investigated the surface radiation effects on flame spread for thermally thick solid in an opposed flow. They claimed that the ratio of the rate of heat transfer by reradiation from the surface to that by conduction from the gas to the solid is proportional to the length over which heat can be conducted forward of the flame to sustain spreading. For thick solid, this length decreases with increasing flow velocity at lower velocities and is determined by gas-phase process. But at higher velocities, the conduction length is determined by solid phase processes and is independent of the gas-phase flow.

Greenberg and Ronney (1993) studied the effect of Lewis number ( $Le$ ) on flame spread. They modified de Ris' analysis ( $Le$  is unity) using their experimental data to include the influences of nonunity Lewis numbers of oxidant and fuel vapors. The deduced flame spread relationship shows that the Lewis number of the oxidant affects the spread rate only through its effect on the flame temperature and the fuel Lewis number plays no role. They have compared their theoretical results with the flame spread data over thin paper samples in a variety of  $O_2$ -diluent atmosphere and good agreements were obtained. They concluded that the assumption of unity  $Le$  can lead to rather inaccurate spread rate and flame temperature predictions.

### 2.1.2 Experimental Work

De Ris (1969) reviewed McAlevy and Magee' (1967) work, where they did extensive experiments for thermally thick materials. Atreya (1984) conducted horizontal flame spread

experiments for wood and also developed a numerical simulation model to predict horizontal flame spread. This model included all necessary components of flame spread phenomena, namely, combustion of pyrolyzing gases, conduction and pyrolysis in the solid, radiation and convection from the flame to the fuel surface. He verified that: 1) forward radiation heat transfer from the flame is the primary accelerating mechanism, 2) forward gas phase heat transfer is a local phenomenon independent of fire size (only material dependent). He solved transient partial differential equations in solid phase which requires large computational time.

Quintiere (1981, 1983 and 1988) used experimental data of flame spread and ignition from the LIFT apparatus to generate material properties data to calculate lateral flame spread rate. He assumed a constant heat flux from the flame to the fuel surface ahead of pyrolysis front extended over a small area. The gas phase conduction from the flame to the fuel surface is the major part of heat flux for the test condition of the LIFT apparatus because flame size is usually small. An analytical solution and a material heat flux characteristic property for flame spread are derived for calculating flame spread speed.

Fernandez-Pello and Hirano (1983) reviewed experimental studies on opposed and concurrent flow flame spread. They realized that flame spread in opposed gas flows frequently occurs at near extinction or non-propagating condition because fires usually spread in atmosphere or vitiated ambient oxygen concentration. The oxygen concentrations are close to the extinction or non-propagation limit. They pointed out that theoretical description, of the flame spread process based solely on heat transfer analysis are inadequate to predict rates of spread near extinctions, unless steps are taken to empirically introduce the effect of gas phase chemical kinetics through one or several of the parameters. Therefore gas phase chemical kinetics plays a critical role while in concurrent flow conditions, heat transfer from the flame to the unburnt fuel is the primary controlling mechanism of flame spread. Ray and Glassman (1983) further investigated the variation of flame propagation rate for a thermally thick solid as a function of opposed flow velocity. They concluded from their analysis and earlier experimental work (Fernandez-Pello et al., 1980) that the opposed flow flame spread comprises of three regimes: at low opposed flow velocities which is dominated by the naturally induced flow, the flame spread rate shows very little variation; the second regime shows a linear increase of propagation rate with opposed flow and is dominated by thermal process alone. In this regime, the laminar premixed flame spread speed at the lean limit is larger than opposed flow velocity. The flame spread speed is determined solely by production of fuel vapor; when the laminar flame spread speed is less than opposed flow velocity, as in the case of the third regime, the chemical effect dominates, the flame spread speed declines. Opposed gas velocity profile has significant influence on the flame spread (Di Blasi et al., 1989).

Fernandez-Pello (1984) reviewed modeling efforts of the flame spread (both opposed and wind assisted flame spreads). He pointed out that most of the early work of flame spread models are based on the opposed flow mode of flame spread because most available experimental information was for this configuration.



Ito and Kashiwagi (1987) conducted PMMA flame spread experiments at various angles ( $-90^\circ$  to  $90^\circ$ ), with  $0^\circ$  being horizontal orientation. Holographic interferometry was used to measure the temperature distributions along the sample surface (flame spread direction) and towards the solid. The net heat flux from the gas phase to sample surface at the pyrolysis front of the PMMA sample was therefore obtained. They concluded that the total net heat transfer rate into the sample from the gas phase is about 56% of the total heat transfer input to the sample at  $\theta = -90^\circ$ , 78% at  $\theta = 0^\circ$ , 87% at  $\theta = +10^\circ$ , and 99% at  $\theta = 90^\circ$ , where  $-90^\circ$  is downward flame spread and  $+90^\circ$  means upward flame spread.

Bhatanger et al. (1990) conducted horizontal flame spread experiments of insulation fibre boards. The samples were moved discretely to insure that the flame front remains at the same location with respect to the external radiating surface. A constant flame spread speed was obtained, effectively eliminating the transient effects of flame spread. They also investigated edge effects on flame spread and found that flame spread speeds for samples with uninhibited edges (edges are not wrapped with non-flammable material) are higher than that of samples with inhibited edges. Fangrat and Wolanski (1991) conducted horizontal flame spread for textile floor coverings made of polypropylene or polyethylene. The flame spread speed as a function of external heat flux was obtained. The surface and bottom temperatures of the sample were measured. Both direct and schlieren photographs of flame front were taken. They clearly observed from their schlieren photographs a hot zone just ahead of the flame front. This zone just extends a comparatively small distance ahead of the flame front. They used exponential profile for radiative and convective heat fluxes from the flame to the fuel surface. The coefficient of these heat flux distributions were first fitted with their experimental data. A general numerical solution and analytical solution for a thermally thin material (such as floor coverings) were developed to predict horizontal flame spread. The result gives right trends though the predictions do not agree with the experiments well because they did not accurately measure the flame heat flux, especially the gas-phase convective heat flux, in addition to over simplicity of their numerical model.

Zhang et al. (1991) experimentally investigated Lewis number effect on flame spread. They measured flame spread rate of thin paper samples and flame temperature as a function of diluent type,  $O_2$  mole fraction, pressure and fuel bed thickness. Since Lewis number has significant influence on temperature of diffusion flame, the flame temperature in turn affect the rate of finite chemistry, consequently, the flame spread rate would be altered from Lewis number of unity as described in de Ris' (1969) work. Experimental data of Zhang et al. (1991) show that the flame spread rate increases with increasing oxygen concentrations for thin paper samples.

Bhattacharjee and Altenkirch (1992) conducted flame spread experiments in a microgravity environment using a sealed chamber filled with 50/50 (volumetric) oxygen/nitrogen mixture. The test samples were thin filter papers. Solid and gas-phase temperatures were measured. The experimental results show that the fuel preheat zone upstream of the gas-phase flame is followed by a constant temperature pyrolysis zone, which



is followed by a large zone of surface reactions. They have also compared their numerical results (Bhattacharjee and Altenkirch, 1990) with the experimental data and suggested that radiation has to be included in their model to accurately predict flame spread.

## 2.2 COMBUSTION AND RADIATION IN FIRES

An important component for modeling and estimating fire spread and fire growth is the heat flux imposed on unpyrolyzed and pyrolyzing materials. Aside from heat fluxes from a hot upper layer or other sources, heat fluxes originate primarily from the flame under consideration or other fires adjacent to a material. Such heat fluxes are mainly due to luminous soot radiation from the flames, because fires in general produce more soot than controlled combustion systems. Thus, it is essential for fire spread and growth predictions to be able to estimate radiative heat fluxes from fires produced from the burning of the pyrolyzing gases of a given material. For this purpose, predictive methods for combustion in fires are needed. Such predictive methods are difficult to develop because fires are turbulent diffusion flame systems dominated by buoyancy. Despite the remarkable progress in turbulent combustion over the last decade, current engineering turbulent models, such as  $k-\epsilon-g$  models, can not provide reliable tools for predicting fluctuation in turbulent buoyant combustion, luminous flame radiation and products of combustion issuing from the burning of an arbitrary material (Bilger, 1976, 1977) (note that  $k-\epsilon-g$  models have been shown to be adequate to account for the dispersion of heat and combustion products after combustion is complete) (Koylu et al., 1990).

Moreover, application of detailed  $k-\epsilon-g$  models in compartment fire growth and smoke movement codes would be rather prohibitive, especially for multi-room or multi-story fires.

Because of such limitations, i.e. scientific and practical, we have put an effort in this project into the development of new integral type models for turbulent fires (such as models by Steward (1970); Tamanini (1981); Delichatsios and Mathews (1989); Cook (1991)). The major innovation in this new integral model concerns the modeling of a) turbulent scalar fluctuations and b) luminous flame radiation, as described in Chapter 4 and Appendix A. Briefly, for the fluctuations in turbulent buoyant fires, we have developed a general correlation by combining analysis and experimental data (See Appendix B) (note: the magnitude of these fluctuations is underpredicted by  $k-\epsilon-g$  models (Koylu et al. (1990))). For the luminous flame radiation in turbulent flames, we have applied a soot formation model (Delichatsios, 1993) that has been derived from measurements of smoke-point data of a given fuel material (gaseous, liquid or solid) (See Section 4.2). It should be pointed out that the chemistry of combustion is reproduced, as it is commonly done, by using so-called state relationships between chemical species and mixture fraction (see Section 4.2 and Appendix A). It still remains a challenge to obtain these state relationships from measurements of product yields from practical material (such measurements can be done in a hood collector (Zukoski et al., 1991, Beyler, 1986) or in a turbulent flow (Tewarson et al., 1993)). The

intended results of the integral model are a) flame radiation distribution in fires and b) products of combustion including soot and even effects of vitiation for an arbitrary material.

## **Chapter 3      Physics of Opposed-Flow Horizontal Flame Spread, Description of the Horizontal Flame Spread Model and Comparison with an Analytical Solution**

### **3.1      PHYSICS OF HORIZONTAL FLAME SPREAD**

Flame spread occurs when fuel surface reaches a characteristic temperature at which material is ignited (Atreya, 1984; Quintiere, 1981). This temperature is called ignition or pyrolysis temperature in the present work (it is assumed that pyrolysis temperature is the same as ignition temperature (Atreya, 1984; Quintiere, 1981)). A study of heat transfer involved in this process is necessary to predict fuel surface temperature histories and flame spread.

There are two types of flame spreads, namely concurrent and opposed-flow flame spreads. Opposed-flow flame spreads include downward, lateral and horizontal flame spreads (see Chapter 2). In this work, we focus on opposed-flow flame spread, in particular horizontal flame spread. Heat transport mechanisms in opposed-flow flame spread include (see Figure 3-1): convection/radiation from the flame to the fuel surface, heat loss from the flame to the ambient environment (by radiation and conduction/convection), radiative/convective heat loss from the fuel surface to the ambient, conduction normal and parallel to the fuel surface. The relative importance of the heat transfer mechanisms depends, among other things, on fuel thickness, ambient oxygen concentration and opposed flow velocity. Heat transfer to the unburnt fuel occurs by conduction through the gas from the flame to the unburnt region, heat conduction from behind the flame through the solid to the solid ahead of the flame, and by radiation from the flame. Radiation from the flame is relatively unimportant in downward flame spread because the view factor for radiation is small. For thermally thin solid, heat conduction through the gas is generally considered as the dominant mode of heat transfer because the path for heat transfer through the solid is very limited (Williams, 1976). For thick solids, both heat conduction through the solid phase and gas phase are important (Fernandez-Pello and Williams, 1975; Fernandez-Pello, 1984).

Solid phase heat transfer is important for flame spread over a solid fuel (di Blasi et al., 1989; Ray and Glassman, 1983). Heat is conducted at directions both normal and parallel to fuel surface and by radiation. The emissivity of the fuel surface, the material properties ( $k$ ,  $\rho$ ,  $c$ ,  $L$  (heat of pyrolysis)), including charring and boundary conditions at the back surface, would also affect the solid heat transfer and flame spread rate (Chen et al., 1993a, 1995).

Gas phase chemical kinetics and gas phase heat transfer to the solid surface are also important factors affecting flame spread. Combustion in the gas phase is controlled both by mass transfer of reactant to flame as well as by chemical kinetics. Combustion also affects radiation from the flame to the fuel surface, flame temperature and gas phase conduction

ahead of the flame front. Chemical kinetics effects depend on opposed flow velocity, oxygen concentration, pyrolysis gas composition and vapor temperature. It is difficult to determine these effects on gas phase conduction because of the complex flow involved near the flame front.

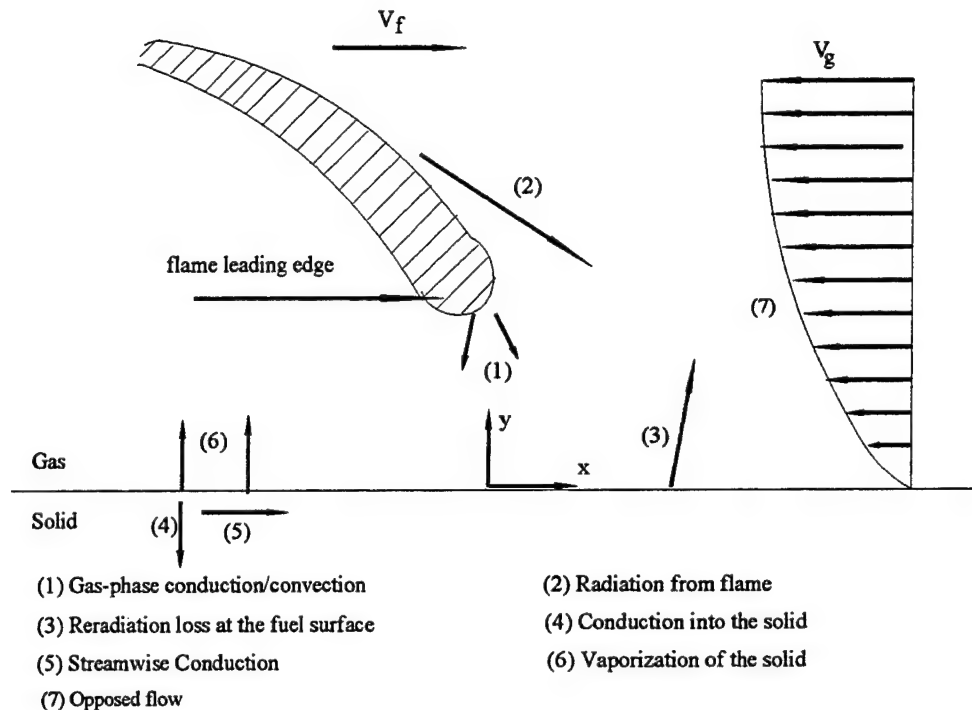


**Figure 3-1** Components of opposed flow horizontal flame spread

Flame spread occurs when fuel surface reaches pyrolysis temperature,  $T_p$  (Atreya, 1984; Quintiere, 1981). Therefore, in order to calculate flame spread as a function of time, the fuel surface temperature ahead of flame front has to be determined. The solid temperature increases because the solid fuel receives various heat fluxes from the flame and other sources as shown in Figure 3-1. There are two stages involved in preheating a point (the preheating process is evaluated by a transient 1-D conduction model) on the fuel surface in horizontal flame spread: 1) this point is heated by external heat flux from other sources or other flames and by radiation from its own flame. A combustion model using heat release rate or pyrolysis rate (therefore a solid pyrolysis model) is thus needed to calculate the radiation from its flame 2) when the flame front approaches the point, a convective heat flux is applied. This heat flux applies to a very short distance ( $O(1 \text{ mm})$ ) and it remains to be determined. We can conclude that a study of horizontal flame spread should include the following components as illustrated in Figure 3-1:

1. A preheat model for calculating the solid temperature rise,
2. A pyrolysis model to provide pyrolysis rate from different materials,

3. A combustion model coupled with the solid phase to compute flame radiation to the fuel surface and coupling to the flame spread phenomena based on flame growth which is affected by ambient condition.
4. A model to evaluate gas-phase conduction near the flame front at gas-solid interface.

Figure 3-2 illustrates the submodels and interconnections of the horizontal flame spread model. An description of models and overview of work involved in current project are presented as follows.

### A. Heat-up and Pyrolysis Model

The process of solid temperature rise ahead of the flame is predicted by an integral heat-up model developed earlier (Chen, 1991, Chen et al., 1993a). An integral pyrolysis model is also used to calculate pyrolysis rate when the fuel surface reaches pyrolysis temperature,  $T_p$ . This 1-D transient conduction model was also developed and validated in earlier works (Chen, 1991, Chen et al., 1993a) and has been developed to predict pyrolysis of charring and non-charring materials. The integral heat-up and pyrolysis models use as inputs, material flammability properties such as  $k$ ,  $\rho$ ,  $c$ , measured in standard flammability apparatus (Chen et al., 1995, Delichatsios and Saito, 1991). Heat fluxes acting on the fuel surface are needed in the model to determine temperature rises or pyrolysis rate of the solid. The pyrolysis rate is required input for the combustion.

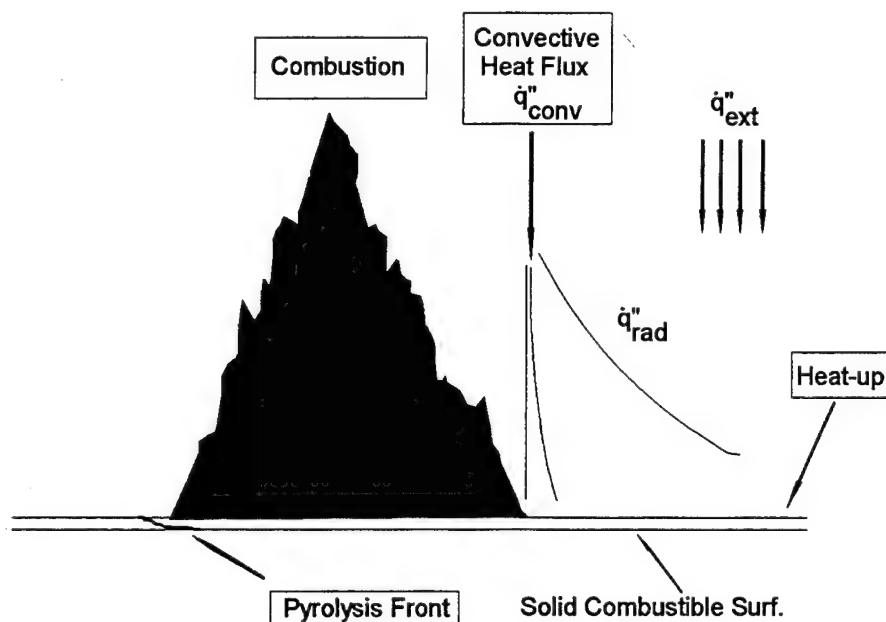


Figure 3-2 A schematic diagram of horizontal flame spread

There are several heat fluxes involved in evaluating surface temperature described as follows: 1)  $\dot{q}_{\text{rad}}''$  is radiative heat flux from the flame originating from burning of the pyrolysis gases. This radiative heat flux is quantified by a radiation-combustion model which uses pyrolysis rate given by the pyrolysis model as an input. 2)  $\dot{q}_{\text{conv}}''$  is called gas-phase conductive heat flux. This heat flux drops from a large value ( $\sim 50 \text{ kW/m}^2$ ) to 0 over a very short distance ( $O(1\text{mm})$ ). Therefore, it is very difficult to measure or calculate. A constant speed horizontal flame spread experiment has been designed and conducted to derive this heat flux profile. These two heat fluxes are major focuses of the current work. The following three heat fluxes are basically inputs to the horizontal flame spread model and can be readily determined: 1)  $\dot{q}_{\text{ext}}''$  is external heat flux originating from other sources, 2)  $\dot{q}_f''$  is convective heat loss from the hot fuel surface to the environment which can be calculated using an empirical correlation of natural convection, 3)  $\dot{q}_{\text{rer}}''$  is reradiation loss from the fuel surface and can be estimated as:

$$\dot{q}_{\text{rer}}'' = \epsilon \sigma (T_s^4 - T_0^4) \quad (3-1)$$

where  $T_s$  is surface temperature and  $T_0$  is ambient temperature;

## B. Combustion Model

The pyrolysis rate,  $\dot{m}''$ , obtained from the integral pyrolysis model is used as an input to an integral combustion model. The combustion model uses state relationship (laminar species concentration as a function of mixture fraction), a correlation to account for turbulent fluctuations of the scalar quantities together with equations of conservation of mass, momentum and energy (in terms of total enthalpy) to solve for the enthalpy, species concentration, centerline velocity and temperature at discrete intervals. This model was validated using jet flame and pool fire experimental data in the current work. It simulates flame radiation and its relation to flame turbulence and the sooting tendency of the fuel. Chemical reaction and combustion is modeled using conservation equations and an ensemble of flamelets. The model can estimate, as a function of the height from the flame base, radiation loss distribution,  $\dot{q}_{\text{R}}''(z)$ , radiation fraction,  $\chi_{\text{R}}$  and heat release rate. Flame length,  $\ell_f$  and major species production rate can also be computed. The radiation loss distribution, heat release rate and flame length are used to calculate heat flux to the fuel surface ahead of the flame front. The combustion model needs to be coupled with the flame spread model. Thus, as the flame grows, the energy input to the fuel surface can change leading to a variation of  $\dot{m}''$ . **This coupling** is a very important development and its completion requires availability of state relations for real fires and an accurate modelling of the radiation to the fuel surface. At the present, a simple coupling using known correlations for mass burning rate and heat release rates (given a burning area) is incorporated. The actual prediction of mass loss rate depends on the flame radiation feed back to the fuel surface. This would require additional data and information on the physics of the soot yield and flow dynamics near the

base of the flame. Such details are difficult to model and the research in this field is still in a developing stage. The integral combustion model, however, is discussed in detail in Chapter 4 and Appendix A.

### C. Heat Flux Model

Using the radiation loss distribution, the heat release rate at height intervals and the flame length, the radiative heat flux,  $\dot{q}_{rad}''$ , from the flame to the fuel surface, both inside and outside the flame, can be determined by a heat flux model. One such model is currently being developed by Vezis (1995) in our research group and the final model can be incorporated into the horizontal flame spread model. This model will not be discussed here. To simulate the radiation ahead of the flame, we have used an exponentially decaying function (discussed next), which is a very good representation of the actual phenomenon.

### D. Constant Speed Horizontal Flame Spread (CSHFS) Experiment

As stated before, the quantification of gas-phase conduction is very difficult. An exponential type profile for the gas-phase conductive (convective) heat flux (this can be supported by the numerical analysis (di Blasi et al., 1987, 1989) and analytical solution (Atreya, 1984)) has been assumed:

$$\dot{q}_{conv}'' = \dot{q}_g'' e^{-\frac{x-x_p}{\delta_g}} \quad (3-2)$$

where  $x$  is distance along the horizontal surface in the direction of flame spread,  $x_p$  is flame front location,  $\delta_g$  is length scale of the gas-phase conductive heat flux and  $\dot{q}_g''$  is the magnitude of this heat flux. A constant speed horizontal flame spread experiment was developed in this work in order to obtain  $\delta_g$  and  $\dot{q}_g''$ .

In the CSHFS experiment, a fuel sample was moved at a constant speed towards the stationary flame or pyrolysis front. The flame is quenched by a cooling plate to maintain a constant (and small) burning area as the sample was moving. In this way, the transient effects of flame spread, pyrolysis rate as well as flame radiation can be eliminated. Surface temperature, total heat flux histories at the fuel surface and flame front locations were measured. The surface temperature histories were used to determine the gas-phase conductive heat flux. The description of the experiment is presented in Chapter 5. Chapter 6 discusses experimental results and derivation of the gas-phase conduction. The comparisons for both flame front and surface temperature between experimental data and numerical simulation using the derived gas-phase conduction are also shown in Chapter 6. More results can also be found in Appendix H.

By using the heat-up model (Chen, 1993a) (which was not the scope of the current work, but has been incorporated in the horizontal flame spread model) that uses material flammability properties and heat fluxes described above, surface temperatures ahead of the flame (pyrolysis front) can be obtained. The flame front location,  $x_p$ , can therefore be derived as described in Section 3.2.

### 3.2 DESCRIPTION OF THE HORIZONTAL FLAME SPREAD MODEL

The heat-up, pyrolysis and combustion models which was briefly described here have been combined to form a comprehensive horizontal flame spread model. This model involves several steps to find flame front location and pyrolysis rate:

1. Obtain external heat fluxes from input or calculated by a compartment fire model, calculate flame radiation and gas-phase conductive heat fluxes derived based on experiments from the flame to each node,
2. Using above heat fluxes, calculate surface temperature for each node using either preheat or pyrolysis model depending on whether the node is at heating or burning, sum pyrolysis rate of each node,
3. For the pyrolysis front, both heat-up and pyrolysis would be calculated,
4. Find new pyrolysis front using surface temperature data obtained in steps 2 and 3,
5. The sum of pyrolysis rate is used as an input to the combustion-radiation model to evaluate flame radiation to the fuel surface, then go back to step 1 for the next time step.

The flow chart of the Horizontal Flame Spread on Compartment Surface (HFSCS) is shown in Figure 3-3 where the interconnections of different subroutines are illustrated. The purpose of each subroutine is described as follows:

- |                |   |
|----------------|---|
| 1.hfscs.f      | The name of the HFSCS code  |
| 2.inputdata    | This routine is used to read the physical properties (e.g. $k$ , $\rho$ , $c$ , $T_p$ , $L$ , etc.) of the fuel that is/will be burning |
| 3.maincal      | The main driver calling all the calculation and output routines   |
| 4.flxte, flxtf | These routines obtain external, flame heat fluxes   |
| 5.preheat      | Driver for heat-up calculation  |
| 6.hpcg         | Hamming's Predictor-Corrector method numerical solver   |
| 7.heatin       | Heat-up calculation for the first time step   |
| 8.heat         | Normal heat-up calculations   |
| 9.qflux        | Combine all the heat fluxes absorbed by the fuel surface  |
| 10.vapor       | The driver for transient pyrolysis process  |
| 11.pyrobb      | The initial pyrolysis calculation   |
| 12.pyrobb      | Normal pyrolysis process calculation  |
| 13.front       | Driver to call routines for combustion  |
| 14.locxp       | Classifying the nodes to see if the node is pyrolysis, heat-up or the section containing the node just starts to pyrolysis              |



- 15.getxp      Interpolation to obtain pyrolysis front
- 16.ftf        Heat release rate and flame height
- 17.loctxb     Locate burnout front
- 18.output     Output results (flame front, flame height, heat release rate, etc.)

This program has been successfully run on Unix and PC systems.

### 3.3 LOCATING THE FLAME (PYROLYSIS) FRONT

The fuel is divided into large number of segments with  $n$  nodes along the fuel length. The surface temperature at each node at each time step is evaluated using the preheat or pyrolysis model (Chen et al., 1993a).

By comparing surface temperature with the pyrolysis temperature, the flame front location can be bracketed into a certain segment. This is called the pyrolysis section. The first section includes the fuel segment between nodes 1 and 2, with node 1 as the beginning of the section while node 2 is excluded from this section. Section 2 would begin with node 2. Section  $I$  would begin with node  $I$  and end with  $I+1$ , but exclude node  $I+1$ ). The pyrolysis front is located between nodes  $x_{i-1}$  and  $x_i$  if surface temperatures of these nodes,  $T_{s,i-1}$  and  $T_{s,i}$  are higher and lower than pyrolysis temperature, respectively. The new pyrolysis front location can be determined either from the two nodal surface temperatures or from the fictitious temperature of the pyrolysis front,  $T_{sp}$  and  $T_{s,i}$  depending on the flame front location previously.

To find new pyrolysis front location,  $x_p$ , one has to determine where the surface temperature is at the pyrolysis temperature,  $T_p$ , i.e.:

$$\theta(x_p^n, t^n) = \theta_p$$

where  $\theta = T_s - T_0$  and  $\theta_p = T_p - T_0$ ,  $T_0$  is initial temperature.  $x_p^n$  is pyrolysis front location at time  $t^n$ .

If  $x_i$  is the nodal location next to  $x_p^n$  where pyrolysis has yet to start, i.e.:

$$\theta(x_i, t^n) < \theta_p$$

at time  $t^{n+1}$ , one calculates by using the heat-up model, the fictitious temperature at  $x_p^n$  (as if pyrolysis did not start) and surface temperature at  $x_i$ , if

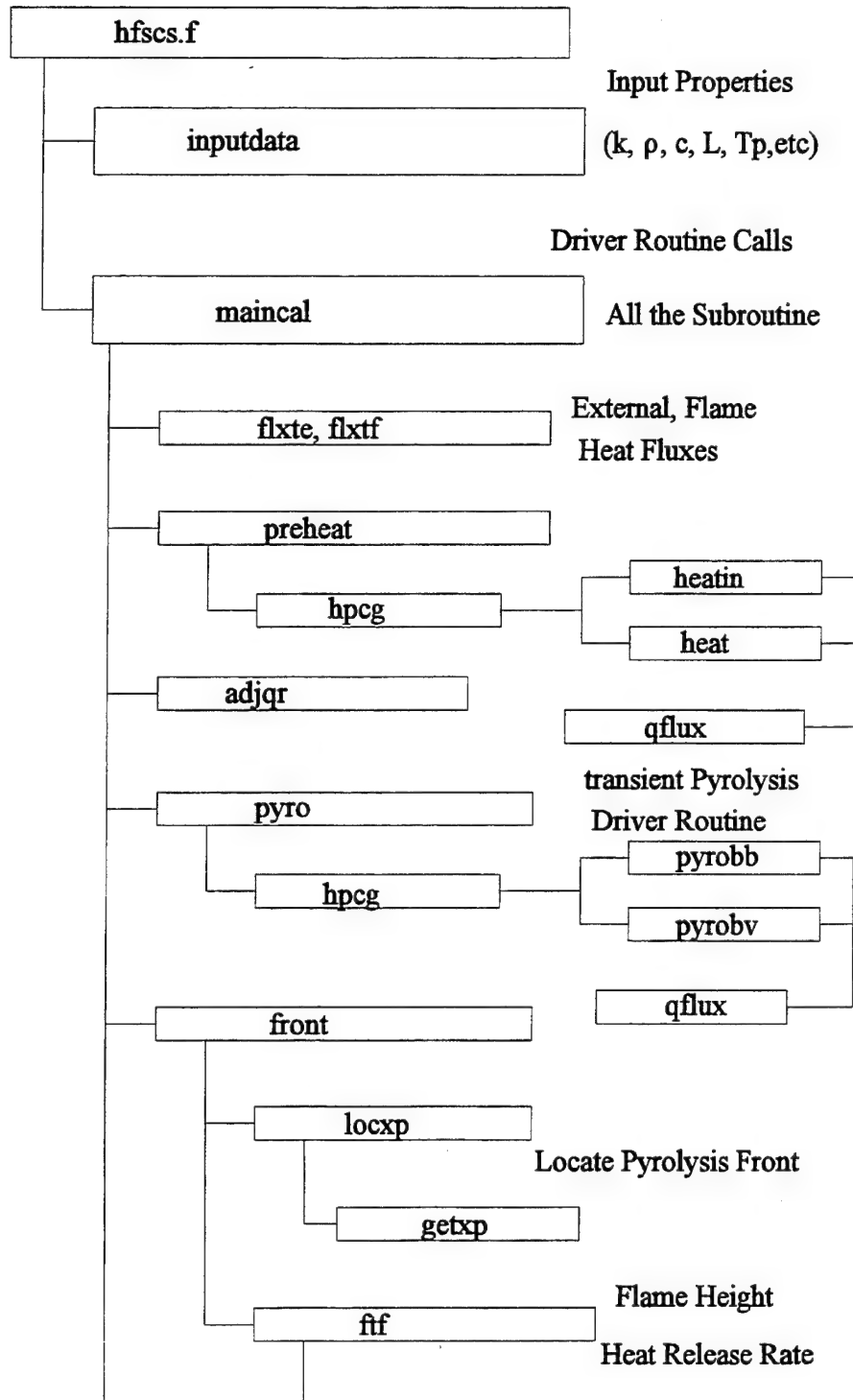
$$\tilde{\theta}(x_p^n, t^{n+1}) > \theta_p \text{ and } \theta(x_i, t^{n+1}) < \theta_p$$

The new pyrolysis front can be obtained by using a linear approximation:

$$x_p^{n+1} = x_p^n + \frac{\tilde{\theta}(x_p^n, t^{n+1}) - \theta_p}{\tilde{\theta}(x_p^n, t^{n+1}) - \theta(x_p, t^{n+1})} \cdot (x_i - x_p^n) \quad (3-3)$$

In reality, the process of finding new pyrolysis front location is: 1) the model figures out whether the pyrolysis front entered the section at the previous time step and 2) If the pyrolysis front was in this section at the previous time step, eqn. (3-3) is used to locate new pyrolysis front, otherwise, the fictitious temperature of node  $x_{i-1}$  and preheat temperature of node  $x_i$  are used to locate the new pyrolysis front, eqn. (3-3) is still used, with  $x_{i-1}$  replacing  $x_p^n$  and  $\theta(x_p^n, t^{n+1})$  being the fictitious temperature at node I-1.

## Flow Chart HFSCS



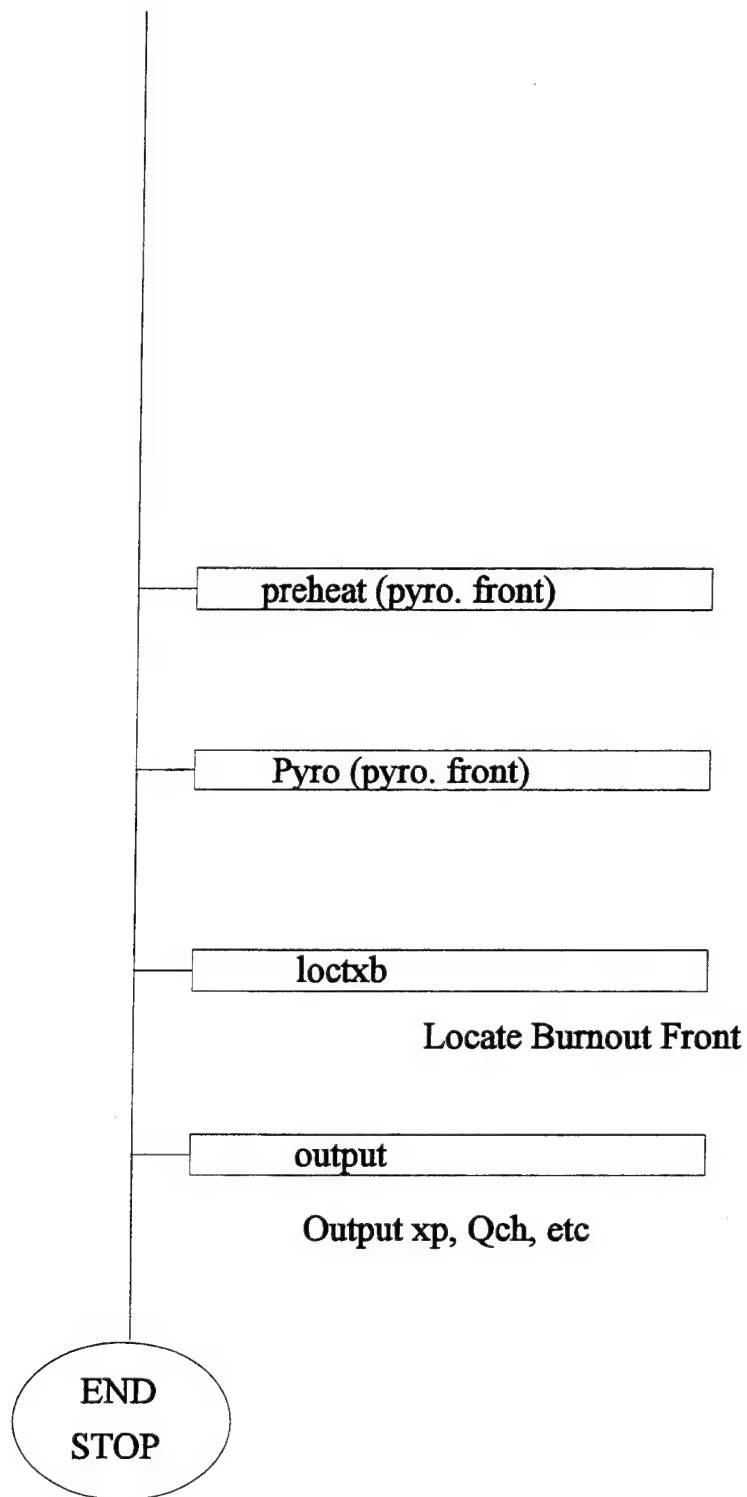


**Figure 3-3** A flowchart and interconnections of the horizontal flame spread on compartment surfaces

### 3.4 SURFACE TEMPERATURE CALCULATIONS USING TWO SOLID TEMPERATURE PROFILES

When a sudden jump of heat flux (e.g. gas phase conduction from flame) starts to apply to a fuel surface which has been heated for a period of time by other heat fluxes (e.g. external, flame radiative heat fluxes), surface temperatures of the fuel and flame front location can not be accurately calculated and estimated by the flame spread code developed initially (see also Delichatsios, M.M. et al., 1990). This problem arises from the fact that there exists actually two different heat-up layers: 1) a new heat-up layer caused by the sudden jump heat flux, and 2) the original heat-up layer caused by other heat fluxes. The original model uses a single temperature exponential decay type profile having a single length scale. This would introduce error in the calculation of surface temperature as well as thermal penetration length (Chen et al., 1993a). Therefore, modification of the original code was made by observing that the heat conduction equation used in the integral heat-up model (Chen et al., 1993a):

$$\frac{\partial \theta}{\partial t} = \alpha \frac{\partial^2 \theta}{\partial z^2} \quad (3-4)$$

can be split into two equations with appropriate initial and boundary conditions for  $t \geq t_1$ , when a sudden jump heat flux,  $\dot{q}_2'' - \dot{q}_1''$  is applied (see eqns. (F-5a), (F-5b), (F-6a) and (F-6b) of the Appendix F):

$$\frac{\partial \theta_1}{\partial t} = \alpha \frac{\partial^2 \theta_1}{\partial z^2} \quad (3-5a)$$

$$-k \frac{\partial \theta_1}{\partial z} \Big|_{z=0} = \dot{q}_1'' \quad (3-5b)$$

$$\frac{\partial \theta_2}{\partial t} = \alpha \frac{\partial^2 \theta_2}{\partial z^2} \quad (3-5c)$$

$$-k \frac{\partial \theta_2}{\partial z} \Big|_{z=0} = \dot{q}_2'' - \dot{q}_1'' \quad (3-5d)$$

@t=t<sub>1</sub>

$$\theta_1(x,t_1)=\theta(x,t_1) \quad (3-5e)$$

$$\theta_2(x,t_1)=0 \quad (3-5f)$$

Therefore two temperature rises,  $\theta_1$  and  $\theta_2$  can be evaluated separately by using two different heat conduction equations and boundary conditions. In other words, two temperature rises in the two different thermal layers caused by two heat fluxes imposed on fuel surface are calculated independently. The actual temperature of the solid would be:

$$\theta=\theta_1+\theta_2 \quad (3-6)$$

In this way, the correct temperatures can be determined. The original code has been modified to account for this situation and for detail see Appendix F. **Hereafter all results from the model are from the modified code using eqn. (3-6) and the described formation.**

Before conducting comparison of the numerical results of the horizontal flame spread model and an analytical solution, the sensitivities of the model will be checked at first, i.e. the numerical results using different time steps, surface nodal spacings and heat flux profiles will be compared and this will be presented in next section. The accuracy of this model will first be checked against an analytical solution which will be presented later in this chapter, and finally, this numerical model will be validated by comparing the numerical results with experimental data of constant speed horizontal flame spread (CSHFS) which we will be described in Chapter 6.

### 3.5 SENSITIVITY ANALYSIS OF THE HORIZONTAL FLAME SPREAD MODEL

Following the completion of the numerical code for horizontal flame spread, a systematic sensitivity analysis is performed by varying: 1) nodal spacings (uniform mesh sizes from small to large and non-uniform mesh size using power series), 2) time steps (from small to large), 3) heat fluxes (constant external heat fluxes of different levels; heat flux distribution at different levels, similar to the experimental conditions which will be described in Chapter 5; different flame heat flux profiles (the magnitudes and length scale of convective (gas-phase conductive) heat fluxes). It is anticipated that the limitation of the numerical code will be revealed from this process.

Figures 3-4 through 3-6 illustrates the effects of nodal spacings, time steps, and heat fluxes. The accuracies of the numerical code, needlessly to say, depend on both nodal spacing and time step. The differences between different nodal spacings are clearly manifested in Figure 3-4. Differences between results of  $\Delta x=0.5, 1, 2$  and  $4$  mm are really small. Fairly large difference from  $\Delta x=10$  mm is observed, so does power series nodal spacings. It can be easily concluded if nodal spacing is shorter than the shortest length scale of heat fluxes (in this case,  $6.67$  mm which is  $1/150$  (m)), the results would not differ much. Therefore  $\Delta x=4$  mm can be used in this case to calculate flame spread.

In Figure 3-5, the results from different time steps ranging from  $\Delta t=0.0625$  to  $\Delta t=1$  seconds are shown. Figure 3-5 shows substantial difference between time steps of  $1$  and  $0.5$  seconds. On the other hand, the difference between the results of two smallest time steps ( $\Delta t=0.0625$  and  $0.125$  seconds) are fairly small. One can see for this case, that the numerical results of  $\Delta t=0.125$  seconds are accurate enough. It can be postulated that if  $\Delta t=\epsilon\Delta x/V$ , where  $\epsilon$  is a number  $\leq 1$  and  $V$  is flame spread speed, the prediction would be accurate. The flame spread speed,  $V$ , in this case is about  $5.3$  mm/s, therefore,  $\epsilon=0.125\times 5.3/4=0.166$ . This can also be supported by Figure 3-7 which will be discussed later.

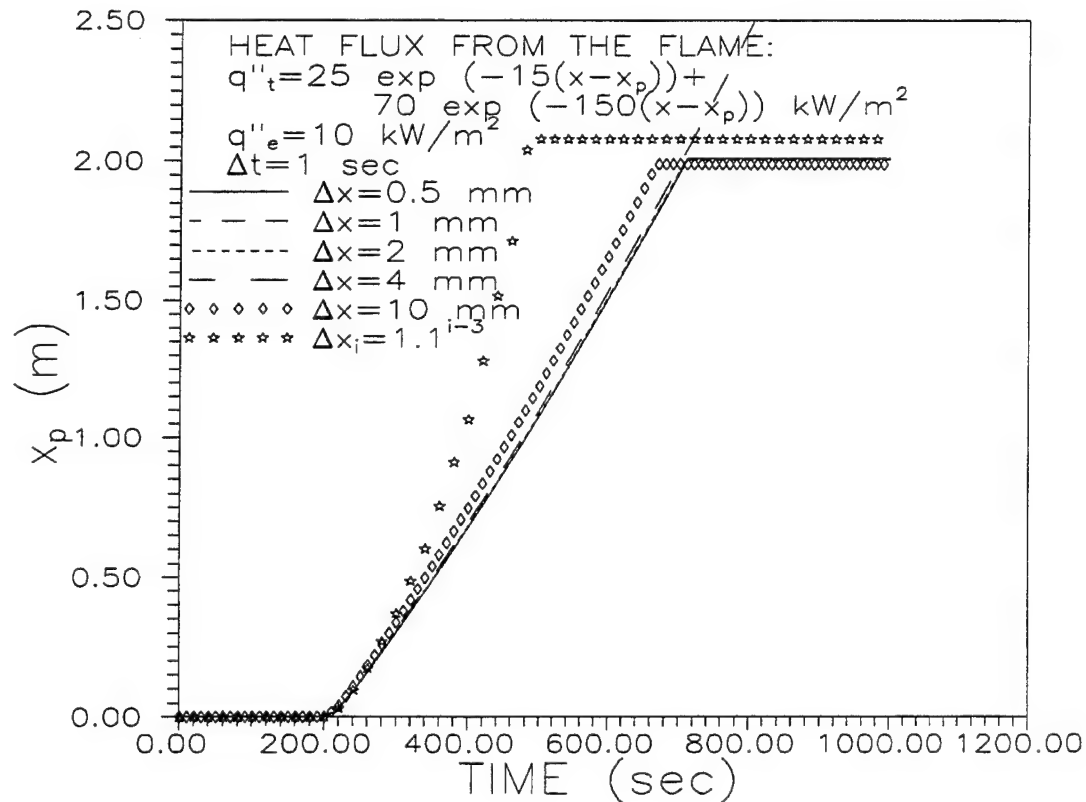


**Figure 3-4** Sensitivity analysis of the horizontal flame spread model-different nodal spacings and  $\Delta t=1$  seconds

Finally, the results from different heat flux profiles are demonstrated in Figure 3-6. Obviously, increasing heat flux and heat flux profile length scale would increase flame spread speed. It has to be pointed out that we use the external heat flux distribution experienced in the experiments (see Chapters 5 and 6) to obtain two sets of results in Figure 3-6. One may also notice that in Figure 3-1,  $\Delta t=1$  second has been used while previous results indicate that in this case,  $\Delta t=0.125$  seconds should be used in order to obtain accurate results. The rational here is that the purpose of Figure 3-6 is to check whether the code would give right trend as one changes heat fluxes, rather to see if the code can give accurate result for each case. In light of this,  $\Delta t=1$  second is sufficient and code does give satisfactory results.

A brief conclusion of above section can help an user to chose correct time step and nodal spacing in order to obtain accurate result from the horizontal flame spread code. The size of nodal spacing,  $\Delta x$ , can be selected as no larger than the smallest length scale of heat fluxes (usually gas-phase convective heat flux). The flame spread speed can be guessed next. A fairly conservative estimate of flame spread speed is 6 mm/s. The time step,  $\Delta t$ , can be chosen as  $\Delta t=0.166 \Delta x/V$ . These time step and nodal spacing are then used in the flame spread model. The flame spread speed can be determined and compared with the value that is guessed. One may need to adjust the time step if the calculated speed is larger than the guessed flame spread speed. Sensitivity of flame spread code has been examined for a similar problem (Delichatsios, M.M., 1991). It can be concluded from their analysis that the stability requirement is less stringent than the accuracy requirement for both time step and nodal

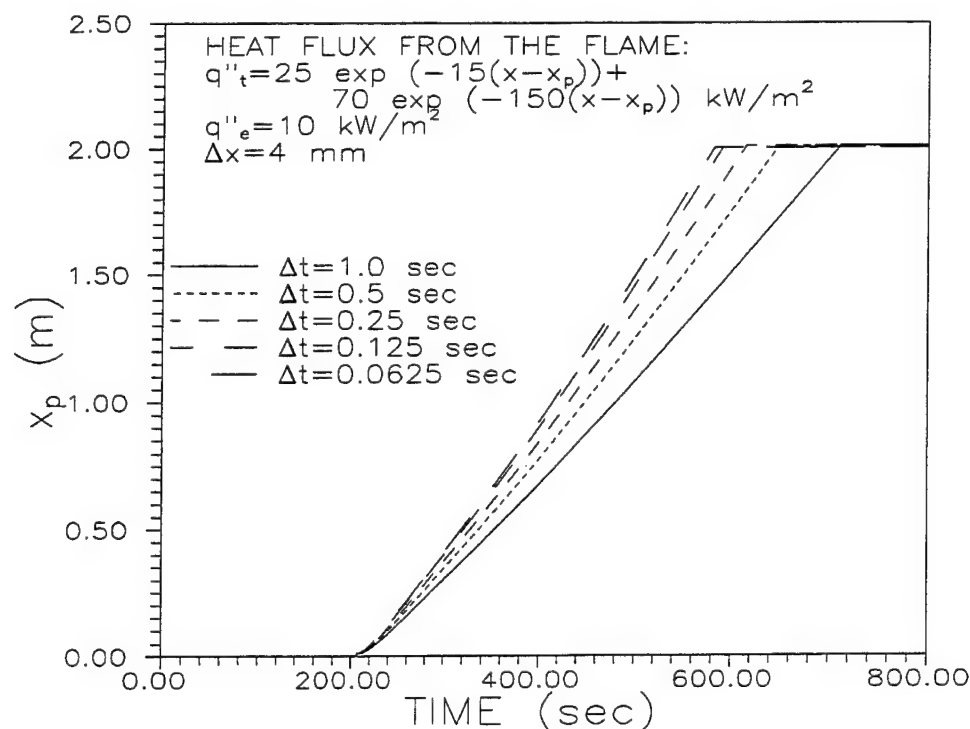


**Figure 3-5** Sensitivity analysis of the horizontal flame spread model-different time steps,  $\Delta x=4$  mm



spacing presented above. Therefore, if one uses time step and nodal spacing that are derived above, there is no stability problem.

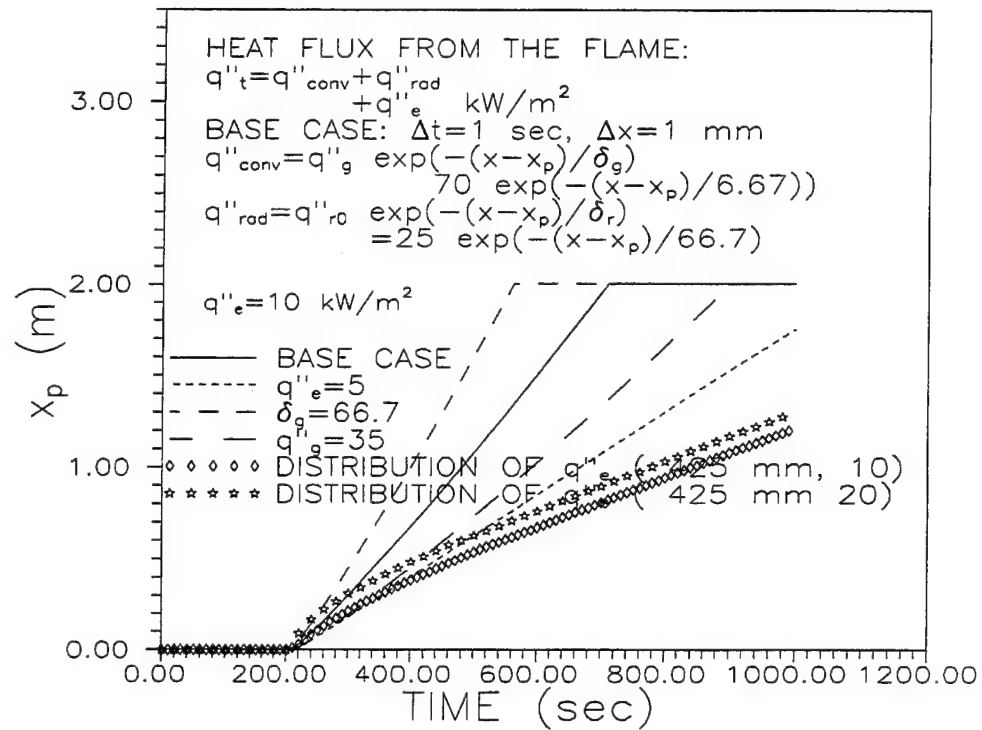


Figure 3-6 Sensitivity analysis of the horizontal flame spread model-different

### 3.6 COMPARISON WITH AN ANALYTICAL SOLUTION

In order to validate the flame spread model, the comparison between numerical results and an analytical solution using Quintiere's postulate (see Appendix D) is carried out. For thermally thick solid with imposed heat flux,  $\dot{q}''$ , at the fuel surface, the surface temperature rise of the solid can be estimated (Carslaw and Jaeger, 1959):

$$T_s - T_0 = \frac{1}{\sqrt{\pi k \rho c}} \int_0^t \frac{\dot{q}''}{\sqrt{t-\tau}} d\tau \quad (3-7)$$

Therefore for a point,  $x$ , on the fuel surface to reach pyrolysis temperature,  $T_p$ , the time,  $t$ , in eqn. (3-7), should be replaced with time to pyrolysis,  $t_p$ . Eqn. (3-7) becomes:

$$T_p - T_0 = \frac{1}{\sqrt{\pi k \rho c}} \int_0^{t_p} \frac{\dot{q}''}{\sqrt{t_p-\tau}} d\tau \quad (3-8)$$

It is assumed that the imposed heat flux,  $\dot{q}''$ , consists of two parts: 1) an external heat flux,  $\dot{q}_e''$ , and 2) a flame heat flux which has an exponential type profile:

$$\dot{q}_{conv}'' = A e^{-\frac{x-x_p}{\delta}} \quad (3-9)$$

One solves eqn. (3-8) together with the heat flux profile (eqn. (3-9)) assuming constant flame spread velocity,  $V$ . The solution of eqn. (3-8) is (eqn. (D-7) of Appendix D):

$$T_p - T_0 = \frac{A \sqrt{\delta} / \sqrt{V}}{\sqrt{\pi k \rho c}} \quad (3-10)$$

where  $T_s$  is surface temperature rise owing to external heat flux,  $\dot{q}_e''$ . It can be shown that the time to pyrolysis (Delichatsios et al., 1991; Quintiere, 1981):

$$t_p = \frac{\pi}{4} \frac{k \rho c (T_p - T_s)^2}{A^2} \quad (3-11)$$

Equation (3-11) can be substituted into eqn. (3-10) and the flame spread velocity,  $V$ , can be solved as:

$$V = \frac{dx_p}{dt} = \frac{\pi \delta}{4 t_p} \quad (3-12)$$

Equation (3-12) is an analytical asymptotic solution for constant flame spread velocity which is also referred to as the Quintiere's postulate. If surface reradiation loss is taken into account, eqn. (3-11) can be modified by (Delichatsios et al., 1991):

$$t_p = \frac{\pi k \rho c (T_p - T_s)^2}{4 (A - C \sigma T_p^4)^2} \quad (3-13)$$

where  $C$  is the coefficient that is less than 1. The flame spread speed can still be calculated using eqn. (3-12).

In the following comparisons, it has been assumed that the fuel surface receives two heat fluxes: 1) a constant external heat flux over the entire length of the fuel and, 2) a flame heat flux with an exponential profile, i.e.

$$\dot{q}_{conv}'' = \dot{q}_0'' e^{-\frac{x-x_p}{\delta}} \quad (3-14)$$

In the analytical solution, the magnitude of this heat flux,  $\dot{q}_0''$ , is used in eqns. (3-11) or (3-13) to calculate the time to pyrolysis while the length scale,  $\delta$ , is used in eqn. (3-12) to quantify flame spread speed. It also has to be pointed out that the instantaneous surface temperature,  $T_s$ , is obtained by using the constant external heat flux together with the one dimensional heat-up model.

Figure 3-7 shows the comparison of flame front location between Quintiere's postulate and the numerical results for constant heat flux:

$$\dot{q}_e'' = 5 \text{ kW/m}^2$$

and the flame heat flux:

$$\dot{q}_{conv}'' = 70 \exp[-150(x-x_p)] \text{ kW/m}^2$$

Three sets of numerical results are illustrated in Figure 3-7 with different time steps and nodal spacings. Surface reradiation is accounted for in this comparison. It can be seen from the figure that all numerical results follow the analytical solution quite well and the numerical

result with  $\Delta x=2$  mm and  $\Delta t=0.1$  seconds (the smallest time step among the three) is fairly close to the analytical solution. This shows the numerical model predicts flame spread accurately, at least for this case. Therefore in the following comparisons, only numerical results for  $\Delta x=2$  mm and  $\Delta t=0.1$  seconds will be shown.

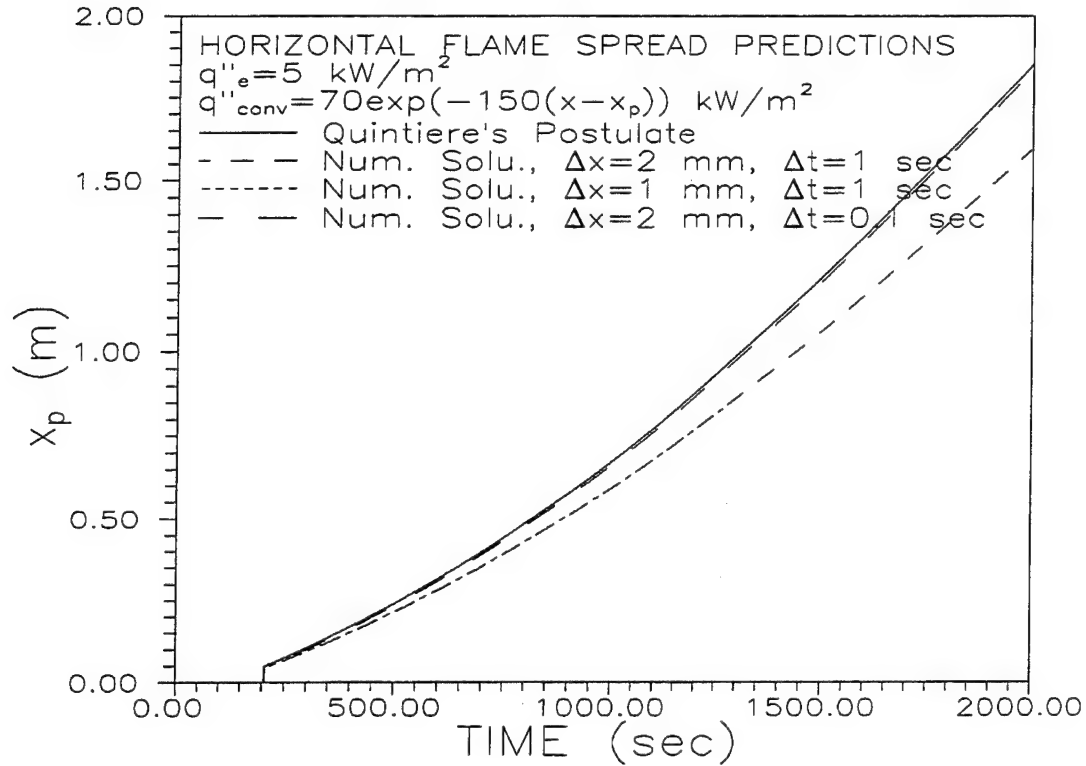


**Figure 3-7** Comparison between numerical solutions of the horizontal flame spread model and an analytical solution with surface reradiation and  $\dot{q}''_e=5$  kW/m<sup>2</sup>

The comparison of the case with no external heat flux ( $\dot{q}''_e=0$ ) is illustrated in Figure 3-8. Two sets of analytical solutions using different  $C$  (see eqn. (3-13)) are also plotted. The numerical results are closer to that of the analytical solution with  $C=0.5$ . The close behavior between the numerical result and the analytical solution shows the validity of the numerical model. It should be pointed out that all the prediction with surface reradiation loss use  $C=0.5$  including Figure 3-7. The comparisons at other external heat fluxes ( $\dot{q}''_e=10$  and  $20$  kW/m<sup>2</sup>) are shown in Figures 3-9 and 3-10 that also manifest the accuracy of the numerical model except more difference is observed for external flux= $20$  kW/m<sup>2</sup>. In that case, the flame spread speed is very higher and from the sensitivity analysis presented earlier, the time step,  $\Delta t$ , should be reduced. An important comment concerning Figures 3-7, 3-9 and 3-10 is that if the external heat flux is less than surface reradiation loss at pyrolysis temperature, i.e.

$$\dot{q}''_e < \dot{q}''_{rer} = \sigma T_p^4$$

the flame spread will be steady after initial transition. The numerical solution should match with the analytical solution asymptotically as shown in Figure 3-7. Otherwise, the flame spread speed will increase continuously, eventually towards infinity (surface flashes) if the flame front does not reach the end of sample as illustrated in Figures 3-9 and 3-10. The surface reradiation loss in this case is about  $10 \text{ kW/m}^2$ .

In Figures 3-11 through 3-14, the same sets of results for no surface reradiation losses are shown. The plots show good agreement between analytical solutions and numerical results. The results from numerical solution at  $\dot{q}_c''=0$  is essentially the same as analytical solution because in this case the analytical solution is exact. Discrepancies between numerical results and the analytical solutions have been observed for external heat fluxes of 10 and 20  $\text{kW/m}^2$  and in these cases, the time steps may have to be reduced.

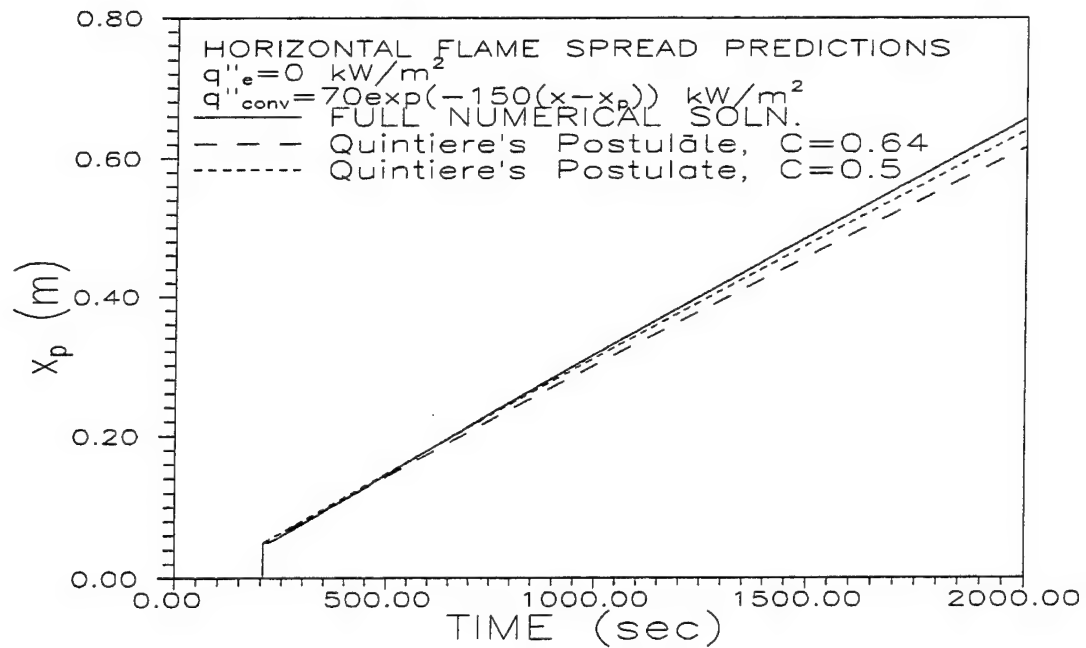


**Figure 3-8** Comparison between numerical solutions of the horizontal flame spread model and an analytical solution with surface reradiation and  $\dot{q}''_e = 0 \text{ kW/m}^2$ .  $C$  is a coefficient accounting for reradiation loss

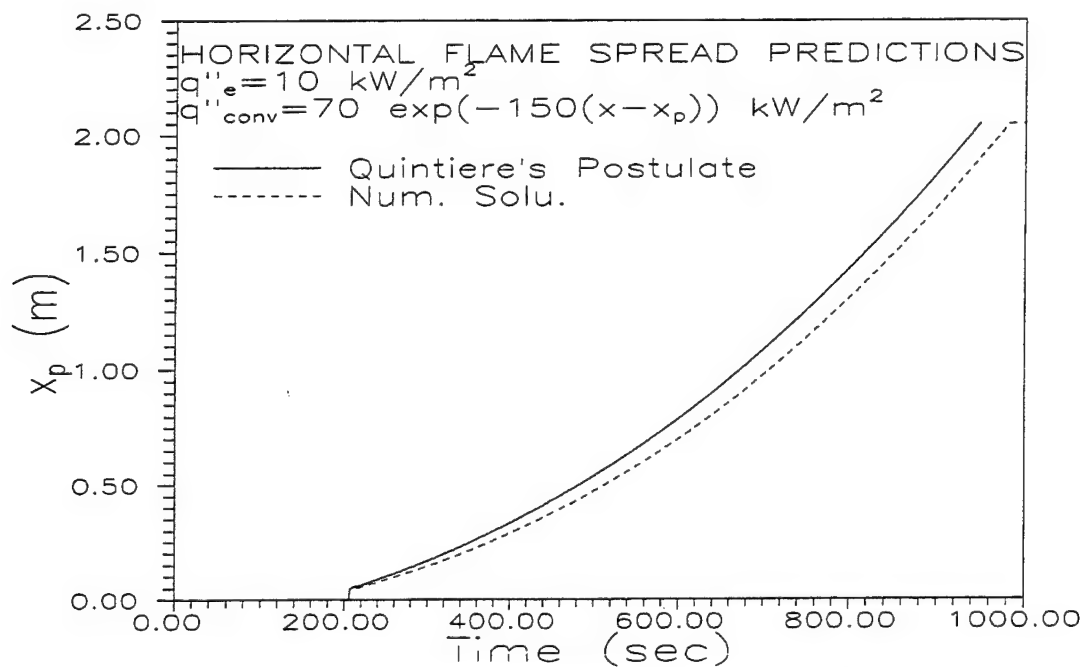


**Figure 3-9** Comparison between numerical solutions of the horizontal flame spread model and an analytical solution with surface reradiation and  $\dot{q}''_e = 10 \text{ kW/m}^2$

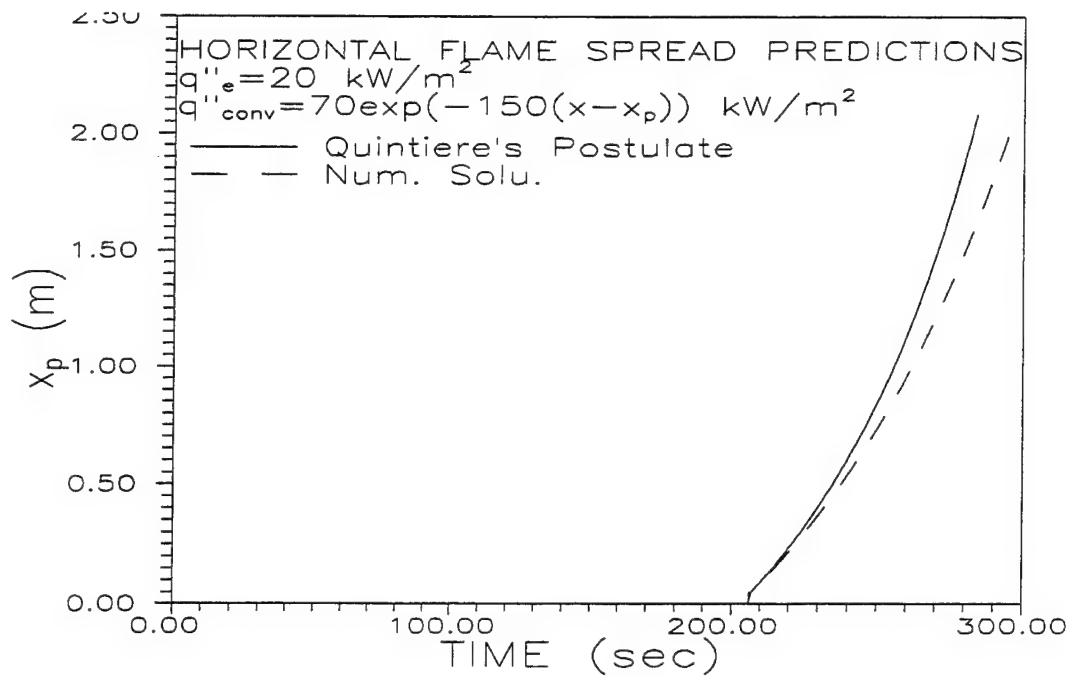


**Figure 3-10** Comparison between numerical solutions of the horizontal flame spread model and an analytical solution with surface reradiation and  $\dot{q}''_e = 20 \text{ kW/m}^2$

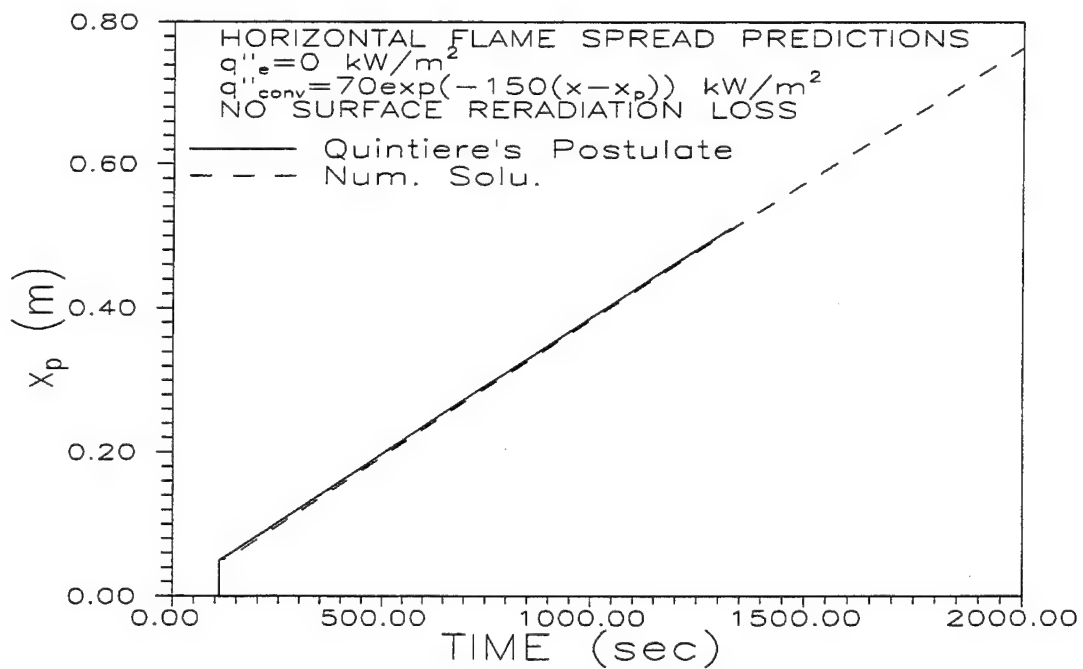


**Figure 3-11** Comparison between numerical solutions of the horizontal flame spread model and an analytical solution with no surface reradiation and  $\dot{q}''_e = 0 \text{ kW/m}^2$

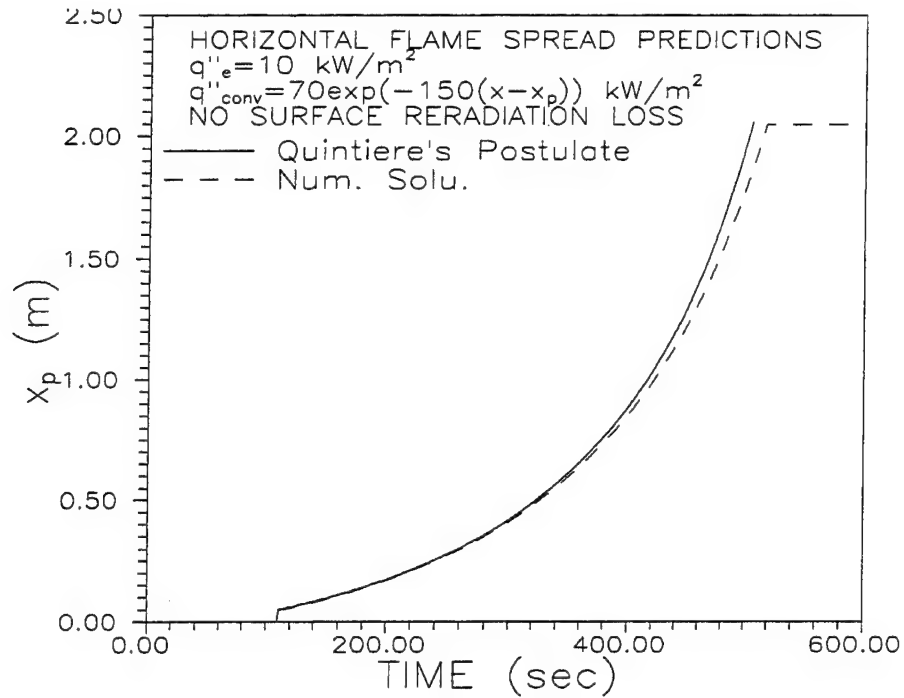


**Figure 3-12** Comparison between numerical solutions of the horizontal flame spread model and an analytical solution with no surface reradiation and  $\dot{q}''_e = 10 \text{ kW/m}^2$

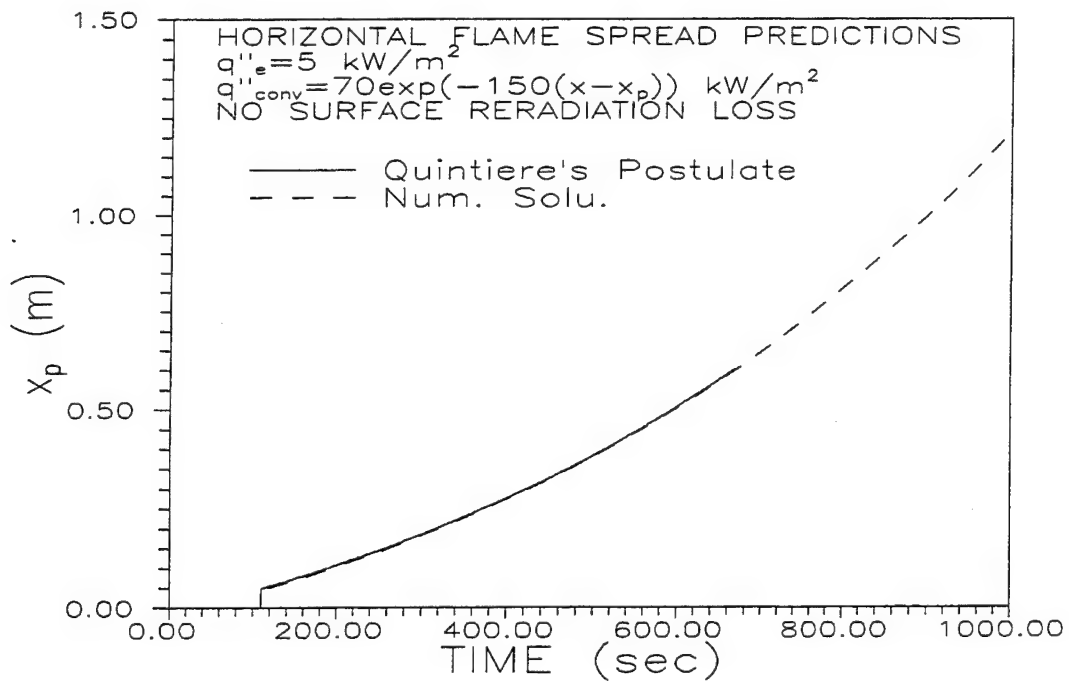


**Figure 3-13** Comparison between numerical solutions of the horizontal flame spread model and an analytical solution with no surface reradiation and  $\dot{q}''_e = 5 \text{ kW/m}^2$



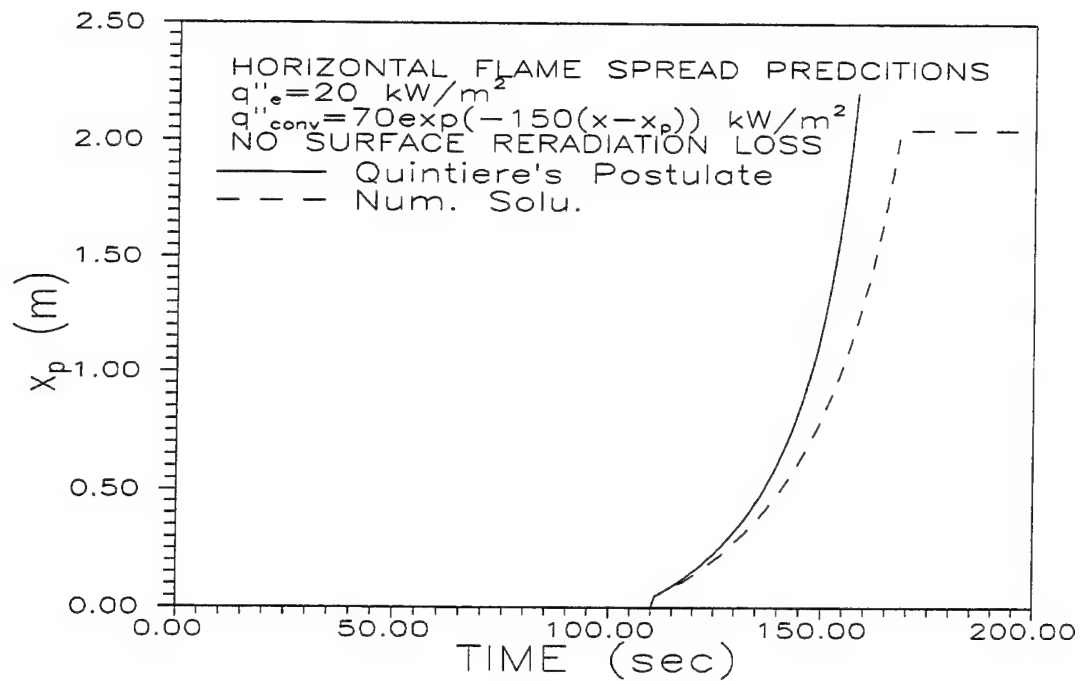


**Figure 3-14** Comparison between numerical solutions of the horizontal flame spread model and an analytical solution with no surface reradiation and  $\dot{q}_e'' = 20 \text{ kW/m}^2$

## Chapter 4      Description of Combustion Model and Comparison with Experimental Data

### 4.1      INTRODUCTION

The primary motivation for the development of the present integral combustion model presented here has been the necessity to predict flame spread behavior from burning of an arbitrary fuel, whose detailed chemical composition would not be known, as a liquid pool or a solid surface. This model would then be coupled with other phenomena such as flame spread or used as a component of enclosure fire models.

Numerical simulation of combustion processes would require a direct numerical solution of the full turbulent Navier-Stokes equation as well as species relations and incorporation of chemical kinetics. Simulation of a turbulent buoyant diffusion flame for an arbitrary burning material, often in enclosures, poses added complexities where fuel geometry, air entrainment into the flame and external parameters have to be modeled. In such flows, large turbulent eddies, normally induced by buoyancy and flame pulsations, make k- $\epsilon$ -g type models prone to errors. Moreover, application of simple correlations (which are currently used in compartment fire models) can not adequately capture the important effects of geometry, flame radiation distribution and vitiation. The use of an integral approach for modeling such phenomena has shown to be promising (Delichatsios and Mathews, 1989; Tamanini, 1981), is accurate within experimental validation errors and computationally much less intensive than full field models. The integral models can include physics of complex combustion flows, such as those encountered for pool fires (i.e. large-scale turbulent fluctuations), via use of experimentally obtained parameters, properties and correlations whereas k- $\epsilon$ -g models, which have been calibrated for isothermal flows having relatively small fluctuations, would simply be unreliable. Prediction of flame temperature for a pool fire by a k- $\epsilon$ -g model may be in error by as much as 200°C, as reported by Nicolette et al. (1993).

Use of an integral combustion model for a turbulent diffusion flame, described in this chapter, has several advantages and characteristics. This approach offers a robust method in order to predict soot formation, flame radiation for optically thin flames (and applicable to optically thick cases), includes turbulent fluctuation effects, major species production, degree of completion of combustion for arbitrary flammable material by using flammability properties. For soot radiation, the laminar smoke-point heat release rate,  $\dot{Q}_{sp}$ , can be utilized to predict soot concentrations (Delichatsios et al., 1992). The model could be applicable to wall, pool and jet fires and incorporate vitiation effects. The use of experimentally determined parameters, properties and correlations (e.g. entrainment rates) allows the model to include the above listed physics and have such a wide range of applicabilities. The major species yield (i.e. CO, CO<sub>2</sub>, etc) are determined by using state relationship for conserved scalar and the flamelet concept. In addition, the turbulent fluctuations of the conserved scalar are modeled

using a direct empirical relationship, which has been tested carefully for buoyant jet diffusion flames with very promising results.

#### 4.2 MODEL DESCRIPTION AND ENERGY BALANCE

The integral combustion model presented earlier (Chen et al., 1993) has been developed for turbulent jet diffusion flames and includes, as its most important component, flame radiation and its relation to flame turbulence and the sooting tendency of the fuel. The buoyant jet is modelled using integral conservation equations and an ensemble of flamelets to model reactions and combustion. The energy equation is simultaneously solved with the flow equations, accounting for radiation losses and employs a simple soot formation model. The model computes the radiant losses, the incompleteness of combustion and the CO-yield by using the following physics: 1) the lower part of the flame is modelled by diffusion flamelets using a probability distribution function and 2) the upper part, as the flame cools due to radiant losses, is modelled as a premixed mixture sustaining CO+soot oxidation (Figure 4-1). The main characteristics of the integral model are the following:

1) Instead of an entrainment equation, a dimensionless correlation for entrainment spanning the range from momentum to buoyant turbulent jet flames has been employed and validated (Chen et al., 1993). 2) A direct relationship for the fluctuation of a conserved scalar,  $\xi$ , inspired by recent work (Chatwin and Sullivan, 1990) and validated by recent experiments is also used (see Appendix B for further detail):

$$\frac{\overline{\xi^2}}{\alpha \overline{\xi} (\beta \overline{\xi_c} - \overline{\xi})} = \frac{1}{1 + \gamma \frac{\alpha (\beta \overline{\xi_c} - \overline{\xi})}{1 - \overline{\xi}}} \quad (4-1)$$

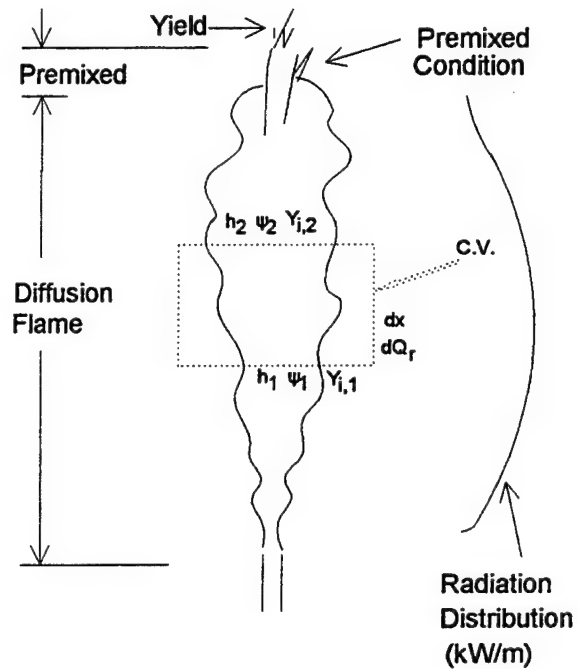


Figure 4-1 A schematic diagram of the integral combustion model

3) In the present model, radial profiles for the mixture fraction and velocity are used in order to preserve the strong nonlinearity of the combustion process (Delichatsios and Mathews, 1989), i.e.:

$$\bar{\xi} = \bar{\xi}_c \left(1 - \frac{\Psi}{\Psi_t}\right) \quad (4-1a)$$

$$\bar{u} = \bar{u}_c \left(1 - \frac{\Psi}{\Psi_t}\right) \quad (4-1b)$$

where  $\bar{u}$  and  $\bar{u}_c$  are the mean local and centerline velocities while  $\Psi$  and  $\Psi_t$  are the stream function and entrainment rate, respectively (Delichatsios and Mathews, 1989).

4) Most importantly, a flame radiation model applicable for luminous (soot radiation) and optically thin flame is presented whose sooting tendency is characterized by the laminar smoke-point height.

The soot radiation model is founded on a phenomenological description for soot formation which has been established from data in laminar diffusion flames (Delichatsios, 1993); the soot concentration can be determined by the following rate equation (Delichatsios, 1993):

$$\frac{dY_s}{dt} = A_1 \rho^2 \frac{\xi - \xi_s}{1 - \xi_s} e^{-E/RT} \quad (4-2a)$$

wherein  $\xi$ ,  $\xi_s$  are the fuel mixture fraction and its stoichiometric value,  $E$  is the activation energy for soot formation and  $T$  is the absolute temperature. As an approximation the destruction of soot can be ignored. The proportionality factor  $A_1$  which includes the fuel structure chemistry effects, is proportional to the inverse of the laminar smoke-point heat release rate (Delichatsios, 1993):

$$A_1 \sim \frac{1}{\dot{Q}_{sp}} \quad (4-2b)$$

The proportionality constant is properly defined in literature (Delichatsios, 1993).

Prior to applying eqn. (4-2a) to turbulent flows, it is useful to know what is required for modelling radiation losses in an optically thin medium. The flame radiation loss due to soot can be treated in this case as an volumetric emission described by an expression which can be reduced to the following form (Delichatsios, 1993):

$$\dot{q}_s''' = 3.26 \cdot 10^{-4} \frac{P}{R \rho_s} Y_s T^4 \text{ W/m}^3 \text{ K}^5 \quad (4-3)$$

where  $P$  is the pressure,  $R$  is the gas constant and  $\rho_s$  is the soot density.

For a turbulent flow, one has to average the volumetric radiant loss (eqn. (4-3)) over the turbulent fluctuating field. Local instantaneous values of the temperature,  $T$ , and the soot concentration,  $Y_s$ , needed for this purpose, are obtained by using the representation of turbulent combustion by an ensemble of flamelets that may also be subjected to a spectrum of turbulent straining rates.

Following such modelling, the instantaneous laminar flamelet temperature,  $T_L$ , would be a function of the mixture fraction,  $\xi$ , as it is customarily done in flamelet models (a modification to this relationship will be presented later in this work to account for the radiant losses). The soot concentration can be obtained by integration of the soot formation rate (eqn. (4-2a)) over the local flow field of a strained diffusion flame (Delichatsis, 1993). The soot concentration becomes:

$$Y_s = \frac{\gamma}{\dot{Q}_{sp}} F(\xi, \xi_s, T_{ad}) \quad \text{for } \xi \geq \xi_s \quad (4-4a)$$

$$\text{while } Y_s = 0, \quad \xi < \xi_s \quad (4-4b)$$

where  $\gamma$  is the inverse straining rate and  $F$  is a function obtained by integrating eqn. (4-2a) over an appropriate streamline (from 0 to  $\Psi_j$ ). Its exact form is not required for the present work, which focuses on optically thin flames. Note that eqn. (4-4b) has been derived from a simplification of the oxidation process according to which the oxidation rate in the fuel lean side ( $\xi < \xi_s$ ) is so fast that soot oxidizes instantaneously there. This situation is applied as long as the (maximum) laminar flamelet temperature (at stoichiometric condition) is greater than a certain value, about (Delichatsis et al., 1992) 1500 K; otherwise, soot can not be further oxidized and is emitted as smoke.

By using eqn. (4-4) and the function of temperature in terms of mixture fraction,  $T(\xi)$ , one obtains from eqn. (4-3) an average volumetric radiation loss:

$$\begin{aligned} \dot{q}_s''' &= 3.26 \cdot 10^{-4} \frac{P}{R\rho_s} Y_s T^4 = \\ &= 3.26 \cdot 10^{-4} \frac{P}{R\rho_s} \int \int \frac{\gamma}{\dot{Q}_{sp}} F(\xi, \xi_s, T_{L,max}) T^4(\xi) P(\xi, \gamma) d\xi d\gamma \end{aligned} \quad (4-5a)$$

wherein  $P(\xi, \gamma)$  is the joint pdf between the mixture fraction,  $\xi$ , and the straining rate,  $\gamma$ . Next, we use the common approximation that mixture fraction and straining rate are statistically independent so that eqn. (4-5a) becomes:

$$\dot{q}_s''' = 3.26 \cdot 10^{-4} \frac{P}{R\rho_s} \frac{\bar{\gamma}}{\dot{Q}_{sp}} \int_0^1 F T^4 P(\xi) d\xi \quad (4-5b)$$

It is this relationship that is applied in the energy balance of the present integral combustion model along the jet axis:

$$\frac{d}{dz} \int h d\psi = - \int_0^{\infty} \dot{q}_s''' 2\pi r dr \quad (4-6a)$$

where  $h$  is the total enthalpy of the product of combustion (i.e. chemical+convective) and  $\Psi$  is the stream function for the mean axial jet velocity. In this form, eqn. (4-6a) is difficult to solve owing to the iterations needed to obtain the flame temperature for the laminar flamelets or for the turbulent flow.

In the spirit of the integral model (and to save computational time), we make the approximation that the laminar flamelet temperature at a given height from the source is uniformly reduced by a constant fraction  $\alpha$  of its adiabatic value, namely:

$$T_L(\xi) - T_{\infty} = \alpha (T_{L,ad}(\xi) - T_{\infty}) \quad (4-6b)$$

while the dependence of species concentrations on  $\xi$  remains the same independent of the radiation losses as long as the maximum flamelet temperature is greater than 1,500 K (this approximation is supported by experiments (Koylu et al., 1992)). With these approximations, the energy conservation equation (4-6a) becomes (see Appendix A):

$$\frac{d}{dz} [(1-\alpha) \dot{Q}_{ch}(z)] = \int_0^{\infty} \dot{q}_s''' 2\pi r dr \quad (4-6c)$$

where  $\dot{Q}_{ch}(z)$  is the chemical (heat of formation flux) heat release at height  $z$  and  $(1-\alpha)$  can also be identified to be equal to the radiant fraction up to height  $z$ :

$$1-\alpha = \chi_R(z) = \frac{\dot{Q}_R(z)}{\dot{Q}_{ch}(z)} \quad (4-6d)$$

where  $\dot{Q}_R(z)$  is the radiation losses from the flame over a length extending from the source to a given height  $z$ . Even in the simplified form, eqn. (4-6c) requires iterations over the whole field in order to obtain the value of  $\alpha$  owing to the complicating dependence of radiant losses on temperature as indicated in eqn. (4-5b). A further simplification of eqn. (4-6c) has been obtained based on overall radiation correlation (Delichatsios et al., 1992) and the specific form of radiations losses (eqn. (4-5b)):

$$\int_0^{\infty} \dot{q}_s''' 2\pi r dr = \frac{C \cdot \sigma T_{ad}^4 \Psi_t}{(1-\alpha)^3 \dot{Q}_{sp}} \int P(\xi_s, \bar{\xi}) \frac{d\psi}{\bar{\rho} \bar{u}} \quad (4-7a)$$

The following remarks are made concerning the derivation of eqn. (4-7a):

1. Most of the contributions to radiation losses originates for values of  $\xi \approx \xi_s + \epsilon$  near the stoichiometric value so that:

$$FT^4 \sim \text{delta function} \sim \delta(\xi - \xi_s) \quad (4-7b)$$

2. The average strain rate  $\bar{\gamma}$  (which can be identified with the Kolmogorov strain rate) is nearly independent of location or total heat release rate for buoyant flames (Delichatsis et al., 1992); therefore it is assumed to have a constant value.
3. The reduction of the term  $FT^4$  due to radiation losses is proportional to  $1/\chi_R^3$ . This dependence has been deduced from global correlations on radiation (Delichatsis et al., 1992).
4. The constant C incorporates all the physical constants associated with the assumptions 1, 2, 3. It has to be determined from experiments.
5. Comparison with experiments demonstrates the applicability of the approximations used to derive eqn. (4-6a). More importantly, the value of the constant C should be independent of the fuel, assuming that the present approximations are adequate.

Finally, with these approximations, the energy balance equation (4-6c) becomes:

$$\frac{d}{dz} [(1-\alpha)\dot{Q}_{ch}(Z)] - \frac{C\sigma T_{ad}^4 \psi_i}{(1-\alpha)^3 \dot{Q}_{sp0}} \int_0^{\psi_i} P(\xi_s, \bar{\xi}) \frac{d\psi}{\rho u} \quad (4-8)$$

- We may also characterize the radiation modelling in eqn. (4-8) in the following way:
- 1). All radiation originates from soot that is near the instantaneous maximum flamelet temperature;
  - 2). This flamelet temperature, however, decreases due to radiant losses as the radiation fraction increases.

Equations (4-8) is singular near the flame base where  $(1-\alpha) \rightarrow 0$ . We can not model the flow conditions near the flame base at this moment. Fortunately, because we have used integrated value over the entire length of the flame, this effect has been eliminated.

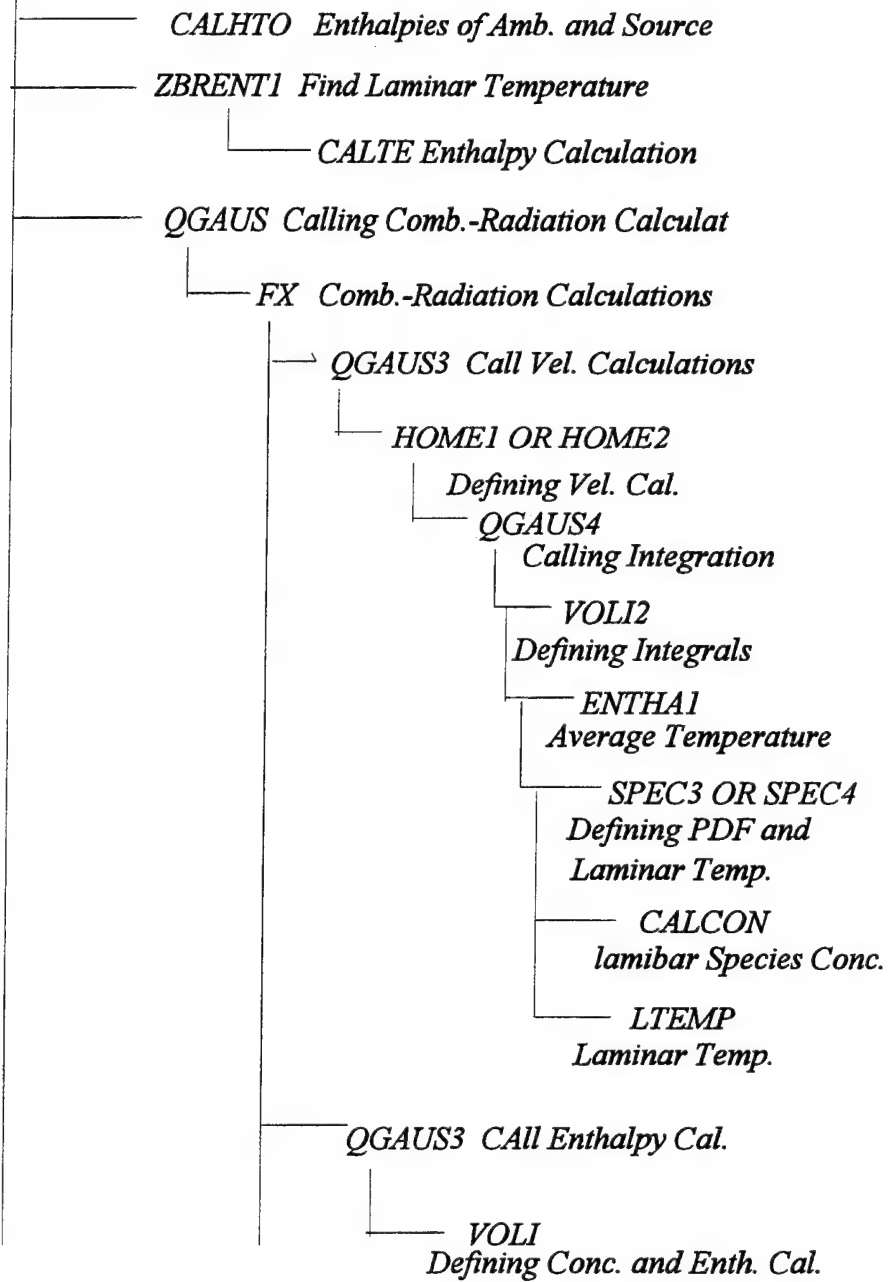
#### 4.3 THE STRUCTURE OF THE COMPUTER CODE

A computer code has been developed based upon the above approach. The flow chart of this code is shown in Figure 4-2.

*PROGRAM RADH.F*

*MAIN*

*DATA INPUT (FILE' combb.dat')*





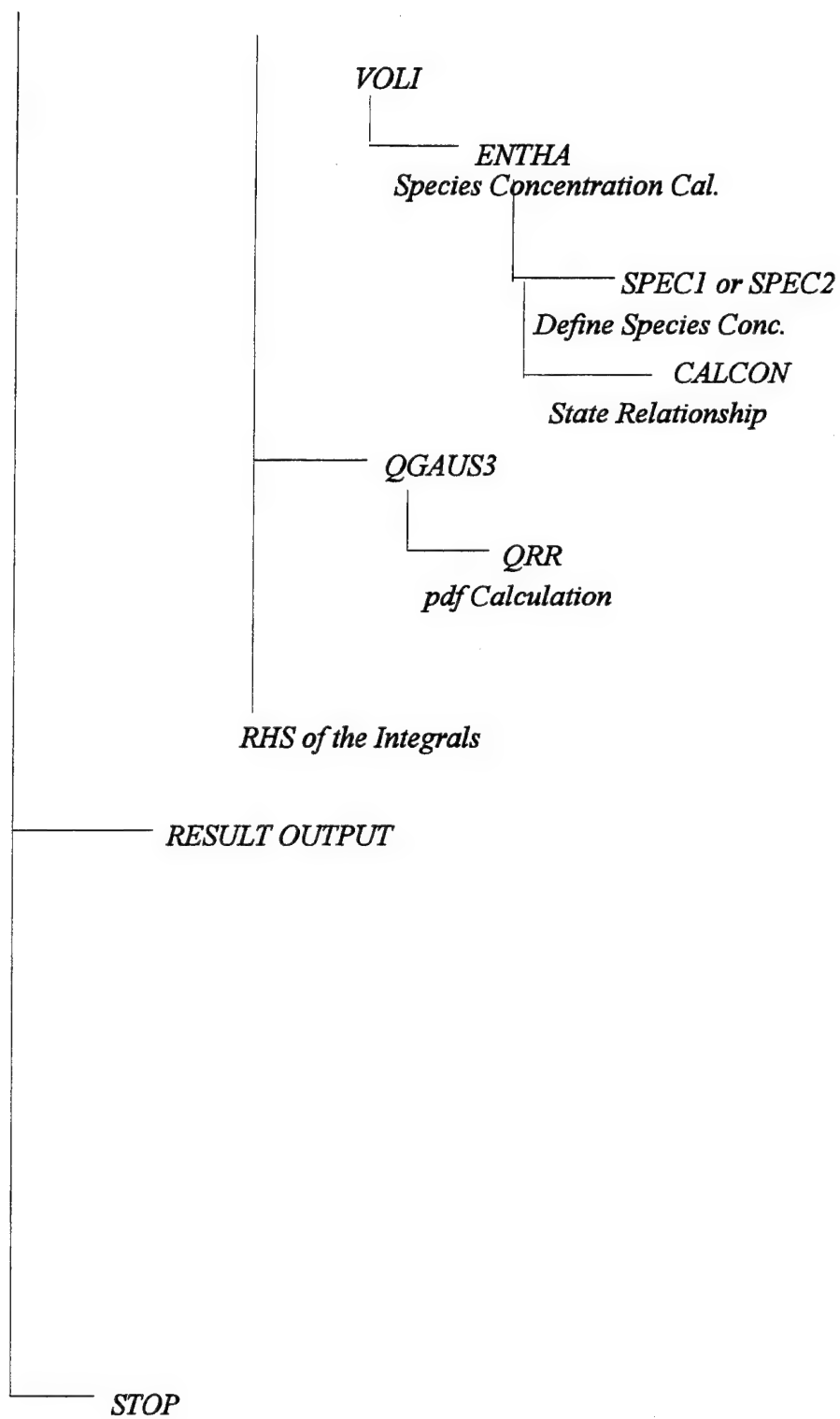


**Figure 4-2** Subroutines and interconnections of the integral combustion model

#### 4.4 COMPARISON OF PREDICTION WITH EXPERIMENTS

Eqn. (4-8) together with the remaining conservation equations (i.e., momentum, mixture fraction), as well as with the flamelet combustion model, form a well-behaved system of equations which have been applied to several cases. Results and comparison for the radiation distribution are presented in this section for turbulent buoyant jets and pool fires of various fuels.

Prediction of heat release rate from the integral combustion model and comparison with experimental data (Tamanini, 1982)

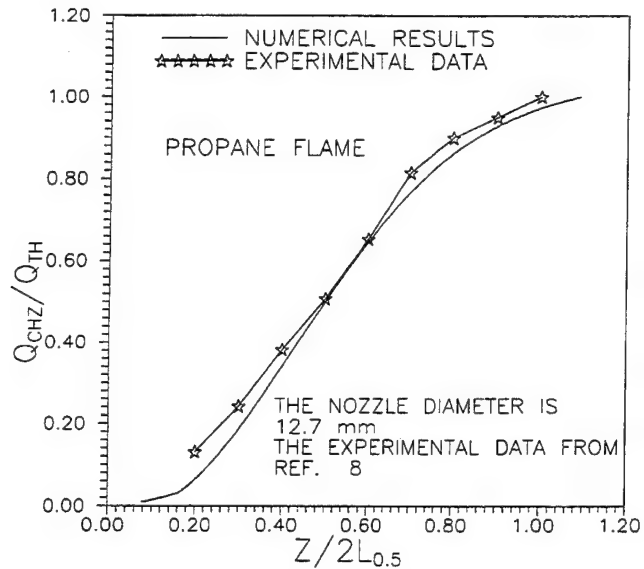


**Figure 4-3** Chemical heat release rate normalized by the total heat release rate versus distance from the nozzle exit, normalized by twice the length,  $L_{0.5}$ , over which half of the combustion has been completed.

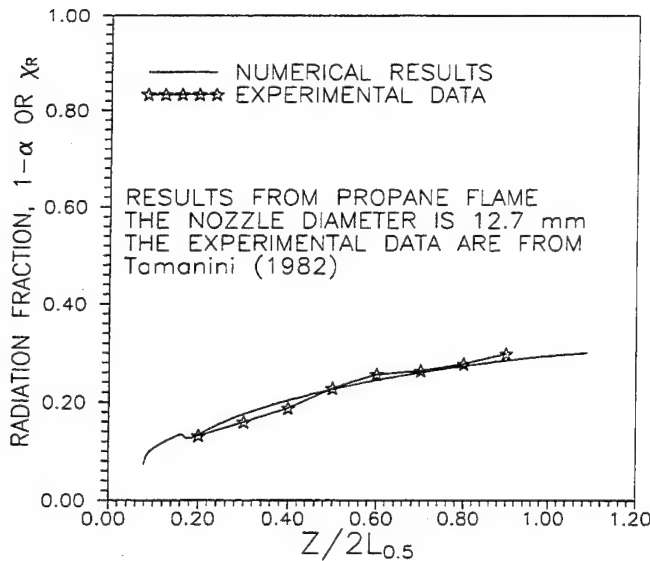


**Figure 4-4a** Radiation fraction at a given height plotted versus the height normalized by twice the length,  $L_{0.5}$ , over which half of the combustion has been completed

for a propane ( $C_3H_8$ ) buoyant jet flame are illustrated in Figure 4-3. The abscissa is the ratio between the height from the nozzle to two times  $L_{0.5}$  ( $L_{0.5}$  is the distance at which one-half of total heat release occurs) and the ordinate is the scaled heat release rate, i.e. the ratio of the heat release rate at that height,  $\dot{Q}_{th}(z)$  to the total heat rate,  $\dot{Q}_{th}$ . The burner diameter used in the experiment was 12.7 mm and the jet flame theoretical heat release rate was 30.8 kW. The comparison in Figure 4-3 shows very good agreement between prediction from the model and the experimental data for heat release rate.

The constant  $C$ , in the energy balance eqn. (4-8), was determined by requiring that at the end of combustion the

radiation fraction ( $1-\alpha$ ) is equal to the total radiation fraction for the fuel, which is known if the smoke-point heat release rate,  $\dot{Q}_{sp}$ , is known (Delichatsis et al., 1992) (for propane,  $\dot{Q}_{sp}=303.4$  W). The value of this constant was found to be,  $C=0.36$  W/s if  $\dot{Q}_{sp}$  is expressed in W. By using this value, the calculated radiation fraction,  $\chi_R$  vs. the scaled height from the nozzle is plotted in Figure 4-4a while the scaled radiation per unit length of the flame is illustrated in Figures 4-4b and 4-4c. All the experimental data were obtained by Tamanini (1981). The close behavior between the prediction and the experiment, shown in Figure 4-4a reinforces the validity of this approach. The prediction does give the right trend of radiation loss distribution (Figures 4-4b and 4-4c) though the difference with experiments is fairly large. It can be noted (may not be obvious) that the area under the curves from the prediction (Figure 4-4b) is the same as that from the experiment.

Finally, Figure 4-5 illustrates the maximum laminar flamelet temperature variation as a function of the height from the flame base. The result shows decreasing laminar flame temperature as radiation losses increase. Near the flame tip ( $\sim 1$  m), the laminar flamelet temperature is about 1680 K indicating that no extinguishment of the flame due to radiation loss occurs. Therefore, soot is probably completely oxidized inside the flames, which agrees with experiments (Tamanini, 1981) that little smoke is emitted from propane flames.

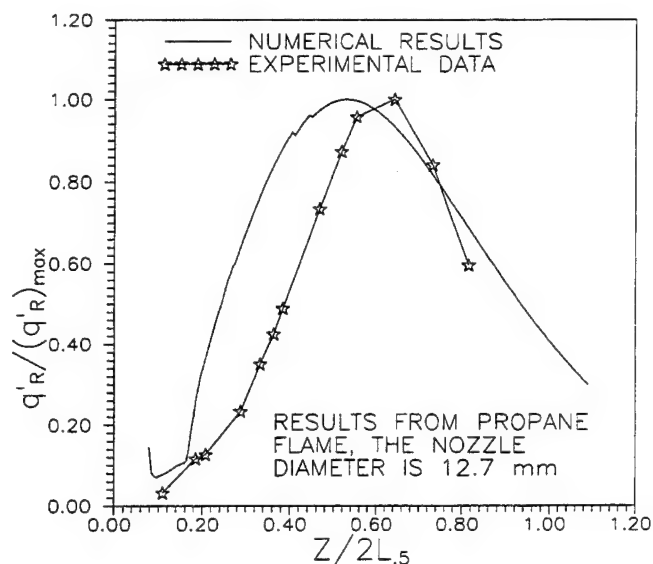


**Figure 4-4b** Radiation distribution per unit height versus normalized distance from the nozzle exit (cf. Fig. 4-4a). The experimental data are from Tamanini (1982)

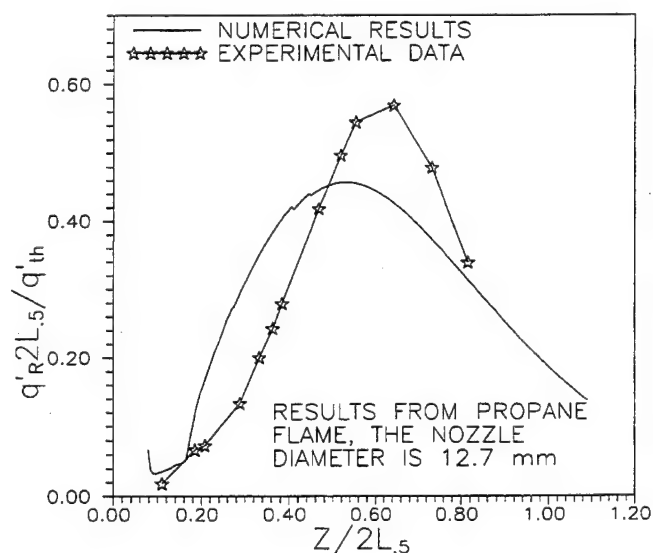


**Figure 4-4c** Same data as in Figure 4-4b, except that the radiation per unit height is normalized by its maximum value. The experimental data are from Tamanini (1982)

The same constant  $C$  ( $\approx 0.36$  W/s), can be used to calculate the combustion and radiation of another fuel, propylene, if the smoke-point heat release rate,  $\dot{Q}_{sp}$  is known (see

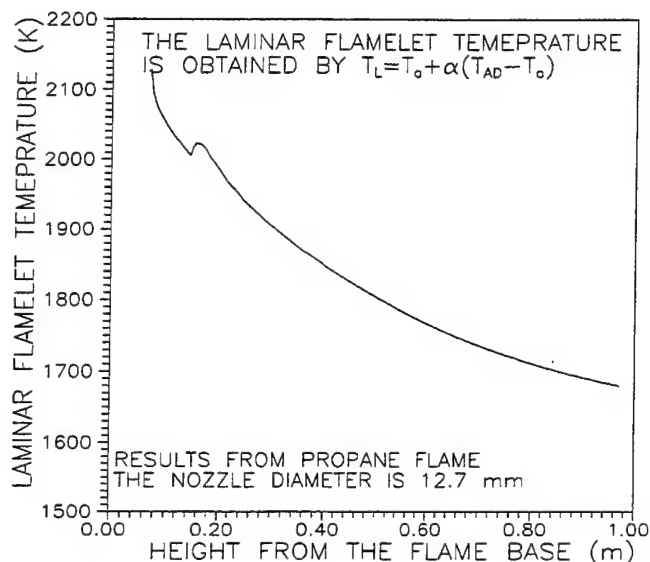


**Figure 4-5** Reduction of laminar flamelet temperature with height owing to radiation losses for the use of Figure 4-3

flamelet temperature for propylene flames is shown in Figure 4-6c. In contrast to the propane flames, Figure 4-5, the temperature drops below 1,500 K at a height at 0.60 m; such a low temperature will result in flame quenching, copious smoke yield and incompleteness of combustion, which might explain the higher calculated value of total radiation fraction, 0.46, relative to the numerical value of 0.44. Incompleteness of combustion will be addressed as the present model is carefully evolved.

The above discussions and results presented in Figures 4-6a and 4-6b have shown that use of a single constant (representing

eqn. (4-8)). We have used this approach to predict the radiation of propylene ( $C_3H_6$ ,  $\dot{Q}_{sp}=46.3$  W). The results are shown in Figures 4-6(a-c). In Figure 4-6a, the prediction of radiation fraction is plotted against the height from the flame; the total radiation fraction is about 0.46 which is close to 0.44 as measured in an experiment (Delichatsis et al., 1992). Figure 4-6b shows a comparison of non-dimensional radiation distribution between the prediction and experiments (Delichatsis et al., 1988). These results show that one can use the smoke-point heat release rate to predict total radiation and radiation distribution from buoyant jet flames. For completeness, the maximum laminar

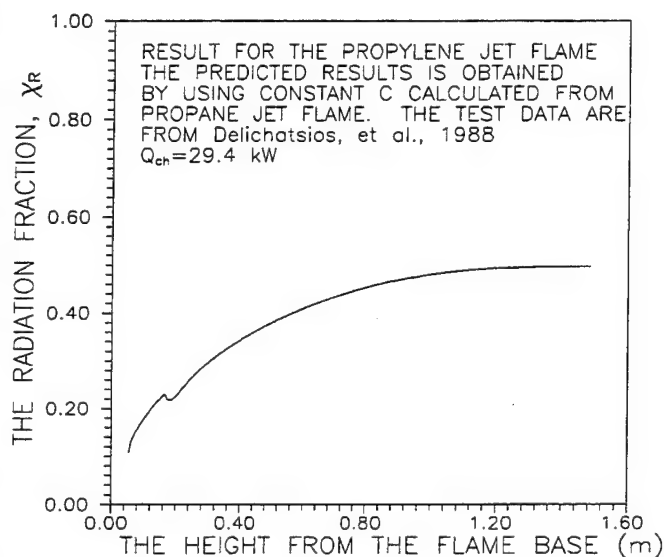


**Figure 4-6a** Prediction of radiation fraction versus height for propylene turbulent buoyant jet flame. No experiments are available except for the total radiation fraction

collective physical parameters) is feasible for radiation modeling. This also points out that the integral model has accurately included the essential physics for buoyant jet flames.

Another ability of the combustion mode is to predict the products of combustion. Figure 4-7 shows the comparison of prediction with experiment of CO production rate for propane jet flame.

A final demonstration that the present model could be extended to combustion and radiation in pool fires is shown in Figures 4-8a, and 4-8b, for a propane fire 0.38 m in diameter. The same conservation equations were used for a turbulent buoyant jet flame including the constant,  $C (=0.36 \text{ W/s})$  for radiation of  $\text{C}_3\text{H}_8$ . The following modifications were made:

- 1) an entrainment rate correlation for pool fires was used (Delichatsis, 1987) and
- 2) the fluctuations were represented by the relationship:

$$\frac{\bar{\xi}^2}{\bar{\xi}(1-\bar{\xi})} = 0.11 \quad (4-9)$$

instead of eqn (4-1) because eqn. (4-9) was shown (Delichatsis and Mathews, 1989) to be the one applicable for pool fires. This expression represents a level of fluctuations,  $(\bar{\xi}^2)^{1/2}/\bar{\xi}$ , which for values of  $\bar{\xi}$  close to 1 is smaller than what eqn. (1a) represents; this behavior is consistent with measurements of fluctuations in pool fires (Gengebre, 1984).

The agreement between predictions and experiments as shown in Figures 4-8a and 5-8b is more encouraging than should be expected, because the elliptic flow field near the pool base is not modeled in the present approach. In fairness to the present work, it

should be pointed out that measurements of  $\chi_R$  in pool fires in Tamanini's (1982) experiments (wherein he used a "catcher-quencher" to measure heat release rates) have large errors ( $\pm 50\%$ ) near the pool base ( $\leq 0.20 \text{ m}$ ) because a) the width of the slit radiometer used to measure the radiation per unit height was 54 mm and b) the "catcher-quencher" might have

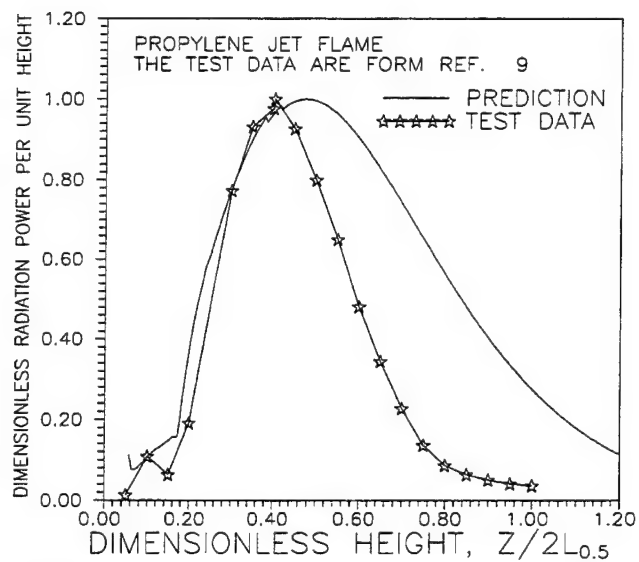


**Figure 4-6b** Radiation distribution per unit height versus height for a propylene turbulent buoyant jet flame

influenced the combustion. A more detailed examination of the shortcoming of pool fire modeling is currently being undertaken.

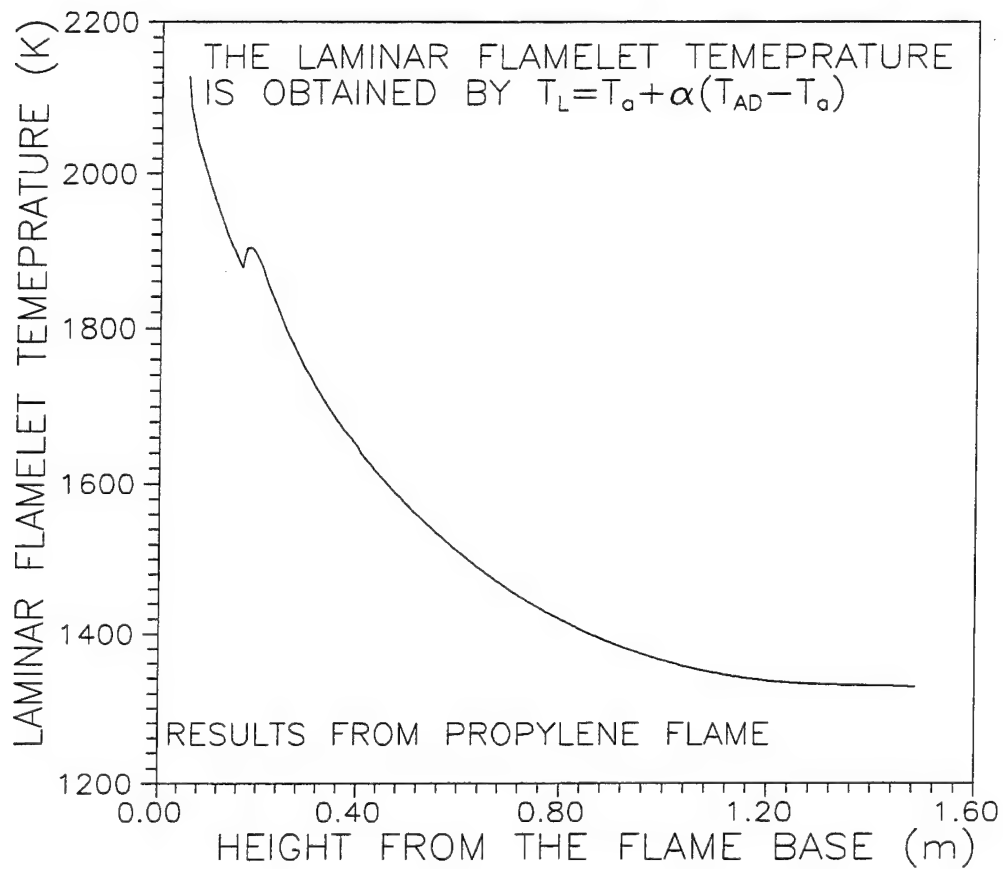


**Figure 4-6c** Reduction of laminar flamelet temperature vs. height owing to radiation loss for the case of Figure 4-6a

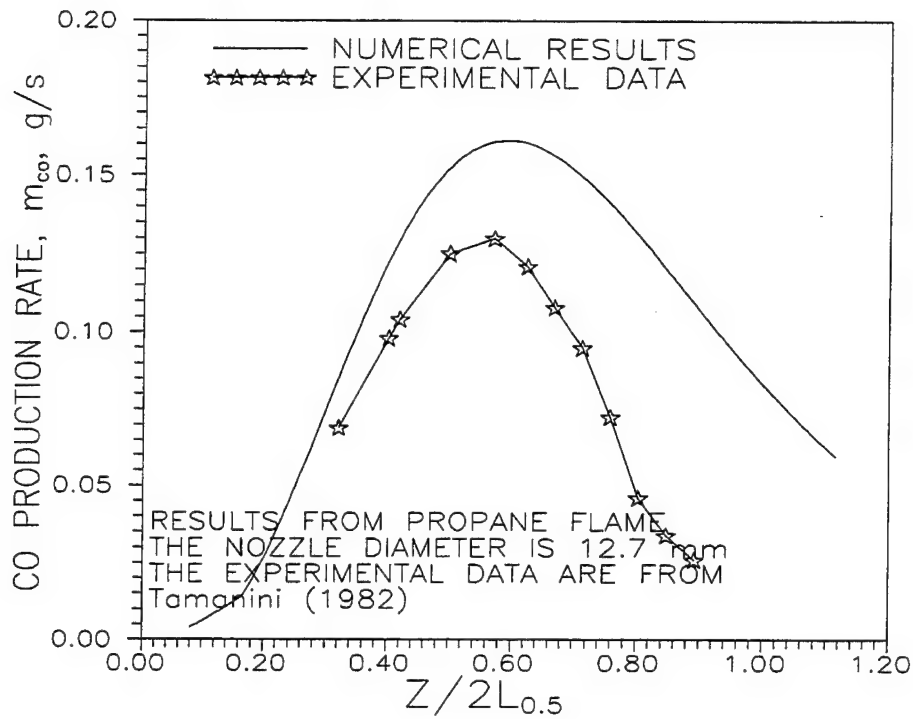


**Figure 4-7** CO production rate vs. scaled height from the flame for a propane jet flame

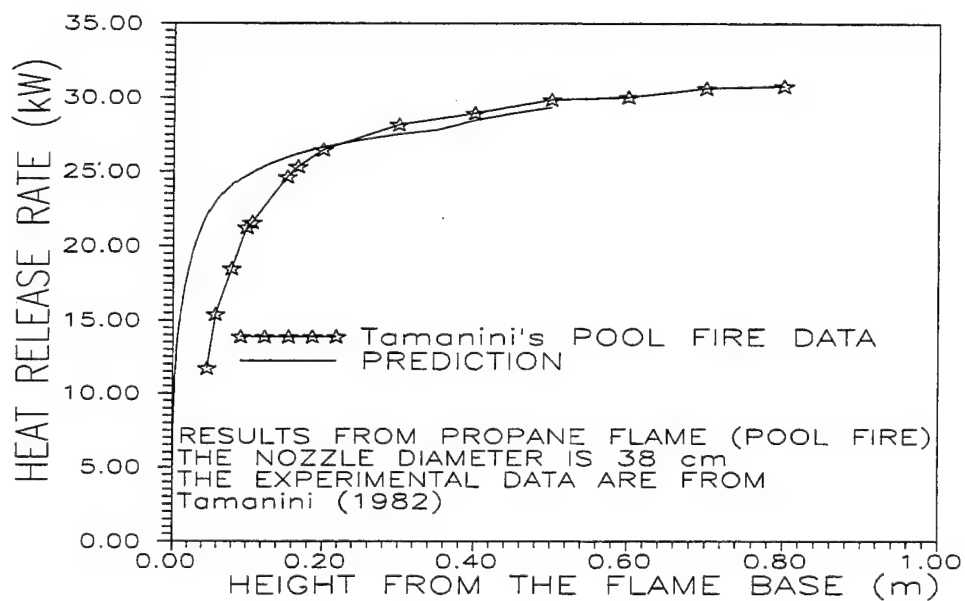


**Figure 4-8a** Chemical heat release rate versus distance from the base of a propane pool fire 0.38 in diameter

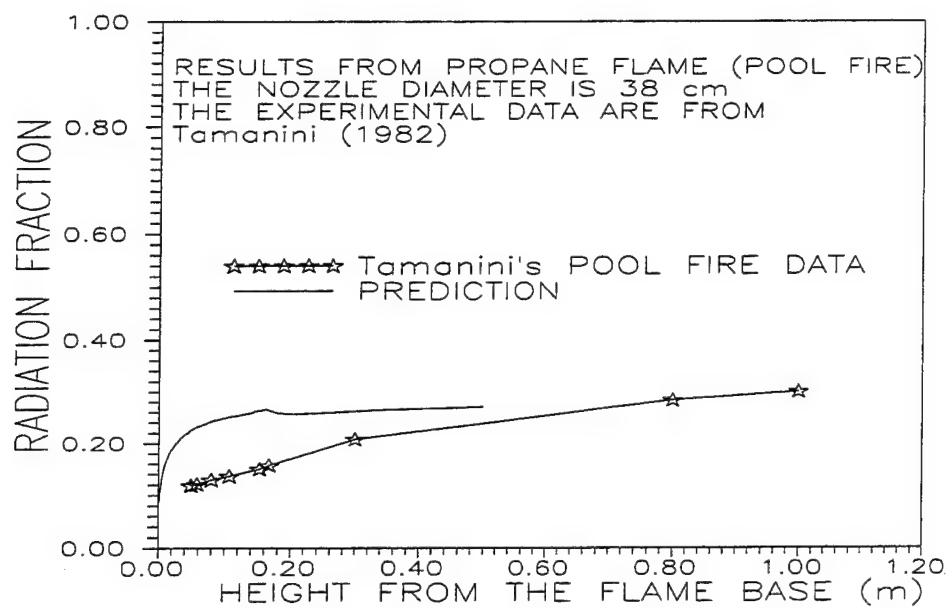


**Figure 4-8b** Radiation fraction at a given height plotted versus the height from the base of a propane pool fire 0.38 m in diameter



## Chapter 5      Description of Constant Speed Horizontal Flame Spread (CSHFS) Experiment

Following the completion of the previous analysis, the horizontal flame spread code is complemented with measurements of gas phase conduction heat flux by conducting a constant speed horizontal flame spread experiment (CSHFS). This includes testing with non-charring (black PMMA, both 19 mm (3/4") and 6.35 mm (1/4") thick, manufactured by the Polycast Technology Corporation) and charring (particle board, 19 mm thick, manufactured by the Potlatch, Inc.) materials.

As discussed previously, the quantification of the total flame heat flux immediately ahead of the flame front is very important. There is a gas-phase conductive flux which applies over a very short distance (in the order of 1 mm) just ahead of flame front. To try to quantify this flux and verify the flame spread model, a particular scheme is accomplished. In this approach, the fuel sample is placed on a movable platform. The platform speed can be controlled using a stepping motor.

The burning sample was moved by a slide (manufactured by the Unislide, Inc.) at a constant speed in the experiments to obtain a constant flame burning area (Figure 5-1). The transient effects can therefore be eliminated. The flame radiation can also be easily deduced from the experiments (flux gage measurements) or predicted from the combustion-radiation model as described in Chapter 4. The only remaining unknown is the gas-phase conduction ahead of the flame front. This conductive heat flux has to be matched with the flame spread speed (also the sample moving speed) and the temperature measurements from the thermocouples as described later.

To create a condition whereby the flame spread speed,  $V_f$ , is equal to the sample speed,  $V_s$ , the flame is being quenched by a water-cooled plate placed above the fuel sample. The quenching serves two purposes. First, the flame impingement on the radiant panel is limited or eliminated. This impingement creates an additional flux which can not be accounted for. Second, the quenching helps to keep the flame spread speed and the burning area constant. The heat release rate would also remain constant for a fixed burning area and a constant external flux distribution by satisfying the condition of  $V_f = V_s$ . The external heat flux at point A (see Fig. 5-1) will always be the same under these conditions since the external heat flux supplied by the radiant panel is decaying along the sample surface as seen in Figure 5-2. We have used the LIFT apparatus to accomplish this. The challenge in this scheme would be to have a very short transient time after ignition and establishing the steady flame, positioning of the pilot flame, instrumentation and measurements and finally the control of the movement of the fuel sample. Thus, it is possible to better quantify the gas-phase conductive heat flux from the flame when the external heat flux and flame radiation are known.

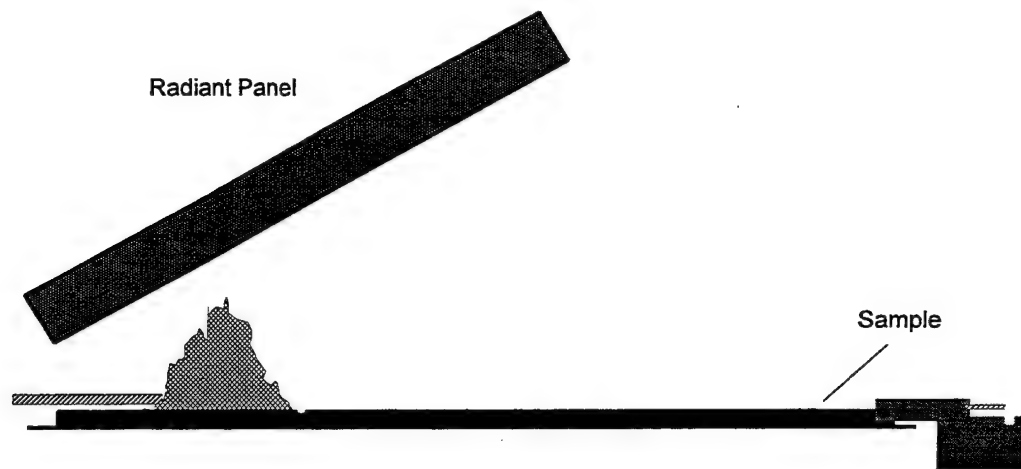


**Figure 5-1** Schematic of the constant speed horizontal flame spread experiment

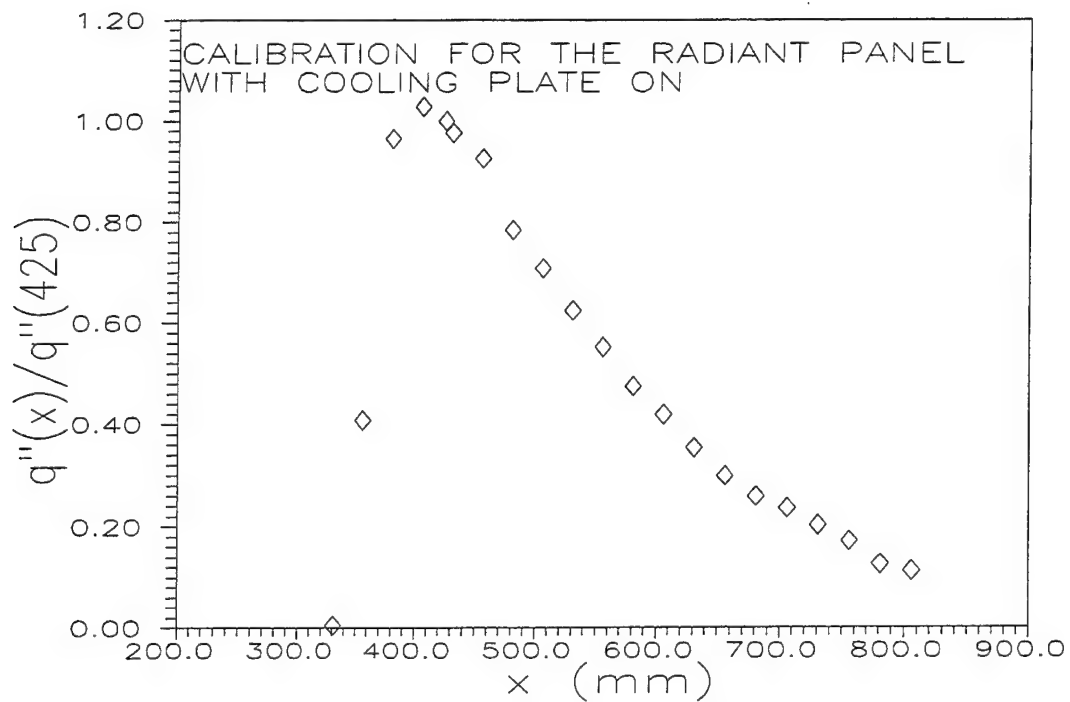


**Figure 5-2** External heat flux from the radiant panel-a decaying profile when  $x > 400$  mm. Ordinate is the ratio between heat fluxes at  $x$  location and 425 mm

Given the constraint of the LIFT apparatus, a slide with a moving distance of 600 mm was used to move the fuel samples. The fuel samples are instrumented with thermocouples and heat flux gages. Three temperature measuring stations situated roughly 200 mm (The exact distances between two stations varies depending on a particular experiment, the variations could be as large as  $\pm 50$  mm and the distances have been listed in Appendix H) apart are used. The first station is about 200 mm from the leading edge of the sample. At the second station, a 1.6 mm (1/16") diameter small heat flux gage is also used. At the third station, which is about 600 mm from the leading edge of the sample, a 25.4 mm (1") diameter (probe size 9.1 mm (23/64") + copper plate) large heat flux gage is instrumented. The flux gages are supported in the bottom of the marinite board insulation to insure their sensors flush with the sample surface. The small flux gage is employed since the flame front can not go over the large sensor (actually, the flame will go around the sensor) due to the cool sensor surface (cooled by water). K-type thermocouples (0.127 mm (0.005") in diameter) are used to measure surface and gas-phase temperatures. The surface thermocouples are imbedded by running two thermocouple wires through two holes and tightening the two wires at the back of the fuel sample to maintain good contacts between thermocouple beads and sample surface. The gas phase thermocouples are placed just above the sample surface (above 1 mm). It is expected that we can use the differences between the surface and gas temperatures to quantify the gas-phase conduction. In each test, video recording was also made to obtain the flame front histories. A constant burning area can be observed from the video tape.

Figures 5-3 through 5-10 are pictures of the experimental set-up and the experiments. Figure 5-3 shows the long view of the LIFT/CSHFS apparatus. Figure 5-4 demonstrates early stage of the experiment. Figures 5-5 and 5-6 illustrate close-up pictures of the experiment. One can see that a metal bracket with scale longitudinally holds a piece of burning material (in this case, it is a 19 mm particle board). On the left of the flame, there is a water cooling plate which is very close to the sample surface so that there is no burning underneath the cooling plate (the sample moves from right to left). At the top left corner of the pictures, the radiant panel is shown (located at a cute angle relevant to the fuel surface). Underneath the sample holder one can see an attachment that has all the thermocouples and heat flux connectors so that the extension wires can be moved more freely with the sample. The flame width is about 7 cm for these tests. The middle stage of the experiment is shown in Figure 5-7 while side view of the experiment is manifested in Figure 5-8. A large heat flux gage probe (circular shape in the middle of the sample) is clearly shown in Figure 5-8. The flux gage probe is flush with the sample surface and it is mounted by drilling a 25.4 diameter hole through the sample, supported at the back of the sample insulation (25.4 thick marinite board). Figure 5-9 shows the experiment is just stopped, and the PMMA samples after the experiments are shown in Figure 5-10.

In order to determine the accuracies of the large and small heat flux gages, we have compared the two heat flux gage readings at the same location for an inert test (no flame, only radiant panel was on). The small heat flux gage gave higher values than the large heat flux gage as shown in Appendix H. The large flux gage was painted by using a known emissivity paint and then calibrated using an Factory Mutual apparatus and the result was not

much different from the calibration newly done by the manufacturer. The large flux gage reading was also compared with a flux gage calibrated at NIST and the difference was negligible. Finally, during the inert test, after exposed both heat gages to the radiant panel, the flux gages were covered. The small flux gage went to a non-zero reading (it varied from time to time!). Therefore it has been determined that small flux gage readings were not accurate and that the measurements of large heat flux gage is more accurate (away from flame front) (see also Figure 6-3 in next Chapter). The cause of non-accurate readings from small flux gage is not fully understood, it may be due to the ineffective cooling of the sensor because of the small sensor/cooling area. The other problem is that because the small heat flux gage nose is fragile, a slightly larger hole was drilled to mount the small flux gage. There was some open space between the gage nose and the wall of the hole. During the experiment, the insulation wall as well as the fuel itself was heated, some heating from the wall to the gage may exist and that would cause some problems for cooling the sensor.

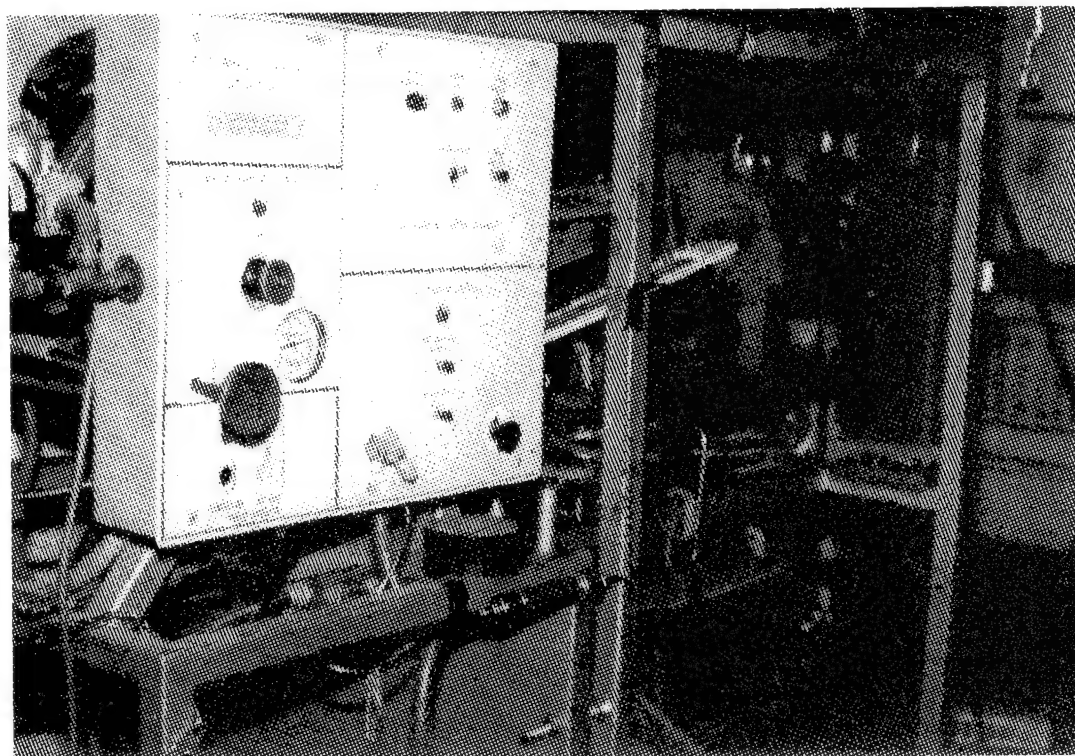


**Figure 5-3** Long view of the flame spread apparatus

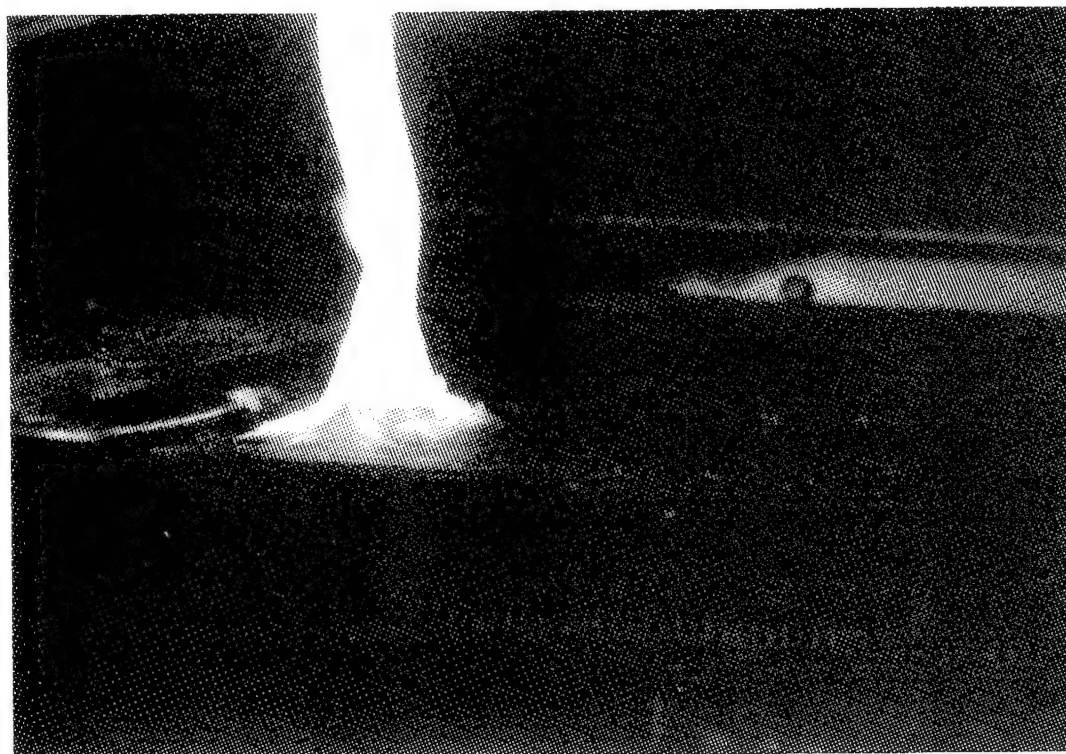


**Figure 5-4** Early stage of flame spread

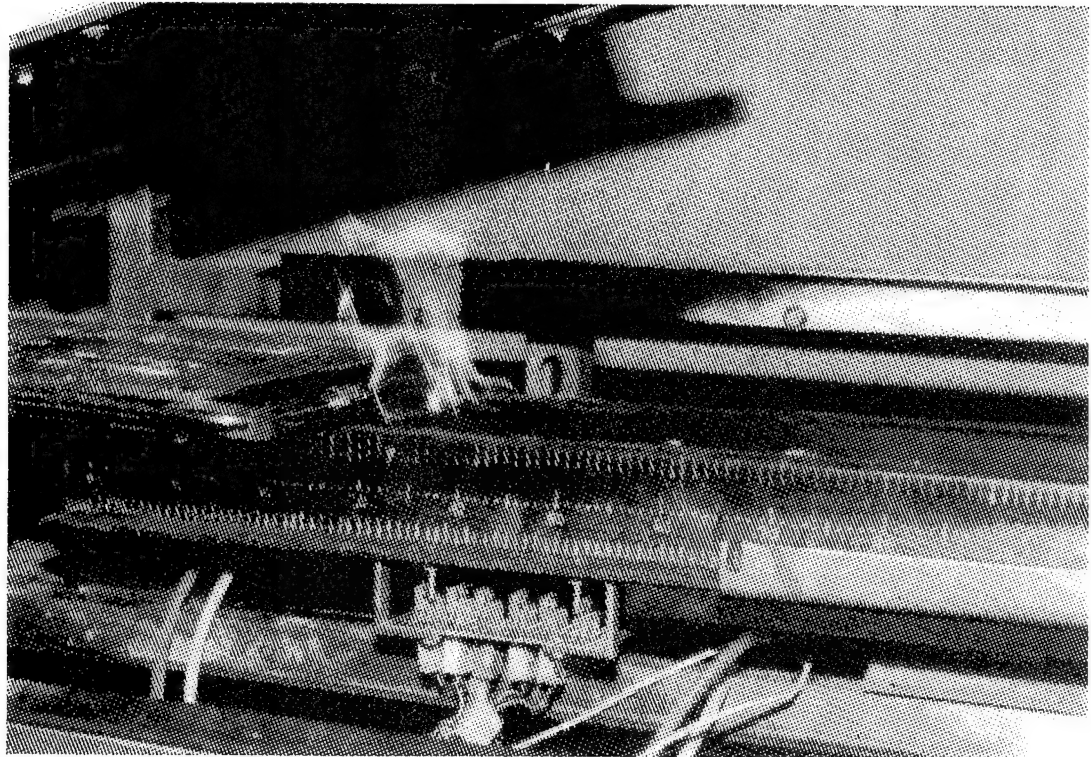


**Figure 5-5** Flame spread after slide has moved about 15 cm

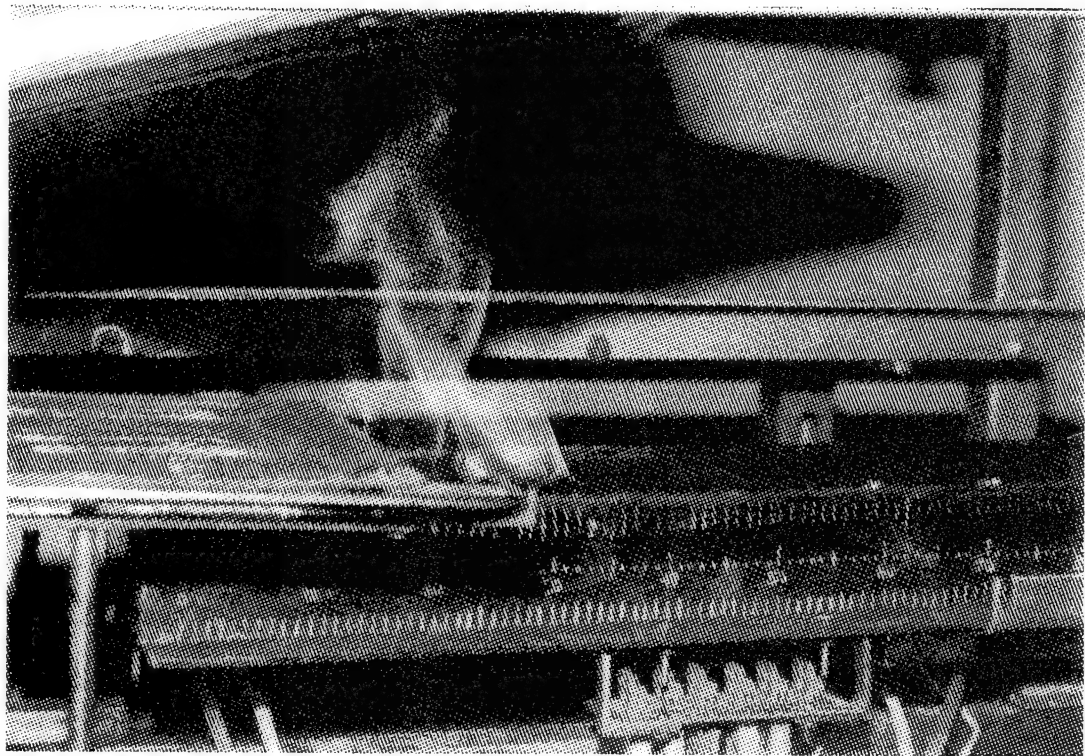


**Figure 5-6** Same as Figure 5-5. but for different test



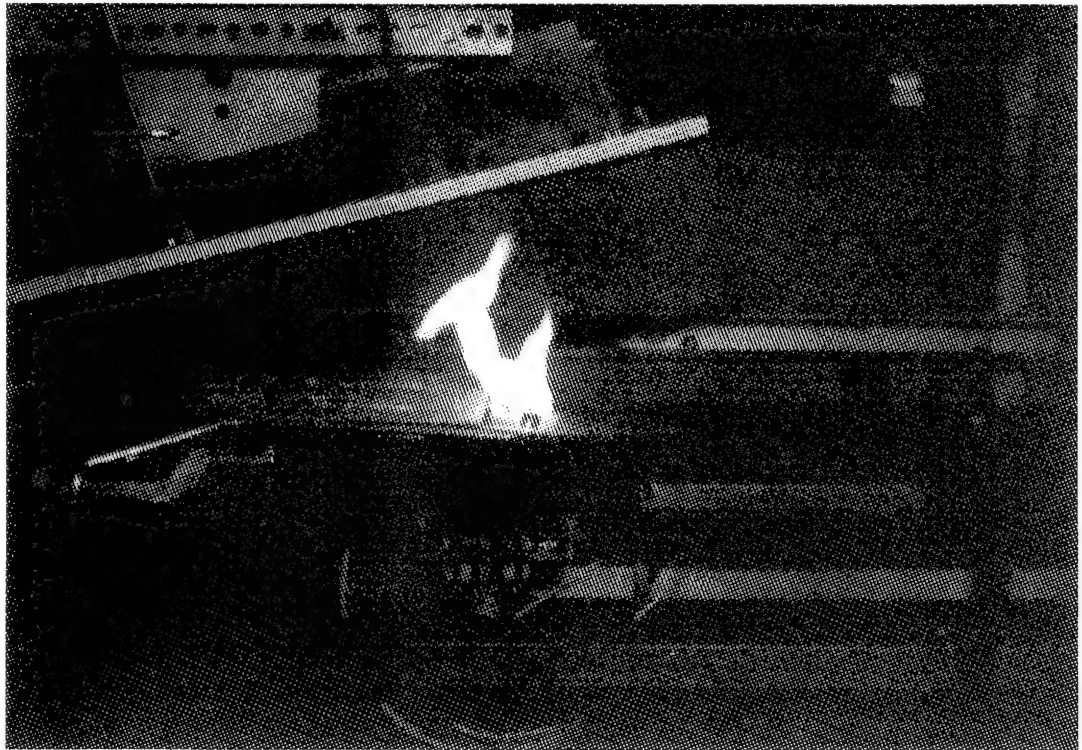


**Figure 5-7** Flame spread at the middle stage of the experiment

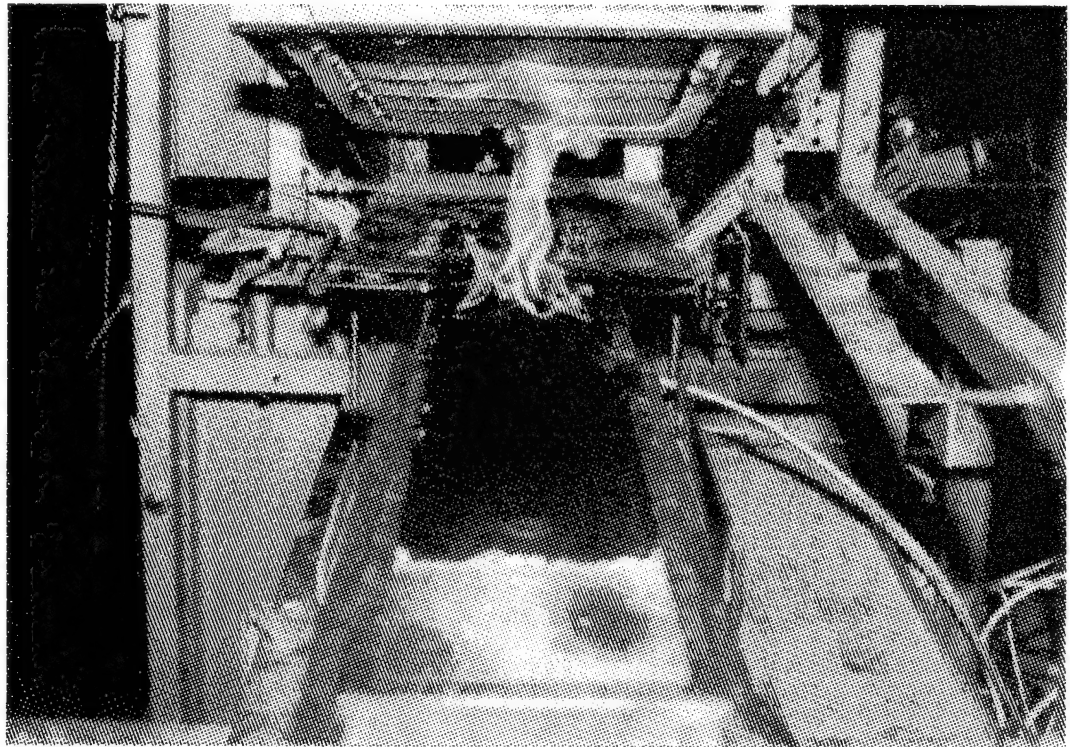


**Figure 5-8** Side view of the flame spread experiment

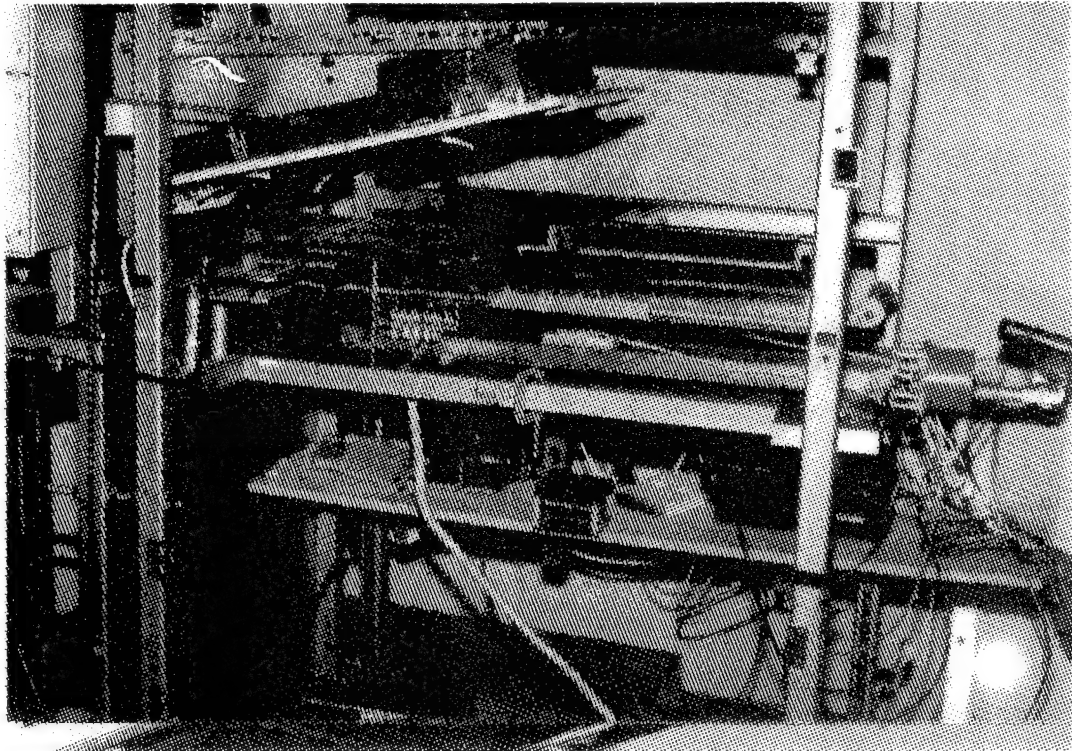


**Figure 5-9** The slide stops, the experiment finishes



**Figure 5-10** The PMMA samples after experiments (6.35 mm (1/4") thick)



## Chapter 6      Experimental Results and Comparison of Simulation of Horizontal Flame Spread Model

### 6.1      EXPERIMENTAL APPROACH AND PROCEDURE

Two fuels, PMMA (non-charring) and particle board (charring materials), for which flammability properties have been known (Chen et al., 1995), were used in the CSHFS experiments described in Chapter 5. Two thicknesses of PMMA (19 mm (3/4") and 6.35 mm (1/4")) and a single thickness of particle board (19 mm) particle board samples were tested. The dimensions of the samples were 152.4×600 (W×L) mm. In the tests, the samples were preheated for a specified time and this time was determined before an experiment using the pre-heat model of the flame spread model discussed in Chapter 3. This time depends on the external heat flux level; then an ignition flame was applied at the leading edge of the sample respectively. The sample (slide) was moved at a pre-determined constant speed after flame has grown to certain size (established flame). This speed was determined by using the flame spread model and assuming flame heat fluxes. This speed was verified or altered based on a preliminary experiment. The criterion for choosing the speed was that the burning area should not be too large (if the speed was too small) such that the flame would not impinge on the radiant panel and create an additional heat flux that can not be quantified. The burning area could not be too small either (if the speed was too large) because relative errors introduced by fluctuations of flame front could become too large or all the flame would be quenched. The proper burning width is 10 cm from experience. There were three measuring stations along the burning sample and they were approximately 200, 400 and 600 mm away from the leading edge of the sample. The surface temperatures at three stations, gas temperatures at first two stations and total heat fluxes at last two stations were measured. At the second station, a small heat flux gage (1.6 mm (1/16") probe diameter) was used and a 9.1 mm (23/64") sensor diameter heat flux gage was used at the third station. All heat flux gages were Gardon type manufactured by Medtherm, Inc.

Data obtained from the experiments described in Chapter 5 include: 1) temperature-time histories from thermocouple measurements, 2) heat flux-time histories from the heat flux gage readings and, 3) flame front location relative to the original leading edge of sample which was obtained from both visual observations and video tape recordings. The difference between the total heat flux measurement and the external heat flux at the measuring stations would be the total flame heat flux incident. The distance from the cooling plate edge to the measuring station at any instant of time is also known because the time to start moving the sample and the slide speed were also recorded. Therefore, the flame heat flux can be plotted versus the distance from the cooling plate to the measuring station.

## 6.2 ANALYSIS OF EXPERIMENTAL DATA

Figure 6-1 shows measured temperatures for a particle board. The external heat flux at 425 mm away from the lower edge of the radiant panel was  $20 \text{ kW/m}^2$  (external heat flux has a distribution as described in Chapter 5). The preheating time before applying the pilot ignition flame was 120 seconds. The time to start moving the slide was 147. seconds. GAS TC1 and SUR TC1 are gas and surface temperatures at the first measuring station. Rest of the curves can be inferred. It can be seen that at the same measuring station, surface temperatures are higher than gas-phase temperatures (though it is somewhat hard to distinguish) when the flame is not close to the measuring station. Gas-phase temperature starts to exceed surface temperature when flame approaches the measuring station and it remains so when the measuring station is immersed in the flame. The reason is that when the flame was far away from the measuring station, the fuel surface received radiation both from the radiant panel and the flame. The hot surface heats the gases above it. Therefore, a thermal layer developed wherein the gas temperature was therefore lower than the surface temperature; when flame approached the measuring station, however, the gases above the fuel surface below involved with the flame, the gas phase temperature became higher. One can observe that there is always a sudden increase of temperature when flame approaches thermocouples. We can employ these periods of sudden increase to obtain flame conductive heat flux profiles as we shall discuss in Section 6.4. We can also observe in Figure 6-1 that the temperature always starts the sudden increase at approximately same temperature (in this case it is about  $270^\circ\text{C}$ ) at all measuring stations. This manifests that the experiment was indeed steady state and this characteristic temperature (e.g.  $T_{\text{ext}}=270^\circ\text{C}$ , note that this is not ignition or pyrolysis temperature, but rather it is the temperature rise caused by external and flame radiative heat fluxes) together with temperature histories during the sudden increase period can be used to derive both the magnitude and length scale of the gas phase conduction (see Section 6.4).

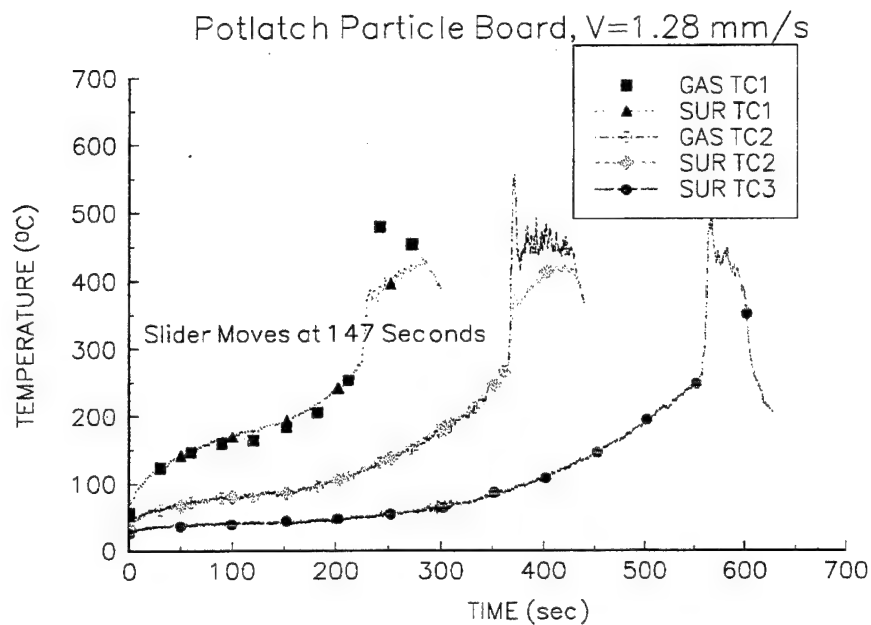


**Figure 6-1** Temperature histories of a particle board test, external heat flux level:  $20 \text{ kW/m}^2$

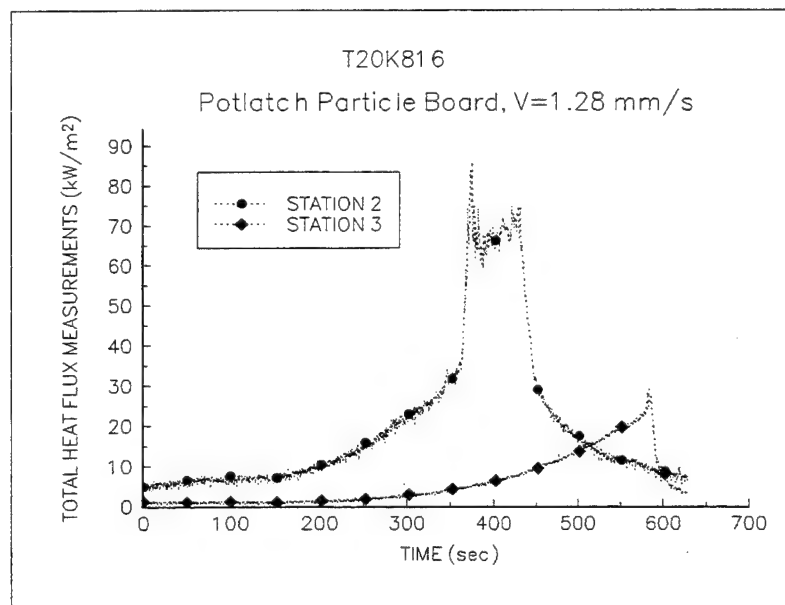


**Figure 6-2** Total heat flux histories of a particle board test, external heat flux level:  $20 \text{ kW/m}^2$

The total heat flux measurement is illustrated in Figure 6-2 where a 1.6 mm diameter small probe flux gage was used at station 2 and a 9.1 mm diameter probe was used in station 3. The total heat flux measured at station 2 shows similar behavior as the temperature measurement demonstrated in Figure 6-1. The peak heat flux is about  $70 \text{ kW/m}^2$  from the small flux gage reading when the flame front reaches the measuring station. This heat flux is the summation of external, flame radiation and gas phase conduction. The total heat flux measurement at station 3 does not show a large size peak for two reasons: 1) the flame quenches and moves around the 25.4 mm diameter gage surface which includes the detector surface and copper cylinder (sink) (see Chapter 5), and, 2) the experiment is stopped once the flame front reaches station 3 because of the length constraint of the LIFT (the sample can not move more than 600 mm because the leading edge of the sample is blocked by the structure of the LIFT). Flame heat flux is determined by subtracting external heat flux from the radiant panel from the total heat flux measurements in Figure 6-2. The result is plotted in Figure 6-3 where the abscissa has been changed from time to distance from the edge of the cooling plate by using the initial location of measuring station and the slider speed. It can be seen from the small flux gage measurement at station 2 that the flame heat flux (flame radiation+gas phase conduction) is about  $50 \text{ kW/m}^2$ . The distance at which the peak flame heat flux occurs is in fact the width of the burning area (if there is no burnout) and in this case is about 100 mm. This length is consistent with video recording.

It is seen in Figure 6-3 that flame heat fluxes are not the same at same distance from the cooling plate edge, namely the reading of small flux gage is much larger than that of large flux gage. The same problem exists for all tests. The possible explanations are offered in Chapter 5.

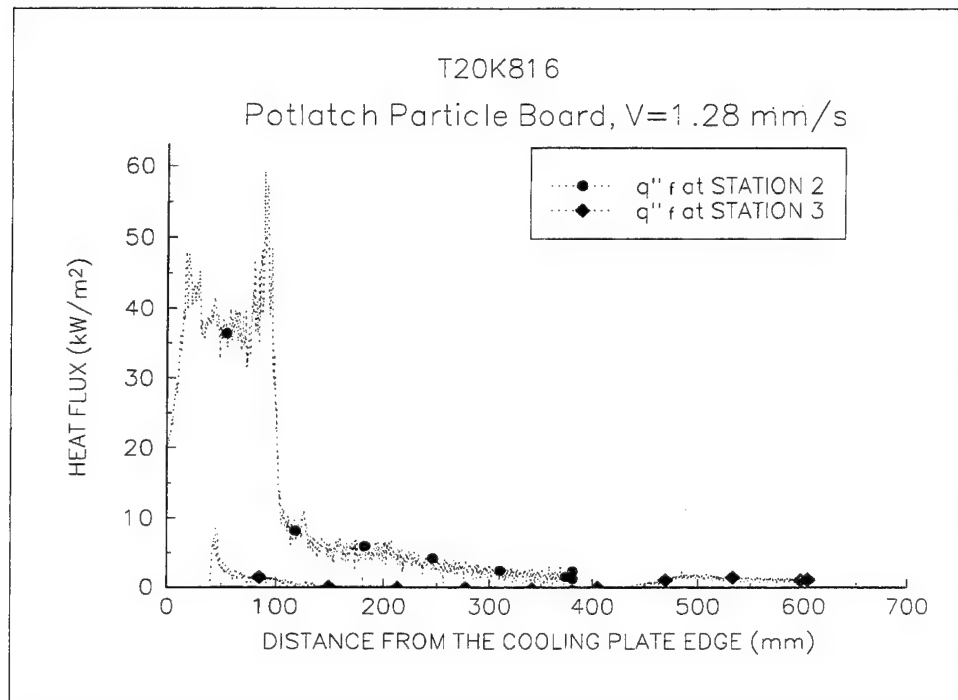


**Figure 6-3** Net flame (radiation+gas-phase conduction) heat flux for a particle board test shown in Figures 6-1 and 6-2

### 6.3 EXAMINATION OF THE FLAMMABILITY PROPERTIES OF PMMA SHEETS AND PARTICLE BOARDS USED IN THE EXPERIMENTS

Before we conduct detailed calculation of gas-phase conductive heat flux and compare results from the numerical model and experimental data, the flammability properties of PMMA and particle boards have to be obtained. The properties derived in earlier work (Chen et al., 1993; 1995) are used as inputs for the heat-up portion of the horizontal flame spread model, using the total heat flux station 3 measured by the large heat flux gage (as stated before, this measurement is reliable). The calculated surface temperature histories are compared with experimental measurement of station 3 surface temperatures. The accuracies of these properties are therefore checked as described below.

Figure 6-4 illustrates the surface temperature histories of a 19 mm particle board experiment and predictions from the heat-up submodel of the HFSCS code. The properties used in the prediction are:  $k=0.25$  kW/m.K,  $\rho=765$  kg/m<sup>3</sup> and  $c=2800$  J/kg.K. The circular line shows the experimental data. The triangle line indicates the prediction without convection loss while the square line illustrates the prediction with convection loss from the fuel surface. The convection loss is evaluated as natural convection on a horizontal plate ( $\dot{q}_{\text{con}}''=h(T_s-T_\infty)$ ). The latter one obviously agrees better with the experimental measurement. The comparison shows that the prediction using convection loss as agrees both with the experiment indicating that the properties used in the prediction are correct. We have used

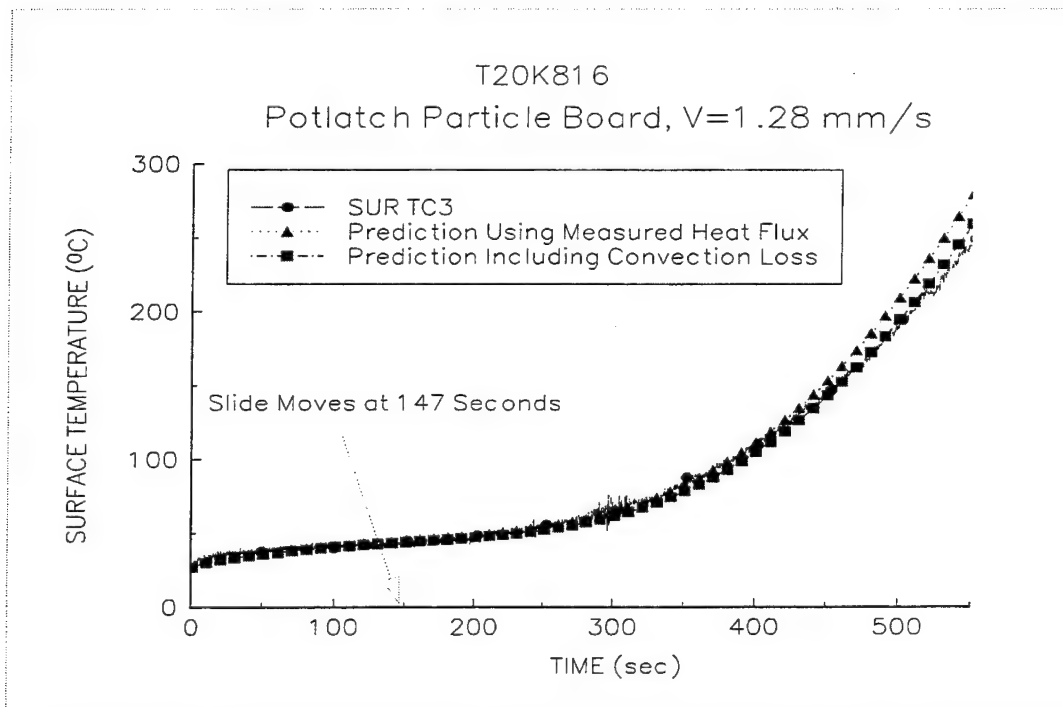


**Figure 6-4** Comparison of surface temperature histories for a particle board test. This comparison is used to check the values of material properties ( $k$ ,  $\rho$ ,  $c$ )

these properties to predict surface temperature histories of other experiments. The predictions all agrees with the experiments. These results are presented in Appendix G where the comparisons of surface temperature histories at the 3rd station between predictions and experiments for 19 mm PMMA sheet are also shown. The PMMA properties used in the predictions are:  $k=0.2798$  kW/m.K,  $\rho=1200$  kg/m<sup>3</sup> and  $c=2200$  J/kg.K. It should be pointed out that all predictions account for convection losses from the surface.

#### 6.4 ESTIMATION OF GAS-PHASE CONDUCTIVE HEAT FLUX

It is the intention that the validation of the horizontal flame spread model (HFSCS) using the data from the constant speed horizontal flame spread experiments (CSHFS) would be carried out. Before doing that, the gas-phase conductive heat flux profiles (ref. discussion of Chapter 3), has to be quantified. Gas-phase conductive heat flux profiles have been shown both experimentally (Babrauskas and Watterlund, 1995) and numerically (di Blasi et al., 1989) to follow an exponential profile:

$$\dot{q}_{conv}'' = \dot{q}_g'' e^{-\frac{x-x_p}{\delta_g}} \quad (6-1)$$

where the magnitude,  $\dot{q}_g''$  and the length scale,  $\delta_g$  have to be obtained. These parameters can be derived from the experimental data of surface temperature histories. The heat flux profiles are essentially the same shape as that of the temperature profiles, if solid conduction is assumed to be one-dimensional into the solid, i.e. conduction parallel to the fuel surface is not important. For justification, readers can refer to Appendix E. The surface temperature rise of the fuel at any location for thermally thick solid can be expressed (eqn. (E-5) of Appendix E):

$$T_s(t) - T_{ext} = \frac{\dot{q}_g''}{\sqrt{k\rho c}} e^{-\frac{V(t-t_p)}{\delta_g}} \sqrt{\frac{\delta_g}{V}} \quad (6-2)$$

where  $t_p$  is the time to pyrolysis and  $V$  is the velocity at which the flame front travels.  $T_{ext}$  is surface temperature rise owing to other heat fluxes (external and flame radiative heat fluxes). It can be easily seen by comparing equations (6-1) and (6-2) that the profile of surface temperature rise also exponentially decays at the same rate as the gas-phase conductive heat flux distribution.

If a point at a fuel surface starts to pyrolyze, i.e.  $T_s = T_p$ , Eqn. (6-2) changes to:

$$T_p - T_{ext} = \frac{\dot{q}_g''}{\sqrt{k\rho c}} \sqrt{\frac{\delta_g}{V}} \quad (6-3)$$

One can carry out simple manipulation by inspecting Eqn. (6-2), assuming two surface temperatures,  $T_{s1}$  and  $T_{s2}$ , at two different times,  $t_1$  and  $t_2$ :

$$T_{s1}(t)-T_{ext} = \frac{\dot{q}_g''}{\sqrt{k\rho c}} e^{-\frac{V(t_p-t_1)}{\delta_g}} \sqrt{\frac{\delta_g}{V}} \quad (6-4a)$$

and

$$T_{s2}(t)-T_{ext} = \frac{\dot{q}_g''}{\sqrt{k\rho c}} e^{-\frac{V(t_p-t_2)}{\delta_g}} \sqrt{\frac{\delta_g}{V}} \quad (6-4b)$$

dividing eqn. (6-4a) by eqn. (6-4b), one has:

$$\frac{T_{s1}-T_{ext}}{T_{s2}-T_{ext}} = e^{-\frac{V(t_2-t_1)}{\delta_g}} \quad (6-5)$$

If we assume the left hand side of eqn. (6-5) equals  $e^{-1}$ , then  $V(t_2-t_1)=\delta_g$ . Therefore we can choose a surface temperature,  $T_{s2}$  during a sudden increase period and read off the time,  $t_2$ , that corresponds to temperature,  $T_{s2}$ , from a detailed plot of surface temperature during a sudden increase period as illustrated in Figure 6-5. By using eqn. (6-5) with  $RHS=e^{-1}$ ,  $T_{s1}$  can be evaluated. One then reads off the time,  $t_1$ , from the same plot. The length scale,  $\delta_g$ , can finally be obtained as  $\delta_g=V(t_2-t_1)$ . Obviously, this can be done only if  $T_s$  is a continuous and smooth function between  $t_1$  and  $t_2$ . Finally one can solve for the magnitude of the heat flux,  $\dot{q}_g''$ , by rearranging eqn. (6-3):

$$\dot{q}_g'' = \sqrt{k\rho c}(T_p-T_{ext}) \sqrt{\frac{V}{\delta_g}} \quad (6-6)$$

where the pyrolysis temperature,  $T_p$ , is obtained from literatures (Chen et al., 1995), i.e.  $T_p=370^\circ\text{C}$  for PMMA and  $T_p=320^\circ\text{C}$  for particle board. The pyrolysis temperature can not be determined from current experiments, but rather should be determined from a separate pyrolysis test (Delichatsios et al., 1991). Again it should be pointed out that this solution is only applicable for thermally thick solid. The materials tested here can all be treated as thermally thick as far as gas-phase conductive heat flux is concerned.



The above analysis of the CSHFS data has been carried out and the results are illustrated in Tables 6-1 through 6-3 (for details, see Appendix G). In Table 6-1, 8 Potlatch particle board (19 mm thick) tests are shown. There are three external heat flux levels at 425 mm away from the radiant panel lower edge (see Figure 5-2): 10, 20 and 30 kW/m<sup>2</sup> (Column 5 in Table 6-1). Three slide (flame spread) speeds (0.32, 1.27 and 2.56 mm/s, Column 4) were used corresponding to the three heat flux levels. The surface temperatures before a sudden increase,  $T_{ext}$  are listed in Column 6. The temperature,  $T_{s2}$  is 320°C. The time differences,  $\tau=t_2-t_1$  (see eqn (6-5)) are presented in Columns 8 and 9 for surface thermocouples at the first and second stations, respectively. For each test, only surface thermocouple measurements at stations 1 and 2 are used since the experiment was stopped when the flame front approached station 3. Columns 10 and 11 show the magnitudes of the

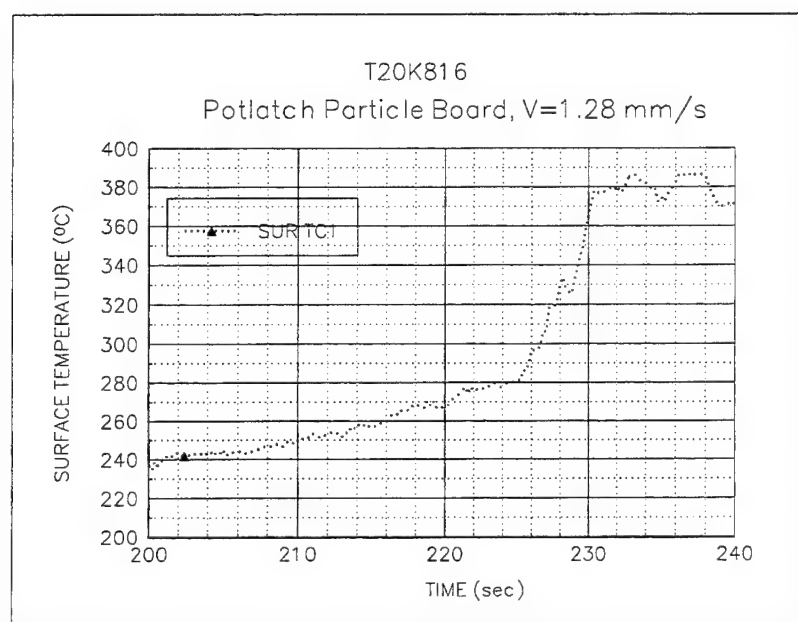


**Figure 6-5** The detailed surface temperature histories during the sudden increase period for a particle board test

heat fluxes. The final three columns of Table 6-1 list average characteristic time, length scale,  $\delta_g$ , and magnitude,  $\dot{q}_g''$ , of the gas phase conduction heat flux. There are considerable differences among  $\delta_g$  and  $\dot{q}_g''$  for different flux levels and even for same flux levels.

The analysis of PMMA test data is shown in Tables 6-2 and 6-3. In 6.35 mm PMMA test (Table 6-2), 0.5 mm/s slide/flame spread speeds were used at the nominal heat flux level of 10 kW/m<sup>2</sup>. The heat flux levels shown in Column 5 are the values at 400 mm from the lower edge of the radiant panel. The 19 mm PMMA test results are demonstrated in Table

6-3 where the slide speeds at 10 kW/m<sup>2</sup> level were not constants (0.5, 0.2 and 0.35 mm/s) because of difficulties of obtaining constant burning areas in the experiments.

It was postulated that the gas phase conductive heat flux profile is independent of fire size (Atreya, 1984) , i.e. for the same material and ambient conditions,  $\delta_g$  and  $\dot{q}_g''$  should be constants. It can be clearly seen that the results are inconsistent and greatly scattered. The wide differences led to the speculation that the derived  $\delta_g$ 's are really the length scales of the gas-phase conductive heat flux profiles. Careful examination has revealed that the  $\delta_g$  are essentially the length scales of the surface temperature distribution along the fuel surface! The more explanation of this abnormal phenomenon will be discussed in the next section and the experimental data will be reprocessed using a new formulation.

Table 6-1 The Experimental Results of 19 mm (3/4") Particle Board

No.	Test No.	File Name	V (mm/s)	Flux @ 425 mm kW/m <sup>2</sup>	T <sub>ext</sub> (°C)	T <sub>s2</sub> (°C)	$\tau_1$ (sec)	$\tau_2$ (sec)	$\dot{q}_1''$ (kW/m <sup>2</sup> )	$\dot{q}_2''$ (kW/m <sup>2</sup> )	$\tau_a$ (sec)	$\delta_g$ (mm)	$\dot{q}_g''$ (kW/m <sup>2</sup> )
1	21	T10K617	0.32	12.76	240	320	7.2	9.7	18.06	15.27	8.45	2.70	16.61
2	22	T10K620	0.32	12.76	238.7	320	4.9	12.81	21.94	13.70	8.86	2.84	16.48
3	23	T10K621	0.32	12.61	225.8	320	11.4	14	16.86	15.15	12.7	4.06	15.95
4	24	T20K621	1.28	25.28	271	320	1.64	1.29	23.09	30.16	1.47	1.88	24.39
5	25	T20K622	1.28	20.44	259.4	320	1.3	1.48	32.09	30.16	1.39	1.78	31.02
6	41	T20K816	1.28	20	274.7	320	1.76	1.26	20.64	24.30	1.51	1.93	22.25
7	43	T20K818	1.28	20.34	271.5	320	2.27	3.33	15.75	13.02	2.8	3.58	14.21
8	27	T30K623	2.56	32.88	289/2 51.5 <sup>1</sup>	320	0.25	0.775	37.71	46.95	0.51	1.31	42.04

<sup>1</sup> The test data show that two surface temperatures start to rise quickly at two different values indicating that flame spread was not steady

Table 6-2 The Experimental Results of 6.35 mm (1/4") PMMA Sheet

No.	Test No.	File Name	V (mm/s)	Flux @ 400 mm kW/m <sup>2</sup>	T <sub>ext</sub> (°C)	T <sub>a2</sub> (°C)	$\tau_1$ (sec)	$\tau_2$ (sec)	$\dot{q}_1''$ (kW/m <sup>2</sup> )	$\dot{q}_2''$ (kW/m <sup>2</sup> )	$\tau_a$ (sec)	$\delta_g$ (mm)	$\dot{q}_g''$ (kW/m <sup>2</sup> )
1	2	P10K418	0.64	10.56	235.4	330	2.45	1.88	73.91	84.48	2.17	1.39	79.62
2	9	P08K511	0.5	9.02	208.2	330	N/A <sup>2</sup>	N/A					
3	11	P10K516	0.5	10.9	221.7	330	2.25	3.00	84.95	73.57	2.62	1.31	78.65
4	31	P10K629	0.5	10.22	228.9	330	3.5	3.48	64.82	65.01	3.49	1.74	64.91
5	4	P20K427	1.27	20.1	232.4	330	1.00	N/A	118.23	N/A	1.00	1.27	118.2
6	5	P20K429	1.27	19.93	245.7	330	N/A	0.83	117.0	N/A	0.83	1.05	117.0
7	6	P20K504	1.27	20	260.4	330	0.83	N/A	103.4	N/A	0.83	1.05	103.4
8	7	P20K506	1.27	19.93	272.0	330	0.48	0.95	121.6	86.42	0.72	0.91	99.61
9	30	P20K628	1.27	19.93	255.5	330	1.17	1.16	91.02	91.41	1.17	1.49	91.02
10	44	P30K822	1.9	30.0	287.8	330	1.29	1.65	80.75	71.40	1.47	2.79	75.64
11	45	P30K823	1.9	30.0	273.8	330	1.96	1.25	59.09	73.99	1.61	3.06	65.40

<sup>2</sup> N/A here means that either surface thermocouple failed to work or the data fluctuate too much to read

Table 6-3 The Experimental Results of 19 mm (3/4") PMMA Sheet

No.	Test No.	File Name	V (mm/s)	Flux @ 425 mm kW/m <sup>2</sup>	T <sub>ext</sub> (°C)	T <sub>s2</sub> (°C)	$\tau_1$ (sec)	$\tau_2$ (sec)	$\dot{q}_1''$ (kW/m <sup>2</sup> )	$\dot{q}_2''$ (kW/m <sup>2</sup> )	$\tau_a$ (sec)	$\delta_g$ (mm)	$\dot{q}_g''$ (kW/m <sup>2</sup> )
1	36	M10K809	0.5	10.0	234.3	330	5.5	8.8	49.73	39.32	7.2	3.6	43.62
2	37	M10K810	0.2	10.0	230.4	330	N/A	7.2	N/A	44.61	7.2	1.44	44.62
3	38	M10K812	0.35	10.34	227.8	330	N/A	6.9	N/A	46.53	6.9	2.42	46.53
4	32	M20K708	1.27	20.52	269.6	330	1.54	1.37	69.49	73.72	1.46	1.85	71.54
5	35	M20K809	1.27	20.34	274.7	330	3.13	2.31	46.3	53.89	2.72	3.45	49.66
6	39	M30K812	1.9	30	269.2 /306	330	3.92	1.12	43.41	52	2.52	4.79	44.61
7	40	M30K816	1.9	30	270.9	330	2.85	2.91	50.45	49.94	2.88	5.47	50.19

## 6.5 ENERGY BALANCE AT THE FLAME LEADING EDGE FOR HORIZONTAL SPREAD; A NEW INTERPRETATION OF EXPERIMENTAL DATA

In an attempt to explain the inconsistencies of gas-phase conduction profiles for the same materials (cf. last two columns of Tables 6-2 and 6-3), we had to reexamine the physics of this process in detail. A schematic diagram of this process is shown in Figure 6-6 where different heat fluxes near the flame front are illustrated. We have derived gas-phase conduction profiles from surface temperature histories based on the postulate that gas-phase conduction profile is the same as the surface temperature profile or in other words, only solid conduction normal to the fuel surface was considered in those calculations while solid conduction upstream of the flame front (parallel to the fuel surface) was not accounted for. This explains why the length scale of gas phase conduction for 6.35 mm PMMA was generally shorter than that for 19 mm PMMA, since the path of conduction is limited for thinner PMMA (Williams, 1976). There is also a uniform heat flux applied in the pyrolyzing region,  $\dot{q}_2''$  which also contributes to the heating upstream of the pyrolysis front because it frees some of the flame heat by assisting in the vaporization process. The new energy balance for the control volume of Figure 6-6 is:

$$\rho_s c_s (T_p - T_\infty) V_s \delta_v = \dot{q}_g'' \delta_g + \dot{q}_2'' \delta_g + \dot{q}_1'' \sqrt{\ell_1 \delta_g} - \epsilon_s \frac{\sigma T_p^4}{4} \delta_H \quad (6-7)$$

where  $\delta_v$  is the vertical thermal length:

$$\delta_v = \sqrt{\alpha_s t} = \sqrt{\alpha_s \frac{\delta_g}{V_s}}$$

and  $\delta_H$  is the vertical thermal scale for the surface temperature distribution:

$$\delta_H = \frac{k_{xx} \alpha_s}{k_{sy} V_s}$$

The coefficient for each term in equation (6-7) may not be exactly equal to one. But there are not much different from one (de Ris, 1969; Delichatsios, 1986).  $\epsilon_s$  is the surface emissivity. The LHS of equation (6-7) represents rate of energy gain by the control volume; the first term on the RHS is the conducted heat from the flame near the pyrolysis front; the second term contributes to the heating upstream of flame front and  $\dot{q}_2''$  is defined as:

$$\dot{q}_2'' = \text{net heat flux} = \dot{q}_{2,ext}'' - \sigma T_p^4 \quad (6-8)$$

the third term is the contribution from the preheating of external heat flux+flame radiation. If an exponential decaying profile of this heat flux is assumed, i.e.  $\dot{q}_1'' \exp(-|x|/\ell_1)$ , the surface temperature rise due to this heat flux can be estimated as:

$$\rho_s c_s (T_s - T_\infty) V_{s_A} \left| \alpha_s \frac{\ell_s}{V_s} = \dot{q}_1'' \ell_s \right. \quad (6-9)$$

$T_s$  is surface temperature due to external heat flux; the last term of the RHS of the equation (6-7) is the reradiation loss for the control volume. One can combine equations (6-9) and (6-7), substitute  $\delta_g$ , arrive at a new energy equation concerning the control volume in Figure 6-6 can be derived as:

$$\rho_s c_s (T_p - T_s) V_{s_A} \sqrt{\alpha_s \frac{\delta_g}{V_s}} = \dot{q}_g'' \cdot \delta_g + \dot{q}_2'' \delta_g - \epsilon_s \frac{\sigma T_p^4}{4} \delta_H \quad (6-10)$$

By examining equation (6-10), one can see that the last term of right hand side is small compared to other terms and therefore it can be ignored for simplicity.

Eqn. (6-10) can be used to derive gas phase conduction profile from the experimental data. The approach is described as follows:

- 1) The flame spread speed,  $V_s$ , of the experiment is known exactly, the surface temperature,  $T_s$ , is measured in the experiment (see Fig. (6-5)). The material properties values are known as described in Section 6.3.  $\dot{q}_2''$  is also known from an experiment.
- 2) By applying eqn. (6-10) for two different experiments (i.e. different external heat flux levels at 425 mm away from the radiant panel edge and different flame spread speeds), two equations with  $\dot{q}_g''$  and  $\delta_g$  are obtained. Subtract the first equation from second equation, one equation with only  $\delta_g$  is derived since the first term on the RHS of eqn. (6-10) is eliminated. The remaining algebraic equation can be simply solved for  $\delta_g$ ,  $\dot{q}_g''$  can be consequently derived.

We have applied above approach to the experimental data discussed above. The results in Tables 6-1 to 6-3 are reprocessed and shown in Tables 6-4 to 6-6. Note that we have used averaged values of surface temperatures,  $T_s$ , for the same external heat flux level and flame spread speed. The derived gas-phase conduction heat flux profiles parameters ( $\dot{q}_g''$  and  $\delta_g$ ) are consistent (cf. the values of  $\delta_g$  and  $\dot{q}_g''$  in Column 4 and 6 of Tables 6-5 and 6-6):  $\dot{q}_g'' \approx 70 \text{ kW/m}^2$  and  $\delta_g \approx 1.4 \text{ mm}$  for PMMA. For particle board,  $\dot{q}_g'' \approx 30 \text{ kW/m}^2$  and  $\delta_g \approx 1.0 \text{ mm}$ . The consistency of the results for different thicknesses of PMMA and different tests for particle board shows the validity of this analytical approach. We will use above values of gas-phase conduction in the flame spread model to simulate flame spread and numerical results will be compared with the experimental data which are discussed in the following section.

Finally, an error analysis is carried out for the 20 kW/m<sup>2</sup> particle board test which is representative of experimental errors. These errors arose mainly from two variables, surface temperature and flame front location (which would cause errors in determining the heat flux behind the flame front,  $\dot{q}_2''$ ). There are many factors that can cause errors in surface temperature measurements, but two factors are particularly important: 1) location of thermocouple, (i.e. it is important to make sure that the thermocouple does measure surface temperature instead of gas-phase or solid temperature inside the solid) 2) the other factor is not really an experimental error, rather it is from the use of the surface temperature at the point of the sudden increase in the above analysis. In the analysis shown above, the surface temperature measurement at the time of the sudden increase is used. In fact, there is still temperature rise due to external heat flux and flame radiation during the sudden increase period which was not accounted for in the above analysis. This uncertainty of surface temperature can be estimated from examining the detailed plot of surface temperature during period (e.g. Figure 6-3). For 20 kW/m<sup>2</sup> particle board test, the uncertainty is estimated to be  $\pm 7.5^\circ$ . Using this uncertainty, the magnitude of the gas phase conduction of  $\dot{q}_g''=27.63$  kW/m<sup>2</sup> is determined with the external imposed flux of 20 kW/m<sup>2</sup> (see Table 6-4). The uncertainty of flame front location is  $\pm 1$  cm from experimental observation and this could be resulted from fluctuations of flame front locations. Accounting for this uncertainty, a value of  $\dot{q}_g''=32.62$  kW/m<sup>2</sup> is obtained. Therefore, we can determine that the overall uncertainty in  $\dot{q}_g''$  is:  $[(27.63-28.69)^2+(32.62-28.69)^2]^{1/2}=4$  kW/m<sup>2</sup> or about 14%. Similarly, the uncertainty in  $\delta_g$  is about 21%.

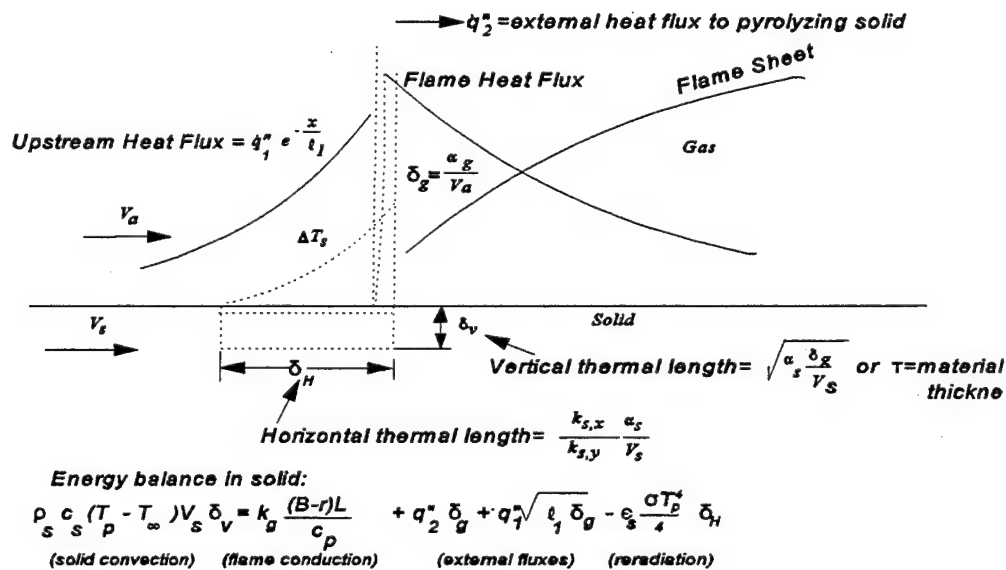


Figure 6-6 A diagram of heat fluxes at the flame leading edge



Table 6-4 19 mm Particle Board Experimental Data-New interpretation

19 mm Particle Board		T20 Case		T30K623	
T10 Case		rho_s=	765	rho_s=	765
rho_s=	765	c_s=	2800	c_s=	2800
c_s=	2800	V_s=	1.28E-03	V_s=	2.56E-03
V_s=	3.20E-04	FW=	1.08E+02	FW=	100
FW=	1.15E+02	ds=	474.5	ds=	467
ds=	482	T_s	2.65E+02	T_s	270.25
T_s	2.35E+02	T_p	320	T_p	320
T_p	320	alpha_s	1.05E-07	alpha_s	1.05E-07
alpha_s	1.05E-07	q_425	2.15E+01	q_425	32.88
q_425	1.27E+01	C_1	0.821272	C_1	0.846988
C_1	0.795644	q_ext	17.66968	q_ext	27.84896
q_ext	10.11264	T_0=	2.25E+01	T_0=	23
T_0=	2.37E+01	q_r	6.058424	q_r	6.055721
q_r	6.052096	q_2	13.61125	q_2	26.79324
q_2	4.060544	LHS=	1365.449	LHS=	1746.711
LHS=	1057.189	LHSD	308.2605	LHSD	689.5219
LHSD		RHSDE3	9550.708	RHSDE3	22732.69
RHSDE3		delta_g(m)	0.001042	delta_g(m)	0.00092
		k_g(T_f-T_p)	29.89195	k_g(T_f-T_p)	28.33061
k_g(T_f-T_p)		q_g'' (kW/m²)	28.6939	q_g'' (kW/m²)	30.79367

Table 6-5 6.35 mm PMMA Experimental Data-New Interpretation

6.35 PMMA Sheet

P10 Case		P20 Case		P30 Case	
rho_s=	1200	rho_s=	1200	rho_s=	1200
c_s=	2200	c_s=	2200	c_s=	2200
V_s=	5.00E-04	V_s=	1.27E-03	V_s=	1.90E-03
FW=	8.00E+01	FW=	8.50E+01	FW=	8.75E+01
ds=	447	ds=	452	ds=	454.5
T_s	2.30E+02	T_s	2.70E+02	T_s	2.75E+02
T_p	370	T_p	370	T_p	370
alpha_s	1.06E-07	alpha_s	1.06E-07	alpha_s	1.06E-07
q_425	1.02E+01	q_425	1.94E+01	q_425	3.00E+01
C_1	0.91564	C_1	0.898498	C_1	0.889917
q_ext	9.357846	q_ext	17.45602	q_ext	26.69752
T_0=	1.90E+01	T_0=	2.29E+01	T_0=	2.15E+01
q_r	8.545232	q_r	8.524531	q_r	8.532057
q_2	0.812614	q_2	11.93149	q_2	23.16547
LHS=	2690.536	LHS=	3062.864	LHS=	3558.986
LHSD		LHSD	372.3275	LHSD	868.4492
RHSDE3		RHSDE3	11118.88	RHSDE3	22352.85
		delta_g (m)	0.001121	delta_g (m)	0.001509
k_g(T_f-T_p)		k_g(T_f-T_p)	89.18426	k_g(T_f-T_p)	103.3057
		q_g'' (kW/m^2)	79.53534	q_g'' (kW/m^2)	68.43859

Table 6-6 19 mm PMMA Experimental Data-New Interpretation

19 mm PMMA Sheet		M20 Case		M30 Case	
M10 Case		rho_s=	1200	rho_s=	1200
rho_s=	1200	c_s=	2200	c_s=	2200
V_s=	5.00E-04	V_s=	1.27E-03	V_s=	1.90E-03
FW=	85	FW=	6.75E+01	FW=	1.28E+02
ds=	452	ds=	434.5	ds=	494.5
T_s	234.3	T_s	2.70E+02	T_s	2.80E+02
T_p	370	T_p	370	T_p	370
alpha_s	1.06E-07	alpha_s	1.06E-07	alpha_s	1.06E-07
q_425	10	q_425	2.04E+01	q_425	3.00E+01
C_1	0.898498	C_1	0.958295	C_1	0.753241
q_ext	8.984983	q_ext	19.57739	q_ext	22.59724
T_0=	23	T_0=	2.33E+01	T_0=	2.18E+01
q_r	8.523989	q_r	8.522632	q_r	8.530721
q_2	0.460994	q_2	12.05475	q_2	20.06652
LHS=	2607.898	LHS=	3062.864	LHS=	3371.671
LHSD		LHSD	454.9654	LHSD	308.8068
RHSDE3		RHSDE3	11593.76	RHSDE3	8011.768
		delta_g (m)	0.00154	delta_g (m)	0.001486
k_g(T_f-T_p)		k_g(T_f-T_p)	101.6299	k_g(T_f-T_p)	100.1463
		q_g''(kW/m²)	65.99539	q_g''(kW/m²)	67.40903

## 6.6 NUMERICAL SIMULATION OF FLAME SPREAD AND COMPARISON WITH THE EXPERIMENTAL DATA

After determining the gas-phase conduction heat flux profile (i.e.  $q''_g$  and  $\delta_g$ ) from the experimental data, the following steps have been taken in order to determine flame spread using the horizontal flame spread model (HFSCS) and to compare with experimental data: 1) the gas-phase conductive heat flux profile was used in the code as an imposed heat flux, 2) the flammability properties examined in Sec. 4.2 were the code input, 3) because the large heat flux measurements were reliable when flame was away from the large heat flux gage, the external and flame radiative heat fluxes at any point on the fuel surface at any instant were inferred from the large heat flux measurement for each experiment. This was possible since the distance between any point on the fuel surface and the cooling plate edge at any instant of time was known, and assuming that the external heat flux+flame radiation were the same for the same distance from the cooling plate edge (see discussion of Fig. 6-3). The inferred heat flux histories are used in the predictions.

Figures 6.7-9 illustrate the comparisons of the measured (via video recording) and predicted flame front locations from the sample leading edge for the 19 mm particle board experiments for three different external heat flux levels. The video recording was used to obtain flame front position at discrete time intervals using frame by frame analysis. One can see that all predictions agree with the experimental data. There are large differences shown in Figure 6-10. This would probably due to 1) the flame spread was not steady at the beginning, 2) no attempt was made to model the exact initial burning area and ignition length. This could result in discrepancies at matching the initial flame front location as seen in Figure 6-7. The main aim is here is to compare the slope of the flame leading edge position vs. time in Figures 6.7-9, which represents the flame spread velocity.

The same approach was used to predict experimental results at three different external heat flux levels for the 19 mm thick PMMA specimens, shown in Figures 6.10-12. Good agreement was observed except for the case M20K809 where there were some problems obtaining a steady flame spread during the experiment. Similarly good agreements can be seen for the comparisons for the 6.35 mm PMMA thick samples shown in Figures 6.13-15.

Finally, we show in Figure 6-16 the comparison of detailed surface temperature histories during the sudden increase period between the prediction and a particle board test at the second measuring station. The temperature history profiles of prediction and experiment are the same. The surface temperatures increase suddenly at almost same value ( $\sim 270^\circ$ ) for both the predication and the experiment indicating that the model follows the surface temperature histories during the flame spread experiment quite well. The flat part of the prediction at  $320^\circ\text{C}$  simply shows the pyrolysis temperature because after pyrolysis starts, the pre-heating model is no longer valid. Therefore, the flat part has no physical meaning. The surface temperature comparison for a 19 mm PMMA is shown in Figure 6-17. Similar results are shown in Appendix L.

Some comments concerning above prediction and the flame spread code should be made to help the reader to better understand the current approach: 1) the use of heat flux measured at the station 3 arrives from the fact that the calculation of the heat flux for the experiments would be difficult due to the presence of the radiant panels (results in additional unknown flux). A radiation model can be used to calculate the heat flux ahead of the flame for an arbitrary condition, 2) for any other materials being modeled, the constant speed horizontal flame spread experiments have to be carried out to derive parameters of gas-phase conductive heat flux profiles,  $q''_g$  and  $\delta_g$ . These parameters then can be used in the flame spread code, 3) material flammability properties have to be determined apriori as input to the model and, 4) the completed horizontal flame spread model can only predict the flame radiative heat flux based on a radiation model, 5) a lumped model (with combustion) can include vitiation in a limited manner.

## 6.7 LIMITATION OF THE HORIZONTAL FLAME SPREAD MODEL

The horizontal flame spread model developed in this work can handle sudden jump of heat flux as described in Section 3.4. The model can also use transient external heat flux with no problems, at least for the cases that have been tested. The transient effect of the flame growth on variation of flame heat fluxes can also be dealt with easily. The model has been designed to accommodate the effects of vitiation (i.e. changes in combustion and flame heat fluxes). The model has not been tested extensively for sudden decrease of heat fluxes, such as heat flux drops due to suppression.

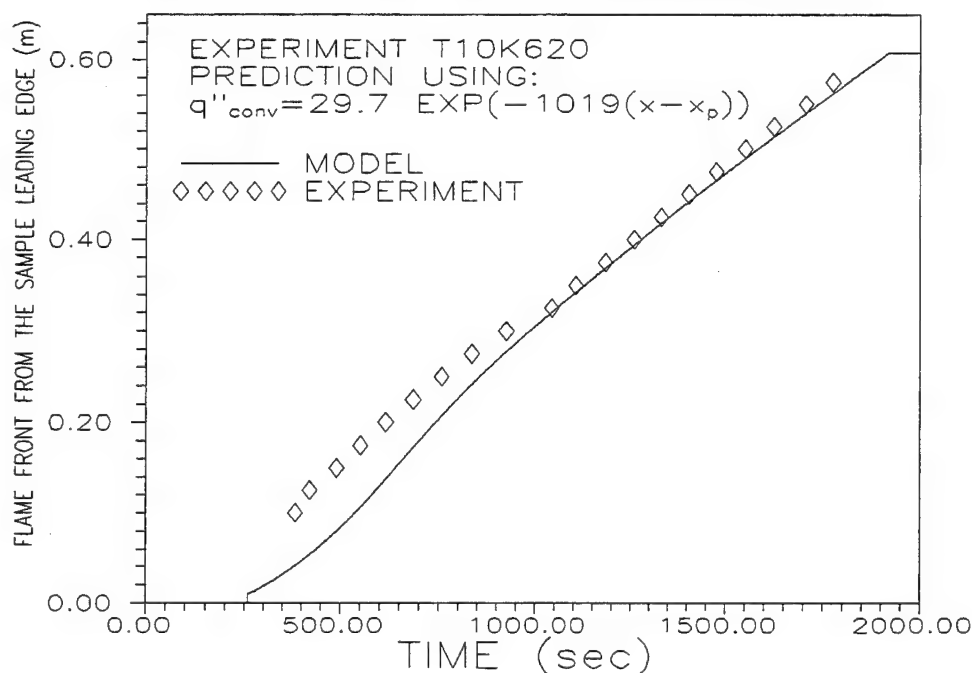


**Figure 6-7** Comparison of predicted and measured flame spread for a particle board experiment. External heat flux level:  $10 \text{ kW/m}^2$

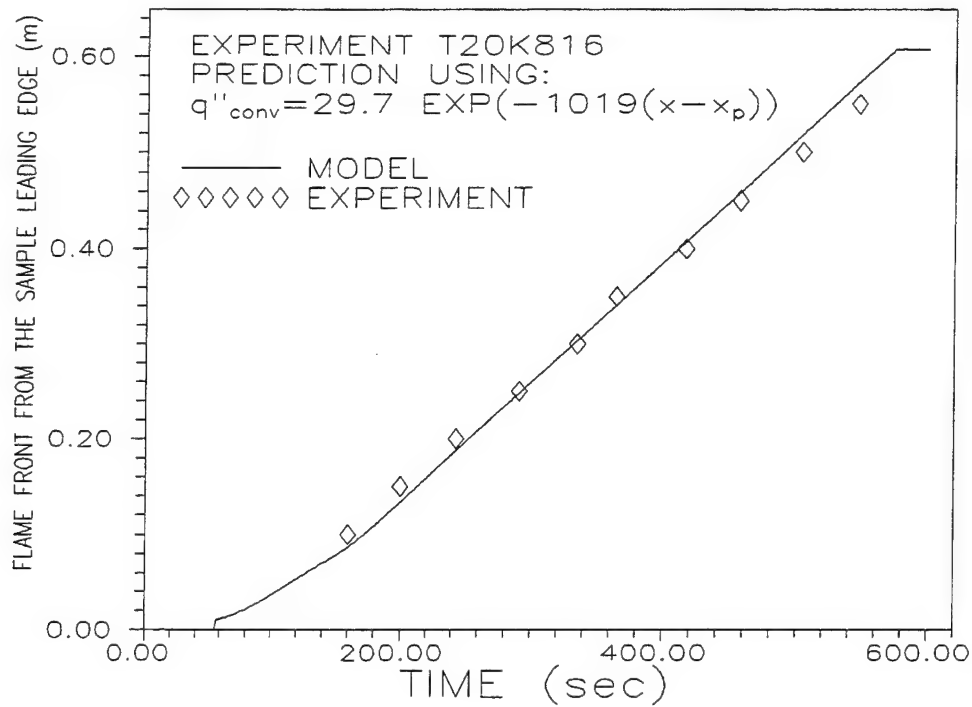


**Figure 6-8** Comparison of predicted and measured flame spread for a particle board experiment. External heat flux level: 20 kW/m<sup>2</sup>

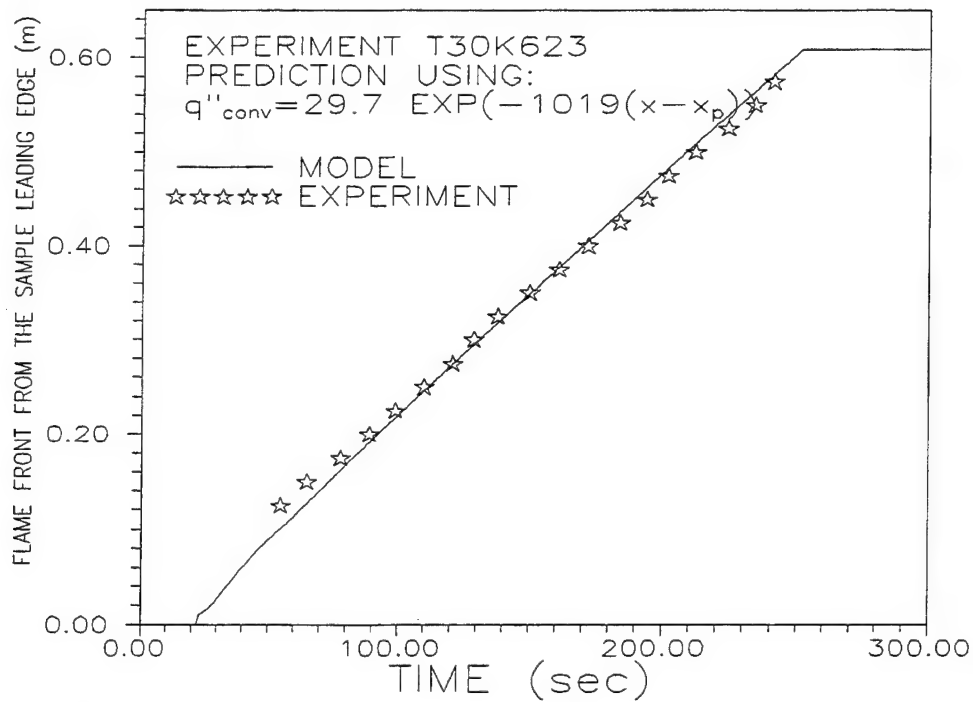


**Figure 6-9** Comparison of predicted and measured flame spread for a particle board experiment. External heat flux level: 30 kW/m<sup>2</sup>

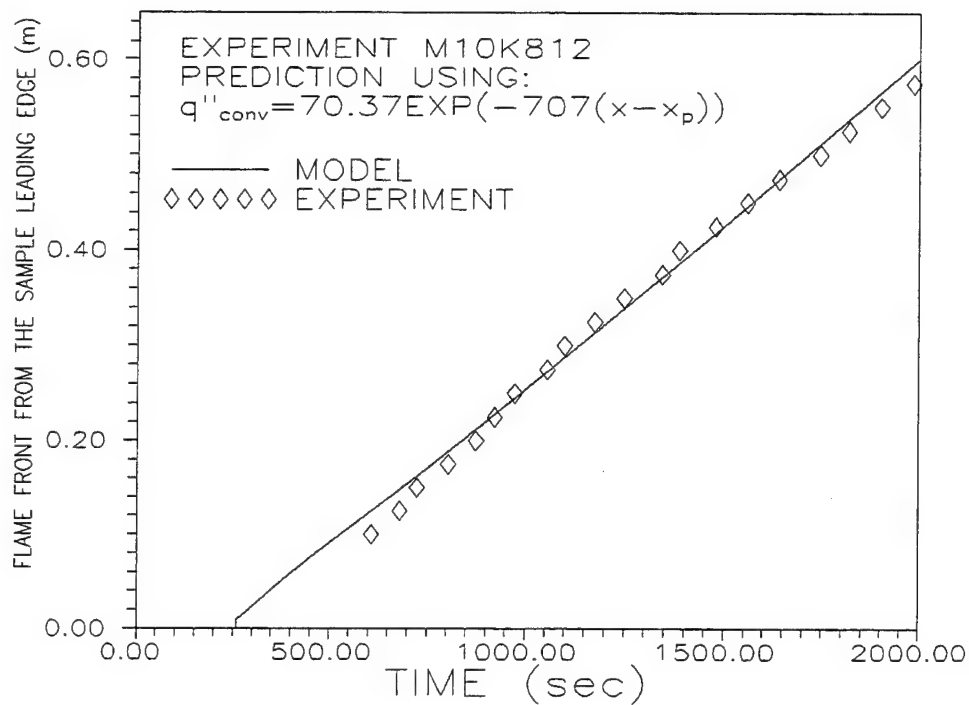


**Figure 6-10** Comparison of predicted and measured flame spread for a 19 mm thick PMMA sample experiment. External heat flux level: 10 kW/m<sup>2</sup>

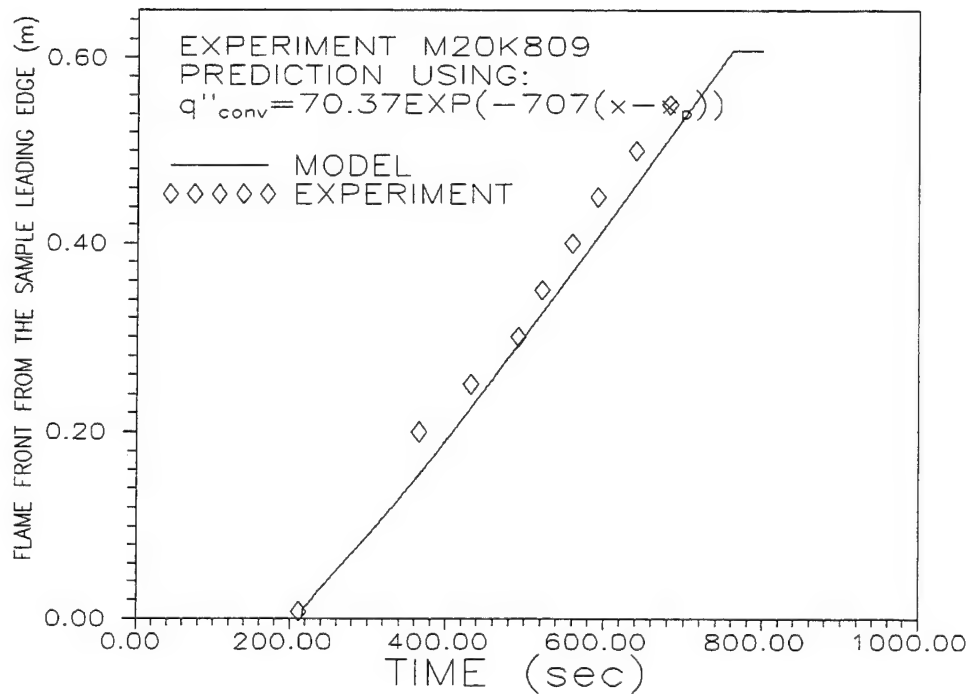


**Figure 6-11** Comparison of predicted and measured flame spread for a 19 mm thick PMMA sample experiment. External heat flux level: 20 kW/m<sup>2</sup>

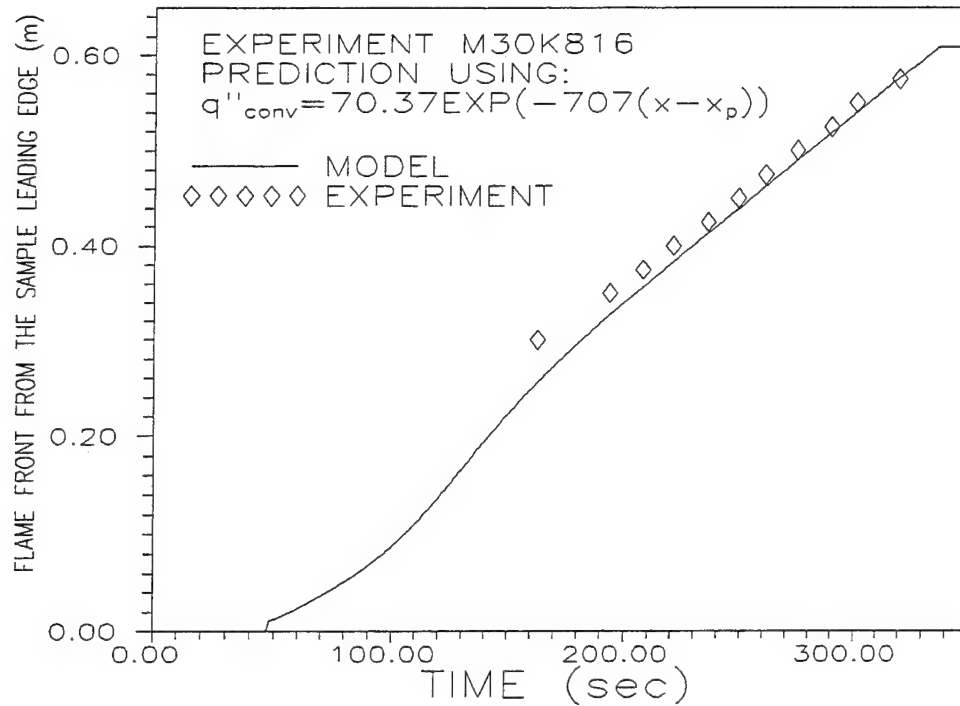


**Figure 6-12** Comparison of predicted and measured flame spread for a 19 mm thick PMMA sample experiment. External heat flux level: 30 kW/m<sup>2</sup>

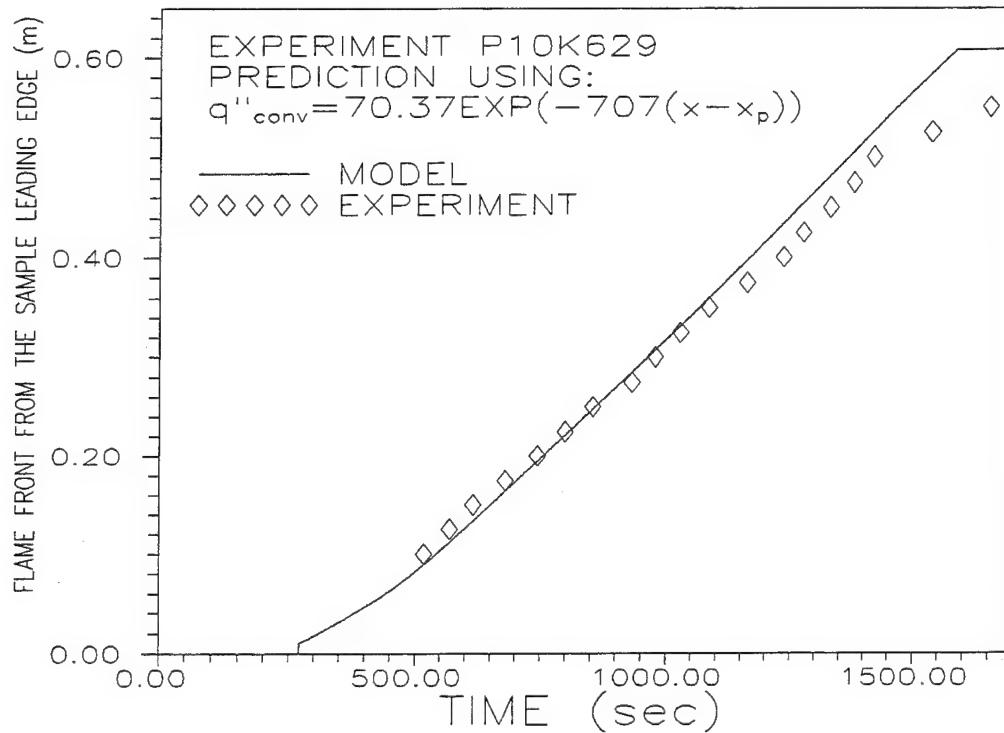


**Figure 6-13** Comparison of predicted and measured flame spread for a 6.35 mm thick PMMA sample experiment. External heat flux level: 10 kW/m<sup>2</sup>



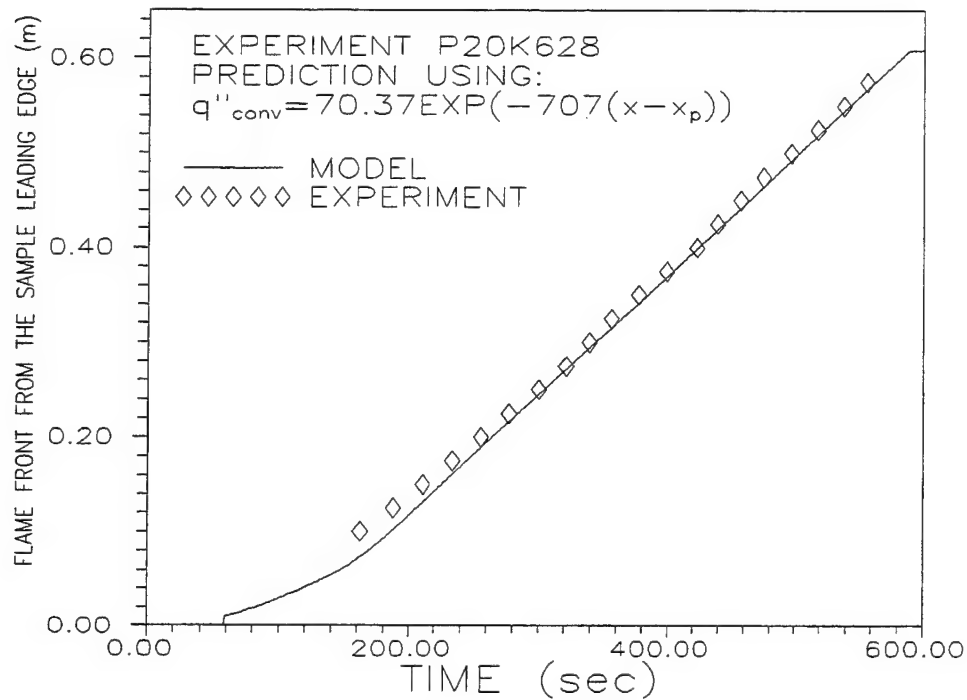


**Figure 6-14** Comparison of predicted and measured flame spread for a 6.35 mm thick PMMA sample experiment. External heat flux level: 20 kW/m<sup>2</sup>

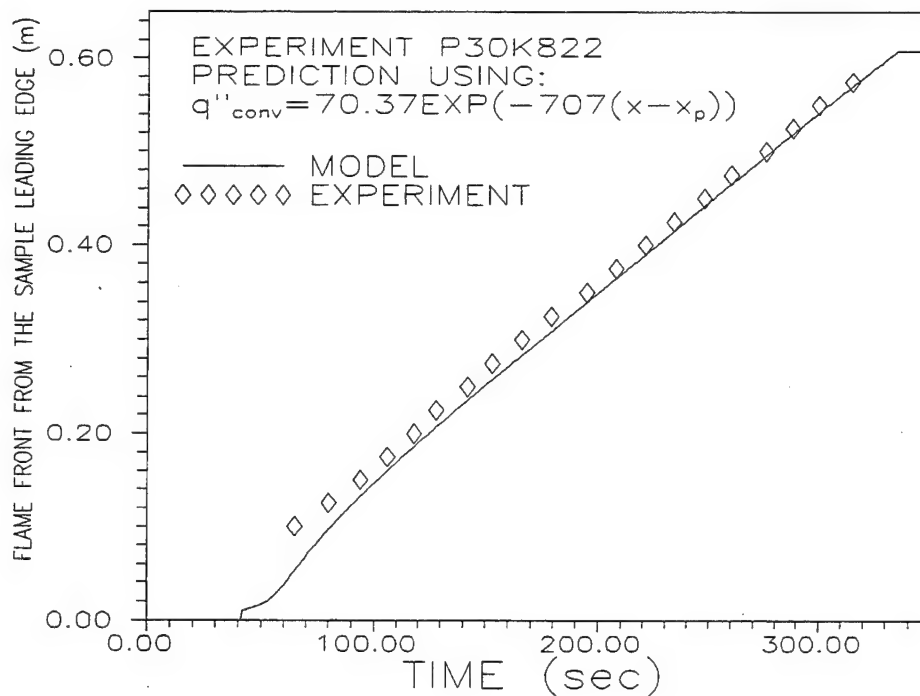


**Figure 6-15** Comparison of predicted and measured flame spread for a 6.35 mm thick PMMA sample experiment. External heat flux level: 30 kW/m<sup>2</sup>

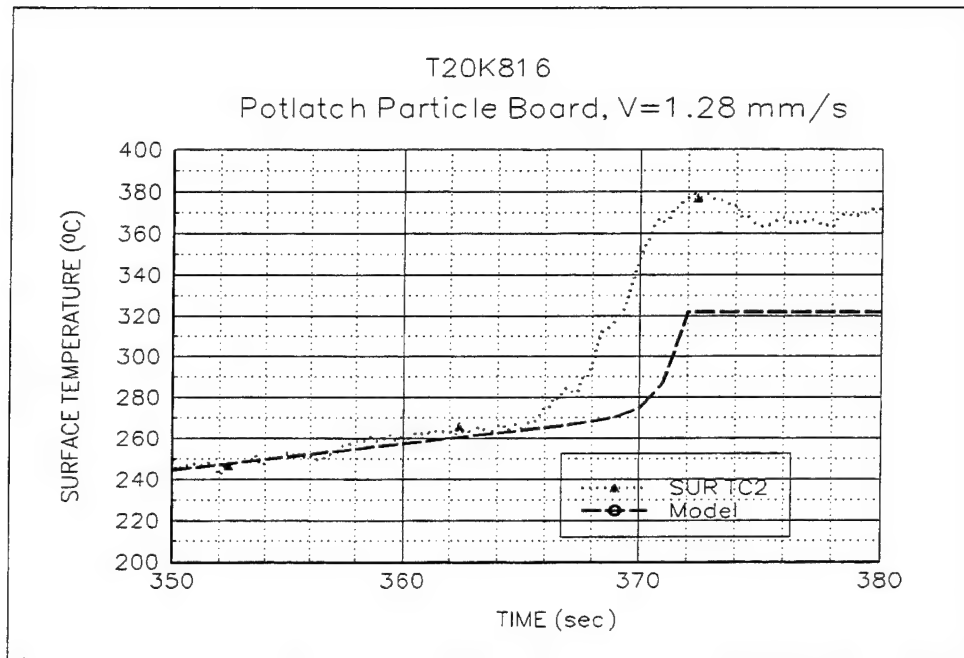


**Figure 6-16** Detailed comparison of surface temperature at the second measuring station during the sudden increase period with the model prediction for the particle board test. External heat flux level:  $20 \text{ kW/m}^2$

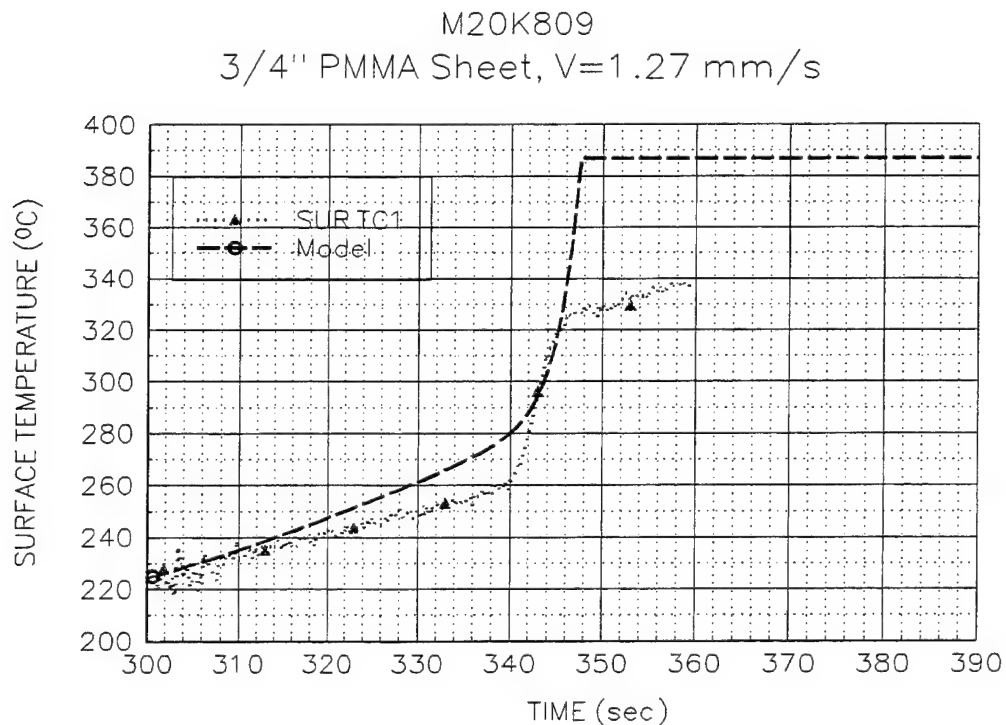


**Figure 6-17** Detailed comparison of surface temperature at the first measuring station during the sudden increase period with the model prediction for the 19 mm thick PMMA. External heat flux level:  $20 \text{ kW/m}^2$

## 6.8 CHAR DEPTH MEASUREMENTS AND ADDITIONAL DISCUSSION

The material charring is an important parameter for determining the material flammability properties and consequently the flame spread prediction. The pyrolysis model that we have developed as part of the horizontal flame spread model can predict the char depth for the material being exposed to external flux. Although the focus of our research was not on in-situ validation of the charring model, the char depth was measured for all the particle board test specimens. The char depth was measured every 5 cm at 3 positions across the material width by cutting the specimen along the width and the three char depth measurements were averaged. The data was collected and tabulated using three specimens for each of the external flux levels (10, 20 and 30 kW/m<sup>2</sup>) and are included in the report for completeness in Appendix M. A plot of the data is shown in Figure 6-18. Tests 1-3 for each of the external flux levels are shown here. Clearly, variations in the material homogeneity, initial material conditions, test conditions and burning area size would affect the char depth. Never-the-less, the three distinct levels of charring is obtained for each external flux levels. Furthermore, the largest variation in the char depth is about 20% from the mean. The scatter seems to be more for the 10 kW/m<sup>2</sup> case, however, the percent variation is no greater. The char depth, as expected, is highest for the lowest flux since the flame spread is slowest in that case and thus the burning zone is being moved under the cooling plate (i.e. the flame is quenched) at a slower rate.

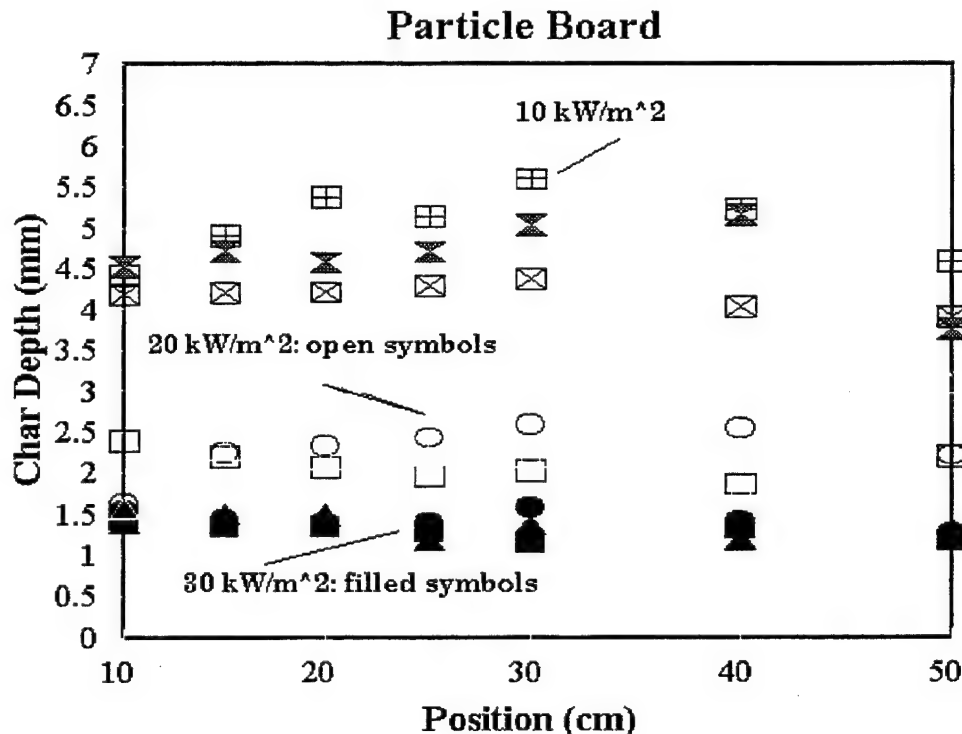


Figure 6-18 Char depth measurements along the particle board specimens exposed to 3 different external flux conditions. Three tests for each condition.

We have shown (Chen, et al., 1995) that the char depth can be characterized by a characteristic char conductance length,  $d_c$ , shown below:

$$d_c = \frac{k_c T^*}{4 \dot{q}_o''} \quad (6-11)$$

where  $k_c$  is the thermal conductivity of the char and  $T^*$  is the maximum surface temperature attained if the imposed external flux,  $\dot{q}_o''$ , is equal to the surface reradiation losses.

The data presented in Figure 6-18 was normalized using equation (6-11). The char depth,  $x_c$ , was averaged for the three tests and normalized by the char conductance length,  $d_c$ , and is shown in Figure 6-19. This plot shows that for a steady state flame spread condition, the char formation is a strong function of the externally imposed flux and does not depend on the flame fluxes. Furthermore, we can conclude that this char conductance length is a reasonable parameter in that all the data collapse approximately on a single curve.

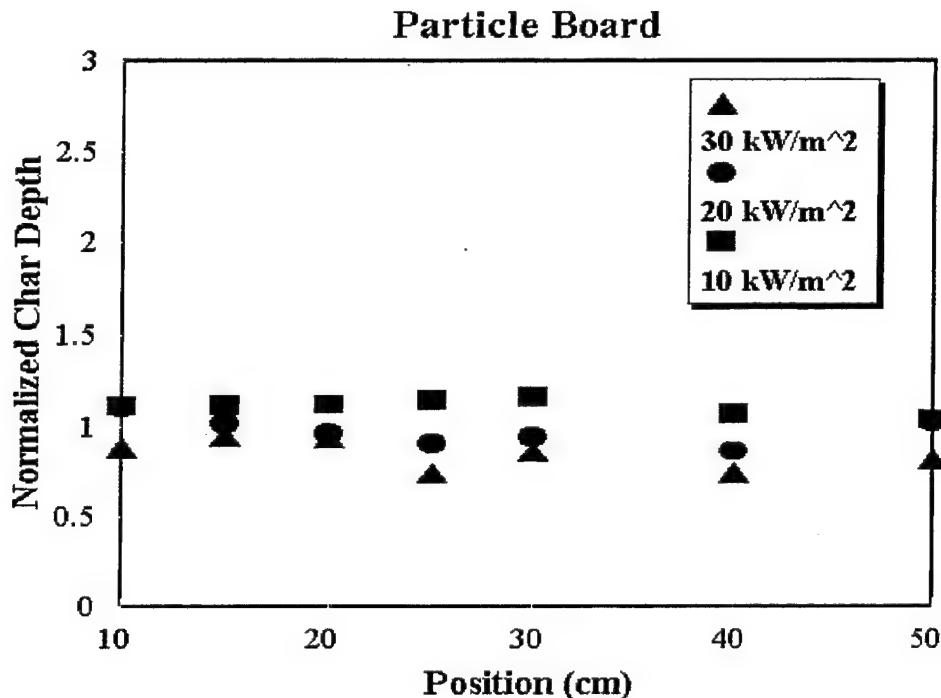


Figure 6-19 Normalized char depth along the specimen for 3 externally imposed conditions, constant flame spread experiments.

## **IR Imaging**

We have shown temperature data in this report obtained from thermocouples. Although, the measurements were relatively reliable, thermocouples only provide local measurements. An alternative measurement approach would be to use IR imaging for surface temperature measurements. The advantage is the field measurements and ability to have evaluate the overall experiment. The disadvantages are the flame interference with the surface measurements, reflections causing errors and the relative uncertainty in the measurement which must be carefully calibrated and dependency on the surface emissivity. In addition, the cost of such system would be much higher than using thermocouples. We used a demonstration system to obtain some preliminary data for a flame spread over a PMMA sample. Figures 6-20 through 6-23 show the thermal images of the sample. The burning zone measurements are totally unreliable since a special filter would be needed to reduce the flame interference. An emissivity of 0.9 was assume for the painted surface of the PMMA. The burning zone is clearly distinguishable. The lateral uniformity of the burning zone is not typical and was improved in actual tests. The last figure is an actual contour plot of the surface temperature generated by the image processing software. The PMMA pyrolysis temperature of 330° is quite closely measured here despite the lack of very careful calibration and relying on the internal calibration of the system.

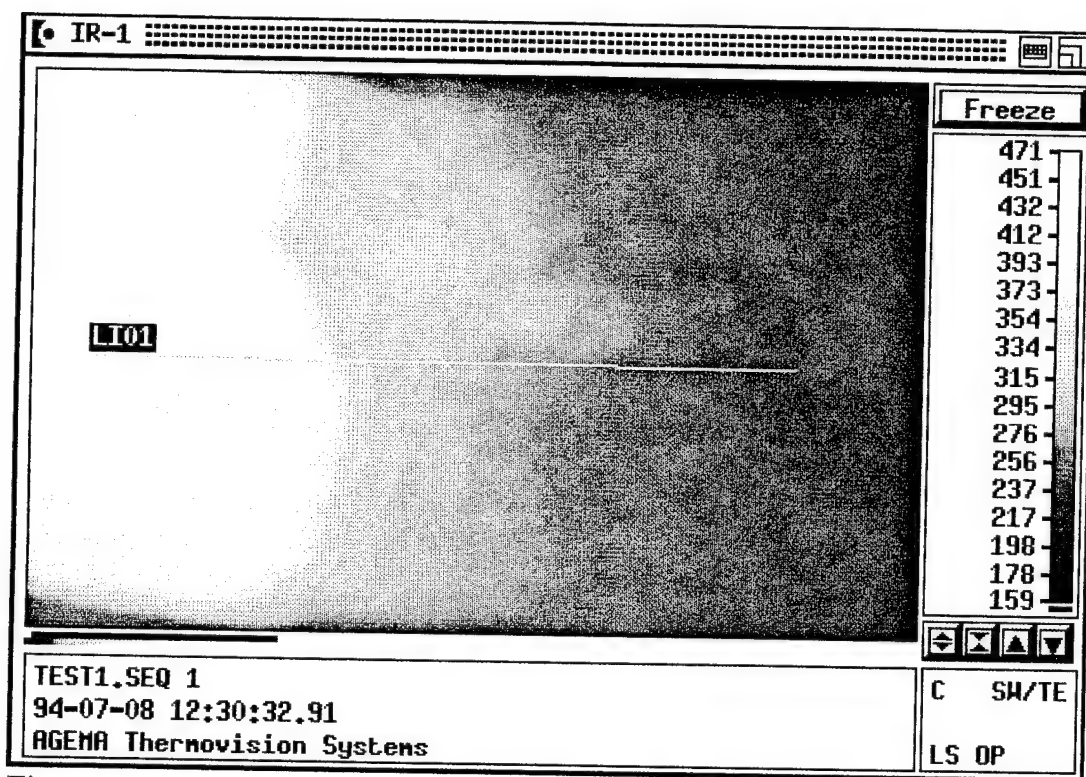


Figure 6-20 - IR Temperature map ( $^{\circ}\text{C}$ ), PMMA Test, 19 mm thick,  $10 \text{ kW/m}^2$

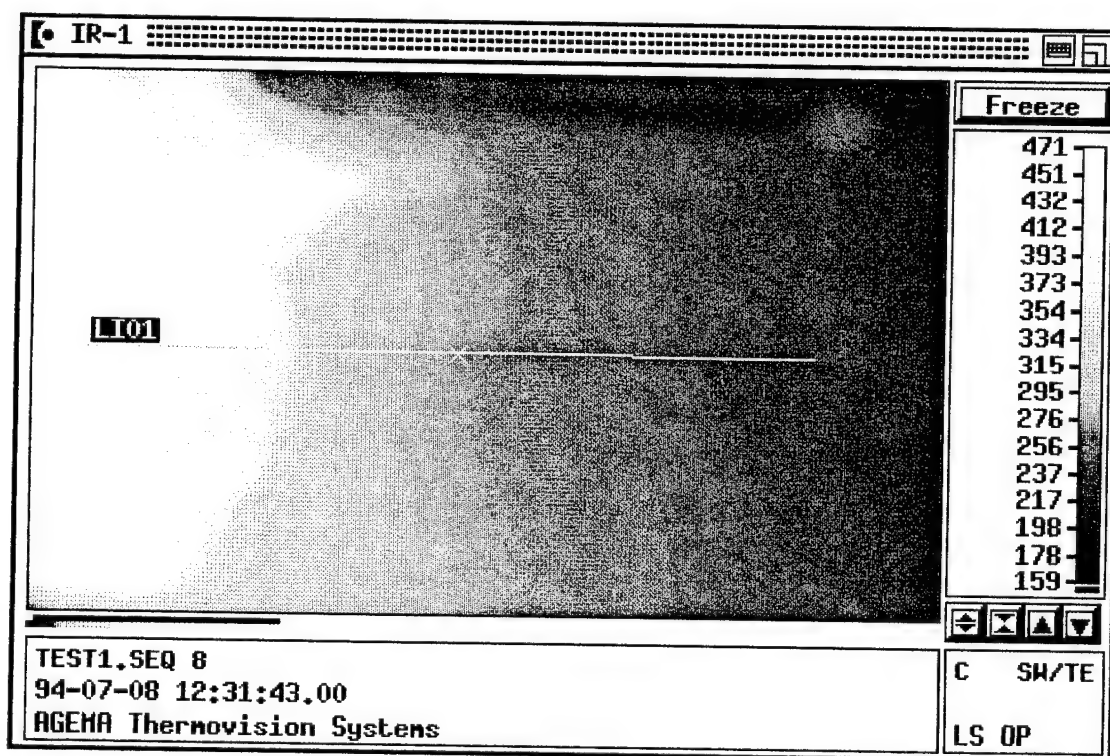


Figure 6-21 - IR Temperature map ( $^{\circ}\text{C}$ ), PMMA Test, 19 mm thick,  $10 \text{ kW/m}^2$

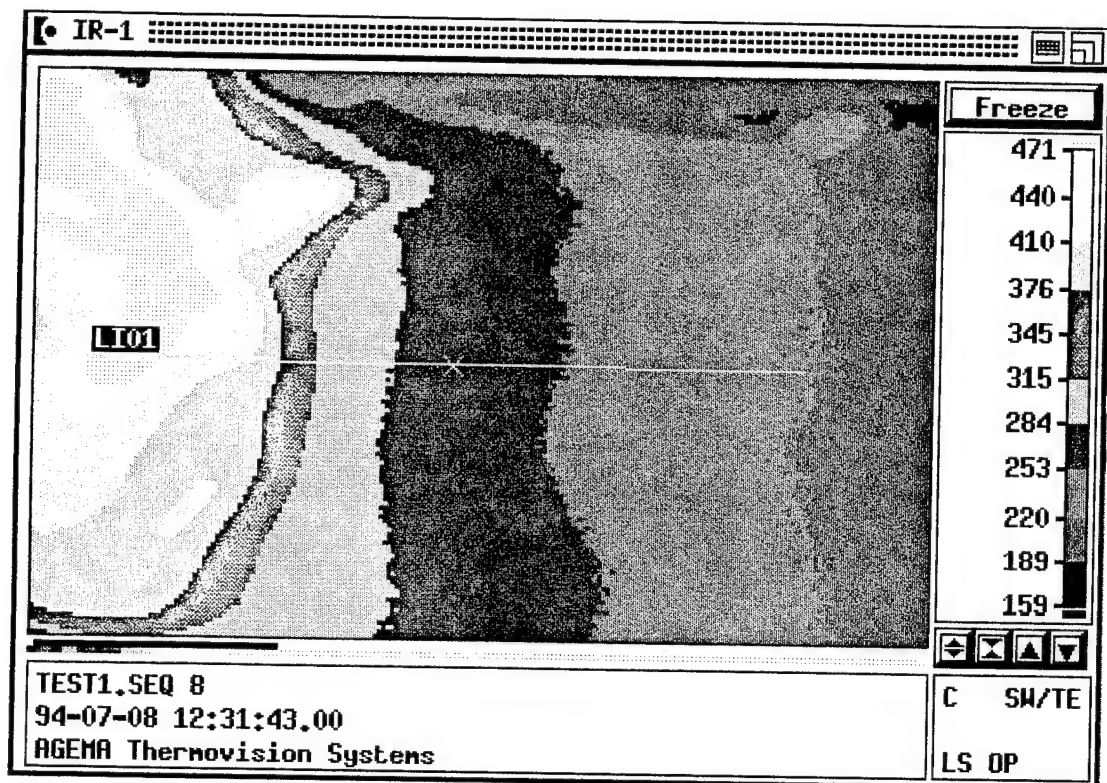


Figure 6-22 - IR Image, Surface temperature ( $^{\circ}\text{C}$ ) contour map of Figure 6-21, PMMA, 19 mm thick,  $10 \text{ kW/m}^2$

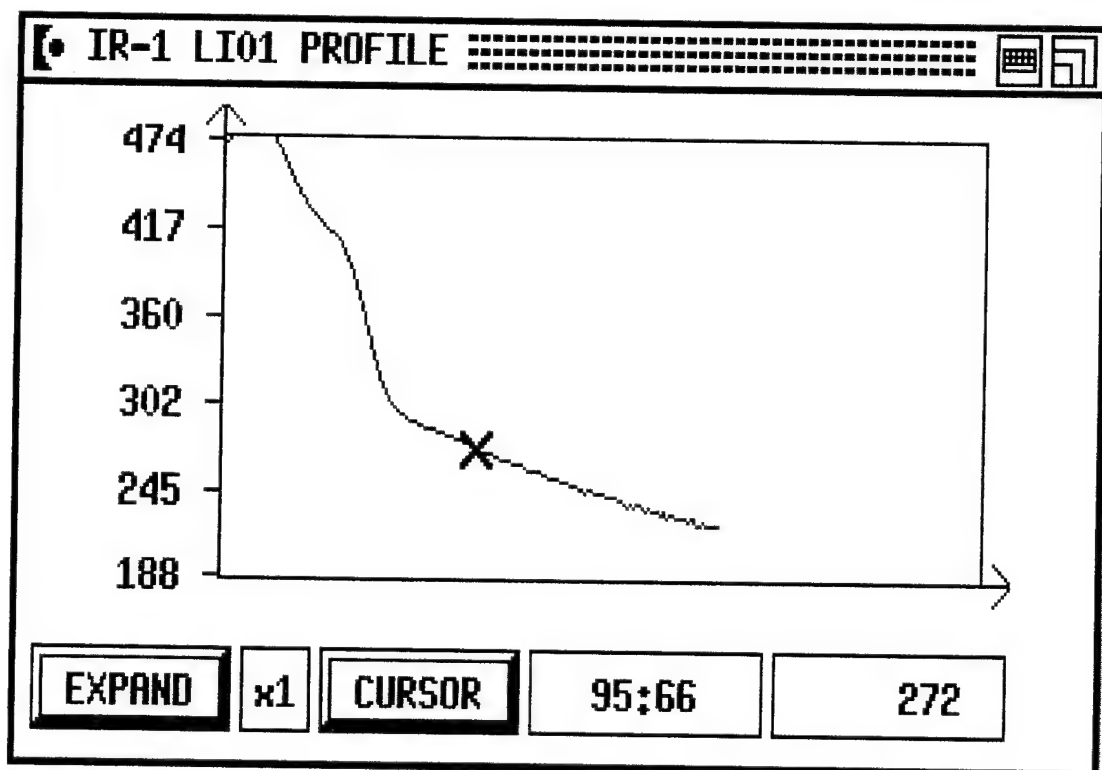


Figure 6-23 - Surface temperature profile of Fig. 6-21 along the designated line.

## Chapter 7      Conclusions and Future Work

A comprehensive opposed flow horizontal flame spread model has been developed and validated by comparison with an analytical solution and experimental data. The model uses measured gas-phase convective heat flux distribution, which has a characteristic exponential decaying profile with a length scale  $\delta_g$  and a maximum flux,  $\dot{q}_g''$ ). The model includes all phenomenon involved in horizontal flame spread as follows:

- 1) Solid conduction and pyrolysis for both charring and non-charring materials is calculated using a one dimensional integral method validated by comparison with experiments.
- 2) Combustion of pyrolysis gases and radiation from turbulent diffusion flame is simulated using a combustion model. A phenomenological soot formation model based on laminar smoke-point height was applied in turbulent combustion to predict soot concentration and flame radiation. As a first step, this soot and radiation model was used for optically thin flames in order to derive an energy equation. Comparison of predictions with radiation measurements in turbulent buoyant jet flames (See Chapter 4) for different fuels provided a partial validation to the present model. For pool fires, application of the model provides encouraging results, but it also points to a need for a) further examination of the flow near the base of the pool fire b) relaxation of the optically thin flame approximation as the pool size increases and c) state relationships for real fuels.
- 3) Derivation of gas-phase convective heat flux from measurements of a constant speed flame spread experiment. A quasi-steady horizontal flame spread experiment (constant speed and burning area) was designed and conducted for two materials: PMMA and particle board. Surface temperature and heat flux histories were measured. The surface temperature histories were analyzed using an analytical solution, to obtain the profiles of gas-phase convective heat flux. It was deduced that the solid conduction from flame front to upstream of the flame front has to be considered (conduction parallel to fuel surface) to correctly derive the gas-phase conductive heat flux profile. A new analytical approach of energy balance has been developed that considers contribution to flame spread from external heat flux in the pyrolyzing region behind the flame front to flame spread (See Chapter 6). Profiles of gas-phase convection was finally determined using this approximation. The uncertainty of the magnitude of the gas-phase convective heat flux from the analysis of the experimental data for a representative particle board test is about 14% for  $\dot{q}_g''$  and 21% for  $\delta_g$ . This profile has incorporated effects on gas phase conductive heat flux, namely, gas phase finite chemistry, complex flow near the flame front as well as ambient condition. The derived profile was finally used in the horizontal flame spread model to calculate flame spread. The model has been validated through experimental data of flame spread and surface temperature histories.



**The future work can include the following items:**

- 1) Complete coupling of the horizontal flame spread model with the integral combustion model should be implemented. Such work would involve:
  - a) validated model of heat flux to the burning surface,
  - b) measurements of state relationships for arbitrary fuel,
  - c) improving numeric of the combustion model, and
  - d) extension of the radiation sub-model to optically intermediate and thick flames.
- 2) Experiments could be performed for other materials (e.g. wood) to derive gas phase conduction heat fluxes.
- 3) Insertion of the horizontal flame spread model into a compartment models (e.g. CFAST) should also be carried out.
- 4) The flame spread should be tested extensively for sudden decrease of heat fluxes.

## References

- Agita, K.C., Ramaker, D.E., Tatem, P.A. and Williams, F.W. (1989), Fire Safety Science- Proceedings of Second International Symposium, Hemisphere Publishing Co., NY, p. 241.
- Atreya, A. (1983), "Pyrolysis, Ignition and Fire Spread on Horizontal Surface of Wood", Ph.D. Dissertation, Harvard University.
- Atreya, A. (1984), "Fire Growth on Horizontal Surfaces of Wood", Combust. Sci. Tech., Vol. 39, pp. 163-194.
- Atreya, A., Carpenter, C. and Harkleroad, M. (1985), "Effect of Sample Orientation on Piloted Ignition and Flame Spread Properties", Fire Safety Sci. 1st Int. Symp.
- Atreya, A., Carpenter, C. and Harkleroad, M. (1986), Fire Safety Science, 1st Int. Symp..
- Babrauskas, V. and Williamson, R.B. (1978), Fire and Materials, 2,39.
- Babrauskas, V. and Watterlund, I. (1995), The Role of Flame Flux in Opposed-flow Flame Spread, Private Communication.
- Beyler, C.L. (1986), Fire Safety Science Proceedings of the First International Symposium, Hemisphere, NY, p. 431.
- Bhatanger, S.K., Varshney, B.S., Mahanty, B. and Agarwal, C.P. (1990), "Steady Flame Spread Rate Measurement at Discrete Levels of External Radiant Heat Flux", 23rd Symp. (Int'l) on Comb., Comb. Inst., pp. 1693-1699.
- Bhattacharjee, S and Altenkirch, R.A. (1990), Radiation-Controlled, Opposed-Flow Flame Spread in a Microgravity Environment, 23rd Symp. (Int'l) on Comb., Comb. Inst., pp. 1627-1633.
- Bhattacharjee, S and Altenkirch, R.A. (1992), A Comparison of Theoretical and Experimental Results in Flame Spread over Thin Condensed Fuels in a Quiescent, Microgravity Environment, 24th Symp. (Int'l) on Comb., Comb. Inst., pp. 1669-1676.
- Bilger, R.W. (1976), Reaction Rates in Diffusion Flame, Combust. Flame, 30 pp. 277-284.
- Bilger, R.W. (1977), Turbulent Jet Diffusion Flame, Prog. Energy Combust. Sci., 1, 87-109.
- Carlsaw, H.S. and Jeager, J.C. (1959), Conduction of Heat in Solids, Oxford Univ. Press.
- Chatwin, P.C. and Sullivan, P.J. (1990), "A Simple and Unifying Physical Interpretation of Scalar Fluctuation Measurements from Many Turbulent Shear Flows, J. Fluid Mech., 212, pp. 533-555.

- Chen, C-H (1990), A Numerical Study of Flame Spread and Blowoff Over a Thermally-Thin Solid Fuel in an Opposed Air Flow, *Combust. Sci. Tech.*, 69, pp. 63-83.
- Chen, Y. (1991), "Development of An Integral Model for Transient Charring Pyrolysis Process and Derivation of Material Flammability Properties", M.S. Thesis, Worcester Polytech. Inst.
- Chen, Y., Delichatsios, M.A. and Motevalli, V. (1993a), "Material Pyrolysis Properties, Part 1: An integral Model for One-dimensional Transient Pyrolysis of Charring and Non-charring Materials", *Comb. Sci. Tech.*, 88, pp. 309-328.
- Chen, Y., Motevalli, V. and Delichatsios, M.A. (1993b), "An Integral Turbulent Radiation and Combustion Model for Diffusion Flames," Proc. of the Eastern and Central Section Meeting of the Combustion Institute, pp. 51-55.
- Chen, Y., Delichatsios, M.A. and Motevalli, V. (1995), "Material Pyrolysis Properties, Part 2: Methodology for Derivation of Pyrolysis Properties for Charring Materials", *Comb. Sci. Tech.*, 104, 4-6, pp.401.
- Cleary, T.G. and Quintiere, J.G. (1991), "Flammability Characterization of Foam Plastics", NISTIR 4664.
- Cook, D.K. (1991), Twenty-Third Symp. (Int'l) on Comb., p. 653, The Comb. Inst.
- de Ris, J.N. (1969), 12th Symp. (Int'l) on Combustion, The Combustion Institute, pp.241-252.
- Delichatsios, M.A. (1986), Exact Solution for the Rate of Creeping Flame Spread Over Thermally Thin Materials, *Combust. Sci. Tech.*, 44, pp. 257-267.
- Delichatsios, M.A. (1987), "Air Entrainment into Buoyant Jet Flames and Pool Fires," *Comb. Flame*, 70, pp. 33-46.
- Delichatsios, M.A. (1988), *SFPE Handbook of Fire Protection Eng.*, p. 1-306.
- Delichatsios, M.A. (1988), *Comb. Sci. and Tech.*, 60, p. 253.
- Delichatsios, M.A. (1993), "Burning Polymer Material Properties for Flame Spread", *Journal of Fire Sciences*, Vol. 11, pp. 2878-295.
- Delichatsios, M.A. (1993), "A Phenomenological Model for Soot Formation in Laminar Flames", accepted for Publication in *Comb. Sci. and Tech.*
- Delichatsios, M.A., Chen, Y., Motevalli, V., and Tatem, P. (1993), "Flame Radiation Distribution from Fires," Accepted for Publication and Presentation at the 4th Int'l Symp. on Fire Safety Science.

Delichatsios, M.A., Markstein, G.H., Orloff, L. and de Ris, J. (1988), "Turbulent Flow Characterization and Radiation From Gaseous Fuel Jets," Gas Research Institute, GRI-88/0100.

Delichatsios, M.A. and Mathews, M.K. (1989), "A New Simplified Method for Calculating Major Species Concentration and Burning in Turbulent Fires", 2nd. Int'l Symp. on Fire Safety Science, pp. 149-158, 1989.

Delichatsios, M.A. and Orloff, L. (1989), 22nd Symposium (International) on Combustion, p. 1271, The Combustion Institute.

Delichatsios, M.A., Orloff, L. and Delichatsios, M.M (1992)., "The Effect of Fuel Sooting Tendency and the Flow on Flame Radiation in Luminous Turbulent Jet Flames," Comb. Sci. and Tech., 84, pp. 199-215, 1992.

Delichatsios, M.A., Panagiotou, Th. and Kiley, F. (1991), "The Use of Time to Ignition Data for Characterizing the Thermal Inertia and the Minimum (Critical) Heat Flux for Ignition or Pyrolysis", Combustion and Flame, 84, 323.

Delichatsios, M.A. and Saito, K. (1991), "Upward Fire Spread: Key Flammability Properties, Similarity Solutions and Flammability indices", presented at the Third Fire Safety Science Conference, Scotland.

Delichatsios, M.M., Mathews, M.K. and Delichatsios, M.A. (1990), "Upward Fire Spread Simulation Code: Version I: Non-Charring Fuels", FMRC Serial No. J.I. 0R0J2.BU, November.

Delichatsios, M.M., Mathews, M.K. and Delichatsios, M.A. (1991), "An Upward Fire Spread and Growth Simulation", presented at the Third Fire Safety Science Conference, Scotland.

Di Blasi, C., Continillo, G., Crescitelli, S. and Russo, G. (1987), Numerical Simulation of Opposed Flow Flame Spread over a Thermally Thick Solid Fuel, Combust. Sci. Tech., 54, pp. 25-36.

Di Blasi, C., Crescitelli, S., Russo, G. and Fernandez-Pello, A.C. (1988), "Model of the Flow Assisted Spread of Flames over a Thin Charring Combustibles", 22d Symp. (Int'l) on Comb., Comb. Inst., pp. 1205-1212.

Di Blasi, C., Crescitelli, S., Russo, G. and Fernandez-Pello, A.C. (1989), Influence of the gas Velocity Profile on the Theoretically Predicted Opposed Flow Flame Spread, Combust. Sci. Tech., 64, pp. 289-294.

Emmons, H.W. (1965), Fundamental Problems of the Free Burning Fire, 10th Symp. (Int'l) on Comb., Comb. Inst., pp. 951-964.

- Fangrat, J. and Wolanski, P. (1991), "One-Dimensional Analytical Model of Flame Spread Over Solids", *Journal of Fire Sci.*, Vol. 9, pp. 425-437.
- Fernandez-Pello, A.C. (1984), "Flame Spread Modeling", *Combust. Sci. Tech.*, 39, pp. 119-134.
- Fernandez-Pello, A.C. and Hirano, T. (1983), "Controlling Mechanism of Flame Spread", *Combust. Tech.*, 32, pp. 1-31.
- Fernandez-Pello, A.C., Ray, S.R. and Glassman, I. (1980), "Flame Spread in an Opposed Forced Flow: the effect of ambient oxygen concentration", 18th Symp. (Int'l) on Combustion, pp. 579-589.
- Fernandez-Pello, A.C. and Santoro, R.J. (1978), "On the Dominant Model of Heat Transfer in Downward Flame Spread", 15th Symp. (Int'l) on Combustion, Comb. Inst., pp. 1201-1209.
- Fernandez-Pello, A.C. and Williams, F.A. (1974), "Laminar Flame Spread Over PMMA Surfaces", 15th Symp. (Int'l) on Combustion, Comb. Inst., pp. 217-231.
- FMRC Annual Report to NIST (1990), Production of Fire Dynamics, GONANB8D0845.
- Frey, Jr., A.E. and T'ien, J.S. (1979), "A Theory of Flame Spread over a Solid Fuel Including Finite Rate Chemical Kinetics", *Combust. Flame*, 36, pp. 263-289.
- Gengebre, E., Cambray, P., Karmed, D. and Bellet, J.C. (1984), "Turbulent Diffusion Flames with Large Buoyant Effects", *Comb. Sci. Tech.*, 41, pp. 55-67.
- Gore, J.P. and Faeth, G.M. (1986), "Structure and Spectral properties of Turbulent Ethylene/Air Diffusion Flames", 21st Symp. (Int'l) on Combustion, The Comb. Inst., pp. 1521-1531.
- Hasemi, Y. and Yasui, N. (1994), "Upward Flame Spread along a Wooden Wall-Part I", Publication and Presentation at the Fourth International Symp. on Fire Safety Science.
- Hasemi, Y. and Yoshida, M. (1991), "Unsteady State Upward Flame Spreading Velocity Along Vertical Combustible Walls and Influence of External Radiation on the Flame Spread", presented at the Third Fire Safety Science Conference, Scotland.
- Heskestad, G. (1983), *Fire Safety J.*, 5.
- Hirano, T. and Suzuki, T. (1993), "Flame Propagation across Liquids-A review of Gas Phase Phenomena", *Fire Safety J.*, 21, pp. 257-267.
- Ito, A. and Kashiwagi, T. (1987), "Characterization of Flame Spread Over PMMA Using Holographic Interferometry Sample Orientation Effects", draft submitted to *Combust. Flame*.

Jeng, S-M, Chen, L-D and Faeth, G.M. (1983), "The tructure of Buoyant methane and Propane Diffusion Flames," 19th Symp. (Int'l) on Combustion, the Combustion Institute, pp.349-358

Jeng, S-M and Faeth, G.M. (1984), "Species Concentration and Turbulent Properties in Buoyant Methane Diffusion Flames," J. Heat Transfer, 106, pp. 721-727.

Jeng, S-M, Lai, M-C and Faeth, G.M. (1984), "Nonluminous Radiation in Turbulent Buoyant Axisymmetric Flames," Comb. Sci. Tech., 40, pp. 41-53

Jeng, S-M, Lai, M-C. and Faeth, G.M. (1984), "An Investigation of Axisymmetric Buoyant Turbulent Diffusion Flames: Flow Structure and Radiation Properties", NBS-GCR-84-458.

Jones, W.W. (1990), "Refinement of a Model for Fire Growth and Smoke Transport," NIST Technical Note 1282.

Kim, C.I. and Kulkarni, A.K. (1990), "Upward Flame Spread Simulation", submitted to Fire Safety Science.

Karlson, B. (1992), "Modeling Fire Growth on Combustible Lining Materials in Enclosures", Lund University, Dept. Of Fire Safety Engineering, Report TVBB-1009.

Kolyu, O.V., Kounalakis, M.E., Sivathanu, Y.R. and Faeth, G.M. (1990), "Carbon Monoxide and Radiation Emissions of Turbulent Diffusion Flames," NIST Technical Report, Grant No. 60NANBD0833.

Kung, H.C. (1972), "A Mathematical Model of Wood Pyrolysis", Combust. Flame, 18, pp. 185.

Loh, H.T. and Fernandez-Pello, A.C. (1984), "A Study of the Controlling Mechanism of the Flow Assisted Flow Flame Spread", 20th Symp. (Int'l) on Comb., Comb. Inst., pp. 1575-1582.

Markstein, G.H. (1986), 21st(Int'l) Symp. on Combustion, The Comb. Inst.

Markstein, G.H. (1989), 22nd Symposium (International) on Combustion, p. 1107, The Combustion Institute.

McAlevy, R.F. and Magee, R.S. (1967), Flame Spreading at Elevated Pressures Over the Surface of Igniting Solid Propellants in Oxygen/Inert Environments, Stevens Institute of Technology, Hoboken, NJ, NASA Grant No. NGR-31-003-014.

Mekki, A. Atreya, A., Agrawal, S. and Wichman, I. (1990), "Wind-Aided Flame Spread Over Charring and Non-Charring Solids: An Experimental Investigation", 23rd Symp. (Int'l) on Comb., Comb. Inst., pp. 1701-1707.

Mitler, H.E. (1990), "Predicting the Spread Rates of Fires on Vertical Surfaces", Presented at the Twenty-Third International Symposium on Combustion, Orleàn, France.

Motevalli, V. and Chen, Y., Conference on Fire and Materials, Washington, D.C., Sepetember, 1992

Motevalli, V., Chen, Y. and Delichatsios, M.A. (1992), Annual Rpt. to NRL..

Motevalli, V., Chen, Y. and Delichatsios, M.A. (1993), Int'l Congress on Computational Methods in Engineering, Ed. Yaghoubi, Shiraz, Iran, May 3-6, 1993, pp. 239-246.

Motevalli, V., Chen, Y., Gallagher, G. and Sheppard, D. (1992), First International Conference on Fire and Materials, Sept. 24-25, Washington, D.C., pp. 23-32.

Nicolette, V.F., Holen, J.H. and Magnussen, B.F. (1993), Annual Conference on Fire Research: Book of Abstracts, (W.J. Duffin, ED), National Inst. of Stand. and Tech., NISTIR 5280.

Panagiotou, Th. and Delichatsios, M.A. (1989), "A Numerical Solution for the Surface Temperature Rise History of a Material Including Surface Reradiation Losses", FMRC Report, J.I.0Q0J1.BU.

Parker, W.J. (1986), "Prediction of the Heat Release Rate of Wood", Proceedings of the First Int'l Symp. on Fire Safety Science, pp. 207.

Pope, S.B. (1991), 23rd Symp. (International) on Combustion, The Combustion Institute.

Quintiere, J.G. (1981), "A Simplified Theory for Generalizing Results from a Radiant Panel Rate of Flame Spread Apparatus", Fire and Materials, 5, 2, pp. 52-60.

Quintiere, J.G. (1988), "The Application of Flame Spread Theory to Predict Material Performance", J. of Research of the National Bureau of Standards, 33, pp. 61-70.

Quintiere, J.G. (1992), Private Communication.

Quintiere, J.G. and Harkleroad, M., "New Concepts for Measuring Flame Spread Properties", NBSIR 84-2943, 1984.

Quintiere, J., Harkleroad, M. and Hasemi, Y (1985), "Wall Flames and Implication for Upward Flame Spread", AIAA Paper No. 85-0456.

Quintiere, J., Harkleroad, M. and Walton, D. (1983), Measurements of Material Flame Spread Properties, 32, pp. 67-89.

Ray, S.R. and Glassman, I. (1983), The Detailed Process Involved in Flame Spread over Solid Fuels, Combust. Tech., 32, pp. 33-48.

Saito, K., Quintere, J.G. and Williams, F.A.: Proceeding of the First Int'l Symp. On Fire Safety Science, 1989.

The SFPE Hand Book of Fire Protection Eng. (1988), NFPA, p. 1-364, 1988.

Sibulkin, M. (1986), "Heat of Gasification for Pyrolysis of Charring Materials", 1st Int'l Symp. on Fire Safety Sci., pp. 391-400.

Sivathanu, Y.R. and Faeth, G.M. (1990), Comb. Flame, 82, pp. 211-230.

Sivathanu, Y.R., Kounalakis, M.E. and Faeth, F.M. (1990), NIST-GCR-90-570.

Steward, F.R. (1970), Comb. Sci. Tech., 2.

Standard for "Determining Material Ignition and Flame Spread Properties", ASTM E1321-90.

Tamanini, F. (1977), Reaction Rates, Air Entrainment and Radiation in Turbulent Fire Plumes, Combust. Flame, 30, pp. 85-101.

Tamanini, F. (1981), "An Integral Model of Turbulent Fire Plumes," 18th (Int'l) Symp. on Comb., The Combustion Institute, pp. 1081-1089.

Tamanini, F. (1982), "Direct Measurements of the Longitudinal Variation of Burning Rate and Product Yield in Turbulent Diffusion Flame," FMRC Technical Report No.J.I.OFON.BU.

Tanaka, T. (1983), A Model of Multicomponent Fire Spread, NBSIR 83-2718.

Tarifa, S.C. and Torralbo, A.M. (1967), Flame Propagation along the Interface Between a Gas and a Reacting Medium, 11th Symp. (Int'l) on Comb., Comb. Inst., pp. 533-544.

Tewarson, A. and Khan, M.M. (1989), 22nd Symposium (International) on Combustion, The Combustion Institute, p. 1231.

Tewarson, A. (1992), Private Communication.

Tewarson, A., Jiang, F.H. and Morikawa, T. (1993), Combust. Flame, 95, pp. 151-169.

Venkatesh, S. and Saito, K (1989). Proc. of 21st Int'l Thermal Conductivity Conference.

Vezi, R. (1995), Master Thesis, Worcester Polytechnic Institute.



West, J., Bhattacharjee, S. and Altenkirch, R.A (1994), Surface radiation Effects on Flame Spread Over Thermally Thick Fuels in an Opposed Flow, *J. of Heat Transfer*, 116, pp. 646-651.

Wichman, I.S. and Williams, F.A. (1983), A Simplified Model of Flame Spread in an Opposed Flow along a Flat Surface of a Semi-infinite Solid, *Combust. Sci. Tech.*, 32, pp. 91-123.

Williams, F.A. (1976), Mechanisms of Fire Spread, 16th Symp. (Int'l) on Combustion, The Combustion Institute, pp. 1281-1294

Zhang, Y., Ronney, P.D., Roegner, E.V. and Greenberg, J.B. (1991), Lewis Number Effects on Flame Spreading over Thin Solid Fuels, Submitted for Publication at the Combust. Flame.

Zhou, L. and Fernandez-Pello, A.C. (1990), "Concurrent Turbulent Flame Spread", 23rd Symp. (Int'l) on Comb., Comb. Inst., pp. 1790-1714.

Zhou, L., Fernandez-Pello, A.C. and Cheng, R. (1990), "Flame Spread in an Opposed Turbulent Flow", *Combust. Flame*, 81, 40-49.

Zukoski, E.E., Morehart, J.H., Kubota, T. and Toner, S.J. (1991), "Species Production and Heat Release Rates in Two-Layered Natural Gas Fires," *Combustion and Flame*, 83, 325.

# Appendix A An Integral Model for Prediction of Radiation and Combustion of Turbulent Diffusion Flames

## 1. The mean species concentration and temperature calculations

Fluctuation correlation<sup>[1]</sup>:

$$\frac{\overline{\xi'^2}}{\alpha \overline{\xi} (\beta \overline{\xi}_c - \overline{\xi})} = \frac{1}{1 + \gamma \frac{\alpha (\beta \overline{\xi}_c - \overline{\xi})}{1 - \overline{\xi}}}$$

where

$\overline{\xi}$ : local mean mixture fraction and

$\overline{\xi}_c$ : mean centerline mixture fraction

The parameter  $\lambda$  used in  $\Gamma$ -function therefore is:

$$\lambda = \frac{\overline{\xi} (1 - \overline{\xi})}{\overline{\xi'^2}} - 1 = \frac{1 - \overline{\xi} + 3 \times 0.16 (5 \overline{\xi}_c - \overline{\xi})}{0.16 (5 \overline{\xi}_c - \overline{\xi})} - 1 \quad (\text{A-1})$$

for  $\alpha=0.16$ ,  $\beta=5$  and  $\gamma=3$

$\xi$  is defined as:

$$\xi = \frac{h - h_\infty}{h_T - h_\infty} \quad (\text{A-2})$$

The method or approach:

At each height of flame,  $z$ , one can calculate the entrainment rate  $\psi_t$  by using appropriate entrainment equations (e.g. whether it is momentum or buoyancy driven flow). Then  $\overline{\xi}_c$  is calculated as:

$$\overline{\xi}_c = 2 \dot{m}_f / \psi_t \quad (\text{A-3})$$

where  $\dot{m}_f$  is the flow rate at the nozzle. The assumed mixture fraction profile is used:

$$\bar{\xi} = \bar{\xi}_c \left(1 - \frac{\psi}{\psi_t}\right)$$

where  $\psi$  is the so-called stream function and is given by:

$$\psi = 2\pi \int_0^r \bar{u} \bar{\rho} r dr$$

Having known  $\bar{\xi}_c$ , one uses eqn. (1) to obtain  $\lambda$ . The probability function  $P(\xi, \bar{\xi}, \bar{\xi}'^2)$  can therefore be calculated by:

$$P(\xi, \bar{\xi}, \bar{\xi}'^2) = \beta(\xi) = \frac{\Gamma(\lambda)}{\Gamma(n) \Gamma(m)} \xi^{n-1} (1-\xi)^{m-1}$$

where  $n = \lambda \bar{\xi}$  and  $m = \lambda(1-\bar{\xi})$ .

Given  $\xi$ , we can use Sivathanu and Faeth's generalized state relationship<sup>[2]</sup> to calculate the laminar species concentration (see the relevant part of the paper).

The average species concentration can be calculated by:

$$\bar{Y}_s(\bar{\xi}) = \int_0^1 Y_{s,L}(\xi) P(\xi, \bar{\xi}, \bar{\xi}'^2) d\xi$$

while the laminal temperature can be easily evaluated by using equation (A-2), noting that:

$h_T$ : enthalpy at the source

$h_\infty$ : enthalpy of the ambient

$h$ : enthalpy in the flame

$$h = \xi (h_t - h_\infty) + h_\infty \quad (\text{A-4})$$

$h$  can be obtained if the laminar species concentration and temperature are known, which is given by:

$$h = \sum_{i=1}^N h_{fi} Y_i + \sum_{i=1}^N \int_{T_0}^T Y_i C_{pi} (T) dT \quad (A-5)$$

where

$h_{fi}$ : heat of formation of species  $i$  at temperature  $T_0$  (usually 298 K)

$T$ : laminar temperature

$C_{pi} (T)$ : heat capacity of species  $i$

On the other hand, knowing  $h$  (i.e. from RHS of eqn. (A-4)), one can evaluate the laminar temperature by trial and error. It is straightforward that the average temperature  $\bar{T}(\bar{\xi})$  can be calculated as:

$$\bar{T}(\bar{\xi}) = \int_0^1 T_L(\xi) P(\xi, \bar{\xi}, \bar{\xi}^2) d\xi \quad (A-6)$$

## 2. Centerline velocity calculations:

Using the momentum equation derived by Delichatsios, et. al<sup>[2]</sup>:

$$\frac{d}{dz} \left[ \frac{1}{2} u_c \psi_t \right] = \int_0^{\psi_t} g \frac{\left( \frac{\Delta \bar{T}}{T_\infty} \right)}{\bar{u}} d\psi \quad (A-7)$$

this equation can also be written as:

$$\frac{1}{2} \psi_t \frac{du_c}{dz} + \frac{1}{2} u_c \frac{d\psi_t}{dz} = \frac{1}{u_c} \int_0^{\psi_t} g \frac{\frac{\Delta \bar{T}}{T_\infty}}{1 - \frac{\psi}{\psi_t}} d\psi$$

Or

$$u_c \frac{du_c}{dz} + \frac{u_c^2}{\psi_t} \frac{d\psi_t}{dz} = \frac{2 RHS}{\psi_t}$$

Or in terms of  $u_c^2$ :

$$\frac{du_c^2}{dz} + \frac{2}{\psi_t} \frac{d\psi_t}{dz} u_c^2 = \frac{4RHS}{\psi_t}$$

This equation takes the form of

$$y' + P(x)y = Q(x)$$

The solution of this type of equation is:

$$y = e^{-\int P(x) dx} \int Q(x) e^{\int P(x) dx} dx + C e^{-\int P(x) dx}$$

Or

$$y = A \int Q(x) e^{\int P(x) dx} dx + CA = Af(x) + CA$$

where

$$A = e^{-\int P(x) dx}$$

$$f(x) = \int Q(x) e^{\int P(x) dx} dx$$

Hence

$$y_1 = A_1 f(x) \big|_{x=x_1} + CA_1 \quad @ \quad x = x_1 \quad (A-8)$$

$$y_2 = A_2 f(x) \big|_{x=x_2} + CA_2 \quad @ \quad x = x_2 \quad (A-9)$$

(9)  $\times A_1 - (8) \times A_2$ :

$$y_2 A_1 - y_1 A_2 = A_1 A_2 [f(x) \big|_{x=x_2} - f(x) \big|_{x=x_1}]$$

$$= A_1 A_2 \int_{x_1}^{x_2} Q(x) e^{\int P(x) dx} dx$$

Therefore:

$$y_2 = \frac{A_2}{A_1} y_1 + A_2 \int_{x_1}^{x_2} Q(x) e^{\int P(x) dx} dx$$

In our case:

$$\psi_t = 0.018 \rho_\infty z^{5/2} \sqrt{\frac{\Delta H_c}{(S+1) C_p T_\infty} g(\chi_a - \chi_R) + \dot{m}_f = a z^{5/2 + \dot{m}_f}}$$

hence:

$$\frac{d\psi_t}{dz} = \frac{5}{2} a z^{3/2}$$

$$P(x) = \frac{2}{\psi_t} \frac{d\psi_t}{dz} = \frac{5 a z^{3/2}}{a z^{5/2 + \dot{m}_f}}$$

$$A = e^{-\int P(x) dx} = e^{-\int \frac{5 a z^{3/2}}{a z^{5/2 + \dot{m}_f}} dz} = \frac{1}{(a z^{5/2 + \dot{m}_f})^2}$$

And

$$Q(x) = \frac{4 RHS}{\psi_t} = \frac{4}{\psi_t} g \int_0^{\psi_t} \frac{\frac{\Delta \bar{T}}{T_\infty}}{1 - \frac{\psi}{\psi_t}} d\psi$$

$$= \frac{4g}{\psi_t} \left[ \int_0^{R\psi_t} \frac{\frac{\Delta \bar{T}}{T_\infty}}{1 - \frac{\psi}{\psi_t}} d\psi + \int_{R\psi_t}^{\psi_t} \frac{\frac{\Delta \bar{T}}{T_\infty}}{1 - \frac{\psi}{\psi_t}} d\psi \right]$$

(Noting @  $\psi = \psi_t$ ,  $1 - \psi/\psi_t = 0$ )

$$= 4g \left[ \int_0^{R\psi_t} \frac{\frac{\Delta \bar{T}}{T_\infty}}{\psi_t - \psi} d\psi + RES \right]$$

The first term can be calculated by using normal integration procedure. The second term has to be handled specifically as follows:

$$RES = \int_{R\psi_t}^{\psi_t} \frac{\frac{\Delta \bar{T}}{T_\infty}}{1 - \frac{\psi}{\psi_t}} d\left(\frac{\psi}{\psi_t}\right) = \int_R^1 \frac{\alpha(1-\phi)}{1-\phi} d\phi$$

$$= \int_R^1 \alpha d\phi = \alpha(1-R)$$

Assuming  $R=0.999$ , then

$$\frac{\Delta \bar{T}}{T_{\infty}} \Big|_{R=0.999} = \alpha (1-\phi) \Big|_{\phi=0.999}$$

Therefore:

$$\alpha = \frac{\frac{\Delta \bar{T}}{T_{\infty}} \Big|_{R=0.999}}{0.001}$$

$$\int Q(x) e^{\int P(x) dx} dx = \int Q(x) (az^{5/2} + \dot{m}_f)^2 dz$$

For buoyancy driven flow:

$$\psi_i = az + \dot{m}_f$$

$$P(x) = \frac{2a}{az + \dot{m}_f}$$

$$A = e^{-\int P(x) dx} = e^{-\int \frac{2a}{az + \dot{m}_f} dz}$$

$$= \frac{1}{(az + \dot{m}_f)^2}$$

3. Generalized state relationship from Sivathanu and Faeth<sup>[3]</sup>:

$$\psi_{N_2} = \frac{Y_{N_2, \infty} - Y_{N_2 S}}{Y_{N_2, \infty} - Y_{N_2}} \left( \frac{Y_{N_2}}{Y_{N_2 S}} \right) \quad (\text{A-10})$$



$$\text{Fuel: } Y_f \quad (\text{A-12})$$

$$\psi_{O_2} = \left( \frac{32n+8m+M_f Y_{O_2,\infty}}{32n+8m+M_f Y_{O_2}} \right) \left( \frac{Y_{CO_2}}{Y_{CO_2S}} \right) \quad (\text{A-11})$$

$$\psi_{CO_2} = \left( \frac{44n-M_f Y_{CO_2S}}{44n-M_f Y_{CO_2}} \right) \left( \frac{Y_{CO_2}}{Y_{CO_2S}} \right) \quad (\text{A-13})$$

$$\psi_{H_2O} = \left( \frac{9m-M_f Y_{H_2OS}}{9m-M_f Y_{H_2O}} \right) \left( \frac{Y_{H_2O}}{Y_{H_2OS}} \right) \quad (\text{A-14})$$

$$\psi_{CO} = \left( \frac{44n-M_f Y_{CO_2S}}{44n-M_f Y_{CO}} \right) \left( \frac{Y_{CO}}{Y_{CO_2S}} \right) \quad (\text{A-15})$$

$$\psi_{H_2} = \left( \frac{9m-M_f Y_{H_2OS}}{9m-M_f Y_{H_2}} \right) \left( \frac{Y_{H_2}}{Y_{H_2OS}} \right) \quad (\text{A-16})$$

One can do some simple algebra transformation to obtain the species concentration  $Y$  as a function of the state function  $\psi_i$ :

$$Y_i = f(\psi_i)$$

$N_2$ :

$$\frac{Y_{N_2, \infty} - Y_{N_2 S}}{Y_{N_2 S}} \frac{1}{\psi_{N_2}} = \frac{Y_{N_2, \infty}}{Y_{N_2}} - 1$$

i.e.

$$\frac{Y_{N_2, \infty}}{Y_{N_2}} = \frac{Y_{N_2, \infty} - Y_{N_2 S} + Y_{N_2 S} \psi_{N_2}}{Y_{N_2 S} \psi_{N_2}}$$

Therefore:

$$Y_{N_2} = \frac{Y_{N_2 S} \psi_{N_2} Y_{N_2, \infty}}{Y_{N_2, \infty} - Y_{N_2 S} + Y_{N_2 S} \psi_{N_2}} \quad (A-17)$$

O<sub>2</sub>:

$$\frac{32n + 8m + M_f Y_{O_2, \infty}}{Y_{O_2, \infty} \psi_{O_2}} = \frac{32 + 8m}{Y_{O_2}} + M_f$$

$$Y_{O_2} = \frac{(32n + 8m) Y_{O_2, \infty} \psi_{O_2}}{32n + 8m + M_f Y_{O_2, \infty} - M_f Y_{O_2, \infty} \psi_{O_2}} \quad (A-18)$$

CH<sub>4</sub>:

$$Y_{CH_4} = \psi_{CH_4} \quad (A-19)$$

CO<sub>2</sub>:

$$\frac{44n - M_f Y_{CO_2 S}}{Y_{CO_2 S} \psi_{CO_2}} = \frac{44n - M_f Y_{CO_2}}{Y_{CO_2}}$$

$$Y_{CO_2} = \frac{Y_{CO_2S} \psi_{CO_2} 44n}{44n - M_f Y_{CO_2S} + M_f Y_{CO_2S} \psi_{CO_2}} \quad (A-20)$$

H<sub>2</sub>O:

$$Y_{H_2O} = \frac{9m Y_{H_2OS} \psi_{H_2O}}{9m - M_f Y_{H_2OS} + M_f Y_{H_2OS} \psi_{H_2O}} \quad (A-21)$$

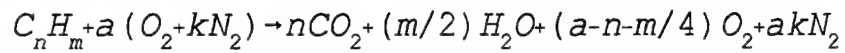
CO:

$$Y_{CO} = \frac{44n Y_{CO_2S} \psi_{CO}}{44n - M_f Y_{CO_2S} + M_f Y_{CO_2S} \psi_{CO}} \quad (A-22)$$

H<sub>2</sub>:

$$Y_{H_2} = \frac{9m Y_{CO_2S} \psi_{CO}}{9m - M_f Y_{H_2OS} + M_f Y_{H_2OS} \psi_{H_2O}} \quad (A-23)$$

For hydrocarbon reaction:



$$Y_i = \frac{v_i M_i}{M_f + a (32 + 28k)}$$

where

$v_i$ : the number of moles of a product species,  $i$ , per mole of fuel.

At stoichiometry:

$$Y_{N_2S} = \frac{(n+m/4) k M_{N_2}}{M_f + (n+m/4) (32+28k)}$$

$$Y_{CO_2S} = \frac{n M_{CO_2}}{M_f + (n+m/4) (32+28k)}$$

$$Y_{H_2OS} = \frac{m/2 M_{H_2O}}{M_f + (n+m/4) (32+28k)}$$

For CH<sub>4</sub> fuel, n=1, m=4.

$$Y_{N_2S} = 0.7247 \quad Y_{CO_2S} = 0.1514 \quad Y_{H_2OS} = 0.1239$$

The following is the correlation of mass fraction with fuel-air equivalence ratio.

Species mass fraction:  $Y_i$

Fuel-air equivalence ratio,  $\phi$

From S and F's paper<sup>[3]</sup>, assuming  $x = \log \phi$ ,  $y_i = \log \psi_i$

1).  $Y_{N_2}$

$$y_{N_2} = 1.446 \times 10^{-5} - 1.0x$$

$$@ \xi = 0, \phi = 0, Y_{N_2} = 0.767$$

$$\xi = 1, \phi = \infty, Y_{N_2} = 0$$

2).  $Y_{O_2}$ :

$$\phi \leq 1, \psi_{O_2} = 0.9898 - 0.9062\phi$$

$$\phi > 1, y_{O_2} = -0.79481 - 3.33465x + 7.74823 x^2 - 8.58911 x^3 + 4.31337 x^4 - 0.810195 x^5$$

$$@ \xi = 0, Y_{O_2} = 0.233$$

$$\xi = 1, Y_{O_2} = 0.0$$

3). Fuel-CH<sub>4</sub>

$$\phi \leq 1, Y_{Fuel} = 0$$

$$\phi > 1, y_{Fuel} = -2.47524 + 3.0703 x - 2.04325 x^2 + 0.406869 x^3$$

$$@ \xi = 0, y_{Fuel} = 0.$$

$$\xi = 1, y_{Fuel} = 1.0$$

4).  $Y_{CO_2}$ :

$$\phi < 1, y_{CO_2} = -0.0332629 + 0.977861 x$$

$$\phi \geq 1, y_{CO_2} = -0.092255 + 0.104665 x - 0.512132 x^2 + 0.110464 x^3$$

$$@ \xi = 0, y_{CO_2} = 0$$

$$\xi=1, Y_{CO_2}=0$$

5).  $Y_{H_2O}$ :

$$\phi \leq 1, y_{H_2O} = -0.0332629 + 0.977861 x$$

$$\phi > 1, y_{H_2O} = -0.032632 + 0.171055 x - 0.301843 x^2$$

@  $\xi=0, Y_{H_2O}=0$

$$\xi=1, Y_{H_2O}=0$$

6).  $Y_{CO}$

$$y_{CO} = -1.00413 + 2.10314 x - 2.80715 x^2 + 1.19247 x^3 - 0.180829 x^4$$

@  $\xi=0, 1, Y_{CO}=0$

7).  $Y_{H_2}$ :

@  $\xi=0, 1, y_{H_2}=0$ .

$$y_{H_2} = -2.08179 + 2.7159 x - 5.80981 x^2 + 5.59833 x^3 - 2.57435 x^4 + 0.445662 x^5$$

4. The entrainment correlations:

1). Buoyancy driven flow:

$$\frac{\psi_t / \rho_\infty}{(\dot{M}_o / \rho_\infty)^{1/2} Z} = 0.018 (z / len)^{3/2} + \frac{\dot{m}_f \rho_\infty}{(\dot{M}_o / \rho_\infty)^{1/2} Z} \quad (A-24)$$

$\dot{M}_o$ : initial momentum

$$\dot{M}_o = \frac{\Pi}{4} d_s^2 u_s^2 \rho_s$$

$$\dot{m}_f = \frac{1}{4} u_s d_s^2 \rho_s$$

$$len^3 = \frac{\dot{M}_o / \rho_\infty}{\frac{\Delta T_f}{T_\infty} g}$$

$d_s$ : the nozzle diameter

$u_s$ : initial velocity of gas flow

therefore:

$$\frac{\Delta \bar{T}_f}{T_\infty} = \frac{\Delta H_c (\chi_A - \chi_R)}{C_p (S+1) T_\infty}$$

if  $z/\text{len} \geq 5$  use correlation in buoyancy driven flow region as above  
if  $z/\text{len} < 5$ , momentum driven flow

$$\frac{\psi_t / \rho_\infty}{(\dot{M}_o / \rho_\infty)^{1/2} z} = .2012 + \frac{\dot{m}_f / \rho_\infty}{(\dot{M}_o / \rho_\infty)^{1/2} z}$$

### 5. Radiation losses in the combustion model

Energy balance:

$$\frac{d}{dz} \int_0^{\psi_t} (\bar{h} - \bar{h}_0) d\psi = -\dot{Q}'_r = -\frac{d\dot{Q}_r}{dz} \quad (\text{A-25})$$

$\bar{h}$ : enthalpy per unit mass at certain location (height)

$\bar{h}_0$ : enthalpy per unit mass of the ambient

$$\psi = 2\pi \int_0^r \rho \bar{u} r dr \quad \text{stream function}$$

$\dot{Q}'_r$ : radiation losses per unit height and it is given by:

$$\frac{\dot{Q}'_r L_f}{\chi_{R,T} \dot{Q}_{ch}} = f \left( \frac{z}{L_f} \right) \quad (\text{A-26})$$

$\chi_{R,T}$ : total turbulent buoyant radiation fraction (for methane,  $\chi_{R,T}=0.18$ ; for propylene,  $\chi_{R,T}=0.40^{[4]}$ ).

Flame height calculations:

$$\frac{L_f}{(S+1) d_s \sqrt{\frac{\rho_s}{\rho_0}}} = \frac{13.5 F_{rf}^{2/5}}{(1+0.7 F_{rf}^2)^{1/5}}$$

where

S: Stoichiometric ratio of air to fuel

$$F_{rf}^2 = \frac{u_s^2}{g d_s \sqrt{\frac{\rho_s}{\rho_0}}} \frac{1}{(S+1)^3} \frac{(S+1) C_p T_0}{\Delta H_c (1-\chi_R)}$$

$u_s$ : velocity at the nozzle

$d_s$ : nozzle diameter

$\rho_s$ : density of fuel at the nozzle

subscript 0: ambient condition

$\chi_R = \chi_{R,T}$

$Q_{ch}$ : total heat release rate =  $\dot{m}_f \Delta H_c$

The  $f(z/L_f)$  in eqn (A-26) can be found from GRI report. By using eqn (A-25), one gets:

$$\int_0^{\psi_t} (\bar{h} - \bar{h}_0) d\psi = (\bar{h} - \bar{h}_0) \dot{m}_f \int_0^z \dot{Q}'_r dz \quad (A-27)$$

where  $(\bar{h} - \bar{h}_0) \dot{m}_f$  is enthalpy at the source.

From this equation, one can determine the temperature of the laminar flamelet.

In reference [4], one has:

$$\frac{\dot{Q}'_r}{(\dot{Q}'_r)_{\max}} = f(z/L_f) \quad (A-28)$$

Or by integration, one gets:

$$\dot{Q}_r = \int \dot{Q}'_r dz = (\dot{Q}'_r)_{\max} \int f(z/L_f) dz$$

Or

$$\dot{Q}_r = (\dot{Q}'_r)_{\max} L_f \int_0^{L_f} f(z/L_f) d(z/L_f)$$

Or

$$\dot{Q}_r = (\dot{Q}'_r)_{\max} L_f C$$

where

$$C = \int_0^{L_f} f(z/L_f) d(z/L_f) \text{ a constant}$$

But

$$\dot{Q}_r = \chi_R \dot{Q}_{ch} = (\dot{Q}'_r)_{\max} L_f C$$

So that:

$$(\dot{Q}'_r)_{\max} = \frac{\chi_R \dot{Q}_{ch}}{L_f C}$$

By inserting this eqn into eqn (A-26), one has:

$$\frac{\dot{Q}_r L_f C}{\chi_R \dot{Q}_{ch}} = f(z/L_f)$$

Thus:



$$\frac{\dot{Q}_f L_f}{\chi_R \dot{Q}_{ch}} = \frac{f(z/L_f)}{C}$$

where  $f(z/L_f)$  is the same as that in Fig. 17 of reference [4], and

$$C = \int_0^1 f(z/L_f) d(z/L_f) = \int_0^1 f(w) dw$$

The idea for incorporating this into the complete model is as follows:

- a. given different  $\xi$ , one can obtain the laminar adiabatic temperature,  $T_{L,ad}$ .
- b. assuming the linear relationship between laminar radiative temperature  $T_L$  and  $T_{L,ad}$ :

$$T_L - T_a = \alpha (T_{L,ad} - T_a)$$

$\alpha$  is assumed to be a constant for each height and in fact is what we are looking for.

c. using  $\bar{\xi}_c$ ,  $\bar{\xi}$  and  $\bar{\xi}'^2$ , the PDF is obtained:

d. calculating average temperature:

$$\bar{T}(\bar{\xi}) = \int_0^1 T(\xi) PDF d\xi$$

e. using eqn (A-27), the  $\alpha$ 's can be evaluated (by trial and error).

The function  $f(z/L_f)$  is obtained as follows:

assuming  $x = z/L_f$

when  $x \leq 0.387637$

$$y = f(z/L_f) = -1.42573E-17 + 1.80933 x - 21.1433 x^2 + 141.767 x^3 - 212.667 x^4$$

when  $x > 0.387637$

$$y = -3.92171 + 28.685 x - 54.3652 x^2 + 35.8018 x^3 - 5.92926 x^4$$

6. Calculation of the radiation constant  $C_1$

Radiation through elemental volume of flame:

$$2\pi \sigma T^4 K_s dr$$

Energy balance:

$$\frac{d}{dz} \int h d\psi = -2\pi \int_0^{\infty} \sigma T^4 K_s r dr = - \int_0^{\infty} \sigma T^4 K_s \frac{d\psi}{\bar{u}\rho}$$

One also knows for optically thin flame:

$$\sigma T^4 K_s \Rightarrow \sigma T^4 Y_s \Rightarrow \sigma T^4 Y_F = C_1 \sigma T^4 \frac{\xi - \xi_s}{1 - \xi_s}$$

The soot formation is assumed occurred somewhere between  $\xi_s$  and  $\xi=1$ .

Taking PDF:

$$\int_{\xi_s}^{\xi^*} \sigma T^4 \frac{\xi - \xi_s}{1 - \xi_s} PDF d\xi$$

Assuming  $\xi = \gamma \xi_s$  where  $\gamma$  is a number larger than 1.

Therefore:

$$\dot{Q}'_r(z) = C_1 \int_0^{\psi_t} \left( \int_{\xi_s}^{\xi^*} \sigma T^4 \frac{\xi - \xi_s}{1 - \xi_s} PDF d\xi \right) \frac{d\psi}{\bar{u}\rho}$$

And at the flame height:

$$\dot{Q}_r(L_f) = C_1 \int_0^{L_f} \dot{Q}'_r(z) dz = \chi_R \dot{Q}_{ch} \quad (A-29)$$

Knowing  $\chi_R$ ,  $\dot{Q}_{ch}$  and  $\int_0^L \dot{Q}'(z) dz$ , one is able to solve for  $C_1$ .

## 7. The simplified combustion model

If there is no radiation loss, the energy balance for combustion process is:

$$\frac{d}{dz} \int_0^{\psi_r(z)} [\Sigma (h_i \bar{Y}_i + \bar{Y}_i \int_{T_0}^{T_a} \bar{C}_{pi} dT) d\psi] = - \frac{d\dot{Q}_r(z)}{dz} \quad (A-30)$$

with radiation taking into account:

$$\frac{d}{dz} \int_0^{\psi_r(z)} [\Sigma (h_i \bar{Y}_i + \bar{Y}_i \int_{T_0}^T \bar{C}_{pi} dT) d\psi] = - \frac{d\dot{Q}_r(z)}{dz} \quad (A-31)$$

where T is the actual temperature after radiation.  
Assuming  $C_{pi}$  is constant, eqn. (A-31)-eqn. (A-30):

$$\frac{d}{dz} \int_0^{\psi_r} \Sigma \bar{Y}_i \left[ \int_{T_a}^T \bar{C}_{pi} dT \right] d\psi = - \frac{d\dot{Q}_r(z)}{dz}$$

where

$T_a$  is adiabatic temperature and T is real temperature:

$$T - T_\infty = \alpha (T_a - T_\infty)$$

Therefore:

$$\frac{d}{dz} \int_0^{\psi_r} \Sigma \bar{Y}_i \bar{C}_{pi} (1-\alpha) T_a d\psi = - \frac{d\dot{Q}_r(z)}{dz}$$

As  $\alpha$  is constant for certain height z.

$$\frac{d}{dz} (1-\alpha) \int_0^{\psi_r} \Sigma \bar{Y}_i \bar{C}_{pi} T_a d\psi = - \frac{d\dot{Q}_r(z)}{dz}$$

Performing integration:

$$(1-\alpha) \int_0^{\psi_r} \Sigma \bar{Y}_i \bar{C}_{pi} T_a d\psi = \dot{Q}_r(z) \quad (A-32)$$

On the other hand, we know:

$$\int_0^{\psi_t} \sum \bar{Y}_i \bar{C}_{pi} T_a d\psi + \int_0^{\psi_t} \sum h_i \bar{Y}_i d\psi = \dot{Q}_{cht}$$

where  $\dot{Q}_{cht}$  is the enthalpy at the source.

Therefore:

$$\int_0^{\psi_t} \sum \bar{Y}_i \bar{C}_{pi} T_a d\psi = \dot{Q}_{cht} - \int_0^{\psi_t} \sum h_i \bar{Y}_i d\psi = \dot{Q}_{ch}(z)$$

$\dot{Q}_{ch}(z)$  is the chemical heat release rate at height  $z$ .

One knows  $\dot{Q}_{cht}$  and

$$\int_0^{\psi_t} \sum \bar{Y}_i \bar{C}_{pi} T_a d\psi$$

$\dot{Q}_{ch}(z)$  can be calculated easily:

$$\int_0^{\psi_t} \sum \bar{Y}_i \bar{C}_{pi} T_a d\psi = \dot{Q}_{ch}(z)$$

Thus from eqn. (A-32), one has:

$$1 - \alpha = \frac{\dot{Q}_r(z)}{\dot{Q}_{ch}(z)} \quad (A-33)$$

8. The combustion model using radiation fraction  $\chi_R$ :

It can be guessed that the left hand side of eqn. (A-29) can be simplified. The LHS of eqn.

(A-29) can also be replaced using eqn. (A-33). Eqn. (A-29) can be changed to:

$$\frac{d}{dz} [(1-\alpha) \dot{Q}_{ch}(z)] = \frac{C}{(1-\alpha)^3} \int_0^{\psi_t(z)} P(\bar{\xi}_s, \bar{\xi}) \frac{d\psi}{\rho \bar{u}}$$

Suppose one is able to obtain  $C$  from total radiation.

Assuming

$$\int_0^{\psi_t(z)} P(\bar{\xi}_s, \bar{\xi}) \frac{d\psi}{\rho \bar{u}} = R(z)$$

Then:

$$\frac{d}{dz} [(1-\alpha) \dot{Q}_{ch}(z)] = \frac{CR(z)}{(1-\alpha)^3}$$

Assuming:  $Y=(1-\alpha)Q_{ch}(z)$ , then:

$$\frac{dY}{dz} = \frac{C\dot{Q}_{ch}^3(z)R(z)}{Y^3}$$

Or:

$$\frac{1}{4} \frac{dY^4}{dz} = C\dot{Q}_{ch}^3(z)R(z) \quad (A-34)$$

Or:

$$Y_2^4 - Y_1^4 = 4C \int_{z_1}^{z_2} \dot{Q}_{ch}^3(z)R(z) dz \quad (A-35)$$

At flame height:

$$(1-\alpha) \dot{Q}_{ch}(z) = \text{total radiation loss} = \dot{m}_f \Delta H_c X_R$$

Thus one can obtain C from eqn. (A-35).

From eqn. (A-35), one has:

$$Y_2^4 - Y_1^4 = 4C \int_{z_1}^{z_2} \dot{Q}_{ch}^3(z)R(z) dz$$

Or:

$$1-\alpha = [Y_1^4 + 4C \int_{z_1}^{z_2} \dot{Q}_{ch}^3(z)R(z) dz]^{1/4} / \dot{Q}_{ch}(z)$$

One can transform  $R(z)$  to more simple form as follows using:

$$\bar{\xi} - \bar{\xi}_c \left(1 - \frac{\psi}{\psi_t}\right)$$

and

$$d\bar{\xi} = -\bar{\xi}_c \frac{d\psi}{\psi_t}$$

Therefore:

$$\int_0^{\psi_t(z)} P(\bar{\xi}_s, \bar{\xi}) \frac{d\psi}{\rho u} = \frac{1}{\rho u_c} \int_0^{\psi_t} P(\bar{\xi}_s, \bar{\xi}) \frac{d\psi}{1 - \frac{\psi}{\psi_t}}$$

$$= \frac{\psi_t}{\rho u_c} \int_0^{\bar{\xi}_c} P(\bar{\xi}_s, \bar{\xi}) \frac{d\bar{\xi}}{\bar{\xi}}$$

where

$$P(\bar{\xi}_s, \bar{\xi}) \equiv \frac{\Gamma(\lambda)}{\Gamma(n)\Gamma(m)} \bar{\xi}_s^{n-1} (1 - \bar{\xi}_s)^{m-1}$$

## References

1. Chatwin, P.C. and Sullivan, P.J., J. Fluid Mech., 212, p. 533, 1990.
2. Delichatsios, M.A. and Mathews, M.K., Second International Symposium on Fire Safety Science, 1989.
3. Sivathanu, Y.R. and Faeth, G.M., Combust. Flame, 82:211-230(1990).
4. Delichatsios, M.A., Markstein, G.H., Orloff L. and de Ris, J., Gas Research Institute, GRI-88/0100, 1988.

## Appendix B    Scalar Fluctuations in a Turbulent Buoyant Jet Flow and Comparison with Experimental Data

The calculation of scalar fluctuations is essential in modeling turbulent flows and combustion. A direct correlation for the fluctuation of a conserved scalar inspired by Chatwin and Sullivan (1990) was used and incorporated in our recent work for a turbulent combustion model (Motevalli et al., 1992). The direct correlation of root-mean-squared fluctuations of mixture fraction is (Chen et al., 1993):

$$\frac{\overline{\xi'^2}}{\alpha \overline{\xi} (\beta \overline{\xi}_c - \overline{\xi})} = \frac{1}{1 + \gamma \frac{\alpha (\beta \overline{\xi}_c - \overline{\xi})}{1 - \overline{\xi}}} \quad (\text{B-1})$$

where  $\alpha$ ,  $\beta$ ,  $\gamma$  are parameters determined from the experiments by Koylu, et al. (1990) and  $\overline{\xi}_c$  and  $\overline{\xi}$  are the centerline and local mean mixture fractions respectively.

A physical interpretation of eqn. (B-1) is as follows: Consider turbulent mixing at a given distance from the origin of the jet where the centerline value for the mixture fraction equals  $\overline{\xi}_c$ . One may visualize that mixing at this height occurs by large scale eddies produced due to concentration gradients between a concentration multiple of the centerline value, i.e.,  $\beta \overline{\xi}_c$  and the concentration of ambient air (where  $\overline{\xi}=0$ ). If molecular mixing is absent, then the fluctuations of the scalar would be (Chatwin and Sullivan, 1990):

$$\overline{\xi'^2} = \overline{\xi} (\beta \overline{\xi}_c - \overline{\xi}) \quad (\text{B-2a})$$

To account for the molecular mixing, we introduce another coefficient  $\alpha$ , so that eqn. (B-2a) becomes:

$$\frac{\overline{\xi'^2}}{\alpha \overline{\xi} (\beta \overline{\xi}_c - \overline{\xi})} = \text{RHS} = \text{Fcn}(\overline{\xi}) \quad (\text{B-2b})$$

We have chosen the right hand side of eqn. (B-2b) to be a function of the scalar,  $\overline{\xi}$ , (and not a constant as it was done in Chatwin and Sullivan (1990)) for two reasons: a) to match the mixing conditions at initial stages near the nozzle and b) to preserve the condition:  $\overline{\xi'^2} \leq \overline{\xi} (1 - \overline{\xi})$ , which must always be satisfied. A simple form was selected as shown in eqn. (B-1) where  $\gamma$  must always be greater than one. Note that near the nozzle where  $\overline{\xi} \approx 1$  eqn.(B-1) becomes:

$$\frac{\bar{\xi}^2}{\bar{\xi}(1-\bar{\xi})} = \frac{1}{\gamma} \quad (\text{B-3})$$

For mixing in non-combusting jets, Chatwin and Sullivan (1990), have suggested, after careful comparison with experiments, the following values:  $\alpha=0.16$ ,  $\beta=1.3$  while the RHS of eqn. (B-2b) is equal to one.

In this work, we compare assumed scalar fluctuations calculated from different combinations of parameters  $\alpha$ ,  $\beta$  and  $\gamma$  (no virtual origin was used) with the experimental data given by Koylu et al. (1990). Koylu et al. (1990) measured root-mean-squared-fluctuations of mixture fraction from a turbulent diffusion flame generated from a mixture of Carbon Monoxide (CO) and Hydrogen ( $\text{H}_2$ ). The experimental data discussed hereafter are for a nozzle diameter of 7.04 mm, CO flow rate of 691 mg/s and  $\text{H}_2$  of 14.3 mg/s. This conditions represent a turbulent buoyant jet flame except very close to the nozzle where the flow is momentum dominated (Delichatsios et al., 1988).

The stream function,  $\Psi$  is related to radial distance,  $r$  as:

$$\psi = \Psi \left( 1 - e^{-\frac{\pi \bar{\rho} \bar{u}_c r^2}{\Psi_t}} \right) \quad (\text{B-4})$$

where  $\bar{u}$  is mean velocity,  $\bar{\rho}$  is mean density and is taken as a constant ( $\bar{\rho}=(\bar{\rho}_c+\bar{\rho}_\infty)/2$ , average density in this height) in the following calculation and  $\bar{u}_c$  is centerline velocity. In the calculation presented here, the velocities from the experiment (Koylu, 1990) at corresponding heights are used.

Figures B-1a, B-1b illustrate comparisons of the experimental data and the results from eqn. (1) with  $\alpha=4.5$ ,  $\beta=1.4$  and  $\gamma=1$  at different heights from the flame base ( $x/d=40$  and  $x/d=50$ ). The abscissa is the normalized radial distance and the ordinate is the scaled root-mean-squared fluctuation normalized by the corresponding centerline mean value. Two numerical results are shown in Figures B-1a, B-1b: 1) using calculated centerline mean mixture fraction,  $\bar{\xi}_c$  (Motevalli et al, 1992) and 2) using the measurement of  $\bar{\xi}_c$  given by Koylu et al. (1990) (therefore, to be consistent,  $\Psi_t=2\dot{m}_f/\bar{\xi}_c$  is incorporated and  $\dot{m}_f$  is fuel flow rate). The value calculated for the centerline mean conserved scalar,  $\bar{\xi}_c$ , does not agree with the experimental values at the same distance from the nozzle, because our integral model does not represent the flow conditions near the nozzle well: no adjustment for virtual origin was used in the present case.

All calculated results show higher fluctuations than the experimental data indicating that adjustment of parameters  $\alpha$ ,  $\beta$  or  $\gamma$  in eqn. (B-1) is necessary in order to match with the experimental data. Therefore, we have changed  $\gamma$  to be 2,  $\alpha$  and  $\beta$  being the same as above,



to calculate fluctuations using eqn. (B-1). The results are shown in Figure B-3 where the experimental data and calculated results of fluctuations using experimental value of  $\bar{\xi}_c$  are plotted. Good agreements are observed in Figure B-2. The same conclusion can be obtained from Figure B-3 where the comparisons of the experimental data and calculated results for  $\alpha=3$ ,  $\beta$  and  $\gamma$  being the same as in Figures B-1a, B-1b, are shown.

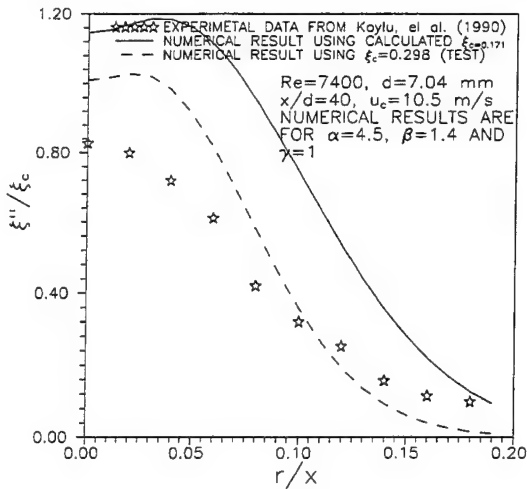


**Figure 1a** Comparison of fluctuations for  $\alpha=4.5$ ,  $\beta=1.4$  and  $\gamma=1$

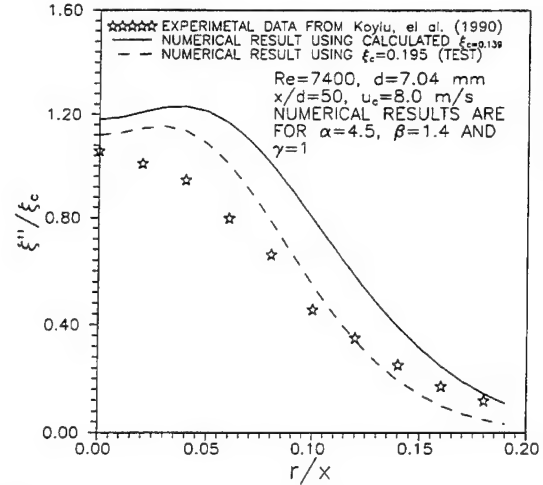


**Figure 1b** Comparison of fluctuations for  $\alpha=4.5$ ,  $\beta=1.4$  and  $\gamma=1$

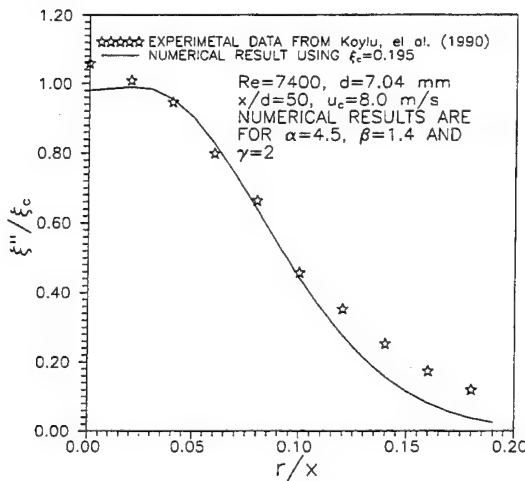


**Figure 2** Comparison of fluctuations for  $\alpha=4.5$ ,  $\beta=1.4$  and  $\gamma=2$

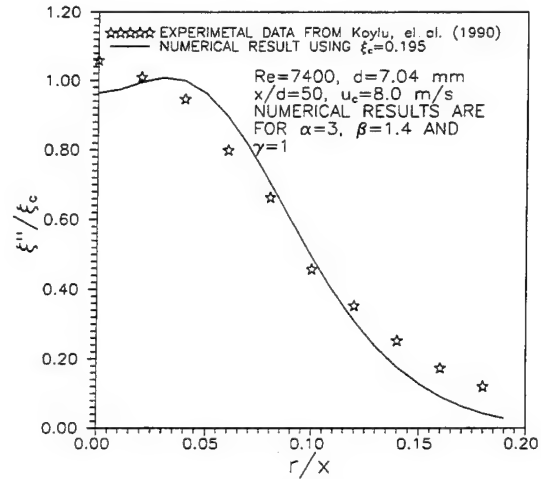


**Figure 3** Comparison of fluctuations for  $\alpha=3$ ,  $\beta=1.4$  and  $\gamma=1$

The comparisons shown above are promising in that one can select a set of parameters  $\alpha$ ,  $\beta$  and  $\gamma$  in order to use a direct general correlation to represent experimental reality.

It is decided to check the sensitivity of selected conserved scalar fluctuation relationships on predications from our integral model. Two of the relationships examined in Figures 1, 2, 3 were used for this purpose: a)  $\alpha=4.5$ ,  $\beta=1.4$ ,  $\gamma=1$  (Figure 1) and b)  $\alpha=4.5$ ,  $\beta=1.4$  and  $\gamma=2$  (Figure 2). The correlation for case b (Figure 3) agrees better with the experiments than the correlation for case a (Figure 1). It should be pointed that the overall predictions for combustion, radiation, and products generation rates based upon the fluctuation relationships we have proposed above do not vary significantly. Figure 4 illustrates the comparison between the data from Tamanini (1982) and numerical calculations of cases a and b. Little difference between predictions for the radiation fraction,  $\chi_R$  was found between  $\gamma=1$  and  $\gamma=2$  indicating the validity of use of the fluctuation correlation shown in eqn. (B-1). We can use any one of the above fluctuation relationships in the integral model for the combustion process.

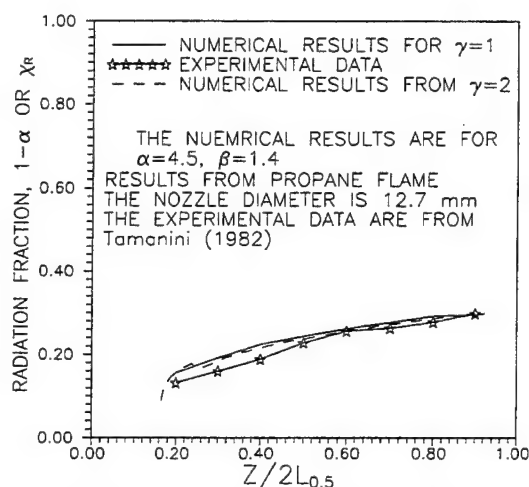


**Figure 4** Comparison of radiation fraction,  $\chi_R$  for different fluctuations

## Appendix C Application of the Combustion Model to Pool Fire

Delichatsios (1988) has derived the entrainment correlations for a pool fires as:

1). For  $z/D \leq 1.0$ , close to the pool surface:

$$\frac{\dot{m}_{ent}}{(S+1)\dot{m}_f} F_{rf} = 0.086 \left( \frac{z}{D} \right)^{1/2} \quad (C-1)$$

2). For  $1.0 < z/D < 4.0$ , around and beyond neck-in area:

$$\frac{\dot{m}_{ent}}{(S+1)\dot{m}_f} F_{rf} = 0.093 \left( \frac{z}{D} \right)^{3/2} \quad (C-2)$$

3). Further downstream but before the flame tip:

$$\frac{\dot{m}_{ent}}{(S+1)\dot{m}_f} F_{rf} = 0.018 \left( \frac{z}{D} \right)^{5/2} \quad (C-3)$$

where the Froude Number is defined as:

$$F_{rf} = \frac{\dot{Q}}{\rho_\infty \frac{\Delta H_c}{S+1} D^2 \sqrt{\frac{\Delta H_c}{(S+1) C_p T_\infty} g D (\chi_A - \chi_R)}}$$

and the theoretic heat release rate:

$$Q = \dot{m}_f \Delta H_c$$

The momentum equation for the flame is (Delichatsios and Mathews, 1989):

$$\frac{d}{dz} \left[ \frac{1}{2} u_c \psi_t \right] = \int_0^{\psi_t} g \frac{\left( \frac{\Delta T}{T_\infty} \right)}{\bar{u}} d\psi$$

This equation can be transformed to (Motevalli et al., 1992):

$$\frac{du_c^2}{dz} + \frac{2}{\psi_t} \frac{d\psi_t}{dz} u_c^2 = \frac{4RHS}{\psi_t}$$

If we specify:  
 $y = u_c^2$

$$P(x) = \frac{2}{\psi_t} \frac{d\psi_t}{dz}$$

and  $Q(x) = 4 RHS/\psi_t$

The solution for the momentum equation is:

$$y_2 = \frac{A_2}{A_1} y_1 + A_2 \int_{x_1}^{x_2} Q(x) e^{\int P(x) dx} dx$$

where;

$$A = e^{-\int P(x) dx}$$

For  $z/D \leq 1.0$

$$\psi_t = \dot{m}_{ent} + \dot{m}_f = \dot{m}_f + 0.086 (S+1) \dot{m}_f \left(\frac{z}{D}\right)^{1/2} + a_1 z^{1/2} \quad (C-4)$$

where;

$$a_1 = \frac{0.086 (S+1) \dot{m}_f}{F_{rf} D^{1/2}}$$

For  $1.0 < z/D < 4.0$ :

$$\psi_t = \dot{m}_f + a_2 z^{3/2}$$

where;

$$a_2 = \frac{0.093 (S+1) \dot{m}_f}{F_{rf} D^{3/2}}$$

For  $z/D > 4.0$ :

$$\psi_t = \dot{m}_f + a_3 z^{5/2}$$

where;

$$a_3 = \frac{0.018 (S+1) \dot{m}_f}{F_{rf} D^{5/2}}$$

For  $z \leq 1.0$ :

$$P(x) = \frac{2}{\psi_t} \frac{d\psi_t}{dz} = \frac{2}{\dot{m}_f + a_1 z^{1/2}} a_1 \frac{1}{2} \frac{1}{z^{1/2}} = \frac{a_1}{(\dot{m}_f + a_1 z^{1/2}) z^{1/2}}$$

and

$$\int P(x) dx = \int \frac{a_1}{(\dot{m}_f + a_1 z^{1/2}) z^{1/2}} dz$$

Assuming  $x = z^{1/2}$ , then  $x^2 = z$ . Therefore:

$$\int P(x) dx = \int \frac{a_1 2x}{(\dot{m}_f + a_1 x) x} dx = \int \frac{2a_1}{\dot{m}_f + a_1 x} dx$$

$$= 2 \ln(\dot{m}_f + a_1 x) = 2 \ln(\dot{m}_f + a_1 z^{1/2})$$

and

$$A = e^{-\int P(x) dx} = \frac{1}{(\dot{m}_f + a_1 z^{1/2})^2}$$

Therefore:

$$\int Q(x) e^{\int P(x) dx} dx = \int Q(z) (\dot{m}_f + a_1 z^{1/2})^2 dz$$

$$Q(z) = \frac{4}{\psi_t} g \int_0^{\psi_t} \frac{\left(\frac{\Delta T}{T_\infty}\right)}{1 - \frac{\psi}{\psi_t}} d\psi$$

For  $1.0 < z/D < 4.0$ :

$$P(x) = \frac{2}{\dot{m}_f + a_2 z^{3/2}} a_2 \frac{3}{2} z^{1/2} = \frac{3 a_2 z^{1/2}}{\dot{m}_f + a_2 z^{3/2}}$$

and

$$\int P(x) dx = 2 \ln (\dot{m}_f + a_2 z^{3/2})$$

$$A = \frac{1}{(\dot{m}_f + a_2 z^{3/2})^2}$$

For  $z/D > 4.0$ :

$$P(x) = \frac{2}{\dot{m}_f + a_3 z^{5/2}} a_3 \frac{5}{2} z^{3/2} = \frac{5 a_3 z^{3/2}}{\dot{m}_f + a_3 z^{5/2}}$$

$$\int P(x) dx = 2 \ln (\dot{m}_f + a_3 z^{5/2})$$

$$A = \frac{1}{(\dot{m}_f + a_3 z^{5/2})^2}$$

## Appendix D Analytical Solution for Constant Horizontal Flame Spread Velocity

For a semi-infinite solid subject to time varying heat flux,  $\dot{q}''$  on the surface, the surface temperature can be evaluated as (Carslaw and Jeager, 1959):

$$T_s - T_0 = \frac{1}{\sqrt{\pi k \rho C}} \int_0^t \frac{\dot{q}''}{\sqrt{t_p - \tau}} d\tau \quad (D-1)$$

where  $T_s$  is the surface and  $T_0$  the initial temperatures.

If the time for a point on the surface to reach pyrolysis temperature is  $t_p$ , then

$$T_p - T_0 = \frac{1}{\sqrt{\pi k \rho C}} \int_0^{t_p} \frac{\dot{q}''}{\sqrt{t_p - \tau}} d\tau \quad (D-2)$$

where  $T_p$  is obviously the pyrolysis temperature.

In the case that  $\dot{q}''$  consists of two heat fluxes: 1) a constant external heat flux,  $\dot{q}_{ext}''$ , and 2) a gas-phase conductive heat flux with exponential profile:  $\dot{q}_{conv}'' = A \exp[-(x - x_p)/\delta]$ , equation (D-2) becomes:

$$T_p - T_0 = \frac{1}{\sqrt{\pi k \rho C}} \int_0^{t_p} \frac{A e^{-(x - x_p)/\delta} + \dot{q}_{ext}''}{\sqrt{t_p - \tau}} d\tau \quad (D-3)$$

Assuming constant flame spread velocity,  $V$ , then  $x = Vt_p$  and  $x_p(t) = Vt$ . Therefore equation (D-3) can be transformed as

$$T_p - T_0 = \frac{1}{\sqrt{\pi k \rho C}} \int_0^{t_p} \frac{A e^{-V(t_p - \tau)/\delta} + \dot{q}_{ext}''}{\sqrt{t_p - \tau}} d\tau \quad (D-4)$$

For the time-being we only deal with the exponential heat flux or the first integral. We assume:

$$t_p - \tau = \omega$$

therefore  $-d\tau=d\omega$

for  $\tau$  from 0 to  $t_p$ ,  $\omega$  from  $t_p$  to 0, we obtain:

$$\int_0^{t_p} \frac{A e^{-V(t_p-\tau)/\delta}}{\sqrt{t_p-\tau}} d\tau = \int_0^{t_p} \frac{A e^{-\frac{V}{\delta}\omega}}{\sqrt{\omega}} d\omega$$

(assuming  $\omega=\phi^2$ ,  $\phi$  from 0 to  $t_p^{1/2}$ )

$$= 2A \int_0^{\sqrt{t_p}} e^{-\frac{V}{\delta}\phi^2} d\phi = 2A \sqrt{\frac{\delta}{V}} \int_0^{\sqrt{\frac{V t_p}{\delta}}} e^{-\beta^2} d\beta$$

where  $\beta=(V/\delta)^{1/2}\phi$

Equation (D-4) can therefore be simplified (for constant external heat flux,  $\dot{q}_{ext}''$ ):

$$T_p - T_0 = \frac{2A}{\sqrt{\pi k \rho C}} \sqrt{\frac{\delta}{V}} \int_0^{\sqrt{\frac{V t_p}{\delta}}} e^{-\beta^2} d\beta + \frac{2}{\sqrt{\pi k \rho C}} \dot{q}_{ext}'' \sqrt{t_p}$$

using  $V t_p = x$ :

$$T_p - T_0 = 2 \frac{A \sqrt{\delta} / \sqrt{V}}{\sqrt{\pi k \rho C}} \int_0^{\sqrt{\frac{x}{\delta}}} e^{-\beta^2} d\beta + \frac{2}{\sqrt{\pi k \rho C}} \dot{q}_{ext}'' \sqrt{\frac{x}{V}} \quad (D-5)$$

The integral is exactly an error function  $\text{erf}[(x/\delta)^{1/2}]$  (including  $2/\pi^{1/2}$ ).

If we  $x$  is large relative to  $\delta$  (this is usually case since  $\delta$  is small (order of 1 mm)), then  $(x/\delta)^{1/2} \rightarrow \infty$  and  $\text{erf}(\infty)=1$ . Therefore equation (D-5) is changed to:

$$T_p - T_0 = \frac{A \sqrt{\delta} / \sqrt{V}}{\sqrt{k \rho C}} + \frac{2}{\sqrt{\pi k \rho C}} \dot{q}_{ext}'' \sqrt{\frac{x}{V}} \quad (D-6)$$

where the second term of the RHS is essentially the surface temperature owing to external heat flux.

Therefore equation (D-6) can be written as:



$$T_p - T_s = \frac{A\sqrt{\delta}/\sqrt{V}}{\sqrt{k\rho C}} \quad (D-7)$$

We can notice that time to reach pyrolysis from the surface temperature,  $T_s$  is:

$$t_{ps} = \frac{\pi}{4} \frac{k\rho C (T_p - T_s)^2}{A}$$

Combining this with equation (7), one has:

$$V = \frac{dx_p}{dt} = \frac{\pi}{4} \frac{\delta}{t_{ps}} \quad (D-8)$$

Equation (D-8) is the analytical asymptotic solution for constant flame spread velocity. On the other hand, if one can obtain constant flame spread velocity,  $V$ , the combination of  $A$  and  $\delta$  ( $A\delta^{1/2}$ ) can be deduced (cf. equation (D-7)).

## Appendix E Justification for Gas-Phase Conductive Heat Flux Profile Being the Same as Surface Temperature History

The surface temperature rise from Carslaw's eqn.:

$$T_s(t) - T_0 = \frac{q}{\sqrt{\pi k \rho c}} \int_0^t \frac{\dot{q}''(\tau)}{\sqrt{t-\tau}} d\tau + T_{\text{ext}} - T_0 \quad (\text{E-1})$$

where  $\dot{q}''(\tau)$  is the flame heat flux, assuming no surface reradiation loss. Therefore:

$$\dot{q}''(\tau) = \dot{q}_0'' e^{-\frac{x-x_p}{\delta}} = \dot{q}_0'' e^{-\frac{x-v\tau}{\delta}}$$

Substituting this into eqn. (E-1) and ignoring  $\dot{q}_0''$  for a moment, one has:

$$T_s(t) - T_0 = \frac{1}{\sqrt{\pi k \rho c}} \int_0^t \frac{e^{-\frac{v(t_p-t)}{\delta}}}{t-\tau} d\tau + T_{\text{ext}} - T_0 \quad (\text{E-2})$$

Ignoring  $T_{\text{ext}} - T_0$  on the right hand side for moment without losing generality:

$$T_s(t) - T_0 = \frac{1}{\sqrt{\pi k \rho c}} e^{-\frac{v(t_p-t)}{\delta}} \int_0^t \frac{e^{-\frac{v(t_p-t)}{\delta}}}{\sqrt{t-\tau}} d\tau \quad (\text{E-3})$$

assuming:

$$\omega^2 = \frac{v(t-\tau)}{\delta}$$

hence:

$$d\tau = -2\omega\delta / v d\omega$$

therefore:

$$\int_0^t \frac{e^{-\omega^2}}{\omega \sqrt{\delta/\nu}} \delta/\nu \cdot 2\omega \, d\omega - 2\sqrt{\delta/\nu} \int_0^{\sqrt{\nu t/\delta}} e^{-\omega^2} d\omega$$

substituting this into eqn. (E-3), the result is:

$$T_s(t) - T_0 = \frac{1}{\sqrt{\pi k \rho c}} e^{-\frac{\nu(t_p-t)}{\delta}} \sqrt{\delta/\nu} \cdot 2 \int_0^{\sqrt{\nu t/\delta}} e^{-\omega^2} d\omega \quad (\text{E-4})$$

As  $t \rightarrow \infty$ ,

$$\frac{2}{\sqrt{\pi}} \int_0^{\sqrt{\nu t/\delta}} e^{-\omega^2} d\omega \rightarrow 1$$

Then putting back all the variables into eqn. (E-4), finally it becomes:

$$T_s(t) - T_{ext} = \frac{\dot{q}_0''}{\sqrt{\pi k \rho c}} e^{-\frac{\nu(t_p-t)}{\delta}} \sqrt{\delta/\nu} \quad (\text{E-5})$$

One can see from above equation that the profile of surface temperature is exactly the same as that of the gas phase conductive heat flux.

## Appendix F    Algorithm of Heat-up Calculation for a Sudden Jump (Drop) in Heat Fluxes at the Surface

When the fuel surface experiences sudden jump (drop) of the heat fluxes (e.g. sharp increase of flame heat flux when flame approaches; sharp decrease of total heat flux when water applies to the fuel surface), the integral heat-up model has problem in calculating surface temperatures (Delichatsios, M.M. et al., 1990). Therefore, the results of flame spread calculation are not reliable. This error arises from the fact that there exists, in essence, two temperature profiles within the solid: one being profile due to previous heat flux without sudden jump (drop) and the other being profile caused by the additional sudden jump (drop) heat flux (es). The following description will show the reader that one can separate the effects of two heat fluxes and superimpose the two surface temperatures calculated independently from these two heat fluxes.

We begin with one dimensional heat conduction equation, boundary and initial conditions:

$$\frac{\partial \theta}{\partial t} = \alpha \frac{\partial^2 \theta}{\partial z^2} \quad (\text{F-1})$$

$$-k \frac{\partial \theta}{\partial z} \Big|_{z=0} = \dot{q}_1 \quad (\text{F-2})$$

$$-k \frac{\partial \theta}{\partial z} \Big|_{z=l} = 0 \quad (\text{F-3})$$

$$\theta(z, 0) = 0 \quad (\text{F-4})$$

where  $\theta = T - T_0$  and  $T_0$  is the initial temperature of the solid;  $\dot{q}_1$  is the total net heat flux at the fuel surface including external, flame as well as surface reradiation loss. We will ignore surface reradiation loss for simplicity of current discussion.

When a sudden jump (drop) of heat flux is applied to the fuel surface at a time,  $t_1$ . The total net heat flux at the fuel surface is  $\dot{q}_2$ , the net increase of the heat flux is  $\dot{q}_2 - \dot{q}_1$ . One can assume there are two temperature rises (drops) ( $\theta_1$  and  $\theta_2$ ) associated with two heat fluxes ( $\dot{q}_2$  and  $\dot{q}_2 - \dot{q}_1$ .) and set similar equations as Equation (F-1 to F-3):

$$\frac{\partial \theta_1}{\partial t} = \alpha \frac{\partial^2 \theta_1}{\partial z^2} \quad (\text{F-5a})$$

$$-k \frac{\partial \theta_1}{\partial z} \Big|_{z=0} = \dot{q}_1 \quad (\text{F-5b})$$

$$-k \frac{\partial \theta_1}{\partial z} \Big|_{z=l} = 0 \quad (\text{F-5c})$$

$$\frac{\partial \theta_2}{\partial t} = \alpha \frac{\partial^2 \theta_2}{\partial z^2} \quad (\text{F-6a})$$

$$-k \frac{\partial \theta_2}{\partial z} \Big|_{z=0} = \dot{q}_2 - \dot{q}_1 \quad (\text{F-6b})$$

$$-k \frac{\partial \theta_2}{\partial z} \Big|_{z=l} = 0 \quad (\text{F-6c})$$

Combining Eqns. (F-5a)-(F-5c) with Eqn. (F-6a)-(F-6c) one can obtain:

$$\frac{\partial \theta}{\partial t} = \alpha \frac{\partial^2 \theta}{\partial z^2} \quad (\text{F-7a})$$

$$-k \frac{\partial \theta}{\partial z} \Big|_{z=0} = \dot{q}_2 \quad (\text{F-7b})$$

$$-k \frac{\partial \theta}{\partial z} \Big|_{z=l} = 0 \quad (\text{F-7c})$$

where  $\theta = \theta_1 + \theta_2$ . It can be seen that equation (F-7a)-(F-7c) are exactly same exactly same except  $\dot{q}_2$  replaces  $\dot{q}_1$ , which is expected because  $\dot{q}_2$  is the net heat flux after time,  $t_1$ .

One can solve equations (F-5a)-(F-5c) and equations (F-6a)-(F-6c) using the same way that solves equations (F-1)-(F-4) with the initial conditions changes to:

$$\theta_1(x, t1) = \theta_1(x, t1) \quad (\text{F-7d})$$

and

$$\theta_2(x, t1) = 0 \quad (\text{F-7e})$$

In the case that reradiation loss is taken into consideration, we can change Eqn. (F-5b) and Eqn. (F-6b) to:

$$-k \frac{\partial \theta_1}{\partial z} \Big|_{z=0} = \dot{q}_1 \epsilon \sigma T_{s1}^4 \quad (\text{F-8a})$$

$$-k \frac{\partial \theta_2}{\partial z} \Big|_{z=0} = \dot{q}_2 \dot{q}_1 \epsilon \sigma (T_s^4 T_{s1}^4) \quad (\text{F-8b})$$

The above equation can be easily implemented into the integral preheat model to calculate flame spread.

## Appendix G The input of the Horizontal Flame Spread Code

There are numerous variables that are used as input to the model. In general, the external heat flux, flame gas-phase conductive heat flux and flame radiation (at least at this moment) have to be prescribed. The material properties have to be known. The input parameters along with their explanations listed below can help interested users to run the model. Two input files are needed to run the flame spread code hfsspv70.f. They are named hflinp and fluxinp. The first input file, hflinp, contains all the necessary input and the second file, fluxinp, is used to specify the external flux.

### hflinp input file listing

```
19.93,1000,1.27,192,371,592,  
2,20.,33.5,  
250,1200.,0.,1100.,2.2,1.,1.,1.06E-4,2.7984E-4,1.,1000.,/N,Rhov,RhoC,Htpyr1,Cpv,Cpc,  
Cpg,tkc,tkv,dt,Timend  
0.1,1., /El,XN  
.30,1.,23400,8.5,296.15,643.15,5.67e-11,.01/CHIR,ChiA,Htcomb,sc,Tinf,Tpyr,epsig,T%  
/(x(i),i=1,n)  
30.,30.,0,0,0.,0,00.,00.,00.,000.,000.,000.,000.,000.,000/(QE(i),i=1,n)
```

### **Nomenclature**

#### Line 1

Line 1 parameters are only used to predict Horizontal Flame Spread experiment, users can ignore this line (but keep it here)

Q42: The nominal heat flux at the 425 mm location from the lower edge of the radiant panel, kW/m<sup>2</sup>

TMV: Time to start moving the slide/sample, seconds

SMV: The slide/sample moving speed, mm/s

N1, N2, N3: the surface temperature output at desired points which corresponds to the experimental conditions

#### Line 2

kchar: The flag for indicating if the fuel is charring or non-charring material, if charring, kchar=1; noncharring, kchar=2

crm: Critical mass flux that can sustain burning (do not use currently)

Qig: The ignition heat used for first two nodes (kW/m<sup>2</sup>)

### Line 3

N: Number of Nodes used for the fuel surface in x direction  
Rhov: The density of the virgin fuel, kg/cu m  
Rhoc: The density of the charred fuel, kg/cu m  
Htpyrl: The heat of pyrolysis, kJ/kg  
Cpv: The specific heat of the virgin fuel, kJ/kg.K  
Cpc: The specific heat of the charred fuel, kJ/kg.K  
Cpg: The specific of the ambient gas, kJ/kg.K  
tkc: The thermal conductivity of the charred fuel, kW/m.K  
tkv: The thermal conductivity of the virgin fuel, kW/m.K  
dt: The initial time step used for the calculation, seconds. If the code is converged within dt, dt is also the output interval  
Timend: The final time of the calculation, seconds

### Line 4

El: The fuel thickness, m  
XN: The fuel length, m (not used currently)  
Xfpowr: power exponent used for Xf computation, if no input, Xfpowr=0.6667  
Xfcof: The coefficient used for Xf computation

### Line 5

CHAIR: The radiation fraction of the flame  
Chi: The combustion efficiency of the flame  
Htcomb: The heat of combustion of the fuel, kJ/kg  
sc: The Mass air/fuel stoichiometric ratio  
Tinf: The initial temperature of the fuel, K  
Tpyl: The pyrolysis temperature of the fuel, K  
epsig: The fuel surface emissivity  $\times$  Stefan-Boltzmann constant, kW/sq m.  $K^4$   
T%: A percentage of  $T_p$ :  $(T_p - T)/T_p$  used for calculation, normally 0.01

### Line 6

x(i): Nodal specification, e.g. node 1, 0, node 2, 0.1, m, if no input in this file, the program calculates x(i) using N

### Line 7

Qe(i): External heat fluxes for the nodes, kW/sq m

### **Comments**

When a non-charring fuel is used in the flame spread calculation (i.e. kchar=2), the density of char (rhoc) is set rhoc=0 inside the program.

When a charring fuel is used (kchar=1), the code sets rhoc=0 only in the pyrolysis subroutine to speed up convergence. Justification for using rhoc=0 is presented in Chen's thesis (Chen, 1991).



### **fluxinp input file listing**

3,0.,20.,0.3/KEFLUX,QCEXT,QE0,XEXT  
10.,0.1,/QFR0,DFRAD  
70.0,0.0015,/QFC0,DFC

#### **Line 1**

KEFLUX: external heat flux option: 1-experiment, 2-constant, 3-exponential

QCEXT: the value of constant external heat flux, kW/m<sup>2</sup> if KEFLUX=2

QE0: the magnitude of exponential external heat flux, kW/m<sup>2</sup> if KEFLUX=3

XEXT: the length scale of exponential external heat flux, m if KEFLUX=3

#### **LINE 2**

QFR0: the magnitude of exponential flame radiative heat flux, kW/m<sup>2</sup>

DFRAD: the length scale of exponential flame radiative heat flux,m

#### **LINE 3**

QFC0: the magnitude of exponential flame conductive heat flux, kW/m<sup>2</sup>

DFC: the length scale of exponential flame conductive heat flux,m

## **Appendix H   Experimental Data and Comparisons with Numerical Predictions**

In this section, processed experimental data and comparisons with the numerical predictions of the horizontal flame spread model are listed. The first page shows the comparison of readings of large and small heat flux gages during a inert test where 86862 is a small flux gages and others are large flux gages (two). The rest of the materials are arranged in the following order: 1) A sheet recording experimental conditions, 2) the temperature history measurements, 3) heat flux history measurement from the two heat flux gages, 4) flame heat fluxes as function of the distance from the cooling plate edge, 5) detailed surface temperature plots for first two stations (if there is any), 6) the comparison of experimental data of surface temperature at the station 3 with the numerical prediction using heat fluxes measured by the large flux gage (not for every case), and 7) the comparison of experimental data of detailed surface temperatures at the stations 1 and 2 (if there is any) with the numerical prediction (not for every case).

C December 9, 1993, the original complete program to calculate  
 C horizontal flame spread.  
 C8/1/94 Modified to handle the sudden jump of the heat flux (e.g.  
 C Exponential profile of gas-phase conduction  
 C9/27/94 Modified again to handle the sudden jump of heat flux by splitting  
 C the external heat flux and flame heat flux in the calculation of  
 C surface temperature and thermal depth using the preheating model  
 C

```

Parameter (Npar=2000)
implicit real*8(a-h,o-z)
Dimension Temp21(Npar),Chard(Npar),ptdptv(npar),
$ Tdpthv1(Npar),tdpthc(Npar),TEMP22(NPAR),TDPthV2 (NPAR)
Common/HT/ x(1:npar+1),dx(npar),El
Common /xpgrp/xpold(npar),xpnew(npar),xptemp(npar),
$ xpgrld(npar),xpqrnw(npar)
Common /htclas/iclass(npar)
Common /Pyr1vr/temp1(npar),Tddot(npar)
Common /Htflcn/CHIR,ChiA,Htcomb,schia,epsig,xfpowr,xfcof
Common /Flux/gr(npar),qe(npar),qinc(npar)
Common /casea/kchar
common/data/rhoc,rhov,cpc,cpv,alphac,alphav,tkc,tkv,cpg,
$ tpyr,tinf,htpyr1,sitp
COMMON/QIGG/QIGN

```

C other variables: N,Rhov,Alphav,RhoC,Alphac,Htpyr1,Cpv,Cpc  
 C  
 C The main Routine  
 C Obtain input data from a data file  
 C Call Inputdata(Temp1,Temp21,TDpthv1,Tdpthc,tddot,Qr,Qe,Chard,  
 \$ N,Rhov,alphav,rhoc,alphac,Cpg,Cpv,Cpc,tkc,tkv, x, Dx,  
 \$ Tpyr,Htpyr1,Time,Dt,Timeend,iclass,Tinf,El,Tprcnt,ptdptv,  
 \$ kchar,crm,QIG,TEMP22,TDPthV2,qinc)  
 QIGN=QIG  
 sitp=tpyr-tinf  
 Call maincal(Temp1,Temp21,TDpthv1,Tdpthc,tddot,Qr,Qe,

```

C
$ Chard,N,x,Dx,Time,Dt,Timeend,iclass,Tprcnt,ptdptv,EL,crm,
$ TEMP22,TDPTHV2)

C
      stop
      End

C
      Subroutine Inputdata(Temp1,Temp21,TDpthv1,TDpthc,tddot,Qr,Qe,
      Chard,N,Rhov,alphav,rhoc,alphac,Cpg,Cpv,Cpc,tkc,tkv,x,Dx,
      Tpyr,Htpyr1,Time,Dt,Timeend,iclass,Tinf,El,tprcnt,ptdptv,
      kchar,crm,QIG,TEMP22,TDPTHV2)
      The required data for the model are inputted in this routine
      implicit real*8(a-h,o-z)
      Parameter (Npar=2000)
      Dimension Temp1(Npar),Temp21(Npar),TDpthv1(Npar),Chard(Npar),
      $   Tdpthc(Npar),TEMP22(NPAR),TDPTHV2(NPAR)
      Dimension tddot(Npar),Qr(Npar),qinc(Npar),    Qe(Npar)
      Dimension x(1:npar+1),dx(npar),iclass(npar),ptdptv(npar)
      Dimension text(20)
      CHARACTER OUTF(20)*2,OUTP(20)*8
      LOGICAL XBL,XPL,XFL,XFL,EMTOL,QCHL,INCFLX
      Common /Htflcn/CHIR,ChiA,Htcomb,schia,epsig,xfpowr,xcof
      Common /xpgrp/xpold(npar),xpnew(npar),xptemp(npar),xpqrld(npar),
      $   xpqrnw(npar)
      COMMON/QMV/Q42,TMV,SMV,N1,N2,N3
      COMMON/OUTPF/XBL,XPL,XFL,EMTOL,QCHL,INCFLX
      COMMON/ETF/QCEXT,QEO,XEXT,QFRO,DFRAD,KEFLUX
      COMMON/QFGASC/QFC0,DFC

C
C other variables: N,Rhov,Alphav,Rhoc,Alphac,Htpyr1,Cpv,Cpc,Cpg
C Initialing
      XBL=.FALSE.
      XPL=.FALSE.
      XFL=.FALSE.
      EMTOL=.FALSE.
      QCHL=.FALSE.
      INCFLX=.FALSE.

```

```

C
KO=0
print*, 'Do You Want to Output Burnout Front Location, Y/N'
READ(5, '(A)') OUTF(1)
OUTF(1)='Y'
IF (OUTF(1).EQ.'Y'.OR.OUTF(1).EQ.'Y') THEN
    XBL=.TRUE.
    KO=KO+1
    OUTP(KO)='XB'
ENDIF
print*, 'Do You Want to Output Flame Front Location, Y/N'
READ(5, '(A)') OUTF(2)
OUTF(2)='Y'
IF (OUTF(2).EQ.'Y'.OR.OUTF(2).EQ.'Y') THEN
    XPL=.TRUE.
    KO=KO+1
    OUTP(KO)='XP'
ENDIF
print*, 'Do You Want to Output Flame Height, Y/N'
READ(5, '(A)') OUTF(3)
OUTF(3)='Y'
IF (OUTF(3).EQ.'Y'.OR.OUTF(3).EQ.'Y') THEN
    XFL=.TRUE.
    KO=KO+1
    OUTP(KO)='XF'
ENDIF
print*, 'Do You Want to Output Mass Pyrolysis Rate, Y/N'
READ(5, '(A)') OUTF(4)
OUTF(4)='Y'
IF (OUTF(4).EQ.'Y'.OR.OUTF(4).EQ.'Y') THEN
    EMTOL=.TRUE.
    KO=KO+1
    OUTP(KO)='EMTOT1'
ENDIF
print*, 'Do You Want to Output Heat Release Rate, Y/N'
READ(5, '(A)') OUTF(5)
OUTF(5)='Y'

```

```

IF (OUTF(5).EQ.'Y'.OR.OUTF(5).EQ.'Y') THEN
  QCHL=.TRUE.
  KO=KO+1
  OUTP(KO)='QCH'
ENDIF
print*, 'Do You the total incident flux at the surface, Y/N'
READ(5,'(A)') OUTF(5)
  OUTF(5)='Y'
IF (OUTF(5).EQ.'Y'.OR.OUTF(5).EQ.'Y') THEN
  INCFLX=.TRUE.
  KO=KO+1
  OUTP(KO)='QINC'
ENDIF
do 10 i=1,npar
  temp1(i)=0.0
  tdpthv1(i)=0.0
  tdpthv2(i)=0.0
  ptdptv(i)=0.0
  temp21(i)=0.0
  temp22(i)=0.0
  chard (i)=0.0
  Qi (i)=0.0
  tddot(i)=0.0
  Qr (i)=0.0
  tdpthc(i)=0.0
  Qe (i)=0.0
  x (i)=0.0
  Dx (i)=0.0
  Iclass(i)=0
10 Continue
C
C Open file for input
open (4,file='hflinp',status='unknown')
open (16,file='fluxinp',status='unknown')
C
C Open files for output

```

```

C
    open(8,file='hfssout',status='unknown')
    open(9,file='hfssprf',status='unknown')

C
C  Copy input onto output
11  read(4,'(20a4)',end=12)(text(i),i=1,20)
    write(8,'(!!',20a4)')text
    write(9,'(!!',20a4)')text
    go to 11

C
12  Continue
    rewind 4

C
    READ (16,*)KEFLUX,QCEXT,QEO,XEXT
    print*,KEFLUX,QCEXT,QEO,XEXT
    READ (16,*) QFR0,DFRAD
    print*,QFR0,DFRAD
    READ (16,*) QFC0,DFC
    print*,QFC0,DFC

C
Q42---The heat flux reading at the 425 mm location (kW/m^2)
TMV---The time start to move the sample
SMV---The sample moving speed
N1-N3---Nodal number for desired surface temperature output to
        compare with the experiment
    READ (4,*) Q42,TMV,SMV,N1,N2,N3
QIG---the ignition heat flux to match the time to ignition from
        the experiment
    READ (4,*) KCHAR,crm,QIG
    Read(4,*)  N,Rhov,Rhoc,Htpyr1,Cpv,Cpc,Cpg,
                tkc,tkv,dt,Timend
    crm=crm*1.0E-3/(rhov-rhoc)
    alphav=tkv/(cpv*rhov)
    if(cpc*rhoc.ne.0.) then
        alphac=tkv/(cpv*rhov)

```

```

else
  alphac=alphav
endif
xn=0.0
xfpowr=0.666667
xfcof=0.052
Read(4,*)      E1,xN,xfpowr,xfcof
Read(4,*)      CHIR,ChIA,Htcomb,sc,Tinf,Tpyr,epsig,Tprcnt
dxi=xn/(n-1.)
x(1)=0.0
x(2)=0.01
do 15 I=3,n
  x(i)=(i-1)*dxi
  x(i)=x(i-1)+0.01
  x(I)=x(I-1)+0.01*(1.005)**(I-3)
  x(i)=x(i-1)+0.004
  Continue
15 read(4,*) (x(i),i=1,n)
  read(4,*) (QE(i),i=1,n)
  Time=0.0
  schia=sc/chia
  Dx(1)=      x(2)-x(1)
  C arbitrary boundary values
  x(n+1)=x(n)+ (x(n)-x(n-1))
  C
  Do 20 i=1,n
    dx(i)=      x(i+1)-x(i)
    temp1(i)=tinf
    temp21(i)=tinf
    TEMP22(I)=tinf
    xpnew(i)=0.0
    xpnew(i)=x(i)
    xptemp(i)=tpyr
    xpgrnw(i)=0.0
    xbnew=0.0
  20 Continue
  CC

```



```

C n th point assumed to be top most
dx(n)=0.0
close(4)

C
100    WRITE(8,100) (OUTP(J),J=1,KO)
        FORMAT('TIME',10(2X,A8))
        return
        end

Subroutine maincal(Temp1,Temp21,TDpthv1,Tdpthc,Tddot,Qr,Qe,
$      Chard,N,x, Dx,Time,Dt,Timeend,Iclass,Tprcnt, ptdptv,EL,
$      crm,TEMP22,TDPTH2)

C
C The main routine to call various subroutines to calculate flame
C spread

        implicit real*8(a-h,o-z)
        Parameter (Npar=2000)
        Dimension temold1(npar),thvold1(npar),thcold(npar),
$      chold(npar), Tdtold(npar), qrold(npar),iclsld(npar)
        Dimension Temp1(Npar),Temp21(Npar),Tdpthv1(Npar),Tdpthc(Npar)
        Dimension tddot (Npar),Qr(Npar),Qe(Npar),qinc(Npar),Temp22(Npar)
        Dimension Tdpth2(Npar),TEMOLD2(NPAR),THVOLD2(NPAR)
        Dimension x(npar),dx(npar),Chard(npar),td(npar),tem(npar)
        Dimension iclass(npar) ,tdotxp(npar) ,ptdptv(npar),ptdold(npar)
        DIMENSION QEIM1(NPAR),QEIM2(NPAR)
        DIMENSION XTEMP1(NPAR),XTEMP2(NPAR)
        DIMENSION TEMP2(NPAR),TDPTHV(NPAR),xptemp1o(npar),
$      xptemp2o(npar)
        dimension tdptvp1(npar),tdptvp2(npar),
$      tdptvp1o(npar),tdptvp2o(npar)
        Common /xpgrp/xpold(npar),xpnew(npar),xptemp(npar),xpqrld(npar),
$      xpqrnw(npar)
        common/khh/T1,khe
        common /indx/i,NT
        common /iterat/iter,itrlim

```

```
$
common/data/rhoc,rhov,cpc,cpv,alphac,alphav,tkc,tkv,cpg,
      tpyr,tinf,htpyr1,sitp
common/casea/kchar
common/flh/xff
common/flammes/nflet
common/flammes1/flmend(6,npar)
common/hor/xp
common/prin/qc1,grad1,qrer1,qelc11
Emtot0=0.0
Emtot1=0.0
percent=Tprcnt
Tpyreg=Tpyr*percent
ercn=2.0
NT=N
```

C

```
Do 20 i=1,n
  temold1(i)=temp21(i)
  temold2(i)=temp22(i)
  tdptvp1(i)=0.
  tdptvp2(i)=0.
  tdptvp1o(i)=0.
  tdptvp2o(i)=0.
  temp2(i)=temp21(i)+temp22(i)-TINF
  tem(i)=temp2(i)
  td(i)=tdpthv(i)
  thvold1(i)=tdpthv1(i)
  thvold2(i)=tdpth2(i)
  ptdold(i)=ptdptv(i)
  thcold(i)=tdpthc(i)
  chroid(i)=chard(i)
  tdtold(i)=tddot(i)
  tdotxp(i)=0.0
  qroid(i)=qr(i)
  xpold(i)=xpnew(i)
  xpgrld(i)=xpgrnw(i)
  iclsld(i)=iclass(i)
```

```

C      xbold=xbnw
C      xtemp1(i)=TINF
C      xtemp2(i)=TINF
C      xtemp1o(i)=TINF
C      xtemp2o(i)=TINF
CC      Call flxt(i),x(1),x(n),time,qe(i),qe1,ts,dq)
CC      QTO(I)=QE1
C      20 Continue
CC      QTZP=QTO(1)
C      Iter=0
C      ITRLIM=2
C
C      5 Continue
C      The 'upcheck' file is for checking the running of the program
C      OPEN (12,FILE='hfcheck',status='unknown')
C
C      iter=iter+1
C      tdzpm1=0.0
C      Start calculation of heat-up or pyrolysis
C      Do 100 I=1,n
C      oldtemp=temp2(i)
C      if(iclsld(i).eq.10) then
C          tddot(i)=0.
C          emtot1=0.
C          goto 100
C      endif
C      if(temp2(i).lt.tpyr) then
C          The surface temperature is below the pyrolysis temperature, the heat-up
C          calculation will be performed
C          if(iclsld(i).eq.2) then
C              temp2(i)=tem(i)
C              tdpthv(i)=td(i)
C          endif
C      Goes to the heat-up subroutine
C      As stated before, the heat flux to the surface is splitted into

```

```

C      two parts: the external heat flux (flxte) and flame heat flux
C      (flxtf) where qe11/2 are the heat fluxes for external and
C      flame flux, respectively.
      Call flxte(x(i),x(1),x(n),time,qe(i),qe11,ts,dq)
      qe1m1(i)=qe11
      Call flxtf(x(i),x(1),x(n),time,qe(i),qe2,ts,dq)
      qe1m2(i)=qe12
C      Total incident flux on the surface (added 5/8/95)
      qinc(i)=qe1+qe2
C      Hence the preheating model will be called twice (if both external
C      and flame heat flux are not zero)
      if(qe1.ne.0.) then
        khe=0
        call preheat(Time,Dt,x(i),Temp1(i),temp21(i),
          Tdpthv1(i),tddot(i),Qr(i),Qold(i),Qe11,EL)
      endif
      T1=TEMP21(I)
C      T1 is stored in order to calculate actual reradiation loss from
C      the fuel surface using flame heat flux as below
      if(qe2.ne.0.) then
        khe=1
        call preheat(Time,Dt,x(i),Temp1(i),temp22(i),
          Tdpth2(i),tddot(i),Qr(i),Qold(i),Qe12,EL)
      endif
C      The two temperature profiles using external and flame heat fluxes
C      have been calculated now
      TEMP2(I)=TEMP21(I)+TEMP22(I)-TINF
C      The real surface temperature would be the sum of the two temperatures
C      calculated from two heat fluxes. Value TINF has to be substrated since
C      both temperatures have initial value of TINF
      if(iter.eq.itrlim) then
        tem(i)=temp2(i)
        td(i)=tdpthv(i)
      endif
      if(oldtemp.lt.tpyr.and.temp2(i).ge.tpyr)ptdptv(i)=tdpthv(i)
      If(oldtemp.lt.tpyrreg.and.Temp2(i).gt.Tpyr .or. tdpthv(i)

```

```

CC      $ .lt. 0.0 ) then
55      Write(12,55)Dt
      Format(//,' DT too large for flux; Dt= ',e12.5// )
      Dt=Dt/2.
      iter=0
      call adjqr(qr,qold,xpqrnw,xpqrld,n)
      go to 105
      endif
      Endif

$      If (temp2(i).ge.Tpyr .and. iclsld(i).ne.10 .and.
      iclsld(i).gt.1 ) then
C      The surafce temperature is higher than the pyrolysis temperature and
C      pyrolysis calculation is performed
      oldtd=tddot(i)
      call flxte(x(i),x(1),x(n),time,qe(i),qe1,ts,dq)
      call flxtf(x(i),x(1),x(n),time,qe(i),qe2,ts,dq)
      QEIM(I)=QEI
      QEI=QEI1+QEI2
C      Pyrolysis routine is called
C3/9/95 at present the pyrolysis routine is not called due to the two heat
C      flux profiles, It is anticipated this will be done easily
C      $      Call vapor(Time,Dt,x(i),temp1(i),temp2(i),ptdptv(i),
      Tdpthc(i),tddot(i), chard(i) ,Qr(i),qold(i),Qei,EL)
      flarea=(xpold(i)-x(i))/(x(i+1)-x(i))
      if (oldtd.ne.0.0.and. iter.eq.2.and.flarea.gt.0.3 ) then
      tdchng=abs((tddot(i)-oldtd)/oldtd )
      if (tdchng.gt.ercn) then
      dtfr=(1-tdchng*2)
      if (dtfr.lt.0.1 ) dtfr=0.1
      Write(12,56) dtfr
      Format(' Iter increased ** difference fact',e14.5)
      itrlim=3
      endif
      endif
      Endif
C      The routine 'front' is used to classify the material section,

```

```

C      obtain total pyrolysis (burning rate), flame height as well as
C      pyrolysis front location
      Call front(Time, x,xbold,xpold,xpnew,temp2,xptemp,tddot(i),
      $tdotxp(i-1),tdotxp(i-2),i,N,iclass,iclslld,emtot0,emtot1,Qr,
      $ chard,Erfalg,iter,ern,xptemp1,xptemp2,temp21,temp22,tdpthv1,
      $ tdpth2,tdptvp1,tdptvp2)
      if(i.eq.n)go to 100
      if(iabs(iclslld(i)).eq.2) then
C      iclslld(i)=2, meaning pyrolysis front is in this section, both heat-up
C      and pyrolysis calculations will be carried out.
      xpfact=(abs(xpold(i))-x(i))/(x(i+1)-x(i))
      tdptv1=(thvold1(i+1)-thvold1(i))*xpfact+thvold1(i)
      tdptv2=(thvold2(i+1)-thvold2(i))*xpfact+thvold2(i)
      Qrzp=xpgrnw(i)
      gezp=(qe(i+1)-qe(i))*xpfact+qe(i)
      Call flxte(xpold(i),x(1),x(n),time,gezp,gezpi1,ts,dq)
      Call flxtf(xpold(i),x(1),x(n),time,gezp,gezpi2,ts,dq)
      xtp=tpyr
      tdptvz=tdptv1
      tdptc=0.0
C      a starting value for tddot; can be improved further 2,-2 etc
      if(tdotxp(i).eq.0.0)tdotxp(i)= tddot(i)*(1.-xpfact)
      charzp=0.0
C      Pyrolysis calculations
      Call vapor(Time,Dt,xpold(i),xtp,xptp,tdptvz,
      $      Tdptc,tdotxp(i),charxp,Qrzp,xpgrld(i),Qezpi,EL)
C      Heat-up calculation
      xptemp1(i)=xptemp1o(i)
      xptemp2(i)=xptemp2o(i)
      tdptv1=tdptvp1o(i)
      tdptv2=tdptvp2o(i)
      if(qezpi1.ne.0.) then
        khe=0
      call preheat(Time,Dt,xpold(i),xtp,xptemp1(i),Tdptv1,
      $      tdotxp(i),Qrzp,xpgrld(i),Qezpi1,EL)
      endif

```

```

T1=xptemp1(i)
if(qezpi2.ne.0.) then
    khe=1
    call preheat(Time,Dt,xpold(i),xptp,xptemp2(i),Tdptv2,
        $      tdotxp(i),Qrzp,xpgrld(i),Qezpi2,EL)
    endif
    tdptvp1(i)=tdptv1
    tdptvp2(i)=tdptv2
    C Need to combine the two thermal depth
      xptemp(i)=xptemp1(i)+xptemp2(i)-TINF
    endif
    100 Continue

    emtot0=emtot1
    Write(12,(' ' iclass ' ',10i4)' ) (iclass(i),i=1,n)
    if(Erflag.gt.ern.and.iter.eq. 2 )then
        dtfr=(1-erflag*2)
        if(dtfr.lt.0.1)dtfr=0.1
        Write(12,57) dtfr
    57 Format('///' 3 ITERATIONS; Chngfct',e14.5,' for EMT-ERR'//)
        itrlim=3
    endif
    105 continue
    do 106 k=1,n
        call locxb(x,xbold,xbnew,k,n,iclass,iclsld,flmend,
            $      tdtold,tddot,dt,chard,chold,el)
        106 continue
    if(iter .lt. itrlim) then
        Do 110 i=1,n
            temp21(i)=temold1(i)
            temp22(i)=temold2(i)
            xptemp1(i)=xptemp1o(i)
            xptemp2(i)=xptemp2o(i)
            xptemp(i)=tpyr

```

```

temp2(i)=temold1(i)+temold2(i)-TINF
tdpthv1(i)=thvold1(i)
tdpth2(i)=thvold2(i)
tdptvp1(i)=tdptvp1o(i)
tdptvp2(i)=tdptvp2o(i)
ptdptv(i)=ptdold(i)
tdpthc(i)=thcold(i)
chard(i)=chroid(i)
C See if averaging done at heatup-pyrol modules
C
    xtemp1(i)=tpyr
    xbnw=xbold
    iclass(i)=iclsld(i)
110    Continue
C
    go to 5
Else
    Time=Time+Dt
    emtot0=emtot1
C    Output result to file 'hfcheck'
60    format(' time,temp1-2,temp2(1),tdp1-2,tddot1'/(7(1x,e10.3)))
CC    write(12,61)time,(temp2(i),i=1,n)
CC    write(12,62)time,(chard(i),i=1,n)
CC    write(12,63)time,(tdpthv(i),i=1,n)
CC    WRITE(12,64)TIME,(XPNEW(I),I=1,N)
64    FORMAT(' TIME,XPNEW',(6E12.5))
61    format(' Time,Temp ',(6E12.5))
62    format(' Time,Char ',(6E12.5))
63    format(' Time,deltv',(6E12.5))

xp=0.0
do 12 k=1,n
    if(iclass(k).eq.2)then
        xp=xpnew(k)
        go to 14
    endif
    if(iclass(k).eq.5)xp=xpnew(k)

```



```

12      continue
14      continue
C      Output result for this time step
      KK=KK+1
      IF (KK.EQ.10) THEN
          Call output(time,Temp2,xbnew,tddot,chard,iclass,
$          xpnew,n,emtot1,tdpthv,x,qinc)
          kk=0
      endif
C      Store current results
      Do 120 i=1,n
          temold1(i)=temp21(i)
          temold2(i)=temp22(i)
          temp2(i)=temold1(i)+temold2(i)-TINF
          thvold1(i)=tdpthv1(i)
          thvold2(i)=tdpth2(i)
          ptdold(i)=ptdptv(i)
          thcold(i)=tdpthc(i)
          chroid(i)=chard(i)
          tdtold(i)=tddot(i)
          xbold=xbnew
          groid(i)=qr(i)
          QTO(I)=QEIM(I)
      try above
          xpgrld(i)=xpgrnw(i)
          xpold(i)=xpnew(i)
          xptemp(i)=tpyr
          if (xptemp1(i).eq.TINF) then
              xptemp1o(i)=temp21(i)
          else
              xptemp1o(i)=xptemp1(i)
          endif
          if (xptemp2(i).eq.TINF) then
              xptemp2o(i)=temp22(i)
          else
              xptemp2o(i)=xptemp2(i)

```

```

endif
if (tdptvp1(i).eq.0.) then
    tdptvplo(i)=tdpthv1(i)
else
    tdptvplo(i)=tdptvp1(i)
endif
if (tdptvp2(i).eq.0.) then
    tdptvp2o(i)=tdpth2(i)
else
    tdptvp2o(i)=tdptvp2(i)
endif
iclsld(i)=iclass(i)
xff=flmnd(3,1)
Continue
QTZP=QEZPI
Iter=0
ITRLIM=2

C
120
C
CLOSE(12)
Go back to calculate for next time step
If(time.lt.Timend)go to 5
Endif
Calculation finished
stop
end

subroutine adjqr(qr,qrold,xpqgrnw,xpqgrld,n)
Adjust radiant heat flux
implicit real*8(a-h,o-z)
dimension qr(n),qrold(n),xpqgrnw(n),xpqgrld(n)
do 10 k=1,n
    qr(k)=(qrold(k)+qr(k))*0.5
    xpqgrnw(k)=(xpqgrld(k)+xpqgrnw(k))*0.5
continue
return
end
10

```

```

subroutine loctxb(x,xbold,xbnew,i,n,iclass,iclslsld,
    flmend,tdtold,tddot,dt,chard,
    chroid,el)
C Locating the burnout front
implicit real*8(a-h,o-z)
dimension x(n),flmend(6,n),tddot(n),iclass(n)
dimension iclslsld(n),tdtold(n),chard(n),chroid(n)

if (iclass(i).eq.10.and.iclass(i+1).ne.10.
    and.i.lt.n) then
    xp=chroid(i)+tdtold(i)*dt
    if (xp.le.el) then
        xbnew=x(i)
    else
        if (xbold.le.x(i)) then
            xbnew=x(i)+(x(i+1)-x(i))*(xp-el)/
                (xp-chard(i+1))
        else
            xbnew=xbold+(x(i+1)-xbold)*(chard(i+1)-
                chroid(i+1))/(el-chroid(i+1))
        endif
    endif
else if (i.eq.n.and.iclass(i).eq.10) then
    write (12,('The material is burnout'))
    stop
else
    return
endif

400 return
end

```

Subroutine front(Time,x,xbold,xpold,xpnew,temp2, xptemp, tddot,  
 \$tdotxp, tdxpm1,i,N,iclass,iclslsld,emtot0,emtot1,Qr,Chard,

```

C      $ Erflag, iter, ercn, xptemp1, xptemp2, temp21, temp22, tdpthv1,
      $ tdpth2, tdptvp1, tdptvp2)
C      Calculating total pyrolysis rate, new pyrolysis front locations, etc.

      implicit real*8(a-h,o-z)
      Parameter (Npar=2000)
      Common /flames/nflet
      Common /flames1/flmend(6,npar)
      Common/data/rhoc,rhov,cpc,cpv,alphac,alphav,tkc,tkv,cpg,
      $      tpyr,tinf,htpyr1,sitp

C      $      Dimension iclass(n),x(n),xpold(n),xpnew(n),temp2(n),xptemp(n),
      $      $      Qr(n),chard(n),iclsld(n),xptemp1(n),xptemp2(n),
      $      $      temp21(n),temp22(n),tdpthv1(n),tdptvp1(n),
      $      $      tdptvp2(n),tdpth2(n)
C      $      goint to the routine to locate new pyrolysis front and classify
C      $      nodes
      call locxp(X,xpold,xpnew,temp2,xptemp,i,n,iclass,iclsld,
      $      flmend,nflet,xptemp1,xptemp2,temp21,temp22,
      $      tdpthv1,tdpth2,tdptvp1,tdptvp2)
C      $      The following is to calculate mass burning rate
      dx1=0.0
      dx2=0.0
      if(i.gt.1.and.iclsld(i-1).eq.-2 )dx1=x(i)+xpold(i-1)
      if(i.gt.1.and.iclsld(i-1).eq.5)dx1=x(i)-x(i-1)
      if(iclsld(i).eq. 2 )dx2=xpold(i)-x(i)
      if(iclsld(i).eq. 5 )dx2=x(i+1)-x(i)
      if(i.gt.1.and.iclsld(i-1).eq.10.and.iabs(iclsld(i)).gt.1)
      $      then
      $      dx1=x(i)-xbold
      $      endif
C      $      dx1 is dx below x & dx2 is dx above x
      If(i.eq.1) then
      $      emtot1=tddot*dx2
C
      Else

```

```

C
C      If( I.lt.N) emtot1=emtot1 + tddot* (dx1+dx2)
C
C      From previous cell, if Xp overflowed in the upward direction
      if(iclass(i-1).eq.2.and.iclsld(i-1).lt.2.and.i.gt.2)then
      if(iclass(i-2).eq.5.and.iclsld(i-2).eq.2)then
      emtot1=emtot1+tdxpm1*(xpnew(i-1)-x(i-1))
      write(12, '( " Overflow emt, tdm, xpn, xi ', 4e12.4) ' )
      emtot1,tdxpm1,xpnew(i-1),x(i-1)
      $
      emtot1=emtot1+tdxpm1*(xpnew(i-1)-x(i-1))*0.5
      endif
      endif
C
C      From old xp to new xp
      if(iclsld(i-1).eq.2)then
C      Forward direction
      dxp1=xpold(i-1)-x(i-1)
      dxp2=xpnew(i-1)-xpold(i-1)
      emtot1=emtot1 +tdotxp *(dxp1+dxp2)
      else
      if(iclsld(i-1).eq.-2)then
C      Backward direction
      If (iclass(i-1).eq.5.and.i.gt.2.and.iclass(i-2)
      .eq.-2 )then
      $      To take account of Xp going into next cell
      dxp1=abs(xpold(i-1)-xpnew(i-2))
      Else
C      Xp & pyrolysing region remaining in same cell
      dxp1=abs(xpold(i-1)-xpnew(i-1))
      endif
      dxp2=x(i)+ xpold(i-1)
      emtot1=emtot1 +tdotxp*(dxp1+dxp2)
      endif
      endif
C
C      When i=N ; The top grid point

```

```

    if(i.eq.n)then
        emtot1=emtot1 +tddot*dx1
        emtot1=emtot1*.5*(rhov-rhoc)
C
C
C      test for convergence
C
        erflag=0
        if(emtot0.ne.0.0.and. iter.eq.2)then
            if((flmend(2,1)-flmend(1,1))/x(n).gt.0.2)then
                Errm=Abs(emtot1-emtot0)/emtot0
                erflag=errm
            endif
        endif
        emtot0=emtot1
C
        call ftf(xbold,Qr,emtot1,flmend,nflet,chard,N,Err)
C
C
C      Endif
C
C      Endif
        return
    end

    Subroutine output(time,Temp2,xbnew,tddot,chard,
        iclass,xpnew,n,emtot1,t dpthv,x,qinc)
C
    Output the calculation results
    Parameter (Npar=2000)
    implicit real*8(a-h,o-z)

    Common/data/rhoc,rhov,cpc,cpv,alphac,alphav,tkc,tkv,cpg,
        tpyr,tinf,htpyr1,sitp
    COMMON/QMV/Q42,TMV,SMV,N1,N2,N3
C
C

```

```

Common /flames/nflet
Common /flames1/flmend(6,npar)
common/hr/qche
added 5/8
common/Flux/qinc
COMMON/OUTPF/XBL,XPL,XFL,EMTOL,QCHL,INCFIX
Logical XBL,XPL,XFL,EMTOL,QCHL,INCFIX

C
$
Dimension Temp2(n),tddot(n),chard(n),iclass(n),xpnew(n),
tdpthv(n),xx(5),tempp(5),x(n),OUTPA(20),qinc(n)
C
C Write flamends for plotting
C
KO=0
xp=0.0
do 12 k=1,n
  if(iclass(k).eq.2)then
    xp=xpnew(k)
    go to 14
  endif
  if(iclass(k).eq.5)xp=xpnew(k)
  continue
  continue
  t0=tnf
  if (time.eq.10000.) then
    open(12,file='temppro.dat',status='unknown')
    xx(1)=0.
    do 16 k=2,5
      xx(k)=xx(k-1)+0.001
      continue
    do 110 i=1,n
      write(12,120) x(i),temp2(i)
      continue
    do 17 i=1,n
      write(12,120) temp2(i),chard(i)
      temp2(1)=temp2(i)
    enddo
  endif
enddo

```

```

if(chard(i).ne.0.) then
  dc=chard(i)/dlog((temp2(i)-t0)/sitp)
else
  dc=0.
endif
do 5 j=2,5
  if(dc.eq.0.) then
    tempp(j)=(temp2(i)-t0)*exp(-xx(j)/tdpthv(i))+t0
  else
    if(xx(j).le.chard(i)) then
      tempp(j)=(temp2(i)-t0)*exp(-xx(j)/dc)+t0
    else
      tempp(j)=sitp*exp(-(xx(j)-chard(i))/tdpthv(i))+t0
    endif
  endif
endif
continue
do 6 j=1,5
  write (12,120) x(i),xx(j),tempp(j)
continue

17
120
      continue
      format(f12.4,2x,f12.4,2x,f12.4)
      close(12)

      endif
      write(8,11)time,qche,tddot(1),tddot(3),
      Added on 3/11/95, users specify output
      IF (IOUTPUT.EQ.1) goto 100,110
      Full output is desired
      write (8,11) time,zbnew,xf,flmnd(3,1),
      if(xbl) then
        ko=ko+1
        outpa(ko)=xbnew
      endif
      if(xpl) then
        ko=ko+1

```



```

        outpa(ko)=xp
    endif
    if(xfl) then
        ko=ko+1
        outpa(ko)=flmend(3,1)
    endif
    if(emptol) then
        ko=ko+1
        outpa(ko)=emtot1
    endif
    if(qchl) then
        ko=ko+1
        outpa(ko)=qche
    endif
    if(incflx) then
        ko=ko+1
        outpa(ko)=qche
    endif
    write(8,11)time,temp2(N1)-273.15,
    $      temp2(N2)-273.15,temp2(N3)-273.15,
    $      xp,nflet,((flmend(k,1),k=1,3),l=1,nflet)
    $      temp2(1)-273.15,nflet,((flmend(k,1),k=1,3),
    $      l=1,1)
    write(8,10) time,(outpa(j),j=1,ko)
    format(10(2x,e12.4))
    format(5(e11.4,1x),i3,7(1x,f10.4))
    nk=n
    if(n.gt.250) nk=250
    write(9,15)time,(temp2(k),k=1,nk,5)
    write(9,1500)(qinc(k),k=1,nk,5)
    format(2x,50(f5.1,2x) )
    format(6x,50(f5.2,2x) )
    Return
    End

```

```

C      Subroutine ftf(xbold,Qr,emtot1,flmend,nflet,chard,N,Err)
      Calculate flame height
      implicit real*8(a-h,o-z)
      Parameter (Npar=2000)
      Dimension chard(n),flmend(6,n),Qi(npar),Qr(n),Xploc1(npar)
      Common /Htflcn/CHIR,ChiA,Htcomb,schia,epsig,xfpowr,xfcof
      Common/HT/ x(1:npar+1),dx(npar),El
      Common /xpgrp/xpold(npar),xpnew(npar),xptemp(npar),xpqrld(npar),
      $ xpqrnw(npar)
      common /iterat/iter,itrlim
      common /htclas/iclass(npar)
      common/hr/qche

C      QCHE=Emtot1*htcomb
C      Xf=.052*qche**.66666
C      Xf=.052*(qche+40.)**xfpowr+xbold
C      Xf = xfcof *qche**xfpowr+Xbold
      Write(12,('( ' Xf, Qche = ' ',3e12.4)' )xf,qche
C
      if(Xf.gt.0.0)then
        do 10 i=1,n
          Qr(i)=Qi(i)* Chir* qche
          Continue
10      write(12,('( ' qr, qi ' '/(4e15.5))')(qr(j),qi(j),j=1,n)
CC      find qr at the xp; at xpold if first iter and at newxp if second iter
C
      if(iter.lt.itrlim)then
        Do 12 i=1,n
          xpocl(i)=xpold(i)
          if(xpocl(i).lt.0.0)xpocl(i)=--xpocl(i)
12      continue
C
      else
        Do 14 i=1,n
          xpocl(i)=xpnew(i)
          if(xpocl(i).lt.0.0)xpocl(i)=--xpocl(i)

```

```

14      continue
C
C      endif
CC      call flmshp(flmend,iclass,n,qi,nflet,xploc1,err,xf)
      do 20 i=1,n
        xpqrnw(i)=qi(i)* Chir * qche
      20      continue
C
      endif
      continue
      Return
      End

Subroutine locxp(X,xpold,xpnew,temp2,xptemp, i,n,iclass,iclslid,
$      flmend,nflet,xptemp1,xptemp2,temp21,temp22,
$      tdpthv1,tdpth2,tdptvp1,tdptvp2)
C  Classifying nodes and obtain pyrolysis front location
      implicit real*8(a-h,o-z)
      common /data/rhoc,rhov,cpc,cpv,alphac,alphav,tkc,tkv,cpg,
$      tpyr,tinf,htpyr1,sitp
      Dimension X(n),xpold(n),xpnew(n),temp2(n),xptemp(n),iclass(n),
$      iclslid(n), flmend(6,n),xptemp1(n),xptemp2(n),
$      temp21(n),temp22(n),tdpthv1(n),tdpth2(n),
$      tdptvp1(n),tdptvp2(n)
C
C      locate routine ****
      write(12,(''loc'',I2,E12.4)) i,temp2(2)
      If(i.eq.1)then
        nflet=0
        if(temp2(1).ge.tpyr)then
          flmend(1,1)=x(1)
          nflet=1
        endif
      return

```

```

      Endif
C IF I NOT Equal To 1 then
CC   Do 100 i=2,n
      Xp=0.0
      If (temp2(i).lt.Tpyr) then
        If (temp2(i-1).ge.Tpyr) then
          C Xp forward
          C
          If (xpol(i-1).eq.0.0) then
            If (xpol(i-1).eq.x(i-1)) then
              call getxp(1,x(i-1),x(i),          iclass(i-1),
              $          iclass(i),xp,temp2(i-1),temp2(i),tpyr
              $          )
              call gettemp(xp,x(i-1),x(i),xptemp1(i-1),
              $          temp21(i-1),temp21(i))
              call gettemp(xp,x(i-1),x(i),xptemp2(i-1),
              $          temp22(i-1),temp22(i))
              call gettemp(xp,x(i-1),x(i),tdptvp1(i-1),
              $          tdpthv1(i-1),tdpthv1(i))
              call gettemp(xp,x(i-1),x(i),tdptvp2(i-1),
              $          tdpth2(i-1),tdpth2(i))
            Else
              call getxp(1,xpol(i-1),x(i),          iclass(i-1),
              $          iclass(i),xp,xptemp(i-1),temp2(i),tpyr
              $          )
              call gettemp(xp,xpol(i-1),x(i),tvp1,
              $          tdptvp1(i-1),tdpthv1(i))
              call gettemp(xp,xpol(i-1),x(i),tvp2,
              $          tdptvp2(i-1),tdpth2(i))
              call gettemp(xp,xpol(i-1),x(i),xptem1,
              $          xptemp1(i-1),temp21(i))
              call gettemp(xp,xpol(i-1),x(i),xptem2,
              $          xptemp2(i-1),temp22(i))
              xptemp1(i-1)=xptem1
              xptemp2(i-1)=xptem2
              tdptvp1(i-1)=tvp1
              tdptvp2(i-1)=tvp2
            Endif
          xpnew(i-1)=xp

```

```

if(nflet.eq.0)nflet=1
flmend(2,nflet)=xp
endif
Else
  If(temp2(i-1).ge.Tpyr)then
    C Classify 5
    C first get xp
    if(iclsld(i-1).eq.2)then
      xp=x(i)
      write(12,'(///' CLASS 5 starts xpold,xi,xptemp,temp2,xp
      $ ' '5e12.5)' )xpold(i-1),x(i),xptemp(i-1),temp2(i),xp
      xpnew(i-1)=xp
    Else
      C
      If(iclsld(i-1).eq.-2)then
        xp=x(i-1)
        xpnew(i-1)=-xp
      Else
        If(iclass(i-1).eq.0)write(12,11)
        Format('///' TWO NODES IN PYROLYSIS TOGETHER '///)
        11
        Endif
      Endif
    Endif
    C Now classify 5
    iclass(i-1)=5
    if(nflet.eq.0)nflet=1
    C Xp Backward
    Else
      If(xpold(i-1).eq.x(i-1) .and.iclsld(i-1).ne.-2)then
        call getxp(-1,x(i),x(i-1),
        $ iclass(i-1),xp,temp2(i),temp2(i-1),tpyr )
        Else
          call getxp(-1,abs(xpold(i-1)),x(i-1),
          $ iclass(i),iclass(i-1),xp,xptemp(i-1),temp2(i-1),tpyr)
          Endif
          xpnew(i-1)=-xp
          nflet=nflet+1
        C

```

```

        if(nflet.eq.0)nflet=nflet+1
        flmend(1,nflet)=xp
      Endif
C   top cell change as boundary cond defined.
      If(i.eq.n )then
        iclass(i)=5
        if(xp.eq.0.0)xp=x(n)
        flmend(2,nflet)=x(n)
      endif
C   above statement tobe modified with different boundary seeting
      Endif
C
CC   write(*, '(' i, icl,xp, xpnew(i-1) ',2i3,2e14.5')i,iclass(i-1)
CC   $, xp,xpnew(i-1)
100  Continue
      Return
      End
      subroutine gettemp(xp,xone,xtwo,xptemp,temone,temtwo)
      implicit real*8 (a-h,o-z)
      xpfact =(abs(xp)-xone)/ (xtwo-xone)
      xptemp= (temtwo-temone)* xpfact +temone
      return
      end
      Subroutine getxp(isn,xone,xtwo,iclas1,iclas2,
      $ xp,temone,temtwo,tpyr)
C   Calculate new pyrolysis front location
      implicit real*8(a-h,o-z)
C
C   Xp= ( xtwo- xone)*(tpyr-temone)/(temtwo-temone) +xone
C
      if(isn.gt.0)iclas1=2
      if(isn.lt.0)iclas2=-2

```

```

C
      return
      end

      Function idzpos(x,n,z )
      implicit real*8(a-h,o-z)
      Dimension z(n)
      C Find the index of x in array x with dx widths
      C
      idzpos=0
      do 10 i=1,n
      write(*,>(' ' i,x, z(i+1) ' ',i3, 2e12.4)') i,x,z(i+1)
      if(x.lt. z(i+1) )then
      idzpos=i
      go to 20
      endif
10    Continue
      idzpos=n
20    Return
      end

      subroutine qflux(t,y,qnet,dq)
      C Combine different heat fluxes
      C implicit real*8(a-h,o-z)
      C
      C Parameter (Npar=2000)
      C
      common /Pyr1vr/temp1(npar),Tddot(npar)
      common/data/rhoc,rhov,cpc,cpv,alphac,alphav,tkc,tkv,cpg,
      $      tpyr,tinf,htpyr1,sitp
      Common/HT/ X(1:npar+1),dx(npar),El
      Common /Htflcn/CHIR,ChiA,Htcomb,schia,epsig,xfpowr,xfcof
      common /Fluxet/qr1cl,qld1cl,qelcl,emdlcl,temper
      Common /htclas/iclass(npar)
      common /indx/i,N
      C !

```

```

common /hpcomn/m
common /hpcomn1/xd1,xd2,dt,use1,use2
common/flh/xf
common/pos/xpp
common/khh/T1,khe
common/hor/xp
common/prin/qc1,grad1,qrer1,qelc11

dimension y(m)

C !
C
C HEAT-FLUX
C
C Qc
C if this cell is the bottom part of flame ????? check??
C Qrer
CC ydf=y(1)-tinf
   ydf=temper-tinf
   if(ydf.eq.0.0) then
       qrer=0.0
   else
       tinsq=tinf*tinf
       tin3=tinsq*tinf
       ydsq=ydf*ydf
       yd3=ydf*ydsq
       yd4=ydsq*ydsq
       qm=tin3*ydf*4.+6.*tinsq*ydsq+4.*tinf*yd3+yd4
       qrer=epsig*qm
   endif
C qrer is the reradiation loss and CONV is the routine to be used
C to obtain heat loss
  IF (KHE.EQ.0) THEN
    CALL CONV(TEMPER,QC)
  ENDIF
  qC=0.
  DQ=-4*EPSIG*TEMPER**3

```



```

C      qrad=0.
C      to obtain ignition and flame radiant heat fluxes
C      Corrected on 2/27/94, xpp is added in place of x(i) since zpp is
C      the real location
C      if (KHE.EQ.1) THEN
C          CALL CONV(T1+TEMPER-TINF,QC)
C              QC=0.
C      qrer=epsig*((T1+TEMPER-TINF)**4-T1**4)
C      endif
C      qrer=0.92*qrer
C      qnet=qrad-qrer+qelcl-qc
C      The net heat flux, qnet is obtained
C      return
C      end

SUBROUTINE FLXTE(X,X1,XN,TIME,QEIN,QEOUT,TS,DQ)
IMPLICIT REAL*8(A-H,O-Z)

PARAMETER (NPAR=1000)
COMMON/hor/xp
COMMON/QIGG/QIGN
COMMON/QMV/Q42,TMV,SMV,N1,N2,N3
COMMON/ETF/QCEXT,QEO,XEXT,QFRO,DFRAD,KEFLUX
IF (KEFLUX.EQ.1) THEN
Q425=Q42*0.92
IF (TIME.LE.TMV) THEN
q1=0.397+X
q1=0.367+X
ELSE
q1=0.397+X-SMV*1.0E-3*(TIME-TMV)
q1=0.367+X-SMV*1.0E-3*(TIME-TMV)
ENDIF
QL=1000*QL
if (QL.GE.1000.) THEN
QE=0.

```

```

10      GOTO 10
      endif
      fc=-0.426427+0.0176022*q1-5.56151E-5*q1**2+6.17988E-8
      $      *q1**3-2.3376E-11*q1**4
      qe=fc*q425
      if(qe.ge.q425) qe=q425
      ELSE IF (KEFLUX.EQ.2) THEN
      QE=QCEXT
      ELSE
      QE=QE0*EXP(-X/XEXT)
      ENDIF
      IF(QFR0.NE.0.) THEN
      IF(XP.NE.0.) THEN
      IF (X.LE.XP) THEN
      QFRAD=QFR0
      ELSE
      IF ((X-XP)/DFRAD.LE.86.) THEN
      QFRAD=QFR0*exp(-(x-xp)/DFRAD)
      ELSE
      QFRAD=0.
      ENDIF
      ENDIF
      ELSE
      QFRAD=0.
      ENDIF
      ENDIF
      IF(qe.LE.0.1) qe=0.
      if(qfrad.le.0.1) qfrad=0.
      IF (X.LE.0.01) THEN
      QEOUT=QIGN
      ELSE
      QEOUT=QE+QFRAD
      ENDIF
      if(qeout.le.0.1) qeout=0.
      RETURN

```

```

END

SUBROUTINE FLXTF(X,X1,XN,TIME,QEIN,QEOUT,TS,DQ)
  Routine to provide ignition, external and flame radiant heat
  fluxes
  IMPLICIT REAL*8 (A-H,O-Z)

  PARAMETER (NPAR=2000)
  common/hor/xp
  COMMON/QFGASC/QFC0,DFC
  IF (XP.NE.0.) THEN
    IF (X.LE.XP) THEN
      QEOUT=QFC0
    ELSE
      qeout=QFC0*exp(-(x-xp)/DFC)
    ENDIF
  ELSE
    QEOUT=0
  ENDIF
  if(qeout.le.0.1) qeout=0.
  RETURN
END

SUBROUTINE CONV(TS,QCON)
  Obtain convective heat losses
  IMPLICIT REAL*8 (A-H,O-Z)
  PARAMETER(NPAR=2000)
  The natural convection model is taken from Tanaka et al.
  Common/HT/ X(1:npar+1),dx(npar),El
  COMMON/INDX/I,N
  common/data/rhoc,rhov,cpc,cpv,alphac,alphav,tkc,tkv,cpg,
  $      tpyr,tinf,htpyr1,sitp
  HL=X(N)

  IF (TINF.EQ.TS) THEN
    QCON=0.

```

N 4.8 x 10<sup>21</sup>

GOTO 400  
ENDIF

T=(TINF+TS)/2.

TLAMDA=the thermal conductivity of Air (W/m.K)  
VU=the kinetic viscosity (m\*\*2/s)

TLAMDA=3.25E-7\*T\*\*0.774

VU=1.14E-9\*T\*\*1.65

GR=9.81\*HL\*\*3\*DABS(TINF-TS)/(VU\*\*2\*TS)

PR=0.7

Anu-Nusselt Number

ANU=0.13\*(GR\*PR)\*\*0.3333

HC=TLAMDA\*ANU/HL

HC=0.4

QCON=HC\*(TS-TINF)

k=0

400 RETURN  
END

SUBROUTINE FLMRAD(X,QRAD)

Obtaining radiant heat flux from the flame and it is not used  
at present

IMPLICIT REAL\*8 (A-H,O-Z)

COMMON/FLM/RADF,H,QCHZ

COMMON/INDX/I

IF (I.LE.2) THEN

QRAD=0.

RETURN

ENDIF

HH=H/3.

R=HH\*\*2+X\*\*2

IF (R.EQ.0.) THEN

QRAD=0.

GOTO 400

ENDIF

```

400      QRAD=RADF*QCHZ/(4.*3.1415927*R)*HH/SQRT(R)
      RETURN
      END

      Subroutine preheat(Time,Dt,x,temp1,temp2,tdepth, tddot,Qr,
      Qold,Qe,EL)
      $ Routine used to call heat-up calculations
      implicit real*8(a-h,o-z)
      dimension prmt(5),aux(16,2), dery(2)
      common/data/rhoc,rhov,cpc,cpv,alphac,alphav,tkc,tkv,cpg,
      $      tpyr,tinf,htpyr1,sitp
      common /Fluxet/qrlcl,qldlcl,qelcl,emdlcl,temper
      common /hpcomn/m
      common /hpcomn1/prmt
      common/av/timea
      common/indx/k
      common/flh/xf
      common/khh/T1,khe
      common/pos/xpp
      COMMON/DN/XI,QRHS,ELS,TQN1
      common/ttt/tdd
      dimension y(2)
      external outph
      external Heat, Heatin
      C setup parametrs for diff eq.solv
      C
      C !!
      TEMP2N=TEMP2-TINF
      DELTN=TDEPTH
      IF (TDEPTH.NE.0.) THEN
      IF (EL/TDEPTH.GE.86.) THEN
      XI=(TEMP2-TINF)*TDEPTH
      ELSE
      XI=(TEMP2-TINF)*TDEPTH*(1.-EXP(-EL/TDEPTH))

```

```

ENDIF
ENDIF
      QRHS=DT*QE/(RHOV*CPV)
      ELS=EL
      xpp=x
      if(xpp.le.xf) then
        ihtgrw=1
      else
        ihtgrw=0
      endif
      c ihtgrw=1 strictly increasing fire. ihtgrw=0 growing or diminishing
        many=1
        m=2

      qrlcl=qr
      qldlcl=qold
      qelcl=qe
      emdlcl=tddot*(rhov-rhoc)

C
CC TRY ALL Heat up computations with emdlcl=0.0 ; most are except Xp
      emdlcl=0.0
      CC -----
        dtry=dt
        Y2I=0.
CModified on 8/1/94
10  Y(1)=TDEPTH
      Y(2)=TEMP2
      TDD=TEMP2
      prmt(1)=time
      prmt(2)=time+dt
      prmt(3)=dtry/4.
      prmt(4)=0.0001
      if(Y(1).eq.0.0.or.Y(2).eq.0.0) prmt(4)=prmt(4)*10.
      dtl=prmt(3)
      sum=0.0
      do 11 i=1,2

```

```

dery(i)=1.
if(y(i).ne.0.0)dery(i)=1./abs(y(i))
sum=sum+dery(i)
11 continue
dery(1)=dery(1)/sum
dery(2)=dery(2)/sum
C Going to heat-up calculations
If(y(1).eq.0.0.or.y(2).eq.0.0)then
call hpcg(prmt, y,dery,m,ihlf,Heatin,outph, Aux )
Else
call hpcg(prmt, y,dery,m,ihlf,Heat,outph, Aux )
Endif
if(ihlf.gt. 10)write(12,('( ' CHECK ihlf = ' ',i4)' )ihlf
if(y(1).lt.0.0 .or. (ihtgrw.eq.1 .and.y(2).lt.temp2)) then
dtry=dtry/4.
many=many+1
if(many .lt. 10)go to 10
write(12,('( ' Too many reduction ?? Dt may change''))' )
endif
temp2=y(2)
tdepth=y(1)
if(temp2.lt.Tpyr)then
temp1=temp2
Else
temp1=Tpyr
Endif
C
Return
END

subroutine outph(x,y,dery,ihlf,m,prmt)
C A routine required by HPCG
implicit real*8(a-h,o-z)
continue
return
end

```

```

Subroutine vapor(Time,Dt,x,temp1,temp2,tdpthv,
  qhthc,tdot, chard, Qr ,Qold, Qe,EL)
  !!!!!!! analysis calculations
  implicit real*8(a-h,o-z)
  !!!!!!!
  common /DATA/GAMAC,GAMAV,CPC,CPV,ALPC,ALPV,TKC,TKV,CPG,
    TP,TO,HTPYRL,SITP
  common /hpcmn/m
  common /hpcmn1/prmt
  common /CASEA/KCHAR
  common /DEX/DXPDT
  common /AV/TIMEA
  common /indx/k
  common /pos/xpp

  Dimension Y(3)
  Dimension prmt(5),dydx(3),aux(16,3),yt(3)
  External outpy
  External PYROBB,PYROBV

C
C set up parameters
C
  xpp=x
  qrlcl=qr
  qlclcl=qold
  qelcl=qe
  emdlcl=tdot*(gamav-gamac)
  temper=temp1
  m=3
  ndim=3
  write(12,(''test'',E12.4)) chard
C

```



```

C right now only pyrolysing & no char formation
  Y(1)=CHARD
  Y(2)=(TEMP2-SITP-T0)/SITP
  Y(3)=tdpthv
  if(chard-el)/Y(3)).le.1.0E-12) goto 400

  xi=time
  xend=time+dt
  prmt(1)=time
  prmt(2)=time+dt
  prmt(3)=dt/4.
  prmt(4)=1.0E-10
  sum=0.0
  do 5 i=1,3
    dydx(i)=1.
    if(Y(i).ne.0.0)dydx(i)=1./abs(Y(i))
    sum=sum+dydx(i)
  continue
  dydx(1)=dydx(1)/sum
  dydx(2)=dydx(2)/sum
  dydx(3)=dydx(3)/sum
  C going to pyrolysis calculations
  IF (CHARD.EQ.0.) THEN
    KF=1
    CALL HPCG(PRMT,Y,DYDX,NDIM,IHLF,PYROBB,OUTPY,AUX)
  ELSE
    KF=0
    CALL HPCG(PRMT,Y,DYDX,NDIM,IHLF,PYROBV,OUTPY,AUX)
  ENDIF
  continue
  write(12,('test2',E12.4)) Y(1)
  if(ihlf.gt. 10)write(12,('CHECK ihlf = ',i4,' )ihlf
    tdpthv=Y(3)
  if(abs((Y(1)-el)/Y(3)).le.1.0E-6) then
    chard=el
  else

```

```

      chard =y(1)
    endif
    IF(KF.EQ.1) THEN
      CALLQ FLUX(XEND,Y,QO,DQ)
      CALL PYROBB(xend,Y,DYDX)
      Y(2)=QO*Y(1)/(SITP*TKC)
    ELSE
      CALL PYROBV(XEND,Y,DYDX)
    ENDIF
    IF(KCHAR.EQ.1) THEN
      TEMP2=Y(2)*SITP+SITP+T0
    ENDIF
    TEMP1=TEMP2
    tddot=DYDX(1)
    tddot=dxpdt
    return
  end

  subroutine outpy(x,y,dery,ihlf,m,prmt)
    implicit real*8(a-h,o-z)
    continue
    return
  end

```

C  
C

```

SUBROUTINE HEATIN(T,Y,DYDX)
  Initial heat-up calculation routine
  IMPLICIT REAL*8(A-H,O-Z)
  PARAMETER (NPAR=2000)
  COMMON/DATA/GAMAC,GAMAV,CPC,CPV,ALPC,ALPV,TKC,TKV,CPG,
    TP,T0,HTPYRL,SITP
  COMMON/PYRLVR/TEMP1(NPAR),TDDOT(NPAR)
  COMMON/HT/X(1:NPAR+1),DX(NPAR),EL
  COMMON/FLUXET/QLCL,QLDLCL,QELCL,EMDLCL,TEMPER
$

```

C

```

COMMON/HTCLAS/ICLASS(NPAR)
COMMON/INDX/I
COMMON/HPCOMN/M
COMMON/HPCOMN1/XD1,XD2,DT,USE1,USE2
COMMON/AV/TIMEA
REAL*8 Y(2),DYDX(2)
IF (Y(2).LE.TO) Y(2)=T0
TEMPER=Y(2)
CALL QFLUX(T,Y,Q0,DQ)
TK3=ALPV*4.0
IF (Q0.EQ.0.AND.Y(1).EQ.0) THEN
DYDX(1)=0.
DYDX(2)=0.
TIMEA=T
RETURN
ENDIF
TIM=T-XD1
if (TIM.LE.0) TIM=0.
IF (TIM.EQ.0.0) TIM=DT
DYDX(1)=0.5*SQRT(0.8*ALPV/TIM)
DYDX(2)=0.5*Q0/(GAMAV*CPV)*SQRT(5./(4.*ALPV*TIM))
TIMEA=T
RETURN
END

SUBROUTINE HEAT(T,Y,DYDX)
Normal heat-up calculations
IMPLICIT REAL*8(A-H,O-Z)
PARAMETER (NPAR=2000)
COMMON/PYRLVR/TEMP1(NPAR),TDDOT(NPAR)
COMMON/DATA/GAMAC,GAMAV,CPC,CPV,ALPC,ALPV,TKC,TKV,CPG,
TP,T0,HTPYRL,SITP
COMMON/HT/X(1:NPAR+1),DX(NPAR),EL
COMMON/FLUXET/QLCL,QLDLCL,QELCL,EMDLCL,TEMPER
COMMON/HTCLAS/ICLASS(NPAR)
COMMON/INDX/I

```

```

COMMON/HPCOMMON/M
COMMON/HPCOMMON1/XD1,XD2,DT,USE1,USE2
COMMON/DEX/DXPDT
COMMON/AV/TIMEA
COMMON/CASEA/KCHAR
COMMON/DEB/KKK
common/ttt/tdd
C T--time, Y(1)--Thermal penetration length of the material,Y(2)--
C The material surface temperature.
REAL*8 Y(2),DYDX(2),C1,C2,Q0,EL,TP,T0,GAMAC,GAMAV,CPC,CPV,ALPC,
$ ALPV
REAL*8 TKC,TKV,HTPVRL
IF(Y(2).LE.T0) Y(2)=TDD
TEMPER=Y(2)
SITS=Y(2)-T0
CALL QFLUX(T,Y,Q0,DQ)
IF(Q0.EQ.0.AND.Y(1).EQ.0) THEN
DYDX(1)=0.
DYDX(2)=0.
TIMEA=T
RETURN
ENDIF
C
IF (2.*EL/Y(1).GE.86.) THEN
C1=1.
DYDX(1)=-2./(C1*SITS)*Q0/(GAMAV*CPV)+2.*ALPV/(C1*Y(1))
C2=-2./(C1*SITS)*Q0/(GAMAV*CPV)+2.
$ *ALPV/(C1*Y(1))
DYDX(2)=(Q0/(GAMAV*CPV)-C2*SITS)/Y(1)
ELSE IF (EL/Y(1).LE.1.0E-2) THEN
DYDX(2)=Q0/(GAMAV*CPV*EL)
ELSE
C1=2.*(1.-EXP(-2.*EL/Y(1)))*(1.-EXP(-EL/Y(1))-EL/Y(1))*
$ EXP(-EL/Y(1))-(1.-EXP(-EL/Y(1)))*
$ (1.-EXP(-2.*EL/Y(1))-2.*EL/Y(1))*EXP(-2.*EL/Y(1))

```

```

DYDX(1)=-2./(C1*SITS)*(1.+EXP(-2.*EL/Y(1))-2.*
EXP(-EL/Y(1)))*Q0/(GAMAV*CPV)+2.*ALPV/
(1.-EXP(-EL/Y(1)))*Q0/(GAMAV*CPV)+
2.*ALPV/(C1*Y(1))*(1.-EXP(-EL/Y(1)))*Q0/(GAMAV*CPV)+
(1.-EXP(-EL/Y(1)))
DYDX(2)=(Q0/(GAMAV*CPV)-C2*SITS)/(Y(1)*(1.-
EXP(-EL/Y(1))))

```

```

ENDIF
TIMEA=T

```

```

RETURN
END

```

```

SUBROUTINE PYROBV(T,Y,DYDX)
Normal pyrolysis calculation routine
IMPLICIT REAL*8 (A-H,O-Z)
PARAMETER (NPAR=2000)
COMMON/PYRLVR/TEMP1(NPAR),TDDOT(NPAR)
COMMON/DATA/GAMAC,GAMAV,CPC,CPV,ALPC,ALPV,TKC,TKV,CPG,
TP,T0,HTPYRL,SITP
COMMON/HT/X(1:NPAR+1),DX(NPAR),EL
COMMON/FLUXET/QLCL,QLDLCL,QELCL,EMDLCL,TEMPER
COMMON/HTCLAS/ICLASS(NPAR)
COMMON/INDX/I
COMMON/HPCOMN/M
COMMON/HPCOMN1/XD1,XD2,DT,USE1,USE2
COMMON/DEX/DXPDT
COMMON/AV/TIMEA
COMMON/CASEA/KCHAR

```



```

C4=2.*(1.+2.*HTPYRL/(CPV*SITP))-4.*(1.+HTPYRL/(CPV*SITP))
LT=2.*ALPV/(C3*Y(3))*(1.+HTPYRL/(CPV*SITP))
NE=-1.
      1.+HTPYRL/(CPV*SITP)
      1.0E-6) .LT.1.0E-6) THEN
      THEN
C3=2.*RATIO*(2./3.*HTPYRL/(CPV*SITP)+(1./6.-0.75*
      HTPYRL/(CPV*SITP))*RATIO)
C4=2.*(-1.+RATIO-7./12.*RATIO**2)
LT=2.*ALPV/(RATIO**2*(2./3.*HTPYRL/(CPV*SITP)+(1./6.-
      0.75*HTPYRL/(CPV*SITP))*RATIO)*Y(3))*(HTPYRL/
      (CPV*SITP)+(1.-HTPYRL/(CPV*SITP))*RATIO+(2./3.*
      HTPYRL/(CPV*SITP)-1.5)*RATIO**2)
NE=-RATIO**2/2.*(1.-2./3.*RATIO)
DE=HTPYRL/(CPV*SITP)+RATIO-RATIO**2/2.
      ELSE
C3=(1.+HTPYRL/(CPV*SITP)-EXP(-(EL-Y(1))/Y(3)))*(-1.+
      EXP(-2.*(EL-Y(1))/Y(3))+2.*(EL-Y(1))/Y(3))*
      EXP(-2.*(EL-Y(1))/Y(3))-2.*(-1.+EXP(-(EL-Y(1))/Y(3))+
      (EL-Y(1))/Y(3)*EXP(-(EL-Y(1))/Y(3)))*(1.+2.*HTPYRL/
      (CPV*SITP)-EXP(-2.*(EL-Y(1))/Y(3)))
C4=2.*(1.+2.*HTPYRL/(CPV*SITP)-EXP(-2.*(EL-Y(1))/Y(3)))-4.*
      (1.+HTPYRL/(CPV*SITP)-EXP(-(EL-Y(1))/Y(3)))
LT=2.*ALPV/(C3*Y(3))*(1.-EXP(-2.*(EL-Y(1))/Y(3)))*(1.+
      HTPYRL/(CPV*SITP)-EXP(-(EL-Y(1))/Y(3)))
NE=-1.+EXP(-(EL-Y(1))/Y(3))+(EL-Y(1))/Y(3)*EXP(-(EL-Y(1))/
      Y(3))
DE=1.+HTPYRL/(CPV*SITP)-EXP(-(EL-Y(1))/Y(3))
ENDIF
IF (Y(2).LE.0.1.OR.(KCHAR.EQ.2)) THEN
a11=C4*DE/C3
a12=-(C4*NE/C3+1.)
D1=0.25*GAMAC*CPC/(GAMAV*CPV)*Y(2)

```

```

D2=-0.5*C4*GAMAC*CPC*Y(1)/(C3*GAMAV*CPV)
RHS1=-LT
PHC0=Q0/(GAMAV*CPV*SITP)
IF (GAMAC*CPC.EQ.0.) THEN
    E1=0.
ELSE
    E1=-1.5/(GAMAV*CPV*SITP)*
        (Q0-TKCA*Y(2)*SITP/Y(1))
ENDIF
E2=-3.*C4/(C3*GAMAV*CPV)*(Q0/SITP-Y(2)*TKCA/Y(1))
RHS3=C4*Q0/(C3*GAMAV*CPV*SITP)+LT
print*,a11,rhs1,a12*(rhs3+c4*e1/c3),'flag'
DYDX(1)=(RHS1-A12*(RHS3+C4*E1/C3))/
        (A11-A12*D1*C4/C3)
IF (GAMAC*CPC.EQ.0.) THEN
    IF (Y(2).EQ.0.) THEN
        DYDX(2)=0.
    ELSE
        DYDX(2)=DYDX(1)*Q0/(SITP*(TKCA-DQ*Y(1)))
    ENDIF
ELSE
    DYDX(2)=(A11*(E2-C4*E1/C3)-D1*C4/C3*(A12*
        (RHS3+E2)-RHS1))/(D2*(A11-A12*D1*C4/C3))
ENDIF
DYDX(3)=(A11*(RHS3+E1*C4/C3)-RHS1*D1*C4/C3)/
        (A11-A12*D1*C4/C3)
ELSE
    G1=Y(1)*SITP/DLOG(1.+Y(2))*(-0.5*(Y(2)-1.)+0.25*Y(2)
        *(Y(2)-2.)/((Y(2)+1.)*DLOG(1.+Y(2))))
    C1=0.5+0.25*Y(2)*(Y(2)-2.)/DLOG(1.+Y(2))
    G2=SITP*(Y(2)-DLOG(1.+Y(2)))/DLOG(1.+Y(2))
    G3=-Y(1)/DLOG(1.+Y(2))/(Y(2)+1.)*
        ((Y(2)-DLOG(1.+Y(2)))/DLOG(1.+Y(2))-Y(2))
    RHS1=-LT

```

C



```

a11=C4*DE/C3
a12=-(NE*C4/C3+1.)
IF (GAMAC*CPC.EQ.0.) THEN
    E1=0.
ELSE
    E1=G3*Y(2)/(G1*GAMAV*CPV)*(Q0-TKCA*SITP*(Y(2)+2.))*
    DLOG(1.+Y(2))/(2.*Y(1))
ENDIF
E2=-C4/(C1*C3)*G2*Y(2)/(GAMAV*CPV*SITP)*(Q0/SITP-
    TKCA*(Y(2)+2.)*DLOG(1.+Y(2))/(2.*Y(1)))
RHS3=C4*Q0/(C3*GAMAV*CPV*SITP)+LT
RHS0=Q0/(GAMAV*CPV*SITP)
D1=G2*GAMAC*CPC/(GAMAV*CPV*SITP)+G3*GAMAC*CPC*SITP*C1/
    (G1*GAMAV*CPV)
D2=-C4*G2*GAMAC*CPC/(C3*GAMAV*CPV*SITP)*G1/(C1*SITP)+
    C4*G3*GAMAC*CPC/(C3*GAMAV*CPV)
DYDX(1)=(RHS1-(RHS3+C4*E1/C3)*A12)/(A11-A12*D1*C4/C3)

IF ((GAMAC*CPC).EQ.0.) THEN
    IF (Y(2).EQ.0.) THEN
        DYDX(2)=0.
    ELSE
        DYDX(2)=Q0*DYDX(1)/(SITP*(TKCA-DQ*Y(1)))
    ENDIF
ELSE
    DYDX(2)=(A11*(E2-C4*E1/C3)-D1*C4/C3*(A12*(RHS3+E2)-
        RHS1))/(D2*(A11-A12*D1*C4/C3))
ENDIF
DYDX(3)=(A11*(RHS3+E1*C4/C3)-(RHS1*D1*C4/C3))/
    (A11-A12*D1*C4/C3)
ENDIF

EMD1=DYDX(1)*(GAMAV-GAMAC)
IF (EMD1.LT.0.0) THEN
    EMD1=0.0

```

C:\FLAME-S\HFS\HFSSPV70.F

```

10  ENDIF
20  IF (EMDLCL*.05.GT.ABS(EMD1-EMDLCL)) GOTO 20
400 EMDLCL=EMD1
    CONTINUE
    EMDLCL=EMD1
    IF (DYDX(1).LE.0.) THEN
        DYDX(1)=0.
    ENDIF
    DXPDT=DYDX(1)
    TIMEA=T

    RETURN
    END

SUBROUTINE PYROBB(T,Y,DYDX)
Pyrolysis calculations for the first time step after pyrolysis
starts
    IMPLICIT REAL*8(A-H,O-Z)
    PARAMETER (NPAR=2000)
    COMMON/PYRLVR/TEMP1(NPAR),TDDOT(NPAR)
    COMMON/DATA/GAMAC,GAMAV,CPC,CPV,ALPC,ALPV,TKC,TKV,CPG,
        TP,T0,HTPYRL,SITP
    COMMON/HT/X(1:NPAR+1),DX(NPAR),EL
    COMMON/FLUXET/QRCL,QLDLCL,QCLCL,EMDLCL,TEMPER
    COMMON/HPCOMN/M
    COMMON/HPCOMN1/XD1,XD2,DT,USE1,USE2
    COMMON/DEX/DXPDT
    COMMON/AV/TIMEA
    COMMON/CASEA/KCHAR
    Virgin layer equations for pyrolysis process
    SITP--The difference between pyrolysis temperature and the
    ambient temperature
    REAL*8 DYDX(M),Y(M),EMD(10),LT,NE

```

```

C
C
C
C
C
C
ALPCA=ALPC
IF (KCHAR.EQ.2) THEN
  TEMPER=TP
ELSE
  TEMPER=Y(2)*SITP+SITP+T0
ENDIF
IF (TEMPER.LE.0.) TEMPER=0.
TKCA=TKC
DO 10 K=1,10
  IF (K.GE.3) THEN
    IF (EMDLCL.NE.0) THEN
      print*, emdkew, 2.*emd(k-1), emd(k-2), emdlcl
      EMDNEW=EMD(K-1)+(EMDLCL-EMD(K-1))*(EMD(K-1)-EMD(K-2))/
        (2.*EMD(K-1)-EMD(K-2)-EMDLCL)
    ENDIF
    IF (EMDNEW.GT.0.0) EMDLCL=EMDNEW
  ENDIF
  EMD(K)=EMDLCL
  CALL QFLUX(T,Y,Q0,DQ)
  IF (Q0.LT.0) THEN
    PAUSE'The external heat flux equals the reradiation loss'
    Q0=0.
  ENDIF
  IF (2.*(EL-Y(1))/Y(3).GE.86.) THEN
    C3=- (1.+HTPYRL/(CPV*SITP))+2.*(1.+2.*HTPYRL/(CPV*SITP))
    C4=2.*(1.+2.*HTPYRL/(CPV*SITP))-4.*(1.+HTPYRL/(CPV*SITP))
    C5=C4/C3*Q0/(SITP*CPV*GAMAV)+2.*ALPV/(C3*Y(3))*(1.+
      HTPYRL/(CPV*SITP))
    DE=(1.+3.*HTPYRL/(CPV*SITP))/3.
    DYDX(1)=(Q0/(GAMAV*CPV*SITP)-2.*ALPV/(3.*Y(3)))/DE
    DYDX(2)=(-C5+Q0/(SITP*GAMAV*CPV))/(1.+HTPYRL/(CPV*SITP))
    DYDX(3)=C4*Q0/(C3*GAMAV*CPV*SITP)+2.*ALPV*(1.+HTPYRL/
      (CPV*SITP))/(Y(3))*(1.+3.*HTPYRL/(CPV*SITP))
  ELSE
    C3=(1.+HTPYRL/(CPV*SITP)-EXP(-(EL-Y(1))/Y(3)))*(-1.+
      EXP(-2.*(EL-Y(1))/Y(3))+2.*(EL-Y(1))/Y(3))*

```

```

$      EXP(-2.*(EL-Y(1))/Y(3))-2.*(-1.+EXP(-(EL-Y(1))/Y(3)))+(
$      (EL-Y(1))/Y(3)*EXP(-(EL-Y(1))/Y(3)))*(1.+2.*HTPYRL/
$      (CPV*SITP)-EXP(-2.*(EL-Y(1))/Y(3)))
$      C4=2.*(1.+2.*HTPYRL/(CPV*SITP)-EXP(-2.*(EL-Y(1))/Y(3)))-4.*
$      (1.+HTPYRL/(CPV*SITP))-EXP(-(EL-Y(1))/Y(3)))
$      C5=C4/C3*Q0/(SITP*GAMAV*CPV)+1./C3*2.*ALPV/Y(3)*
$      (1.-EXP(-2.*(EL-Y(1))/Y(3)))*(1.+HTPYRL/(CPV*SITP)-
$      EXP(-(EL-Y(1))/Y(3)))
$      DE=1.+HTPYRL/(CPV*SITP)-EXP(-(EL-Y(1))/Y(3))
$      NE=-1.+EXP(-(EL-Y(1))/Y(3))+(EL-Y(1))/Y(3)
$      *EXP(-(EL-Y(1))/Y(3))
$      LT=2.*ALPV/(C3*Y(3))*(1.-EXP(-2.*(EL-Y(1))/Y(3)))*
$      (1.+HTPYRL/(CPV*SITP)-EXP(-(EL-Y(1))/Y(3)))
$      DYDX(3)=C4*Q0/(C3*GAMAV*CPV*SITP)+LT
$      DYDX(1)=(Q0/(GAMAV*CPV*SITP)+NE*(LT+C4/C3*Q0/
$      (CPV*SITP*GAMAV)))/DE
$      CLT*NE/(C4*NE/C3+1.)/
$      (DE/(C4*NE/C3+1.))
$      ENDIF
$      EMD1=DYDX(1)*(GAMAV-GAMAC)
$      IF(EMD1.LE.0) EMD1=0.
$      IF(EMDLCL*.05.GT.ABS(EMD1-EMDLCL)) GOTO 20
$      EMDLCL=EMD1
$      CONTINUE
$      EMDLCL=EMD1
$      DXPDY=DYDX(1)
$      TIMEA=T
$      RETURN
$      END

```

10  
20

C



CHANGE PRMT(5) TO NON-ZERO BY MEANS OF SUBROUTINE  
 OUTP. FURTHER COMPONENTS OF VECTOR PRMT ARE  
 FEASIBLE IF ITS DIMENSION IS DEFINED GREATER  
 THAN 1. IF HPCG DOES NOT REQUIRE  
 THESE VALUES THEY MAY BE USEFUL  
 FOR HANDING RESULT VALUES TO THE MAIN PROGRAM  
 (CALLING HPCG) WHICH ARE OBTAINED BY SPECIAL  
 MANIPULATIONS WITH OUTPUT DATA IN SUBROUTINE OUTP.

Y - INPUT VECTOR OF INITIAL VALUES. (DESTROYED)  
 LATERON Y IS THE RESULTING VECTOR OF DEPENDENT  
 VARIABLES COMPUTED AT INTERMEDIATE POINTS X.

DERY - INPUT VECTOR OF ERROR WEIGHTS. (DESTROYED)  
 THE SUM OF ITS COMPONENTS MUST BE EQUAL TO 1.  
 LATERON DERY IS THE VECTOR OF DERIVATIVES, WHICH  
 BELONG TO FUNCTION VALUES Y AT A POINT X.

NDIM - AN INPUT VALUE, WHICH SPECIFIES THE NUMBER OF  
 EQUATIONS IN THE SYSTEM.

IHLF - AN OUTPUT VALUE, WHICH SPECIFIES THE NUMBER OF  
 BISECTIONS OF THE INITIAL INCREMENT. IF IHLF GETS  
 GREATER THAN 10, SUBROUTINE HPCG RETURNS WITH  
 ERROR MESSAGE IHLF=11 INTO MAIN PROGRAM.  
 ERROR MESSAGE IHLF=12 OR IHLF=13 APPEARS IN CASE  
 PRMT(3)=0 OR IN CASE SIGN(PRMT(3)).NE.SIGN(PRMT(2)) -  
 PRMT(1)) RESPECTIVELY.

FCT - THE NAME OF AN EXTERNAL SUBROUTINE USED. IT  
 COMPUTES THE RIGHT HAND SIDES DERY OF THE SYSTEM  
 TO GIVEN VALUES OF X AND Y. ITS PARAMETER LIST  
 MUST BE X,Y,DERY. THE SUBROUTINE SHOULD NOT  
 DESTROY X AND Y.

OUTP - THE NAME OF AN EXTERNAL OUTPUT SUBROUTINE USED.  
 ITS PARAMETER LIST MUST BE X,Y,DERY,IHLF,NDIM,PRMT.  
 NONE OF THESE PARAMETERS (EXCEPT, IF NECESSARY,  
 PRMT(4),PRMT(5),...) SHOULD BE CHANGED BY  
 SUBROUTINE OUTP. IF PRMT(5) IS CHANGED TO NON-ZERO,  
 SUBROUTINE HPCG IS TERMINATED.

AUX - AN AUXILIARY STORAGE ARRAY WITH 16 ROWS AND NDIM



SUBROUTINE HPCG(PRMT,Y,DERY,NDIM,IHLF,FCT,OUTP,AUX)  
implicit real\*8(a-h,o-z)

C  
C

dimension PRMT(1),Y(1),DERY(1),AUX(16,1)  
N=1

IHLF=0

X=PRMT(1)

H=PRMT(3)

PRMT(5)=0.

do 1 I=1,NDIM

AUX(16,I)=0.

AUX(15,I)=DERY(I)

1 AUX(1,I)=Y(I)

IF(H\*(PRMT(2)-X))3,2,4

C  
C

ERROR RETURNS

2 IHLF=12

GOTO 4

3 IHLF=13

C  
C

COMPUTATION OF DERY FOR STARTING VALUES

4 CALL FCT(X,Y,DERY)

C  
C

RECORDING OF STARTING VALUES

CALL OUTP(X,Y,DERY,IHLF,NDIM,PRMT)

IF(PRMT(5))6,5,6

5 IF(IHLF)7,7,6

6 RETURN

7 DO 8 I=1,NDIM

8 AUX(8,I)=DERY(I)

C  
C

COMPUTATION OF AUX(2,I)

ISW=1

GOTO 100

C



```

9 X=X+H
DO 10 I=1,NDIM
10 AUX(2,I)=Y(I)
C
C          FUNCTION H IS TESTED BY MEANS OF BISECTION
11 IHLF=IHLF+1
X=X-H
DO 12 I=1,NDIM
12 AUX(4,I)=AUX(2,I)
H=.5*H
N=1
ISW=2
GOTO 100
C
13 X=X+H
CALL FCT(X,Y,DERY)
N=2
DO 14 I=1,NDIM
AUX(2,I)=Y(I)
14 AUX(9,I)=DERY(I)
ISW=3
GOTO 100
C
C          COMPUTATION OF TEST VALUE DELT
15 DELT=0.
DO 16 I=1,NDIM
16 DELT=DELT+AUX(15,I)*ABS(Y(I)-AUX(4,I))
DELT=.066666667*DELT
IF(DELT-PRMT(4))19,19,17
17 IF(IHLF-10)11,18,18
C
C          NO SATISFACTORY ACCURACY AFTER 10 BISECTIONS. ERROR MESSAGE.
18 IHLF=11
X=X+H
GOTO 4
C

```

C        THERE IS SATISFACTORY ACCURACY AFTER LESS THAN 11 BISECTIONS.

```

19 X=X+H
   CALL FCT(X,Y,DERY)
   DO 20 I=1,NDIM
     AUX(3,I)=Y(I)
20  AUX(10,I)=DERY(I)
   N=3
   ISW=4
   GOTO 100

```

C

```

21 N=1
   X=X+H
   CALL FCT(X,Y,DERY)
   X=PRMT(1)
   DO 22 I=1,NDIM
     AUX(11,I)=DERY(I)
22  Y(I)=AUX(1,I)+H*(.375*AUX(8,I)+.7916667*AUX(9,I)
      1-.2083333*AUX(10,I)+.04166667*DERY(I))
23 X=X+H
   N=N+1

```

```

   CALL FCT(X,Y,DERY)
   CALL OUTP(X,Y,DERY,IHLF,NDIM,PRMT)
   IF (PRMT(5)) 6,24,6

```

```

24 IF (N-4) 25,200,200
25 DO 26 I=1,NDIM
   AUX(N,I)=Y(I)
26 AUX(N+7,I)=DERY(I)
   IF (N-3) 27,29,200

```

C

```

27 DO 28 I=1,NDIM
   DELT=AUX(9,I)+AUX(9,I)
   DELT=DELT+DELT
28 Y(I)=AUX(1,I)+.3333333*H*(AUX(8,I)+DELT+AUX(10,I))
   GOTO 23

```

C

```

29 DO 30 I=1,NDIM

```

```

DELT=AUX(9,I)+AUX(10,I)
DELT=DELT+DELT+DELT
      CALL FCT(X,Y,DERY)
      GOTO 23
C
C
C *****
C THE FOLLOWING PART OF SUBROUTINE HPCG COMPUTES BY MEANS OF
C RUNGE-KUTTA METHOD STARTING VALUES FOR THE NOT SELF-STARTING
C PREDICTOR-CORRECTOR METHOD.
      DO 101 I=1,NDIM
        Z=H*AUX(N+7,I)
        AUX(5,I)=Z
        101 Y(I)=AUX(N,I)+.4*Z
      Z IS AN AUXILIARY STORAGE LOCATION
C
C
      Z=X+.4*H
      CALL FCT(X,Y,DERY)
      DO 102 I=1,NDIM
        Z=H*DERY(I)
        AUX(6,I)=Z
        102 Y(I)=AUX(N,I)+.2969776*AUX(5,I)+.1587596*Z
C
      Z=X+.4557372*H
      CALL FCT(X,Y,DERY)
      DO 103 I=1,NDIM
        Z=H*DERY(I)
        AUX(7,I)=Z
        103 Y(I)=AUX(N,I)+.2181004*AUX(5,I)-3.050965*AUX(6,I)+3.832865*Z
C
      Z=X+H
      CALL FCT(X,Y,DERY)
      DO 104 I=1,NDIM
        104 OY(I)=AUX(N,I)+.1747603*AUX(5,I)-.5514807*AUX(6,I)
        1+.205536*AUX(7,I)+.1711848*H*DERY(I)
      GOTO(9,13,15,21),ISW

```



```

C
C
C DERIVATIVE OF MODIFIED PREDICTOR IS GENERATED IN DERY
C
DO 208 I=1,NDIM
    DERY(I)=AUX(N-3,I)+3.*H*(DERY(I)+AUX(N+6,I)+
    &AUX(N+5,I))-AUX(N+4,I))
    Y(I)=AUX(16,I)-DELT
208 Y(I)=DELT+.07438017*AUX(16,I)
C
C TEST WHETHER H MUST BE HALVED OR DOUBLED
C
DELT=0.
DO 209 I=1,NDIM
    DELT=DELT+AUX(15,I)*ABS(AUX(16,I))
    IF(DELT-PRMT(4))210,222,222
C
C H MUST NOT BE HALVED. THAT MEANS Y(I) ARE GOOD.
C
210 CALL FCT(X,Y,DERY)
    CALL OUTP(X,Y,DERY,IHLF,NDIM,PRMT)
    IF(PRMT(5))212,211,212
211 IF(IHLF-11)213,212,212
212 RETURN
213 IF(H*(X-PRMT(2)))214,212,212
214 IF(ABS(X-PRMT(2))-.1*ABS(H))212,215,215
215 IF(DELT-.02*PRMT(4))216,216,201
C
C
C H COULD BE DOUBLED IF ALL NECESSARY PRECEDING VALUES ARE
C AVAILABLE
C
216 IF(IHLF)201,201,217
217 IF(N-7)201,218,218
218 IF(ISTEP-4)201,219,219
219 IMOD=ISTEP/2
    IF(ISTEP-IMOD-IMOD)201,220,201
220 H=H+H
    IHLF=IHLF-1
    ISTEP=0
    DO 221 I=1,NDIM

```

```

AUX(N-1,I)=AUX(N-2,I)
AUX(N-2,I)=AUX(N-4,I)
X(N-3,I)=AUX(N-6,I)
X(N-6,I)=AUX(N-15,I)
X(N-5,I)=AUX(N-3,I)
X(N-4,I)=AUX(N-1,I)
DELT=AUX(N+6,I)+AUX(N+5,I)
DELT=DELT+DELT+DELT
2210AUX(16,I)=8.962963*(Y(I)-AUX(N-3,I))-3.361111*H*(DERY(I)+DELT
1+AUX(N+4,I))
GOTO 201

C
C
C H MUST BE HALVED
222 IHLF=IHLF+1
IF(IHLF-10)223,223,210
223 H=.5*H
ISTEP=0
DO 224 I=1,NDIM
OY(I)=.00390625*(80.*AUX(N-1,I)+135.*AUX(N-2,I)+40.*AUX(N-3,I)+
1AUX(N-4,I))-1171875*(AUX(N+6,I)-6.*AUX(N+5,I)-AUX(N+4,I))*H
OAX(N-4,I)=.00390625*(12.*AUX(N-1,I)+135.*AUX(N-2,I)+
1108.*AUX(N-3,I)+AUX(N-4,I))-0234375*(AUX(N+6,I)+18.*AUX(N+5,I)-
29.*AUX(N+4,I))*H
AUX(N-3,I)=AUX(N-2,I)
224 AUX(N+4,I)=AUX(N+5,I)
X=X-H
DELT=X-(H+H)
CALL FCT(X,Y,DERY)
DO 225 I=1,NDIM
AUX(N-2,I)=Y(I)
AUX(N+5,I)=DERY(I)
225 Y(I)=AUX(N-4,I)
DELT=DELT-(H+H)
CALL FCT(X,Y,DERY)
DO 226 I=1,NDIM

```

C:\FLAME-S\HFS\HFSSPV70.F

```
DELT=AUX(N+5,I)+AUX(N+4,I)
DELT=DELT+DELT+DELT
      AUX(N+3,I)=DERY(I)
      GOTO 206
END
SUBROUTINE OUTPG(PRMT,NDIM,IHLF,ISTEP,X,Y,TY)
  continue
  return
end
```

7, 0.28963194E01,0.15154866E-02,-0.57235277E-06,0.99807393E-10,-0.65223555E-14,  
0.36748261E01,-0.12081500E-02,0.23240102E-05,-0.63217559E-09,-0.22577253E-12,  
0.36219535E01,0.73618264E-03,-0.19652228E-06,0.36201558E-10,-0.28945627E-14,  
0.36255985E01,-0.18782184E-02,0.70554544E-05,-0.67635137E-08,0.21555993E-11,  
0.42948342E+1,0.19538024E-1,0.32109452E-5,-0.84809778E-8,0.24872618E-11,  
0.74188008E00,0.26778804E-1,0.78425850E-5,-0.25901330E-7,0.11588147E-10,  
0.44608041E01,0.30981719E-02,-0.12392571E-05,0.22741325E-09,-0.15525954E-13,  
0.24007797E01,0.87350957E-02,-0.66070878E-05,0.20021861E-08,0.63274039E-15,  
0.27167633E01,0.29451374E-02,-0.80224374E-06,0.10226682E-09,-0.48472145E-14,  
0.40701275E01,-0.11084499E-02,0.41521180E-05,-0.29637404E-08,0.80702103E-12,  
0.29840696E01,0.14891390E-02,-0.57899684E-06,0.10364577E-09,-0.69353550E-14,  
0.37100928E01,-0.16190964E-02,0.36923594E-05,-0.20319674E-08,0.23953344E-12,  
0.31001901E01,0.51119464E-03,0.52644210E-07,-0.34909973E-10,0.36945345E-14,  
0.30574451E01,0.26765200E-02,-0.58099162E-05,0.55210391E-08,-0.18122739E-11,  
0.,0.,-2.3545E3,-8945.93,-13438.01,-3948.25,0.,  
0.0,0.,1,0.0,0.0,0.0,0.,  
0.79,0.21,0.0,0.0,0.0,0.0,0.0,  
0.663e-3,15.58,1,0.3,4.645e04,1,298.,1.23,10,0.38,1,  
1.800,  
298.,298.,  
3,8,3.76,44.,0.0632,

# Propane (C3H8) Pool Fire Input File

## Nomenclature

Line 1:

The number of components counted in reaction/production gas.

Line 2-Line 15:



The polynomial coefficients of specific heats of the chemical components (kJ/kmol).W  
The even lines are the coefficients used when temperature  $\leq 3000$  C and  
The odd lines are those for temperature  $> 3000$  C for each species.

There are seven (7) components in this input. The order of these components  
are: 1) N<sub>2</sub>, 2) O<sub>2</sub>, 3) Fuel (e.g. CH<sub>4</sub>, C<sub>3</sub>H<sub>8</sub>), 4) CO<sub>2</sub>, 5) H<sub>2</sub>O, 6) CO and 7) H<sub>2</sub>.

Line 16:

The standard heats of formation of each component (kJ/kmol).

Line 17:

The composition of the initial fuel (mass fraction).

Line 18:

The composition of the ambient oxidizer (mass fraction).

Line 19:

The initial fuel flow rate, stoichiometric air/fuel ratio (mass based),  
the combustion efficiency, the total radiation fraction of the fuel,  
the heat of combustion of the fuel (J/kg), the ambient air specific heat  
(kJ/kg.K), the ambient air temperature (K), ambient air density (kg/m<sup>3</sup>),  
the height of the flame (not used now), the diameter of the pool diameter  
(or jet flame nozzle, m), the height interval for calculation (m)

Line 20:

Initial fuel density (kg/m<sup>3</sup>)

Line 21:

Ambient temperature (K), initial fuel temperature (K)

Line 22:

Number of hydrogen (H) atoms, number of carbon (C) atoms, the N<sub>2</sub>/O<sub>2</sub>  
ratio in the air (3.76 usually), molecular weight of the fuel (kg/kmol),  
stoichiometric fuel mixture fraction.

7, 0.28963194E01,0.15154866E-02,-0.57235277E-06,0.99807393E-10,-0.65223555E-14,  
0.36748261E01,-0.12081500E-02,0.23240102E-05,-0.63217559E-09,-0.22577253E-12,  
0.36219535E01,0.73618264E-03,-0.19652228E-06,0.36201558E-10,-0.28945627E-14,  
0.36255985E01,-0.18782184E-02,0.70554544E-05,-0.67635137E-08,0.21555993E-11,  
0.42948342E+1,0.19538024E-1,0.32109452E-5,-0.84809778E-8,0.24872618E-11,  
0.74188008E00,0.26778804E-1,0.78425850E-5,-0.25901330E-7,0.11588147E-10,  
0.44608041E01,0.30981719E-02,-0.12392571E-05,0.22741325E-09,-0.15525954E-13,  
0.24007797E01,0.87350957E-02,-0.66070878E-05,0.20021861E-08,0.63274039E-15,  
0.27167633E01,0.29451374E-02,-0.80224374E-06,0.10226682E-09,-0.48472145E-14,  
0.40701275E01,-0.11084499E-02,0.41521180E-05,-0.29637404E-08,0.80702103E-12,  
0.29840696E01,0.14891390E-02,-0.57899684E-06,0.10364577E-09,-0.69353550E-14,  
0.37100928E01,-0.16190964E-02,0.36923594E-05,-0.20319674E-08,0.23953344E-12,  
0.31001901E01,0.51119464E-03,0.52644210E-07,-0.34909973E-10,0.36945345E-14,  
0.30574451E01,0.26765200E-02,-0.58099162E-05,0.55210391E-08,-0.18122739E-11,  
0.,0.,-2.3545E3,-8945.93,-13438.01,-3948.25,0.,  
0.0,0.,1.,0.0,0.0,0.0,0.0,  
0.79,0.21,0.0,0.0,0.0,0.0,0.0,  
0.663e-3,15.58,1.,0.3,4.645e04,1.,298.,1.23,10.,0.0127,1,  
1.800,  
298.,298.,  
3,8,3.76,44.,0.0632,  
388.117,30706.3,3028.11,-12242.5,24544.,-23323.3,8319.02,

Propane (C3H8) Jet Flame Input File

Nomenclature

Line 1:

The number of components counted in reaction/production gas.

Line 2-Line 15:

The polynomial coefficients of specific heats of the chemical components (kJ/kmol). W  
The even lines are the coefficients used when temperature  $\leq 3000$  C and  
The odd lines are those for temperature  $> 3000$  C for each species.

There are seven (7) components in this input. The order of these components  
are: 1) N<sub>2</sub>, 2) O<sub>2</sub>, 3) Fuel (e.g. CH<sub>4</sub>, C<sub>3</sub>H<sub>8</sub>), 4) CO<sub>2</sub>, 5) H<sub>2</sub>O, 6) CO and 7) H<sub>2</sub>.

Line 16:

The standard heats of formation of each component (kJ/kmol).

Line 17:

The composition of the initial fuel (mass fraction).

Line 18:

The composition of the ambient oxidizer (mass fraction).

Line 19:

The initial fuel flow rate, stoichiometric air/fuel ratio (mass based),  
the combustion efficiency, the total radiation fraction of the fuel,  
the heat of combustion of the fuel (J/kg), the ambient air specific heat  
(kJ/kg.K), the ambient air temperature (K), ambient air density (kg/m<sup>3</sup>),  
the height of the flame (not used now), the diameter of the jet flame nozzle  
(or pool diameter, m), the height interval for calculation (m)

Line 20:

Initial fuel density (kg/m<sup>3</sup>)

Line 21:

Ambient temperature (K), initial fuel temperature (K)

Line 22:

Number of hydrogen (H) atoms, number of carbon (C) atoms, the N<sub>2</sub>/O<sub>2</sub>  
ratio in the air (3.76 usually), molecular weight of the fuel (kg/kmol),  
stoichiometric fuel mixture fraction.

```

C 10/11/91, calculating the radiation at different height, using
C a simplified model (do not do temperature^4 calculation for radiation)
C 3/9/93, modification, calculation of CO yield when (1-alpha)T_ad
C (adiabatic temperature at stoichiometric condition)
C 5/7/93 Apply the combustion model to a pool fire. The entrainment
C Correlation have to be changed to accomodate the diameter of the pool.
C 9/3/93 Change the fluctuation correlation since the original
C fluctuation is too high and we use a simple fluctuation correlation
C psi''/psi bar(1-pai bar)
PARAMETER (NPAR=64,NPAR1=1000)
IMPLICIT REAL*8(A-H,O-Z)

REAL*8 A(NPAR,5),B(NPAR,5),DELH(NPAR),TB,
$ YMASSF(NPAR),YI(NPAR),YO(NPAR),
$ emtot1,s,chia,chir,hitcomb,tinf,gamag
REAL*8 bbi(NPAR1),tei(NPAR1),siti(NPAR1),cosci(NPAR1),
$ ymcoi(NPAR1),qchzi(NPAR1),ycoci(NPAR1),RE(NPAR1),
$ summ(npar1),UCI(NPAR1)
COMMON/BASIS/A,B,DELH
COMMON/NOCOMP/N
COMMON/COMP/YMASSF
COMMON/INIT/DELH0,DELHB
COMMON/STOICH/YN2S,YCO2S,YH2OS,CS
COMMON/COSS/COSM
COMMON/AMB/TA
COMMON/FLOW1/SIT
COMMON/FLOW2/COSC
COMMON/CONCC/emtot1,s,chia,chir,hitcomb,cpga,tinf,gamag,ACO
COMMON/RAD/TL
COMMON/OUT/RHS1
COMMON/TOT/CONS,FLH
COMMON/VOL/UC20,UC21,UC22,UC23
COMMON/IC/IFLAG1
COMMON/COE/A1,A2,A3,ZM1,ZM2
COMMON/RT/QCHZ
COMMON/FI/TE2,UC,TE1,RHOC

```

```

COMMON/RQ/QCHT
COMMON/ACOMP/NN,MM,WMF
COMMON/INDEC/ICOUNT
EXTERNAL HOME1,HOME,FX,VOL1,VOL3,VOCO,QRR,CALTE,HOME2
OPEN (2,FILE='combb.dat',status='old')
READ (2,*) N
DO 100 I=1,N
  READ (2,*) (A(I,J),J=1,5)
  READ (2,*) (B(I,J),J=1,5)
100 CONTINUE
  READ (2,*) (DELH(I),I=1,N)
  READ (2,*) (YI(I),I=1,N)
  READ (2,*) (YO(I),I=1,N)
  READ (2,*) emtot1,s,chia,chir,htcomb,cpga,tinf,gamag,h,DS,DZ
  READ (2,*) PHS
  READ (2,*) TA,TB
  READ(2,*) NN,MM,AK,WMF,CS
  CLOSE(2)

  DEM=WMF+(NN+MM/4.)*(32+28*AK)
  YN2S=(NN+MM/4.)*AK*28./DEM
  YCO2S=NN*44/DEM
  YH2OS=MM/2.*18./DEM
C   Calculate the adiabatic temperature at stoichiometric condition
  PRINT*,YN2S,YCO2S,YH2OS
C   di=(emtot1/(0.785*gamag*voi))*0.5
  VOI=EMTOT1/(PHS*0.785*DS**2)
  UC20=VOI**2
  DO 110 I=1,N
    YMASSF(I)=YO(I)
110 CONTINUE
    CALL CALHT0(TA,DELH0)
    DO 115 I=1,N
      YMASSF(I)=YI(I)
115 CONTINUE
      CALL CALHT0(TB,DELHB)

```

```

OPEN (11,FILE='pool2.dat',status='unknown')
OPEN (21,FILE='pool3.dat',status='unknown')
SQTT=SQRT(HTCOMB/((S+1.)*CPGA*TA)*9.81*DS*(CHIA-CHIR))
C   SFRN, THE FROUDE NUMBER
SFRN=EMTOT1*HTCOMB/(GAMAG*HTCOMB*DS**2/(S+1.)*SQTT)
C   FLH, THE FLAME HEIGHT
FLH=(S+1.)*DS*(PHS/GAMAG)**0.5*13.5*SFRN**0.4/
C   $   (1.+0.07*SFRN**2)**0.2
IF (SFRN.LE.8.6E-3) THEN
  FLH=1.35E4*SFRN**2*DS
ELSE IF(SFRN.GT.7.44E-2) THEN
  FLH=12.52*SFRN**0.4*DS
ELSE
  FLH=22.54*SFRN**0.6667*DS
ENDIF
C   Calculate the integral of  $f(Z/Lf)$ 
AA=0.
BB=1.
FLH=1.2
C   CALL QGAUS1(HOME,AA,BB,CONS)
Z=0.1
FMO=EMTOT1*VOI
C9/21/93
A1=0.086*(S+1.)*EMTOT1/(SFRN*DS**0.5)
A1=0.04*(S+1.)*EMTOT1/(SFRN*DS**0.5)
A2=0.093*(S+1.)*EMTOT1/(SFRN*DS**1.5)
A3=0.018*(S+1.)*EMTOT1/(SFRN*DS**2.5)
C   PLEN=(FMO*CPGA*(S+1.)*TINF/(GAMAG*9.81*HTCOMB*(CHIA-
C   $   CHIR)))*0.3333
QCHT=DELHB*EMTOT1
AA=0.1
BB=FLH
IFLAG1=1
Cc   CALL QGAUS10(FX,AA,BB,TE)
Cc   CSM=(CHIR*CHIA*EMTOT1*HTCOMB)**4/(4.*TE)
TEO=0.

```

```

AA=0.
BB=AA+0.001
sum=0.
i=1
C  Calculate the velocity*2 at ZM1 and ZM2 locations
    ZM1=(A1/A2)
    ZM2=(A2/A3)
    ACO=A1
    SIT=ACO*(ZM1)**0.5+EMTOT1
    COSC=2.*EMTOT1/SIT
C9/21/93    COSC=4.*EMTOT1*(1.-EXP(-4.))/SIT
    IF (COSC.GT.1.) GOTO 116
    AI=(EMTOT1/A1)**2.
    UC21=UC20
    FV1=0.
C    IF(ZM1.GT.DS) THEN
C        CALL QGAUS3(HOME1,AI,DS,FV1)
C        UCZD=(ACO*(AI)**0.5+EMTOT1)**2*(UC21/(ACO*
C            (ZM1)**0.5+EMTOT1)**2)+FV1/(ACO*(ZM1)
C            **0.5+EMTOT1)**2
C        UCZ=4.*UCZD
C        CALL QGAUS3(HOME1,DS,ZM1,FV1)
C        UC22=(ACO*(AI)**0.5+EMTOT1)**2*(UCZ/(ACO*
C            (ZM1)**0.5+EMTOT1)**2)+FV1/(ACO*(ZM1)
C            **0.5+EMTOT1)**2
C        ELSE
C            CALL QGAUS3(HOME1,AI,ZM1,FV1)
C            UC22=(ACO*(AI)**0.5+EMTOT1)**2*(UC21/(ACO*
C                (ZM1)**0.5+EMTOT1)**2)+FV1/(ACO*(ZM1)
C                **0.5+EMTOT1)**2
C9/21/93    UC22=4.*UC22
116    ACO=A2
        AI=ZM1
    IF(COSC.GT.1.) THEN
        AI=(EMTOT1/A2)**0.6667
        UC22=4.*UC20

```

```

ENDIF
SIT=ACO*(ZM2)**1.5+EMTOT1
IF(ZM2.LE.DS) THEN
C   COSC=4.*EMTOT1*(1.-EXP(-4.))/SIT
C   ELSE
C   COSC=2.*EMTOT1/SIT
C   ENDIF
FV1=0.
CALL QGAUS3(HOME2,AI,ZM2,FV1)
UC23=(ACO*(AI)**1.5+EMTOT1)**2*(UC22/(ACO*
$   (ZM2)**1.5+EMTOT1)**2)+FV1/(ACO*(ZM2)
$   **1.5+EMTOT1)**2
150  IFLAG1=1
OPEN(20,FILE='pro2.dat',status='unknown')
C   Calculate the total radiation losses
      CALL QGAUS(FX,AA,BB,TE)
CC  TEN=4.*CSM*TE
CC  TEO=TEO+TEN
C   Calculate the mass flow rate of the flame (psi_t)=entrainment rate +
C   mass burning rate (m_f), Delichatsios' correlations
      IF(BB.LT.ZM1) THEN
C   Close to the pool
          ICOUNT=1
          ACO=A1
          SIT=ACO*(BB)**0.5+EMTOT1
          ELSE IF (BB.GE.ZM2) THEN
C   Far field
          ICOUNT=2
          ACO=A3
          SIT=ACO*(BB)**2.5+EMTOT1
          ELSE
C   Neck-in area
          ICOUNT=3
          ACO=A2
          SIT=ACO*(BB)**1.5+EMTOT1
          ENDIF

```



```

AA1=0.
BB1=SIT
COSC=2.*EMTOT1/SIT
IF(COSC.GT.1.) GOTO 201
CALL CTEMP(COSC,TC)
call ctemp1(cosc,vlamda)
C WRITE (15,12) BB,COSC,TC,vlamda
12 FORMAT(4(2X,F14.4))
C GOTO 201
CALL QGAUS2(VOL1,AA1,BB1,QL)
C Calculate CO Production Rate
CALL QGAUS(VOCO,AA1,BB1,YMCO)
QCHZ=QCHT-QL
AA2=0.
BB2=COSC
CALL QGAUS3(QRR,AA2,BB2,RE1)
RE2=RE1*SIT/(RHOC*UC)
C Calculate CO at centerline
zc=0.
YCOC=VOCO(zc)
Cc ALL=1.-TEO**0.25/QCHZ
C Calculate the constant related to the smoke point heat release rate
C CSM=CHIA*CHIR*HTCOMB/TE
C PRINT*,bb,all,te,UC,'constant'
WRITE (20,200) BB,UC,RHOC,TE1,TE2
C WRITE(20,200) BB,ALL,SIT,TE,TE2,TCE,UC
C WRITE(11,200) BB,(1.-ALL),SIT,COSC,YMCO*1.0E3,QCHZ,YCOC
Cc WRITE(11,200) BB,SIT,COSC,YMCO*1.0E3,QCHZ,YCOC,TE
kcount=kcount+1
Cc if(bb.lt.zm) then
Cc sum1=sum1+te
Cc else
Cc sum2=sum2+te
Cc endif
sum=sum+te
UCI(KCOUNT)=UC

```

```

bbi(kcount)=bb
tei(kcount)=te
RE(KCOUNT)=RE2
siti(kcount)=sit
cosci(kcount)=csc
ymcoi(kcount)=ymco*1.0E3
qchzi(kcount)=qchz
ycoci(kcount)=ycoc
WRITE(21,200) BB,UC,(1.-ALL),SIT,RE2,YMCO*1.0E3,
$ QCHZ,COSC,TE,QCHZ/(EMTOT1*HTCOMB)
close(20)
200 FORMAT(F10.6,9(2X,E12.6))
CCC 201 IF(QCHZI(KCOUNT).GT.QCHZI(KCOUNT-1)) THEN
201 IF (BB.LT.FLH.AND.(FLH-BB)/FLH.GE.0.01) THEN
AA=BB
IF(AA.LE.0.2) THEN
BB=AA+0.001
ELSE
BB=AA+0.05
ENDIF
i=i+1
GOTO 150
ENDIF
Cc close(12)
C CLOSE(15)
C STOP
Cc CSM=(CHIR*CHIA*EMTOT1*HTCOMB)**4/(2.*sum1+4.*SUM2)
do 250 j=1,kcount
Cc if(bbi(j).lt.zm) then
Cc ten=2.*csm*tei(j)
Cc teo=teo+ten
Cc all=1.-teo**0.5/qchzi(j)
Cc else
TEN=4.*CSM*TEI(j)
TEO=TEO+TEN

```

```

C      ALL=1.-TEO**0.25/QCHZI(J)
      endif
      WRITE(11,200) BBI(J),UCI(J),(1.-ALL),SITI(J),RE(J),
$      YMCOI(J),QCHZI(J),COSCI(J),TEI(J),QCHZI(J)/
$      (EMTOT1*HTCOMB)
C      WRITE (11,210) SUM,CSM
C 210  FORMAT (E16.8,4X,E16.8)
C      BB=0.15
C      DO 250 J=1,I
C      BM(J)=CSM*BM(J)
C      WRITE(11,200) BB,BM(J)
C      BB=BB+0.02
250  continue
251  continue
252  format(f12.4,4x,F16.6)
      CLOSE(11)
      OPEN(21,FILE='radf.dat',status='unknown')
      SUM=0.
      DO 254 J=1,KCOUNT
      SUM=SUM+TEI(J)
      SUMM(J)=SUM
254  CONTINUE
      CSM=(CHIR*QCHZI(KCOUNT))/SUM**0.25
      WRITE(21,256) CSM
      DO 255 J=1,KCOUNT
      ALL1=SUMM(J)**0.25/QCHZI(J)*CSM
      WRITE (21,256) BBI(J),ALL1,CSM**4/4.*RE(J)/ALL1**3,QCHZI(J)/
$      (EMTOT1*HTCOMB)
255  CONTINUE
      CLOSE(21)
256  FORMAT(F12.4,3(2X,E16.6))
      STOP
      END

      FUNCTION FX(Z)

```

```

IMPLICIT REAL*8(A-H,O-Z)
COMMON/FLOW1/SIT
COMMON/FLOW2/COSC
COMMON/CONCC/emtot1,s,chia,chir,htcomb,cpga,tinf,gamag,ACO
COMMON/RAD/TL
COMMON/TOT/CONS,FLH
COMMON/VOL/UC20,UC21,UC22,UC23
COMMON/IC/IFLAG1
COMMON/COE/A1,A2,A3,ZM1,ZM2
COMMON/INIT/DELH0,DELHB
COMMON/RT/QCHZ
COMMON/FI/TE2,UC,TE1,RHOC
COMMON/RQ/QCHT
COMMON/INDEC/ICOUNT
COMMON/KCC/KC
EXTERNAL VOLI,QRR,HOME,HOME1,HOME2,VOLI3,HOME3
EPS=1.0E-3
CCC IF (IFLAG1.EQ.1) THEN
CCC   UC21=UC20
CCC   ACO=A1
CCC   AI=0.1+(EMTOT1)/A1
CCC   ZM=(A1/A2)**(0.6667)+0.1
CCC   AA=0.03/FLH
CCC   BB=(ZM-0.07)/FLH
CCC   SIT=ACO*(ZM-0.1)+EMTOT1
CCC   COSC=2.*EMTOT1/SIT
Cc   CALL QGAUS2(HOME,AA,BB,QR1)
Cc   TL=CHIR*EMTOT1*HTCOMB*QR1/CONS
C   RADP=ALPHA, TL-T0=ALPHA*(TL,ad-T0)
CCC   AMIN=0.
CCC   AX=1.
C   RADP=ZBRENT1(SEARA,AMIN,AX,EPS)
C   ALL=RADP
CCC   FV1=0.
CCC   CALL QGAUS3(HOME1,AI,ZM,FV1)
CCC   UC22=(A1*(AI-0.1)+EMTOT1)**2*(UC21/(ACO*

```

```

CCC $      (ZM-0.1)+EMTOT1)**2)+FV1/(A1*(ZM-0.1)+
CCC $      EMTOT1)**2
CCC      ENDIF
      UC=UC21**0.5
      BI=Z
      IF(Z.LT.ZM1) THEN
        ACO=A1
        SITI=ACO*(Z)**0.5+EMTOT1
        IF(2.*EMTOT1.GT.SITI) THEN
          C9/21/93  IF(4.*EMTOT1.GT.SITI*(1.-EXP(-4.))) THEN
            FX=0.
            GOTO 140
          ELSE
            KC=1
            GOTO 128
          ENDIF
        ELSE IF (Z.GE.ZM1.AND.Z.LT.ZM2) THEN
          ACO=A2
          SITI=ACO*(Z)**1.5+EMTOT1
          IF(2.*EMTOT1.GT.SITI) THEN
            FX=0.
            IS=1
            GOTO 140
          ELSE
            KC=2
            GOTO 128
          ENDIF
        ELSE
          ACO=A3
          SITI=ACO*(Z)**2.5+EMTOT1
          IF(2.*EMTOT1.GT.SITI) THEN
            FX=0.
            GOTO 140
          ELSE
            KC=3
            GOTO 128

```

```

      ENDIF
    ENDIF
128  CONTINUE
      AA=0.03/FLH
      BB=(Z-0.07)/FLH
      Cc CALL QGAUS2(HOME,AA,BB,QR)
      Cc TL=CHIR*EMTOT1*HTCOMB*QR/CONS
      C  RADP=ALPHA, TL-T0=ALPHA(TL,ad-T0)
      AMIN=0.
      AX=1.
      EPS=1.0E-3
      C  RADP=ZBRENT1(SEARA,AMIN,AX,EPS)
      C  ALL=RADP
      C  Calculate the centerline temperature at Z
      SIT=SITI
      C9/21/93 IF(Z.LT.ZM1) THEN
      C9/21/93   COSC=4.*EMTOT1/((1.-EXP(-4.))*SIT)
      C9/21/93 ELSE
      C9/21/93   COSC=2.*EMTOT1/SIT
      C9/21/93 ENDIF
      CALL CT(TCE)
      RHOC=1.2*298./TCE
      IF(KC.EQ.1) THEN
      C  KC equals 1, meaning close to the pool surface
      UC2=UC21
      AI=(EMTOT1/ACO)**2.
      FV1=0.
      CALL QGAUS3(HOME1,AI,BI,FV1)
      UC2=(ACO*(AI)**0.5+EMTOT1)**2*(UC21/(ACO*
$      (BI)**0.5+EMTOT1)**2)+FV1/(ACO*(BI
$      **0.5+EMTOT1)**2
      ELSE IF (KC.EQ.2) THEN
      C  KC equals 2, meaning around to the neck-in area
      UC2=UC22
      AI=ZM1
      IF(1S.EQ.1) THEN

```

```

AI=(EMTOT1/ACO)**0.6667
ENDIF
CALL QGAUS3(HOME2,AI,BI,FV1)
UC2=(ACO*(AI)**1.5+EMTOT1)**2*(UC2/(ACO*
$ (BI)**1.5+EMTOT1)**2)+FV1/(ACO*(BI)
$ **1.5+EMTOT1)**2
ELSE
C KC equals 3, meaning far field
AI=ZM2
UC2=UC23
CALL QGAUS3(HOME3,AI,BI,FV1)
UC2=(ACO*(AI)**2.5+EMTOT1)**2*(UC2/(ACO*
$ (BI)**2.5+EMTOT1)**2)+FV1/(ACO*(BI)
$ **2.5+EMTOT1)**2
ENDIF
UC=UC2**0.5
C The centerline velocity has been obtained
C Calculate the radiation losses at each location
SIT=SITI
C9/21/93 IF(Z.LT.ZM1) THEN
C9/21/93 COSC=4.*EMTOT1/((1.-EXP(-4.))*SIT)
C9/21/93 ELSE
COSC=2.*EMTOT1/SIT
C9/21/93 ENDIF
AA2=0.
BB2=1.
C ALL=RADP
C Calculate the integral of radiation
AA=0.
BB=SIT
CALL QGAUS3(VOLI,AA,BB,QL)
QCHZ=QCHT-QL
AA2=0.
BB2=COSC
ERRABS=0.

```

```

ERRREL=0.001
IRULE=2
C  CALL DQDAG(QRR,AA2,BB2,ERRABS,ERRREL,IRULE,TE1,ERREST)
CALL  QGAUS3(QRR,AA2,BB2,TE1)
TE2=TE1*SIT/(UC*RHOC)

C  if((1.-all).le.0.08) then
C    all=0.92
C  endif
C  TE2=TE1*SIT/((1.-ALL)**2*UC*RHOC)
Cc  if (icount.eq.1) then
Cc    fx=qchz*te2
Cc  else
Cc    FX=QCHZ**3*TE2
Cc  endif
140  IFLAG1=0

      RETURN
      END

      FUNCTION HOME(ZL)
      IMPLICIT REAL*8(A-H,O-Z)
      CALL REL(ZL,FCN)
      HOME=FCN

      RETURN
      END

      FUNCTION HOME1(Z2)
      IMPLICIT REAL*8(A-H,O-Z)

      EXTERNAL VOLII
      Common/CONCC/emtot1,s,chia,chir,hitcomb,cpga,tinf,gamag,aCO
      COMMON/FLOW1/SIT
      COMMON/FLOW2/COSC
      COMMON/COE/A1,A2,A3,ZM1,ZM2

```



```

SIT = A1*(Z2)**0.5 + EMTOT1
C9/21/93  COSC=4.*EMTOT1/((1.-EXP(-4.))*SIT)
COSC=2.*EMTOT1/SIT
IF(COSC.GT.1.) THEN
  HOME1=0.
  RETURN
ENDIF
AA=0.
BB=0.999*SIT
CALL QGAUS4(VOLI,AA,BB,TOT)
SCF=0.999*SIT
VO = VOLI(SCF)
HOME1=4*9.81*(SIT**2)*(tot+0.001*SIT*VO)
400  RETURN
      END

```

FUNCTION HOME2(Z2)

IMPLICIT REAL\*8(A-H,O-Z)

EXTERNAL VOLI2

Common/CONCC/emtot1,s,chia,chir,htcomb,cpga,tinf,gamag,aCO

COMMON/FLOW1/SIT

COMMON/FLOW2/COSC

COMMON/COE/A1,A2,A3,ZM1,ZM2

SIT = A2\*(Z2)\*\*1.5 + EMTOT1

COSC=2.\*EMTOT1/SIT

AA=0.

BB=0.999\*SIT

CALL QGAUS4(VOLI2,AA,BB,TOT)

SCF=0.999\*SIT

VO = VOLI2(SCF)

HOME2=4\*9.81\*(sit\*\*2)\*(tot+0.001\*SIT\*VO)

400 RETURN

END

```

FUNCTION HOME3(Z2)
  IMPLICIT REAL*8(A-H,O-Z)

  EXTERNAL VOLI2
  Common/CONCC/emtot1,s,chia,chir,htcomb,cpga,tinf,gamag,aCO
  COMMON/FLOW1/SIT
  COMMON/FLOW2/COSC
  COMMON/COE/A1,A2,A3,ZM1,ZM2
  SIT = A3*(Z2)**2.5 + EMTOT1
  COSC = 2.*EMTOT1/SIT
  AA = 0.
  BB = 0.999*SIT
  CALL QGAUS4(VOLI2,AA,BB,TOT)
  SCF = 0.999*SIT
  VO = VOLI2(SCF)
  HOME3 = 4*9.81*(sit**2)*(tot + 0.001*SIT*VO)
  400 RETURN
  END

SUBROUTINE REL(X,FCN)
  IMPLICIT REAL*8(A-H,O-Z)
  COMMON/TOT/CONS,FLH
  C Routine for the expressions of radiate loss versus height
  C X = X-0.05/FLH
  IF(X.LT.0) X = 0.
  IF (X.GT.0.387637) THEN
    FCN = -3.92171 + 28.685*X-54.3652*X**2 + 35.8018*X**3 -
    $ 5.92926*X**4
  ELSE
    FCN = -1.42573E-17 + 1.80933*X-21.1433*X**2
    $ + 141.767*X**3-212.667*X**4
  ENDIF

```

```

RETURN
END

SUBROUTINE CT(TCE)
  IMPLICIT REAL*8(A-H,O-Z)
  CALCULATE THE FLAME ENTHALPY AT HIGHT Z, MIXTURE FRACTION COSM
  PARAMETER(NPAR=64)
  REAL*8 YMASS(NPAR), DELH(NPAR), A(NPAR,5), B(NPAR,5)
  Common/CONCC/emtot1,s,chia,chir,htcomb,cpga,tinf,gamag,aCO
  COMMON/ROOT/ALL
  COMMON/AMB/TA
  COMMON/FLOW1/SIT
  COMMON/FLOW2/COSC
  COMMON/COMP/YMASSF
  COMMON/NOCOMP/N
  COMMON/INIT/DELH0,DELHB
  COMMON/BASIS/A,B,DELH
  EXTERNAL CALTE
  EPS=1.0E-2
  COSM=COSC
  C   VLAMDA=(1.-COSM)/(0.16*(1.31*COSC-COSM))
  C   VLAMDA=8.09
  C   VLAMDA=(1.-COSM+3.*0.16*(5.*COSC-COSM))/(0.16*
  C     $ (5.*COSC-COSM))
  C   VLAMDA=(1.-COSM+1.*4.5*(1.4*COSC-COSM))/(4.5*
  C     $ (1.4*COSC-COSM))-1.
  C 9/3/93
  IF(COSM.LE.0.068) THEN
    VLAMDA=(1.-COSM)/(1.5*COSM)-1.
  ELSE
    VLAMDA=8.09
  ENDIF
  CALL ENTHA2(COSM,VLAMDA,TCE)
  RETURN
END

```

```

FUNCTION QRR(SF)
IMPLICIT REAL*8(A-H,O-Z)
C  CALCULATE THE FLAME ENTHALPY AT HIGHT Z, MIXTURE FRACTION COSM
PARAMETER(NPAR=64)
REAL*8 YMASSF(NPAR),DELH(NPAR),A(NPAR,5),B(NPAR,5)
Common/CONCC/emtot1,s,chia,chir,hicomb,cpga,tinf,gamag,aCO
COMMON/STOICH/YN2S,YCO2S,YH2OS,CS
COMMON/ROOT/ALL
COMMON/AMB/TA
COMMON/FLOW1/SIT
COMMON/FLOW2/COSC
COMMON/COMP/YMASSF
COMMON/NOCOMP/N
COMMON/INIT/DELH0,DELHB
COMMON/BASIS/A,B,DELH
EXTERNAL CALTE
EPS=1.0E-2
TMAX=5000.
TMIN=298.
COSM=SF
C  VLAMDA=(1.-COSM+3.*0.16*(5.*COSC-COSM))/(0.16*
C  $ (5.*COSC-COSM))
VLAMDA=(1.-COSM+1.*4.5*(1.4*COSC-COSM))/(4.5*
$ (1.4*COSC-COSM))-1.
C  9/3/93
IF(COSM.LE.0.068) THEN
VLAMDA=(1.-COSM)/(1.5*COSM)-1.
ELSE
VLAMDA=8.09
ENDIF
IF(VLAMDA.LT.0.) VLAMDA=0.
VN=VLAMDA*COSM
VM=VLAMDA*(1.-COSM)
GLAMDA=GAMMLN(VLAMDA)

```

```

GN=GAMMLN(VN)
GM=GAMMLN(VM)
DIV1=GLAMDA-GN-GM
DIV=EXP(DIV1)
PO1=1.-VN
PO2=1.-VM
QRR=DIV*CS**(-PO1)*(1.-CS)**(-PO2)/SF
VLAMDA=(1.-COSM)/(0.16*(1.31*COSC-COSM))
C   The integral of radiation per unit volume
C
C   CALL TCC(COSM,VLAMDA,RI)
C   QRR=RI/((1.-CS)*(1.-SF))
C   RETURN
C   END

FUNCTION VOL11(SCC)
IMPLICIT REAL*8(A-H,O-Z)
C   CALCULATE THE FLAME ENTHALPY AT HIGHT Z, MIXTURE FRACTION COSM
PARAMETER(NPAR=64)
REAL*8 YMASSF(NPAR)
Common/CONCC/emtot1,s,chia,chir,htcomb,cpga,tinf,gamag,aCO
COMMON/ROOT/ALL
COMMON/AMB/TA
COMMON/FLOW1/SIT
COMMON/FLOW2/COSC
COMMON/COMP/YMASSF
EPS=1.0E-2
IF (SCC.GE.SIT) SCC=SIT
COSM=COSC*EXP(-4.*SCC/SIT)
C   VLAMDA=(1.-COSM)/(0.16*(1.31*COSC-COSM))
C   VLAMDA=(1.-COSM+3.*0.16*(5.*COSC-COSM))/(0.16*
C   $      (5.*COSC-COSM))
C   VLAMDA=(1.-COSM+1.*4.5*(1.4*COSC-COSM))/(4.5*
C   $      (1.4*COSC-COSM))-1.
C   9/3/93
IF(COSM.LE.0.068) THEN

```

```

VLAMDA=(1.-COSM)/(1.5*COSM)-1.
ELSE
  VLAMDA=8.09
ENDIF
CALL ENTHA1(COSM,VLAMDA,TC)
VOL11=(TC-TA)/(TA*(SIT-SCC))
RETURN
END

FUNCTION VOL12(SCC)
IMPLICIT REAL*8(A-H,O-Z)
C  CALCULATE THE FLAME ENTHALPY AT HIGHT Z, MIXTURE FRACTION COSM
PARAMETER(NPAR=64)
REAL*8 YMASSF(NPAR)
Common/CONCC/emtot1,s,chia,chiir,hitcomb,cpga,tinf,gamag,aCO
COMMON/ROOT/ALL
COMMON/AMB/TA
COMMON/FLOW1/SIT
COMMON/FLOW2/COSC
COMMON/COMP/YMASSF
EPS=1.0E-2
IF (SCC.GE.SIT) SCC=SIT
COSM=COSC*(1.-SCC/SIT)
C  VLAMDA=(1.-COSM)/(0.16*(1.31*COSC-COSM))
C  VLAMDA=(1.-COSM+3.*0.16*(5.*COSC-COSM))/(0.16*
C  $    (5.*COSC-COSM))
C  VLAMDA=(1.-COSM+1.*4.5*(1.4*COSC-COSM))/(4.5*
C  $    (1.4*COSC-COSM))-1.
C  9/3/93
IF(COSM.LE.0.068) THEN
  VLAMDA=(1.-COSM)/(1.5*COSM)-1.
ELSE
  VLAMDA=8.09
ENDIF
CALL ENTHA1(COSM,VLAMDA,TC)
VOL12=(TC-TA)/(TA*(SIT-SCC))

```

```

RETURN
END

FUNCTION VOLK(SCC)
IMPLICIT REAL*8(A-H,O-Z)
C  CALCULATE THE FLAME ENTHALPY AT HIGHT Z, MIXTURE FRACTION COSM
PARAMETER(NPAR=64)
REAL*8 YMASSF(NPAR), DELH(NPAR), A(NPAR,5), B(NPAR,5), Y(NPAR)
Common/CONCC/emtotl,s,chia,chir,htcomb,opga,tinf,gamag,aCO
COMMON/ROOT/ALL
COMMON/AMB/TA
COMMON/FLOW1/SIT
COMMON/FLOW2/COSC
COMMON/COMP/YMASSF
COMMON/NOCOMP/N
COMMON/BASIS/A,B,DELH
COMMON/KCC/K
EXTERNAL CALTE
EPS=1.0E-2
TMAX=5000.
TMIN=298.
IF (SCC.GE.SIT) SCC=SIT
C9/21/93  IF(K.EQ.1) THEN
C9/21/93  COSM = COSC*EXP(-4.*SCC/SIT)
C9/21/93  ELSE
COSM = COSC*(1.-SCC/SIT)
C9/21/93  ENDIF
C  VLAMDA=(1.-COSM)/(0.16*(1.31*COSC-COSM))
C  VLAMDA=8.09
C  VLAMDA=(1.-COSM+3.*0.16*(5.*COSC-COSM))/(0.16*
C  $ (5.*COSC-COSM))
C  VLAMDA=(1.-COSM+1.*4.5*(1.4*COSC-COSM))/(4.5*
C  $ (1.4*COSC-COSM))-1.
C  9/3/93
IF(COSM.LE.0.068) THEN
VLAMDA=(1.-COSM)/(1.5*COSM)-1.

```

```

ELSE
  VLAMDA = 8.09
ENDIF
CALL ENTHA(COSM, VLAMDA, Y)
DELH0 = 0.
DO 100 K = 1, N
  DELH0 = DELH0 + DELH(K) * Y(K)
  CONTINUE
VOLI = DELH0
RETURN
END

100

SUBROUTINE CTEMP(COSC, TC)
  IMPLICIT REAL*8(A-H, O-Z)
  C  CALCULATE THE FLAME ENTHALPY AT HIGHT Z, MIXTURE FRACTION COSM
  PARAMETER(NPAR = 64)
  REAL*8 YMASSF(NPAR), DELH(NPAR), A(NPAR, 5), B(NPAR, 5)
  Common/CONCC/emitot1, s, chia, chir, hitcomb, cpga, tinf, gamag, aCO
  COMMON/ROOT/ALL
  COMMON/AMB/TA
  COMMON/FLOW1/SIT
  COMMON/COMP/YMASSF
  COMMON/NOCOMP/N
  COMMON/BASIS/A, B, DELH
  EXTERNAL CALTE
  COSM = COSC
  VLAMDA = (1. - COSM + 1. * 4.5 * (1.4 * COSC - COSM)) / (4.5 *
    $ (1.4 * COSC - COSM)) - 1.
  C  9/3/93
  IF(COSM.LE.0.068) THEN
    VLAMDA = (1. - COSM) / (1.5 * COSM) - 1.
  ELSE
    VLAMDA = 8.09
  ENDIF
  CALL ENTHA1(COSM, VLAMDA, TC)
  RETURN

```



END

```

SUBROUTINE CTEMP1(COSC,sqi)
  IMPLICIT REAL*8(A-H,O-Z)
  C  CALCULATE THE FLAME ENTHALPY AT HIGHT Z, MIXTURE FRACTION COSM
    PARAMETER(NPAR=64)
    REAL*8 YMASSF(NPAR),DELH(NPAR),A(NPAR,5),B(NPAR,5)
    Common/CONCC/emtot1,s,chia,chir,htcomb,cpga,tinf,gamag,aCO
    COMMON/ROOT/ALL
    COMMON/AMB/TA
    COMMON/FLOW1/SIT
    COMMON/COMP/YMASSF
    COMMON/NOCOMP/N
    COMMON/BASIS/A,B,DELH
    EXTERNAL CALTE
    COSM = COSC
    VLAMDA = (1.-COSM + 1.*4.5*(1.4*COSC-COSM))/(4.5*
      $ (1.4*COSC-COSM))-1.
  C  9/3/93
    IF(COSM.LE.0.068) THEN
      VLAMDA = (1.-COSM)/(1.5*COSM)-1.
    ELSE
      VLAMDA = 8.09
    ENDIF
    sqi = (1.-cosm)/(vlamda + 1.)*cosm
    sqi = sqi**0.5/cosm
    RETURN
  END

```

```

FUNCTION VOCO(SCC)
  IMPLICIT REAL*8(A-H,O-Z)
  C  CALCULATE THE FLAME ENTHALPY AT HIGHT Z, MIXTURE FRACTION COSM

```

```

PARAMETER(NPAR=64)
REAL*8 YMASSF(NPAR), DELH(NPAR), A(NPAR,5), B(NPAR,5), Y(NPAR)
Common/CONCC/emtot1,s,chia,chir,htcomb,cpga,tinf,gamag,aCO
COMMON/ROOT/ALL
COMMON/AMB/TA
COMMON/FLOW1/SIT
COMMON/FLOW2/COSC
COMMON/COMP/YMASSF
COMMON/NOCOMP/N
COMMON/BASIS/A,B,DELH
EXTERNAL CALTE
EPS=1.0E-2
TMAX=5000.
TMIN=298.
IF (SCC.GE.SIT) SCC=SIT
COSM = COSC*(1.-SCC/SIT)
C   VLAMDA=(1.-COSM)/(0.16*(1.31*COSC-COSM))
C   VLAMDA=8.09
C   VLAMDA=(1.-COSM+3.*0.16*(5.*COSC-COSM))/(0.16*
C   $   (5.*COSC-COSM))
C   VLAMDA=(1.-COSM+1.*4.5*(1.4*COSC-COSM))/(4.5*
C   $   (1.4*COSC-COSM))-1.
C 9/3/93
IF(COSM.LE.0.068) THEN
  VLAMDA=(1.-COSM)/(1.5*COSM)-1.
ELSE
  VLAMDA=8.09
ENDIF
CALL ENTHA(COSM,VLAMDA,Y)
VOCO=Y(6)
RETURN
END

FUNCTION VOLI3(SCC)
IMPLICIT REAL*8(A-H,O-Z)

```

```

C  CALCULATE THE FLAME ENTHALPY AT HIGHT Z, MIXTURE FRACTION COSM
PARAMETER(NPAR=64)
REAL*8 Y(NPAR),DELH(NPAR),A(NPAR,5),B(NPAR,5)
Common/CONCC/emtot1,s,chia,chir,htcomb,cpga,tinf,gamag,aCO
COMMON/ROOT/ALL
COMMON/AMB/TA
COMMON/FLOW1/SIT
COMMON/FLOW2/COSC
COMMON/COMP/Y
COMMON/NOCOMP/N
COMMON/BASIS/A,B,DELH
EXTERNAL CALTE
EPS=1.0E-2
TMAX=5000.
TMIN=298.
IF (SCC.GE.SIT) SCC=SIT
COSM = COSC*(1.-SCC/SIT)
C  VLAMDA=(1.-COSM)/(0.16*(1.31*COSC-COSM))
C  VLAMDA=8.09
C  VLAMDA=(1.-COSM+3.*0.16*(5.*COSC-COSM))/(0.16*
C  $ (5.*COSC-COSM))
C  VLAMDA=(1.-COSM+1.*4.5*(1.4*COSC-COSM))/(4.5*
C  $ (1.4*COSC-COSM))-1.
C  9/3/93
IF(COSM.LE.0.068) THEN
  VLAMDA=(1.-COSM)/(1.5*COSM)-1.
ELSE
  VLAMDA=8.09
ENDIF
CALL ENTHA(COSM,VLAMDA,Y)
CALL ENTHA1(COSM,VLAMDA,TC)
CALL CALCP(CPT,TC)
VOL13=CPT
RETURN
END

```

```

SUBROUTINE CALHT0(T,DELH0)
PARAMETER(NPAR=64)
IMPLICIT REAL*8(A-H,O-Z)
REAL*8 A(NPAR,5),B(NPAR,5),DELH(NPAR),
$ YMASSF(NPAR)
COMMON/BASIS/A,B,DELH
COMMON/NOCOMP/N
COMMON/COMP/YMASSF
DELH0=0.
DO 100 I=1,N
    DELH0=DELH0+YMASSF(I)*DELH(I)
100 CONTINUE
CALL CALCP(CPT,T)
DELH0=CPT+DELH0
RETURN
END

```

```

FUNCTION CALTE(T)
PARAMETER(NPAR=64)
IMPLICIT REAL*8(A-H,O-Z)
REAL*8 A(NPAR,5),B(NPAR,5),DELH(NPAR),YMASSF(NPAR)
COMMON/BASIS/A,B,DELH
COMMON/NOCOMP/N
COMMON/COMP/YMASSF
COMMON/INIT/DELH0,DELHB
COMMON/CONCC/EMTOT1,S,CHIA,CHIR,HTCOMB,CPGA,TINF,GAMAG,ACO
COMMON/COSS/COSM
DELHF=0.
DO 100 I=1,N
    DELHF=DELHF+YMASSF(I)*DELH(I)

```

```

100    CONTINUE

      IF(T.EQ.298.)GOTO 400
      CALL CALCP(CPT,T)
      DELHF=DELHF+CPT
400    CALTE=COSM*(DELHB-DELH0)-DELHF+DELH0
      RETURN
      END

SUBROUTINE CALCP(CPT,T)
PARAMETER (NPAR=64)
IMPLICIT REAL*8(A-H,O-Z)
REAL*8 CPG(NPAR),A(NPAR,5),B(NPAR,5),DELH(NPAR),YMASSF(NPAR)
COMMON/BASIS/A,B,DELH
COMMON/NOCOMP/N
COMMON/COMP/YMASSF
DO 100 I=1,N
  CPG(I)=0.
  DO 100 J=1,5
    COE=1./J
    IF(T.LE.1000.) THEN
      CPG(I)=CPG(I)+COE*B(I,J)*(T**J-298.**J)
    ELSE
      CPG(I)=CPG(I)+COE*A(I,J)*(T**J-298.**J)
    ENDIF
  ENDIF
100  CONTINUE
DO 200 I=1,7
  IF(CPG(I).LT.0.) CPG(I)=0.
  CPG(I)=CPG(I)*1.9872*4.185
200  CONTINUE
C    Now the unit of CPG(I) is in KJ/Kmol.K. This should be changed
C    as KJ/kg.K
  CPG(I)=CPG(I)/28.

```

```

CPG(2)=CPG(2)/32.
CPG(3)=CPG(3)/16.
CPG(4)=CPG(4)/44.
CPG(5)=CPG(5)/18.
CPG(6)=CPG(6)/28.
CPG(7)=CPG(7)/2.
CPT=0.
DO 220 I=1,N
  CPT=CPT+YMASSF(I)*CPG(I)
220 CONTINUE

```

```

RETURN
END

```

```

SUBROUTINE ENTHA(COSM,VLAMDA,Y)

```

```

C   This is the program of the combustion model, it needs the fuel flow rate
C   emtot1 as a input. The output of this program is the mean temperature
C   at various positions of the fire plume Z.

```

```

PARAMETER (NPAR=64)

```

```

IMPLICIT REAL*8(A-H,O-Z)

```

```

real*8 emtot1,s,chia,chir,htcomb,tinf,gamag,sit

```

```

real*8 Y(NPAR)

```

```

common/total/DIV

```

```

COMMON/STOICH/YN2S,YCO2S,YH2OS,CS

```

```

COMMON/NOCOMP/N

```

```

COMMON/NO/K

```

```

COMMON/CONCC/emtot1,s,chia,chir,htcomb,cpga,tinf,gamag,ACO

```

```

COMMON/INDI/IFLAG

```

```

common/pw/po1,PO2

```

```

C   COMMON/COSS/COSM

```

```

COMMON/FLOW1/SIT

```

```

EXTERNAL SPEC1,SPEC2

```

```

C   EXTERNAL MIDSQU1

```

```

C   EXTERNAL MIDSQU2

```

```

IF(VLAMDA.LT.0.) VLAMDA=0.
VN=VLAMDA*COSM
VM=VLAMDA*(1.-COSM)
GLAMDA=GAMMLN(VLAMDA)
GN=GAMMLN(VN)
GM=GAMMLN(VM)
DIVI=GLAMDA-GN-GM
DIV=EXP(DIVI)
PO1=1.-VN
PO2=1.-VM
AA=0.

IF(PO1.GE.0..AND.PO1.NE.1.) THEN
BB1=0.5**VN
ELSE
BB1=0.5
ENDIF
IF(PO2.GE.0..AND.PO2.NE.1.) THEN
BB2=0.
CC=0.5**VM
ELSE
BB2=0.5
CC=1.
ENDIF
DO 120 K=1,N
IFLAG=1
C  print*,aa,bb1
CALL QGAUS7(SPEC1,AA,BB1,CON1)
C  print*,con1,'con1'
CALL QGAUS8(SPEC2,BB2,CC,CON2)
C  print*,con2,'con2'
Y(K)=CON1+CON2
120 CONTINUE
RETURN
END

```

```

FUNCTION SPEC1(CO)
PARAMETER (NPAR=64)
IMPLICIT REAL*8(A-H,O-Z)
REAL*8 YS(NPAR), DELH(NPAR), A(NPAR,5), B(NPAR,5)
COMMON/BASIS/A,B,DELH
COMMON/TOTAL/DIV
COMMON/NOCOMP/N
COMMON/NO/K
common/pw/po1,PO2
COMMON/COMP/YS

C   IF(CO.LE.EXP((1.-PO1)*(-86.))) CO1=0.
IF(PO1.LT.0.) THEN
C   CO1=CO**(1./(1.-PO1))
CO1=CO
ENDIF
IF(PO1.GE.0.) THEN
IF (CO.LE.EXP((1.-PO1)*(-86.))) THEN
CO1=0.
ELSE
CO1=CO**(1./(1.-PO1))
ENDIF
ENDIF
CALL CALCON(CO1,YS)
IF (YS(K).LT.0.) STOP
IF (ABS(YS(K)).LE.1.0E-30.OR.DIV.LE.1.0E-30) THEN
SPEC1=0.
ELSE IF (PO1.GE.0.) THEN
SPEC1=YS(K)*DIV*(1.-CO1)**(-PO2)/(1.-PO1)
ELSE
SPEC1=YS(K)*DIV*CO**(-PO1)*(1.-CO)**(-PO2)
ENDIF
RETURN
END

```



```

FUNCTION SPEC2(CO)
PARAMETER (NPAR=64)
IMPLICIT REAL*8(A-H,O-Z)
REAL*8 YS(NPAR),DELH(NPAR),A(NPAR,5),B(NPAR,5)
COMMON/BASIS/A,B,DELH
COMMON/TOTAL/DIV
COMMON/NOCOMP/N
COMMON/NO/K
COMMON/COMP/YS
common/pw/po1,PO2
CALL CALCON(CO,YS)
IF (PO2.GE.0.) THEN
CO1=1.-CO**(1./(1.-PO2))
ELSE
CO1=CO
ENDIF
CALL CALCON(CO1,YS)
print*,co,po2,'po2'
IF (YS(K).LT.0.) STOP
IF (ABS(YS(K)).LE.1.0E-30.OR.DIV.LE.1.0E-30) THEN
SPEC2=0.
ELSE IF (PO2.GE.0.) THEN
IF (-PO1*DLOG(CO1).LE.(-86.)) THEN
SPEC2=0.
ELSE
SPEC2=YS(K)*DIV*CO1**(-PO1)/(1.-PO2)
ENDIF
ELSE
IF (-PO1*DLOG(CO1).LE.(-86.)) OR.(-PO2)*DLOG(1.-CO1).
$ LE.(-86.)) THEN
SPEC2=0.
ELSE
SPEC2=YS(K)*DIV*CO1**(-PO1)*(1.-CO1)**(-PO2)
ENDIF
ENDIF
PRINT*,co1,po1

```

```
RETURN
END
```

```
SUBROUTINE ENTHA1(COSM, VLAMDA, TC)
```

```
C      This is the program of the combustion model, it needs the fuel flow rate
C      emtot1 as a input. The output of this program is the mean temperature
C      at various positions of the fire plume Z.
```

```
PARAMETER (NPAR=64)
```

```
IMPLICIT REAL*8(A-H,O-Z)
```

```
real*8 emtot1,s,chia,chir,htcomb,tinf,gamag,sit
```

```
real*8 cosm
```

```
common/total/DIV
```

```
COMMON/STOICH/YN2S,YCO2S,YH2OS,CS
```

```
COMMON/NOCOMP/N
```

```
COMMON/NO/K
```

```
COMMON/CONCC/emtot1,s,chia,chir,htcomb,cpga,tinf,gamag,ACO
```

```
COMMON/INDI/IFLAG
```

```
common/pw/po1,PO2
```

```
COMMON/FLOW1/SIT
```

```
EXTERNAL SPEC3,SPEC4
```

```
IF(VLAMDA.LT.0.) VLAMDA=0.
```

```
VN=VLAMDA*COSM
```

```
VM=VLAMDA*(1.-COSM)
```

```
GLAMDA=GAMMLN(VLAMDA)
```

```
GN=GAMMLN(VN)
```

```
GM=GAMMLN(VM)
```

```
DIVI=GLAMDA-GN-GM
```

```
DIV=EXP(DIVI)
```

```
PO1=1.-VN
```

```
PO2=1.-VM
```

```
AA=0.
```

```
IF(PO1.GE.0..AND.PO1.NE.1.) THEN
```

```
BB1=0.5**VN
```

```

ELSE
BB1=0.5
ENDIF
IF(PO2.GE.0..AND.PO2.NE.1.) THEN
BB2=0.
CC=0.5**VM
ELSE
BB2=0.5
CC=1.
ENDIF
IFLAG=1
CALL QGAUS5(SPEC3,AA,BB1,TC1)
CALL QGAUS6(SPEC4,BB2,CC,TC2)
TC=TC1+TC2
120 CONTINUE
RETURN
END

FUNCTION SPEC3(CO)
PARAMETER (NPAR=64)
IMPLICIT REAL*8(A-H,O-Z)
REAL*8 YS(NPAR),DELH(NPAR),A(NPAR,5),B(NPAR,5)
COMMON/BASIS/A,B,DELH
COMMON/TOTAL/DIV
COMMON/NOCOMP/N
COMMON/NO/K
common/pw/po1,PO2
COMMON/COMP/YS

IF(PO1.LT.0.) THEN
CO1=CO
ENDIF
IF(PO1.GE.0.) THEN
IF (CO.LE.EXP((1.-PO1)*(-86.))) THEN
CO1=0.
ELSE

```

```

CO1=CO**(1./(1.-PO1))
ENDIF
ENDIF
CALL CALCON(CO1,YS)
CALL LTEMP(CO1,YS,TEMP)
IF(ABS(TEMP).LE.1.0E-30.OR.(DIV.LE.1.0E-30)) THEN
  $  OR.(PO2.LE.(-80.)) THEN
  SPEC3=0.
ELSE IF (PO1.GE.0) THEN
  IF(ABS(PO2).LE.85./DLOG(1-CO1)) THEN
    SPEC3 = TEMP*DIV/(1-PO1)
  ELSE
    SPEC3 = TEMP*DIV*(1.-CO1)**(-PO2)/(1.-PO1)
  ENDIF
ELSE
  SPEC3 = TEMP*DIV*CO**(-PO1)
ELSE
  SPEC3 = TEMP*DIV*CO**(-PO1)*(1.-CO)**(-PO2)
ENDIF
ENDIF
RETURN
END

FUNCTION SPEC4(CO)
PARAMETER (NPAR=64)
IMPLICIT REAL*8(A-H,O-Z)
REAL*8 YS(NPAR),DELH(NPAR),A(NPAR,5),B(NPAR,5)
COMMON/BASIS/A,B,DELH
COMMON/TOTAL/DIV
COMMON/NOCOMP/N
COMMON/NO/K
COMMON/COMP/YS
common/pw/po1,PO2
IF (PO2.GE.0.) THEN
  CO1 = 1.-CO**(1./(1.-PO2))

```

```

ELSE
COI=CO
ENDIF
CALL CALCON(COI,YS)
CALL LTEMP(COI,YS,TEMP)
IF(ABS(TEMP).LE.1.0E-30.OR.(DIV.LE.1.0E-30)) THEN
C $ OR.(PO2.LE.(-80.))) THEN
SPEC4=0.
ELSE IF (PO2.GE.0) THEN
IF(-PO1*DLOG(COI).LE.(-86.)) THEN
SPEC4=0.
ELSE
SPEC4=TEMP*DIV*COI**(-PO1)/(1.-PO2)
ENDIF
ELSE
IF(-PO1*DLOG(CO).LE.(-86.).OR.(-PO2)*DLOG(1.-CO).
$ LE.(-86.)) THEN
SPEC4=0.
ELSE
SPEC4=TEMP*DIV*CO**(-PO1)*(1.-CO)**(-PO2)
ENDIF
ENDIF
RETURN
END

SUBROUTINE TCC(COSM,VLAMDA,RI)

C This is the program of the combustion model, it needs the fuel flow rate
C emtot1 as a input. The output of this program is the mean temperature
C at various positions of the fire plume Z.
PARAMETER (NPAR=64)
IMPLICIT REAL*8(A-H,O-Z)
real*8 emtot1,s,chia,chir,htcomb,tinf,gamag
real*8 cosm
common/total/DIV

```

```

COMMON/STOICH/YN2S,YCO2S,YH2OS,CS
COMMON/NOCOMP/N
COMMON/NO/K
COMMON/CONCC/emtot1,s,chia,chir,htcomb,cpga,tinf,gamag,ACO
COMMON/INDI/IFLAG
common/pw/po1,PO2
EXTERNAL SPEC5
IF(VLAMDA.LT.0.) VLAMDA=0.
VN=VLAMDA*COSM
VM=VLAMDA*(1.-COSM)
GLAMDA=GAMMLN(VLAMDA)
GN=GAMMLN(VN)
GM=GAMMLN(VM)
DIVI=GLAMDA-GN-GM
DIV=EXP(DIVI)
PO1=1.-VN
PO2=1.-VM
BB=CS
CC=3.*CS
RI=DIV*CS**(-PO1)*(1.-CS)**(-PO2)
CALL QGAUS10(SPEC5,BB,CC,RI)
RETURN
END

C
FUNCTION SPEC5(CO)
PARAMETER (NPAR=64)
IMPLICIT REAL*8(A-H,O-Z)
REAL*8 YS(NPAR)
COMMON/TOTAL/DIV
COMMON/NOCOMP/N
common/pw/po1,PO2
COMMON/NO/K
COMMON/STOICH/YN2S,YCO2S,YH2OS,CS
IF(PO1.LT.0.) THEN
C   CO1=CO
C   ENDIF

```

```

C      IF(PO1.GE.0.) THEN
C      IF (CO.LE.EXP((1.-PO1)**(-86.))) THEN
C      CO1=0.
C      ELSE
C      CO1=CO**((1./(1.-PO1))
C      ENDIF
C      ENDIF
C      CALL CALCON(CO,YS)
C      CALL LTEMP(CO,YS,TEMP)
C      IF (TEMP.LT.0.) STOP
C      IF(TEMP.LE.1.0E-30.OR.DIV.LE.1.0E-30) THEN
C      SPEC5=0.
C      ELSE
C      SPEC5=5.67E-08*(TEMP**4)*(CO-CS)*DIV*CO**(-PO1)*
C      $ (1.-CO)**(-PO2)
C      ENDIF
C      RETURN
C      END

```

# SUBROUTINE ENTHA2(COSM,VLAMDA,TCE)

```

C      This is the program of the combustion model, it needs the fuel flow rate
C      emtot1 as a input. The output of this program is the mean temperature
C      at various positions of the fire plume Z.
C      PARAMETER (NPAR=64)
C      IMPLICIT REAL*8(A-H,O-Z)
C      real*8 emtot1,s,chia,chir,htcomb,tinf,gamag,sit
C      real*8 cosm
C      common/total/DIV
C      COMMON/STOICH/YN2S,YCO2S,YH2OS,CS
C      COMMON/NOCOMP/N
C      COMMON/NO/K
C      COMMON/CONCC/emtot1,s,chia,chir,htcomb,cpga,tinf,gamag,ACO
C      COMMON/INDI/FLAG
C      common/pw/po1,PO2
C      COMMON/COSS/COSM

```

```

COMMON/FLOW1/SIT
C  COMMON/FLOW2/COSC
EXTERNAL SPEC6,SPEC7
IF(VLAMDA.LT.0.) VLAMDA=0.
VN=VLAMDA*COSM
VM=VLAMDA*(1.-COSM)
GLAMDA=GAMMLN(VLAMDA)
GN=GAMMLN(VN)
GM=GAMMLN(VM)
DIVI=GLAMDA-GN-GM
DIV=EXP(DIVI)
PO1=1.-VN
PO2=1.-VM
AA=0.

IF(PO1.GE.0..AND.PO1.NE.1.) THEN
BB1=0.5**VN
ELSE
BB1=0.5
ENDIF
IF(PO2.GE.0..AND.PO2.NE.1.) THEN
BB2=0.
CC=0.5**VM
ELSE
BB2=0.5
CC=1.
ENDIF
C  DO 120 K=1,N
IFLAG=1
CALL QGAUS5(SPEC6,AA,BB1,CON1)
CALL QGAUS6(SPEC7,BB2,CC,CON2)
TCE=CON1+CON2
120 CONTINUE
RETURN
END

```



```

FUNCTION SPEC6(CO)
PARAMETER (NPAR=64)
IMPLICIT REAL*8(A-H,O-Z)
REAL*8 YS(NPAR),DELH(NPAR),A(NPAR,5),B(NPAR,5)
COMMON/BASIS/A,B,DELH
COMMON/TOTAL/DIV
COMMON/NOCOMP/N
COMMON/NO/K
common/pw/po1,PO2
COMMON/COMP/YS

C IF(CO.LE.EXP((1.-PO1)*(-86.))) CO1=0.
IF(PO1.LT.0.) THEN
C CO1=CO**((1./(1.-PO1))
CO1=CO
ENDIF
IF(PO1.GE.0.) THEN
IF (CO.LE.EXP((1.-PO1)*(-86.))) THEN
CO1=0.
ELSE
CO1=CO**((1./(1.-PO1))
ENDIF
ENDIF
CALL CALCON(CO1,YS)
CALL LTEMP(CO1,YS,TEMP)
CALL CALCP(CPT,TEMP)
DELHF=0.
C DO 100 I=1,N
C DELHF=DELHF + YS(I)*DELH(I)
C100 CONTINUE
C HP=DELHF+CPT
IF(TEMP.LE.1.0E-30.OR.DIV.LE.1.0E-30) THEN
SPEC6=0.
ELSE IF (PO1.GE.0) THEN
SPEC6=TEMP*DIV*(1.-CO1)**(-PO2)/(1.-PO1)
ELSE

```

```

SPEC6=TEMP*DIV*CO**(-PO1)*(1.-CO)**(-PO2)
ENDIF
RETURN
END

FUNCTION SPEC7(CO)
PARAMETER (NPAR=64)
IMPLICIT REAL*8(A-H,O-Z)
REAL*8 YS(NPAR),DELH(NPAR),A(NPAR,5),B(NPAR,5)
COMMON/BASIS/A,B,DELH
COMMON/TOTAL/DIV
COMMON/NOCOMP/N
COMMON/NO/K
COMMON/COMP/YS
common/pw/po1,PO2
CALL CALCON(CO,YS)
IF (PO2.GE.0.) THEN
CO1=1.-CO**(1./(1.-PO2))
ELSE
CO1=CO
ENDIF
CALL CALCON(CO1,YS)
CALL LTEMP(CO1,YS,TEMP)
CALL CALCP(CPT,TEMP)
DELHF=0.
DO 100 I=1,N
DELHF=DELHF+YS(I)*DELH(I)
100 CONTINUE
HP=CPT+DELHF
IF (HP.LT.0.) STOP
IF (TEMP.LE.1.0E-30.OR.DIV.LE.1.0E-30) THEN
SPEC7=0.
ELSE IF (PO2.GE.0) THEN
IF(-PO1*DLOG(CO1).LE.(-86.)) THEN
SPEC7=0.

```

```

ELSE
SPEC7=TEMP*DIV*CO1**(-PO1)/(1.-PO2)
ENDIF
ELSE
IF(-PO1*DLOG(CO).LE.(-86.).OR.(-PO2)*DLOG(1.-CO).
LE.(-86.)) THEN
SPEC7=0.
ELSE
SPEC7=TEMP*DIV*CO**(-PO1)*(1.-CO)**(-PO2)
ENDIF
ENDIF
RETURN
END

```

```

SUBROUTINE LTEMP(CO,YMASSF,TEMP)
IMPLICIT REAL*8(A-H,O-Z)
PARAMETER (NPAR=64)
REAL*8 CO,YMASSF(NPAR),YMA(NPAR)
COMMON/NOCOMP/N
COMMON/INIT/DELH0,DELHB
COMMON/COMP/YMA
COMMON/COSS/COSMM
COMMON/ROOT/ALPHA
COMMON/AMB/TA
EXTERNAL CALTE
DO 10 I=1,N
YMA(I)=YMASSF(I)
10 CONTINUE
T0=298.
TMAX=5000.
EPS=1.0E-3
COSMM=CO
ALPHA=1.
TEMP1=ZBRENT2(CALTE,T0,TMAX,EPS)

```

```

TEMP=ALPHA*(TEMP1-TA)+TA
RETURN
END

SUBROUTINE CALCON(CO,Y)
IMPLICIT REAL*8(A-H,O-Z)
PARAMETER (NPAR=64)
REAL*8 CO,Y(NPAR),YM(NPAR)
COMMON/NOCOMP/N
COMMON/STOICH/YN2S,YCO2S,YH2OS,CS
COMMON/NO/K
COMMON/ACOMP/NN,MM,WMF
C IF(CO.EQ.0) THEN
C   Y(1)=0.767
C   Y(2)=0.233
C   DO 100 I=3,N
C100   Y(I)=0.
C ELSE IF (CO.EQ.1.) THEN
C   DO 110 I=1,N
C   IF (I.EQ.3) THEN
C     Y(I)=1.
C   ELSE
C     Y(I)=0.
C   ENDIF
C110 CONTINUE
C ELSE
C   IF((1.-CO).LE.1.0E-5) THEN
C     IF(CO.EQ.1.) THEN
C       DO 10 I=1,N
C       IF(I.EQ.3) THEN
C         Y(I)=1.0
C       ELSE
C         Y(I)=0.
C       ENDIF
C10 CONTINUE
C     RETURN

```

```

END IF
PHI=CO/(1.-CO)*(1.-CS)/CS
IF (PHI.LE.1.0E-30) THEN
IF (PHI.EQ.0.) THEN
DO 50 I=1,N
IF(L.NE.1.AND.I.NE.2) THEN
Y(I)=0.
ELSE IF (I.EQ.1) THEN
Y(I)=0.767
ELSE
Y(I)=0.233
ENDIF
CONTINUE
GOTO 400
ENDIF
XM=DLOG(PHI)/2.3026
IF((1.446E-5-1.0*XM).LE.(-43.)) THEN
YM(1)=0.
ELSE
YM(1)=EXP(2.3026*(1.446E-5-1.0*XM))
ENDIF
Y(1)=YN2S*YM(1)*0.767/(0.767-YN2S+YN2S*YM(1))
IF(PHI.LE.1) THEN
YM(2)=0.9898-0.9062*PHI
IF((-0.0332629+0.977861*XM).LE.(-43.)) THEN
YM(4)=0.
YM(5)=0.
ELSE
YM(4)=EXP(2.3026*(-0.0332629+0.977861*XM))
YM(5)=EXP(2.3026*(-0.0332629+0.977861*XM))
ENDIF
ELSE
P2=(-0.79481-3.33465*XM+7.74823*XM**2-
$ 8.58911*XM**3+4.31337*XM**4-0.810195*XM**5)
IF (P2.LE.(-43.)) THEN
YM(2)=0.

```

```

ELSE
  YM(2)=EXP(2.3026*P2)
ENDIF
IF(PH1.LE.100.) THEN
  P4=(-0.0922555+0.104665*XM-0.512132*
    $ XM**2+0.110464*XM**3)
  IF (P4.LE.(-43.)) THEN
    YM(4)=0.
  ELSE
    YM(4)=EXP(2.3026*P4)
  ENDIF
ELSE
  YM(4)=0.
ENDIF
C Print*,co,YM(4),xm
P5=(-0.032632+0.171055*XM-0.301843*
  $ XM**2)
  IF (P5.LE.(-43.)) THEN
    YM(5)=0.
  ELSE
    YM(5)=EXP(2.3026*P5)
  ENDIF
ENDIF
IF (PH1.LE.0.2) THEN
  YM(6)=0.
ELSE
  P6=(-1.00413+2.10314*XM-2.80715*XM**2+
    $ 1.19247*XM**3-0.180829*XM**4)
  IF(P6.LE.(-43.)) THEN
    YM(6)=0.
  ELSE
    YM(6)=EXP(P6*2.3026)
  ENDIF
ENDIF
IF(PH1.LE.0.5) THEN
  YM(7)=0.

```

```

ELSE
  P7=(-2.08179+2.7159*XM-5.80981*XM**2+
$   5.59883*XM**3-2.57435*XM**4-0.445662*XM**5)
  IF(P7.LE.(-43.)) THEN
    YM(7)=0.
  ELSE
    YM(7)=EXP(2.3026*P7)
  ENDIF
ENDIF
C   PRINT*,CO,YM(3),Y(3)

Y(2)=((32*NN+8.*MM)*0.233*YM(2))/(32.*NN+8.*MM+
$   WMF*0.233-WMF*0.233*YM(2))
Y(4)=(44.*NN*YM(4)*YCO2S)/(44.*NN-WMF*YCO2S+WMF*YCO2S*YM(4))
Y(5)=(9.*MM*YH2OS*YM(5))/(9.*MM-WMF*YH2OS+WMF*YH2OS*
$   YM(5))
Y(6)=(44.*NN*YCO2S*YM(6))/(44.*NN-WMF*YCO2S+
$   WMF*YCO2S*YM(6))
Y(7)=(9.*MM*YH2OS*YM(7))/(9.*MM-WMF*YH2OS+WMF*YH2OS*
$   YM(7))
C   ENDIF
IF(PH.LE.1.5) THEN
  Y(3)=0.
  ELSE
    P3=(-2.47524+3.6703*XM-2.04325*XM**2+
$   0.406869*XM**3)
    IF (P3.LE.(-43.)) THEN
      Y(3)=0.
    ELSE
      Y(3)=EXP(2.3026*P3)
    ENDIF
  ENDIF
  comm=Y(2)
  DO 120 I=1,N
  IF (Y(I).GT.1.0) THEN
    Y(I)=1.

```

```

      ENDIF
120  CONTINUE
      IF (CO.LE.0.02) THEN
        Y(4)=3.*CO
        Y(5)=72./44.*CO
      ENDIF

      C  print*,CO,PHI,YM(4)
400  RETURN
      END

FUNCTION GAMMLN(XX)
  IMPLICIT REAL*8 (A-H,O-Z)
  C  Returns the value ln[GAMMA(XX)] for XX > 0. Fu accuracy is
  C  obtained for XX > 1. For 0 < XX < 1, the reflection formula(6.1.4)
  C  can be used first.
      REAL*8 COF(6),STP,HALF,ONE,FPF,X,TMP,SER
  C  Internal arithmetic will be done in double precision, a nicety
  C  that you can omit if five-figure accuracy is good enough.
  DATA COF,STP/76.18009173D0,-86.50532033D0,24.01409822D0,
$    -1.231739516D0,.120858003D-2,-.536382D-5,
$    2.50662827465D0/
  DATA HALF,ONE,FPF/0.5D0,1.0D0,5.5D0/
  X=XX-ONE
  TMP=X+FPF
  TMP=(X+HALF)*LOG(TMP)-TMP
  SER=ONE
  DO 11 J=1,6
    X=X+ONE
    SER=SER+COF(J)/X
  11 CONTINUE
      GAMMLN=TMP+LOG(STP*SER)
  RETURN
  END

```



```

SUBROUTINE QGAUS(FUNC,A,B,SS)
IMPLICIT REAL*8(A-H,O-Z)
C Returns as SS the integral of the function FUNC between A and B,
C by ten-point Gauss-Legendre integration: the function is
C evaluated exactly ten times at interior points in the range of
C integration
DIMENSION X(5),W(5)
EXTERNAL FUNC
C The abscissa and weights.
DATA X/.1488743389,.4333953941,.6794095682,.8650633666,
$ .9739065285/
DATA W/.2955242247,.2692667193,.2190863625,.1494513491,
$ .0666713443/
XM=0.5*(B+A)
XR=0.5*(B-A)
SS=0.
DO 11 J=1,5
DX=XR*X(J)
SS=SS+W(J)*(FUNC(XM+DX)+FUNC(XM-DX))
11 CONTINUE
SS=XR*SS
RETURN
END

```

```

SUBROUTINE QGAUS1(FUNC,A,B,SS)
IMPLICIT REAL*8(A-H,O-Z)
C Returns as SS the integral of the function FUNC between A and B,
C by ten-point Gauss-Legendre integration: the function is
C evaluated exactly ten times at interior points in the range of
C integration
DIMENSION X(5),W(5)

```

## EXTERNAL FUNC

C The abscissa and weights.

DATA X/.1488743389,.4333953941,.6794095682,.8650633666,  
\$ .9739065285/

DATA W/.2955242247,.2692667193,.2190863625,.1494513491,  
\$ .0666713443/

XM=0.5\*(B+A)

XR=0.5\*(B-A)

SS=0.

DO 11 J=1,5

DX=XR\*X(J)

SS=SS+W(J)\*(FUNC(XM+DX)+FUNC(XM-DX))

11 CONTINUE

SS=XR\*SS

RETURN

END

## SUBROUTINE QGAUS6(FUNC,A,B,SS)

IMPLICIT REAL\*8(A-H,O-Z)

C Returns as SS the integral of the function FUNC between A and B,

C by ten-point Gauss-Legendre intergration: the function is

C evaluated exactly ten times at interior points in the range of

C integration

DIMENSION X(5),W(5)

EXTERNAL FUNC

C The abscissa and weights.

DATA X/.1488743389,.4333953941,.6794095682,.8650633666,  
\$ .9739065285/

DATA W/.2955242247,.2692667193,.2190863625,.1494513491,  
\$ .0666713443/

XM=0.5\*(B+A)

XR=0.5\*(B-A)

SS=0.

```

DO 11 J=1,5
  DX=XR*X(J)
  SS=SS+W(J)*(FUNC(XM+DX)+FUNC(XM-DX))
11  CONTINUE
  SS=XR*SS
  RETURN
  END

SUBROUTINE QGAUS2(FUNC,A,B,SS)
  IMPLICIT REAL*8(A-H,O-Z)
  C Returns as SS the integral of the function FUNC between A and B,
  C by ten-point Gauss-Legendre intergration: the function is
  C evaluated exactly ten times at interior points in the range of
  C integration
  DIMENSION X(5),W(5)
  EXTERNAL FUNC
  C The abscissa and weights.
  DATA X/.1488743389,.4333953941,.6794095682,.8650633666,
  $ .9739065285/
  DATA W/.2955242247,.2692667193,.2190863625,.1494513491,
  $ .0666713443/
  XM=0.5*(B+A)
  XR=0.5*(B-A)
  SS=0.
  DO 11 J=1,5
    DX=XR*X(J)
    SS=SS+W(J)*(FUNC(XM+DX)+FUNC(XM-DX))
11  CONTINUE
  SS=XR*SS
  RETURN
  END

SUBROUTINE QGAUS3(FUNC,A,B,SS)

```

```

C IMPLICIT REAL*8(A-H,O-Z)
C Returns as SS the integral of the function FUNC between A and B,
C by ten-point Gauss-Legendre integration: the function is
C evaluated exactly ten times at interior points in the range of
C integration
C
C DIMENSION X(5),W(5)
C EXTERNAL FUNC
C The abscissa and weights.
C DATA X/.1488743389,.4333953941,.6794095682,.8650633666,
C $.9739065285/
C DATA W/.2955242247,.2692667193,.2190863625,.1494513491,
C $.0666713443/
C XM=0.5*(B+A)
C XR=0.5*(B-A)
C SS=0.
C DO 11 J=1,5
C   DX=XR*X(J)
C   SS=SS+W(J)*(FUNC(XM+DX)+FUNC(XM-DX))
C 11 CONTINUE
C SS=XR*SS
C RETURN
C END

SUBROUTINE QGAUS4(FUNC,A,B,SS)
IMPLICIT REAL*8(A-H,O-Z)
C Returns as SS the integral of the function FUNC between A and B,
C by ten-point Gauss-Legendre integration: the function is
C evaluated exactly ten times at interior points in the range of
C integration
C
C DIMENSION X(5),W(5)
C EXTERNAL FUNC
C The abscissa and weights.
C DATA X/.1488743389,.4333953941,.6794095682,.8650633666,
C $.9739065285/

```

```

DATA W/.2955242247,.2692667193,.2190863625,.1494513491,
$ .0666713443/
XM=0.5*(B+A)
XR=0.5*(B-A)
SS=0.
DO 11 J=1,5
DX=XR*X(J)
SS=SS+W(J)*(FUNC(XM+DX)+FUNC(XM-DX))
11 CONTINUE
SS=XR*SS
RETURN
END

```

# SUBROUTINE QGAUSS5(FUNC,A,B,SS)

IMPLICIT REAL\*8(A-H,O-Z)

C Returns as SS the integral of the function FUNC between A and B,  
 C by ten-point Gauss-Legendre intergration: the function is  
 C evaluated exactly ten times at interior points in the range of  
 C integration

DIMENSION X(5),W(5)

EXTERNAL FUNC

C The abscissa and weights.

```

DATA X/.1488743389,.4333953941,.6794095682,.8650633666,
$ .9739065285/

```

```

DATA W/.2955242247,.2692667193,.2190863625,.1494513491,
$ .0666713443/

```

XM=0.5\*(B+A)

XR=0.5\*(B-A)

SS=0.

DO 11 J=1,5

DX=XR\*X(J)

SS=SS+W(J)\*(FUNC(XM+DX)+FUNC(XM-DX))

11 CONTINUE

SS=XR\*SS

RETURN

END

SUBROUTINE QGAUS7(FUNC,A,B,SS)

IMPLICIT REAL\*8(A-H,O-Z)

C Returns as SS the integral of the function FUNC between A and B,  
C by ten-point Gauss-Legendre integration: the function is  
C evaluated exactly ten times at interior points in the range of  
C integration

DIMENSION X(5),W(5)

EXTERNAL FUNC

C The abscissa and weights.

DATA X/.1488743389,.4333953941,.6794095682,.8650633666,  
\$ .9739065285/

DATA W/.2955242247,.2692667193,.2190863625,.1494513491,  
\$ .0666713443/

XM=0.5\*(B+A)

XR=0.5\*(B-A)

SS=0.

DO 11 J=1,5

DX=XR\*X(J)

SS=SS+W(J)\*(FUNC(XM+DX)+FUNC(XM-DX))

11

CONTINUE

SS=XR\*SS

RETURN

END

SUBROUTINE QGAUS8(FUNC,A,B,SS)

IMPLICIT REAL\*8(A-H,O-Z)

C Returns as SS the integral of the function FUNC between A and B,  
C by ten-point Gauss-Legendre integration: the function is  
C evaluated exactly ten times at interior points in the range of  
C integration

```

DIMENSION X(5),W(5)
EXTERNAL FUNC
C The abscissa and weights.
DATA X/.1488743389,.4333953941,.6794095682,.8650633666,
$ .9739065285/
DATA W/.2955242247,.2692667193,.2190863625,.1494513491,
$ .0666713443/
XM=0.5*(B+A)
XR=0.5*(B-A)
SS=0.
DO 11 J=1,5
DX=XR*X(J)
SS=SS+W(J)*(FUNC(XM+DX)+FUNC(XM-DX))
11 CONTINUE
SS=XR*SS
RETURN
END

```

```

SUBROUTINE QGAUS9(FUNC,A,B,SS)
IMPLICIT REAL*8(A-H,O-Z)
C Returns as SS the integral of the function FUNC between A and B,
C by ten-point Gauss-Legendre intergration: the function is
C evaluated exactly ten times at interior points in the range of
C integration

```

```

DIMENSION X(5),W(5)
EXTERNAL FUNC
C The abscissa and weights.
DATA X/.1488743389,.4333953941,.6794095682,.8650633666,
$ .9739065285/
DATA W/.2955242247,.2692667193,.2190863625,.1494513491,
$ .0666713443/
XM=0.5*(B+A)
XR=0.5*(B-A)
SS=0.
DO 11 J=1,5

```

```

DX=XR*X(J)
SS=SS+W(J)*(FUNC(XM+DX)+FUNC(XM-DX))

```

```

11 CONTINUE

```

```

SS=XR*SS
RETURN
END

```

```

SUBROUTINE QGAUS10(FUNC,A,B,SS)

```

```

IMPLICIT REAL*8(A-H,O-Z)

```

```

C Returns as SS the integral of the function FUNC between A and B,
C by ten-point Gauss-Legendre integration: the function is
C evaluated exactly ten times at interior points in the range of
C integration

```

```

DIMENSION X(5),W(5)
EXTERNAL FUNC

```

```

C The abscissa and weights.

```

```

DATA X/.1488743389,.4333953941,.6794095682,.8650633666,
$ .9739065285/

```

```

DATA W/.2955242247,.2692667193,.2190863625,.1494513491,
$ .0666713443/

```

```

XM=0.5*(B+A)

```

```

XR=0.5*(B-A)

```

```

SS=0.

```

```

DO 11 J=1,5

```

```

DX=XR*X(J)

```

```

SS=SS+W(J)*(FUNC(XM+DX)+FUNC(XM-DX))

```

```

11 CONTINUE

```

```

SS=XR*SS

```

```

RETURN

```

```

END

```

```

FUNCTION ZBRENT1(FUNC,X1,X2,TOL)

```

```

IMPLICIT REAL*8(A-H,O-Z)

```



```

C      Using Brent's method, find the root of a function FUNC known to lie
C      between X1 and X2. The root, returned as ZBRENT, will be refined until
C      its accuracy is TOL.
      EXTERNAL FUNC
      PARAMETER (ITMAX=100, EPS=3.E-8)
      Maximum allowed number of iterations, and machine floating point
      precision.
      A=X1
      B=X2
      FA=FUNC(A)
      FB=FUNC(B)
      IF(FB*FA.GT.0.) PAUSE 'Root must be bracketed for ZBRENT.'
      FC=FB
      DO 11 ITER=1, ITMAX
      IF(FB*FC.GT.0.) THEN
C      Rename A, B, C and adjust bounding interval D
        C=A
        FC=FA
        D=B-A
        E=D
      ENDIF
      IF(ABS(FC).LT.ABS(FB)) THEN
        A=B
        B=C
        C=A
        FA=FB
        FB=FC
        FC=FA
      ENDIF
      TOL1=2.*EPS*ABS(B)+0.5*TOL
      Convergence check
      XM=.5*(C-B)
      IF(ABS(XM).LE.TOL1.OR.FB.EQ.0.) THEN
        ZBRENT1=B
        RETURN
      ENDIF

```

```

C      IF(ABS(E).GE.TOL1.AND.ABS(FA).GT.ABS(FB)) THEN
C      Attempt inverse quadratic interpolation
      S=FB/FA
      IF(A.EQ.C) THEN
        P=2.*XM*S
        Q=1.-S
      ELSE
        Q=FA/FC
        R=FB/FC
        P=S*(2.*XM*Q*(Q-R)-(B-A)*(R-1.))
        Q=(Q-1.)*(R-1.)*(S-1.)
      ENDIF
      Check whether in bounds
      IF(P.GT.0) Q=-Q
      P=ABS(P)
      IF(2.*P.LT.MIN(3.*XM*Q-ABS(TOL1*Q),ABS(E+Q))) THEN
C      Accept interpolation
        E=D
        D=P/Q
      ELSE
C      Interpolation failed, use bisection
        D=XM
        E=D
      ENDIF
C      Bounds decreasing too slowly, use bisection
      ELSE
        D=XM
        E=D
      ENDIF
C      Move last best guess to A
      A=B
      FA=FB
      IF(ABS(D).GT.TOL1) THEN
C      Evaluate new trial root.
        B=B+D
      ELSE

```

```

      B=B+SIGN(TOL1,XM)
    ENDIF
    FB=FUNC(B)
    CONTINUE
    PAUSE 'ZBRENT exceeding maximum iteration.'
    ZBRENT1=B
    RETURN
  END

```

11

```

FUNCTION ZBRENT2(FUNC,X1,X2,TOL)
  IMPLICIT REAL*8(A-H,O-Z)

```

C Using Brent's method, find the root of a function FUNC known to lie  
 C between X1, and X2. The root, returned as ZBRENT1, will be refined until  
 C its accuracy is TOL.

```
EXTERNAL FUNC
```

```
PARAMETER (ITMAX=100, EPS=3.E-8)
```

C Maximum allowed number of iterations, and machine floating point  
 C precision.

```
A=X1
```

```
B=X2
```

```
FA=FUNC(A)
```

```
FB=FUNC(B)
```

```
IF(FB*FA.GT.0.) PAUSE 'Root must be bracketed for ZBRENT.'
```

```
FC=FB
```

```
DO 11 ITER=1,ITMAX
```

```
  IF(FB*FC.GT.0.) THEN
```

```
    C Rename A, B, C and adjust bounding interval D
```

```
      C=A
```

```
      FC=FA
```

```
      D=B-A
```

```
      E=D
```

```
    ENDIF
```

```
  IF(ABS(FC).LT.ABS(FB)) THEN
```

```
    A=B
```

```
    B=C
```

```

C=A
FA=FB
FB=FC
FC=FA
ENDIF
TOL1=2.*EPS*ABS(B)+0.5*TOL
C
Convergence check
XM=.5*(C-B)
IF(ABS(XM).LE.TOL1.OR.FB.EQ.0.) THEN
  ZBRENT2=B
  RETURN
ENDIF
IF(ABS(E).GE.TOL1.AND.ABS(FA).GT.ABS(FB)) THEN
  Attempt inverse quadratic interpolation
  S=FB/FA
  IF(A.EQ.C) THEN
    P=2.*XM*S
    Q=1.-S
  ELSE
    Q=FA/FC
    R=FB/FC
    P=S*(2.*XM*Q*(Q-R)-(B-A)*(R-1.))
    Q=(Q-1.)*(R-1.)*(S-1.)
  ENDIF
  Check whether in bounds
  IF(P.GT.0) Q=-Q
  P=ABS(P)
  IF(2.*P.LT.MIN(3.*XM*Q-ABS(TOL1*Q),ABS(E+Q))) THEN
    Accept interpolation
    E=D
    D=P/Q
  ELSE
    Interpolation failed, use bisection
    D=XM
    E=D
  ENDIF

```

```

C   Bounds decreasing too slowly, use bisection
ELSE
    D=XM
    E=D
ENDIF
C   Move last best guess to A
A=B
FA=FB
IF(ABS(D).GT.TOL1) THEN
C   Evaluate new trial root.
    B=B+D
ELSE
    B=B+SIGN(TOL1,XM)
ENDIF
FB=FUNC(B)
CONTINUE
11 PAUSE 'ZBRENT exceeding maximum iteration.'
ZBRENT2=B
RETURN
END

```

## Appendix K Description of Execution of the Program and Output

The main code of the HFSCS is named *hfsspv70.f*. This program is written in FORTRAN 77 and consist of a large number of subroutines. The input files for the program are *hflinp* and *fluxinp* which are described in details in Appendix G. A small number of input may be required to change the parameters within the code and if the output needs to be modified. The nodal spacing,  $\Delta x$ , can be either fixed or variable and is set in the code or specified in the input file *hflinp*. The external radiative flux distribution is specified by the *fluxinp* file where 3 choices, experimental (HIFT distribution profile), constant or exponential are available as described in Appendix G. The flame radiative and gas-phase conductive flux profiles are also specified using peak and length scale values for exponentially decaying profiles by *fluxinp*.

There are two output files currently active in the program, although a number of other output files have been set-up (and are documented in the code) for debugging and special data outputs (e.g. to make contour plots of temperature) are commented out and can be readily used. The primary output files are:

*hfssprf*: is the main output file reporting the temperature and flux distribution on the fuel surface, respectively, at specified spatial distribution by the user. The time interval of the output is also user specified. These specifications are made in the code at the *output subroutine*.

*hfssout*: is another output file containing some of the key parameters that are selected by the user when the code is initially executed. These are the burn-out front,  $X_b$ , pyrolysis or flame front,  $X_p$ , flame height,  $X_f$ , rate of mass burning,  $E_{mtot1}$ , the chemical heat release rate,  $Q_{ch}$  and the incident flux,  $Q_{inc}$ . The parameters  $X_f$  and  $Q_{ch}$  are based on a calculated mass loss rate,  $E_{mtot1}$  and are calculated using an empirical relation for  $X_f$  and the heat of combustion for  $Q_{ch}$ . However,  $E_{mtot1}$  would need an accurate value for the radiation feed-back from the flame to the burning surface. This can be accomplished using a combustion model and a radiation model that could account for the soot concentration near the flame base. Since such models are still under development, a true coupling between the combustion model and the flame spread can not be accomplished without further work.

The combustion model, *pool2.f* (Appendix J), relies on the *combb.dat* (Appendix I) file for input and a modified program *radh8.f* (listing not provided but included on a diskette) can be used for jet flames with an input file *combb1.dat* (Appendix Ia).

The combustion model can be pseudo coupled to the HFSCS by using the radiation vertical profile output of the combustion model to estimate the flame radiative profile. The HFSCS can be simply modified to vary the peak radiative flux as the burning area grows. As noted before, lack of basic data for state relationships for real fuels, time intensive calculation of the combustion model and difficulty in developing a robust and accurate radiation model prevents a true coupling of the HFSCS with the combustion model.

## **Appendix L Complete Set of Plots of Experimental Measurements of Temperature and Fluxes, Data Sheets and External Flux Profile. Plots are results after significant processing of the raw data**

The first plot shows the comparison of the external flux profile measured by three different flux gages as the sample holder was moved at a speed of 0.5 m/s. Flux gages 27844 and 525842 are the large gages. They were placed at different locations, but the data was processed to show the plot as a function of distance from the leading edge. These two gages measured approximately the same flux level (there may be some small variations in time of the radiant panel). The small gage (86862) clearly measures a higher flux level. It is noisier and does not drop to a near zero when reaches the leading edge of the cooling plate (as other two gages do). This indicated that the small gage was not reliable. We also used a large gage (1 inch in diameter and the same type as 27844 and 525842) calibrated at NIST to check the measurements.

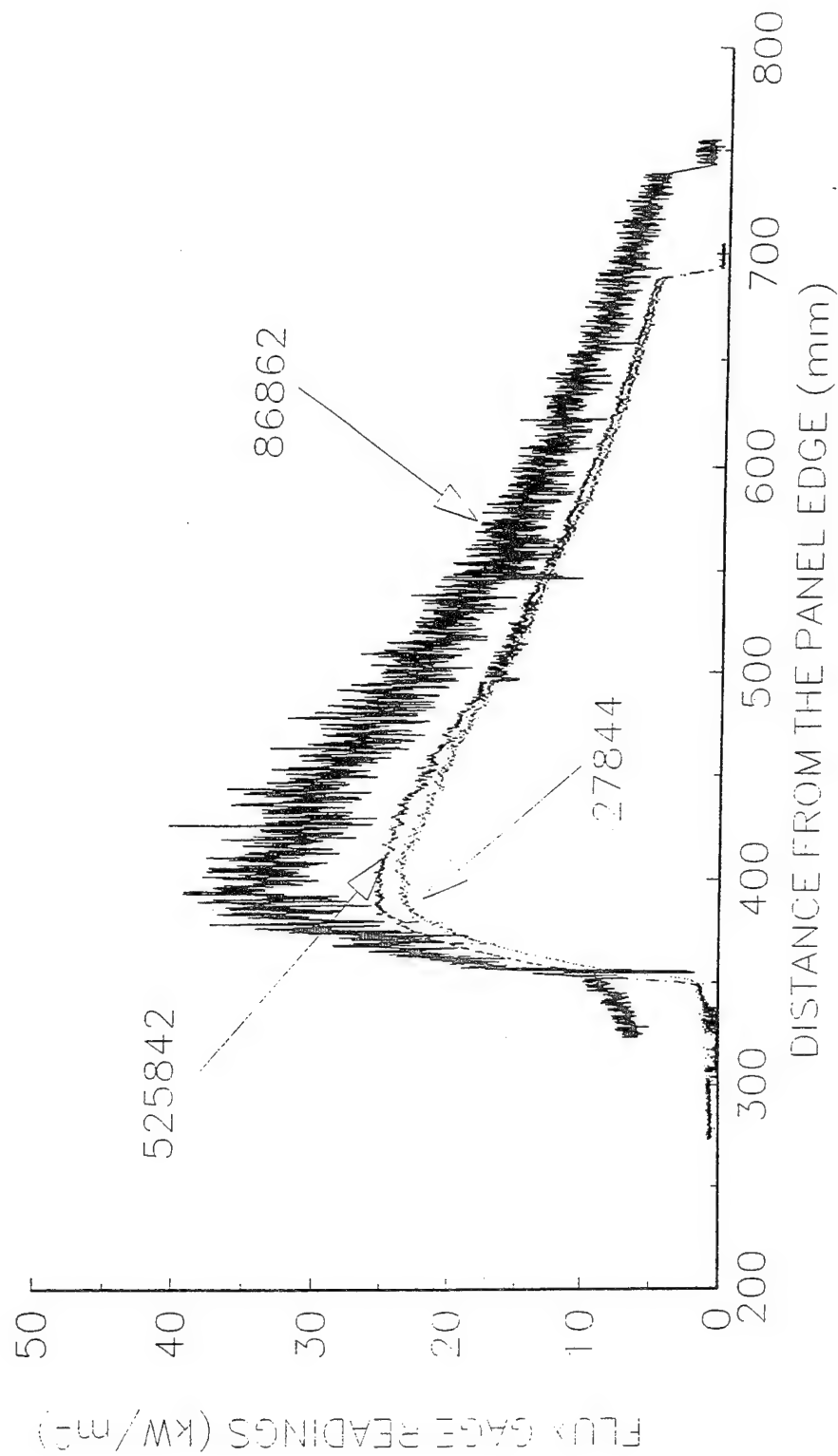
### **Arrangement of the information**

For each test, the following is contained in this appendix:

1. Data sheet, listing all the pertinent information
2. Plot of surface and gas temperatures measured vs. Time, noting the time of slide movement and speed of movement.
3. Total heat flux measured at the surface as a function of time.
4. Flame heat flux (total - externally imposed radiation) profile ahead of the flame. It is obtained by transforming the flux vs. time data using the traversing speed of the slide.
5. Prediction vs. measurement of the surface temperature during heat-up using the flame flux measurement (which would be all flame radiation at some finite distance before the flame leading edge region). This procedure was used to determine the material thermal inertia, kpc.
6. Detailed plots of the surface temperature measurements near the flame front to estimate the pyrolysis temperature and perform the analysis described in 6.5 and Appendix E.



0.5 mm/s Moving Forwards, FLX-CAL3.PRN  
86862 Window OFF



**Data Sheet**  
**Constant Horizontal Flame Spread Experiment**

Experimental No.: 21                      Date: 6/17/94 Tu                      Time: 10:30 pm

**Pre-Experiment**

Heat Flux at 425 mm Location (Planned) (kW/m<sup>2</sup>): 10  
Slider Speed (mm/s): 0.32 mm/s

**Burning Sample Data**

Material: 3/4" Potlatch Particle Board                      Dimension(LxWxH, mm): 600x152x18.85

**Instrumentation**

Number of Thermocouples: 5                      Number of Heat Flux Gauges: 2

Station	Sensor	x (mm)	z (mm)	File Column	Note
1	TC	175	0.79	B	GAS TC1
1	TC	175	0	C	SURFACE
2	TC	350	0.41	D	GAS TC2
2	TC	350	0	E	SURFACE
2	HG	350	0	G	SER. 84501
3	TC	573	0	F	SURFACE
3	HG	573	0	H	SER. 525842

**Experiment**

Flux Gauge Reading @ 425 mm (Serial No. 27844, mV): 3.70-12.7576 kW/m<sup>2</sup>

Preheating Time without Pilot Flame (seconds): 270

Time to Sample Ignition After Applying the Pilot Flame (seconds): 20

Speed Used (S1M"Steps"): 50

Number of Steps (I1M"Steps"): 80000

File Names (.PRN): T10K617

Set-up File Name:

Sampling Rate (Hz): 5      Duration of Sampling (sec): 2500

Time to Start Moving the Sample (sec): 402.2

Ignition Heat Flux (Calculated, kW/m<sup>2</sup>):

**Ambient Conditions**

Temperature (°C): 23

**Observations** Burning area ~10 cm

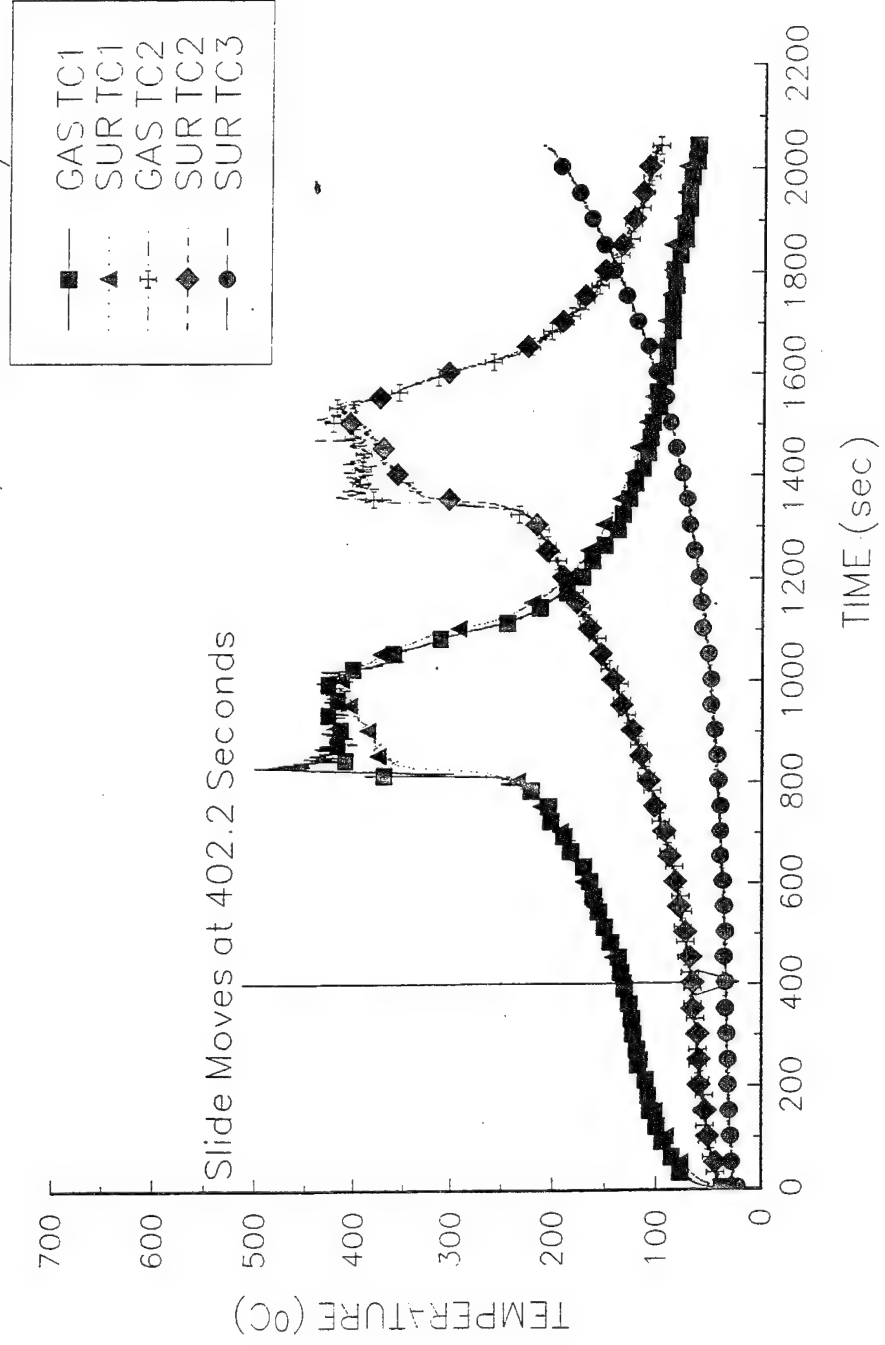
Personnel V.M., Y.C

Processing of Data:  $T_p=320^{\circ}\text{C}$ , Surface TC1,  $1/\tau=0.14$ ,  $T_{ext}=240^{\circ}\text{C}$ ,  $k_{pc}=0.17 \times 765 \times 2800=364140$ ,  
 $q''_0=(k_{pc})^{1/2}(T_p-T_{ext})(1/\tau)^{1/2}=(364140)^{1/2} \times (320-240)(0.14)^{1/2}=18.06 \text{ kW/m}^2$

Surface TC2,  $1/\tau=0.10$ ,  $T_{ext}=240^{\circ}\text{C}$ ,  $q''_0=(364140)^{1/2} \times (320-240)(0.10)^{1/2}=15.27 \text{ kW/m}^2$

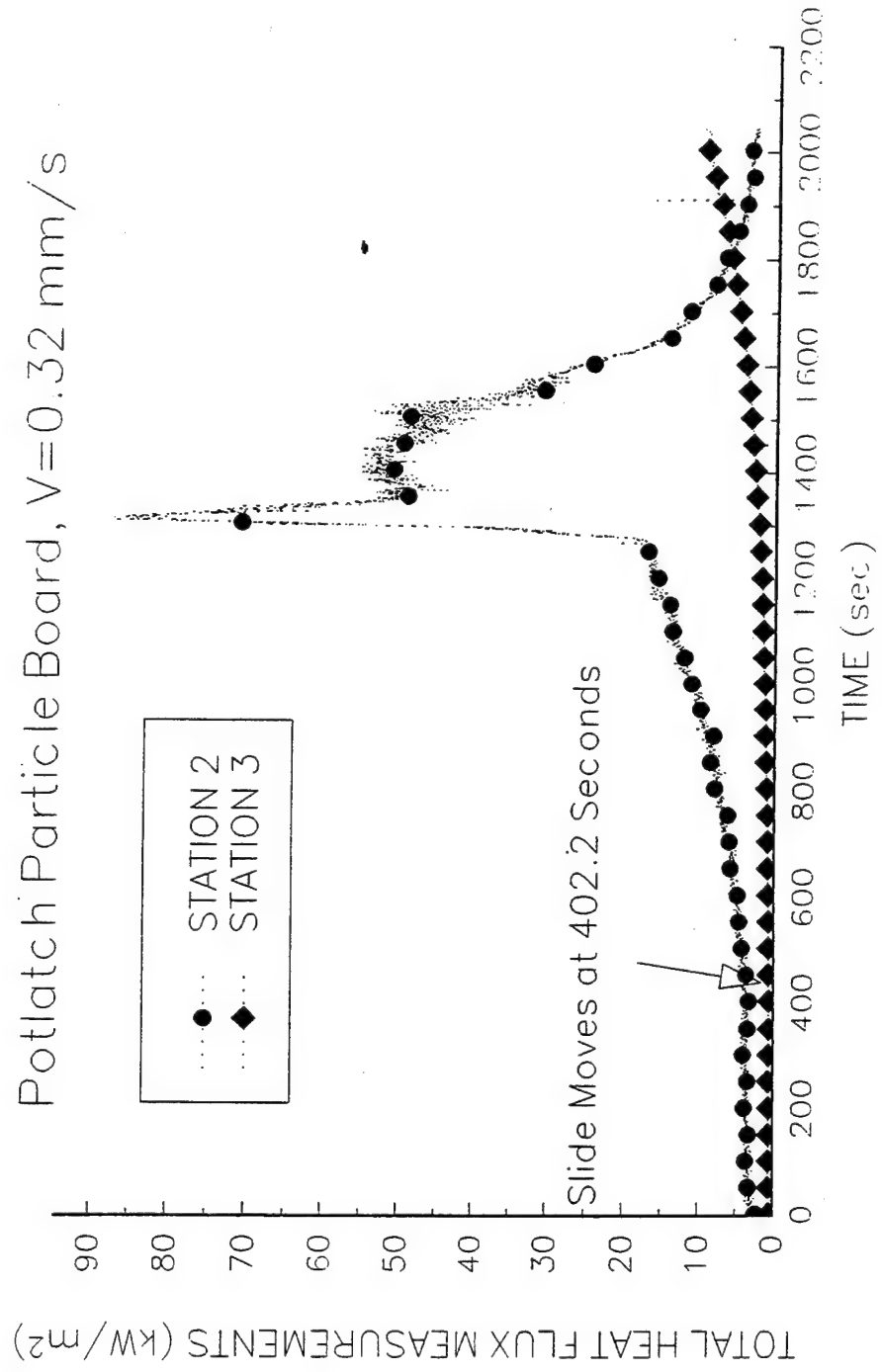
T10K617

Potlatch Partical Board, V=0.32 mm/s

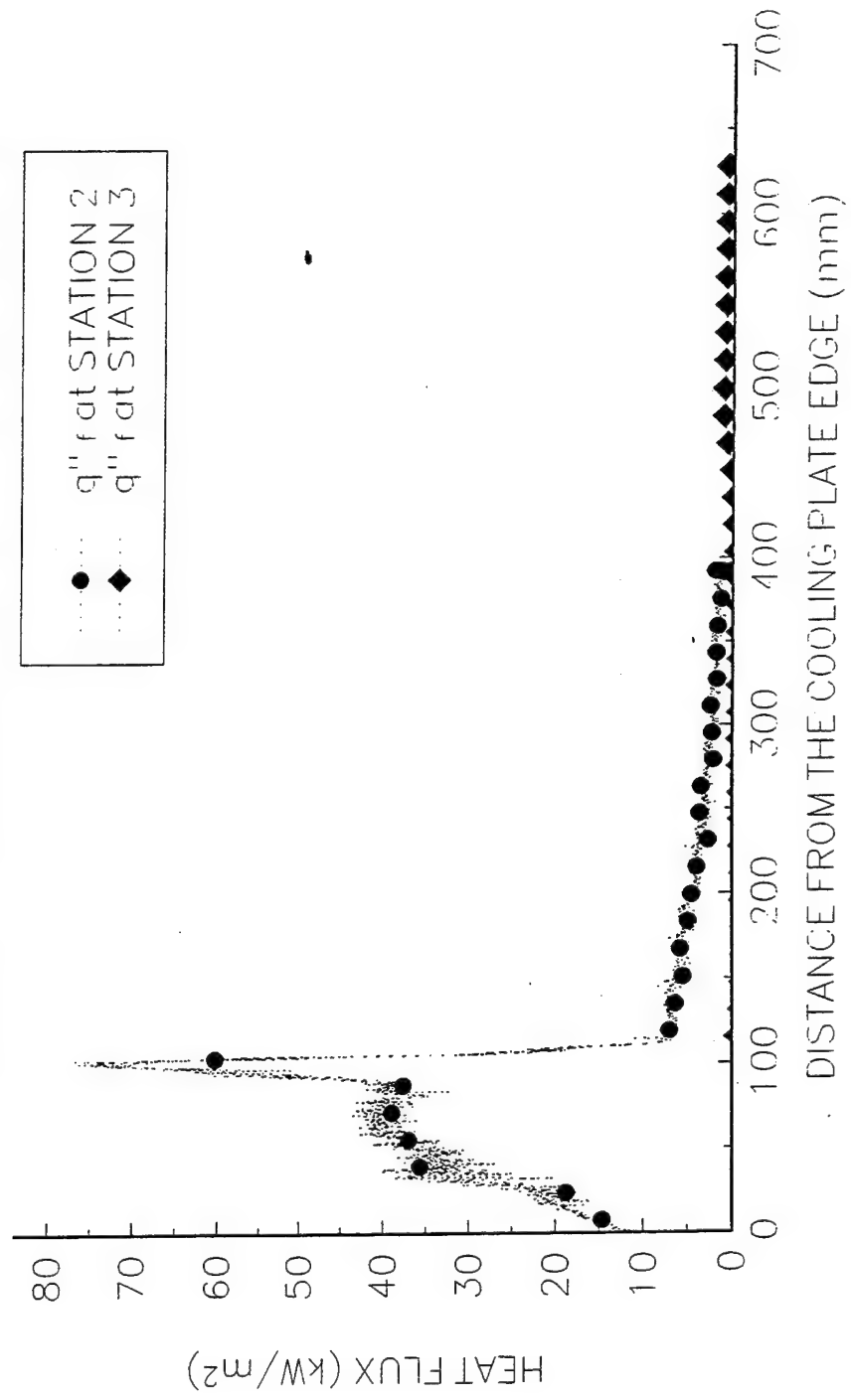


T10K617

Potlatch Particle Board,  $V=0.32$  mm/s

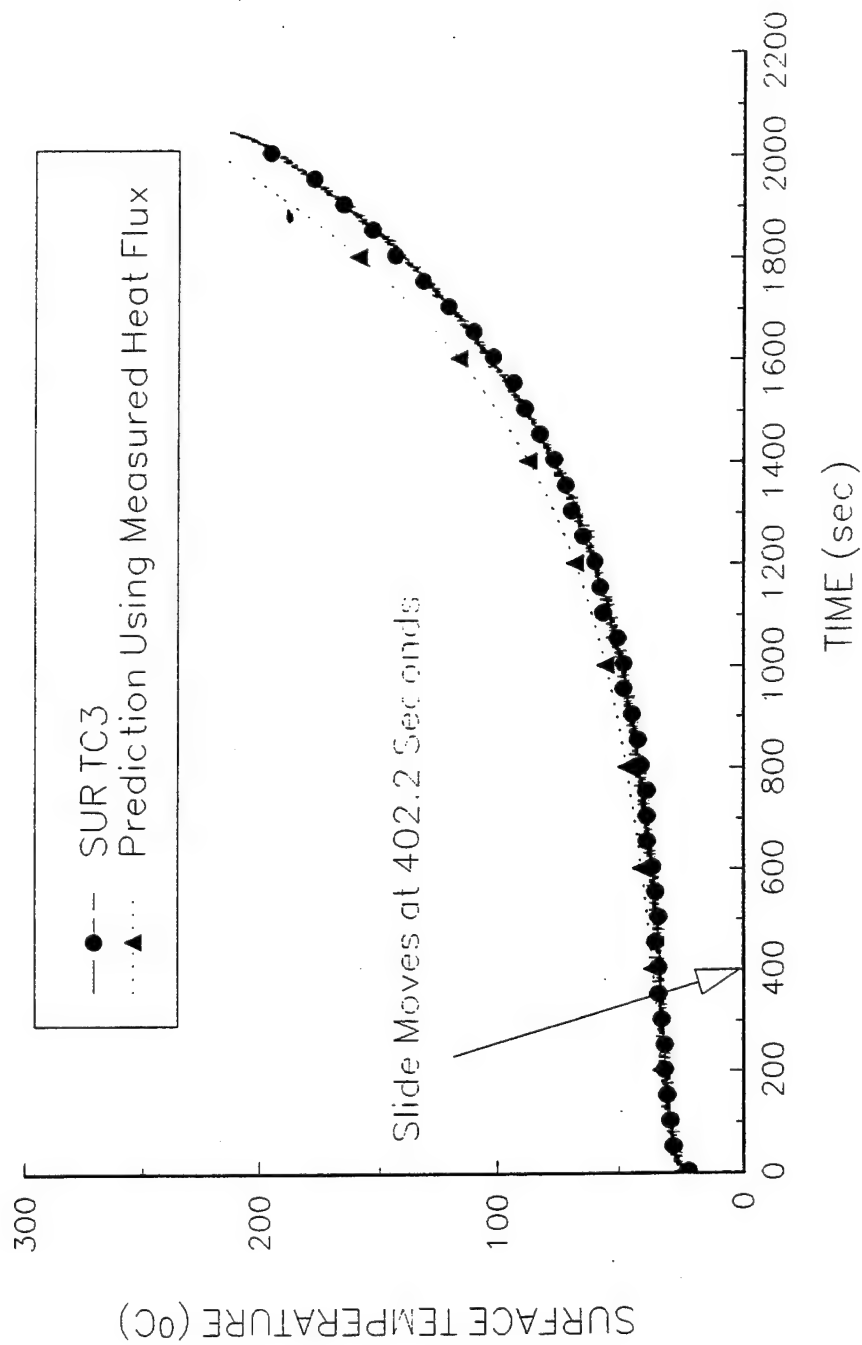


T10K617  
Potlatch Particle Board,  $V=0.32$  mm/s



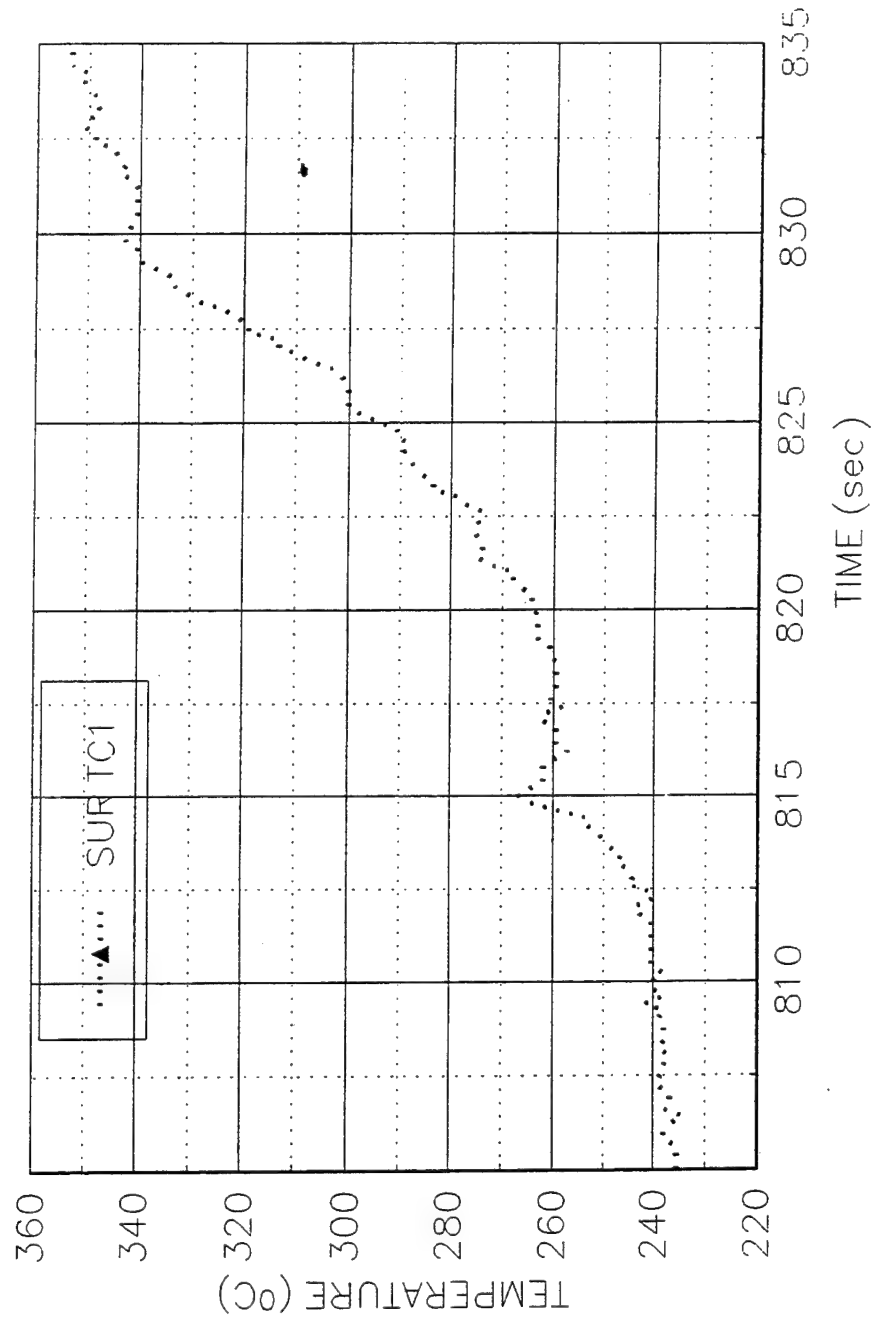
T10K617

Potlatch Particle Board,  $V=0.32$  mm/s



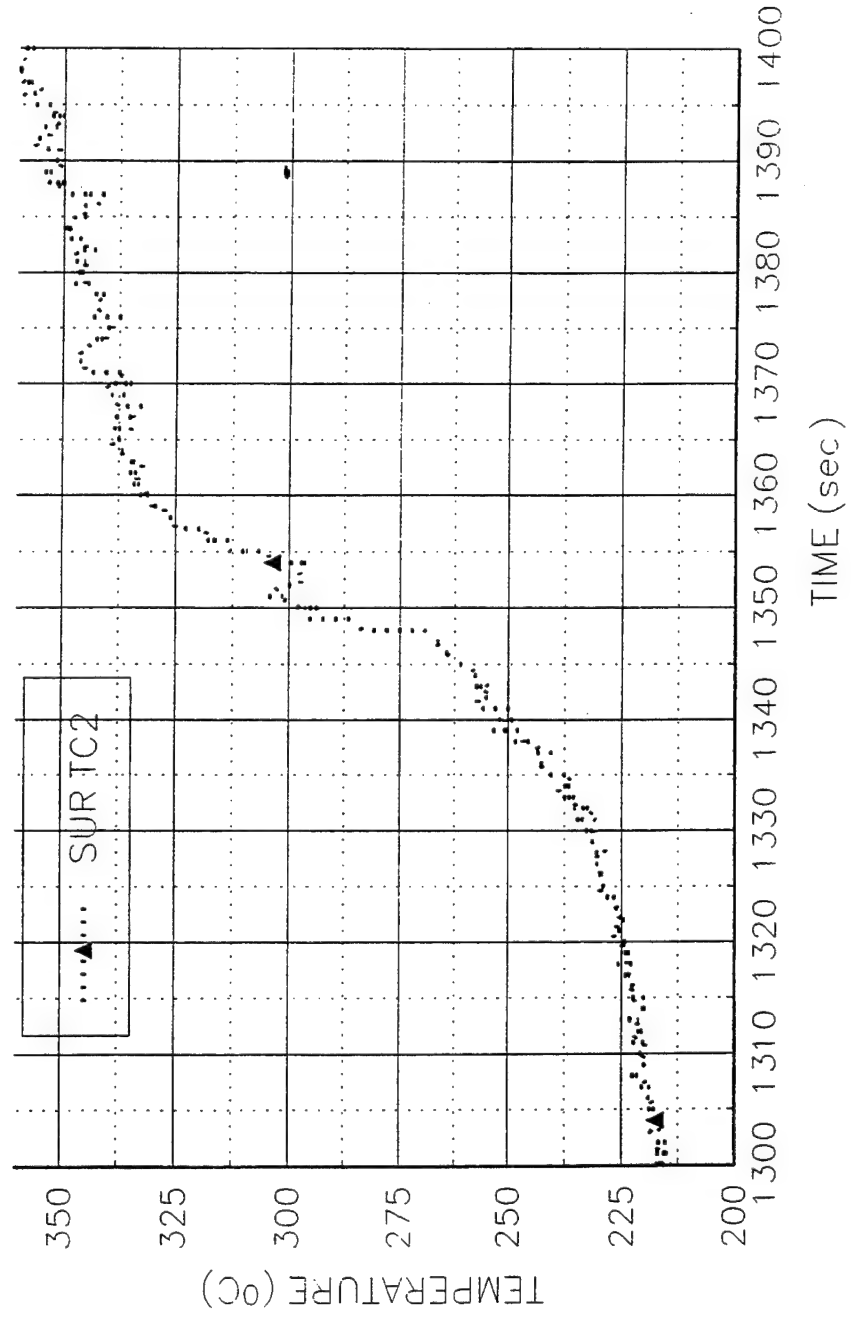
T10K617

Potlatch Partical Board, V=0.32 mm/s



T10K617

Potlatch Partical Board, V=0.32 mm/s





**Data Sheet**  
**Constant Horizontal Flame Spread Experiment**

Experimental No.: 22

Date: 6/20/94 Tu

Time: 8:30 pm

**Pre-Experiment**

Heat Flux at 425 mm Location (Planned) (kW/m<sup>2</sup>): 10

Slider Speed (mm/s): 0.32 mm/s

**Burning Sample Data**

Material: 3/4" Potlatch Particle Board

Dimension(LxWxH, mm): 600x152x18.85

**Instrumentation**

Number of Thermocouples: 5

Number of Heat Flux Gauges: 2

Station	Sensor	x (mm)	z (mm)	File Column	Note
1	TC	170	0.8	B	GAS TC1
1	TC	170	0	C	SURFACE
2	TC	333	0.41	D	GAS TC2
2	TC	333	0	E	SURFACE
2	HG	333	0	G	SER. 84501
3	TC	569	0	F	SURFACE
3	HG	569	0	H	SER. 525842

**Experiment**

Flux Gauge Reading @ 425 mm (Serial No. 27844, mV): 3.70-12.7576 kW/m<sup>2</sup>

Preheating Time without Pilot Flame (seconds): 240

Time to Sample Ignition After Applying the Pilot Flame (seconds): 20

Speed Used (S1M"Steps"): 50

Number of Steps (I1M"Steps"): 80000

File Names (.PRN): T10K620

Set-up File Name:

Sampling Rate (Hz): 5      Duration of Sampling (sec): 2500

Time to Start Moving the Sample (sec): 309.8

Ignition Heat Flux (Calculated, kW/m<sup>2</sup>): 16.7

**Ambient Conditions**

Temperature (°C): 24

**Observations** Burning area: -10 cm, -2 cm burnout area so the burning width is in fact 8 cm.

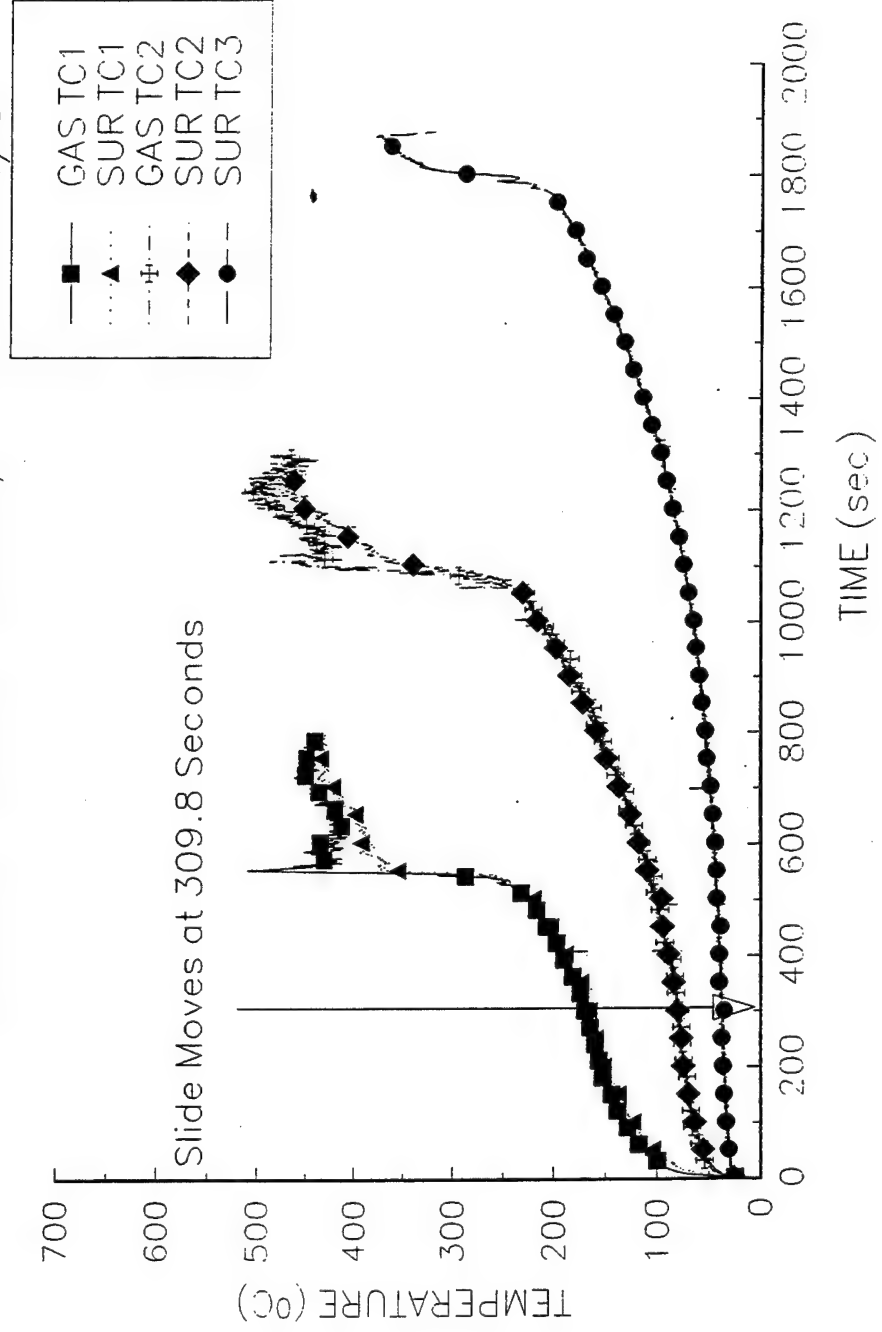
Personnel J.C, Y.C

Processing of Data:  $T_p = 320^\circ\text{C}$ , Surface TC1,  $1/\tau = 0.20$ ,  $T_{ext} = 238.7^\circ\text{C}$ ,  $k_{pc} = 0.17 \times 765 \times 2800 = 364140$ ,

$q_0'' = (k_{pc})^{1/2} (T_p - T_{ext}) (1/\tau)^{1/2} = (364140)^{1/2} \times (320 - 238.7) (0.20)^{1/2} = 21.94 \text{ kW/m}^2$

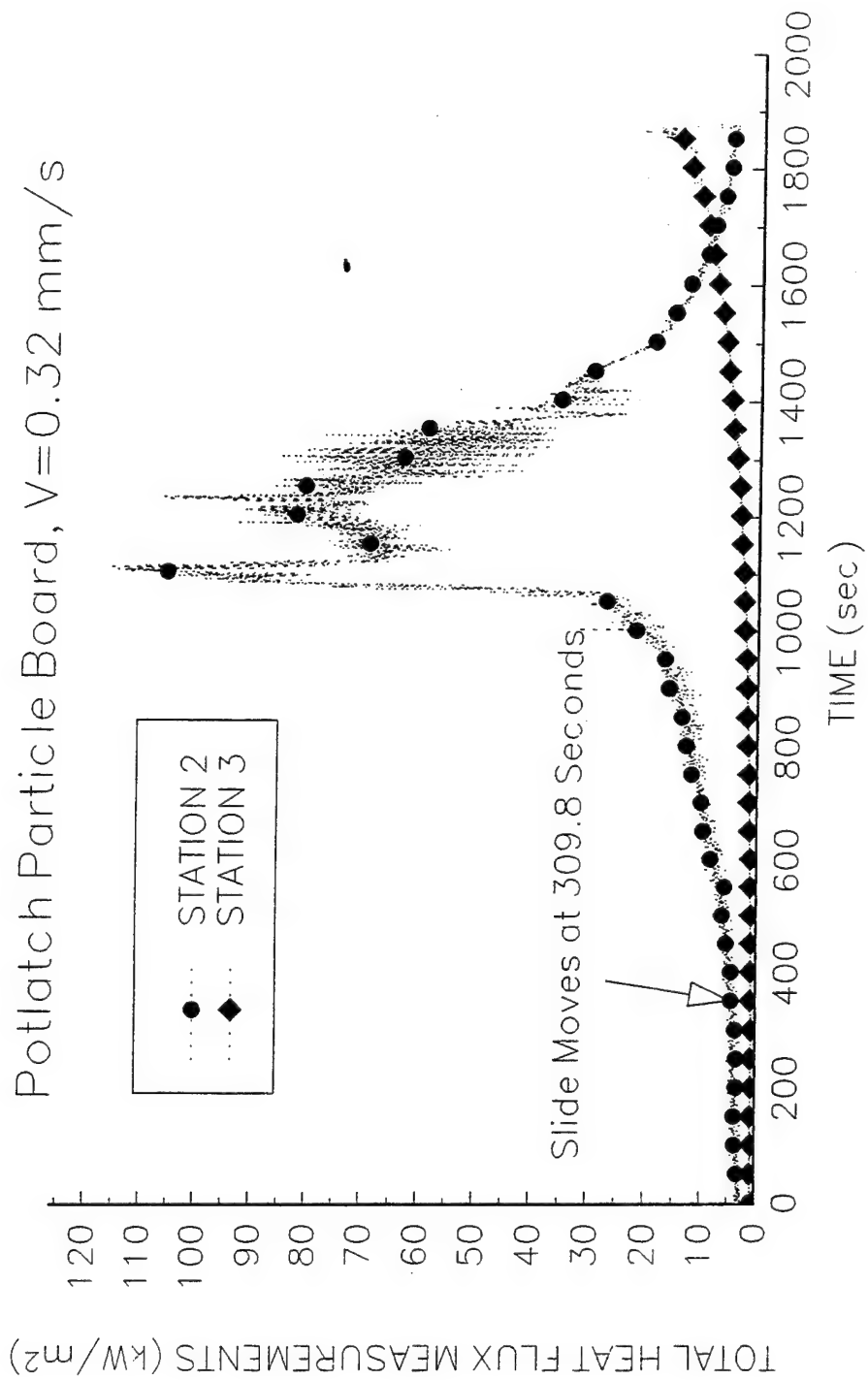
Surface TC2,  $1/\tau = 0.078$ ,  $T_{ext} = 238.7^\circ\text{C}$ ,  $q_0'' = (364140)^{1/2} \times (320 - 238.7) (0.078)^{1/2} = 13.70 \text{ kW/m}^2$

T10K620  
Potlatch-Partical Board, V=0.32 mm/s

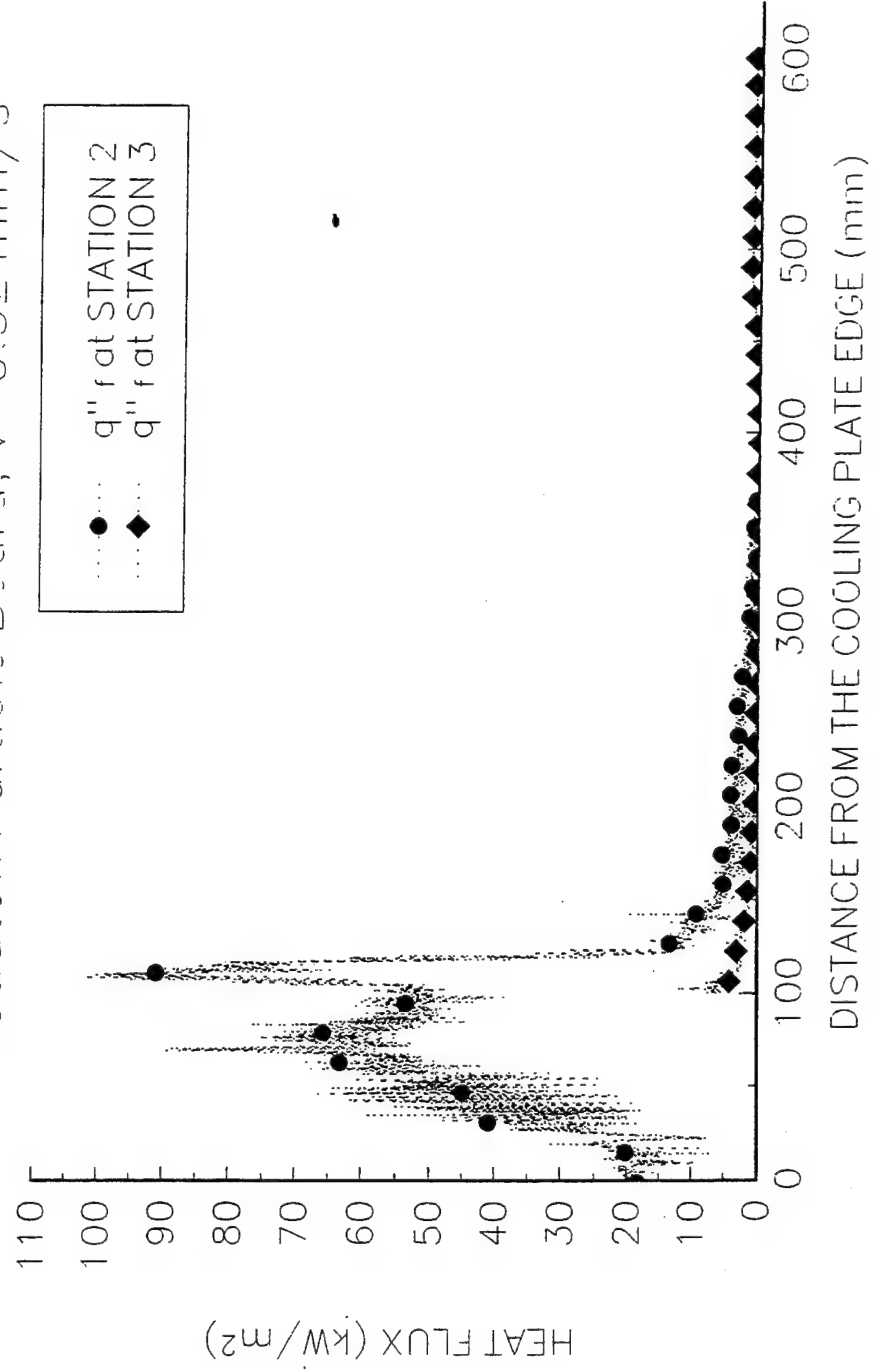


T10K620

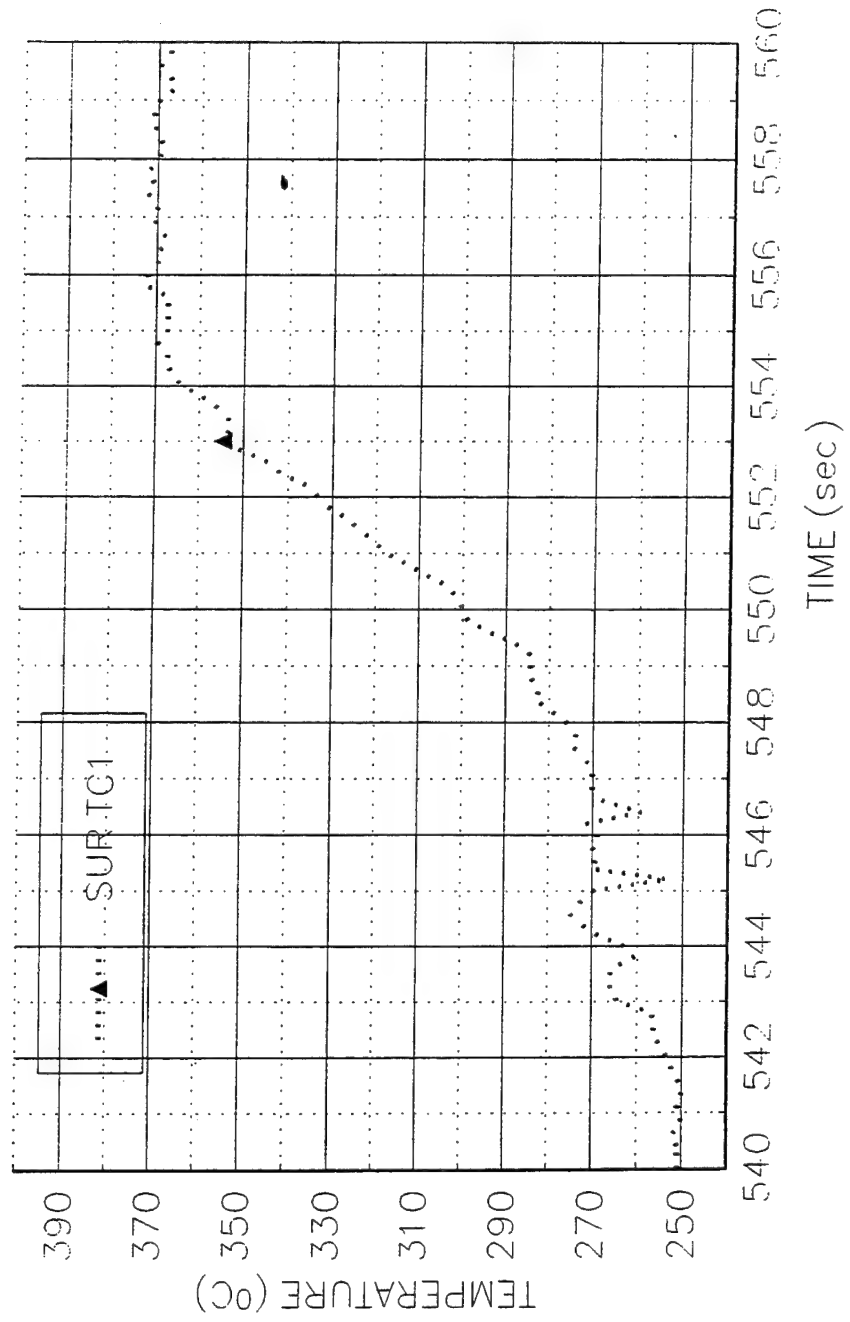
Potlatch Particle Board,  $V=0.32$  mm/s



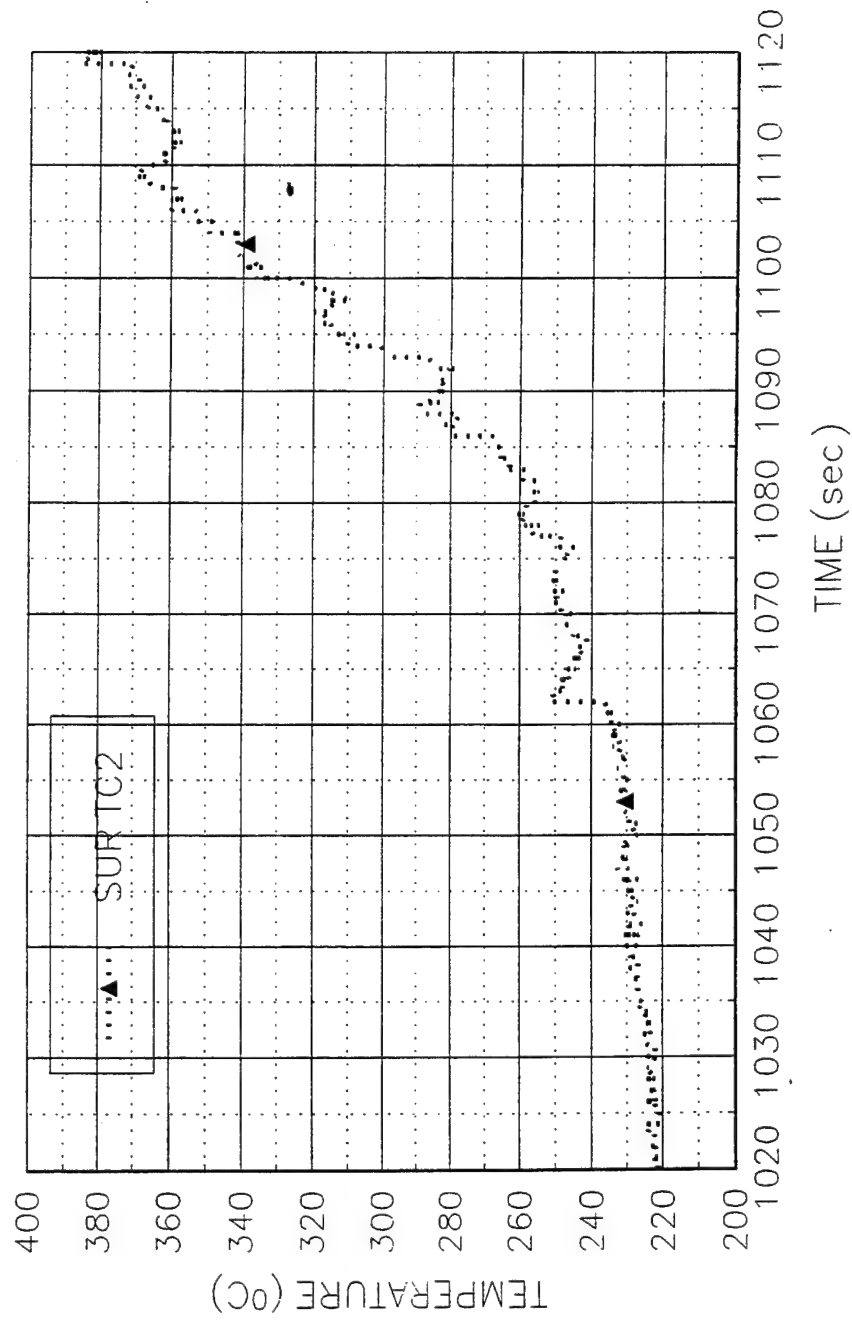
T10K620  
Potlatch Particle Board,  $V=0.32$  mm/s



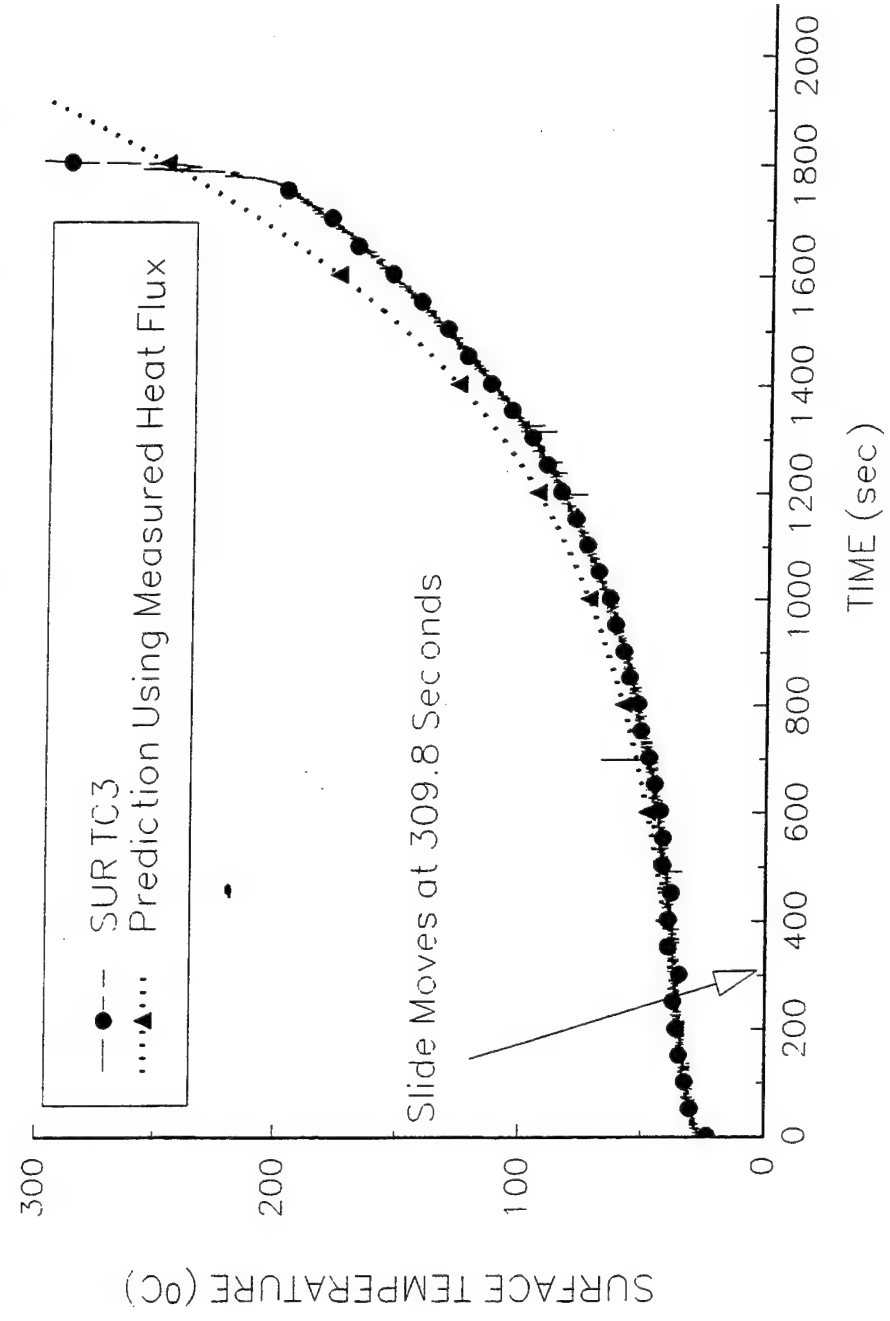
T10K620  
Potlatch Partical Board, V=0.32 mm/s



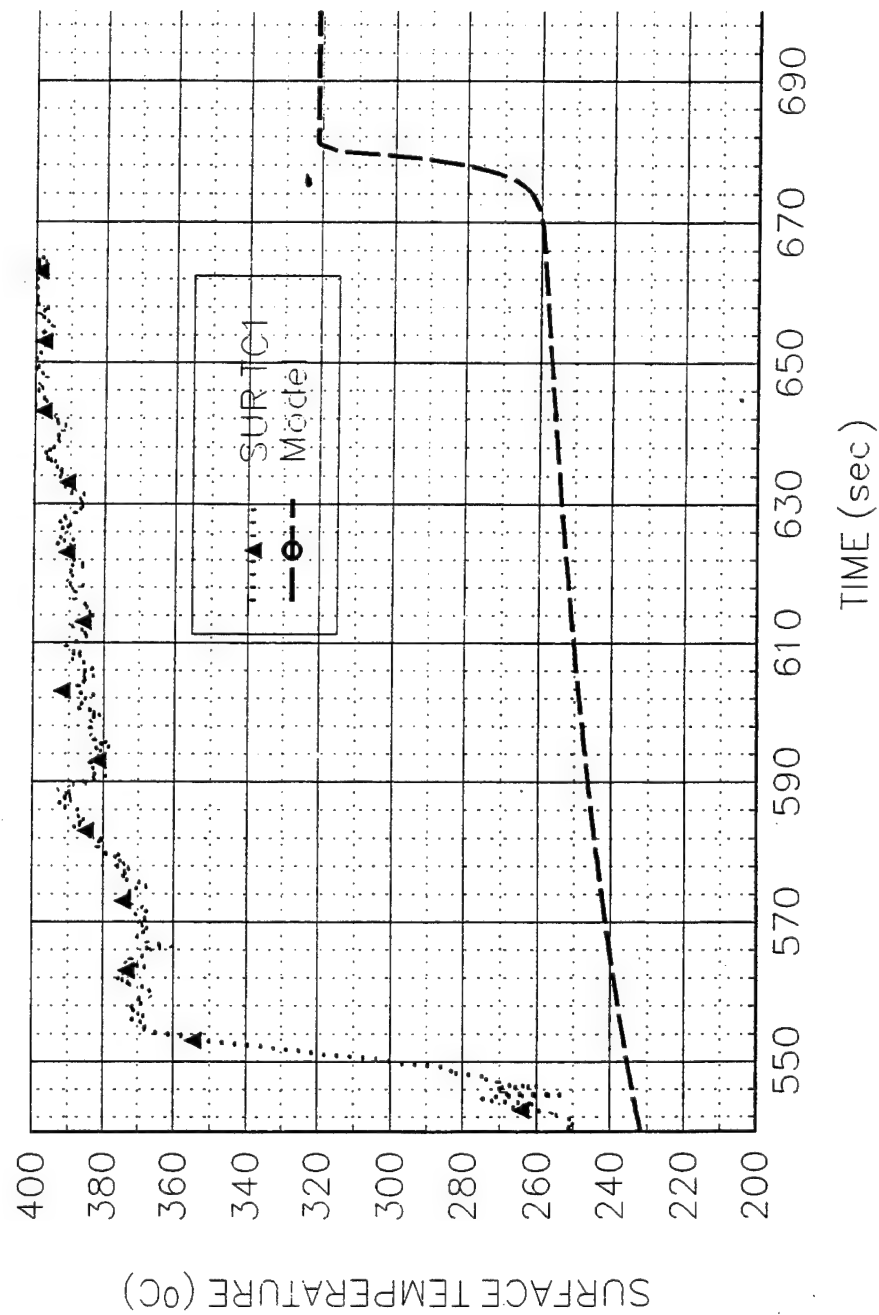
T10K620  
Potlatch Partical Board, V=0.32 mm/s



T10K620  
Potlatch Particle Board,  $V=0.32$  mm/s

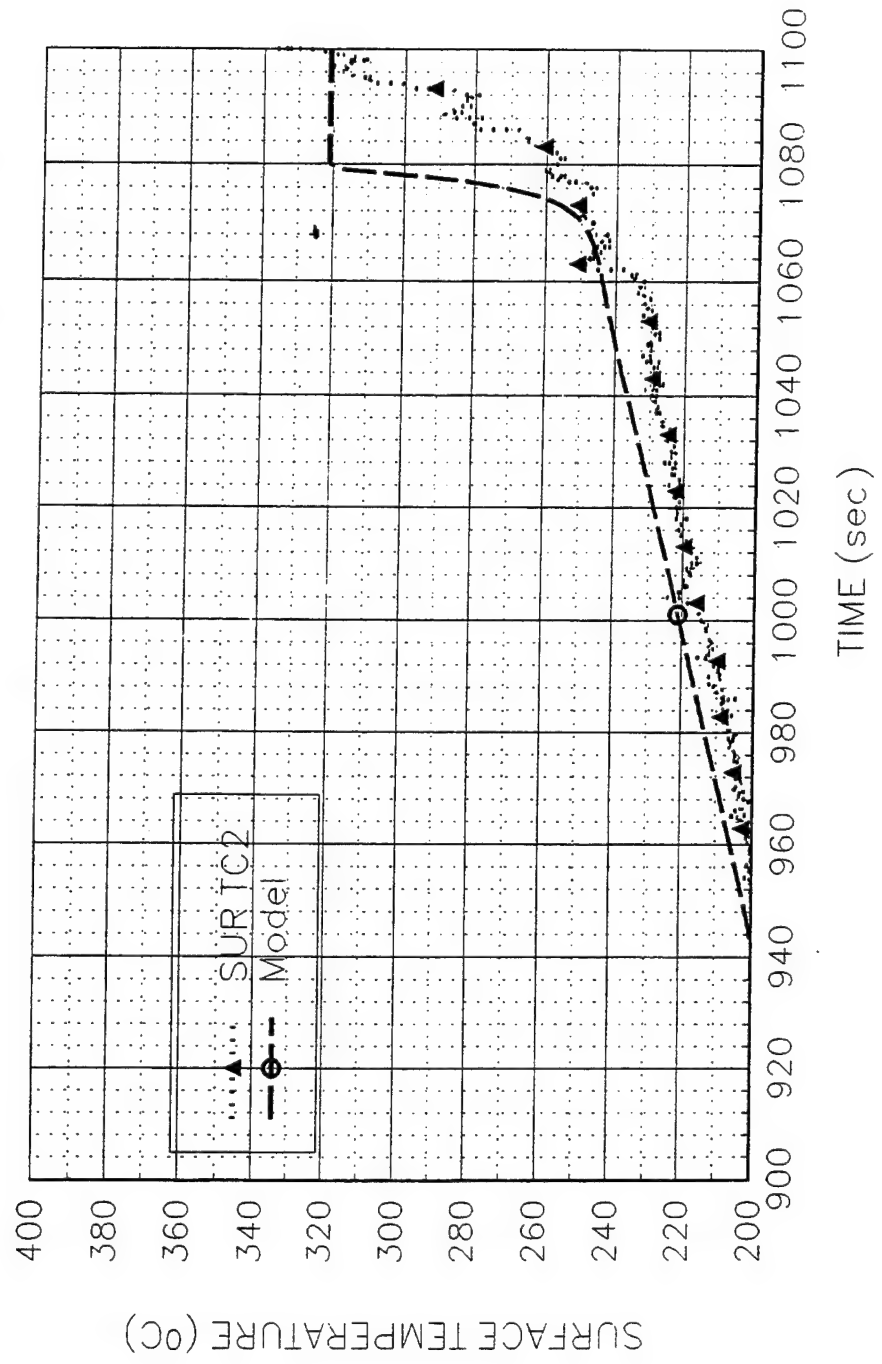


T10K620  
Potlatch Particle Board, V=0.32 mm/s





T10K620  
Potlatch Particle Board, V=0.32 mm/s



**Data Sheet**  
**Constant Horizontal Flame Spread Experiment**

Experimental No.: 23

Date: 6/21/94 Wed

Time: 10:30 am

**Pre-Experiment**

Heat Flux at 425 mm Location (Planned) (kW/m<sup>2</sup>): 10

Slider Speed (mm/s): 0.32 mm/s

**Burning Sample Data**

Material: 3/4" Potlatch Particle Board

Dimension (LxWxH, mm): 600x152x18.85

**Instrumentation**

Number of Thermocouples: 5

Number of Heat Flux Gauges: 2

Station	Sensor	x (mm)	z (mm)	File Column	Note
1	TC	167	0.7	B	GAS TC1
1	TC	167	0	C	SURFACE
2	TC	332	05	D	GAS TC2
2	TC	332	0	E	SURFACE
2	HG	332	0	G	SER. 84501
3	TC	568	0	F	SURFACE
3	HG	568	0	H	SER. 525842

**Experiment**

Flux Gauge Reading @ 425 mm (Serial No. 27844, mV): 3.70-12.61 kW/m<sup>2</sup>

Preheating Time without Pilot Flame (seconds): 252

Time to Sample Ignition After Applying the Pilot Flame (seconds): 18

Speed Used (S1M"Steps"): 50

Number of Steps (I1M"Steps"): 80000

File Names (.PRN): T10K621

Set-up File Name:

Sampling Rate (Hz): 5      Duration of Sampling (sec): 2500

Time to Start Moving the Sample (sec): 355.8

Ignition Heat Flux (Calculated, kW/m<sup>2</sup>):

**Ambient Conditions**

Temperature (°C): 24

**Observations** Burning area: 14-4=10 cm, -4 cm burnout area, HG1 did not flush with the surface and SUR TC3 had some problems in the middle of the test

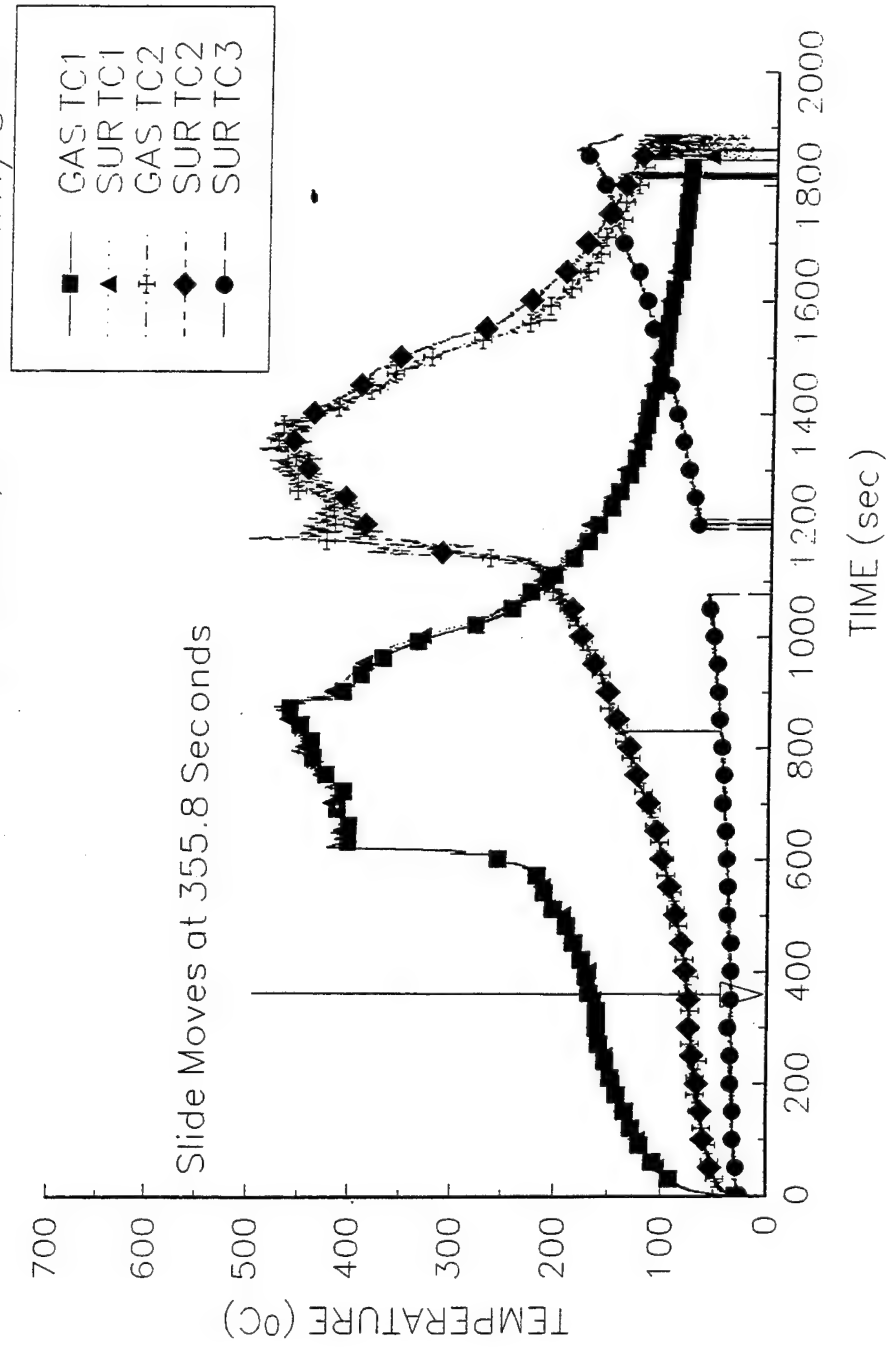
Personnel J.C, Y.C

Processing of Data:  $T_p = 320^\circ\text{C}$ , Surface TC1,  $1/\tau = 0.088$ ,  $T_{ext} = 225.8^\circ\text{C}$ ,  $k_{pc} = 0.17 \times 765 \times 2800 = 364140$ ,  
 $q_0'' = (k_{pc})^{1/2} (T_p - T_{ext}) (1/\tau)^{1/2} = (364140)^{1/2} \times (320 - 225.8) (0.088)^{1/2} = 16.86 \text{ kW/m}^2$

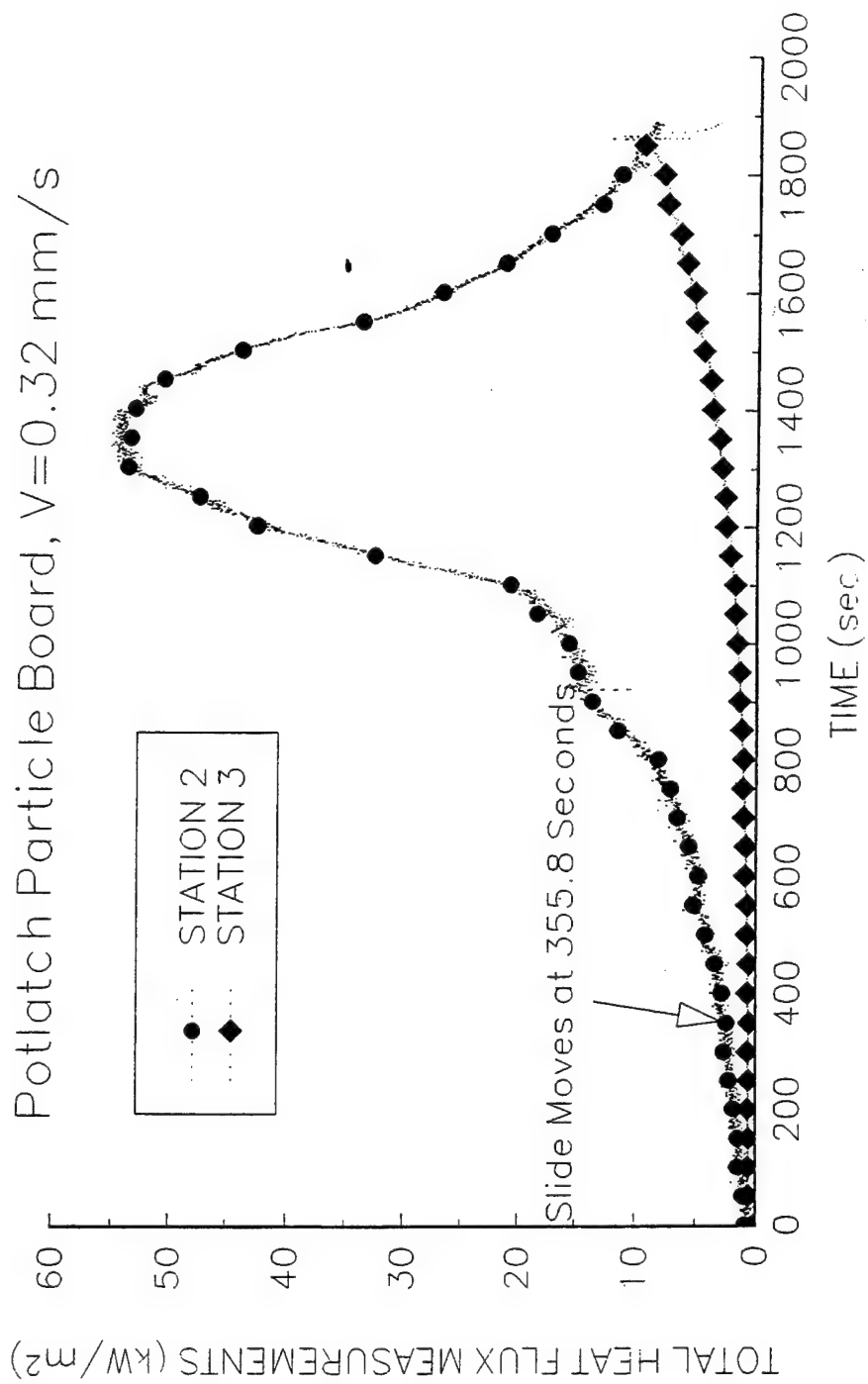
Surface TC2,  $1/\tau = 0.071$ ,  $T_{ext} = 225.8^\circ\text{C}$ ,  $q_0'' = (364140)^{1/2} \times (320 - 225.8) (0.071)^{1/2} = 15.15 \text{ kW/m}^2$

T10K621

Potlatch Partical Board, V=0.32 mm/s

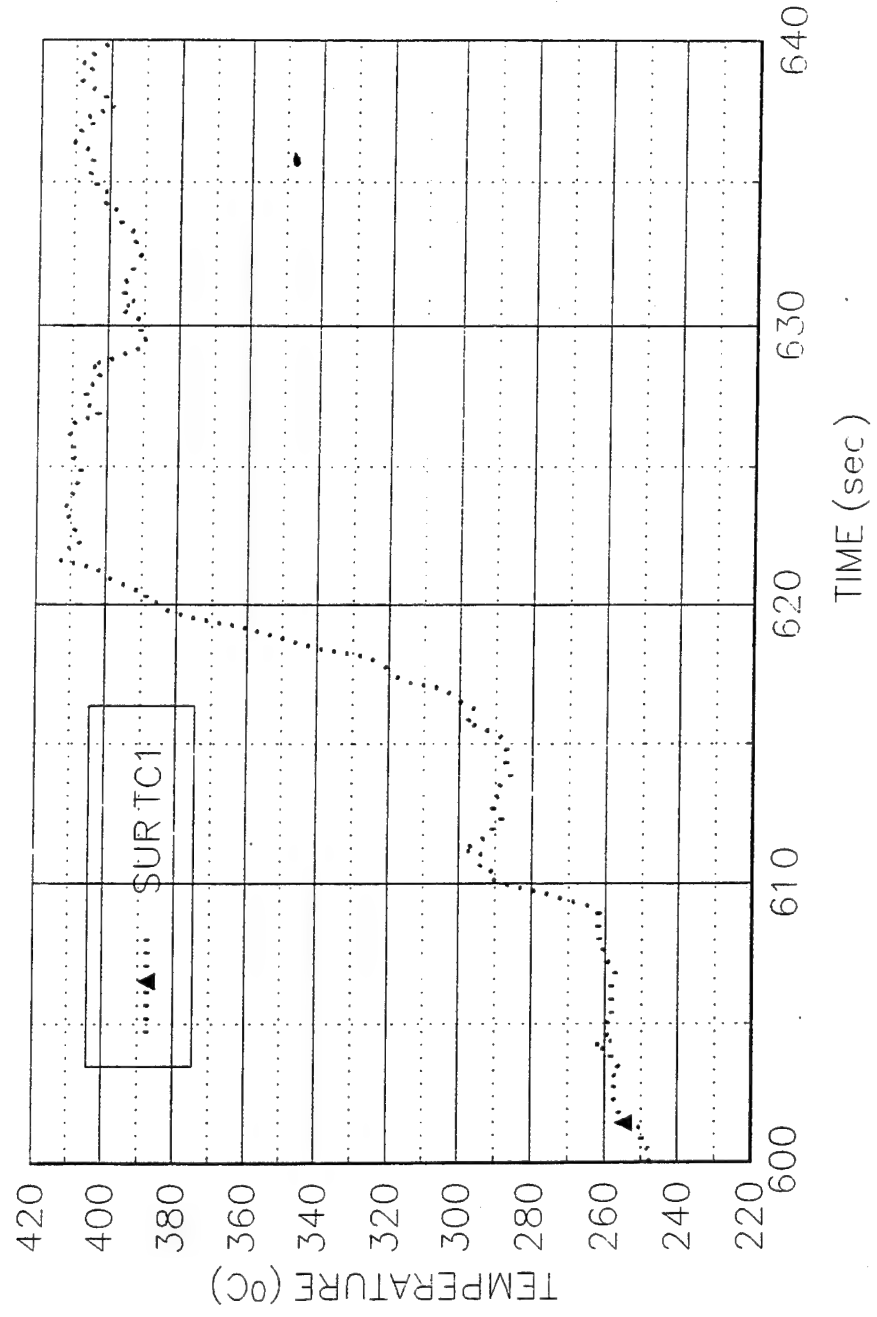


T10K621



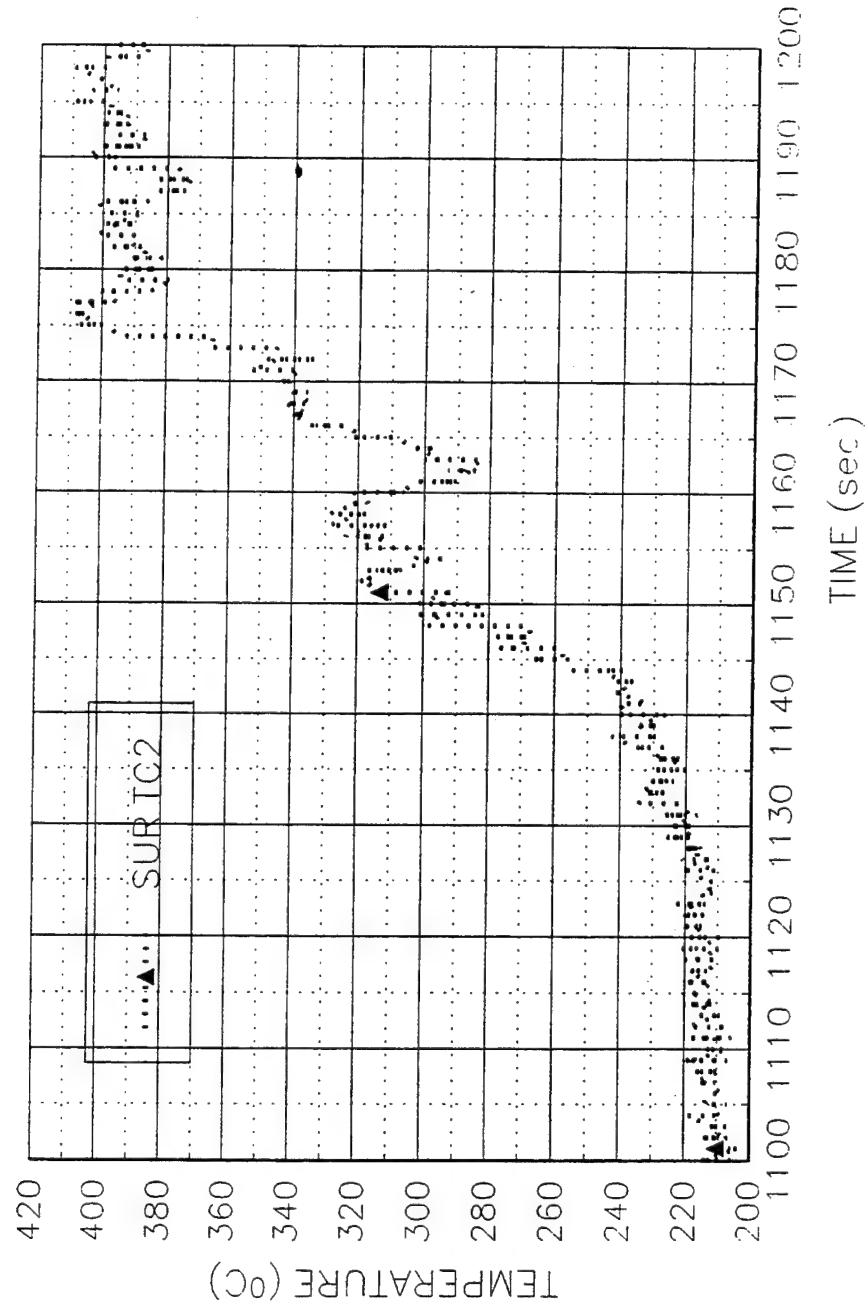
T10K621

Potlatch Partical Board, V=0.32 mm/s



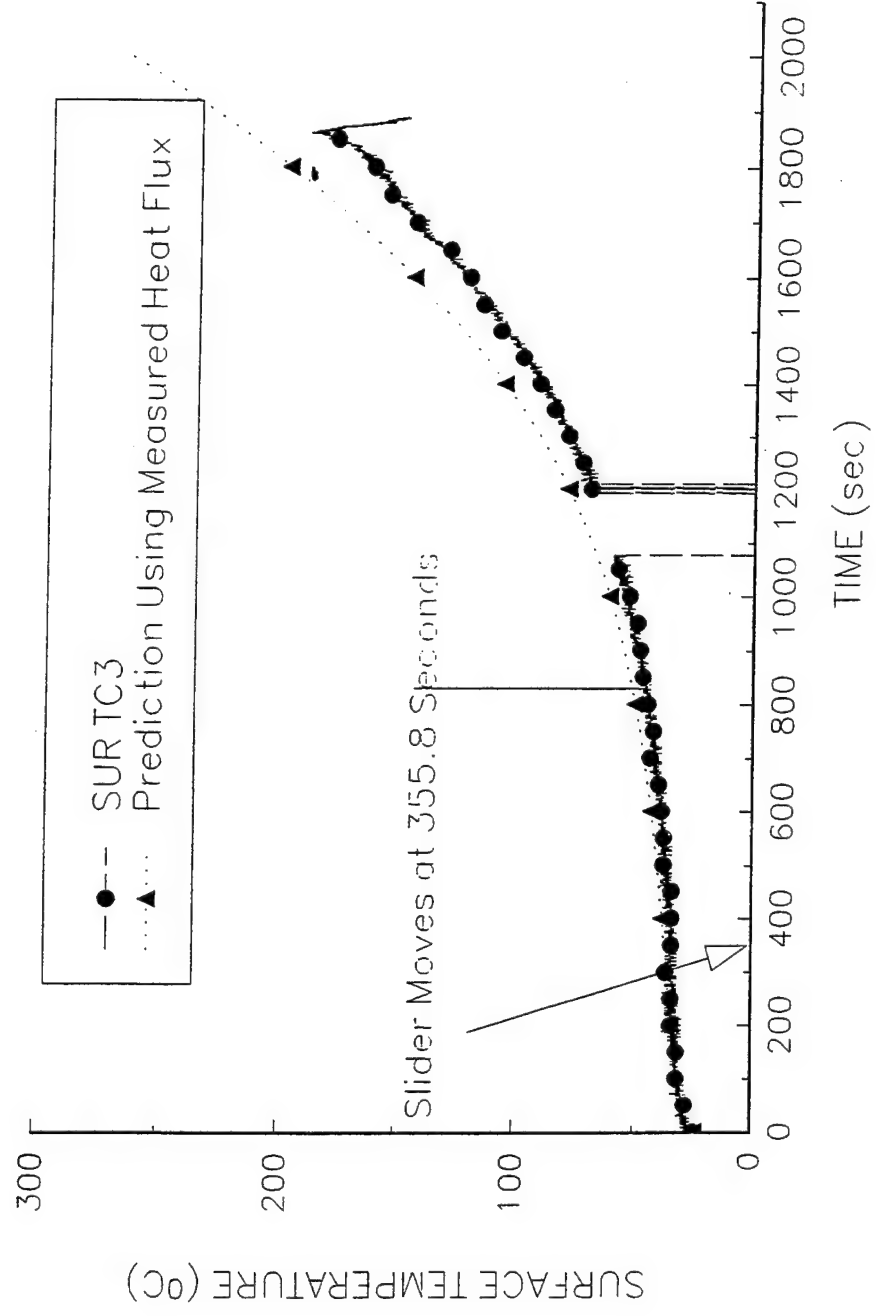
T10K621

Potlatch Partical Board, V=0.32 mm/s



T10K621

Potlatch Particle Board,  $V=0.32 \text{ mm/s}$



**Data Sheet**  
**Constant Horizontal Flame Spread Experiment**

Experimental No.: 24

Date: 6/21/94 Wed

Time: 8:30 pm

**Pre-Experiment**

Heat Flux at 425 mm Location (Planned) (kW/m<sup>2</sup>): 20

Slider Speed (mm/s): 1.28 mm/s

**Burning Sample Data**

Material: 3/4" Potlatch Particle Board

Dimension(LxWxH, mm): 600x152x18.85

**Instrumentation**

Number of Thermocouples: 5

Number of Heat Flux Gauges: 2

Station	Sensor	x (mm)	z (mm)	File Column	Note
1	TC	174	1	B	GAS TC1
1	TC	174	0	C	SURFACE
2	TC	338	0.6	D	GAS TC2
2	TC	338	0	E	SURFACE
2	HG	338	0	G	SER. 84501
3	TC	574	0	F	SURFACE
3	HG	574	0	H	SER. 525842

**Experiment**

Flux Gauge Reading @ 425 mm (Serial No. 27844, mV): 7.45-25.38 kW/m<sup>2</sup>

Preheating Time without Pilot Flame (seconds): 120

Time to Sample Ignition After Applying the Pilot Flame (seconds): 0

Speed Used (S1M"Steps"): 200

Number of Steps (I1M"Steps"): 80000

File Names (.PRN): T20K621

Set-up File Name:

Sampling Rate (Hz): 5      Duration of Sampling (sec): 2500

Time to Start Moving the Sample (sec): 126.8

Ignition Heat Flux (Calculated, kW/m<sup>2</sup>):

**Ambient Conditions**

Temperature (°C): 24

**Observations** Burning width: 12 cm, no burnout area, SUR TC3 is not good

Personnel J.C, Y.C

Processing of Data:  $T_p = 320^\circ\text{C}$ , Surface TC1,  $1/\tau = 0.61$ ,  $T_{ext} = 271^\circ\text{C}$ ,  $k_{pc} = 0.17 \times 765 \times 2800 = 364140$ ,

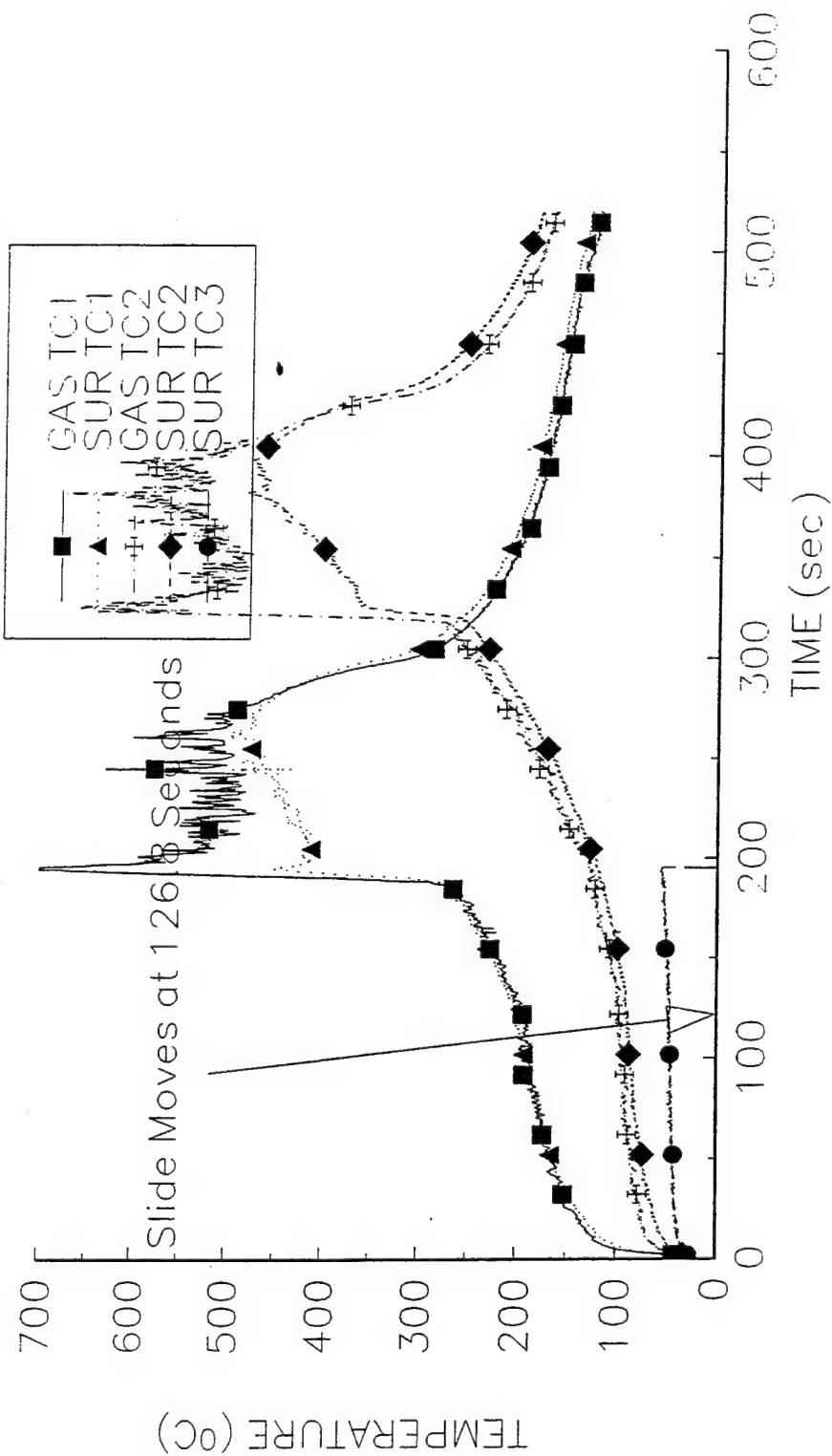
$q_o'' = (k_{pc})^{1/2} (T_p - T_{ext}) (1/\tau)^{1/2} = (364140)^{1/2} \times (320 - 271) (0.61)^{1/2} = 23.09 \text{ kW/m}^2$

Surface TC2,  $1/\tau = 0.077$ ,  $T_{ext} = 271^\circ\text{C}$ ,  $q_o'' = (364140)^{1/2} \times (320 - 271) (0.77)^{1/2} = 30.16 \text{ kW/m}^2$



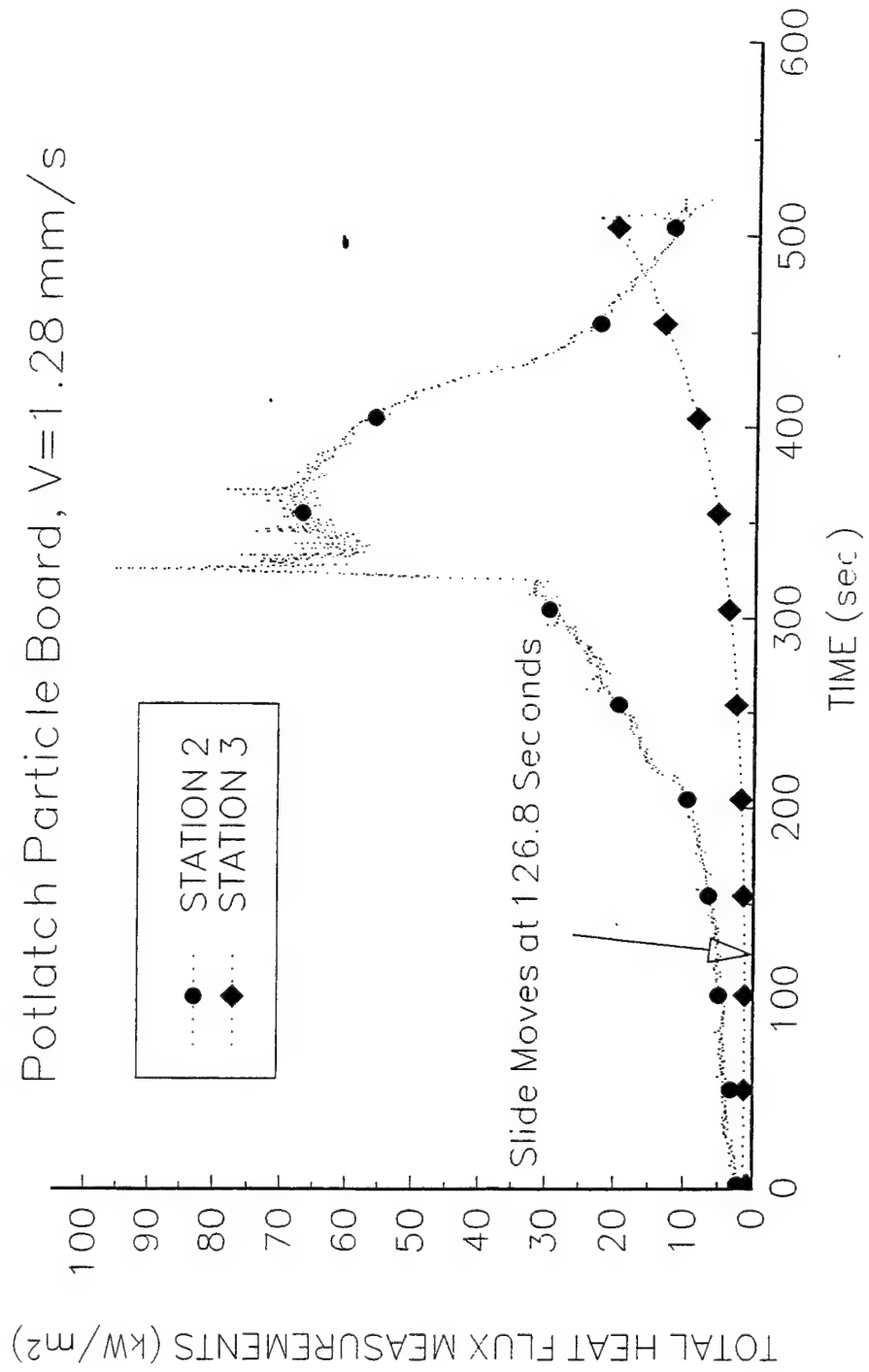
T20K621

Potlatch Partical Board, V=1.28 mm/s



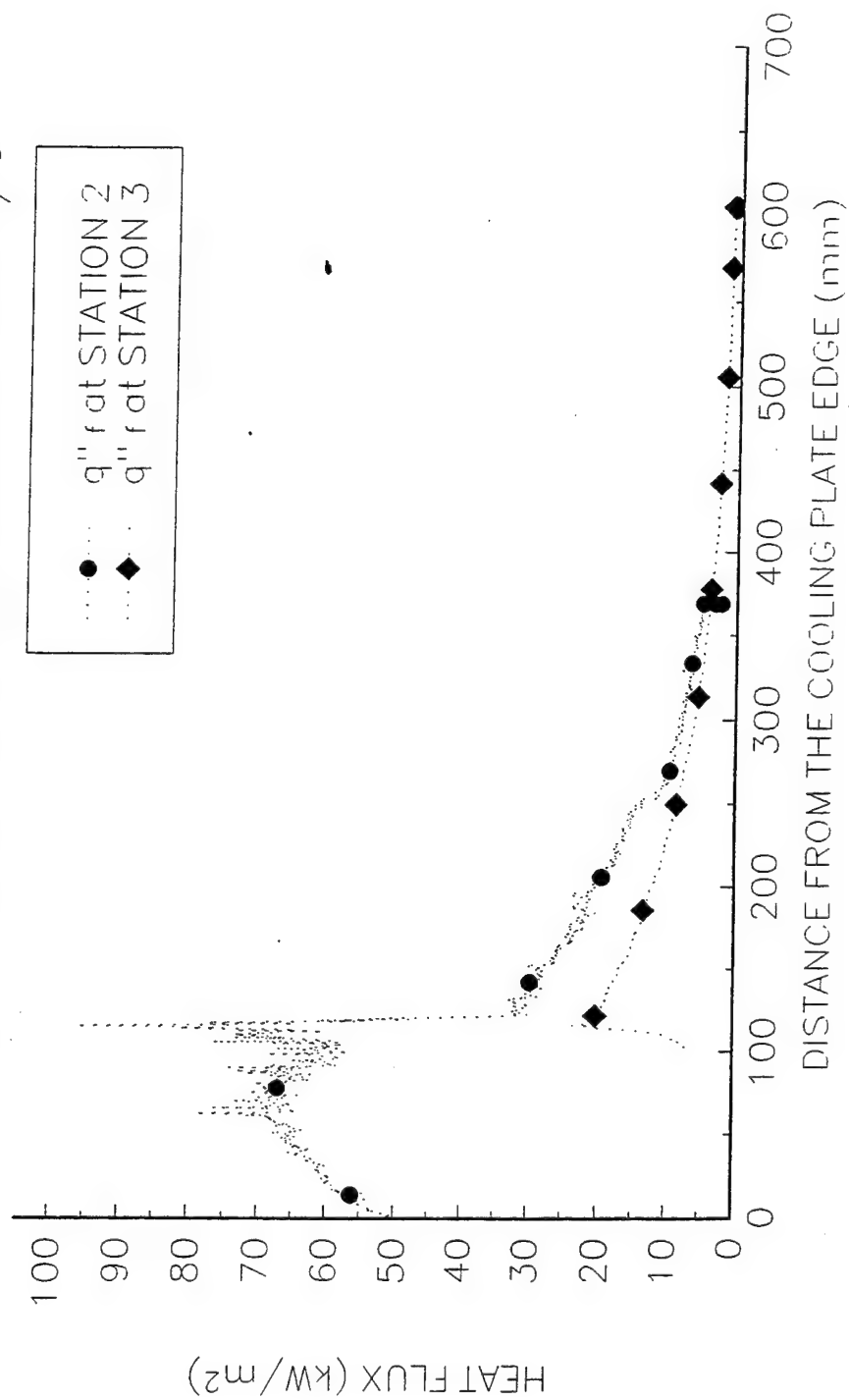
T20K621

Potlatch Particle Board,  $V=1.28 \text{ mm/s}$



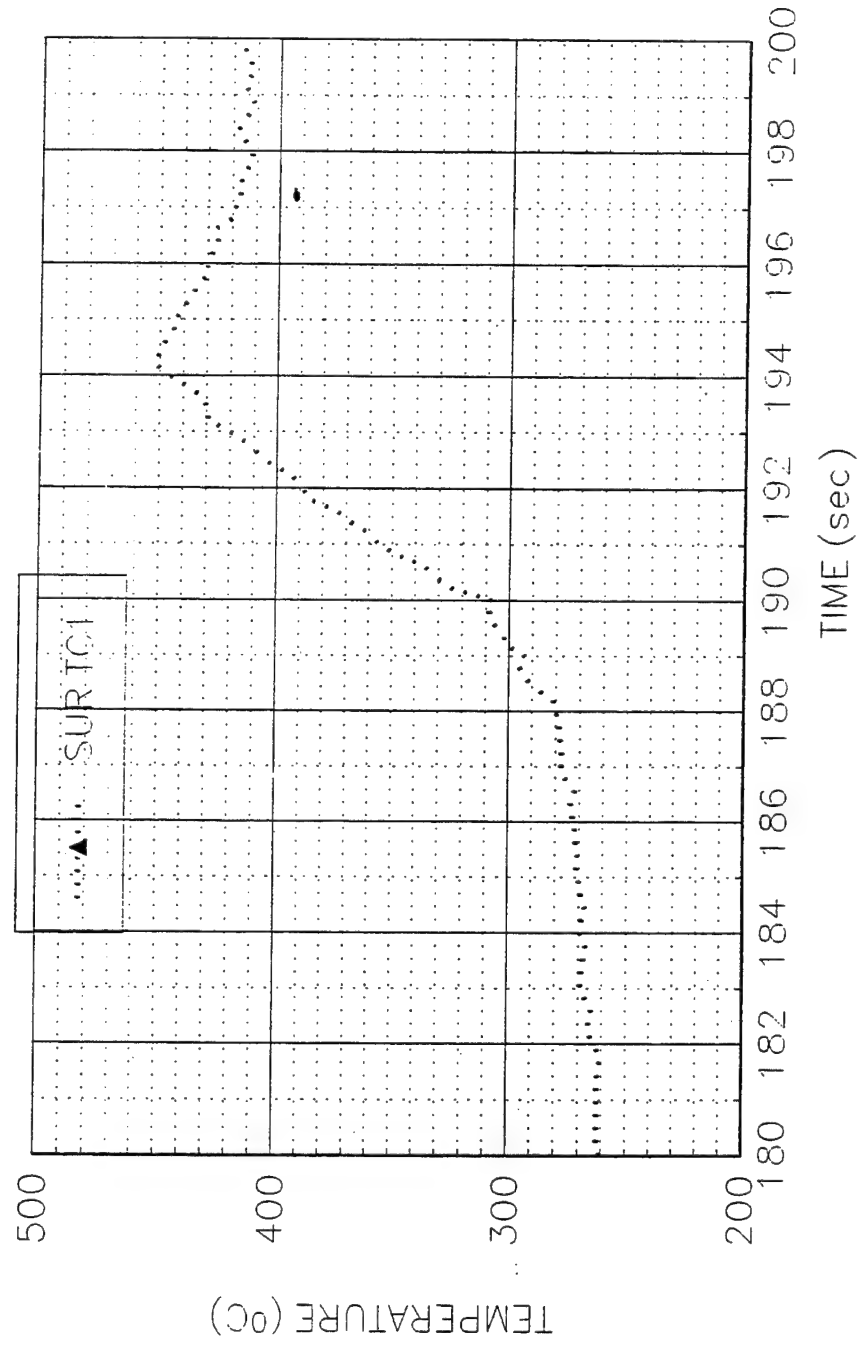
T20K621

Potlatch Particle Board,  $V=1.28 \text{ mm/s}$



T20K621

Potlatch Partical Board, V=1.28 mm/s



**Data Sheet**  
**Constant Horizontal Flame Spread Experiment**

Experimental No.: 25

Date: 6/22/94 Wed

Time: 8:30 pm

**Pre-Experiment**

Heat Flux at 425 mm Location (Planned) (kW/m<sup>2</sup>): 20

Slider Speed (mm/s): 1.28 mm/s

**Burning Sample Data**

Material: 3/4" Potlatch Particle Board

Dimension(LxWxH, mm): 600x152x18.85

**Instrumentation**

Number of Thermocouples: 5

Number of Heat Flux Gauges: 2

Station	Sensor	x (mm)	z (mm)	File Column	Note
1	TC	176	0.9	B	GAS TC1
1	TC	176	0	C	SURFACE
2	TC	342	0.4	D	GAS TC2
2	TC	342	0	E	SURFACE
2	HG	342	0	G	SER. 84501
3	TC	578	0	F	SURFACE
3	HG	578	0	H	SER. 525842

**Experiment**

Flux Gauge Reading @ 425 mm (Serial No. 27844, mV): 6.00 mV- 20.44 kW/m<sup>2</sup>

Preheating Time without Pilot Flame (seconds): 120

Time to Sample Ignition After Applying the Pilot Flame (seconds): 0

Speed Used (S1M"Steps"): 200

Number of Steps (I1M"Steps"): 80000

File Names (.PRN): T20K622

Set-up File Name:

Sampling Rate (Hz): 5      Duration of Sampling (sec): 2500

Time to Start Moving the Sample (sec): 129.2

Ignition Heat Flux (Calculated, kW/m<sup>2</sup>):

**Ambient Conditions**

Temperature (°C): 23

**Observations** Burning width ~7 cm

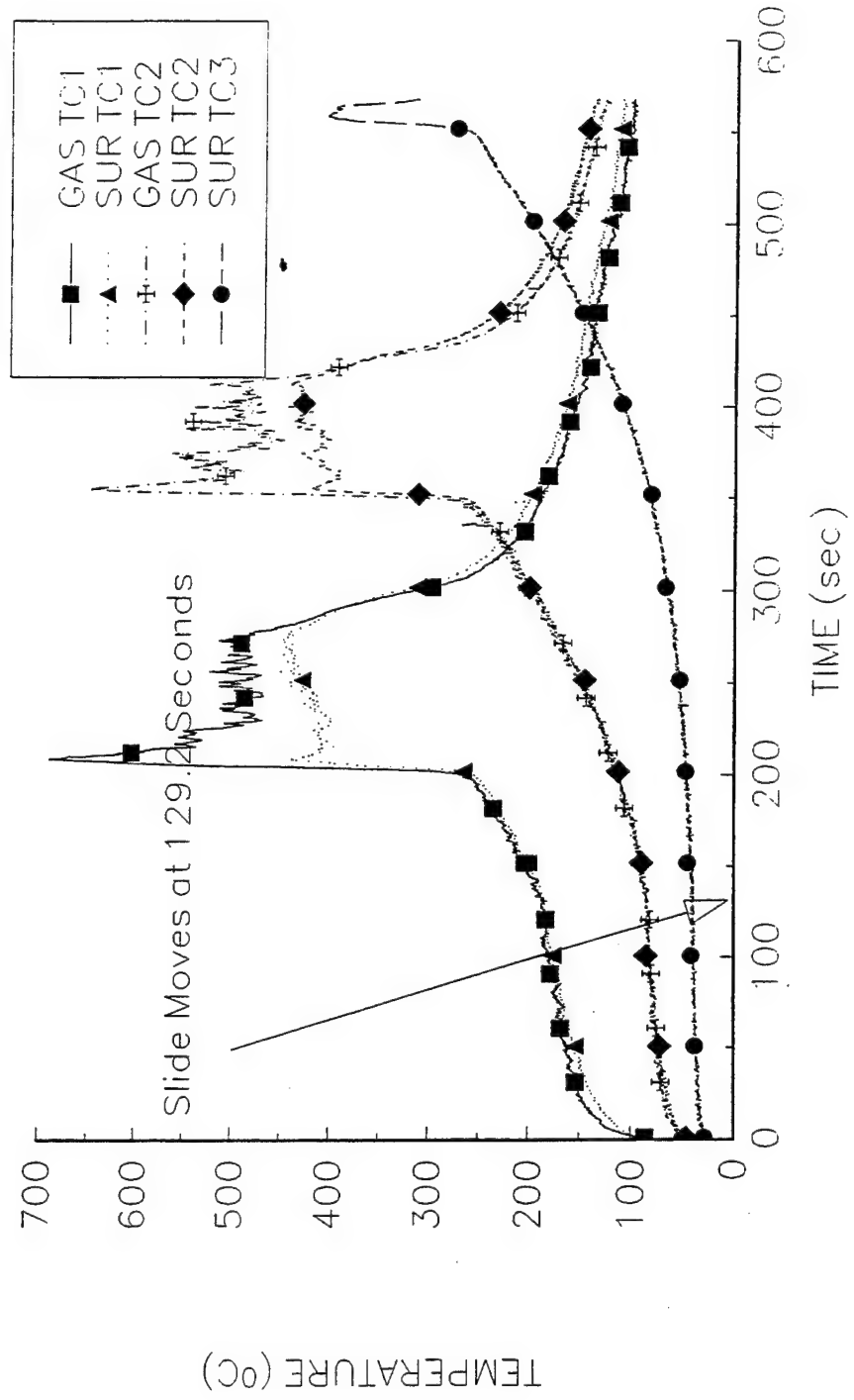
Personnel J.C, Y.C

Processing of Data:  $T_p = 320^\circ\text{C}$ , Surface TC1,  $1/\tau = 0.77$ ,  $T_{ext} = 259.4^\circ\text{C}$ ,  $k_{pc} = 0.17 \times 765 \times 2800 = 364140$ ,  
 $q_0'' = (k_{pc})^{1/2} (T_p - T_{ext}) (1/\tau)^{1/2} = (364140)^{1/2} \times (320 - 259.4) (0.77)^{1/2} = 32.09 \text{ kW/m}^2$

Surface TC2,  $1/\tau = 0.68$ ,  $T_{ext} = 259.4^\circ\text{C}$ ,  $q_0'' = (364140)^{1/2} \times (320 - 259.4) (0.68)^{1/2} = 30.16 \text{ kW/m}^2$

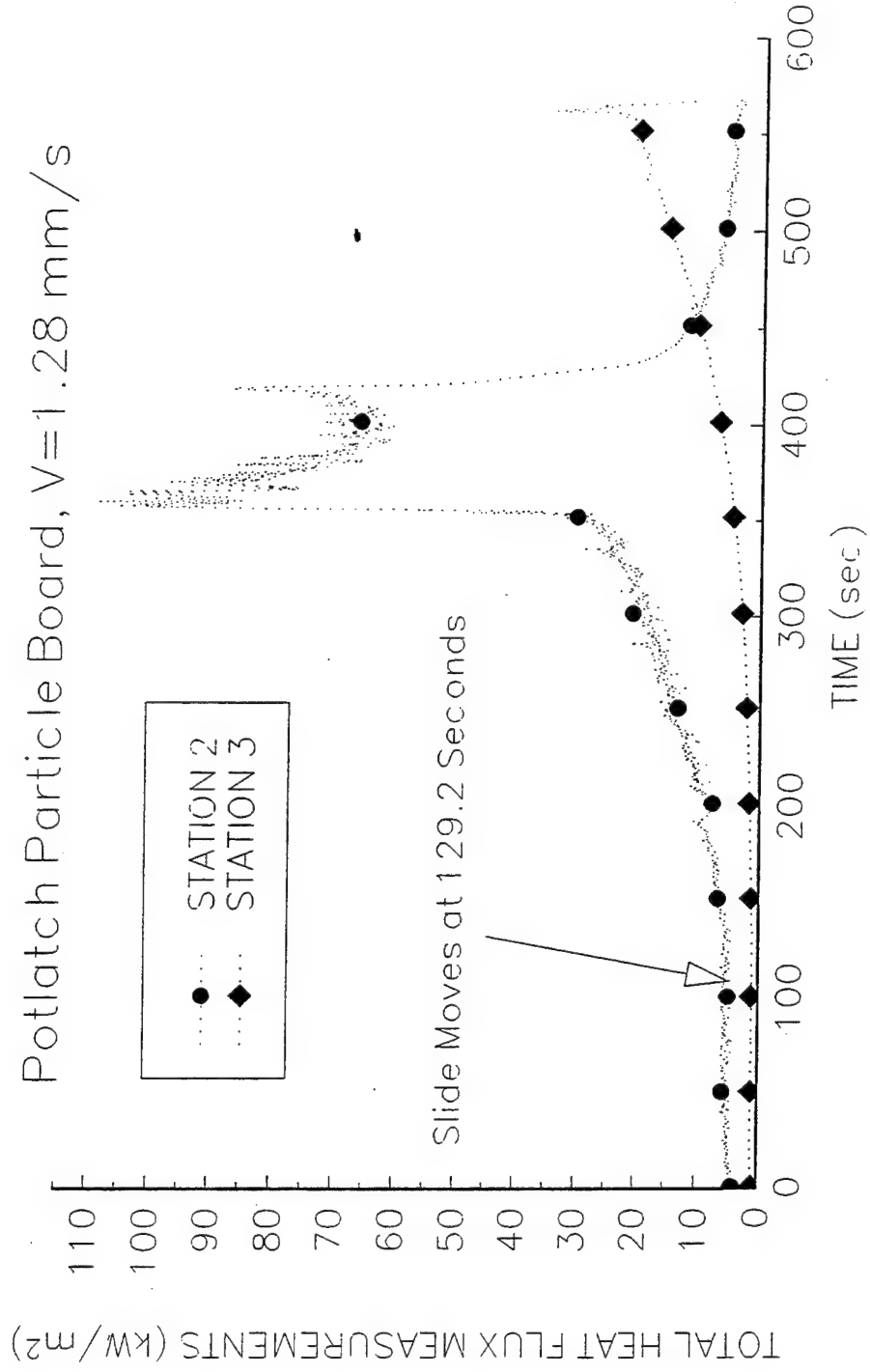
T20K622

Potlatch Partical Board, V=1.28 mm/s



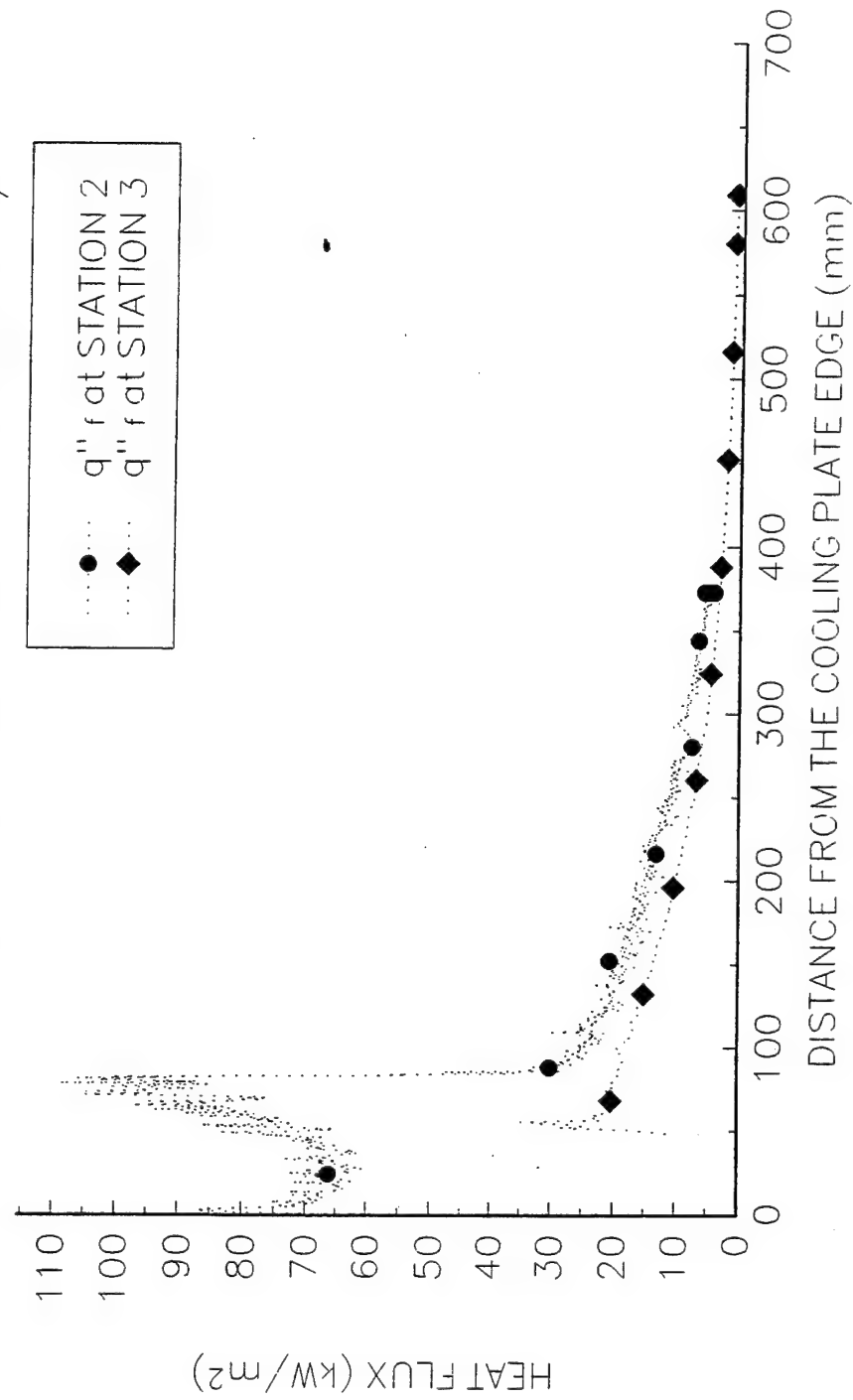
T20K622

Potlatch Particle Board,  $V=1.28 \text{ mm/s}$



T20K622

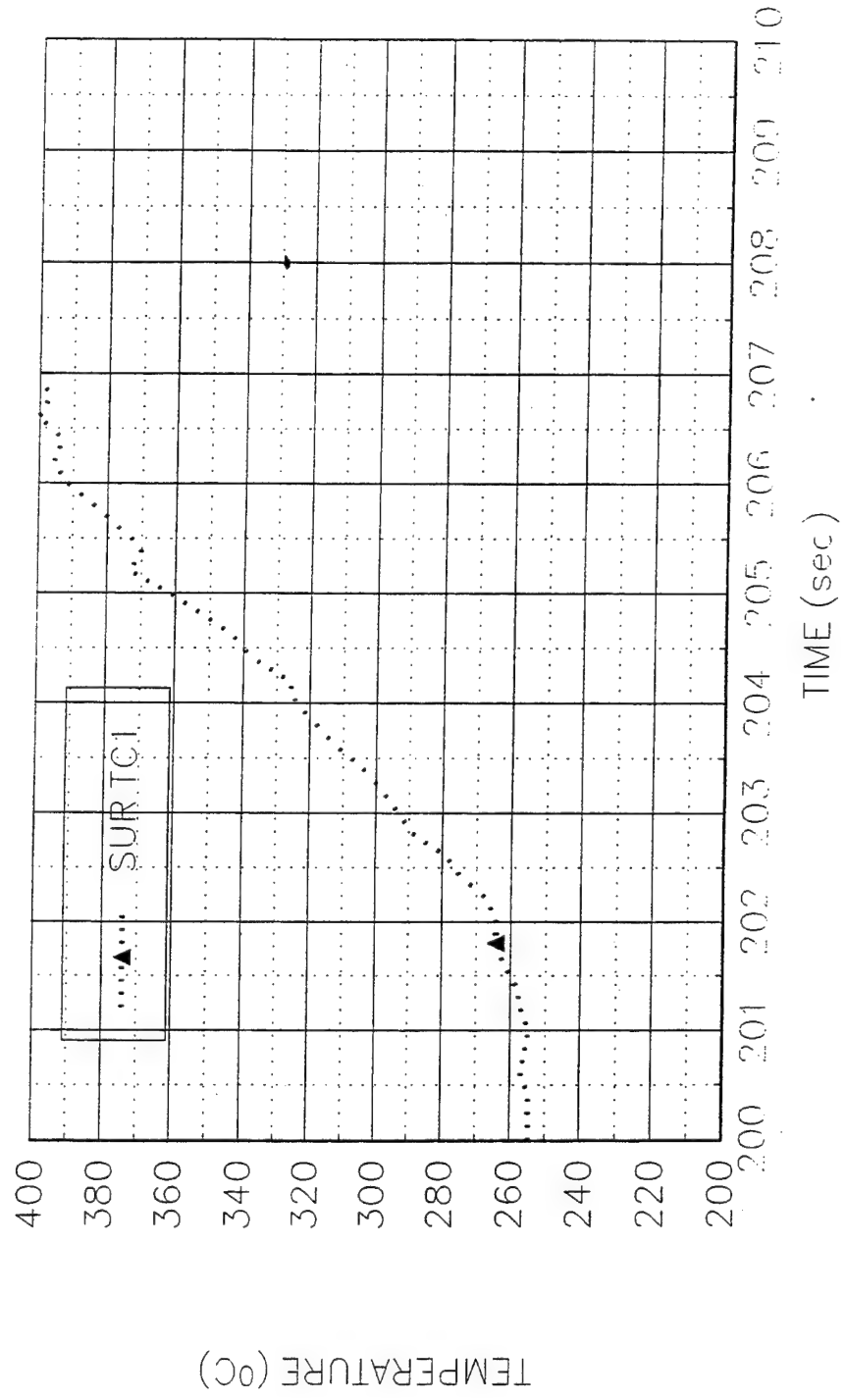
Potlatch Particle Board,  $V=1.28 \text{ mm/s}$





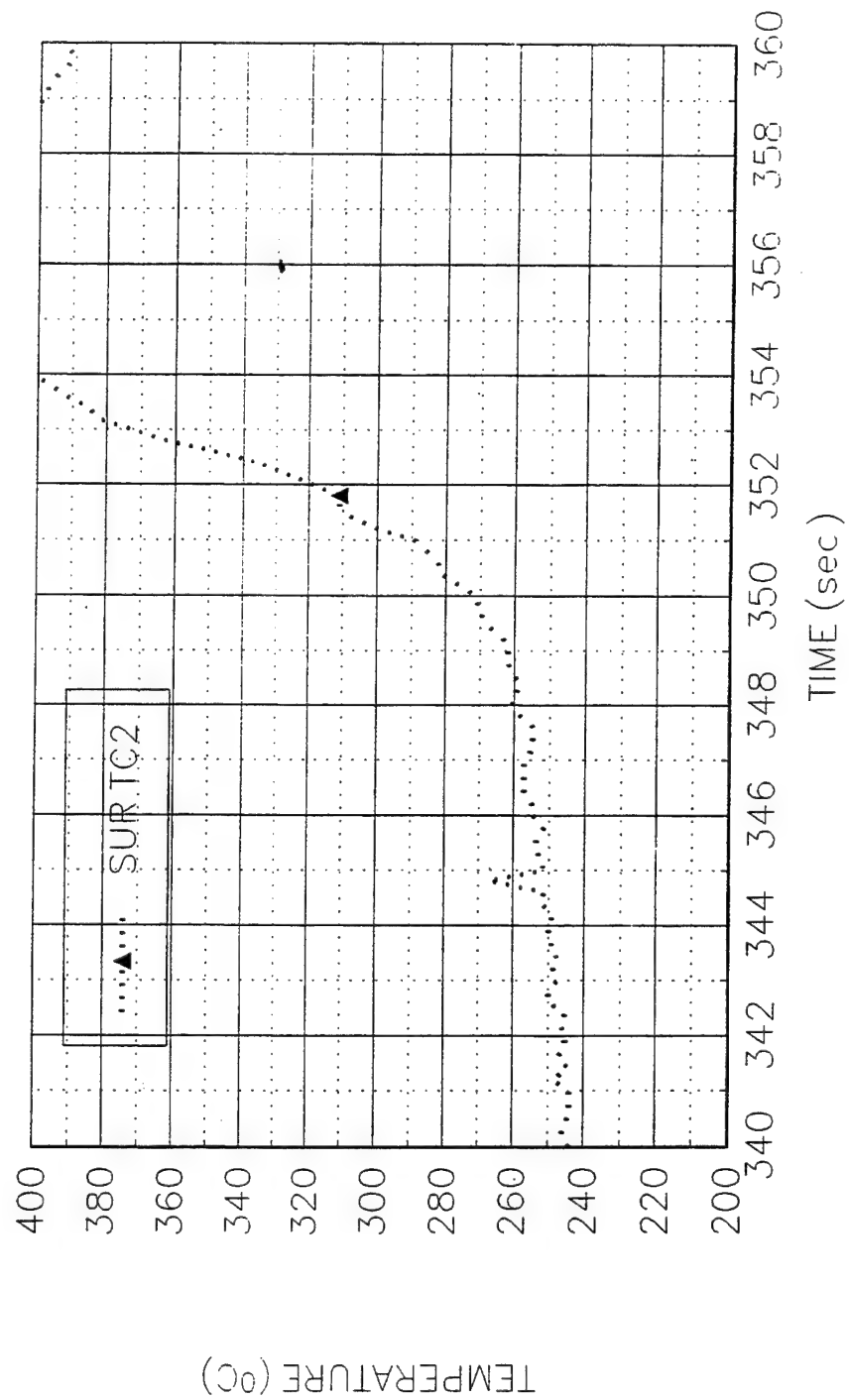
T20K622

Potlatch Partical Board, V=1.28 mm/s



T20K622

Potlatch Partical Board, V=1.28 mm/s



**Data Sheet**  
**Constant Horizontal Flame Spread Experiment**

Experimental No.: 41

Date: 8/16/94 Tu

Time: 4.00 pm

**Pre-Experiment**

Heat Flux at 425 mm Location (Planned) (kW/m<sup>2</sup>): 20

Slider Speed (mm/s): 1.28 mm/s

**Burning Sample Data**

Material: 3/4" Potlatch Particle Board

Dimension(LxWxH, mm): 600x152x18.85

**Instrumentation**

Number of Thermocouples: 5

Number of Heat Flux Gauges: 2

Station	Sensor	x (mm)	z (mm)	File Column	Note
1	TC	175	1.47	B	GAS TC1
1	TC	175	0	C	SURFACE
2	TC	350	1.09	D	GAS TC2
2	TC	350	0	E	SURFACE
2	HG	350	0	G	SER. 86862
3	TC	573	0	F	SURFACE
3	HG	573	0	H	SER. 525842

**Experiment**

Flux Gauge Reading @ 425 mm (Serial No. 27844, mV): 5.80-19.9984 kW/m<sup>2</sup>

Preheating Time without Pilot Flame (seconds): 120

Time to Sample Ignition After Applying the Pilot Flame (seconds): 7

Speed Used (S1M"Steps"): 200

Number of Steps (I1M"Steps"): 80629

File Names (.PRN): T20K816

Set-up File Name:

Sampling Rate (Hz): 5      Duration of Sampling (sec): 2500

Time to Start Moving the Sample (sec): 147.0

Ignition Heat Flux (Calculated, kW/m<sup>2</sup>): 29.4

**Ambient Conditions**

Temperature (°C): 22

**Observations** Burning area ~10 cm

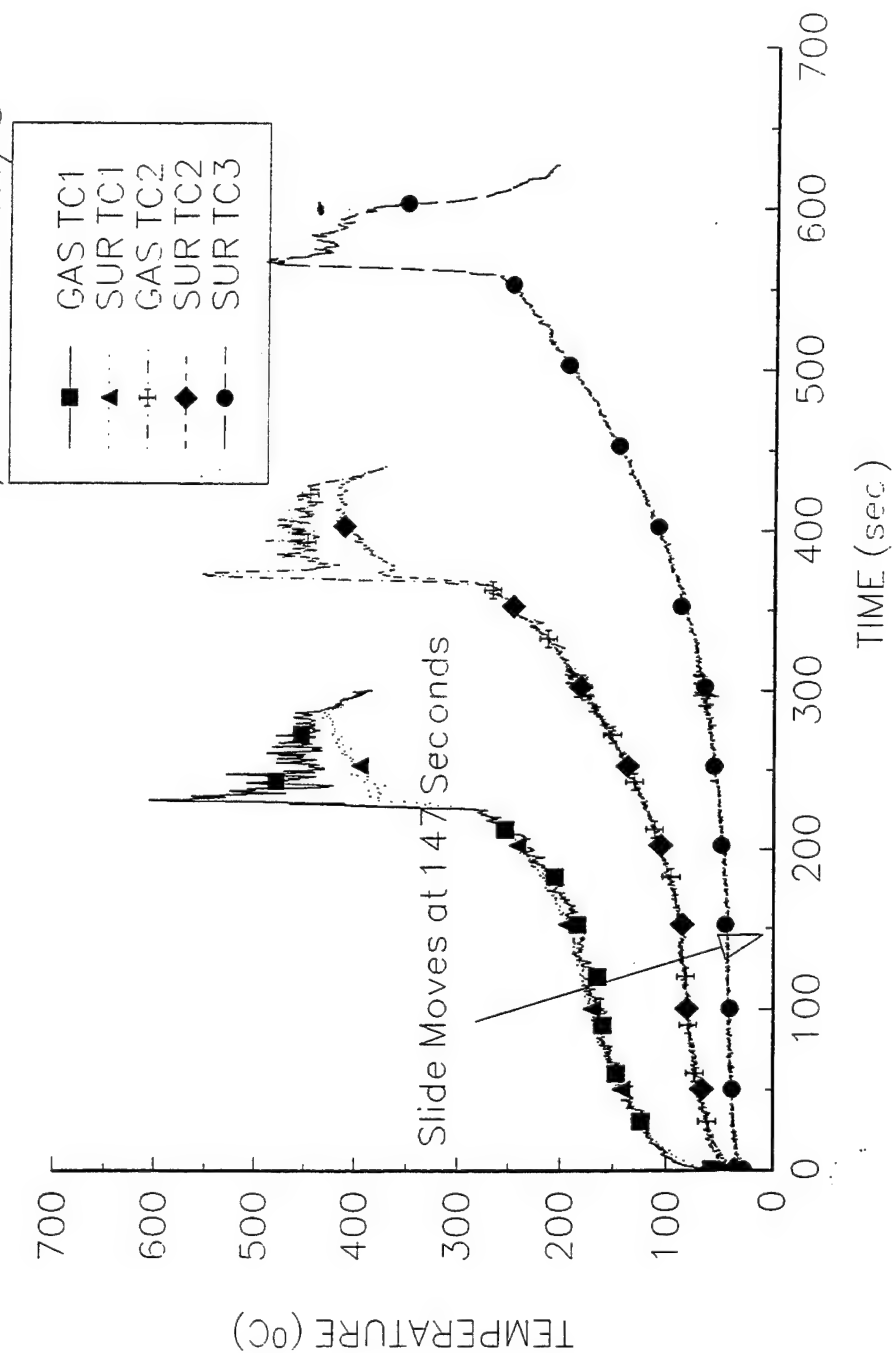
Personnel V.M., Y.C

Processing of Data:  $T_p = 320^\circ\text{C}$ , Surface TC1,  $1/\tau = 0.57$ ,  $T_{ext} = 274.7^\circ\text{C}$ ,  $k_{pc} = 0.17 \times 765. \times 2800 = 364140$ ,  
 $q_0'' = (k_{pc})^{1/2} (T_p - T_{ext}) (1/\tau)^{1/2} = (364140)^{1/2} \times (320 - 274.7) (0.57)^{1/2} = 20.64 \text{ kW/m}^2$

Surface TC2,  $1/\tau = 0.79$ ,  $T_{ext} = 274.7^\circ\text{C}$ ,  $q_0'' = (364140)^{1/2} \times (320 - 274.7) (0.79)^{1/2} = 24.30 \text{ kW/m}^2$

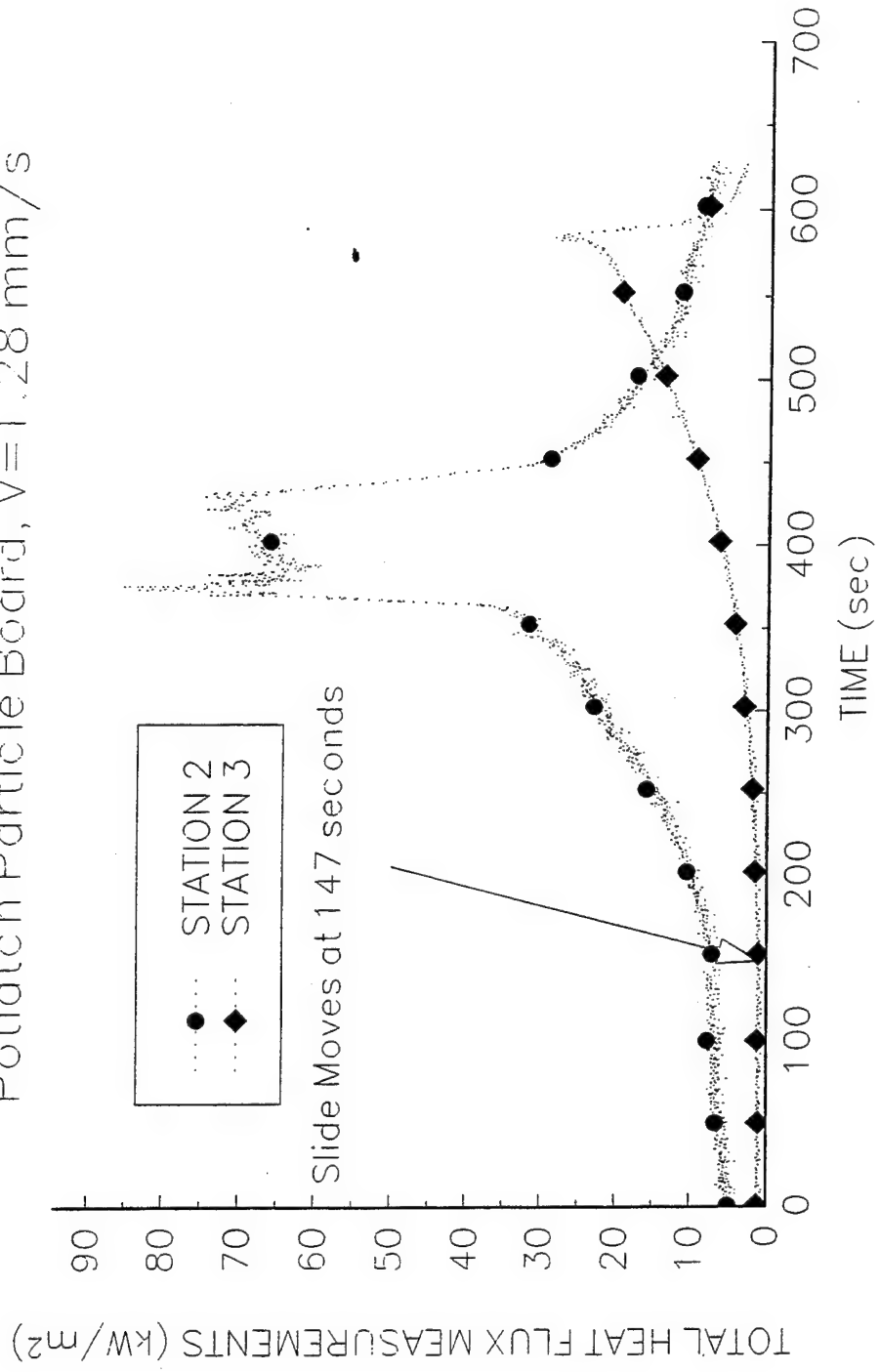
T20K816

Potlatch Particle Board,  $V=1.28 \text{ mm/s}$



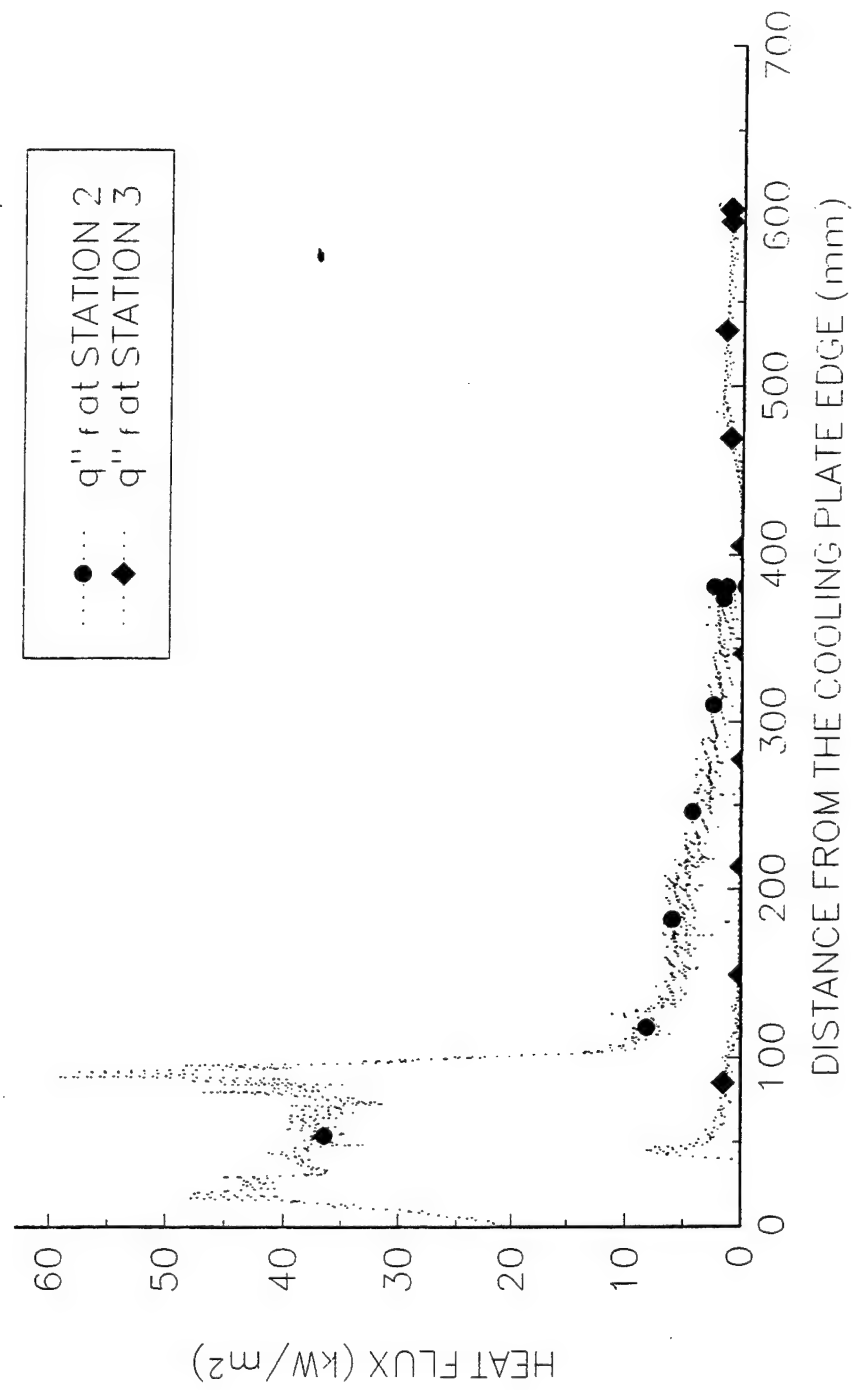
T20K816

Potlatch Particle Board,  $V=1.28 \text{ mm/s}$

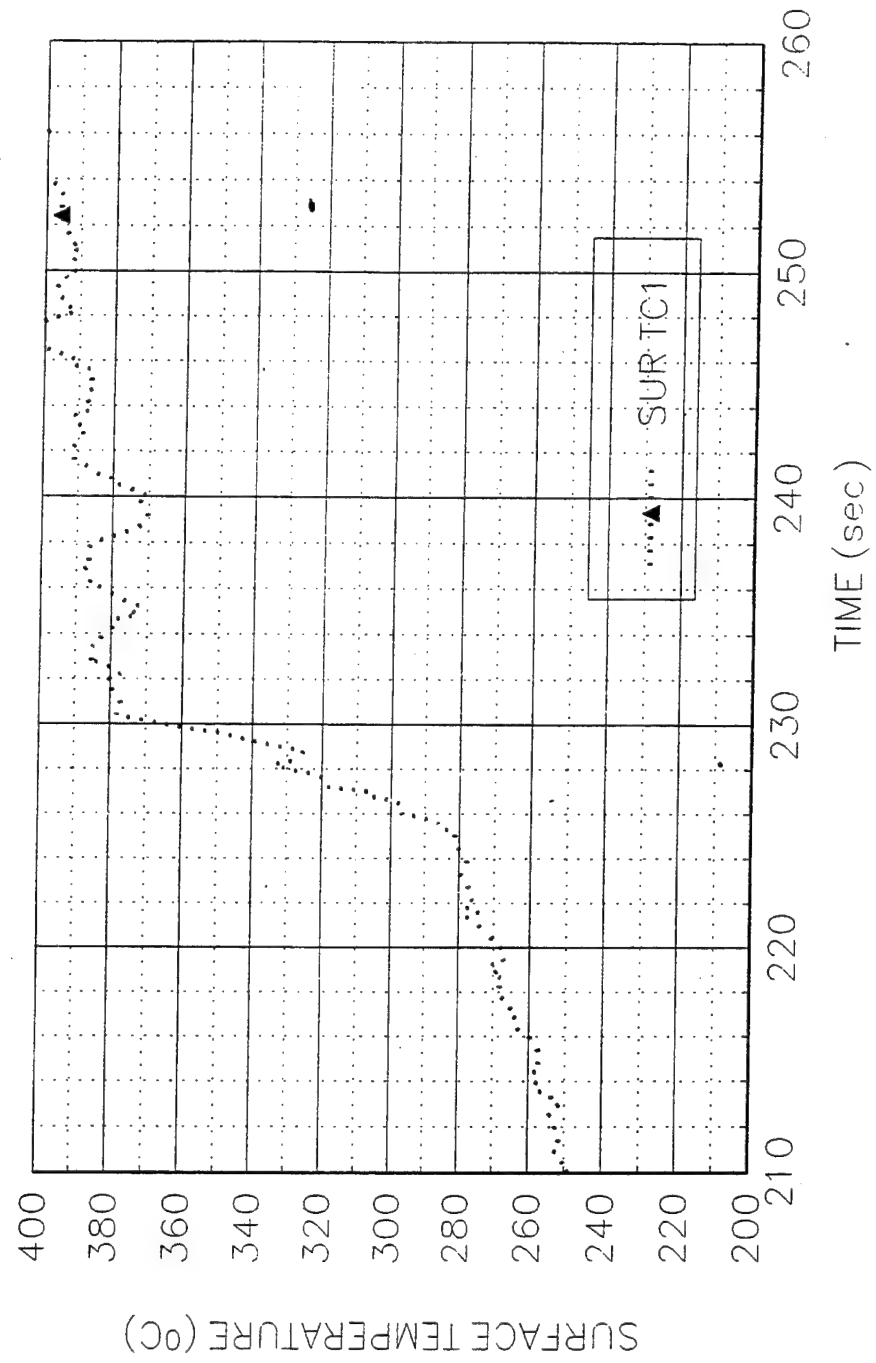


T20K816

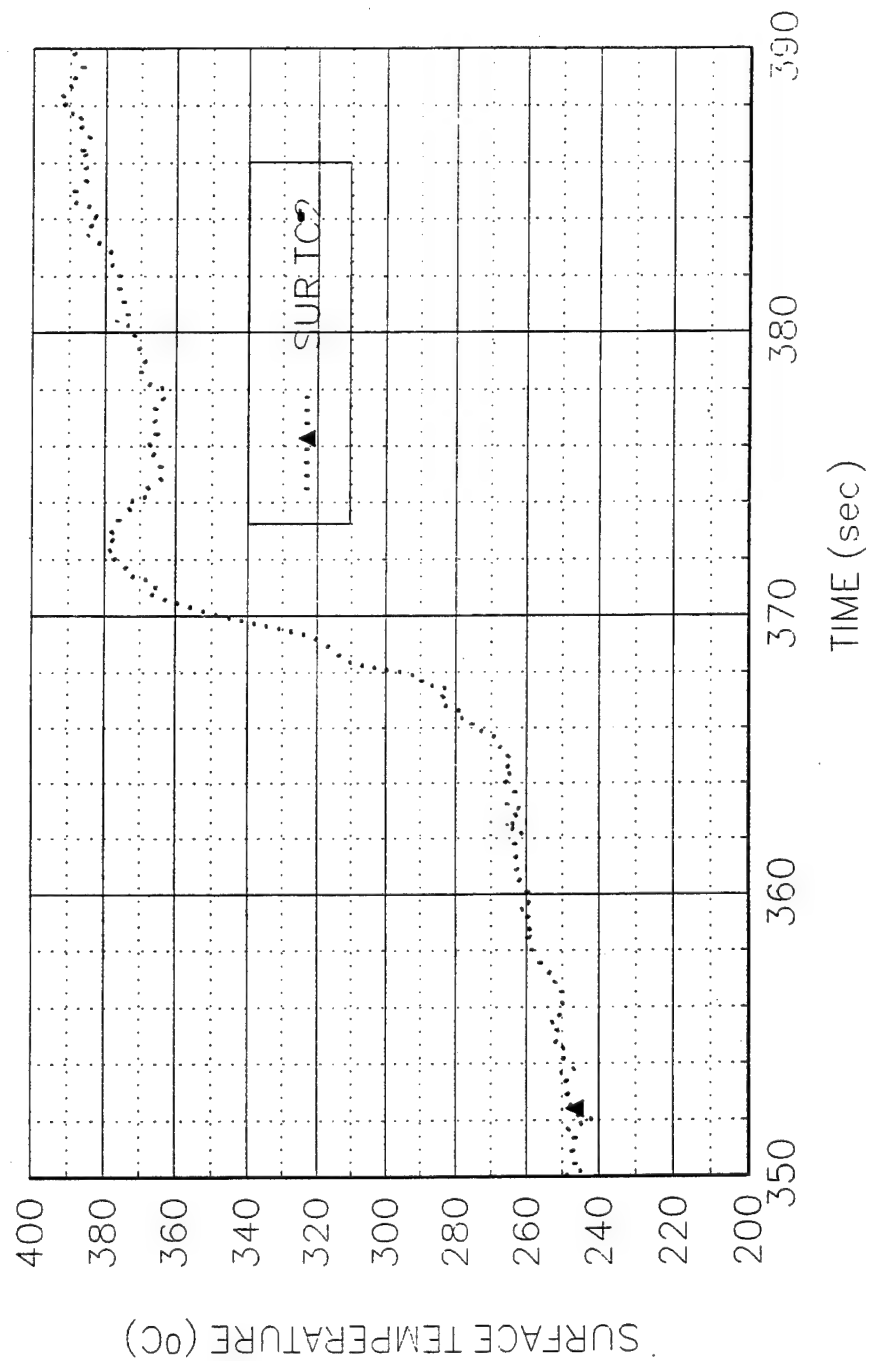
Potlatch Particle Board,  $V=1.28 \text{ mm/s}$



T20K816  
Potlatch Particle Board, V=1.28 mm/s

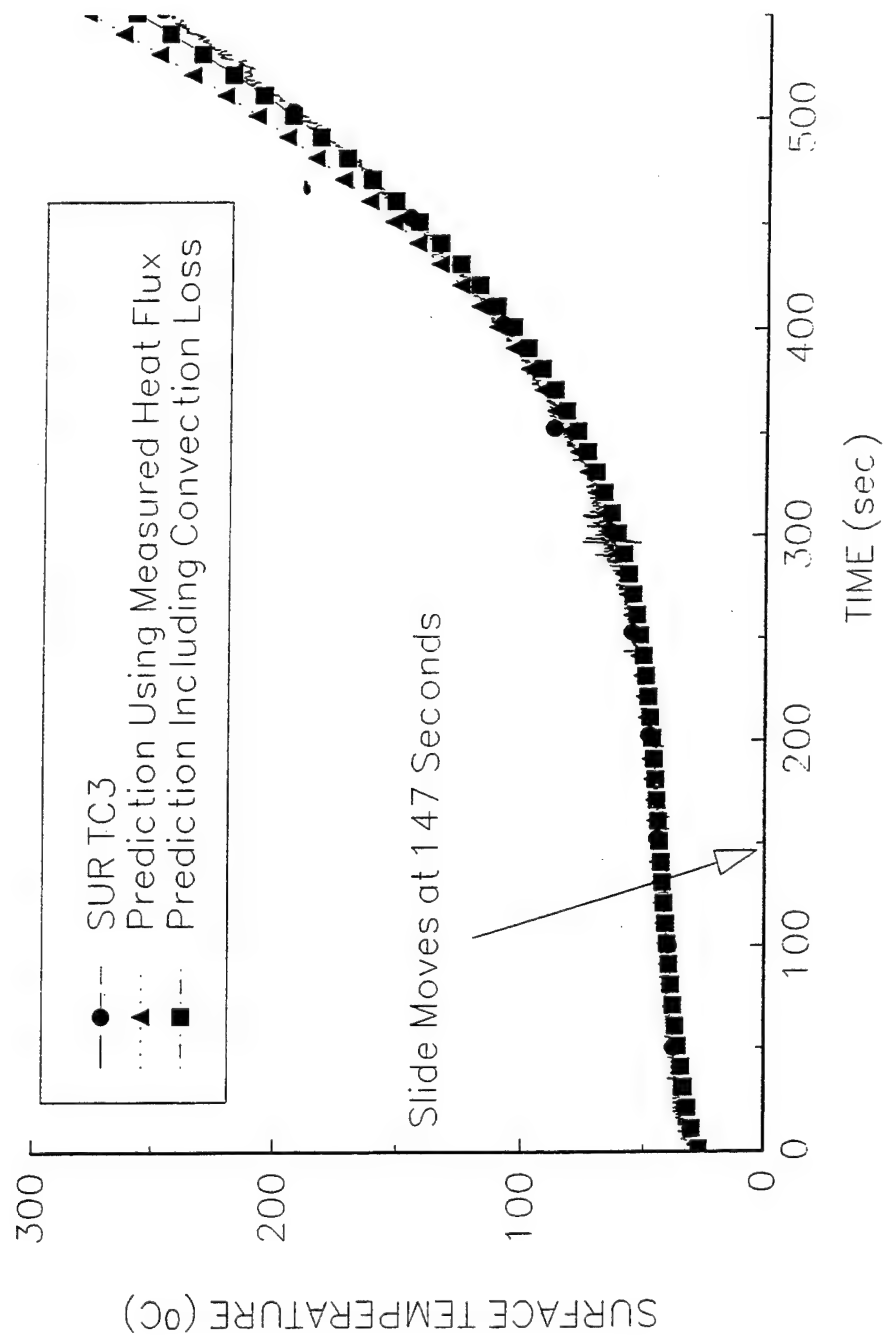


T20K816  
Potlatch Particle Board, V=1.28 mm/s

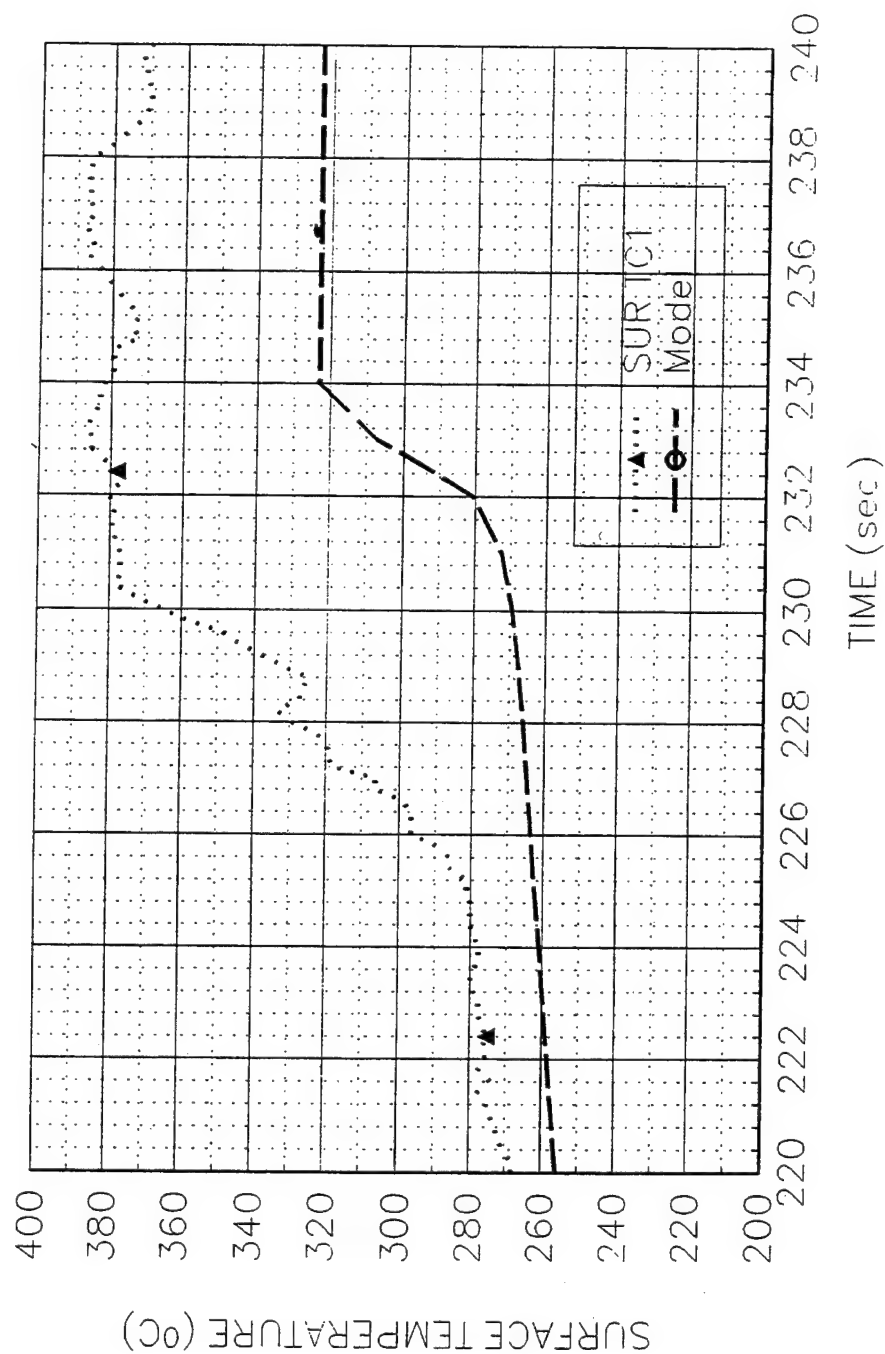




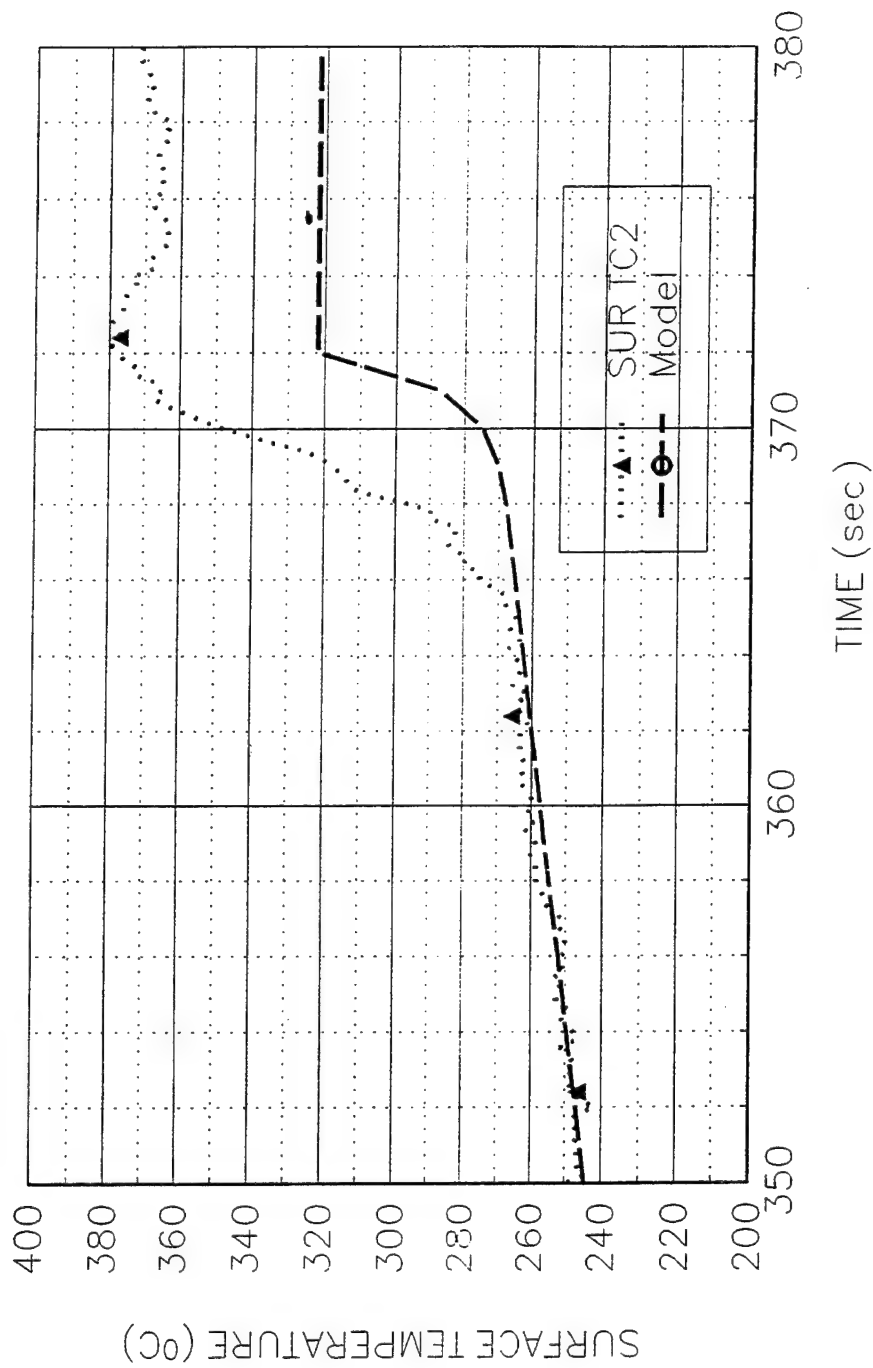
T20K816  
Potlatch Particle Board,  $V=1.28 \text{ mm/s}$



T20K816  
Potlatch Particle Board, V=1.28 mm/s



T20K816  
Potlatch Particle Board, V=1.28 mm/s



**Data Sheet**  
**Constant Horizontal Flame Spread Experiment**

Experimental No.: 43

Date: 8/18/94 Th.

Time: 9:30 pm

**Pre-Experiment**

Heat Flux at 425 mm Location (Planned) (kW/m<sup>2</sup>): 20

Slider Speed (mm/s): 1.28 mm/s

**Burning Sample Data**

Material: 3/4" Potlatch Particle Board

Dimension (LxWxH, mm): 600x152x18.85

**Instrumentation**

Number of Thermocouples: 5

Number of Heat Flux Gauges: 2

Station	Sensor	x (mm)	z (mm)	File Column	Note
1	TC	174	1.47	B	GAS TC1
1	TC	174	0	C	SURFACE TC1
2	TC	352	1.27	D	GAS TC2
2	TC	352	0	E	SURFACE TC2
2	HG	352	0	G	SERIAL 86862
3	TC	575	0	F	SURFACE TC3
3	HG	575	0	H	SERIAL 525842

**Experiment**

Flux Gauge Reading @ 425 mm (Serial No. 27844, mV): 5.90 mV - 20.3432 kW/m<sup>2</sup>

Preheating Time without Pilot Flame (seconds): 120

Time to Sample Ignition After Applying the Pilot Flame (seconds): 0

Speed Used (S1M"Steps"): 200

Number of Steps (I1M"Steps"): 80629

File Names (.PRN): T20K818

Set-up File Name:

Sampling Rate (Hz): 5      Duration of Sampling (sec): 2500

Time to Start Moving the Sample (sec): 141.2

Ignition Heat Flux (Calculated, kW/m<sup>2</sup>): 23.4

**Ambient Conditions**

Temperature (°C): 22

**Observations** Burning width ~7.5 cm, constant

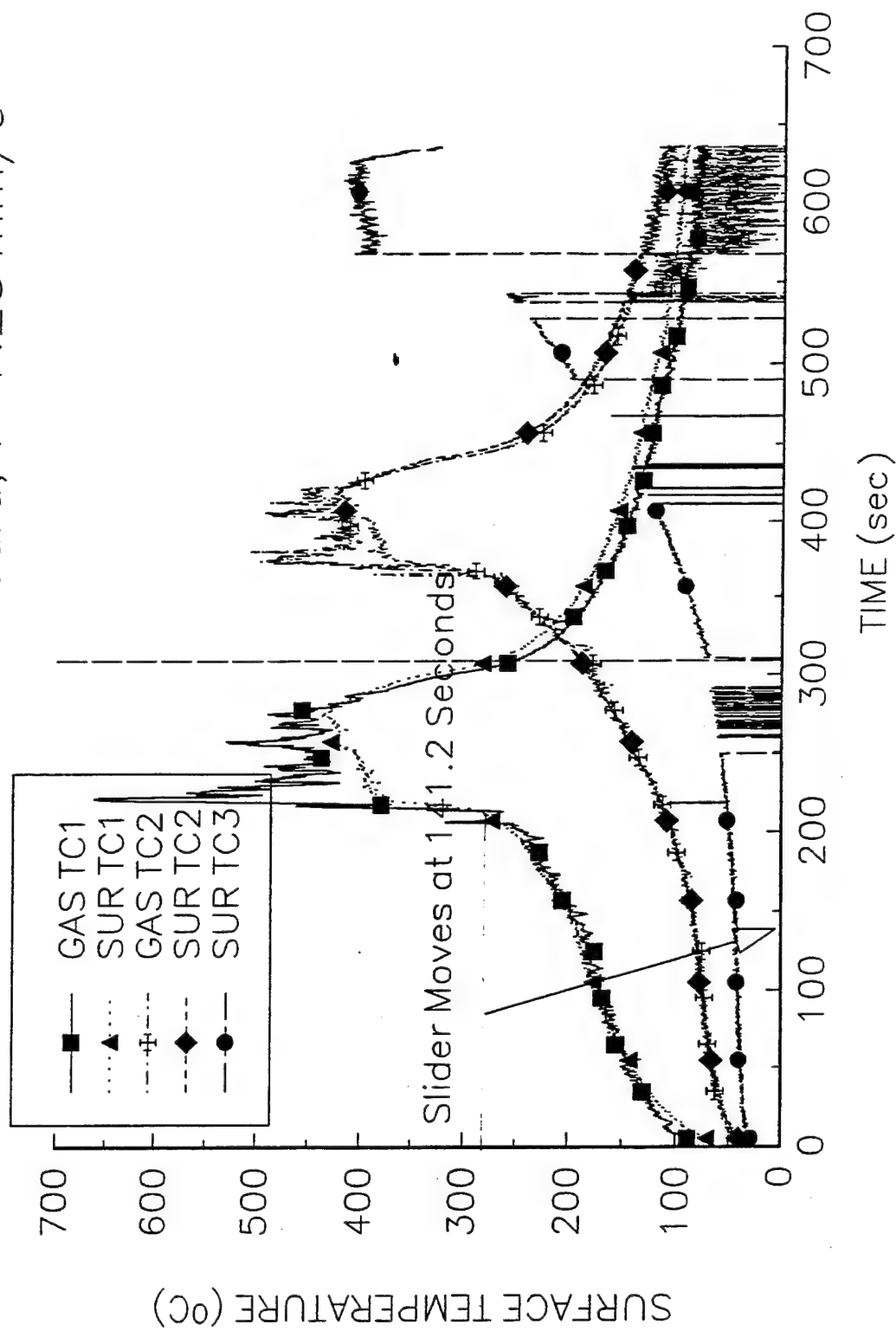
Personnel J.C, Y.C

Processing of Data:  $T_p = 320^\circ\text{C}$ , Surface TC1,  $1/\tau = 0.44$ ,  $T_{ext} = 280.6^\circ\text{C}$ ,  
 $k_{pc} = 0.17 \times 765 \times 2800 = 364140$ ,  $q_0'' = (k_{pc})^{1/2} (T_p - T_{ext}) (1/\tau)^{1/2} = (364140)^{1/2} \times (320 - 280.6) (0.44)^{1/2} = 15.75$   
 kW/m<sup>2</sup>

Surface TC2,  $1/\tau = 0.30$ ,  $T_{ext} = 280.6^\circ\text{C}$ ,  $q_0'' = (364140)^{1/2} \times (320 - 280.6) (0.30)^{1/2} = 13.02$  kW/m<sup>2</sup>

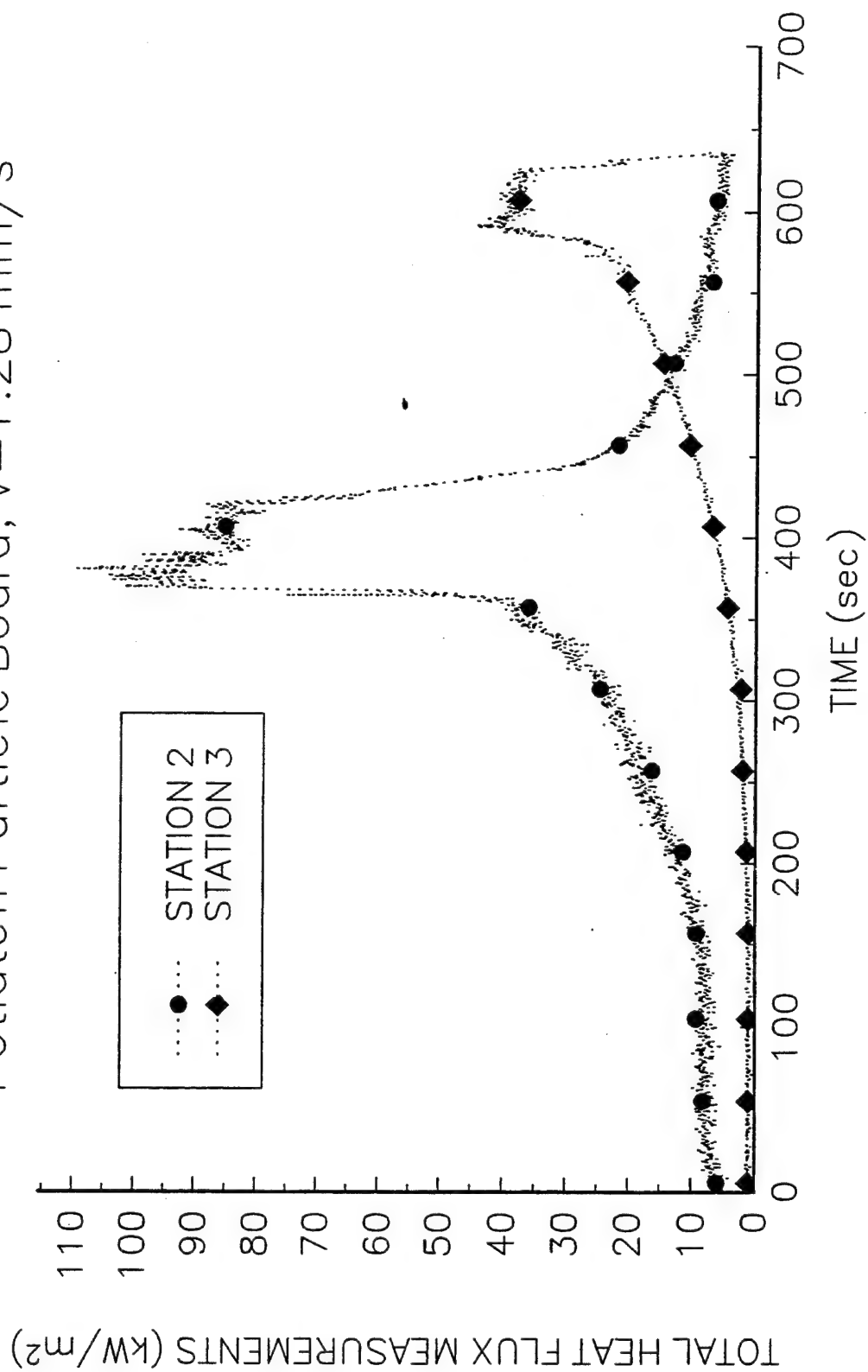
T20K818

Potlatch Particle Board,  $V=1.28 \text{ mm/s}$



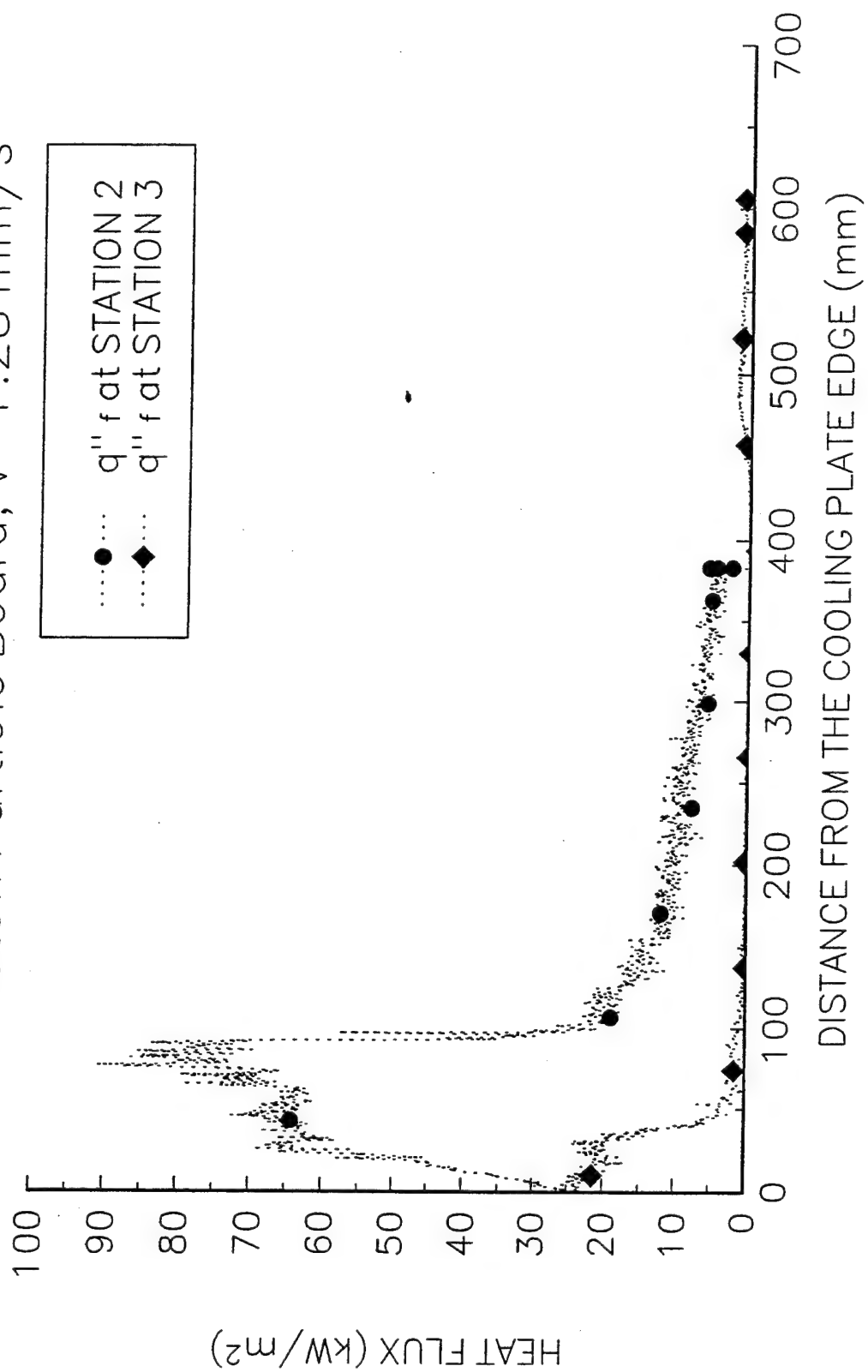
T20K818

Potlatch Particle Board,  $V=1.28 \text{ mm/s}$



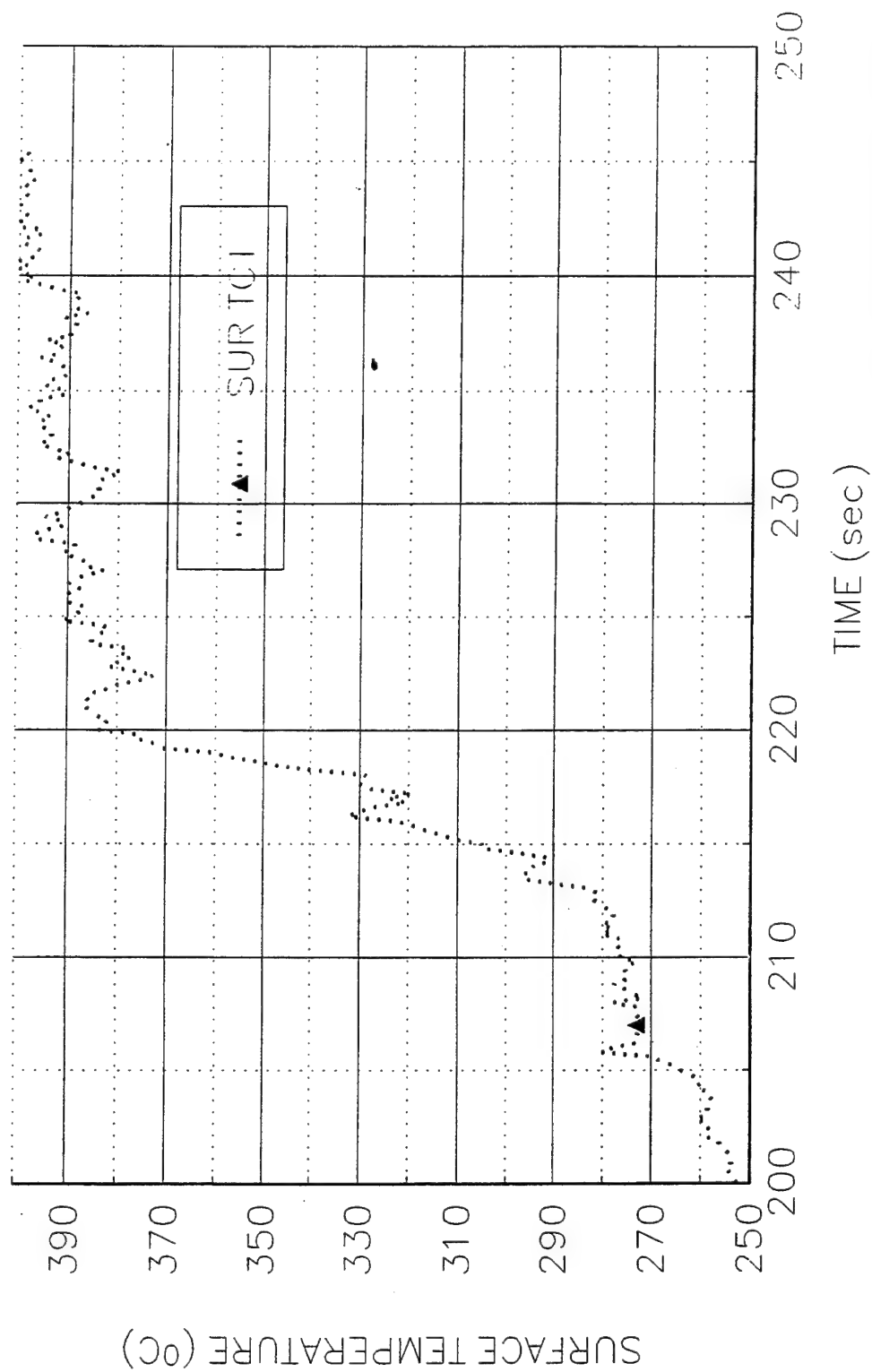
T20K818

Potlatch Particle Board,  $V=1.28 \text{ mm/s}$



T20K818

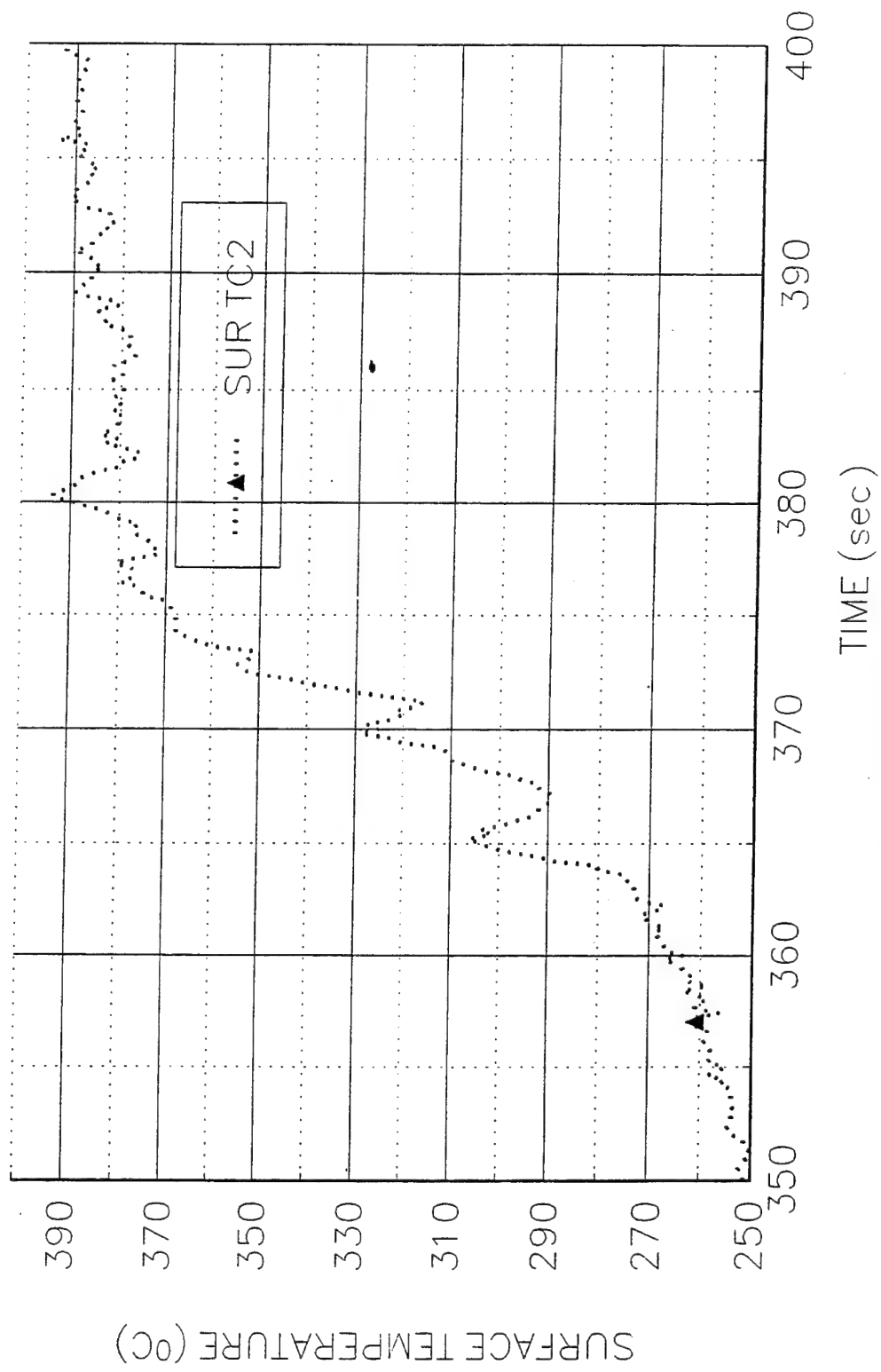
Potlatch Particle Board, V=1.28 mm/s





T20K818

Potlatch Particle Board, V=1.28 mm/s



**Data Sheet**  
**Constant Horizontal Flame Spread Experiment**

Experimental No.: 27

Date: 6/23/94 Th.

Time: 8:30 pm

**Pre-Experiment**

Heat Flux at 425 mm Location (Planned) (kW/m<sup>2</sup>): 30

Slider Speed (mm/s): 2.56 mm/s

**Burning Sample Data**

Material: 3/4" Potlatch Particle Board

Dimension(LxWxH, mm): 600x152x18.85

**Instrumentation**

Number of Thermocouples: 5

Number of Heat Flux Gauges: 2

Station	Sensor	x (mm)	z' (mm)	File Column	Note
1	TC	174	0.5	B	GAS TC1
1	TC	174	0	C	SURFACE TC1
2	TC	339	0.9	D	GAS TC2
2	TC	339	0	E	SURFACE TC2
2	HG	339	0	G	SERIAL 84501
3	TC	575	0	F	SURFACE TC3
3	HG	575	0	H	SERIAL 525842

**Experiment**

Flux Gauge Reading @ 425 mm (Serial No. 27844, mV): 9.65 mV- 32.88 kW/m<sup>2</sup>

Preheating Time without Pilot Flame (seconds): 50

Time to Sample Ignition After Applying the Pilot Flame (seconds): 0

Speed Used (S1M"Steps"): 400

Number of Steps (I1M"Steps"): 80000

File Names (.PRN): T30K623

Set-up File Name:

Sampling Rate (Hz): 5

Duration of Sampling (sec): 2500

Time to Start Moving the Sample (sec): 55

Ignition Heat Flux (Calculated, kW/m<sup>2</sup>): 40

**Ambient Conditions**

Temperature (°C): 23

**Observations** Burning width ~10 cm, flame size little bit large

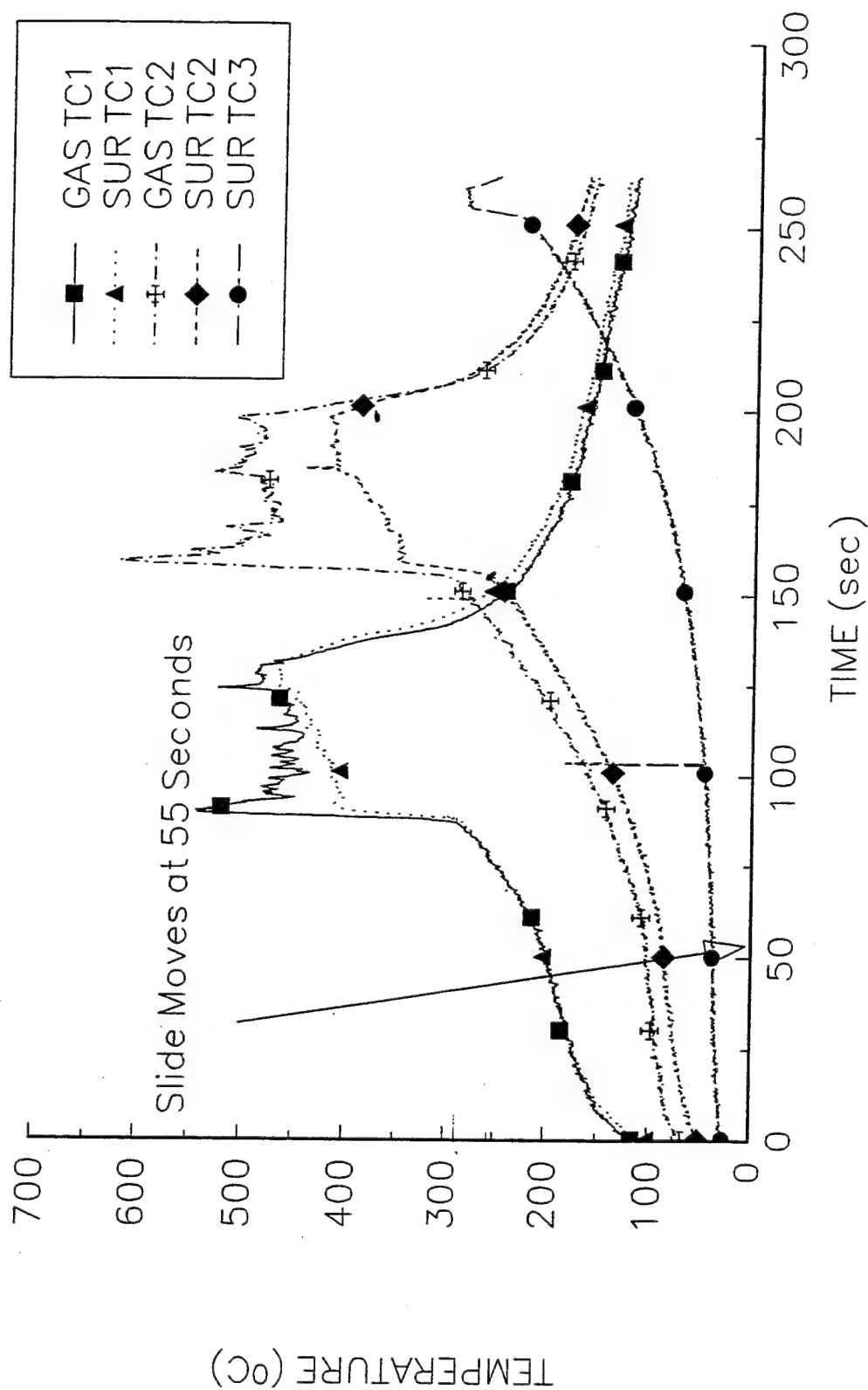
Personnel J.C, Y.C

Processing of Data:  $T_p = 320^\circ\text{C}$ , Surface TC1,  $1/\tau = 4.0$ ,  $T_{ext} = 289^\circ\text{C}$ ,  $k_{pc} = 0.17 \times 765 \times 2800 = 364140$ ,  
 $q_0'' = (k_{pc})^{1/2} (T_p - T_{ext}) (1/\tau)^{1/2} = (364140)^{1/2} \times (320 - 289) (4.0)^{1/2} = 37.71 \text{ kW/m}^2$

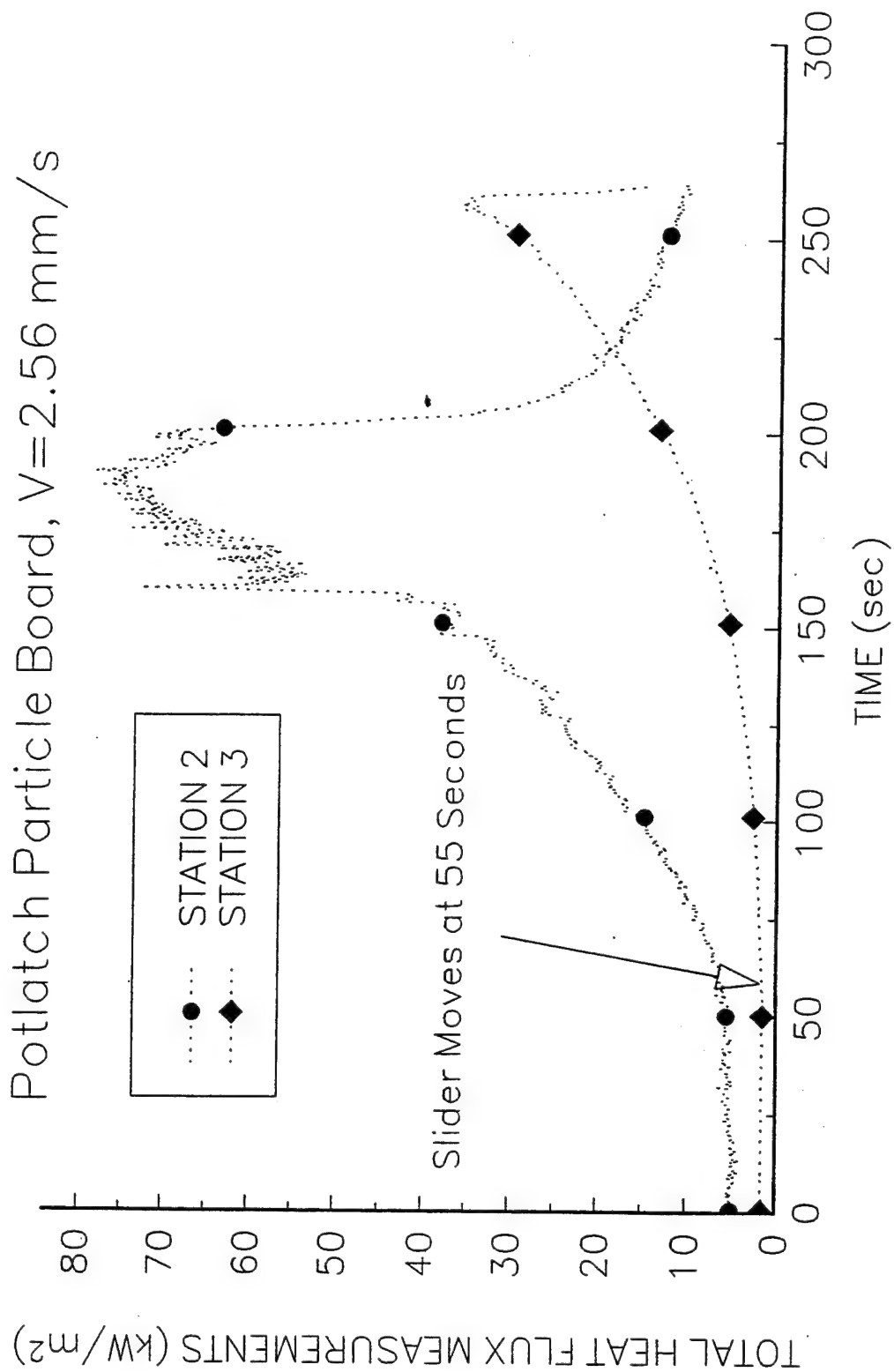
Surface TC2,  $1/\tau = 1.29$ ,  $T_{ext} = 251.5^\circ\text{C}$ ,  $q_0'' = (364140)^{1/2} \times (320 - 251.5) (1.29)^{1/2} = 46.95 \text{ kW/m}^2$

T30K623

Potlatch Partical Board, V=2.56 mm/s

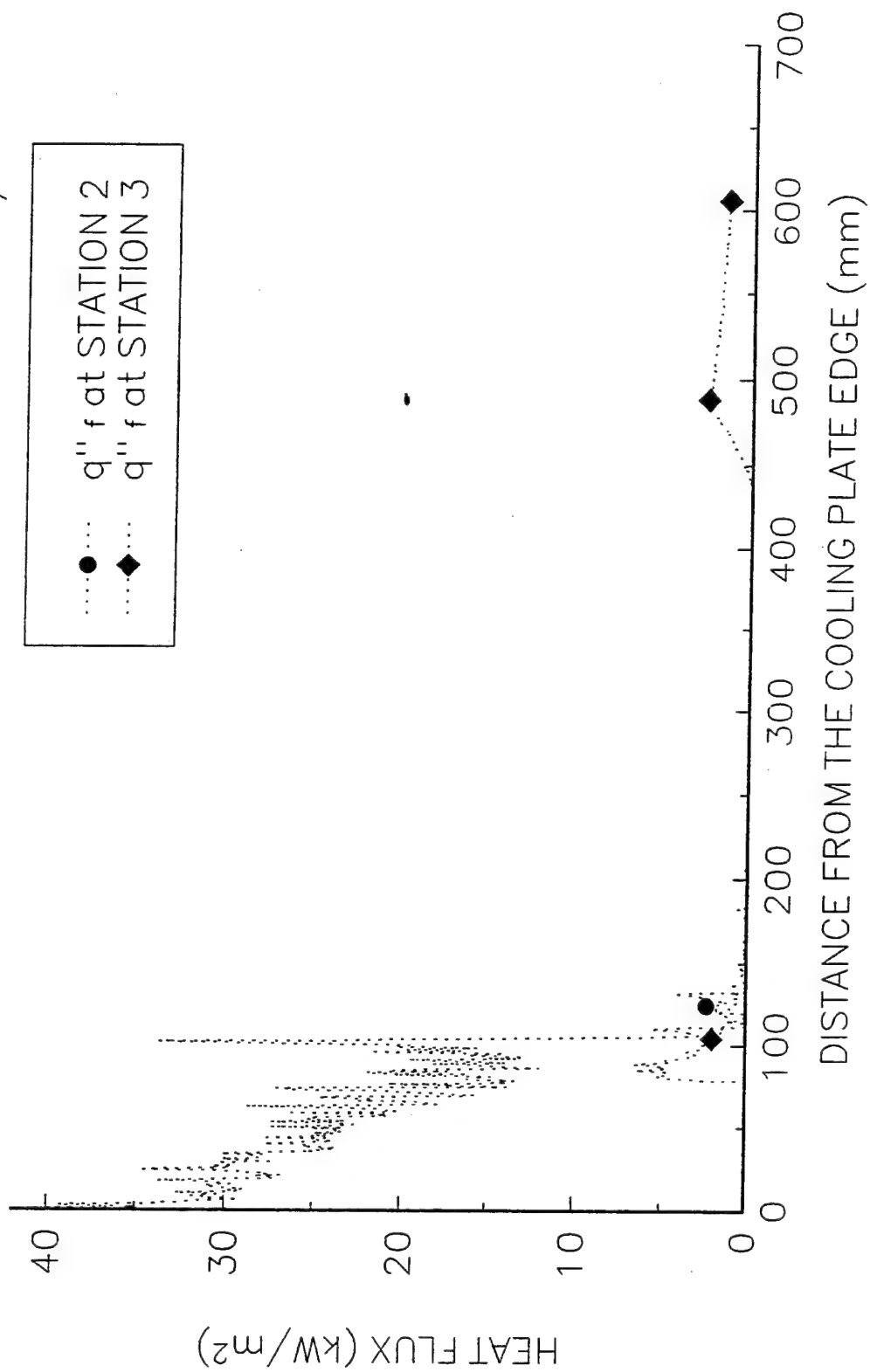


T30K623



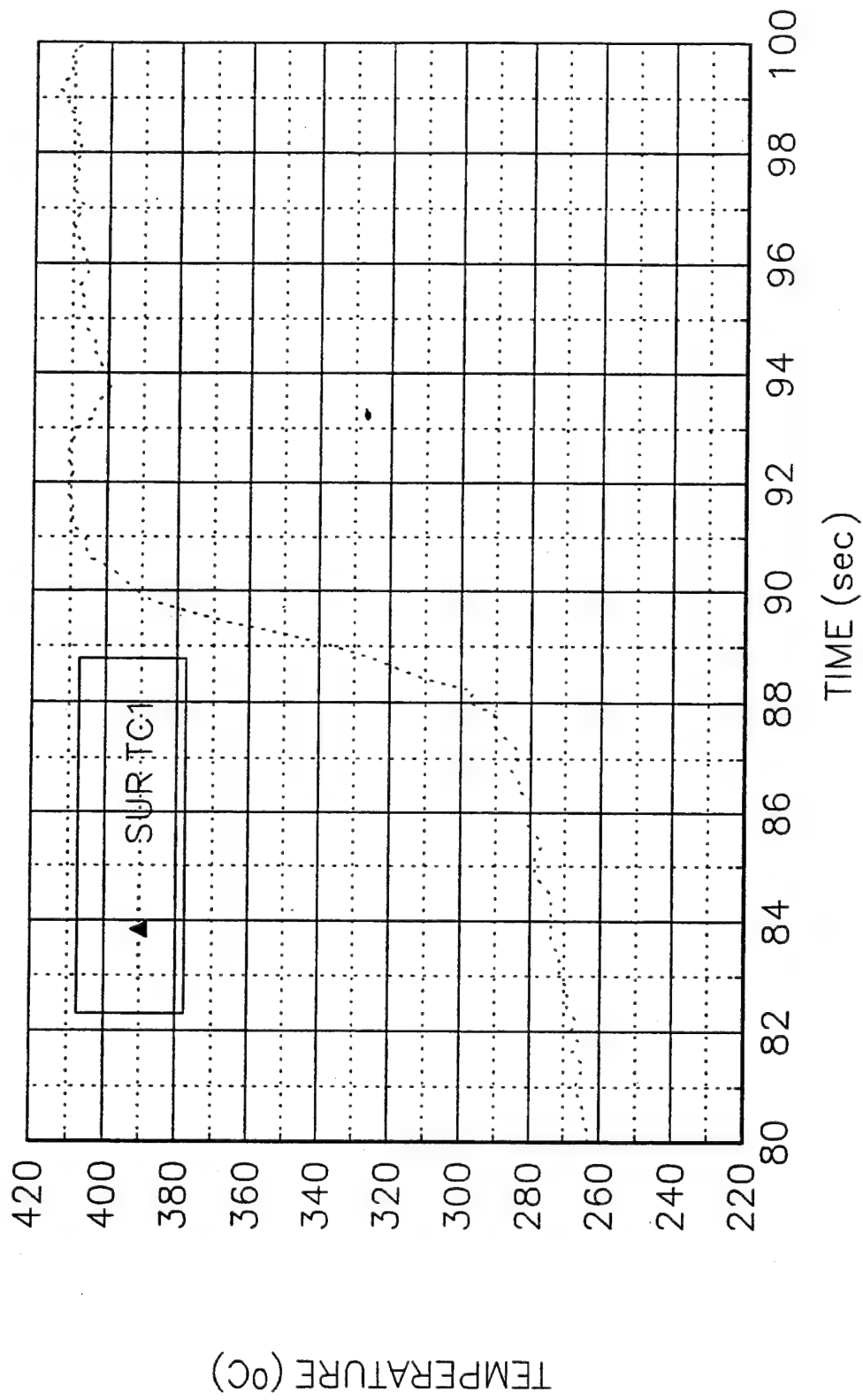
T30K623

Potlatch Particle Board,  $V=2.56$  mm/s



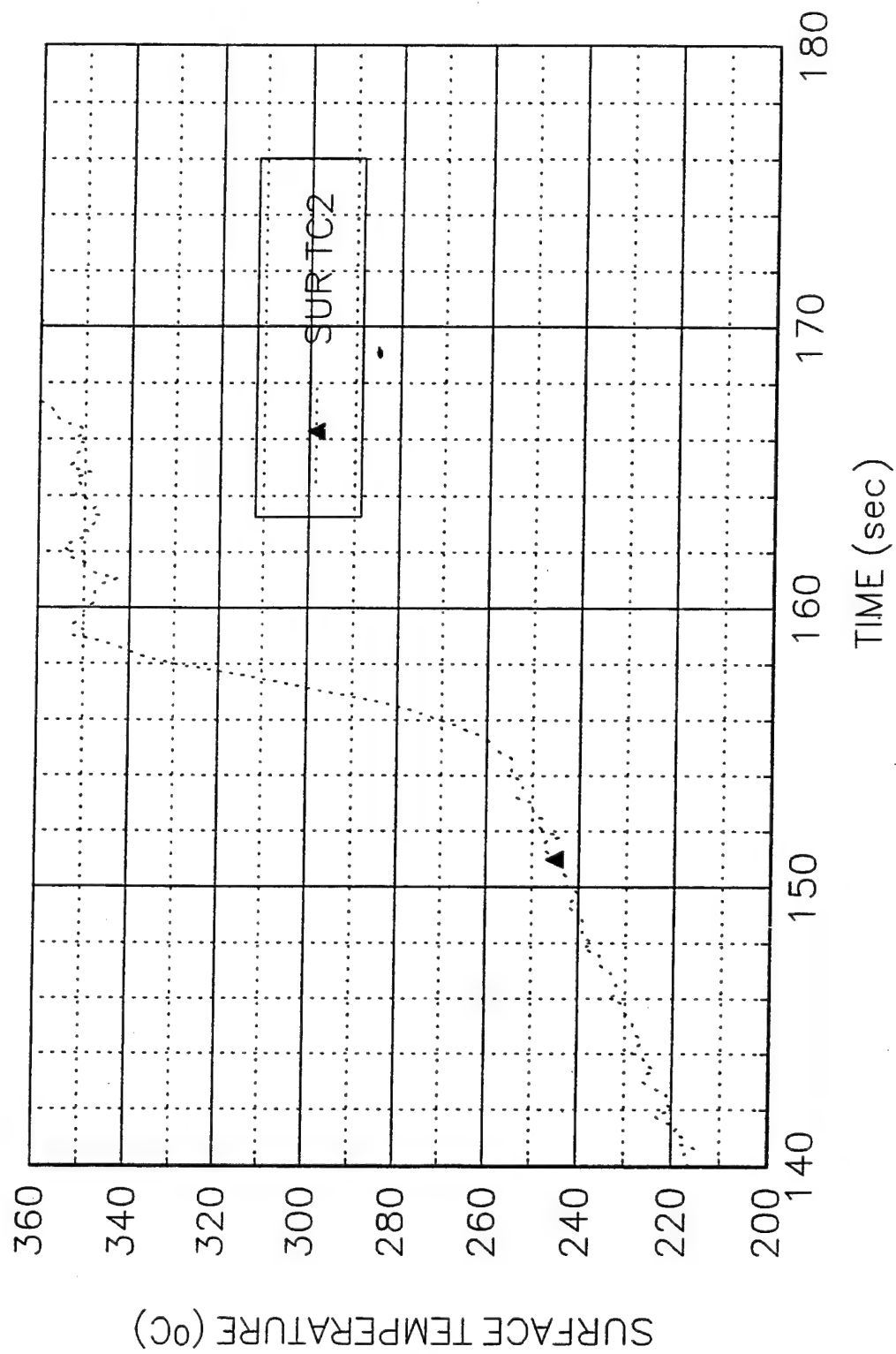
T30K623

Potlatch Partical Board, V=2.56 mm/s



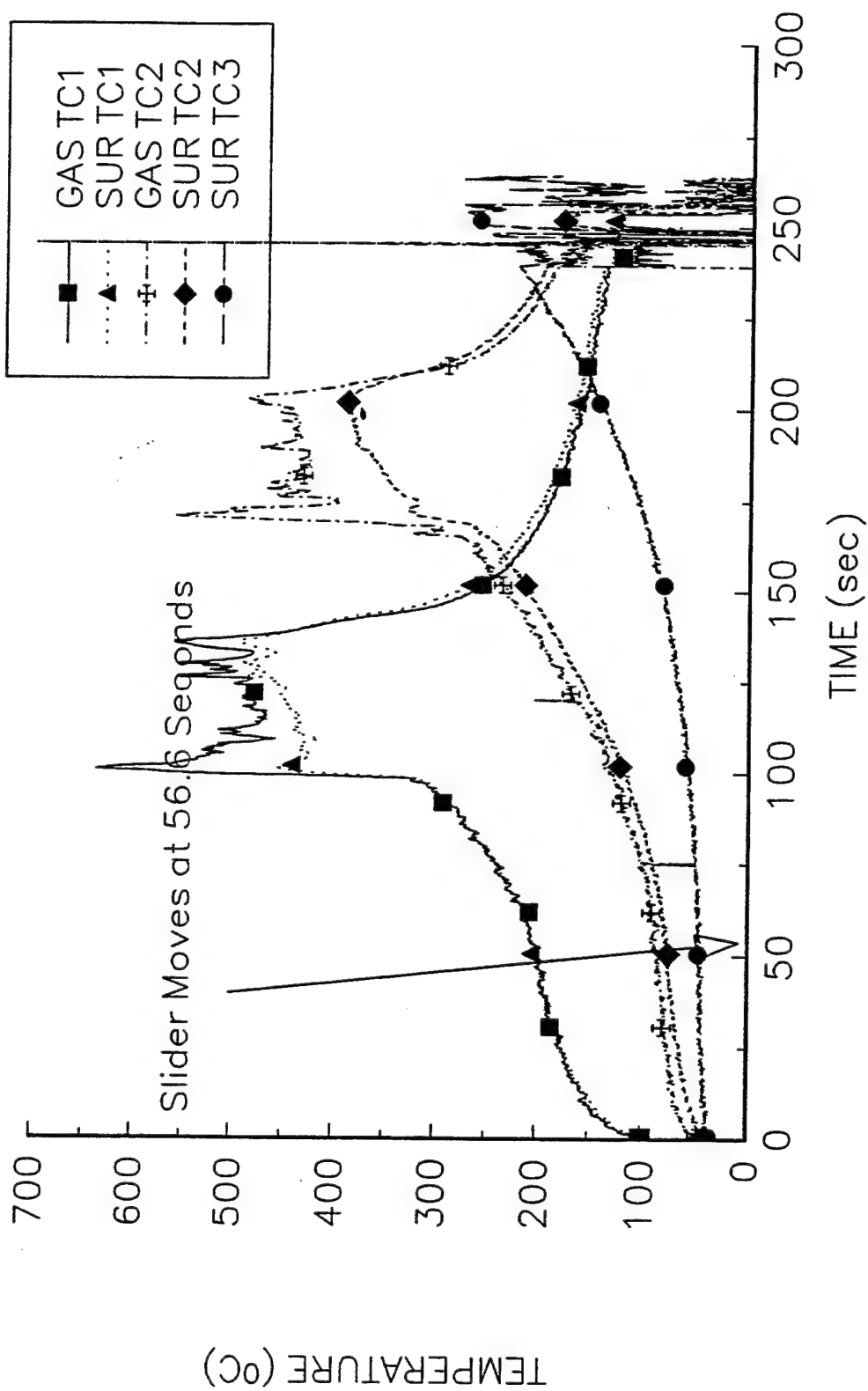
T30K623

Potlatch Particle Board, V=2.56 mm/s



T30K624

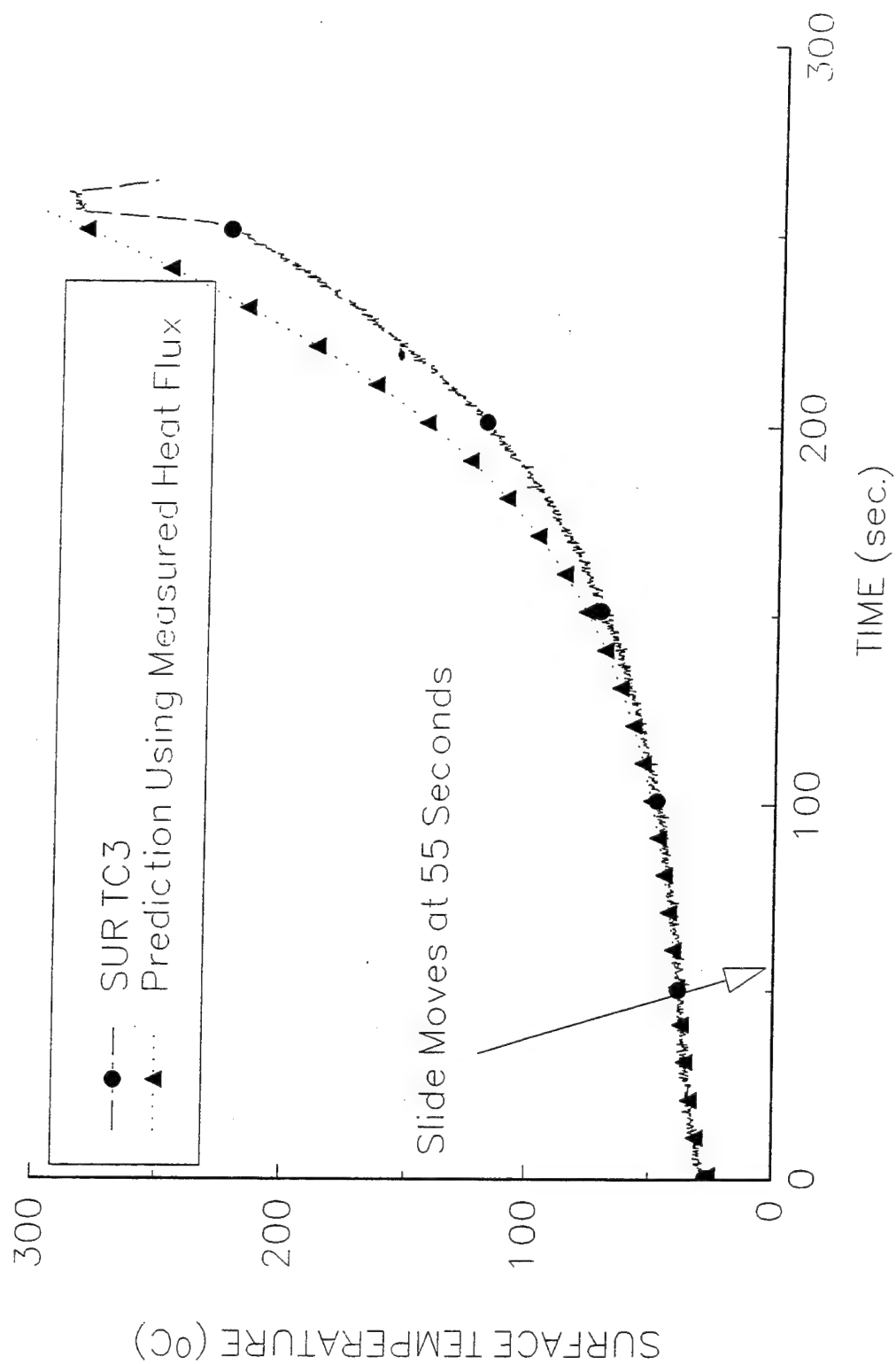
Potlatch Partical Board, V=2.56 mm/s





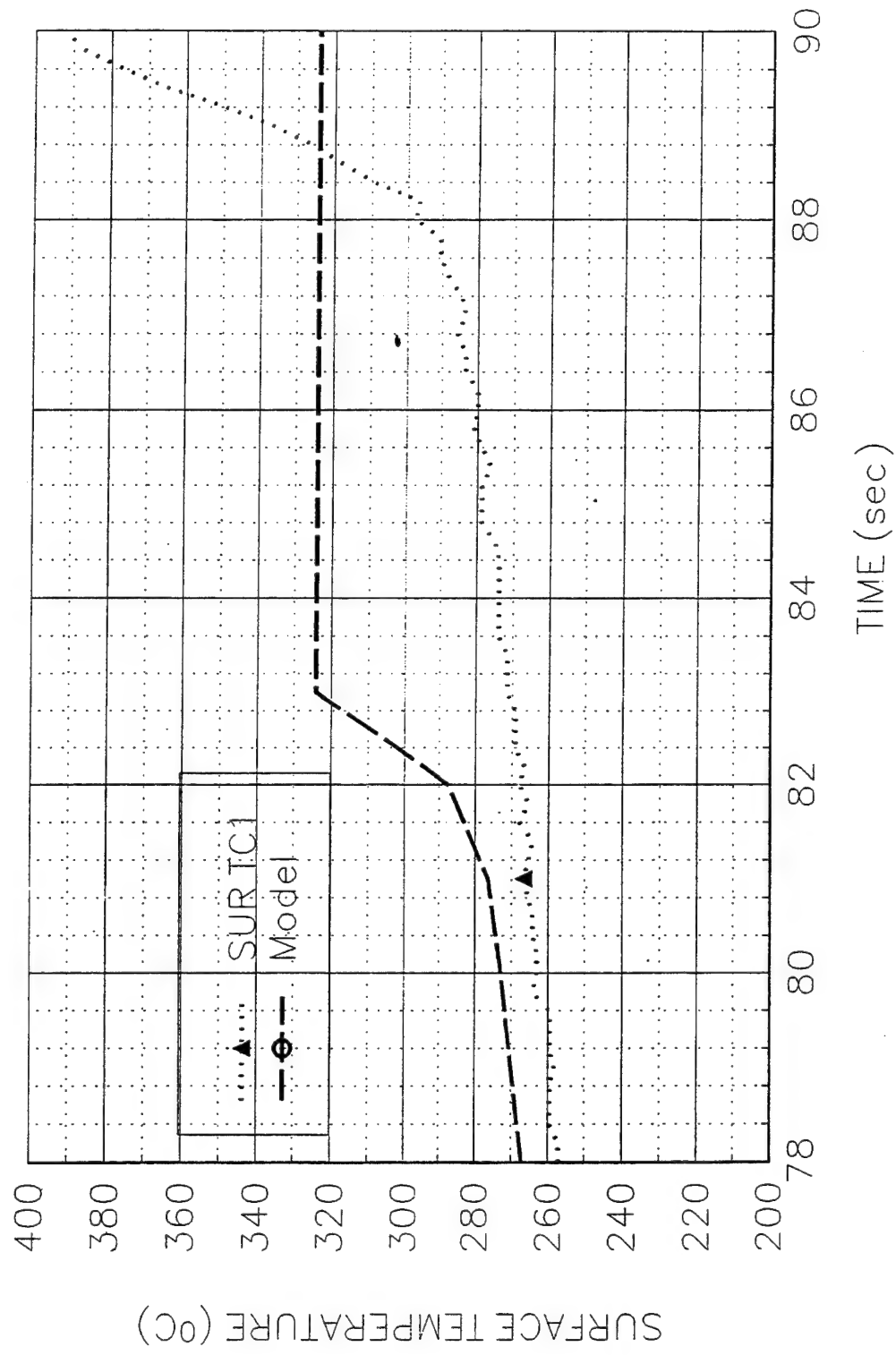
T30K623

Potlatch Particle Board,  $V=2.56 \text{ mm/s}$



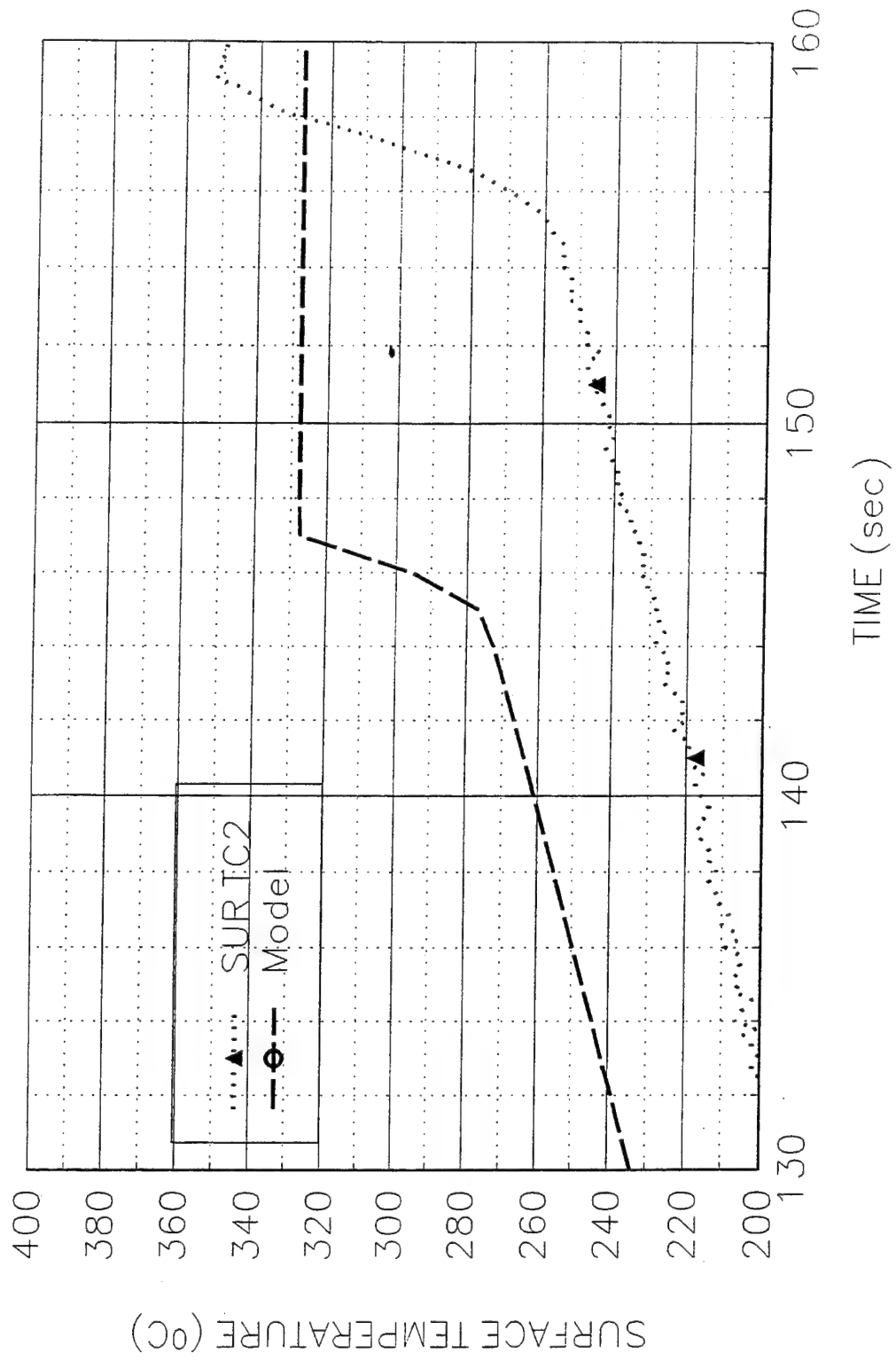
T30k623

Potlatch Particle Board, V=2.56 mm/s



T30K623

Potlatch Particle Board,  $V=2.56$  mm/s



**Data Sheet**  
**Constant Horizontal Flame Spread Experiment**

Experimental No.: 2

Date: 4/18/94 Mon.

Time: 10:30 pm

**Pre-Experiment**

Heat Flux at 400 mm Location (Planned) (kW/m<sup>2</sup>): 10

Slider Speed (mm/s): 0.64 mm/s

**Burning Sample Data**

Material: 1/4" PMMA Sheet

Dimension(LxWxH, mm): 800x152x6.35

**Instrumentation**

Number of Thermocouples: 6

Number of Heat Flux Gauges: 2

Station	Sensor	x (mm)	z (mm)	File Column	Note
1	TC	197	0.76	B	GAS TC1a
1	TC	197	?	C	Ready_Made TC
1	TC	197	0	D	SURFACE TC1
2	TC	378	0.76	E	GAS TC2
2	TC	378	0	F	SURFACE TC2
2	HG	378	0	H	SERIAL 84501
3	TC	599	0	G	SURFACE TC3
3	HG	599	0	I	SERIAL 525842

**Experiment**

Flux Gauge Reading @ 400 mm (Serial No. 27844, mV): 3.10-10.56 kW/m<sup>2</sup>~10.16 kW/m<sup>2</sup> @425 mm

Preheating Time without Pilot Flame (seconds): 150

Time to Sample Ignition After Applying the Pilot Flame (seconds): 20

Speed Used (S1M"Steps"): 100

Number of Steps (I1M"Steps"): 60000

File Names (.PRN): P10K418a, P10K418b

Set-up File Name:

Sampling Rate (Hz): 10      Duration of Sampling (sec): 600

Time to Start Moving the Sample (sec): -170

Ignition Heat Flux (Calculated, kW/m<sup>2</sup>):

**Ambient Conditions**

Temperature (°C): 18.

**Observations** Burning width remains at about 6 cm, slide stops @60000 steps (travels over 381 mm) then stops the data acquisition for 10, seconds, begin data file P10K418b which is the data file when the slide stops

Personnel Jeff Cote, Y.C.

Processing of Data: SUR TC1:  $1/\tau = 0.41$ ,  $T_p = 370^\circ\text{C}$ ,  $T_{ext} = 235.4^\circ\text{C}$ ,  
 $k_{pc} = 0.2798 \times 1200 \times 2200 = 738672$ ,

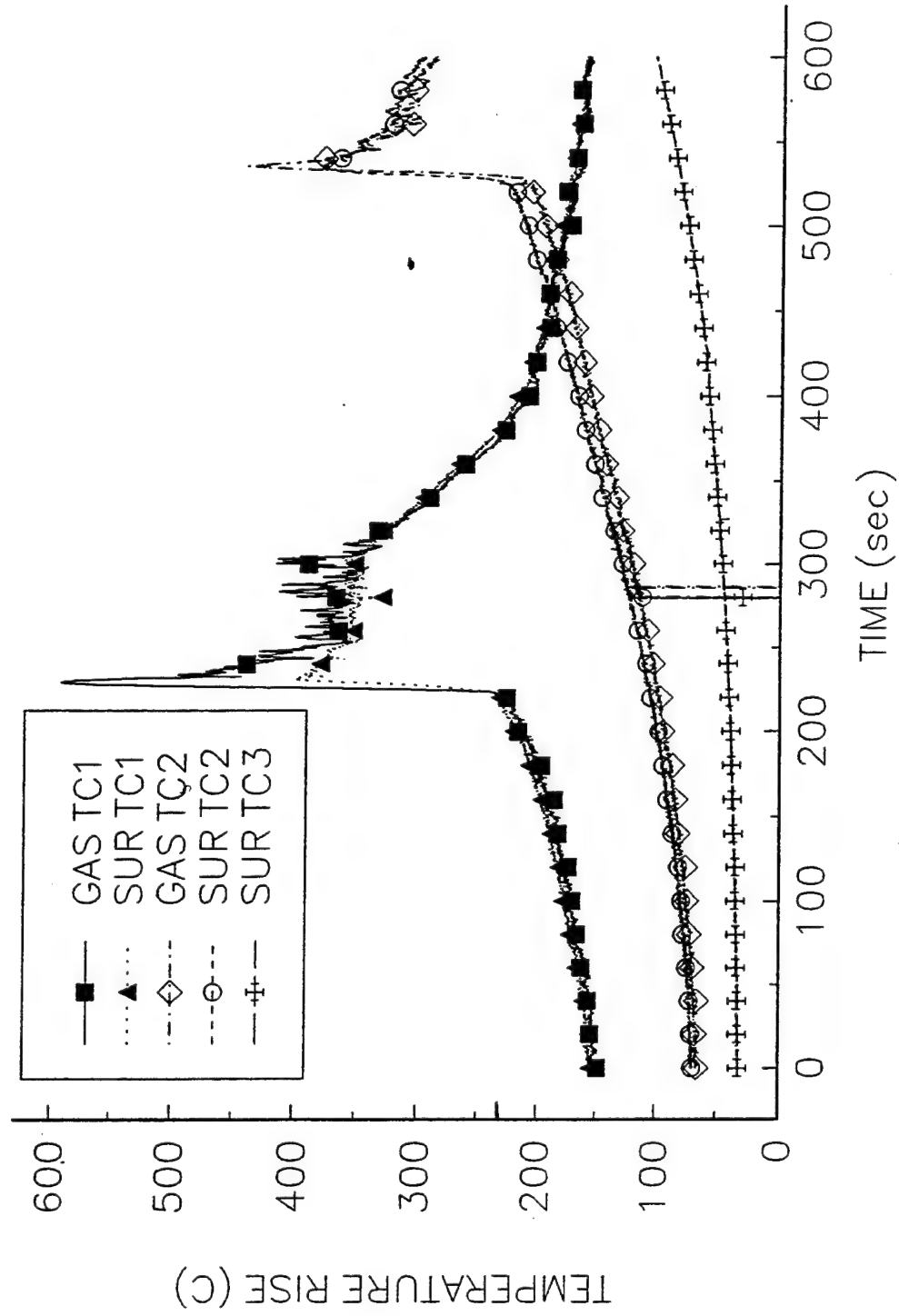
$q_0'' = (\pi k_{pc})^{1/2} (T_p - T_{ext})(V/\delta)^{1/2} = (738672)^{1/2} \times (370 - 235.4)(0.41)^{1/2} = 73.91 \text{ kW/m}^2$

SUR TC2:  $1/\tau = 0.53$ ,  $T_p = 370^\circ\text{C}$ ,  $T_{ext} = 235.4^\circ\text{C}$ ,

$q_0'' = (\pi k_{pc})^{1/2} (T_p - T_{ext})(V/\delta)^{1/2} = (738672)^{1/2} \times (370 - 235.4)(0.53)^{1/2} = 84.48 \text{ kW/m}^2$

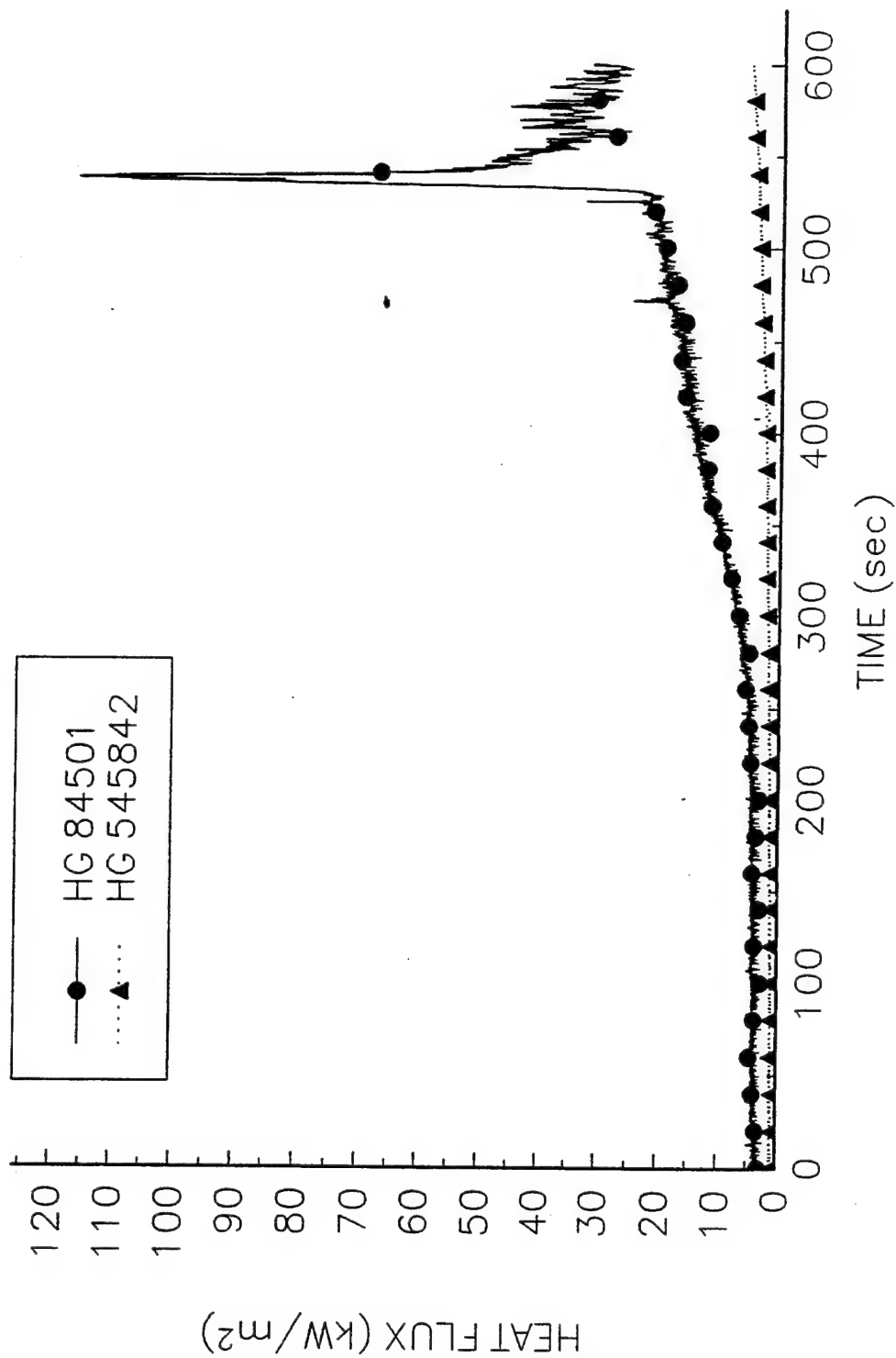
P10K418A

1/4" PMMA Sheet,  $V=0.64$  mm/s



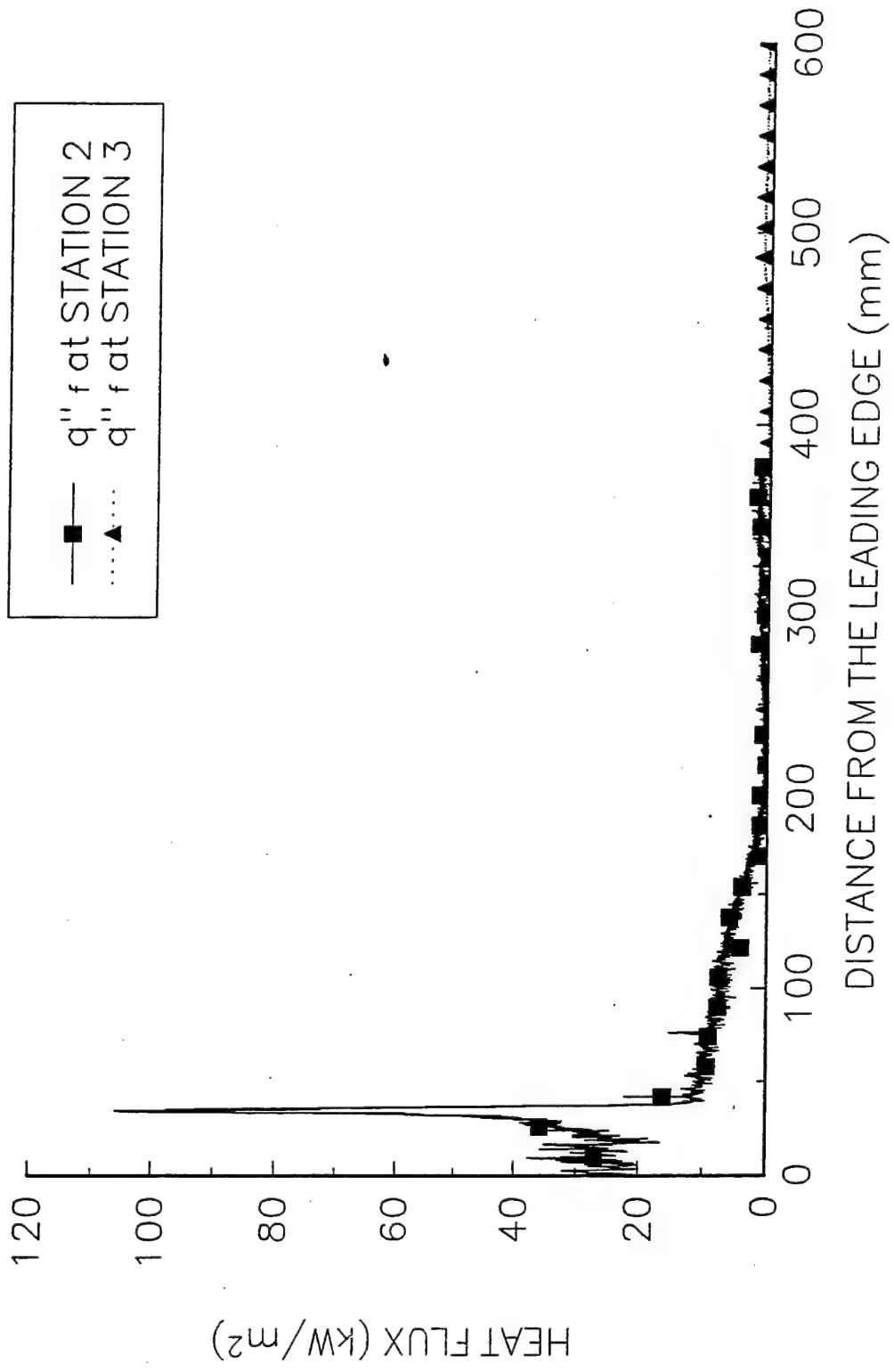
P10K418a

1/4" PMMA Sheet,  $V=0.64$  mm/s



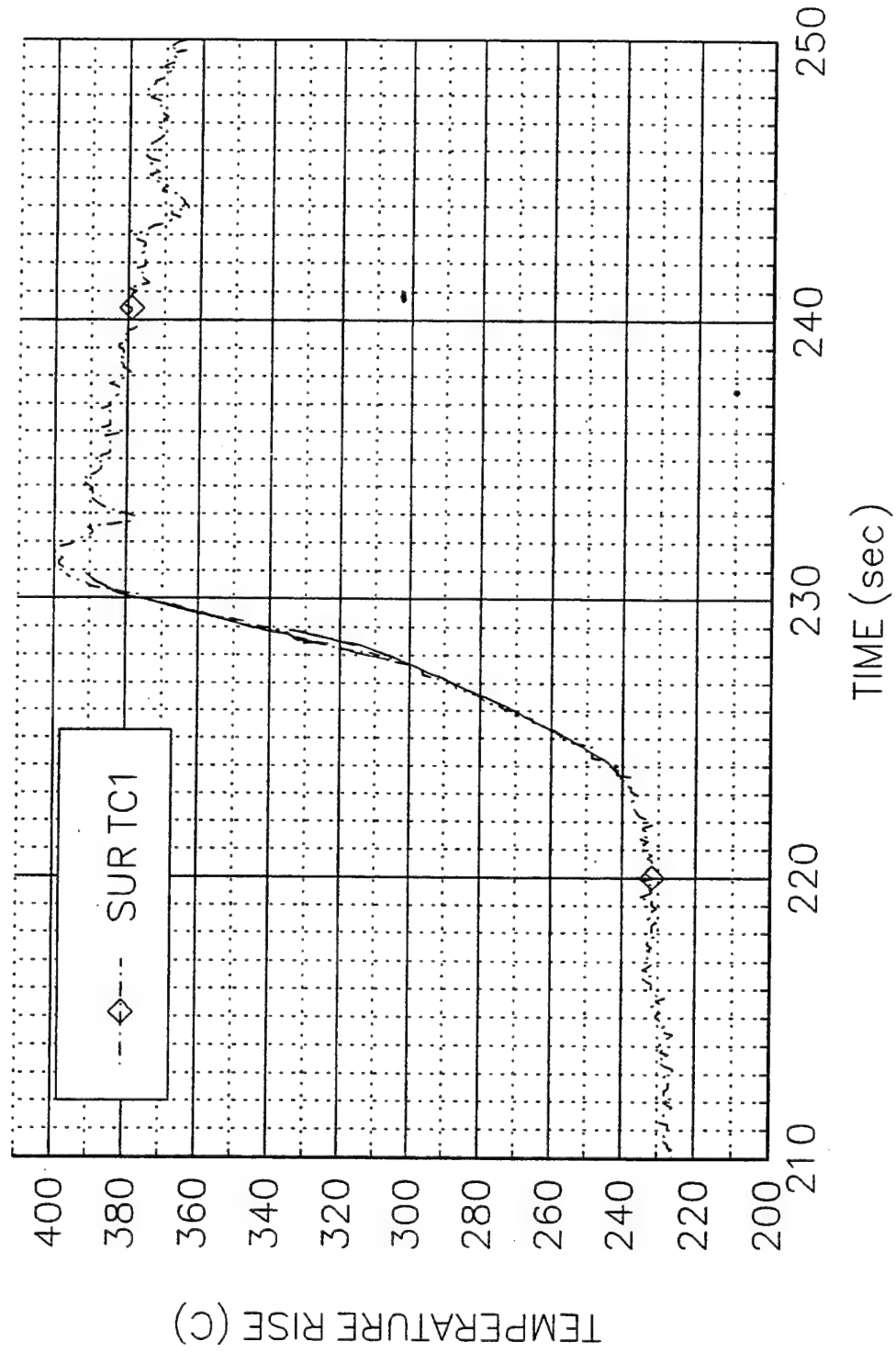
P10K418A

1/4" PMMA Sheet,  $V=0.64$  mm/s



P10K418A

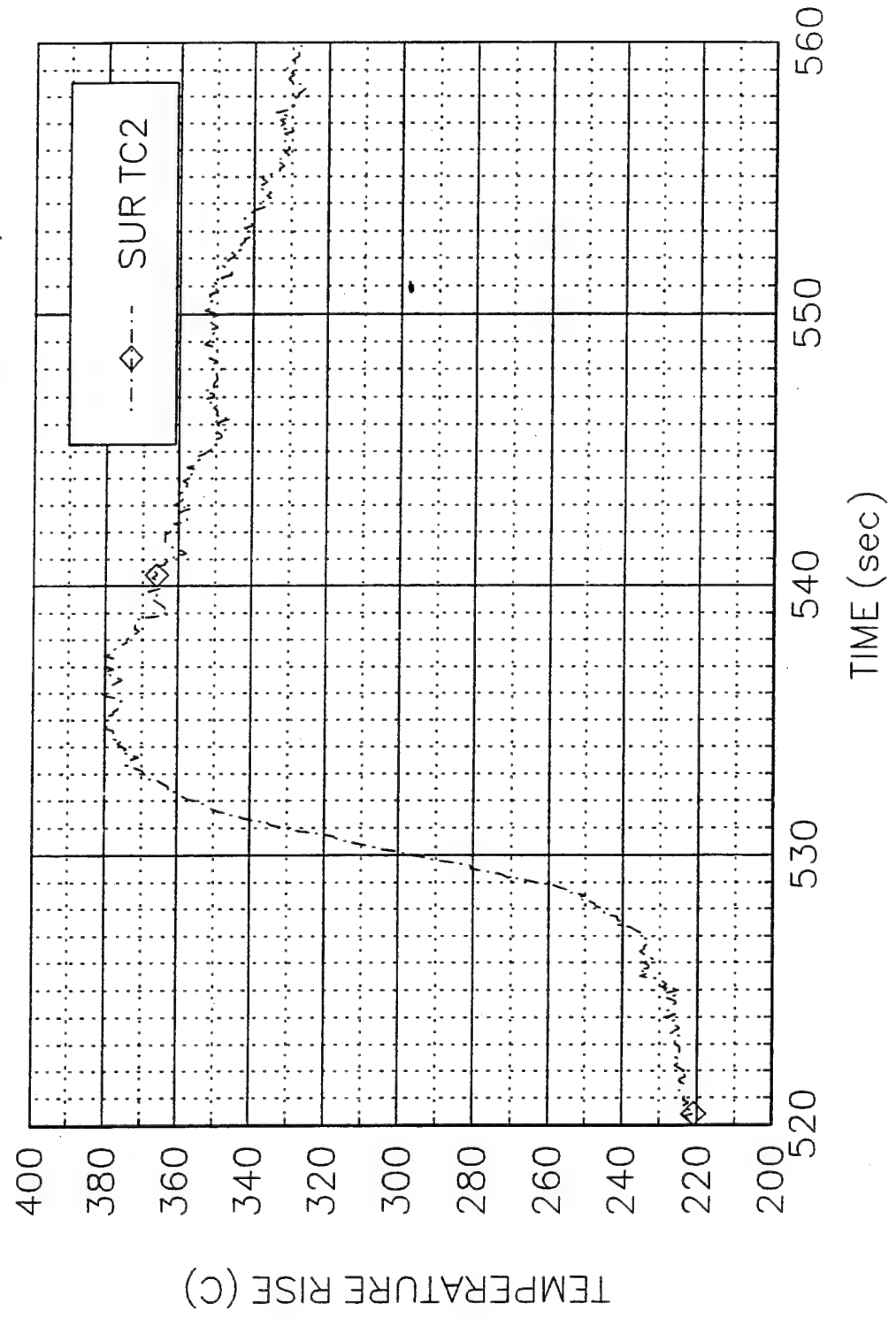
1/4" PMMA Sheet, V=0.64 mm/s





P10K418A

1 / 4" PMMA Sheet, V=0.64 mm/s



**Data Sheet**  
**Constant Horizontal Flame Spread Experiment**

Experimental No.: 11

Date: 5/16/94 Mon.

Time: 2:30 pm

**Pre-Experiment**

Heat Flux at 400 mm Location (Planned) (kW/m<sup>2</sup>): 10

Slider Speed (mm/s): 0.50 mm/s

**Burning Sample Data**

Material: 1/4" PMMA Sheet

Dimension(LxWxH, mm): 800x152x6.35

**Instrumentation**

Number of Thermocouples: 5

Number of Heat Flux Gauges: 2

Station	Sensor	x (mm)	z (mm)	File Column	Note
1	TC	201	0.05	C	GAS TC1a
1	TC	201	0	B	SURFACE TC1
2	TC	381	0.05	E	GAS TC2
2	TC	381	0	D	SURFACE TC2
2	HG	381	0	G	SERIAL 84501
3	TC	602	0	F	SURFACE TC3
3	HG	602	0	H	SERIAL 525842

**Experiment**

Flux Gauge Reading @ 400 mm (Serial No. 27844, mV): 3.20-10.90 kW/m<sup>2</sup>-10.58 kW/m<sup>2</sup> @425 mm

Preheating Time without Pilot Flame (seconds): 240

Time to Sample Ignition After Applying the Pilot Flame (seconds): 80

Speed Used (S1M"Steps"): 79

Number of Steps (I1M"Steps"): 80000

File Names (.PRN): P10K516

Set-up File Name:

Sampling Rate (Hz): 5      Duration of Sampling (sec): 1500

Time to Start Moving the Sample (sec): ~376

Ignition Heat Flux (Calculated, kW/m<sup>2</sup>):

**Ambient Conditions**

Temperature (°C): 16.

**Observations** Surface & TC, HG all are unpainted. Area is constant (10 cm wide). 84501 water outlet temperature: 16°C, about constant.

Personnel Jeff Cote, Y.C.

Processing of Data: SUR TC1:  $1/\tau = 0.444$ ,  $T_p = 370^\circ\text{C}$ ,  $T_{ext} = 221.7^\circ\text{C}$ ,  
 $k_{pc} = 0.2798 \times 1200 \times 2200 = 738672$ ,

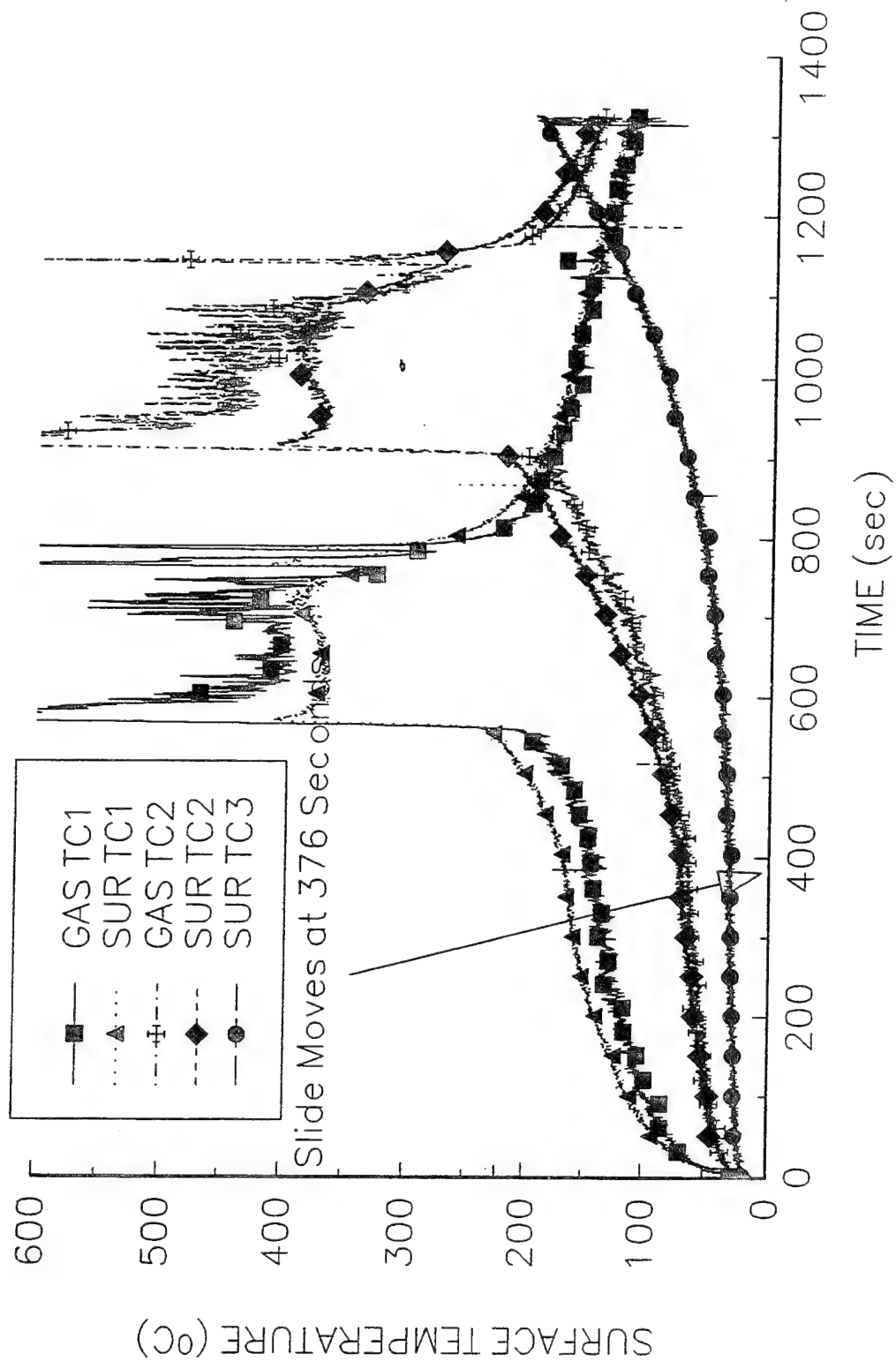
$$q_0'' = (\pi k_{pc})^{1/2} (T_p - T_{ext}) (V/\delta)^{1/2} = (738672)^{1/2} \times (370 - 221.7) (0.444)^{1/2} = 84.95 \text{ kW/m}^2$$

SUR TC2:  $1/\tau = 0.333$ ,  $T_p = 370^\circ\text{C}$ ,  $T_{ext} = 221.7^\circ\text{C}$ ,

$$q_0'' = (\pi k_{pc})^{1/2} (T_p - T_{ext}) (V/\delta)^{1/2} = (738672)^{1/2} \times (370 - 235.4) (0.333)^{1/2} = 73.57 \text{ kW/m}^2$$

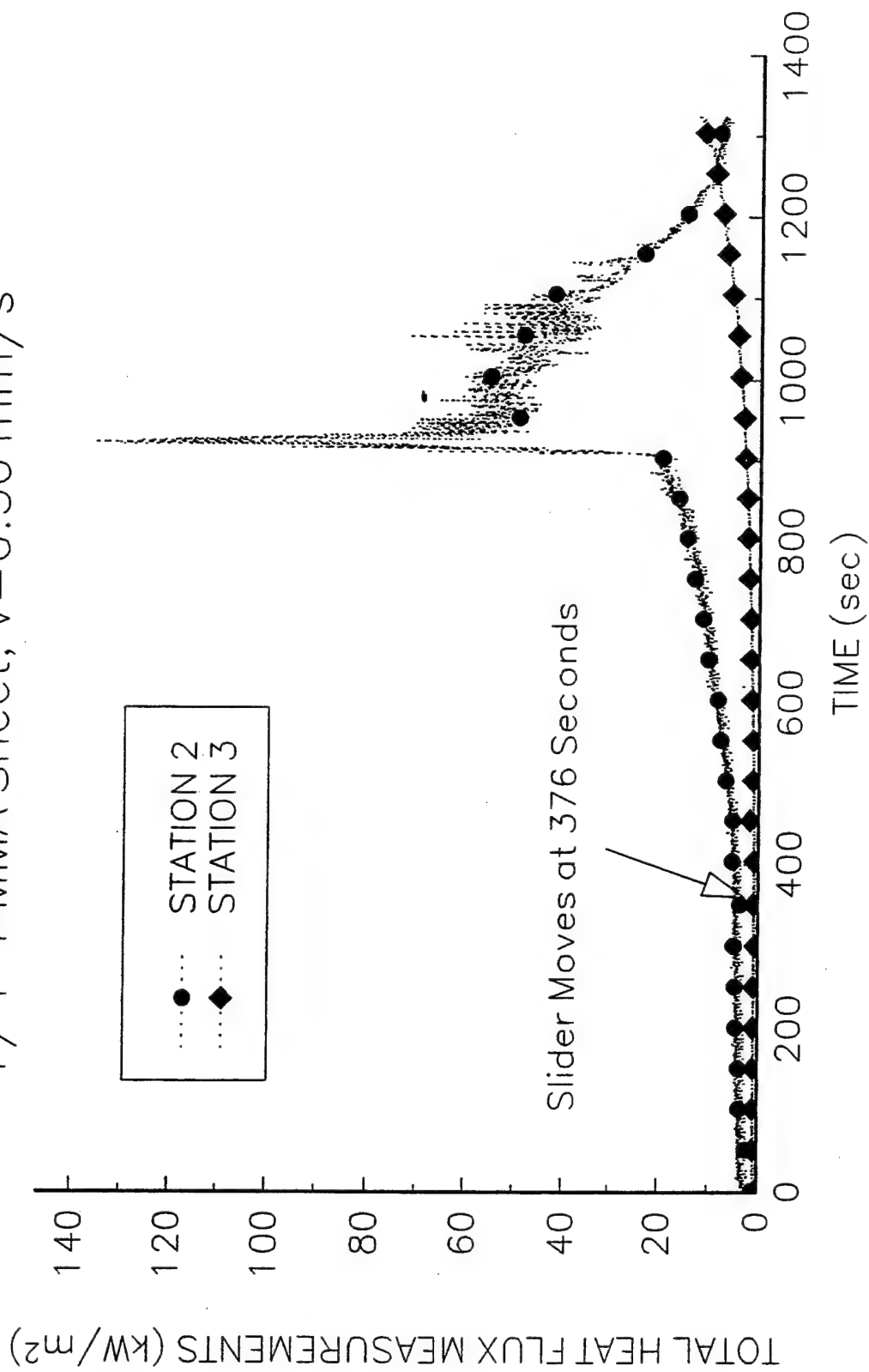
P10K516

1/4" PMMA Sheet, V=0.5 mm/s



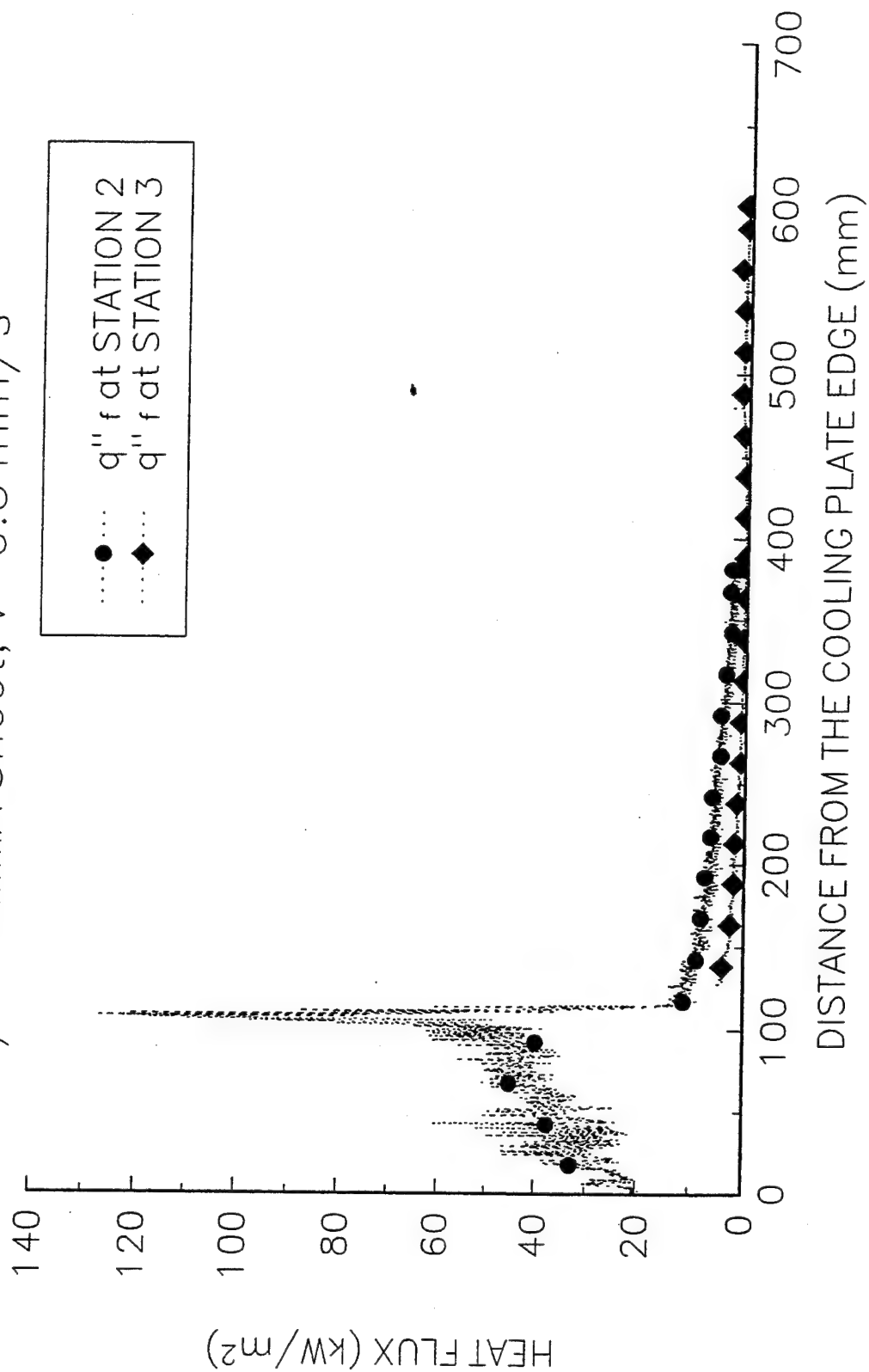
P10K516

1/4" PMMA Sheet,  $V=0.50$  mm/s



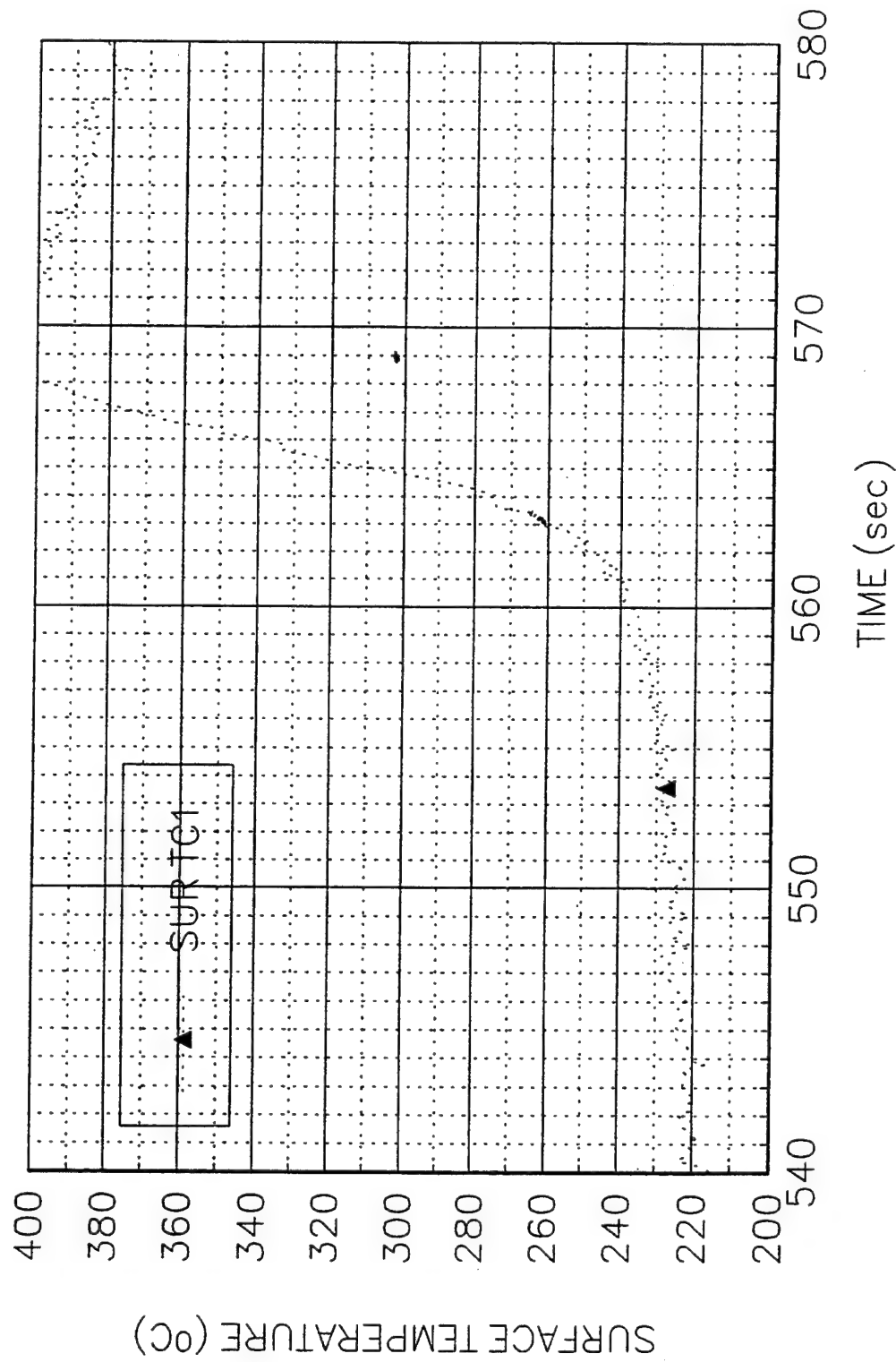
P10K516

1/4" PMMA Sheet,  $V=0.5 \text{ mm/s}$



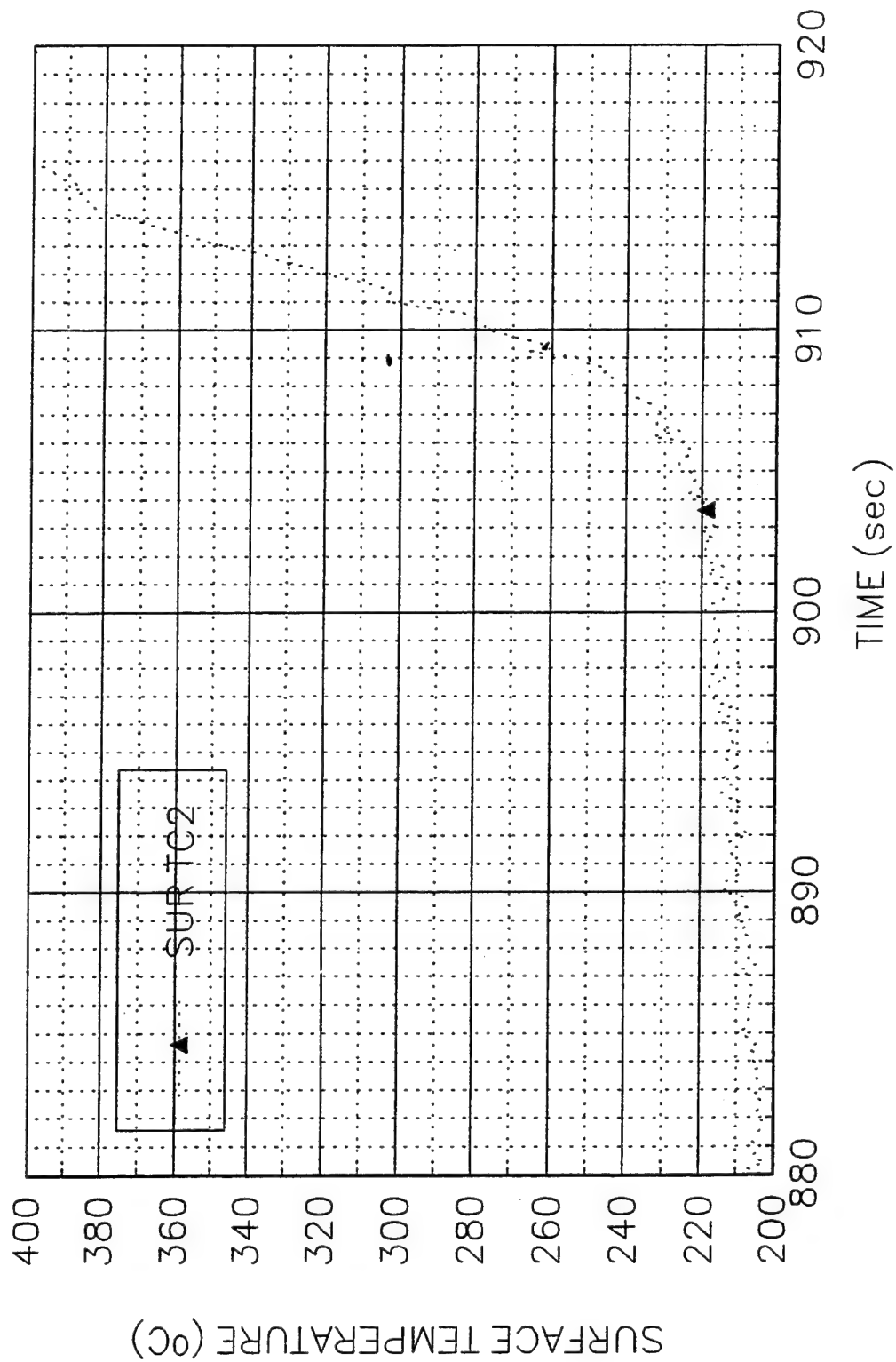
P10K516

1/4" PMMA Sheet, V=0.5 mm/s



P10K516

1/4" PMMA Sheet, V=0.5 mm/s



**Data Sheet**  
**Constant Horizontal Flame Spread Experiment**

Experimental No.: 5

Date: 4/29/94 Fr.

Time: 10:30 pm

**Pre-Experiment**

Heat Flux at 400 mm Location (Planned) (kW/m<sup>2</sup>): 20

Slider Speed (mm/s): 1.27 mm/s

**Burning Sample Data**

Material: 1/4" PMMA Sheet

Dimension(LxWxH, mm): 800x152x6.35

**Instrumentation**

Number of Thermocouples: 5

Number of Heat Flux Gauges: 2

Station	Sensor	x (mm)	z (mm)	File Column	Note
1	TC	195	1.57	B	GAS TC1a
1	TC	195	0	C	SURFACE TC1
2	TC	377	1.22	D	GAS TC2
2	TC	377	0	E	SURFACE TC2
2	HG	377	0	G	SERIAL 84501
3	TC	598	0	F	SURFACE TC3
3	HG	598	0	H	SERIAL 525842

**Experiment**

Flux Gauge Reading @ 400 mm (Serial No. 27844, mV): 5.85-19.93 kW/m<sup>2</sup>-19.35 kW/m<sup>2</sup> @425 mm

Preheating Time without Pilot Flame (seconds): 90

Time to Sample Ignition After Applying the Pilot Flame (seconds): 30

Speed Used (S1M"Steps"): 200

Number of Steps (I1M"Steps"): 80000

File Names (.PRN): P20K429

Set-up File Name:

Sampling Rate (Hz): 5      Duration of Sampling (sec): 1500

Time to Start Moving the Sample (sec):

Ignition Heat Flux (Calculated, kW/m<sup>2</sup>):

**Ambient Conditions**

Temperature (°C): 24.5

**Observations** Burning area is good (~6 cm). Data acquisition starts @35 seconds after starting up of preheating, connection to TC not good. Connection to HG2 discontinues after flame front gets to second station

Personnel Y. C.

Processing of Data: SUR TC1:  $k_{pc} = 0.2798 \times 1200 \times 2200 = 738672$ ,

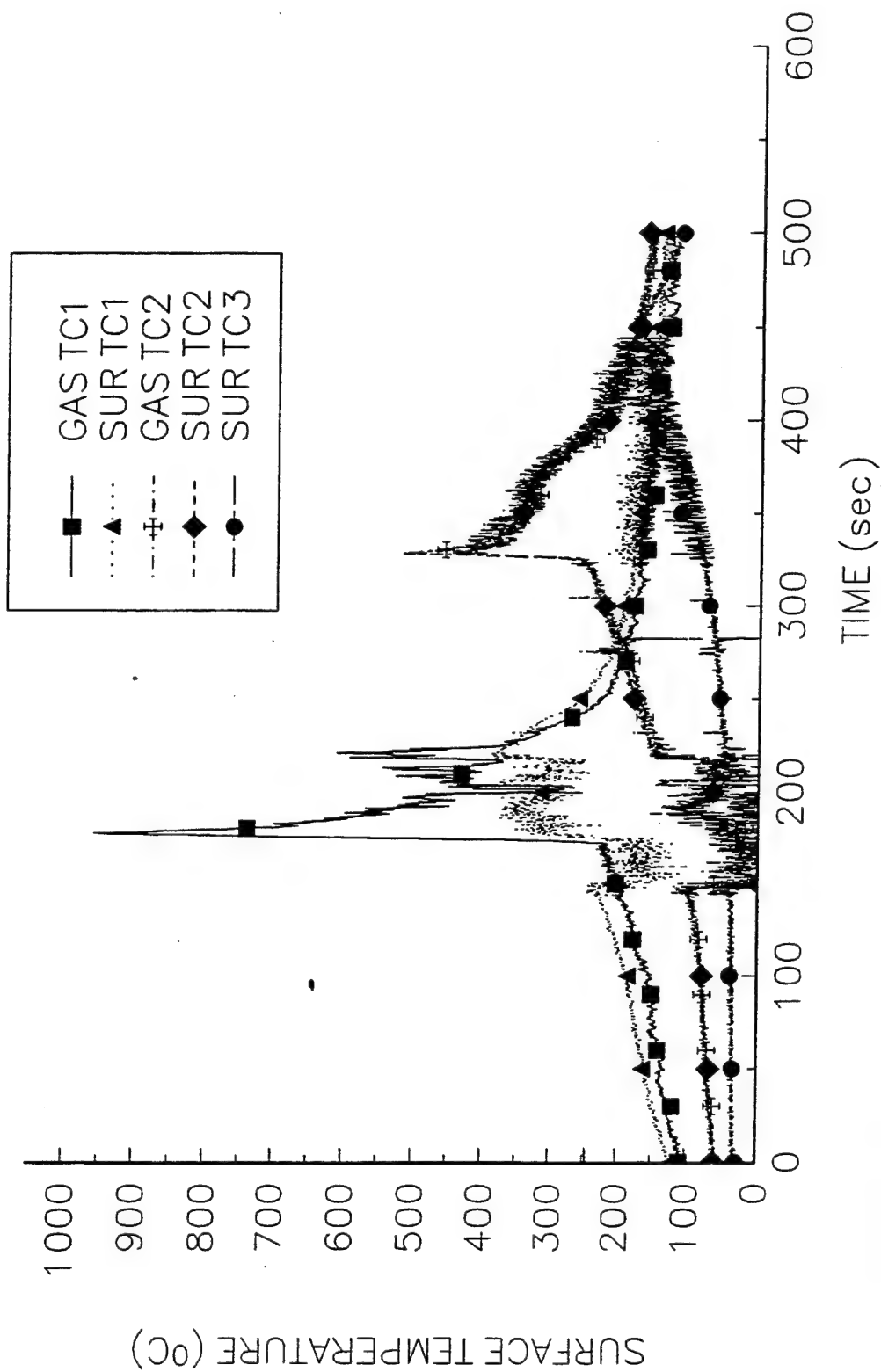
SUR TC2:  $1/\tau = 1.20$ ,  $T_p = 370^\circ\text{C}$ ,  $T_{ext} = 245.7^\circ\text{C}$ ,

$$q_0'' = (\pi k_{pc})^{1/2} (T_p - T_{ext}) (V/\delta)^{1/2} = (738672)^{1/2} \times (370 - 245.7) (1.20)^{1/2} = 117.0 \text{ kW/m}^2$$



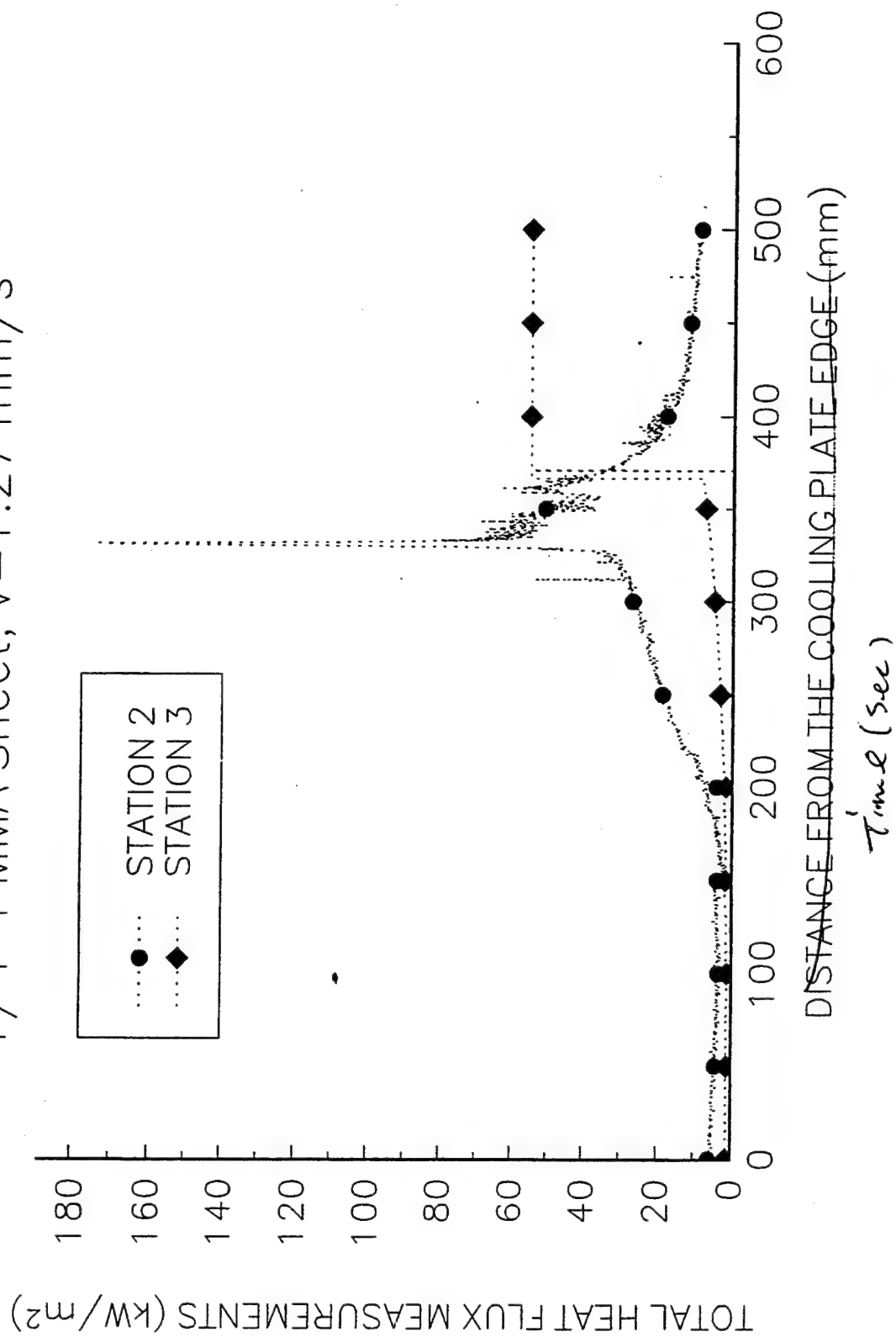
P20K429

1/4" PMMA Sheet, V=1.27 mm/s



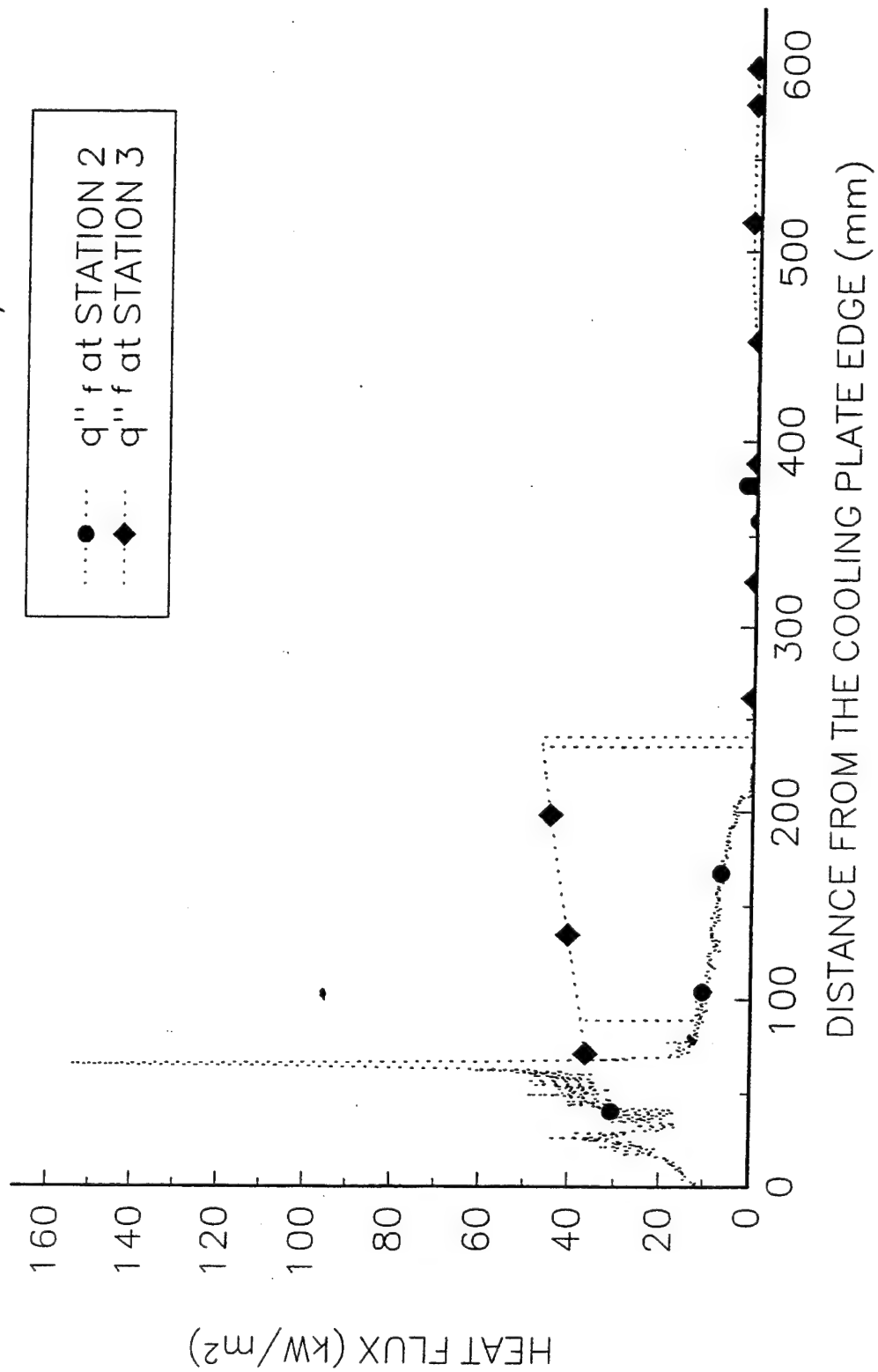
P20K429

1/4" PMMA Sheet,  $V=1.27$  mm/s



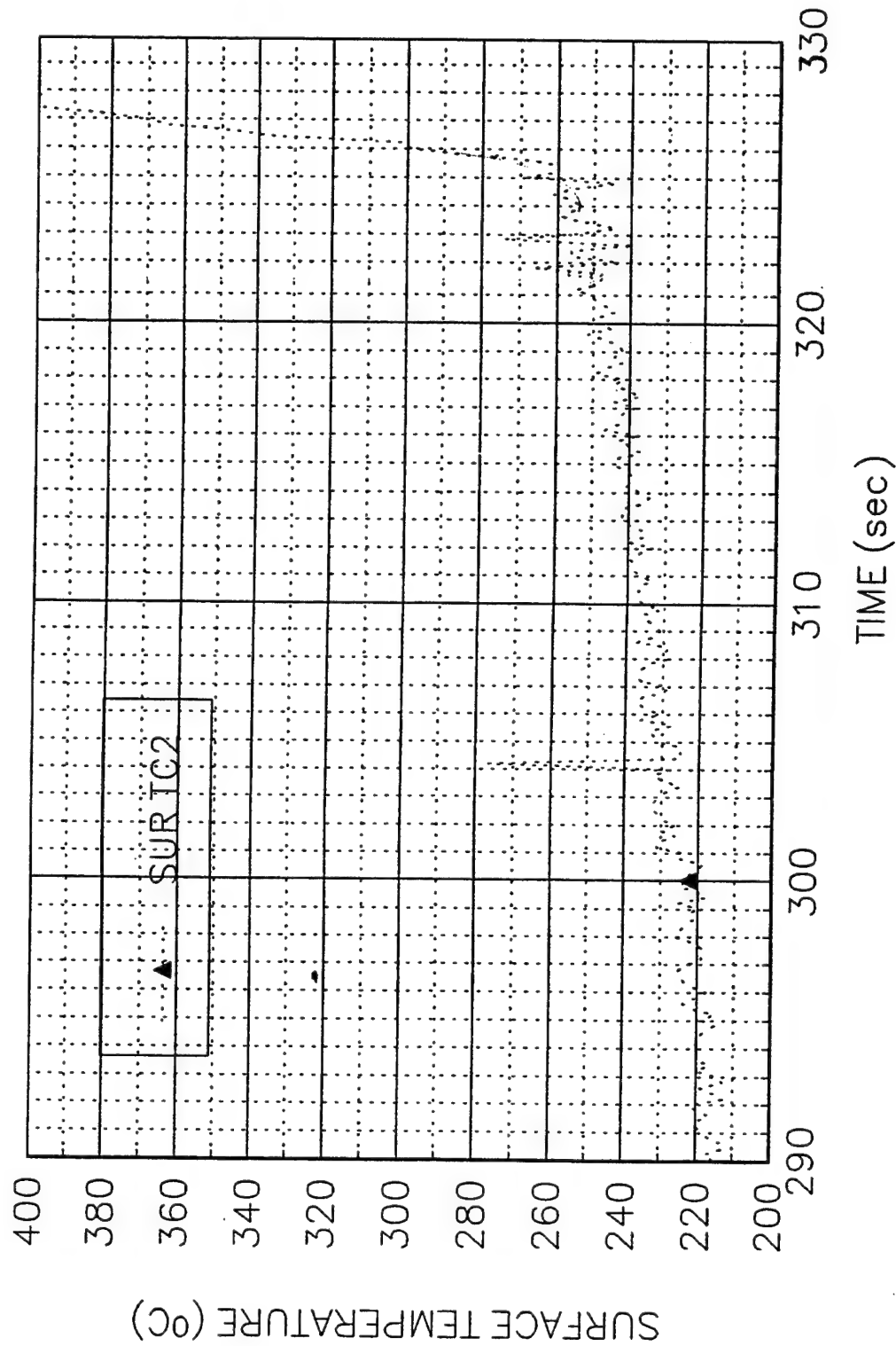
P20K429

1/4" PMMA Sheet,  $V=1.27$  mm/s



P20K429

1 / 4" PMMA Sheet, V=1.27 mm/s



**Data Sheet**  
**Constant Horizontal Flame Spread Experiment**

Experimental No.: 6

Date: 5/04/94 Wed.

Time: 11:30 am

**Pre-Experiment**

Heat Flux at 400 mm Location (Planned) (kW/m<sup>2</sup>): 20

Slider Speed (mm/s): 1.27 mm/s

**Burning Sample Data**

Material: 1/4" PMMA Sheet

Dimension(LxWxH, mm): 800x152x6.35

**Instrumentation**

Number of Thermocouples: 5

Number of Heat Flux Gauges: 2

Station	Sensor	x (mm)	z (mm)	File Column	Note
1	TC	201	0.77	C	GAS TC1
1	TC	201	0	B	SURFACE TC1
2	TC	379	0.34	E	GAS TC1
2	TC	379	0	D	SURFACE TC2
2	HG	379	0	G	SERIAL 84501
3	TC	600	0	F	SURFACE TC3
3	HG	600	0	H	SERIAL 525842

**Experiment**

Flux Gauge Reading @ 400 mm (Serial No. 27844, mV): 5.87-20.00 kW/m<sup>2</sup>-19.42 kW/m<sup>2</sup> @425 mm

Preheating Time without Pilot Flame (seconds): 90

Time to Sample Ignition After Applying the Pilot Flame (seconds): 20

Speed Used (S1M"Steps"): 200

Number of Steps (I1M"Steps"): 80000

File Names (.PRN): P20K504

Set-up File Name:

Sampling Rate (Hz): 5

Duration of Sampling (sec): 800

Time to Start Moving the Sample (sec):

Ignition Heat Flux (Calculated, kW/m<sup>2</sup>):

**Ambient Conditions**

Temperature (°C): 23.

**Observations** Surface TC3 seems fluctuating at the end of the test. 84501 reading low. High heat spray paint was applied on the fuel surface

Personnel Jeff Cote, Y.C.

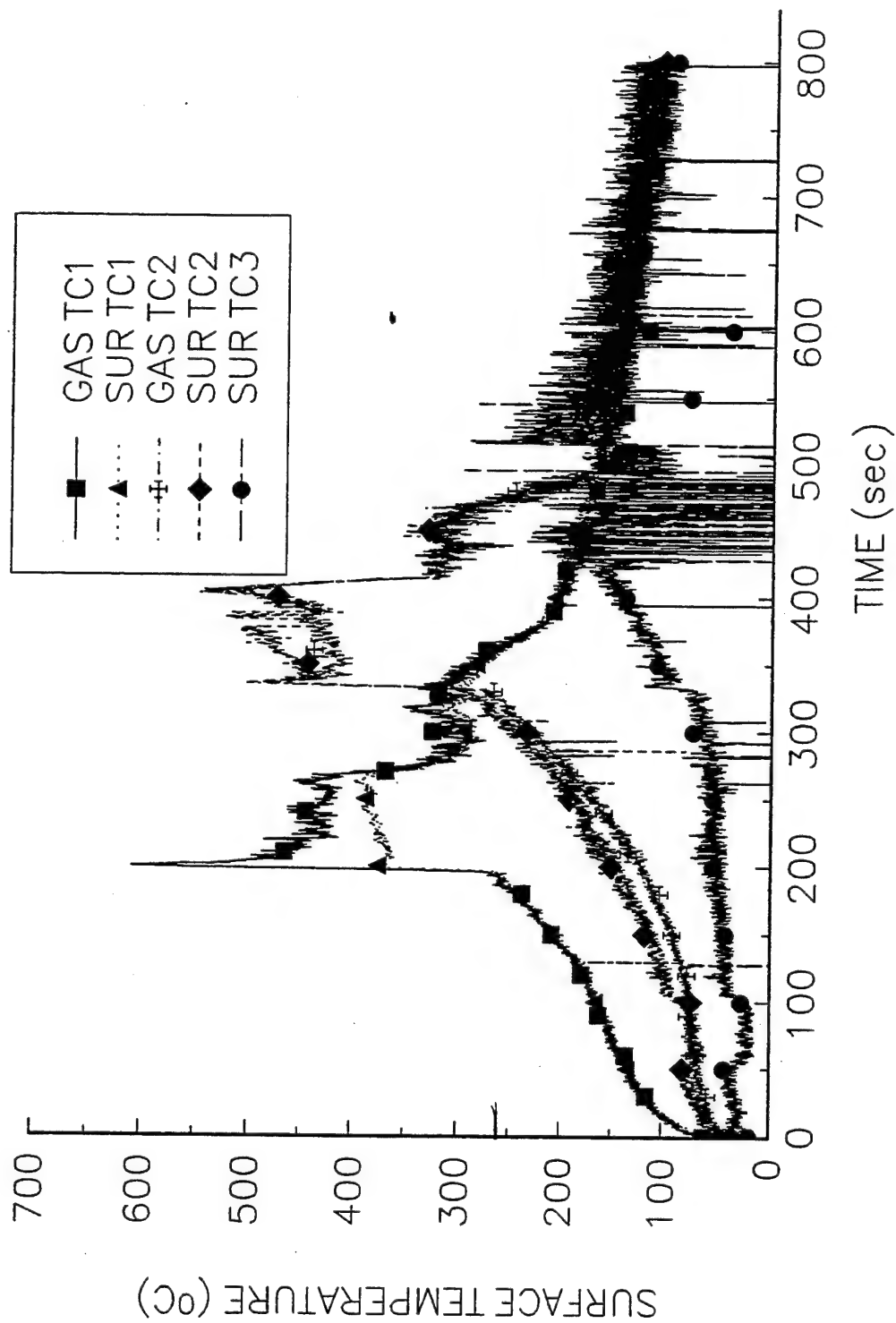
Processing of Data: SUR TC1:  $1/\tau = 1.20$ ,  $T_p = 370^\circ\text{C}$ ,  $T_{ext} = 260.4^\circ\text{C}$ ,

$k_{pc} = 0.2798 \times 1200 \times 2200 = 738672$ ,

$q_0'' = (\pi k_{pc})^{1/2} (T_p - T_{ext}) (V/\delta)^{1/2} = (738672)^{1/2} \times (370 - 260.4) (1.2)^{1/2} = 103.4 \text{ kW/m}^2$

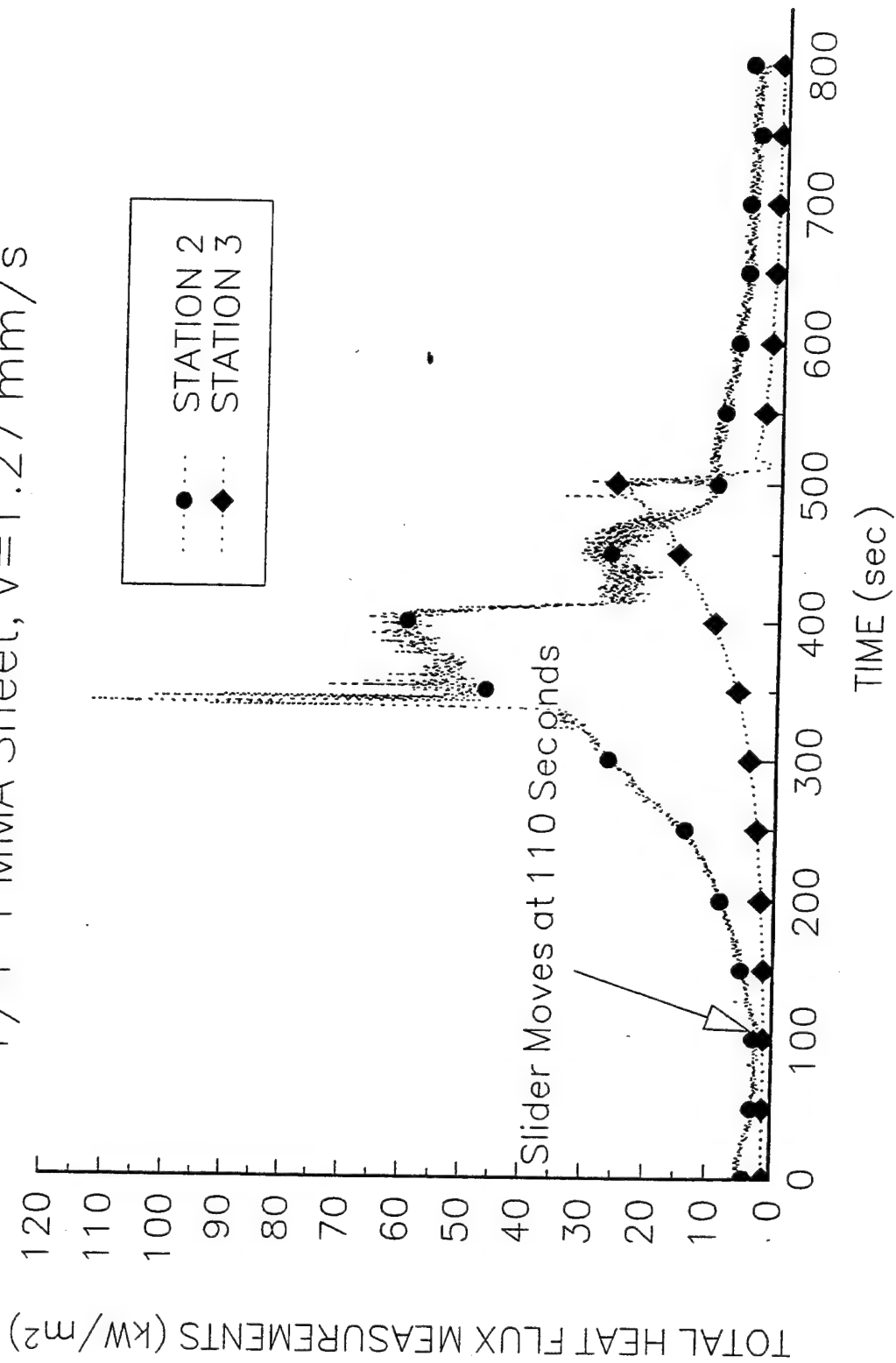
P20K504

1/4" PMMA Sheet, V=1.27 mm/s



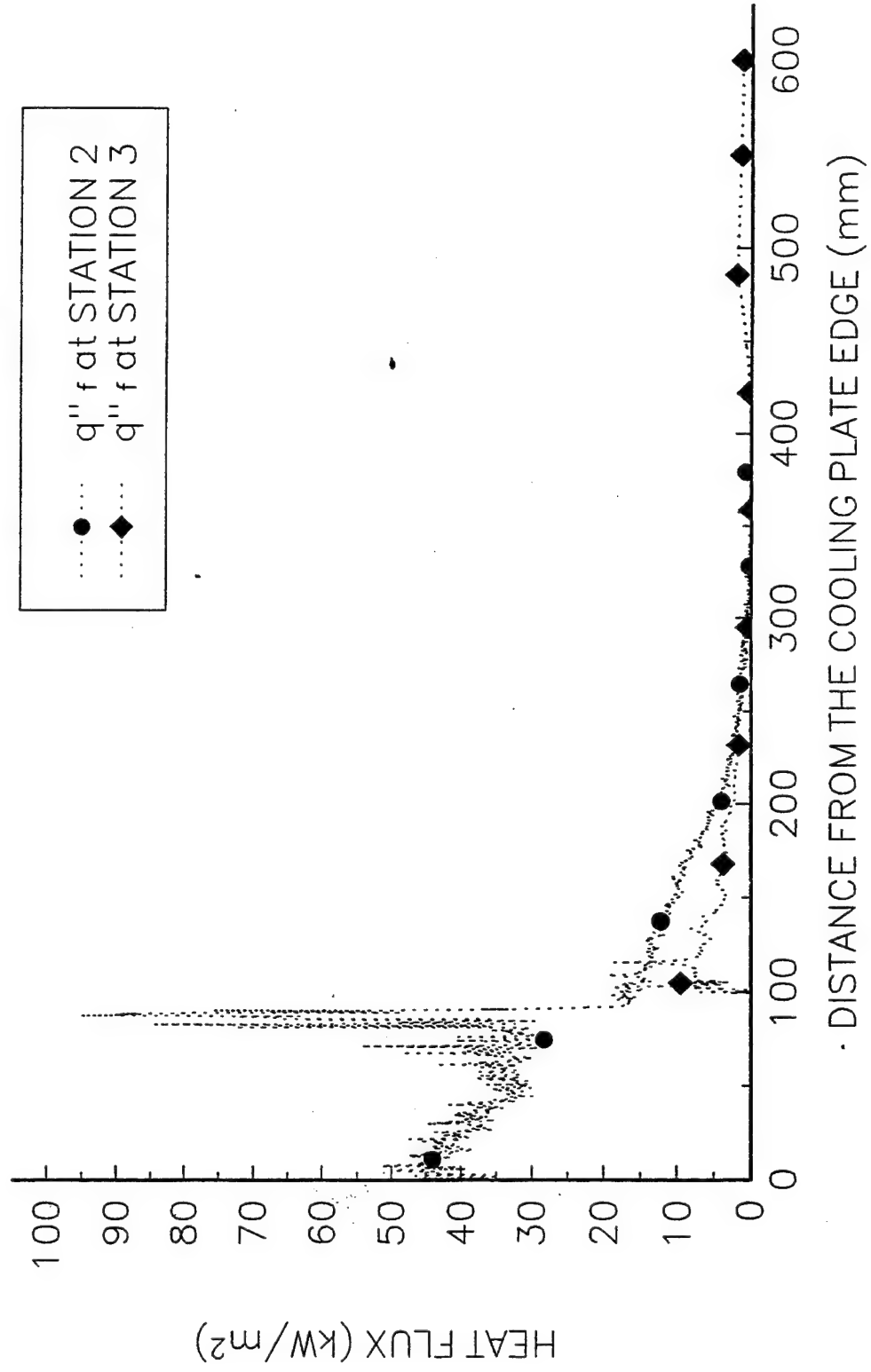
P20K504

1/4" PMMA Sheet,  $V=1.27$  mm/s



P20K504

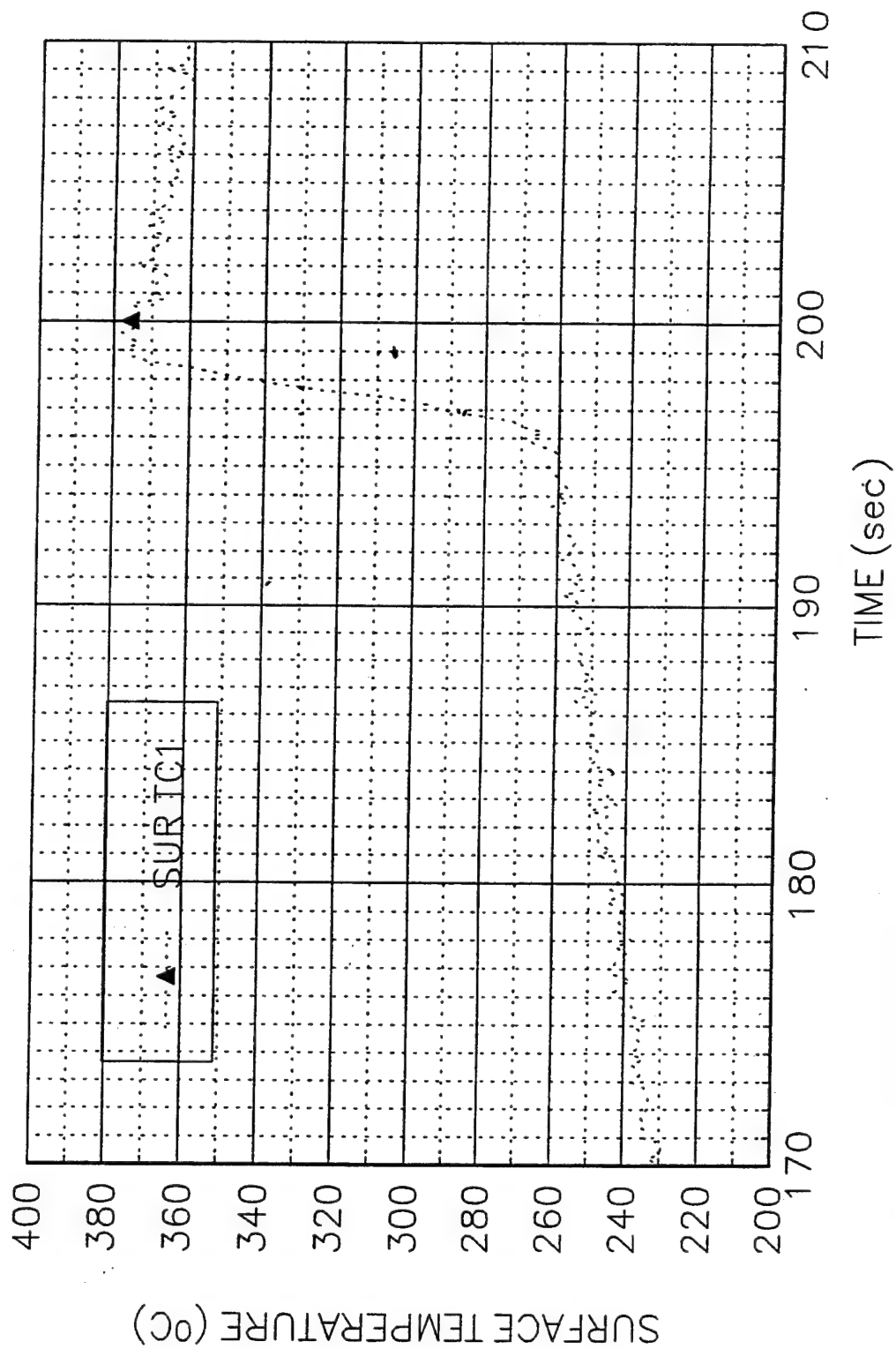
1/4" PMMA Sheet,  $V=1.27$  mm/s





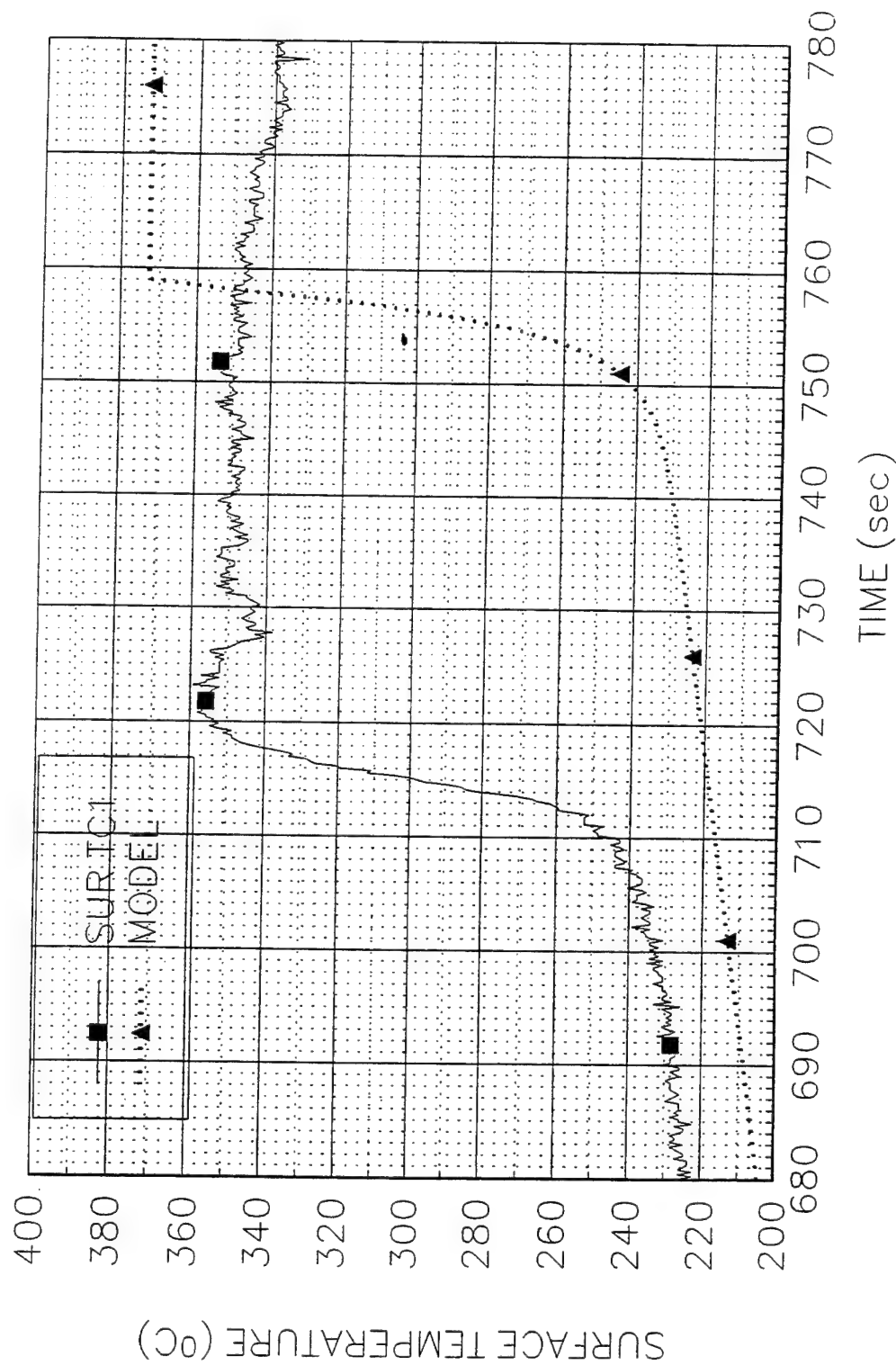
P20K504

1/4" PMMA Sheet, V=1.27 mm/s



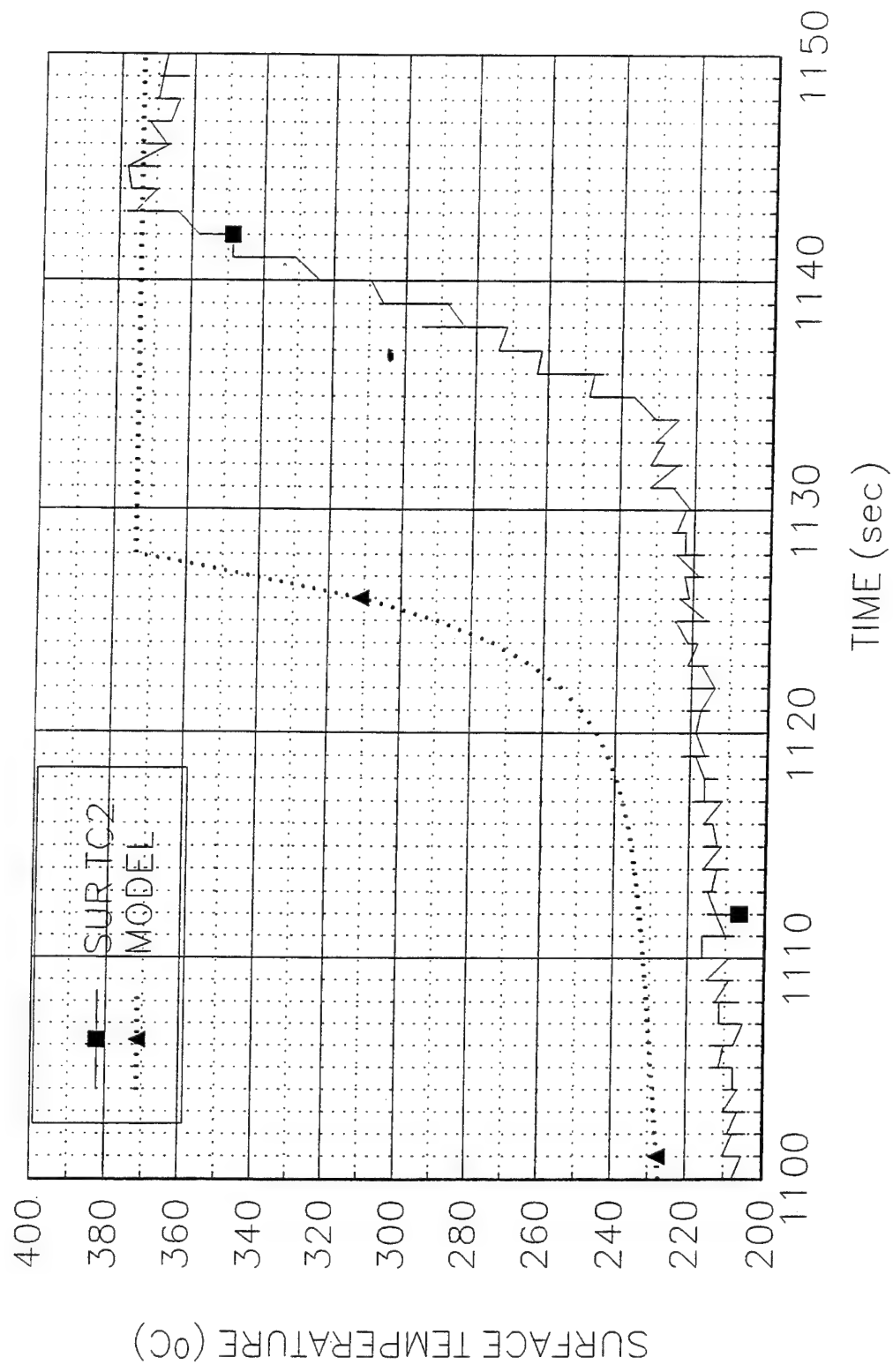
P10K629

1/4" PMMA Sheet,  $V=0.50$  mm/s



PI0K629

1/4" PMMA Sheet, V=0.50 mm/s



**Data Sheet**  
**Constant Horizontal Flame Spread Experiment**

Experimental No.: 4

Date: 4/27/94 Wed.

Time: 11:30 am

**Pre-Experiment**

Heat Flux at 400 mm Location (Planned) (kW/m<sup>2</sup>): 20

Slider Speed (mm/s): 1.27 mm/s

**Burning Sample Data**

Material: 1/4" PMMA Sheet

Dimension(LxWxH, mm): 800x152x6.35

**Instrumentation**

Number of Thermocouples: 5

Number of Heat Flux Gauges: 2

Station	Sensor	x (mm)	z (mm)	File Column	Note
1	TC	200	0.85	B	GAS TC1
1	TC	200	0	C	SURFACE TC1
2	TC	378	0.64	D	GAS TC1
2	TC	378	0	E	SURFACE TC2
2	HG	378	0	G	SERIAL 84501
3	TC	599	0	F	SURFACE TC3
3	HG	599	0	H	SERIAL 525842

**Experiment**

Flux Gauge Reading @ 400 mm (Serial No. 27844, mV): 5.90-20.10 kW/m<sup>2</sup>-19.68 kW/m<sup>2</sup> @425 mm

Preheating Time without Pilot Flame (seconds): 90

Time to Sample Ignition After Applying the Pilot Flame (seconds): 60

Speed Used (S1M"Steps"): 200

Number of Steps (I1M"Steps"): 80000

File Names (.PRN): P20K427

Set-up File Name:

Sampling Rate (Hz): 5      Duration of Sampling (sec): 800

Time to Start Moving the Sample (sec):

Ignition Heat Flux (Calculated, kW/m<sup>2</sup>):

**Ambient Conditions**

Temperature (°C): 21.

**Observations** Stops at 70481, HG1 wire disconnects, burning width too large (8 cm), constant burning area is obtained

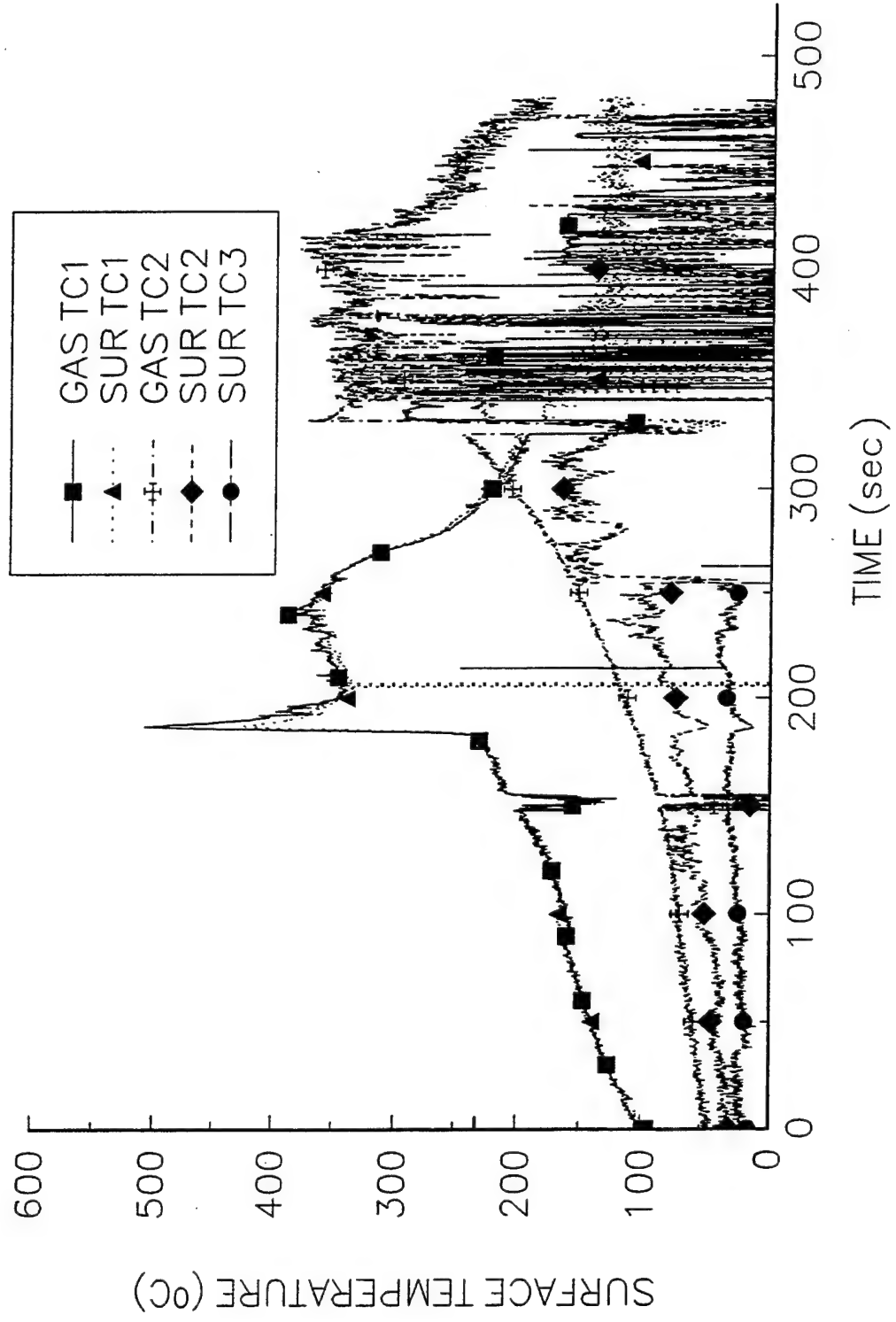
Personnel Jeff Cote, Y.C.

Processing of Data: SUR TC1:  $1/\tau = 1.0$ ,  $T_p = 370^\circ\text{C}$ ,  $T_{ext} = 232.4^\circ\text{C}$ ,  
 $k_{pc} = 0.2798 \times 1200 \times 2200 = 738672$ ,

$q_0'' = (\pi k_{pc})^{1/2} (T_p - T_{ext}) (V/\delta)^{1/2} = (738672)^{1/2} \times (370 - 232.4) (0.2857)^{1/2} = 118.23 \text{ kW/m}^2$

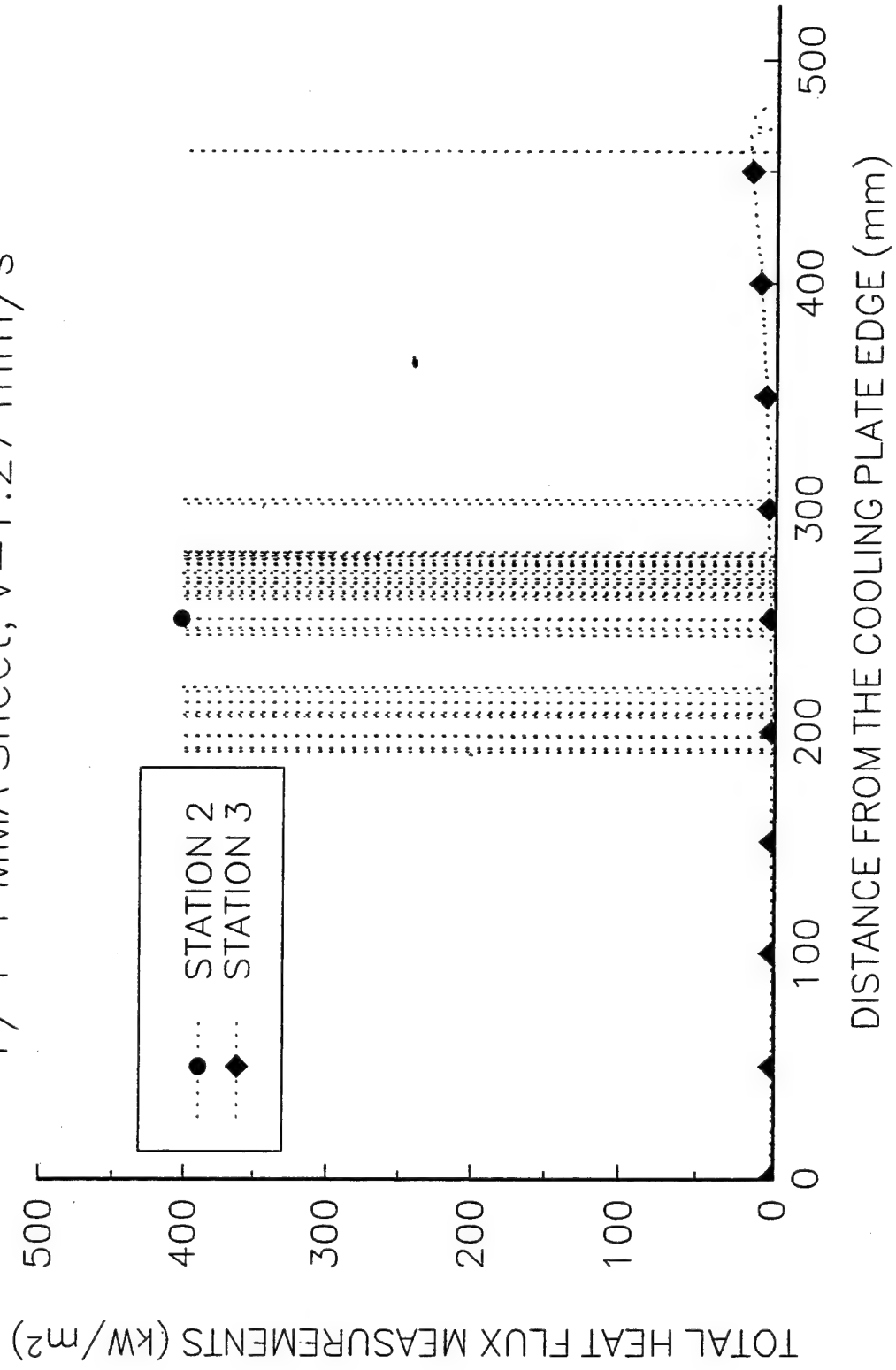
P20K427

1/4" PMMA Sheet, V=1.27 mm/s



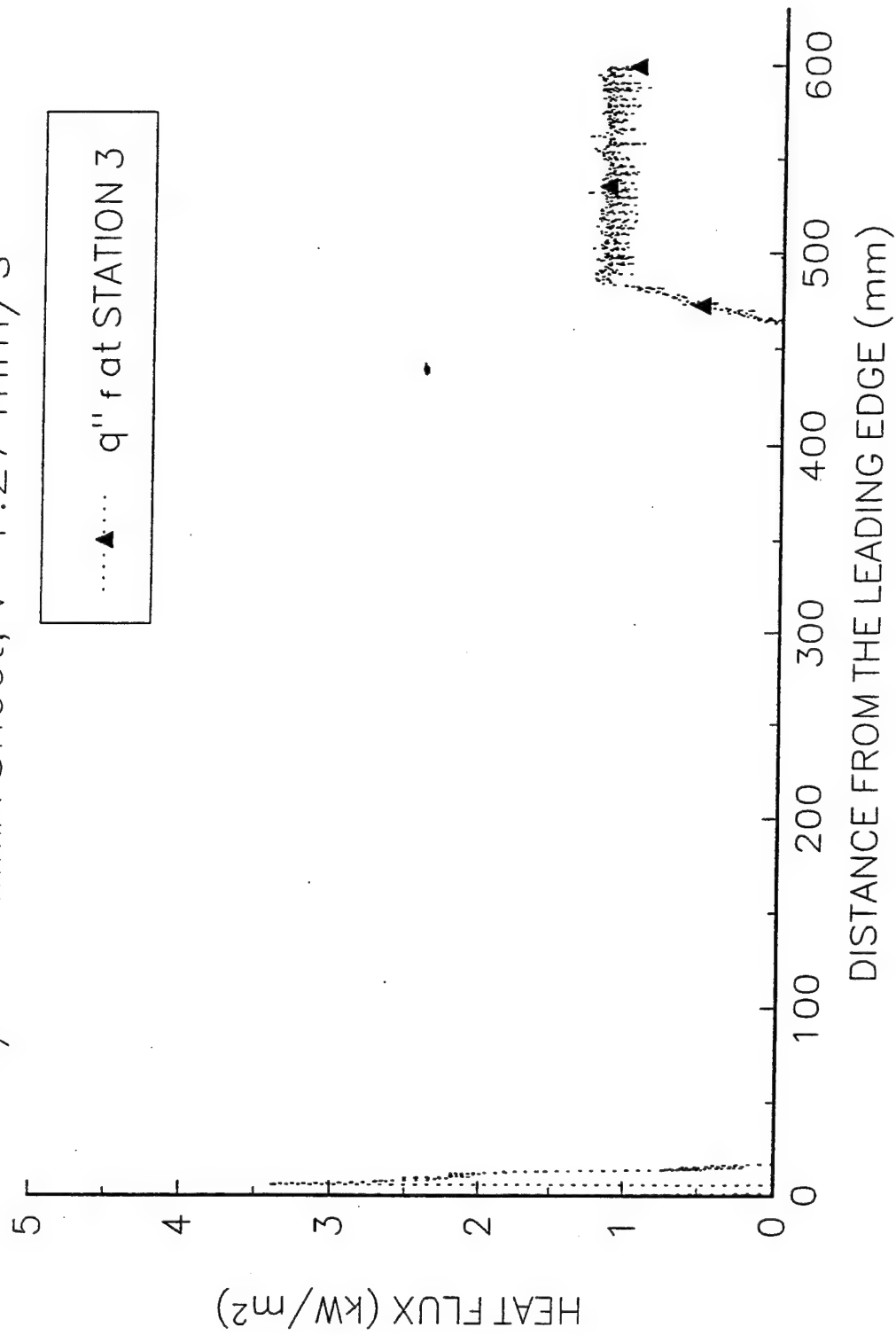
P20K427

1/4" PMMA Sheet,  $V=1.27$  mm/s



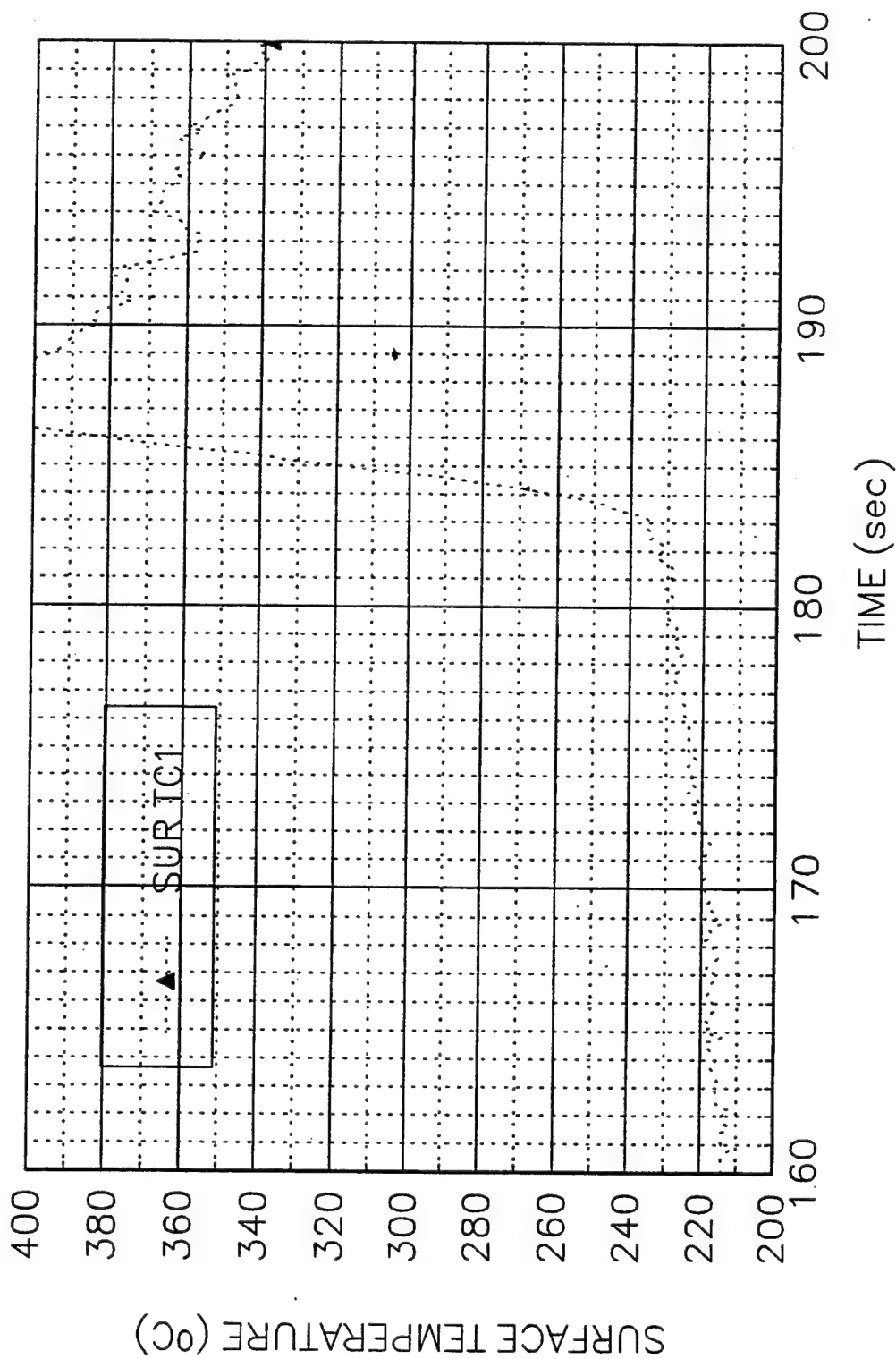
P20K427

1/4" PMMA Sheet,  $V=1.27$  mm/s



P20K427

1/4" PMMA Sheet, V=1.27 mm/s





**Data Sheet**  
**Constant Horizontal Flame Spread Experiment**

Experimental No.: 7

Date: 5/06/94 Wed.

Time: 11:30 am

**Pre-Experiment**

Heat Flux at 400 mm Location (Planned) (kW/m<sup>2</sup>): 20

Slider Speed (mm/s): 1.27 mm/s

**Burning Sample Data**

Material: 1/4" PMMA Sheet unpainted

Dimension(LxWxH, mm): 800x152x6.35

**Instrumentation**

Number of Thermocouples: 5

Number of Heat Flux Gauges: 2

Station	Sensor	x (mm)	z (mm)	File Column	Note
1	TC	196		F	GAS TC1
1	TC	196	0	G	SURFACE TC1
2	TC	377		E	GAS TC1
2	TC	377	0	D	SURFACE TC2
2	HG	377	0	H	SERIAL 84501
3	TC	598	0	B	SURFACE TC3
3	HG	598	0	I	SERIAL 525842

**Experiment**

Flux Gauge Reading @ 400 mm (Serial No. 27844, mV): 5.85-19.93 kW/m<sup>2</sup>-19.35 kW/m<sup>2</sup> @425 mm

Preheating Time without Pilot Flame (seconds): 90

Time to Sample Ignition After Applying the Pilot Flame (seconds): 27

Speed Used (S1M"Steps"): 200

Number of Steps (I1M"Steps"): 80000

File Names (.PRN): P20K506

Set-up File Name:

Sampling Rate (Hz): 5      Duration of Sampling (sec): 800

Time to Start Moving the Sample (sec):

Ignition Heat Flux (Calculated, kW/m<sup>2</sup>):

**Ambient Conditions**

Temperature (°C): 23.

**Observations** HG2 polarity wrong, surface TC2 short circuit, surface TC2 was painted 10 cm up and down streams. All TC's are painted. Note that the file column numbers were messed up at the beginning.

Personnel Jeff Cote, Y.C.

Processing of Data: SUR TC1:  $1/\tau = 2.08$ ,  $T_p = 370^\circ\text{C}$ ,  $T_{ext} = 272.0^\circ\text{C}$ ,  
 $k_{pc} = 0.2798 \times 1200 \times 2200 = 738672$ ,

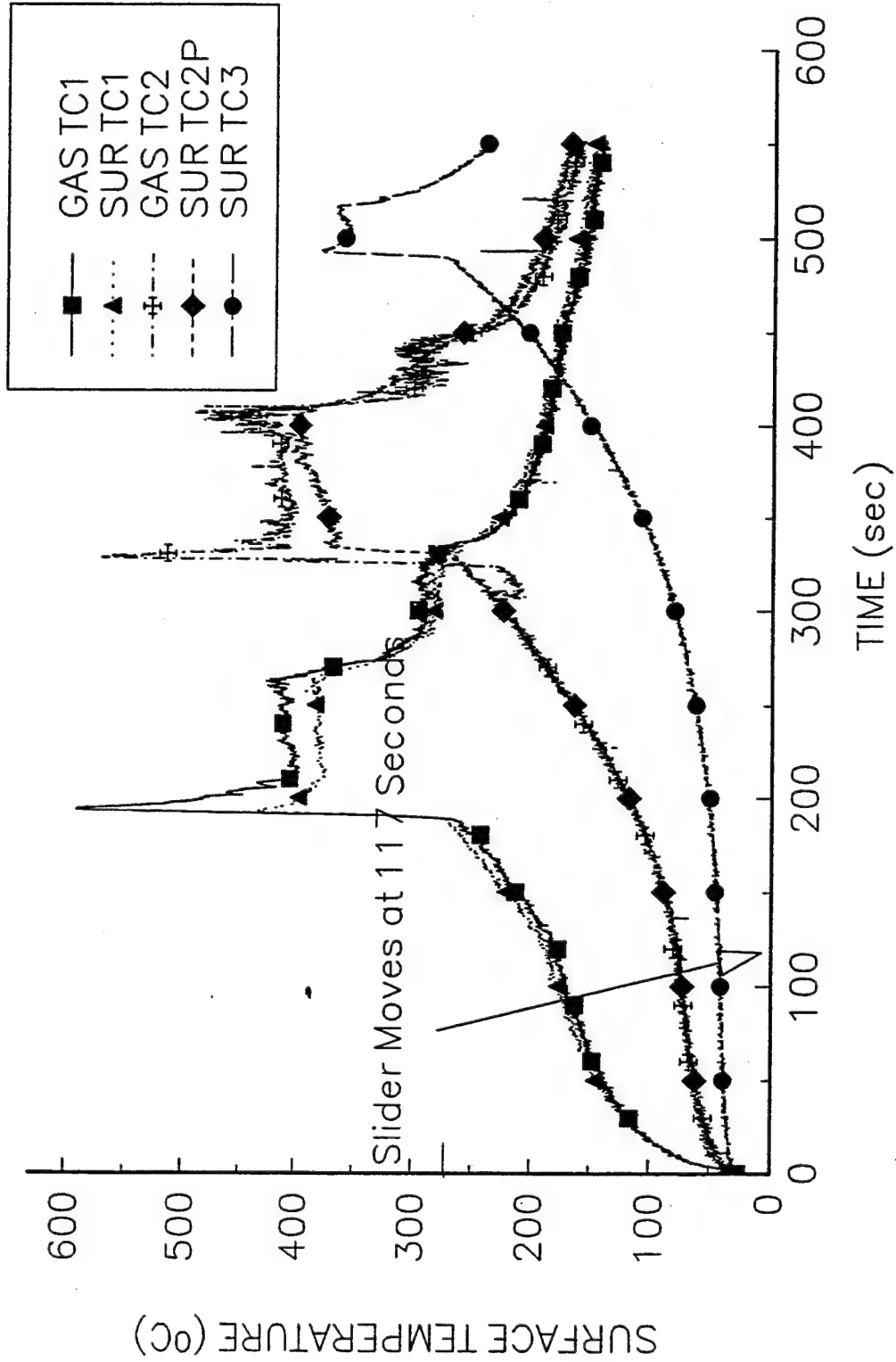
$q_0'' = (\pi k_{pc})^{1/2} (T_p - T_{ext}) (V/\delta)^{1/2} = (738672)^{1/2} \times (370 - 272.0) (2.08)^{1/2} = 121.6 \text{ kW/m}^2$

SUR TC2:  $1/\tau = 1.05$ ,  $T_p = 370^\circ\text{C}$ ,  $T_{ext} = 272.0^\circ\text{C}$ ,  $k_{pc} = 0.2798 \times 1200 \times 2200 = 738672$ ,

$q_0'' = (\pi k_{pc})^{1/2} (T_p - T_{ext}) (V/\delta)^{1/2} = (738672)^{1/2} \times (370 - 272.0) (1.05)^{1/2} = 86.42 \text{ kW/m}^2$

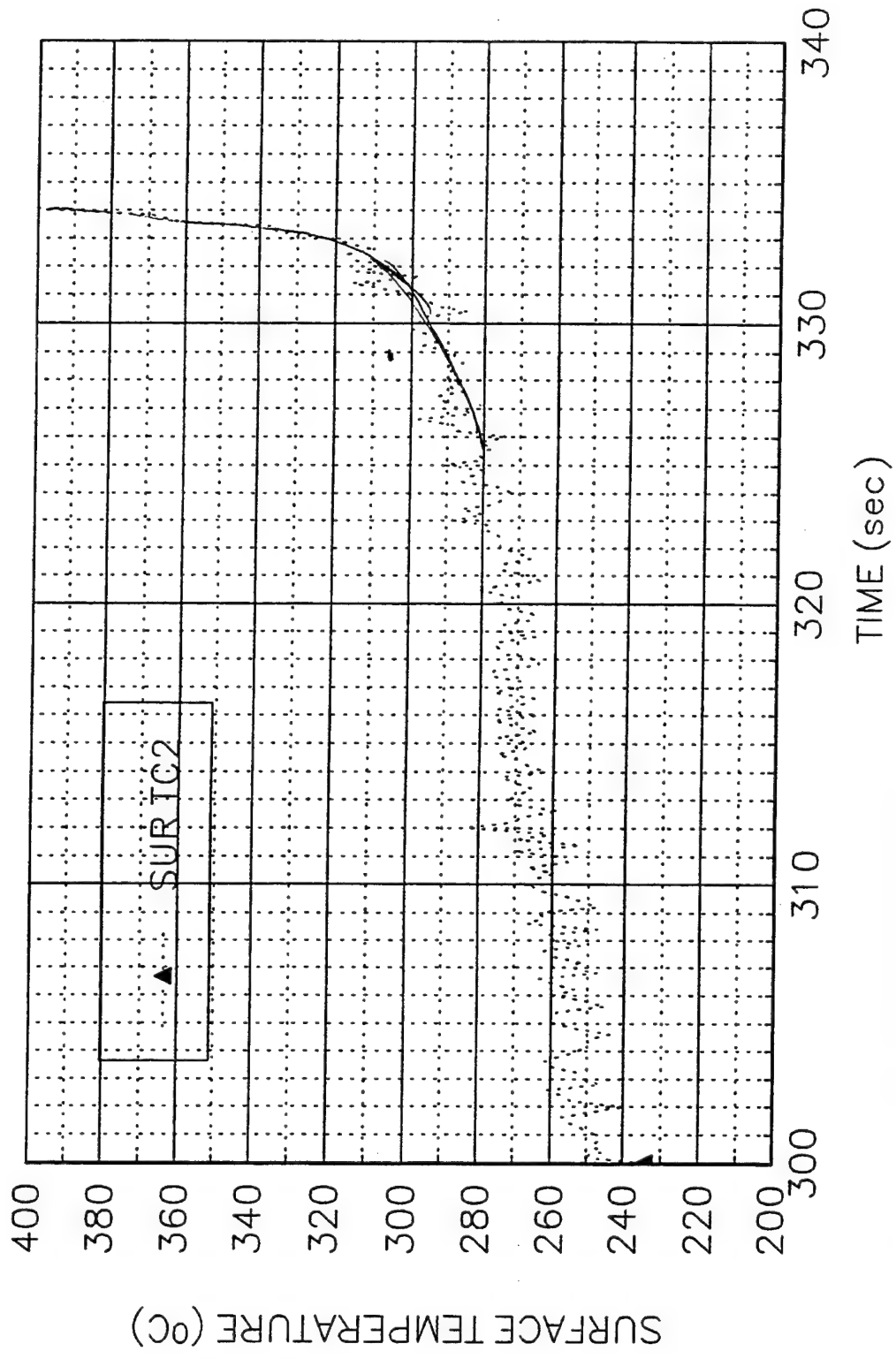
P20K506

1/4" PMMA Sheet, V=1.27 mm/s



P20K504

1/4" PMMA Sheet, V=1.27 mm/s



**Data Sheet**  
**Constant Horizontal Flame Spread Experiment**

Experimental No.: 31

Date: 6/29/94 Wed.

Time: 8:30 pm

**Pre-Experiment**

Heat Flux at 400 mm Location (Planned) (kW/m<sup>2</sup>): 10

Slider Speed (mm/s): 0.50 mm/s

**Burning Sample Data**

Material: 1/4" PMMA Sheet

Dimension(LxWxH, mm): 800x152x6.35

**Instrumentation**

Number of Thermocouples: 3

Number of Heat Flux Gauges: 2

Station	Sensor	x (mm)	z (mm)	File Column	Note
1	TC	N/A			
1	TC	201	0	B	SURFACE TC1
2	TC	N/A			
2	TC	380	0	C	SURFACE TC2
2	HG	380	0	E	SERIAL 84501
3	TC	601	0	D	SURFACE TC3
3	HG	601	0	F	SERIAL 525842

**Experiment**

Flux Gauge Reading @ 400 mm (Serial No. 27844, mV): 3.20-10.22 kW/m<sup>2</sup>-9.92 kW/m<sup>2</sup> @425 mm

Preheating Time without Pilot Flame (seconds): 240

Time to Sample Ignition After Applying the Pilot Flame (seconds): 30

Speed Used (S1M"Steps"): 79

Number of Steps (I1M"Steps"): 100000

File Names (.PRN): P10K629

Set-up File Name:

Sampling Rate (Hz): 5      Duration of Sampling (sec): 2500

Time to Start Moving the Sample (sec): -422.4

Ignition Heat Flux (Calculated, kW/m<sup>2</sup>): 23.1

**Ambient Conditions**

Temperature (°C): 23.

**Observations** Burning width~10 cm but is reduces somewhat~7.5 cm, eventually to 5 cm

Personnel Jeff Cote, Y.C.

Processing of Data: SUR TC1:  $1/\tau = 0.2857$ ,  $T_p = 370^\circ\text{C}$ ,  $T_{ext} = 228.9^\circ\text{C}$ ,

$k_{pc} = 0.2798 \times 1200 \times 2200 = 738672$ ,

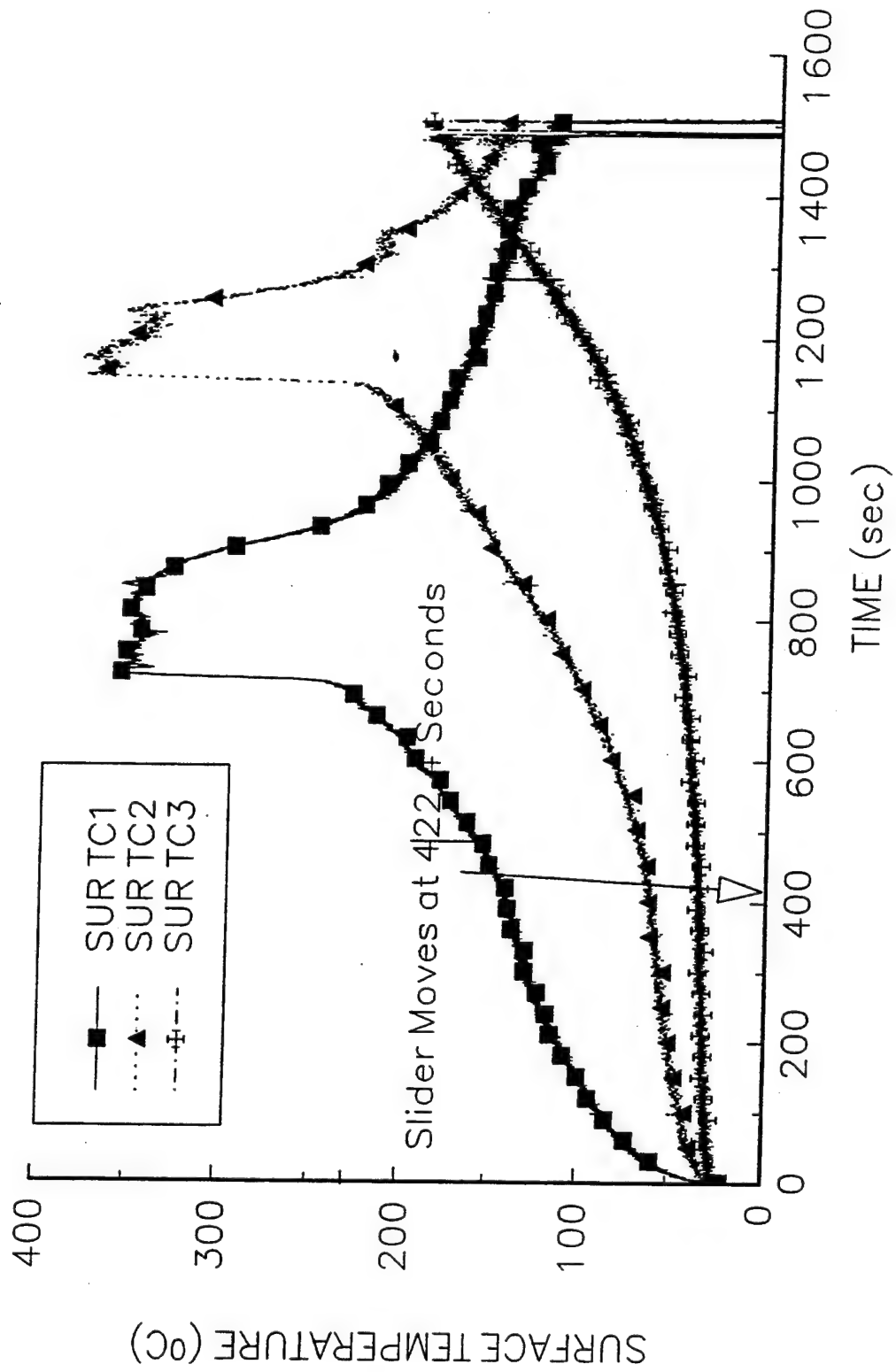
$q_0'' = (\pi k_{pc})^{1/2} (T_p - T_{ext}) (V/\delta)^{1/2} = (738672)^{1/2} \times (370 - 228.9) (0.2857)^{1/2} = 64.82 \text{ kW/m}^2$

SUR TC2:  $1/\tau = 0.2874$ ,  $T_p = 370^\circ\text{C}$ ,  $T_{ext} = 228.9^\circ\text{C}$ ,

$q_0'' = (\pi k_{pc})^{1/2} (T_p - T_{ext}) (V/\delta)^{1/2} = (738672)^{1/2} \times (370 - 228.9) (0.2874)^{1/2} = 65.01 \text{ kW/m}^2$

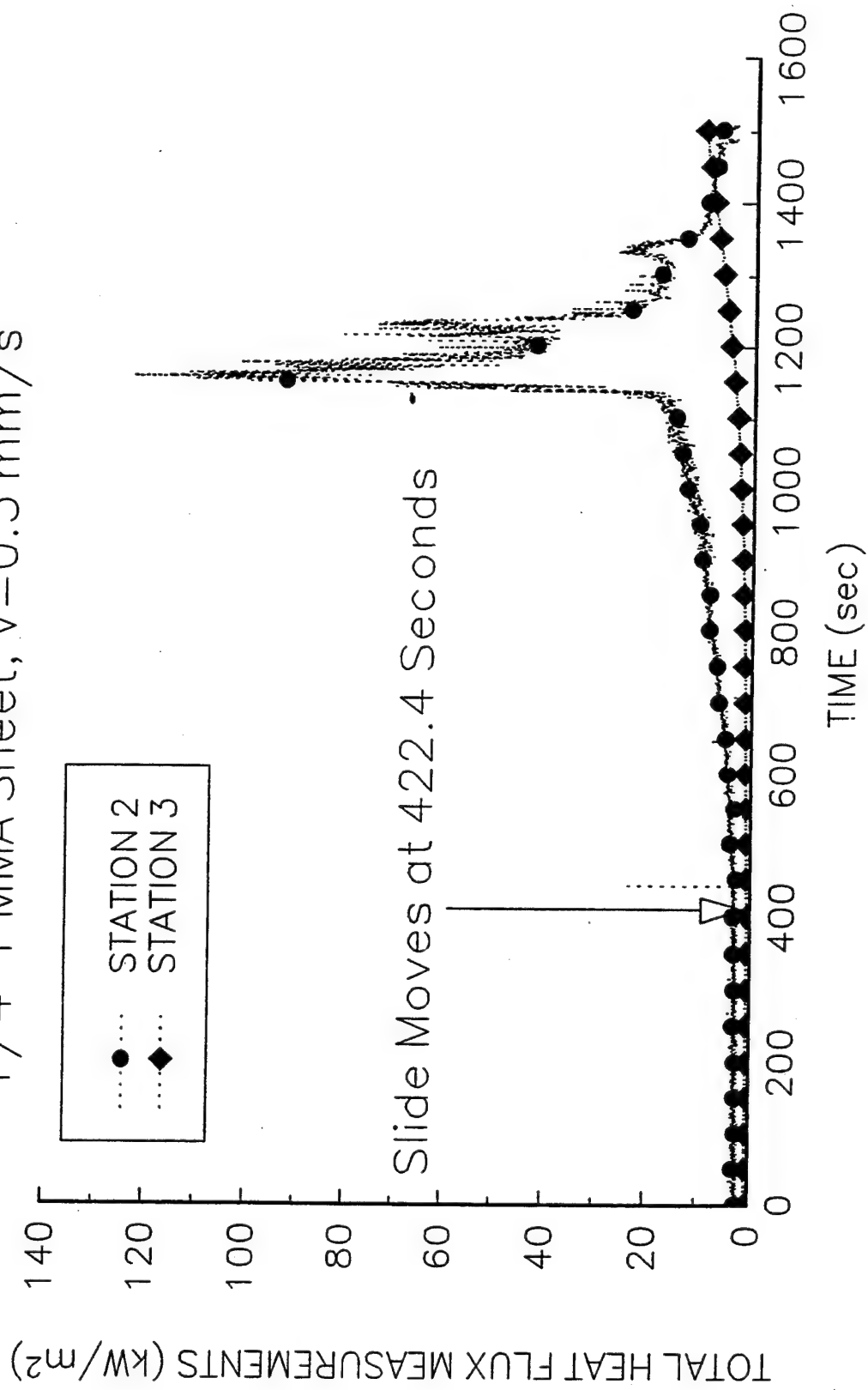
P10K629

1 / 4" PMMA Sheet,  $V=0.50$  mm/s



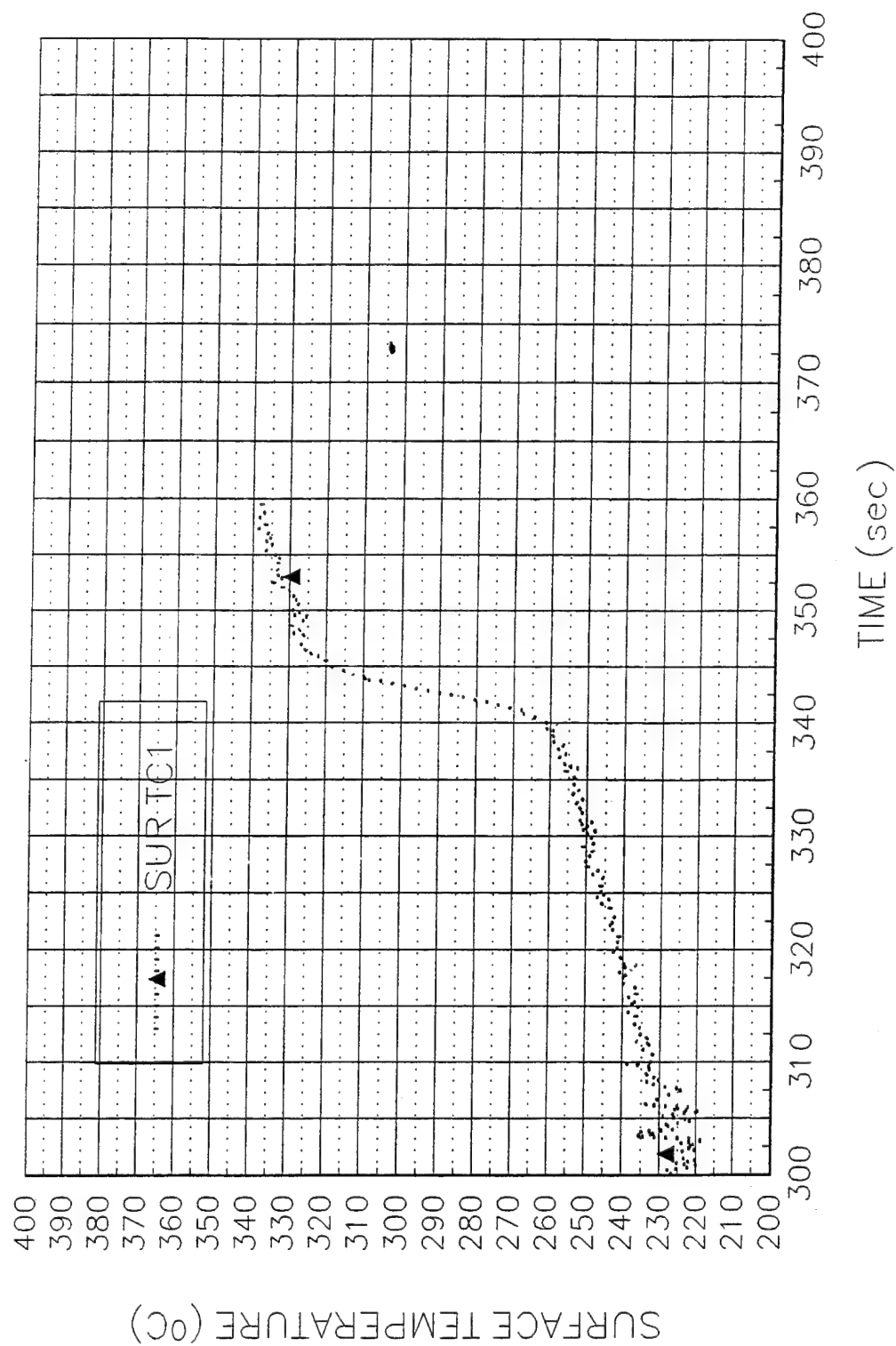
P10K629

1/4" PMMA Sheet,  $V=0.5 \text{ mm/s}$



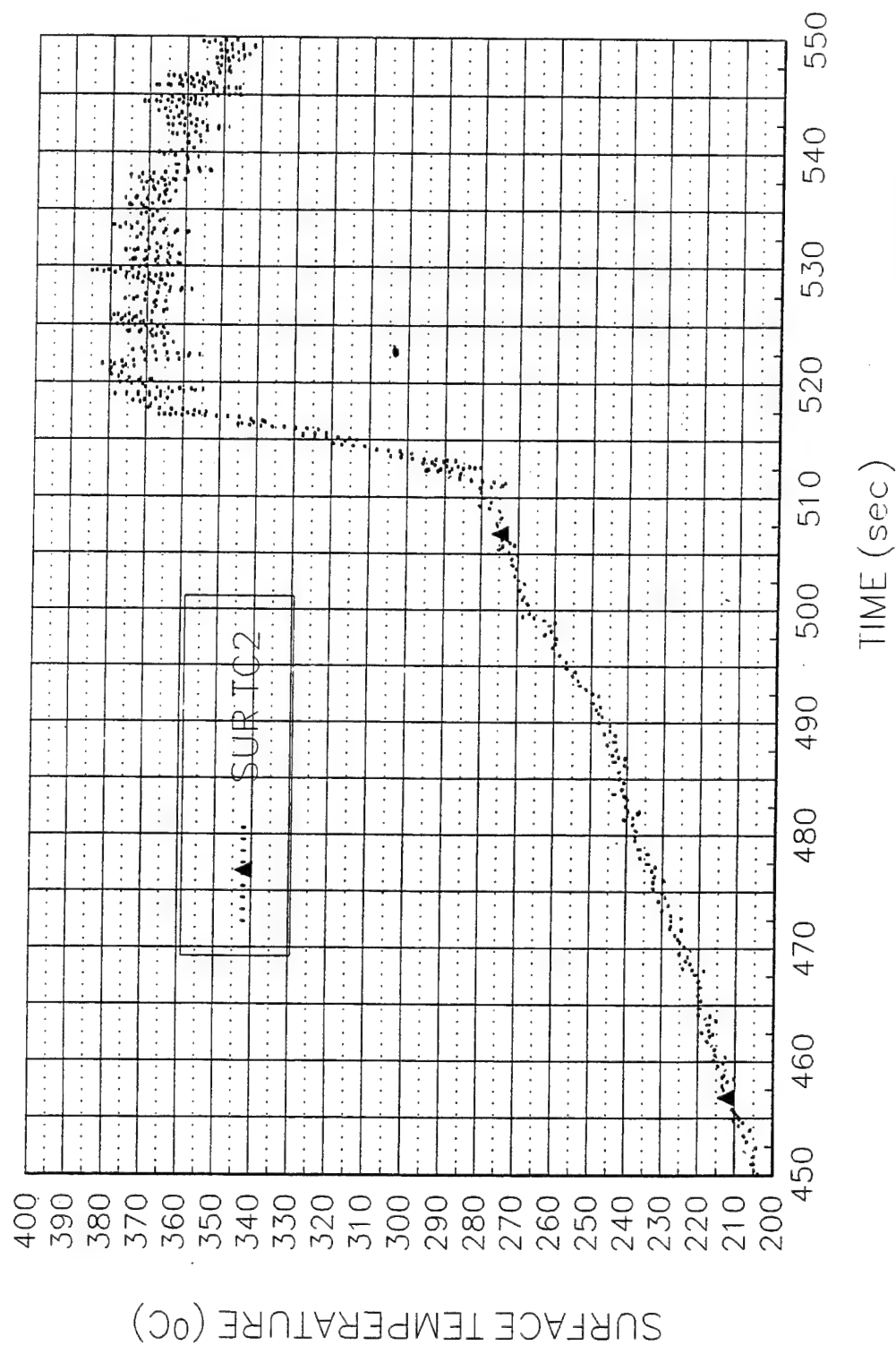
M20K809

3/4" PMMA Sheet, V=1.27 mm/s



M20K809

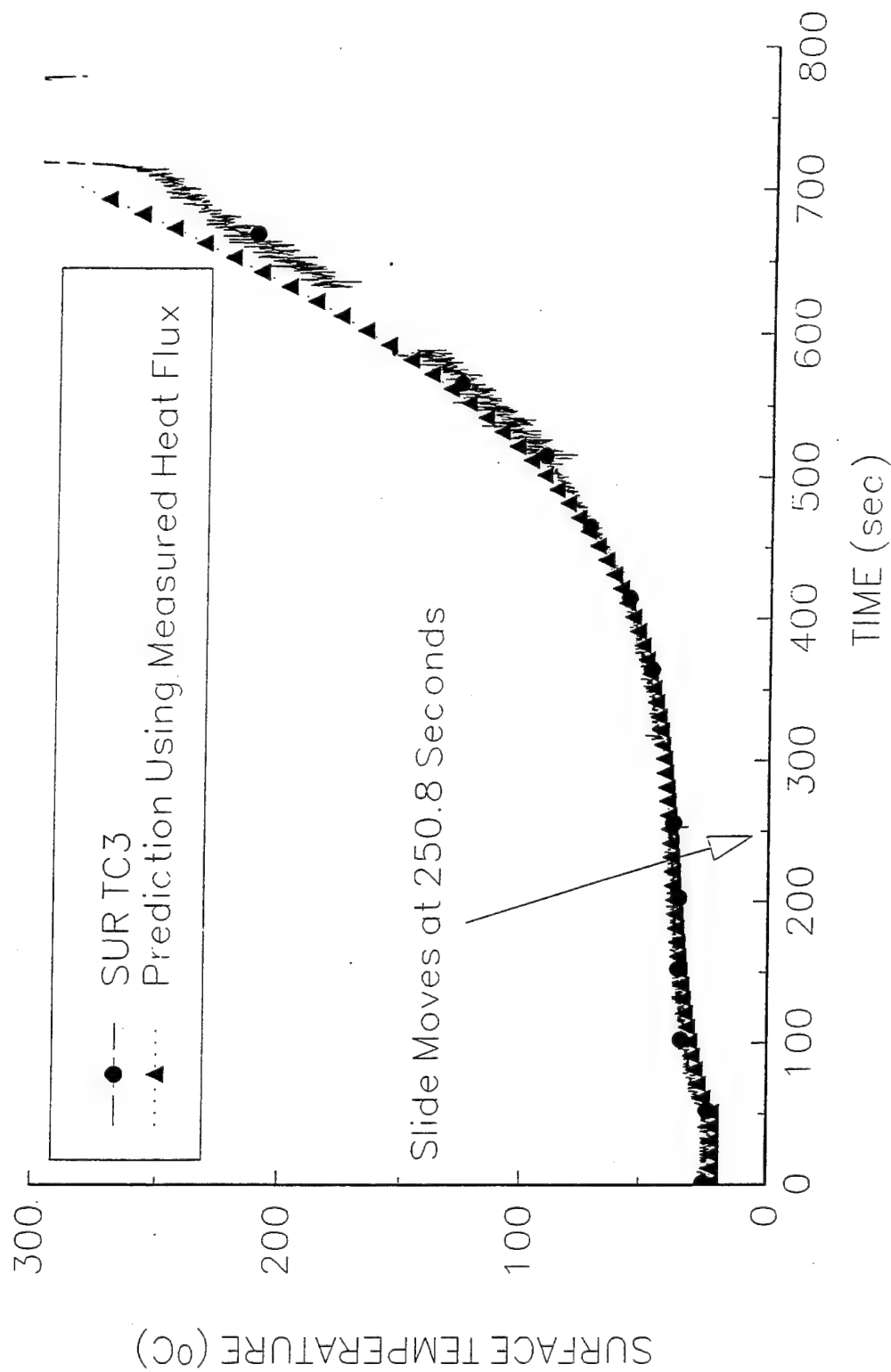
3/4" PMMA Sheet, V=1.27 mm/s





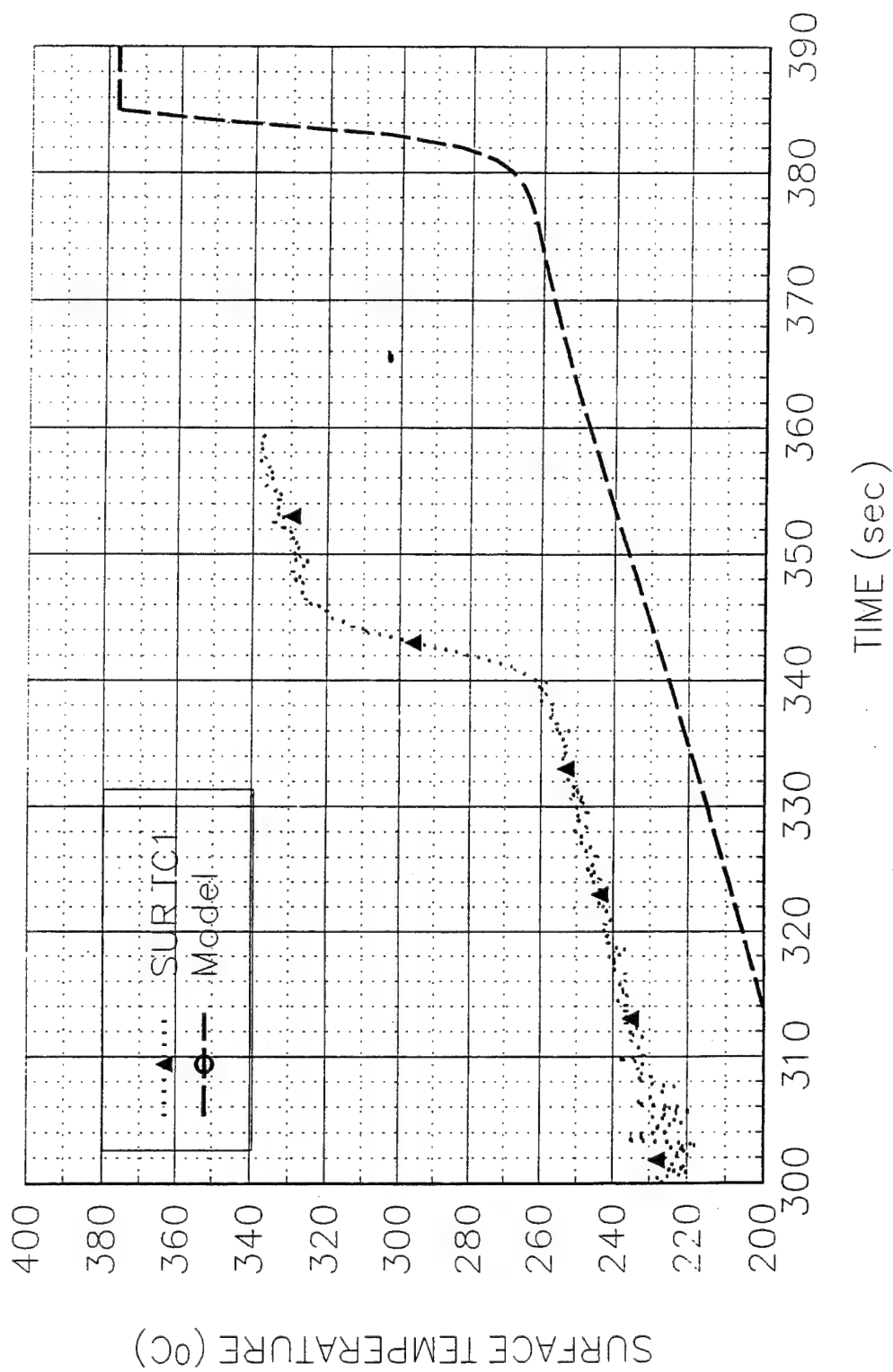
M20K809

3/4" PMMA Sheet,  $V=1.27 \text{ mm/s}$



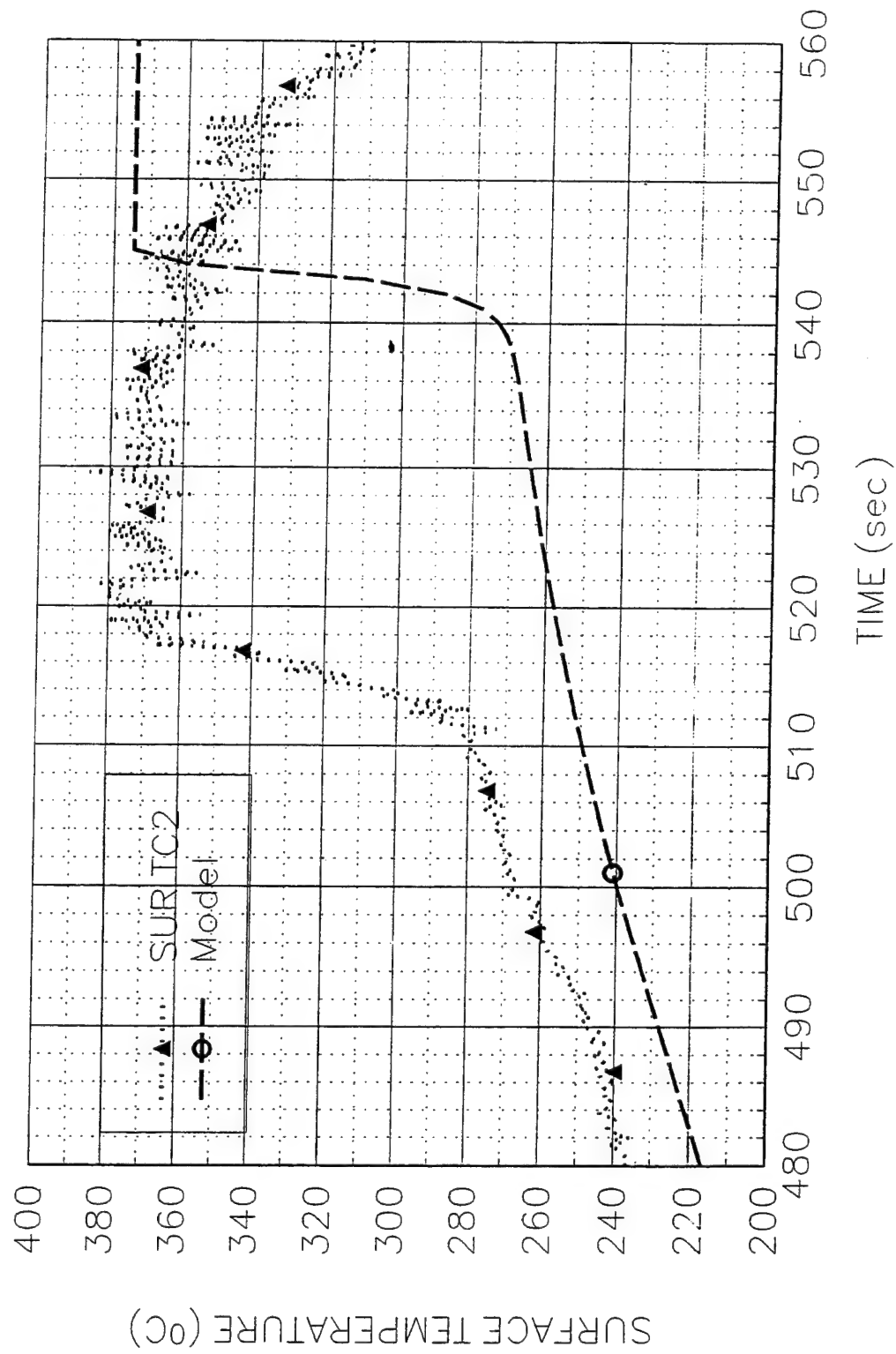
M201809

3/4" PMMA Sheet,  $V=1.27$  mm/s



M20k809

3/4" PMMA Sheet,  $V=1.27 \text{ mm/s}$



**Data Sheet**  
**Constant Horizontal Flame Spread Experiment**

Experimental No.: 39

Date: 8/12/94 Fri

Time: 6.30 pm

**Pre-Experiment**

Heat Flux at 425 mm Location (Planned) (kW/m<sup>2</sup>): 30

Slider Speed (mm/s): 1.90 mm/s

**Burning Sample Data**

Material: 3/4" PMMA Sheet

Dimension(LxWxH, mm): 600x152x6.35

**Instrumentation**

Number of Thermocouples: 5

Number of Heat Flux Gauges: 2

Station	Sensor	x (mm)	z (mm)	File Column	Note
1	TC	176	1.38	B	GAS TC1
1	TC	176	0	C	SURFACE TC1
2	TC	350	1.43	D	GAS TC2
2	TC	350	0	E	SURFACE TC2
2	HG	350	0	G	SERIAL 86862
3	TC	573	0	F	SURFACE TC3
3	HG	573	0	H	SERIAL 525842

**Experiment**

Flux Gauge Reading @ 425 mm (Serial No. 27844, mV): 8.7-29.9976 kW/m<sup>2</sup>

Preheating Time without Pilot Flame (seconds): 60

Time to Sample Ignition After Applying the Pilot Flame (seconds): 0

Speed Used (S1M"Steps"): 300

Number of Steps (I1M"Steps"): 80629

File Names (.PRN): M30K812

Set-up File Name:

Sampling Rate (Hz): 5      Duration of Sampling (sec): 2500

Time to Start Moving the Sample (sec): 121.4

Ignition Heat Flux (Calculated, kW/m<sup>2</sup>): 40.1

**Ambient Conditions**

Temperature (°C): 23.5

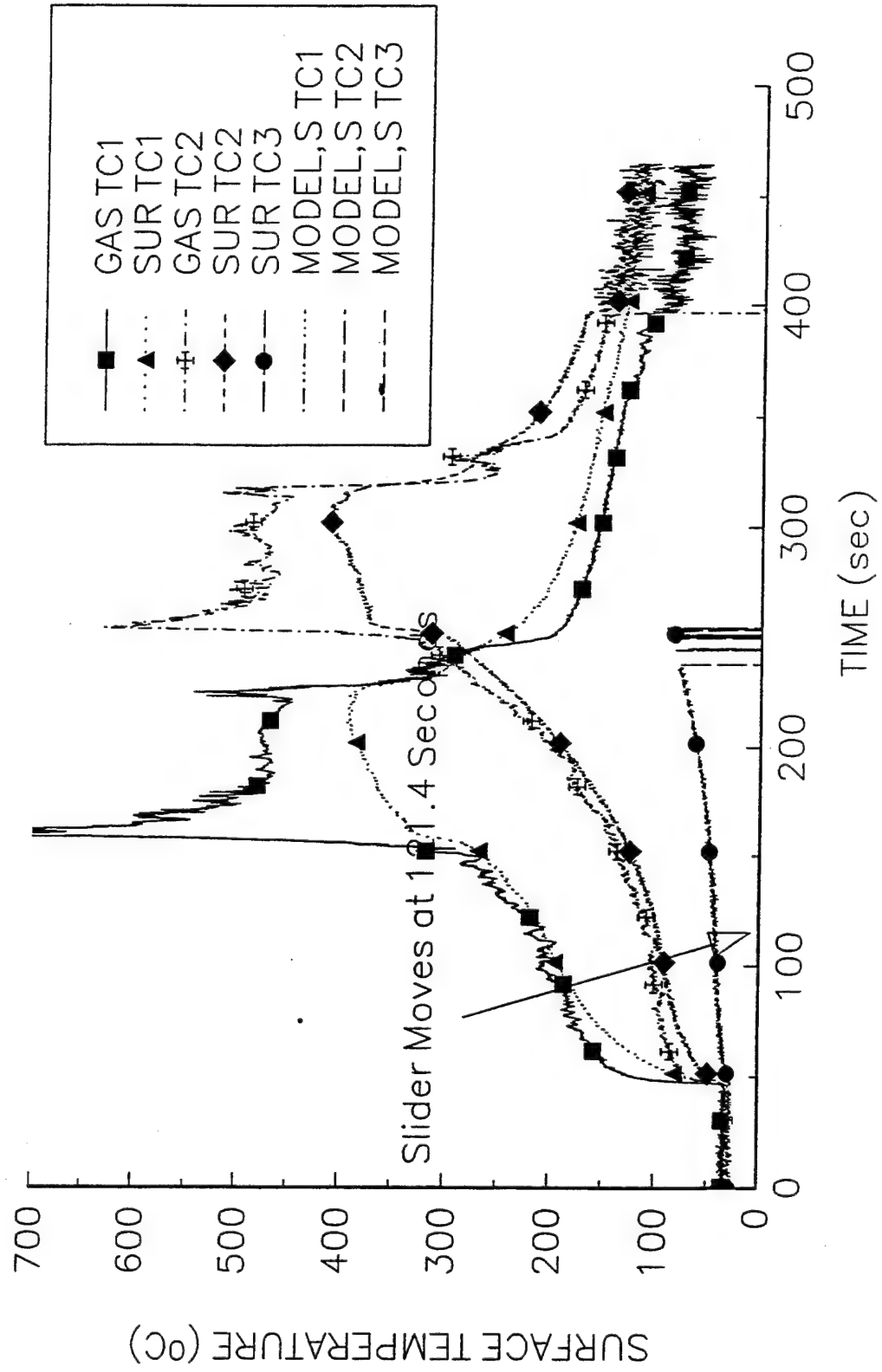
**Observations** Burning area 11 cm, constant

Personnel Rich Kashian, Y.C.

Processing of Data: SUR TC1,  $1/\tau=0.26$ ,  $T_p=370^\circ\text{C}$ ,  $T_{ext}=269.2^\circ\text{C}$ ,  
 $k\rho c=0.2798 \times 1200 \times 2200 = 738672$ ,  $\dot{q}_0'' = (k\rho c)^{1/2}(T_p - T_{ext})(V/\delta)^{1/2} = (738672)^{1/2} \times (370 - 269.2)(0.26)^{1/2} = 43.41 \text{ kW/m}^2$

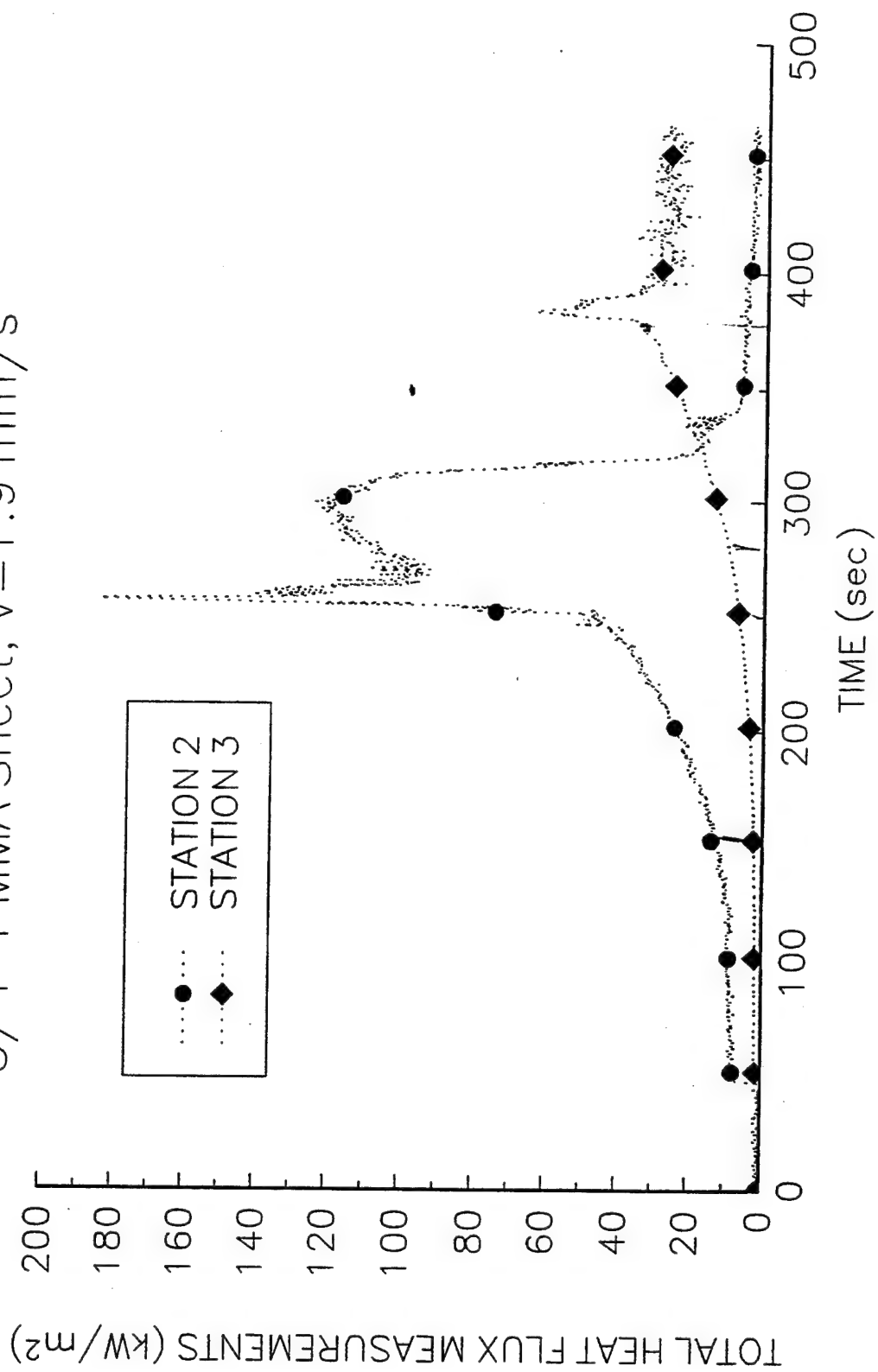
SUR TC2,  $1/\tau=0.83$ ,  $T_p=370^\circ\text{C}$ ,  $T_{ext}=306.3^\circ\text{C}$ ,  $\dot{q}_0'' = (k\rho c)^{1/2}(T_p - T_{ext})(V/\delta)^{1/2} = (738672)^{1/2} \times (370 - 306.3)(0.83)^{1/2} = 52.00 \text{ kW/m}^2$

3/4" PMMA Sheet,  $V=1.9 \text{ mm/s}$



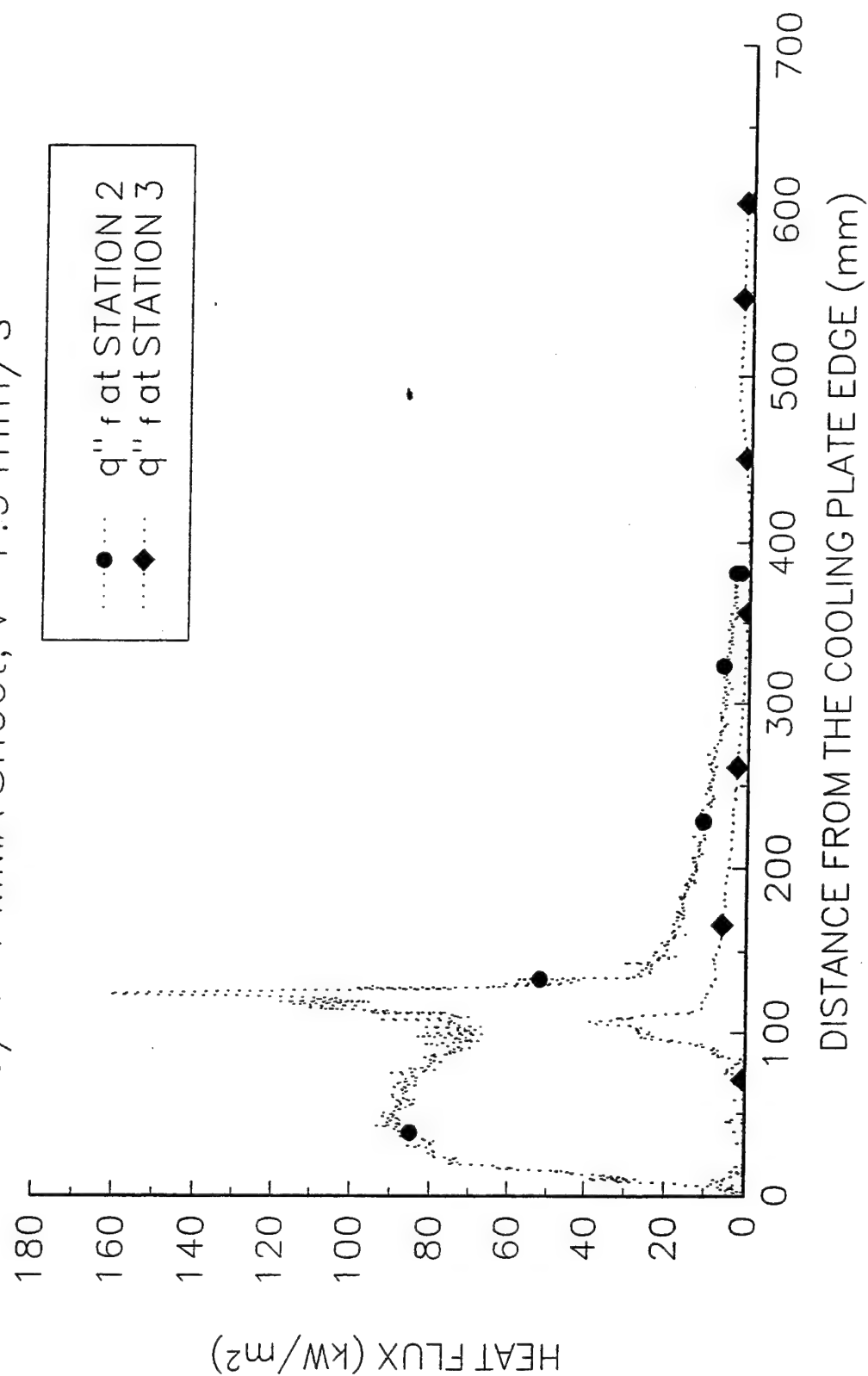
M30K812

3/4" PMMA Sheet,  $V=1.9 \text{ mm/s}$



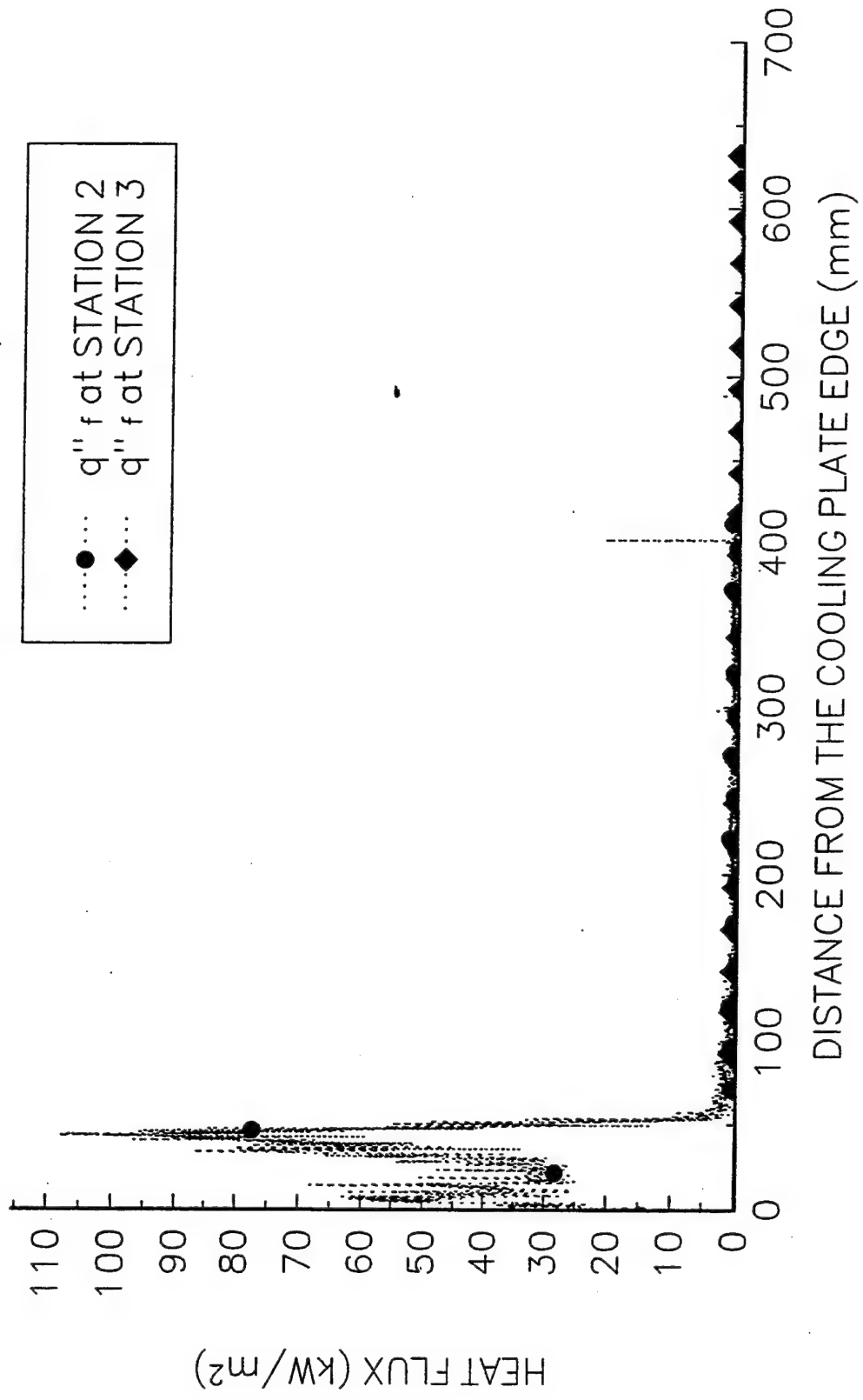
M30K812

3/4" PMMA Sheet,  $V=1.9 \text{ mm/s}$



P10K629

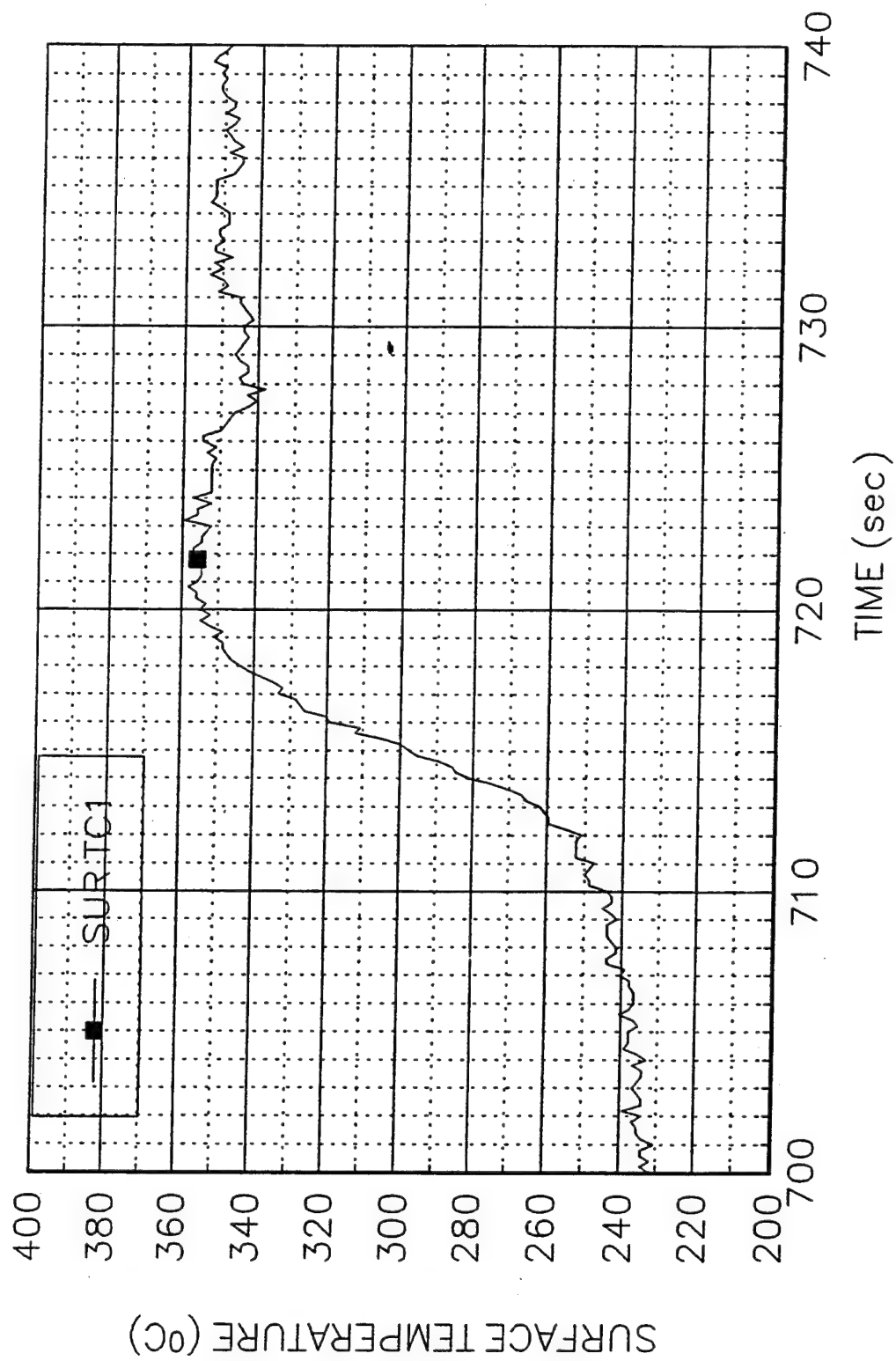
1 / 4" PMMA Sheet,  $V=0.50$  mm/s





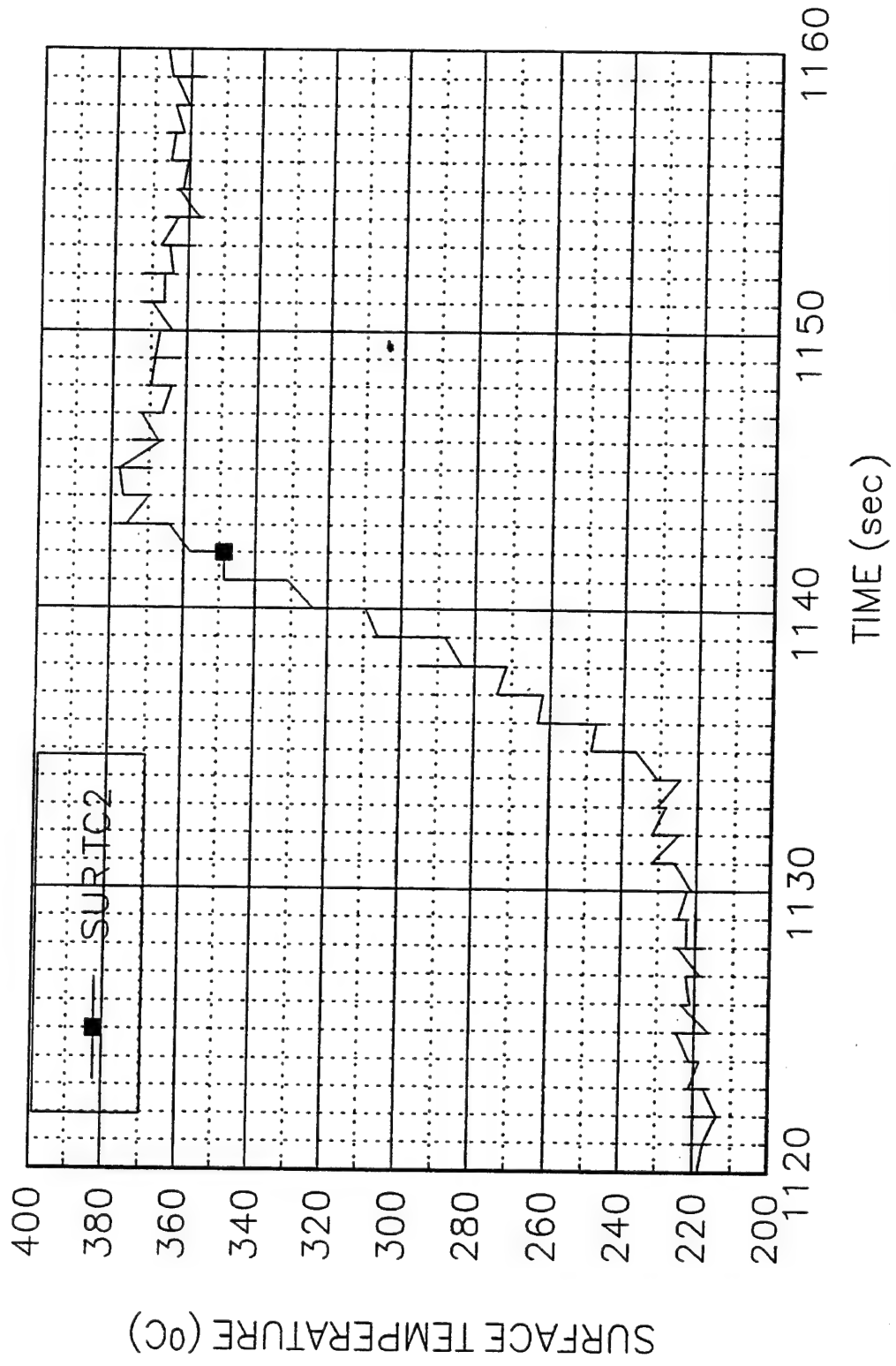
P10K629

1 / 4" PMMA Sheet, V=0.50 mm/s



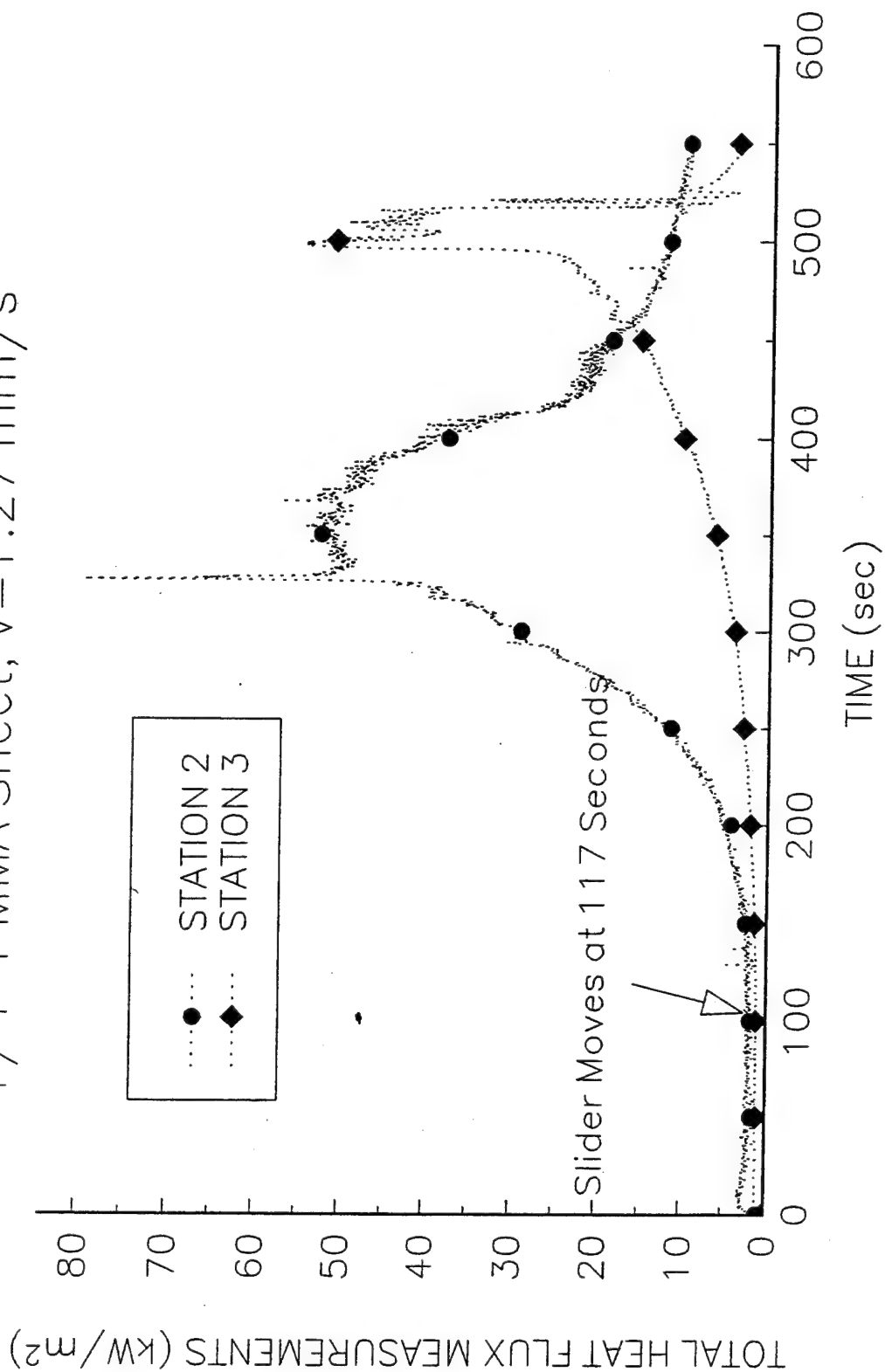
P10K629

1/4" PMMA Sheet, V=0.50 mm/s



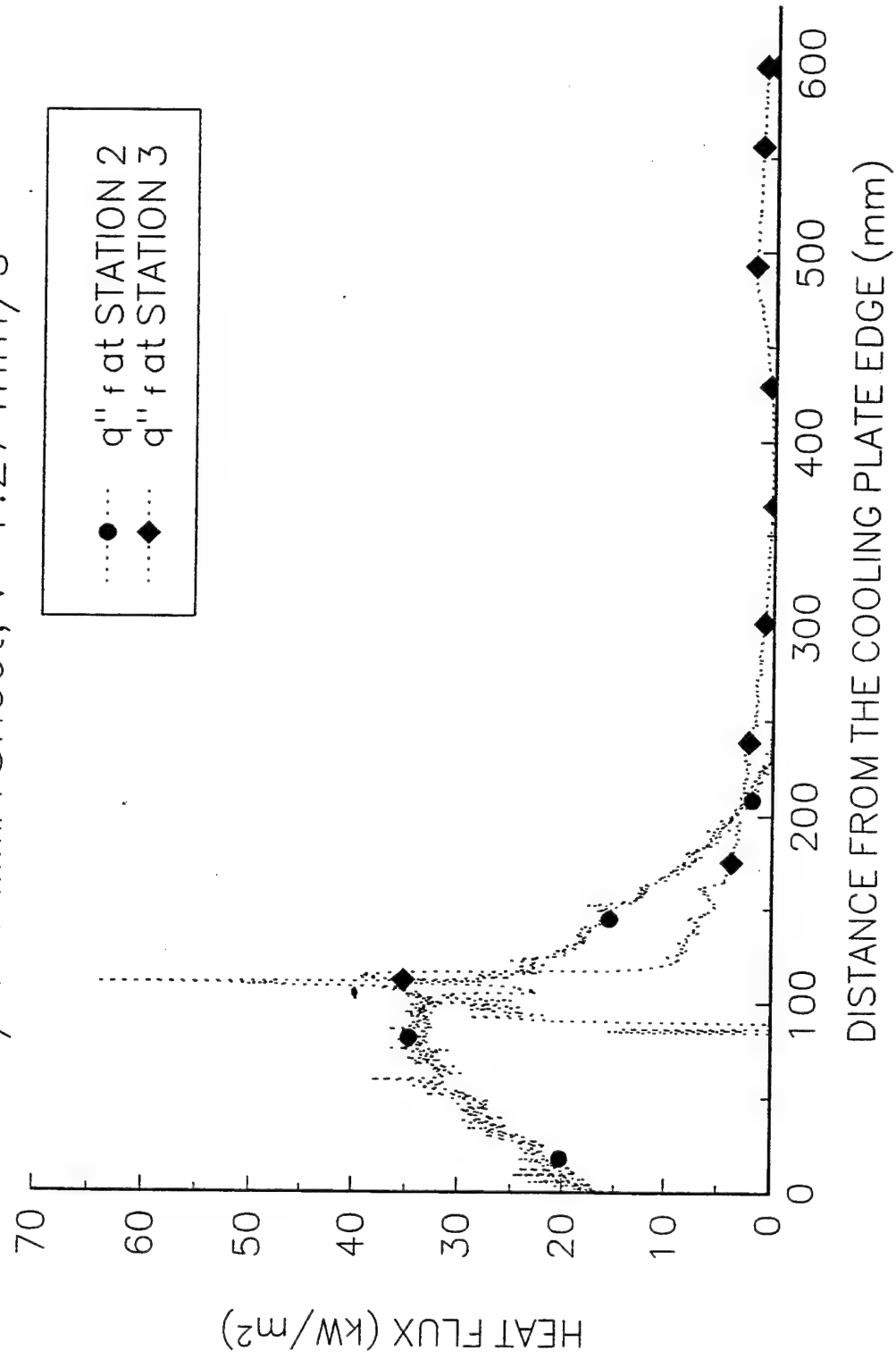
P20K506

1/4" PMMA Sheet,  $V=1.27 \text{ mm/s}$



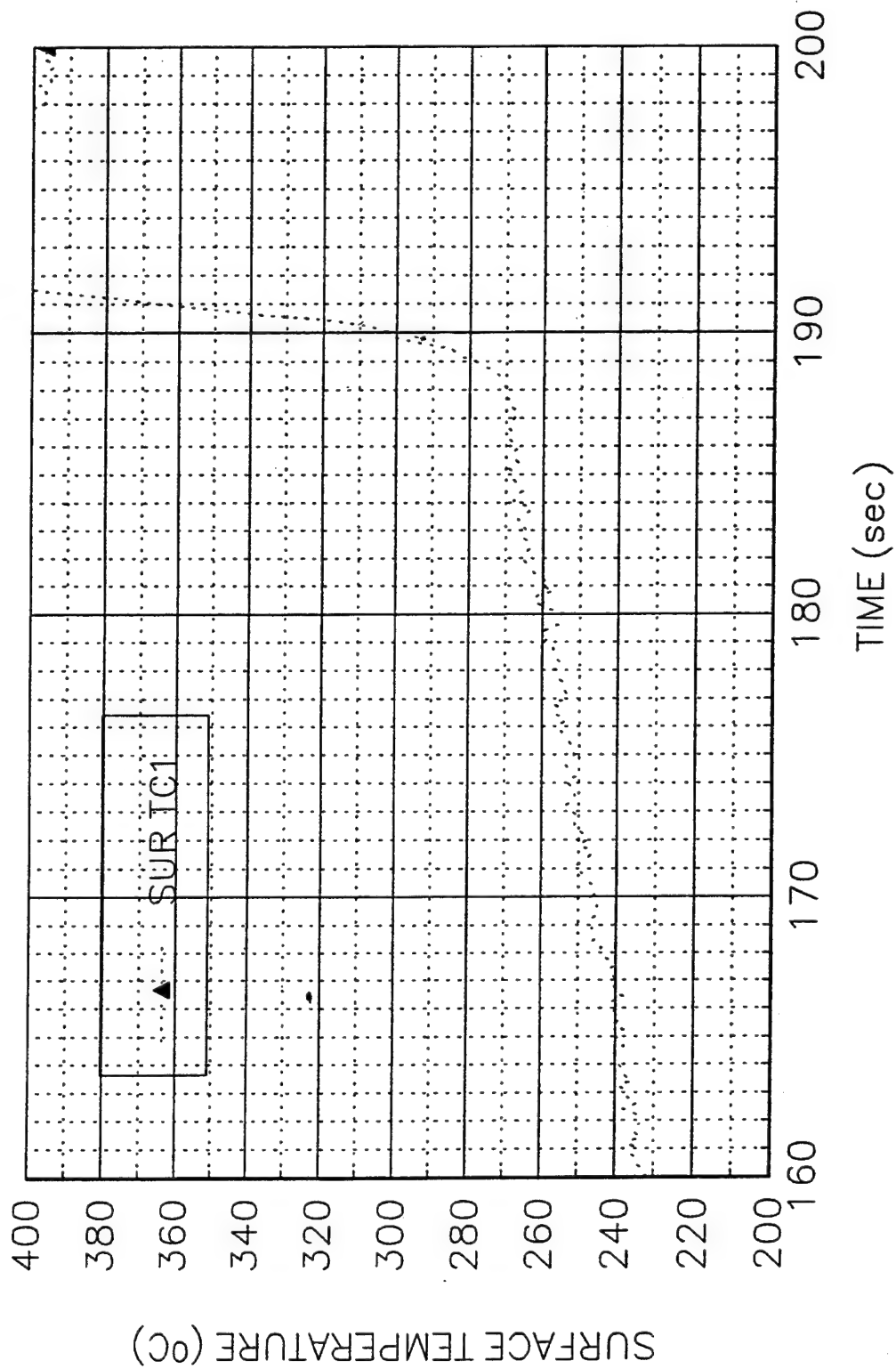
P20K506

1/4" PMMA Sheet,  $V=1.27$  mm/s



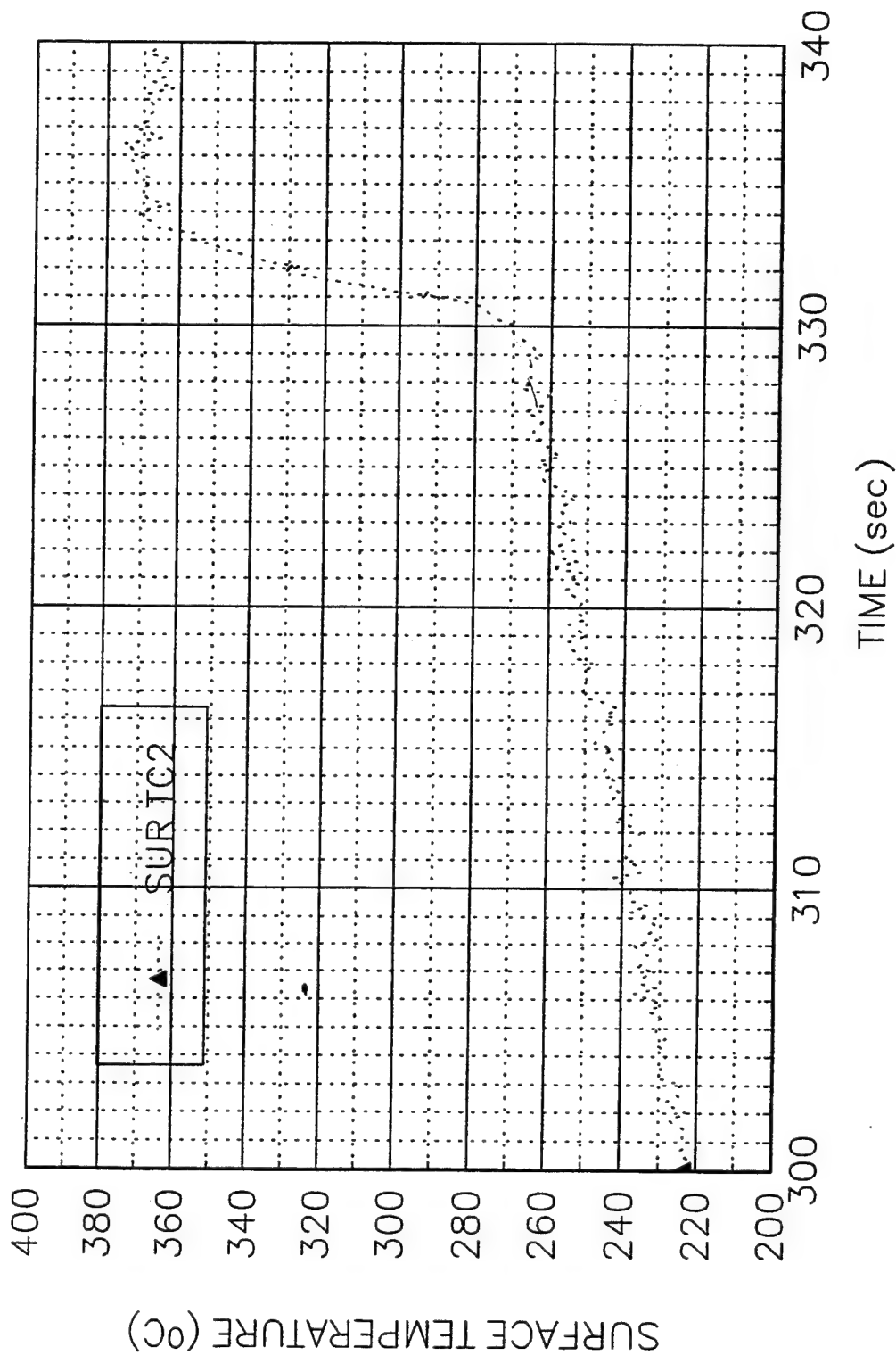
P20K506

1/4" PMMA Sheet, V=1.27 mm/s



P20K506

1/4" PMMA Sheet, V=1.27 mm/s



**Data Sheet**  
**Constant Horizontal Flame Spread Experiment**

Experimental No.: 30

Date: 6/28/94 Wed.

Time: 8:30 pm

**Pre-Experiment**

Heat Flux at 400 mm Location (Planned) (kW/m<sup>2</sup>): 20

Slider Speed (mm/s): 1.27 mm/s

**Burning Sample Data**

Material: 1/4" PMMA Sheet unpainted

Dimension(LxWxH, mm): 800x152x6.35

**Instrumentation**

Number of Thermocouples: 5

Number of Heat Flux Gauges: 2

Station	Sensor	x (mm)	z (mm)	File Column	Note
1	TC	N/A			GAS TC1
1	TC	200	0	B	SURFACE TC1
2	TC	N/A			GAS TC1
2	TC	379	0	C	SURFACE TC2
2	HG	379	0	E	SERIAL 84501
3	TC	600	0	D	SURFACE TC3
3	HG	600	0	F	SERIAL 525842

**Experiment**

Flux Gauge Reading @ 400 mm (Serial No. 27844, mV): 5.85-19.93 kW/m<sup>2</sup>-19.35 kW/m<sup>2</sup> @425 mm

Preheating Time without Pilot Flame (seconds): 90

Time to Sample Ignition After Applying the Pilot Flame (seconds): 27

Speed Used (S1M"Steps"): 200

Number of Steps (I1M"Steps"): 80000

File Names (.PRN): P20K628

Set-up File Name:

Sampling Rate (Hz): 5

Duration of Sampling (sec): 2500

Time to Start Moving the Sample (sec): ~138.80

Ignition Heat Flux (Calculated, kW/m<sup>2</sup>): 41.5

**Ambient Conditions**

Temperature (°C): 23.

**Observations** Burning width ~10 cm

Personnel Jeff Cote, Y.C.

Processing of Data: SUR TC1:  $1/\tau=0.85$ ,  $T_p=370^\circ\text{C}$ ,  $T_{ext}=255.5^\circ\text{C}$ ,

$k_{pc}=0.2798 \times 1200 \times 2200 = 738672$ ,

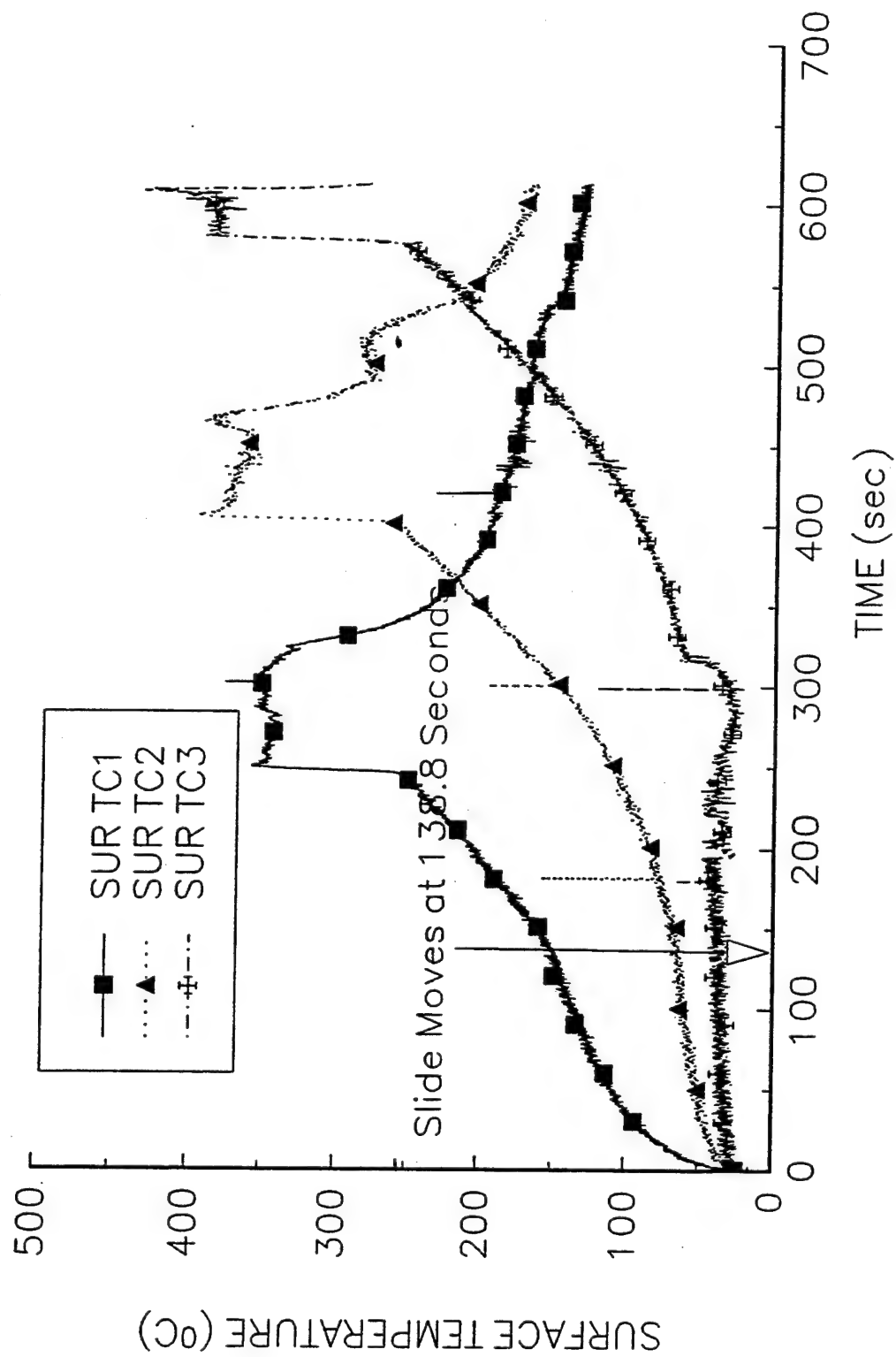
$q_0'' = (\pi k_{pc})^{1/2} (T_p - T_{ext}) (V/\delta)^{1/2} = (738672)^{1/2} \times (370 - 255.5) (0.85)^{1/2} = 91.02 \text{ kW/m}^2$

SUR TC2:  $1/\tau=0.86$ ,  $T_p=370^\circ\text{C}$ ,  $T_{ext}=272.0^\circ\text{C}$ ,

$q_0'' = (\pi k_{pc})^{1/2} (T_p - T_{ext}) (V/\delta)^{1/2} = (738672)^{1/2} \times (370 - 255.5) (0.86)^{1/2} = 91.41 \text{ kW/m}^2$

P20K628

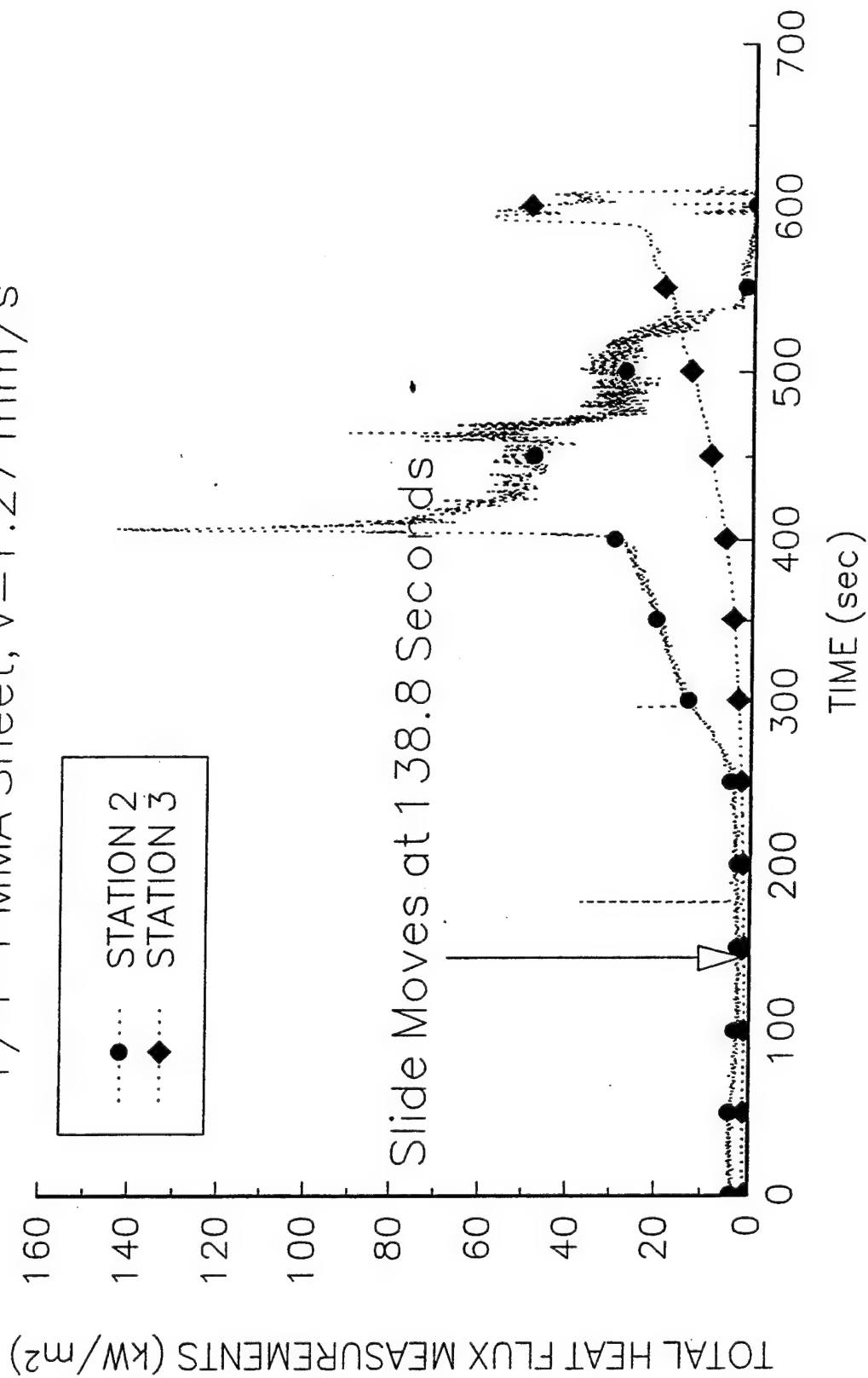
1/4" PMMA Sheet, V=1.27 mm/s





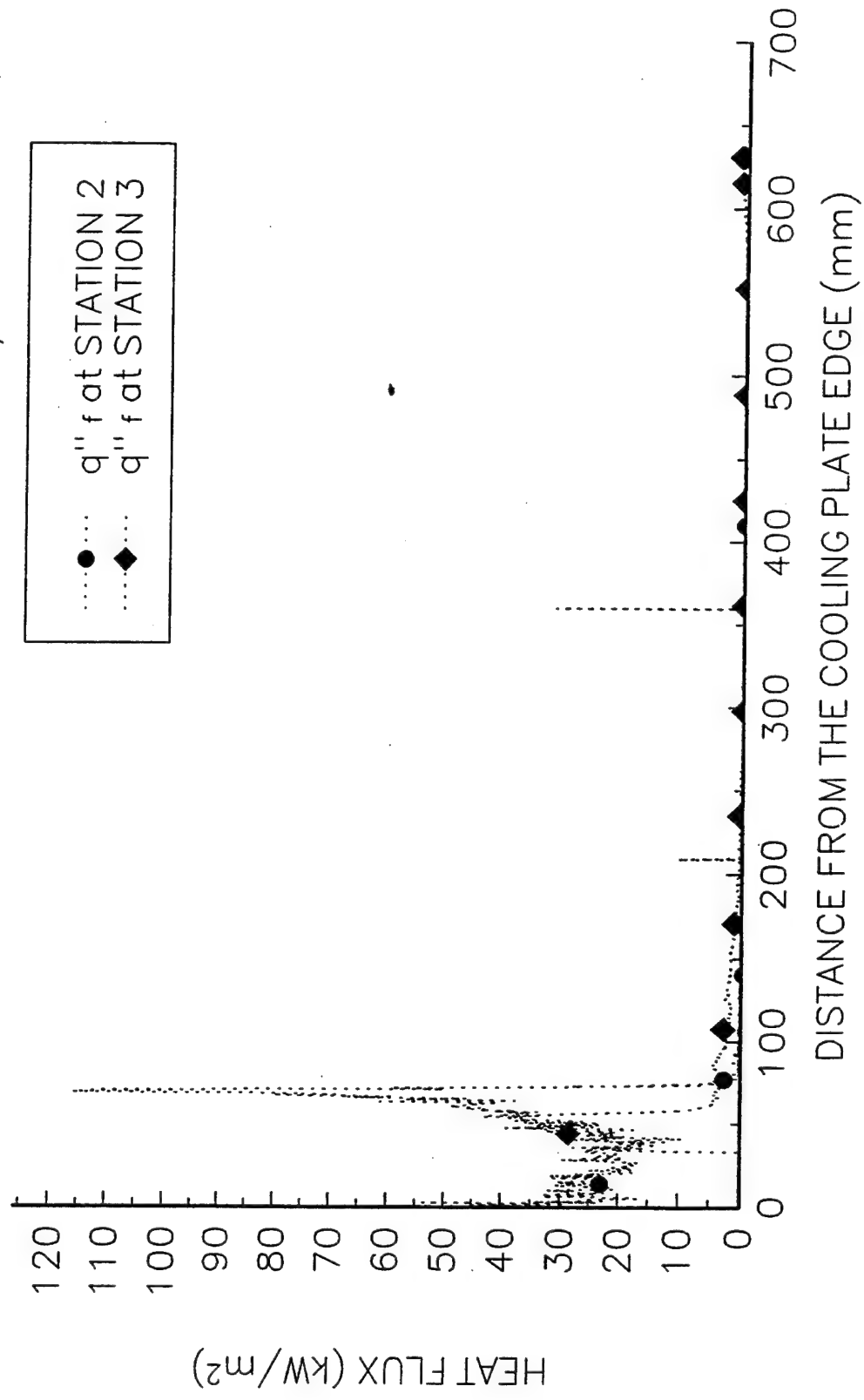
P20K628

1/4" PMMA Sheet,  $V=1.27$  mm/s



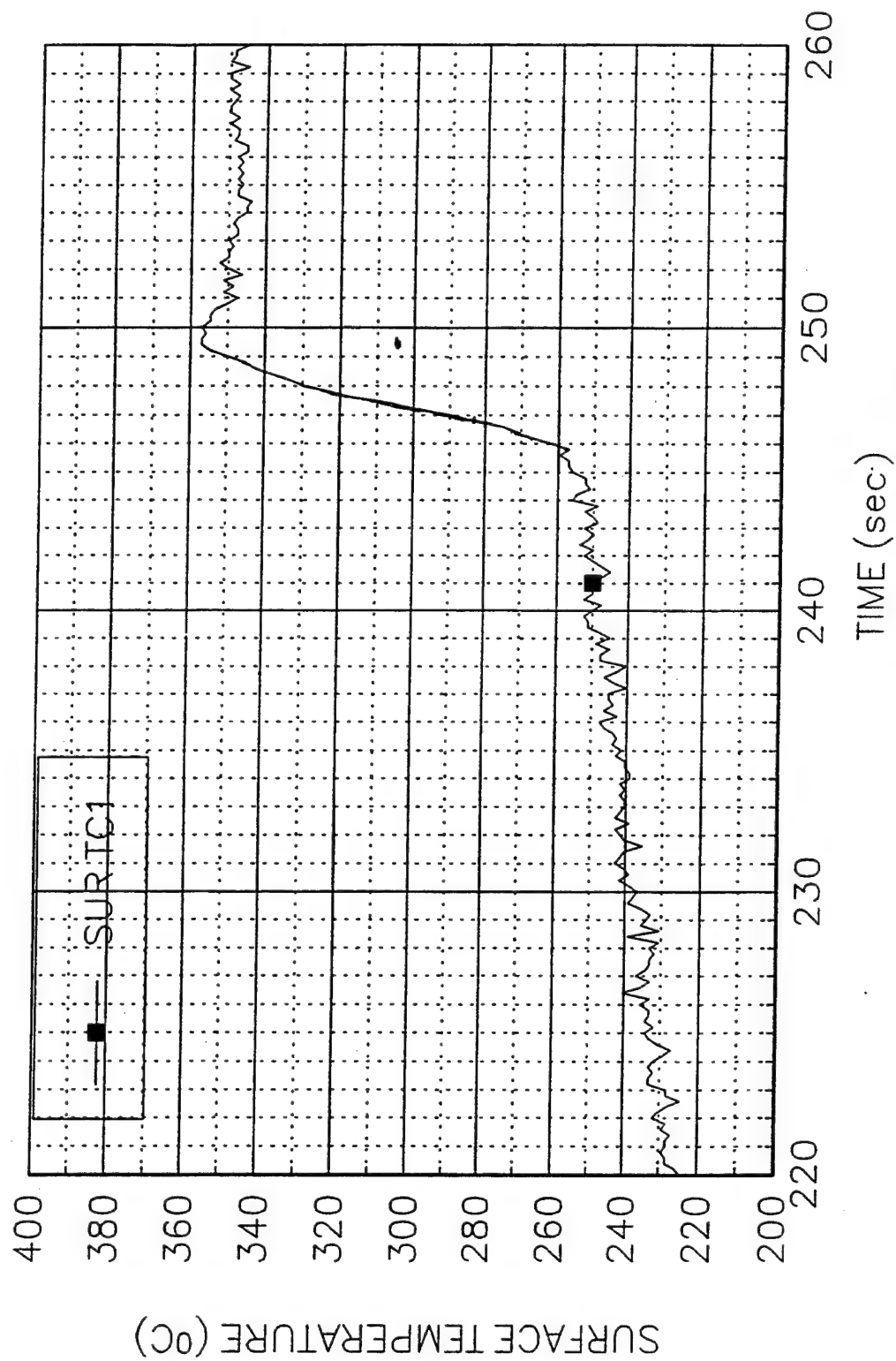
P20K628

1/4" PMMA Sheet,  $V=1.27 \text{ mm/s}$



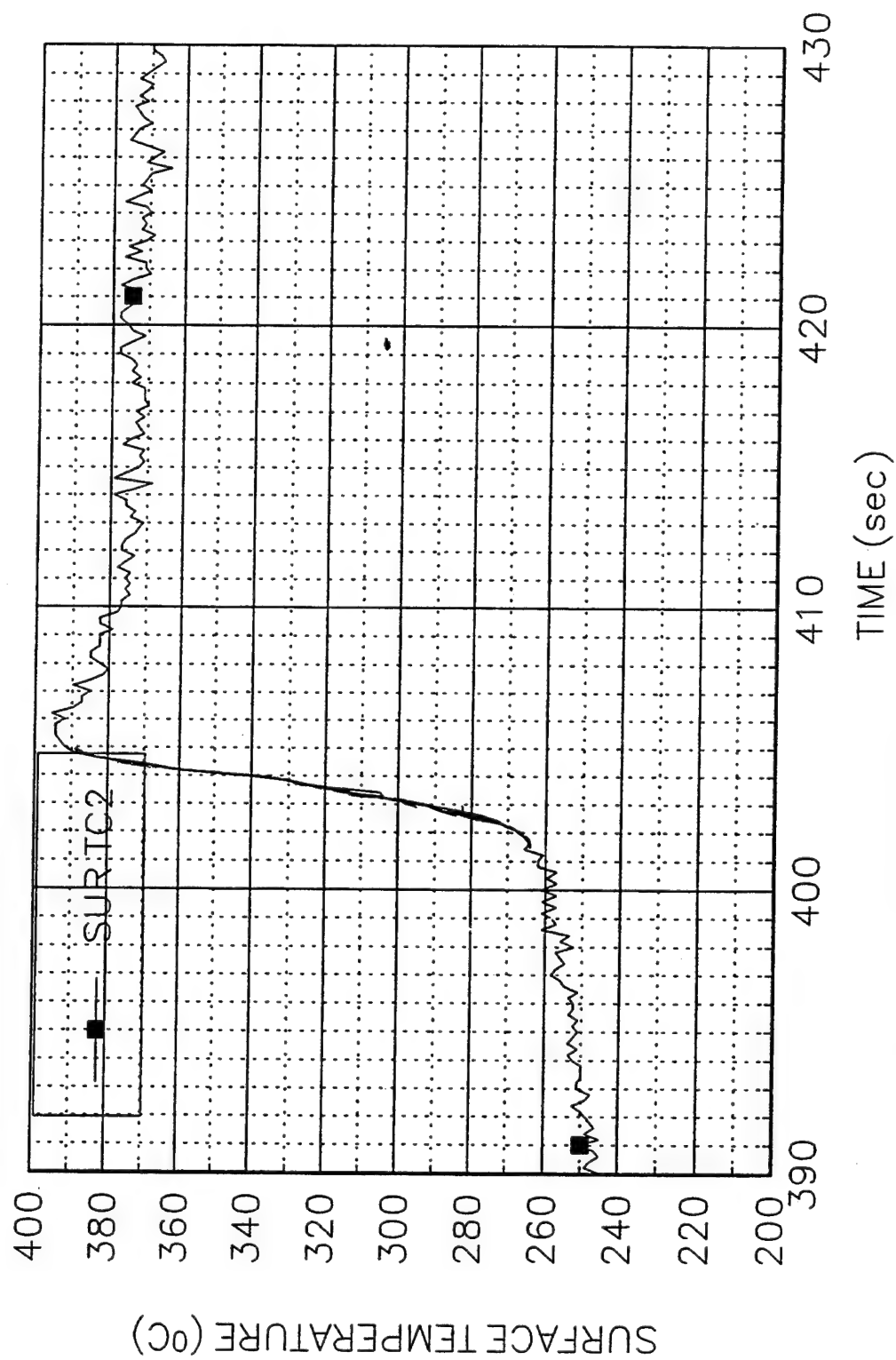
P20K628

1/4" PMMA Sheet, V=1.27 mm/s



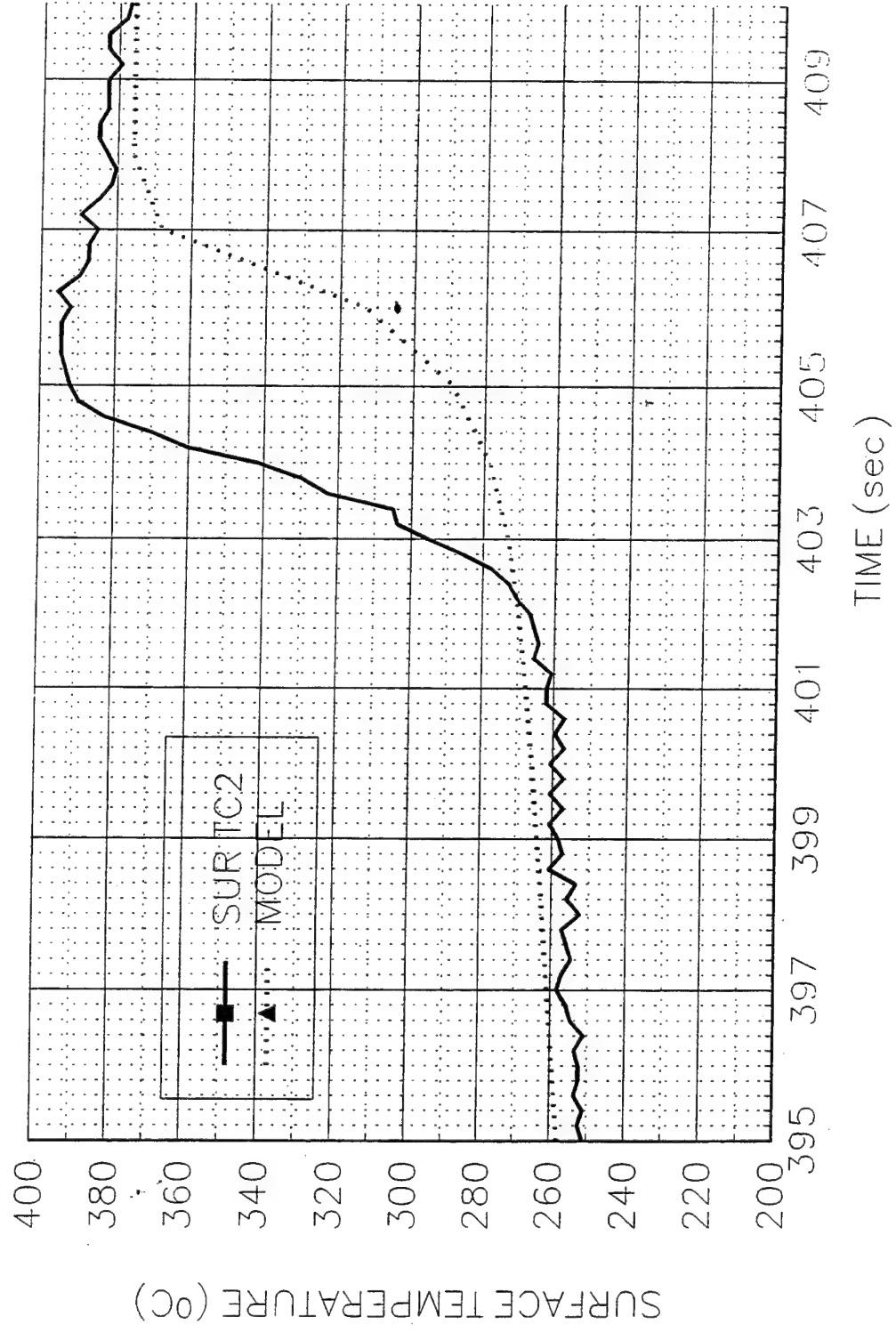
P20K628

1/4" PMMA Sheet, V=1.27 mm/s



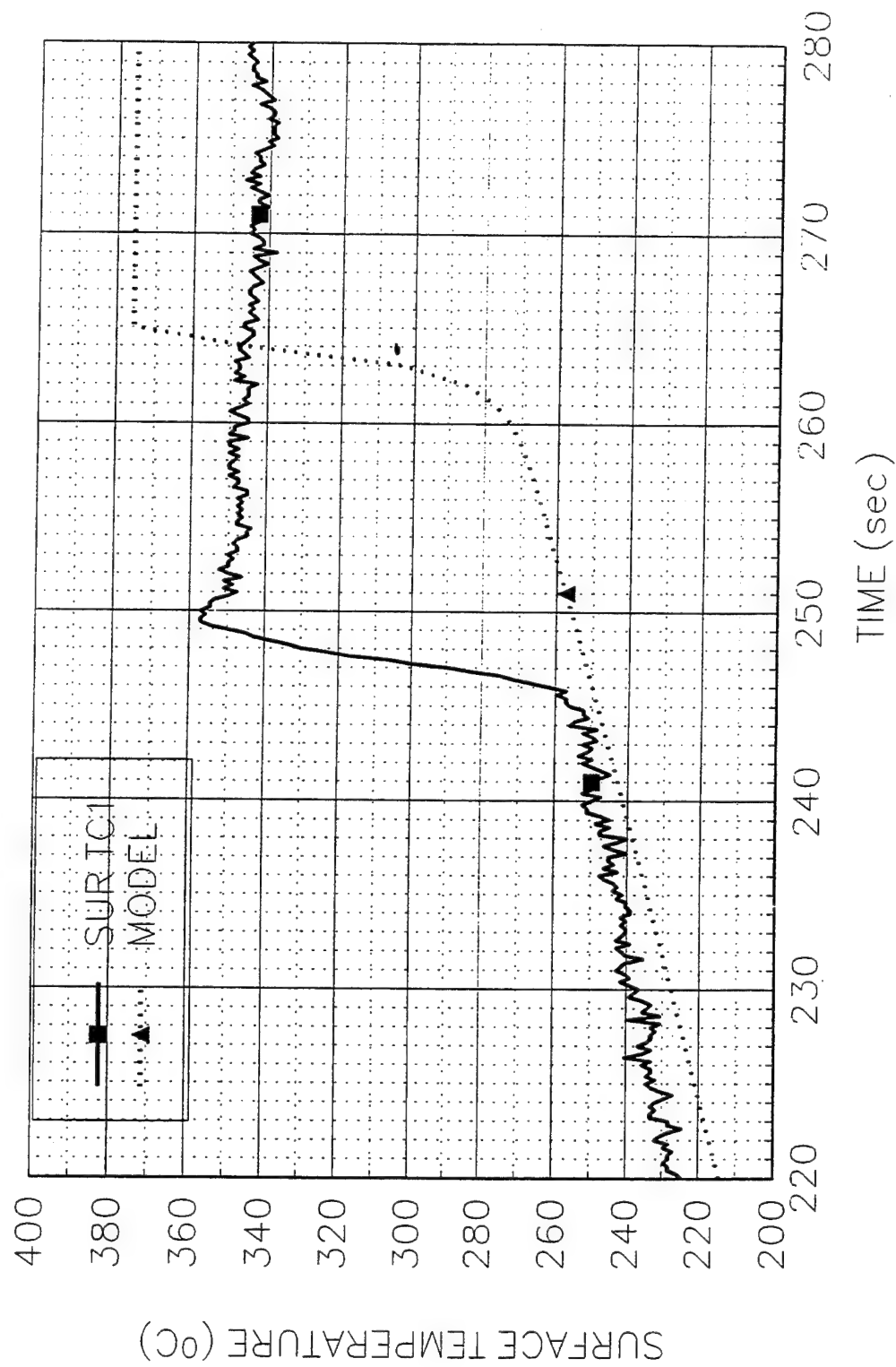
P20K628

1 / 4" PMMA Sheet, V=1.27 mm/s.



P201N628

1 / 4" PMMA Sheet, V=1.27 mm/s



**Data Sheet**  
**Constant Horizontal Flame Spread Experiment**

Experimental No.: 44

Date: 8/22/94 Wed.

Time: 9:30 pm

**Pre-Experiment**

Heat Flux at 400 mm Location (Planned) (kW/m<sup>2</sup>): 30

Slider Speed (mm/s): 1.90 mm/s

**Burning Sample Data**

Material: 1/4" PMMA Sheet unpainted

Dimension(LxWxH, mm): 800x152x6.35

**Instrumentation**

Number of Thermocouples: 5

Number of Heat Flux Gauges: 2

Station	Sensor	x (mm)	z (mm)	File Column	Note
1	TC	191	1.37	B	GAS TC1
1	TC	191	0	C	SURFACE TC1
2	TC	371	1.70	D	GAS TC1
2	TC	371	0	E	SURFACE TC2
2	HG	371	0	G	SERIAL 86862
3	TC	594	0	F	SURFACE TC3
3	HG	594	0	H	SERIAL 525842

**Experiment**

Flux Gauge Reading @ 425 mm (Serial No. 27844, mV): 8.70-29.9976 kW/m<sup>2</sup>

Preheating Time without Pilot Flame (seconds): 42

Time to Sample Ignition After Applying the Pilot Flame (seconds): 0

Speed Used (S1M"Steps"): 300

Number of Steps (I1M"Steps"): 80629

File Names (.PRN): P30K822

Set-up File Name:

Sampling Rate (Hz): 5      Duration of Sampling (sec): 2500

Time to Start Moving the Sample (sec): -50

Ignition Heat Flux (Calculated, kW/m<sup>2</sup>): 50.

**Ambient Conditions**

Temperature (°C): 23.

**Observations** Burning width ~15 cm, constant

Personnel Hui Fang, Y.C.

Processing of Data: SUR TC1:  $1/\tau = 0.78$ ,  $T_p = 370^\circ\text{C}$ ,  $T_{ext} = 287.8^\circ\text{C}$ ,  
 $k_{pc} = 0.2798 \times 1200 \times 2200 = 738672$ ,

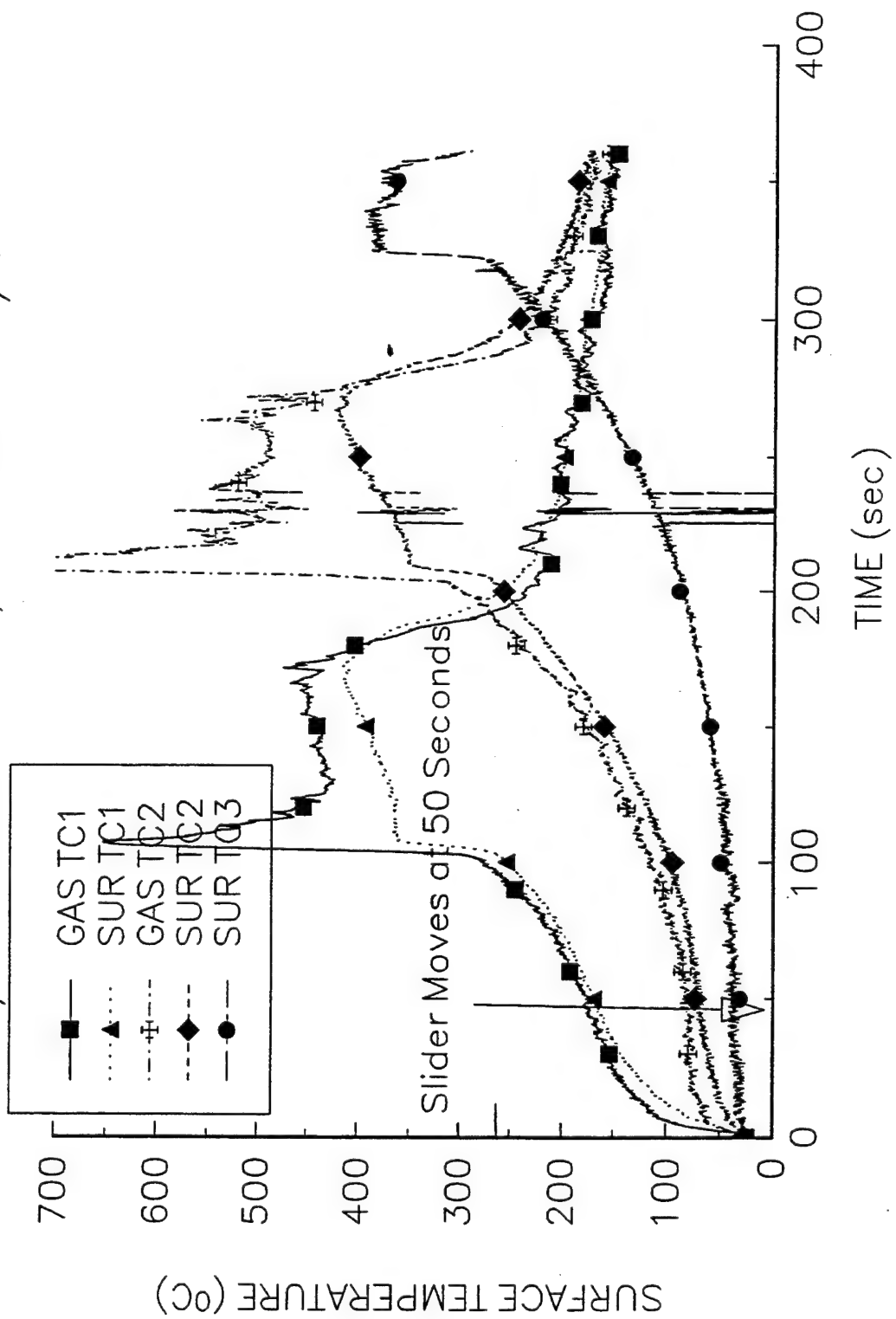
$q_0'' = (\pi k_{pc})^{1/2} (T_p - T_{ext}) (V/\delta)^{1/2} = (738672)^{1/2} \times (370 - 287.8) (0.78)^{1/2} = 80.75 \text{ kW/m}^2$

SUR TC2:  $1/\tau = 0.61$ ,  $T_p = 370^\circ\text{C}$ ,  $T_{ext} = 287.8^\circ\text{C}$ ,

$q_0'' = (\pi k_{pc})^{1/2} (T_p - T_{ext}) (V/\delta)^{1/2} = (738672)^{1/2} \times (370 - 287.8) (0.61)^{1/2} = 71.4 \text{ kW/m}^2$

P30K822

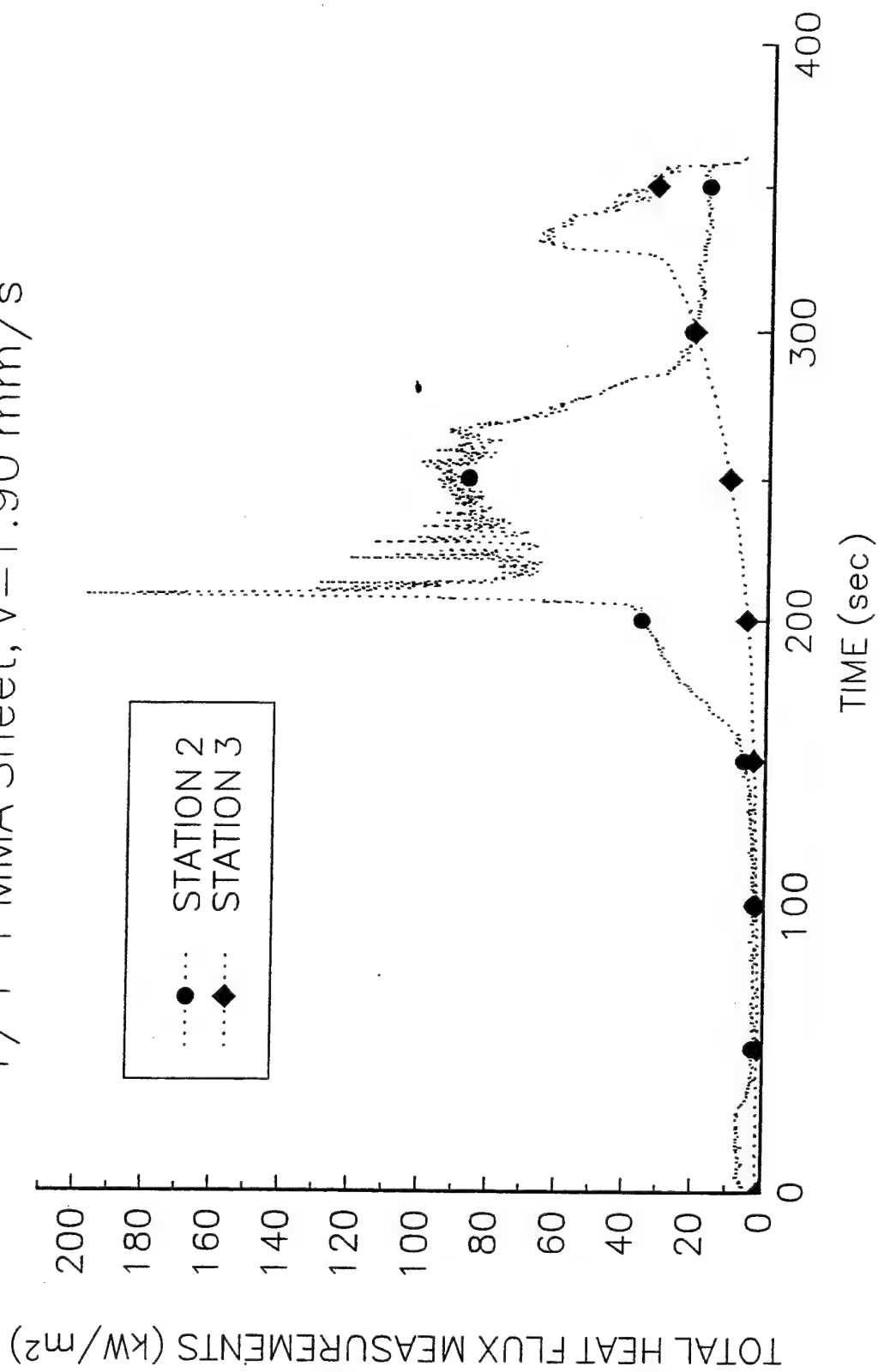
1/4" PMMA Sheet, V=1.90 mm/s





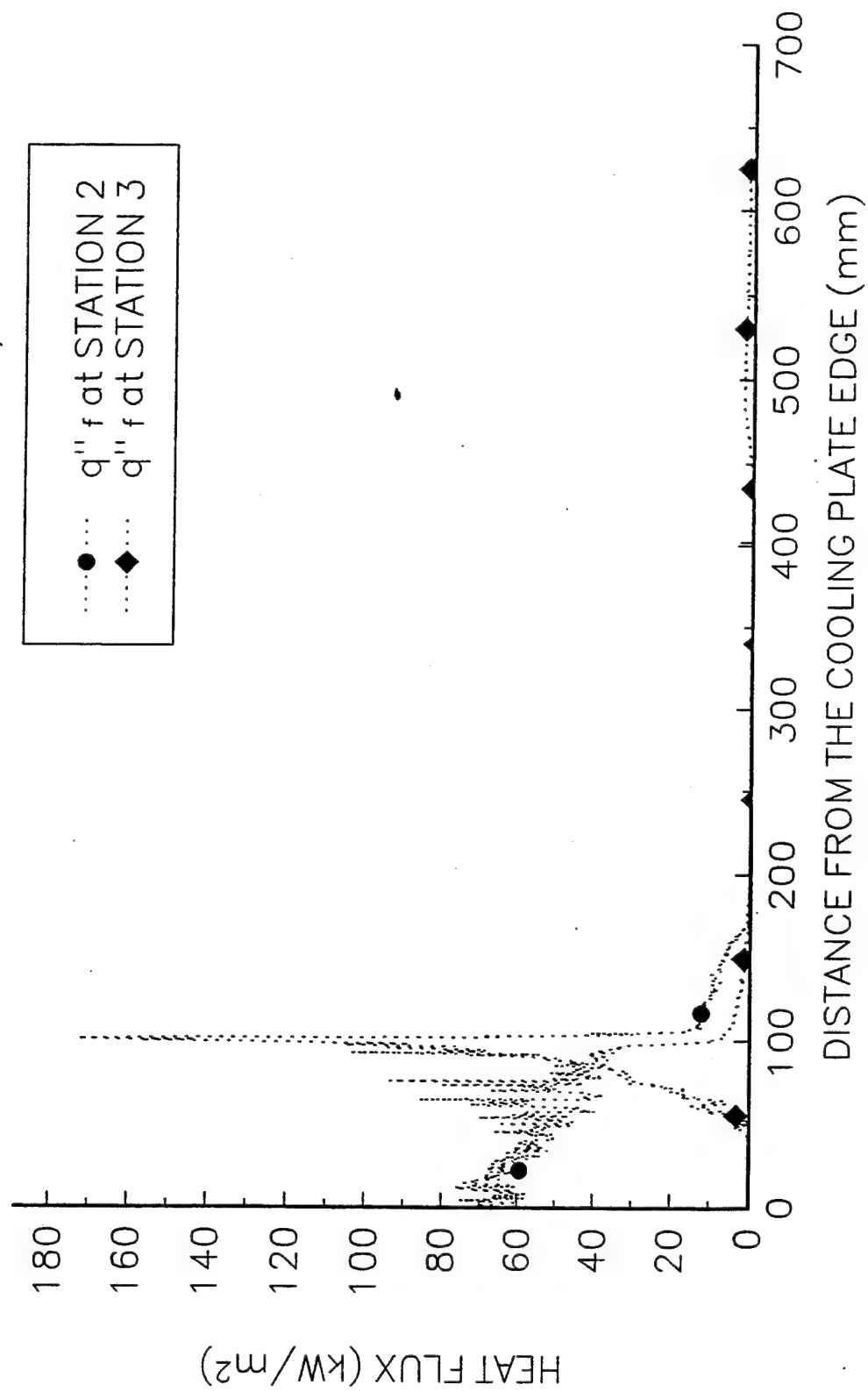
P30K822

1/4" PMMA Sheet,  $V=1.90 \text{ mm/s}$



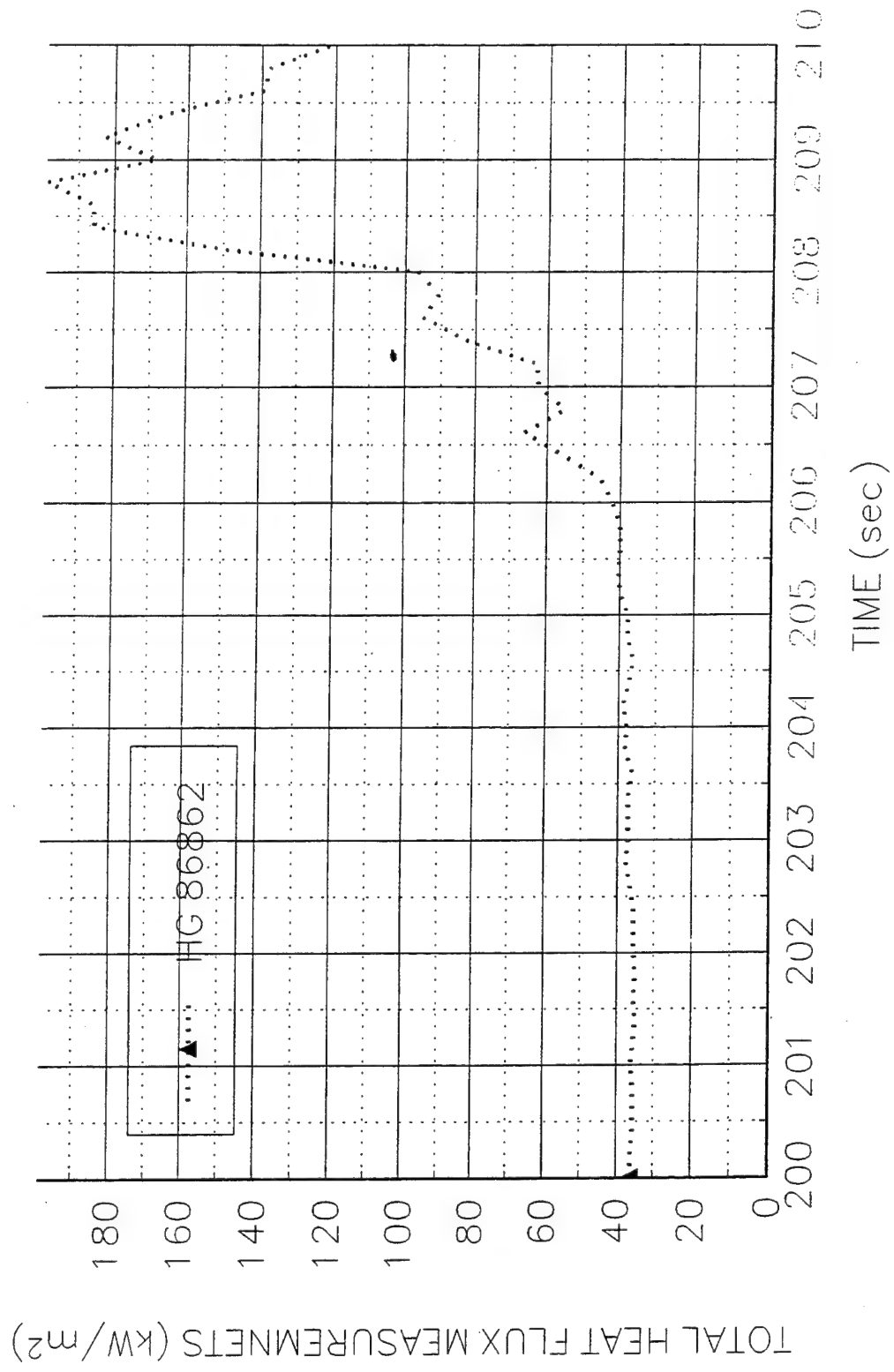
P30K822

1/4" PMMA Sheet,  $V=1.90 \text{ mm/s}$



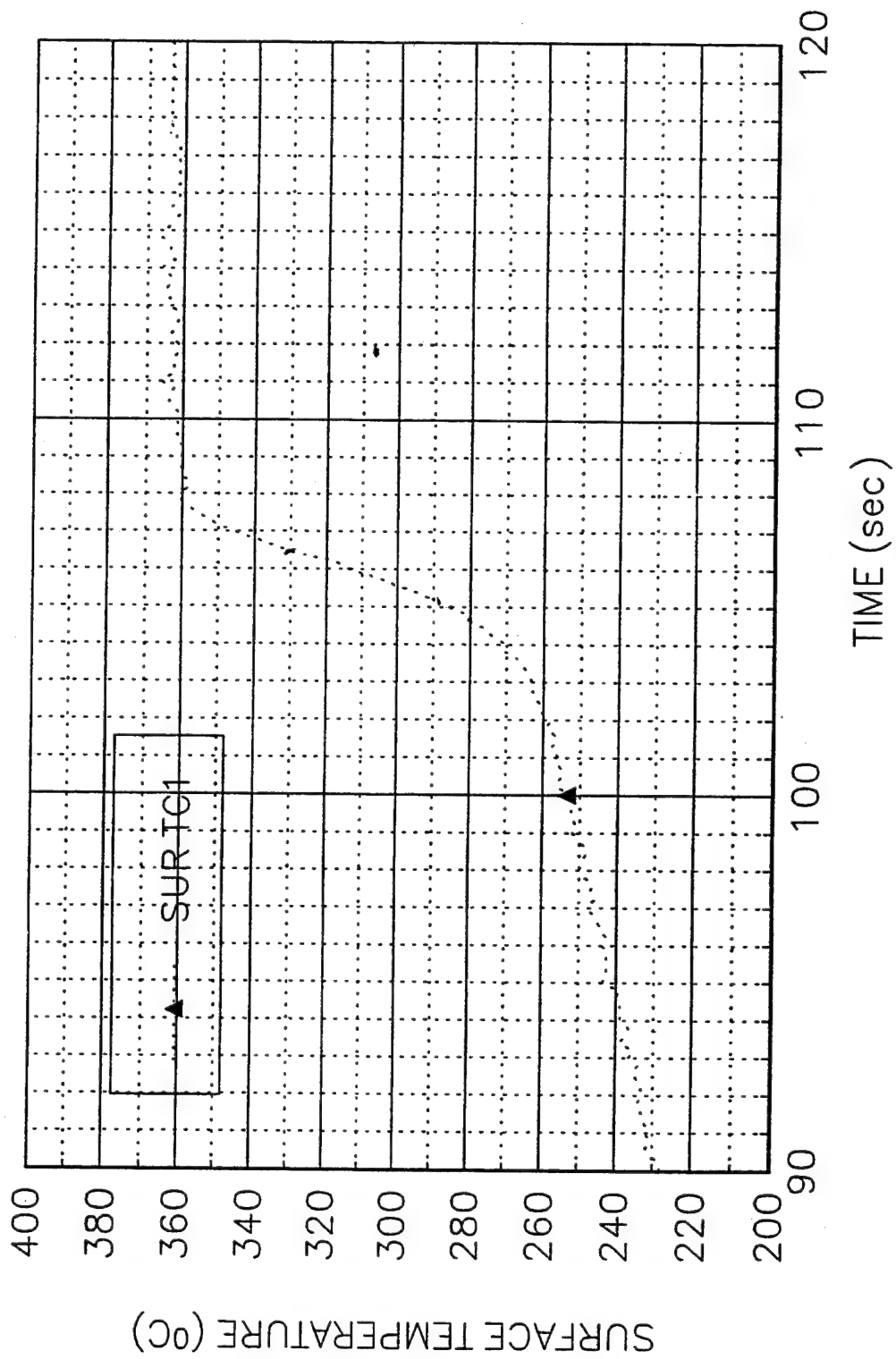
P30K822

1/4" PMMA Sheet, V=1.90 mm/s



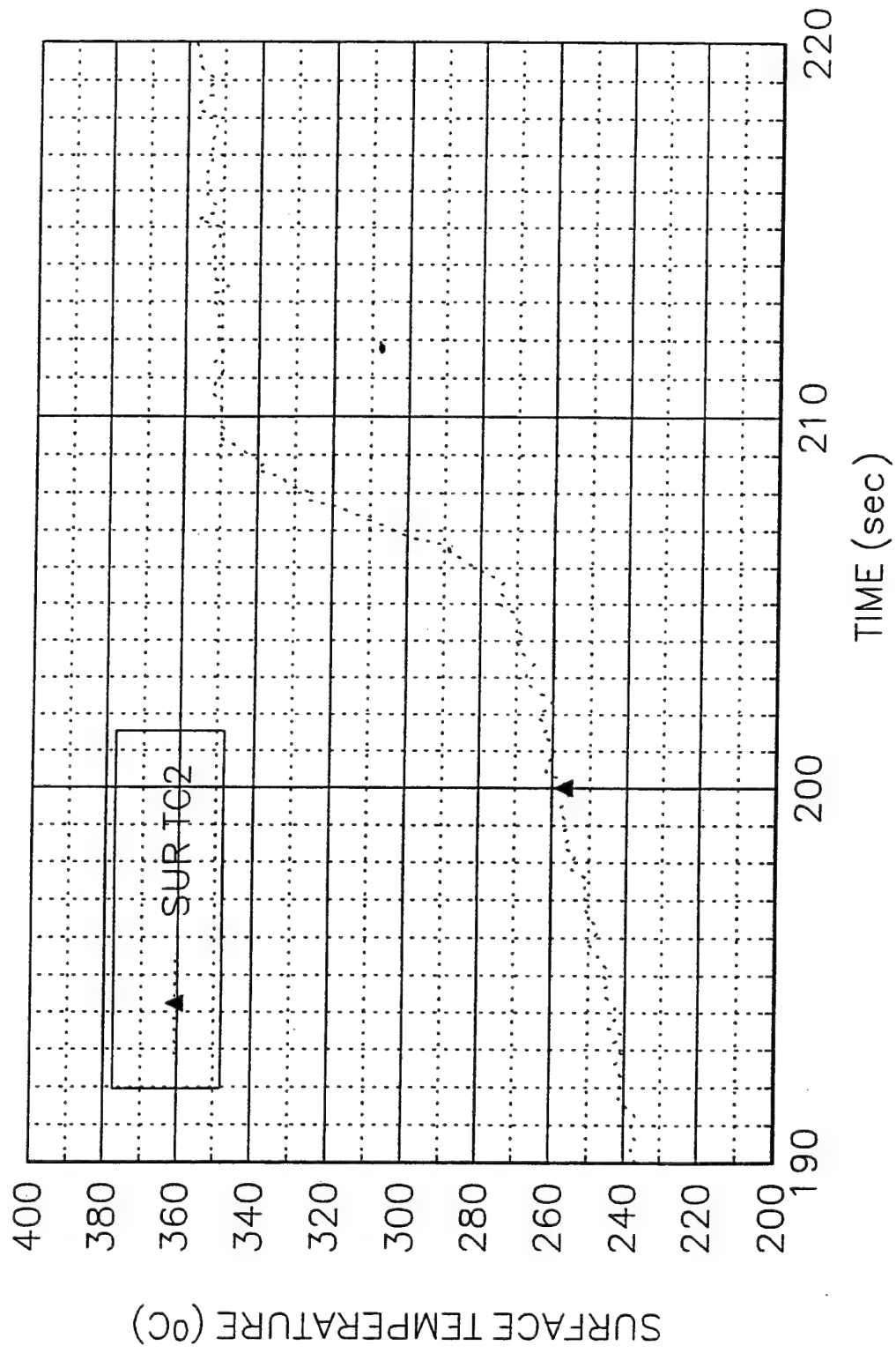
P30K822

1/4" PMMA Sheet, V=1.90 mm/s



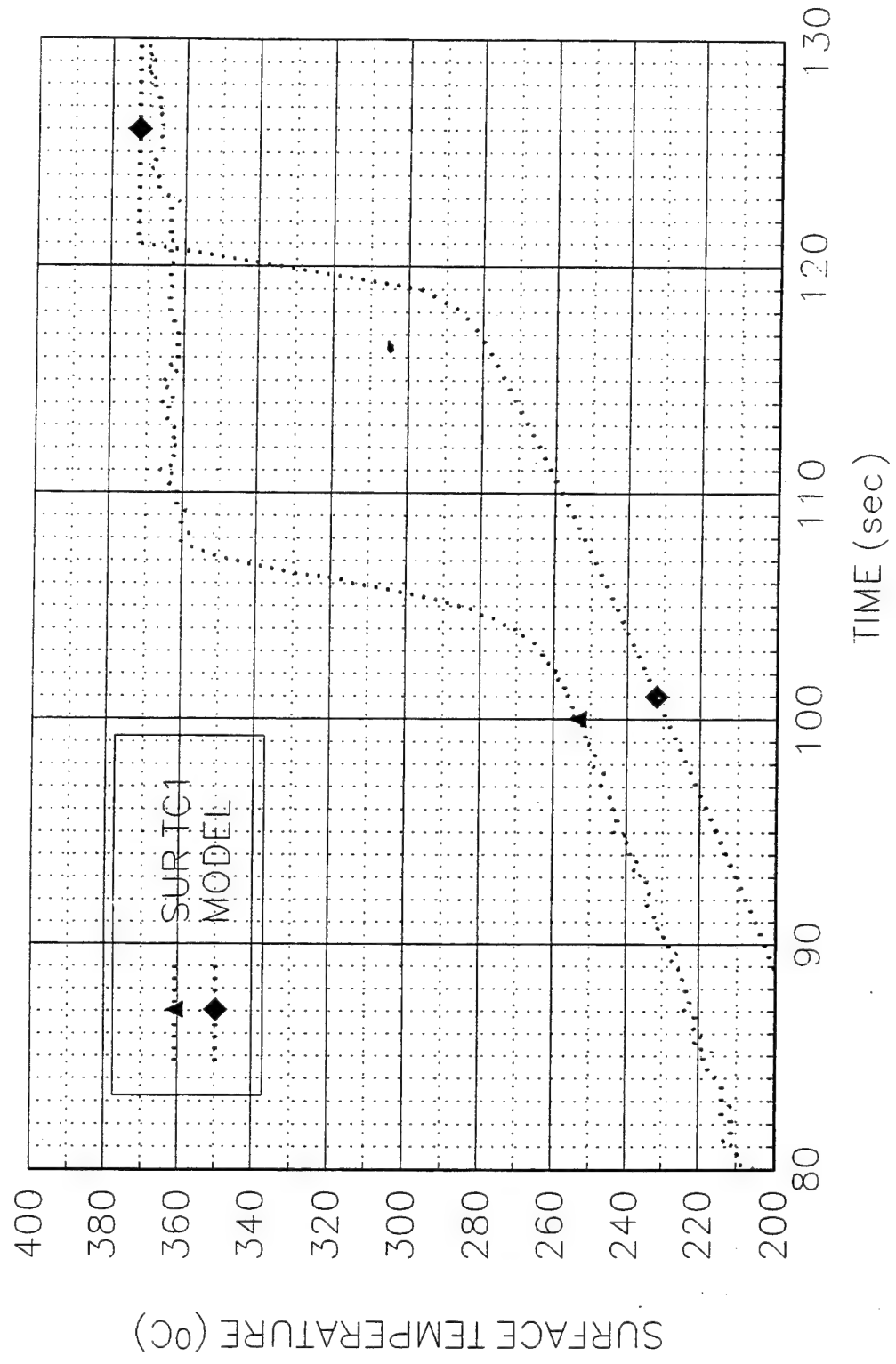
P30K822

1/4" PMMA Sheet, V=1.90 mm/s



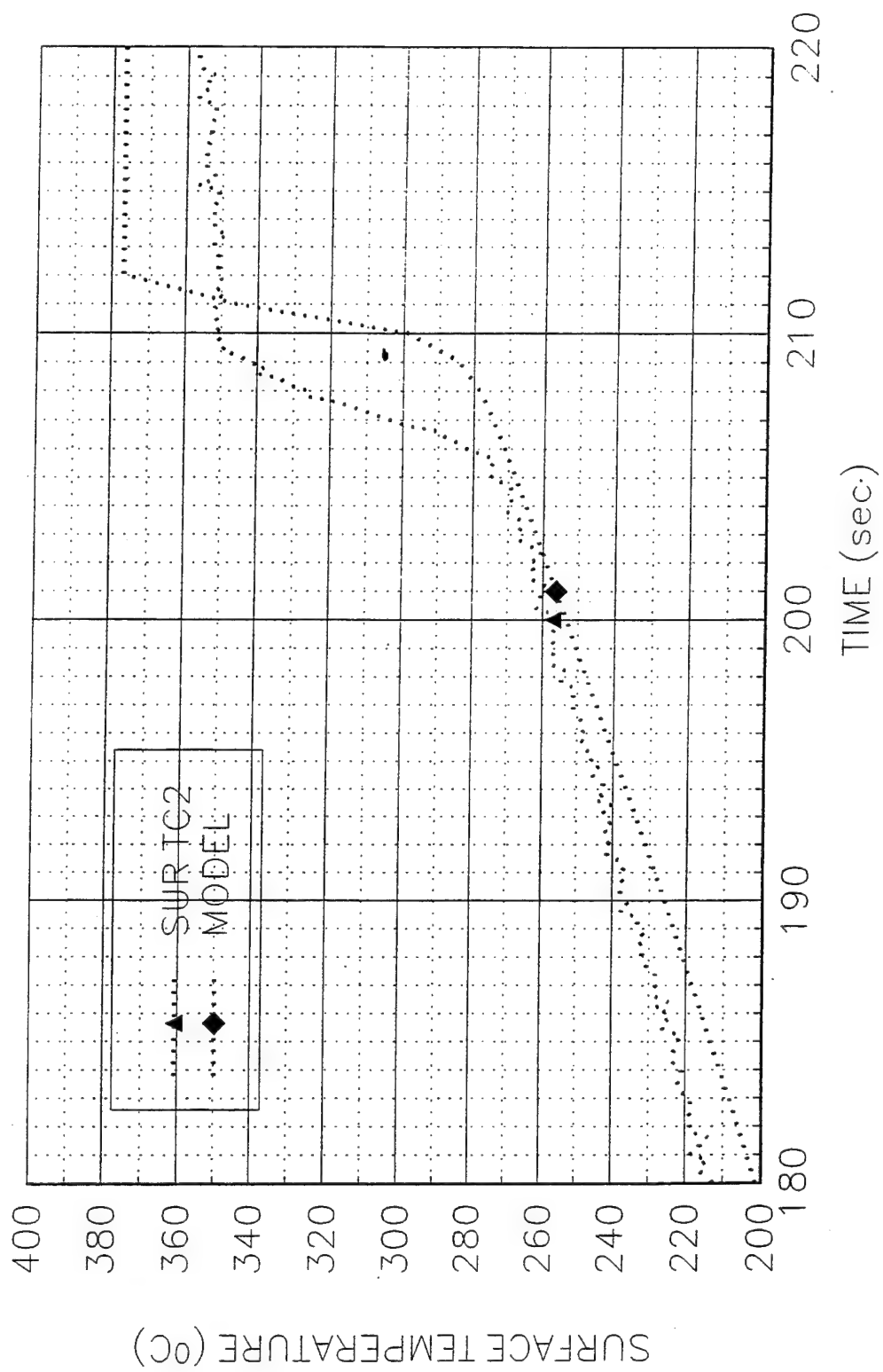
P30K822

1/4" PMMA Sheet, V=1.90 mm/s



P30K822

1/4" PMMA Sheet, V=1.90 mm/s



**Data Sheet**  
**Constant Horizontal Flame Spread Experiment**

Experimental No.: 45

Date: 8/23/94 Wed.

Time: 10:30 pm

**Pre-Experiment**

Heat Flux at 400 mm Location (Planned) (kW/m<sup>2</sup>): 30

Slider Speed (mm/s): 1.90

**Burning Sample Data**

Material: 1/4" PMMA Sheet unpainted

Dimension(LxWxH, mm): 800x152x6.35

**Instrumentation**

Number of Thermocouples: 5

Number of Heat Flux Gauges: 2

Station	Sensor	x (mm)	z (mm)	File Column	Note
1	TC	199	1.12	B	GAS TC1
1	TC	199	0	C	SUREFACE TC1
2	TC	378	1.70	D	GAS TC1
2	TC	378	0	E	SUREFACE TC2
2	HG	378	0	G	SERIAL 86862
3	TC	598	0	F	SUREFACE TC3
3	HG	598	0	H	SERIAL 525842

**Experiment**

Flux Gauge Reading @ 425 mm (Serial No. 27844, mV): 8.70-29.9976 kW/m<sup>2</sup>

Preheating Time without Pilot Flame (seconds): 30

Time to Sample Ignition After Applying the Pilot Flame (seconds): 0

Speed Used (S1M"Steps"): 300

Number of Steps (I1M"Steps"): 80629

File Names (.PRN): P30K823

Set-up File Name:

Sampling Rate (Hz): 5

Duration of Sampling (sec): 2500

Time to Start Moving the Sample (sec): -45

Ignition Heat Flux (Calculated, kW/m<sup>2</sup>):

**Ambient Conditions**

Temperature (°C): 20.

**Observations** Burning width ~7.5 cm, constant

Personnel Hui Fang, Y.C.

Processing of Data: SUR TC1:  $1/\tau=0.51$ ,  $T_p=370^\circ\text{C}$ ,  $T_{ext}=273.8^\circ\text{C}$ ,  
 $k_{pc}=0.2798 \times 1200 \times 2200 = 738672$ ,

$q''_0 = (\pi k_{pc})^{1/2} (T_p - T_{ext}) (V/\delta)^{1/2} = (738672)^{1/2} \times (370 - 273.8) (0.51)^{1/2} = 59.09 \text{ kW/m}^2$

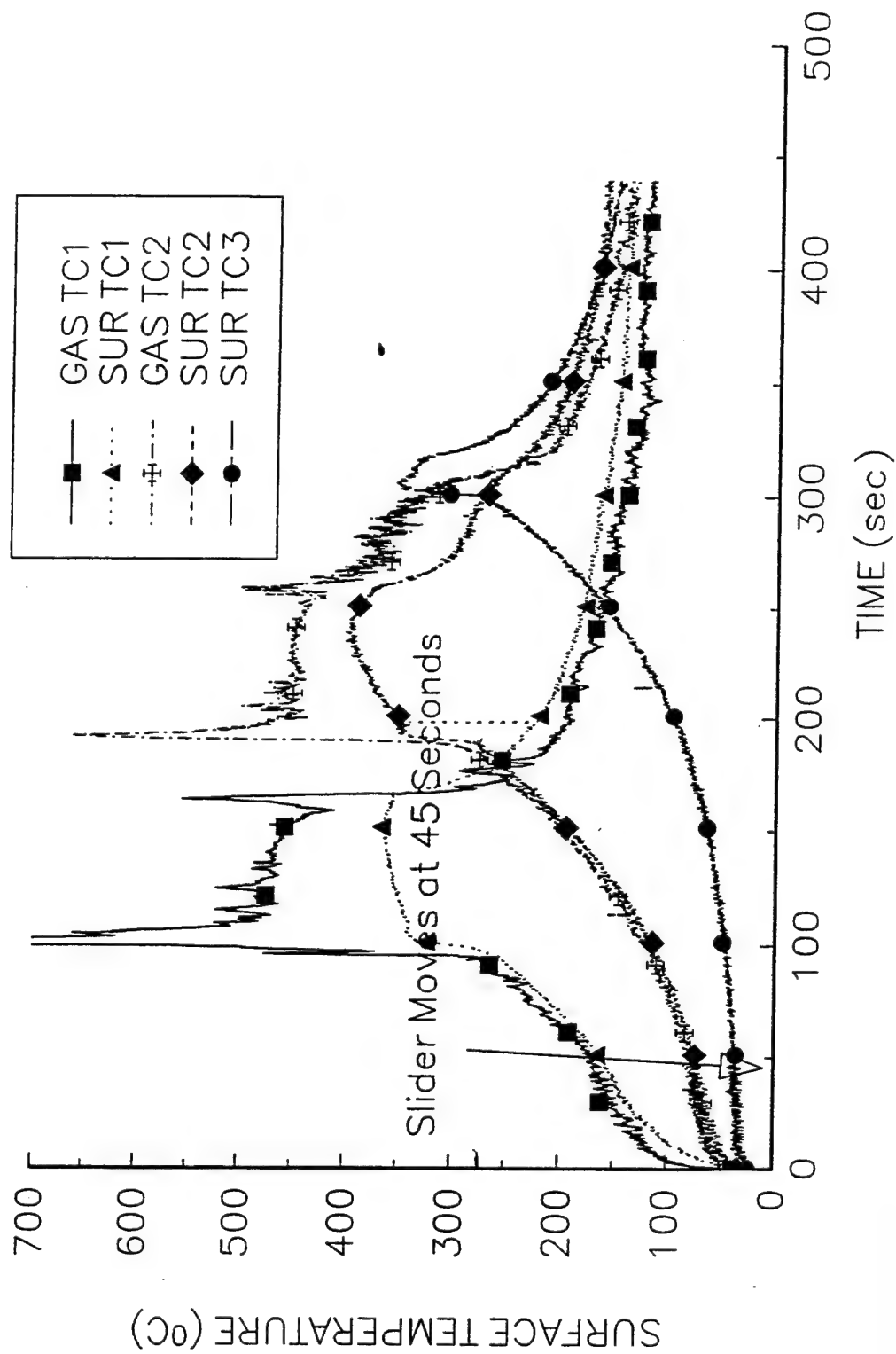
SUR TC2:  $1/\tau=0.8$ ,  $T_p=370^\circ\text{C}$ ,  $T_{ext}=273.8^\circ\text{C}$ ,

$q''_0 = (\pi k_{pc})^{1/2} (T_p - T_{ext}) (V/\delta)^{1/2} = (738672)^{1/2} \times (370 - 273.8) (0.8)^{1/2} = 73.99 \text{ kW/m}^2$



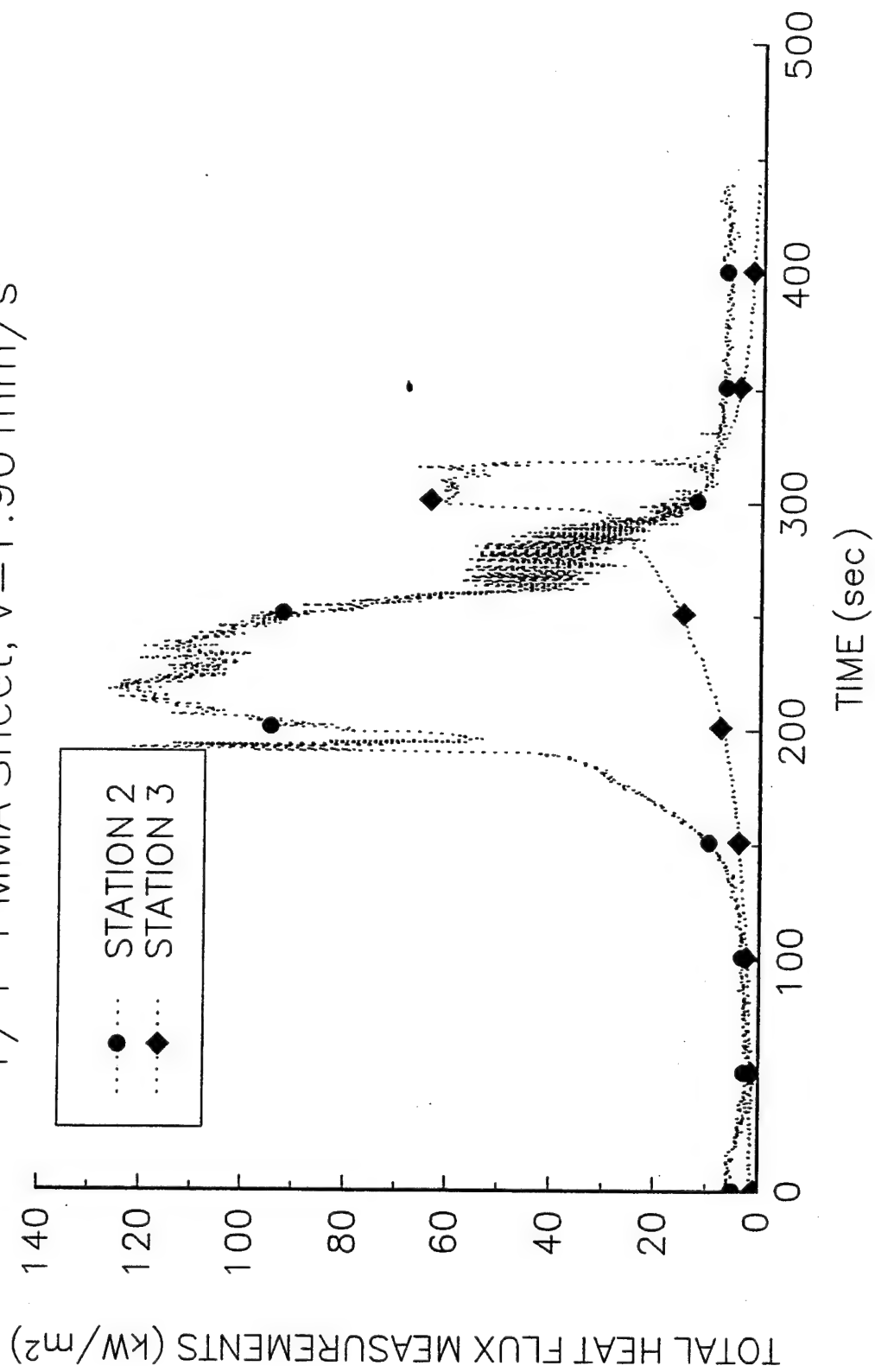
P30K823

1/4" PMMA Sheet, V=1.90 mm/s



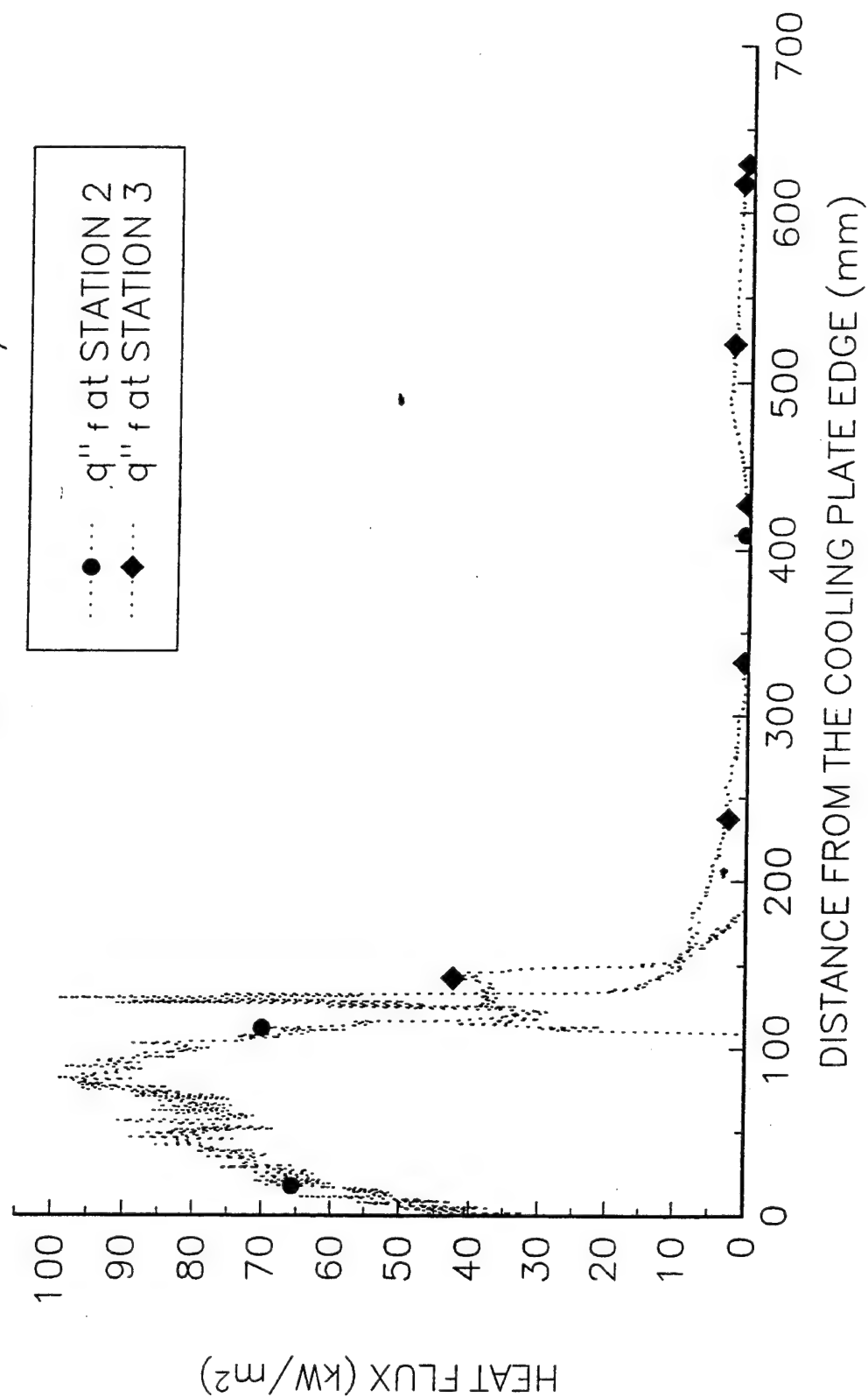
P30K823

1/4" PMMA Sheet,  $V=1.90 \text{ mm/s}$



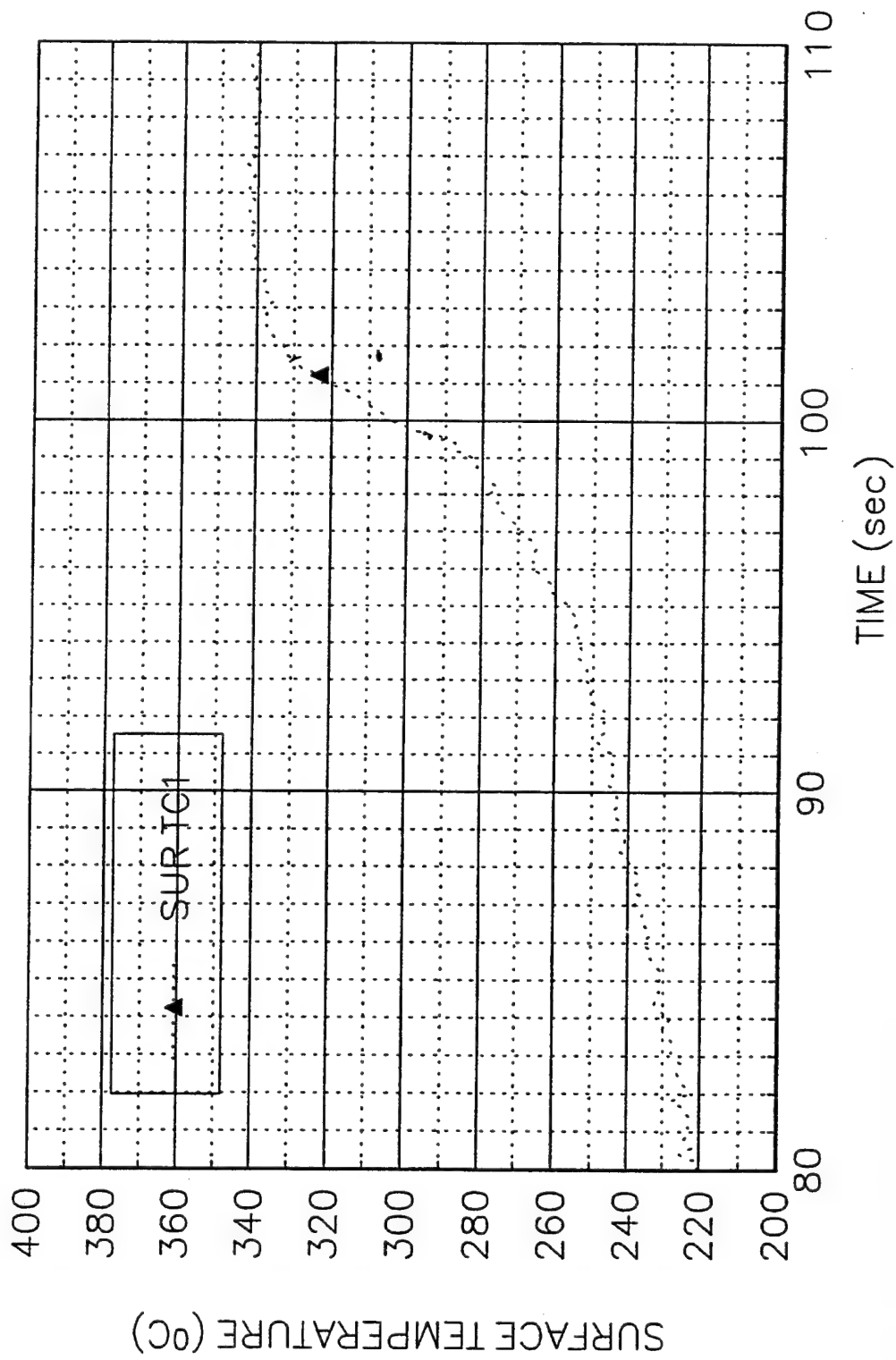
P30K823

1/4" PMMA Sheet,  $V=1.90 \text{ mm/s}$



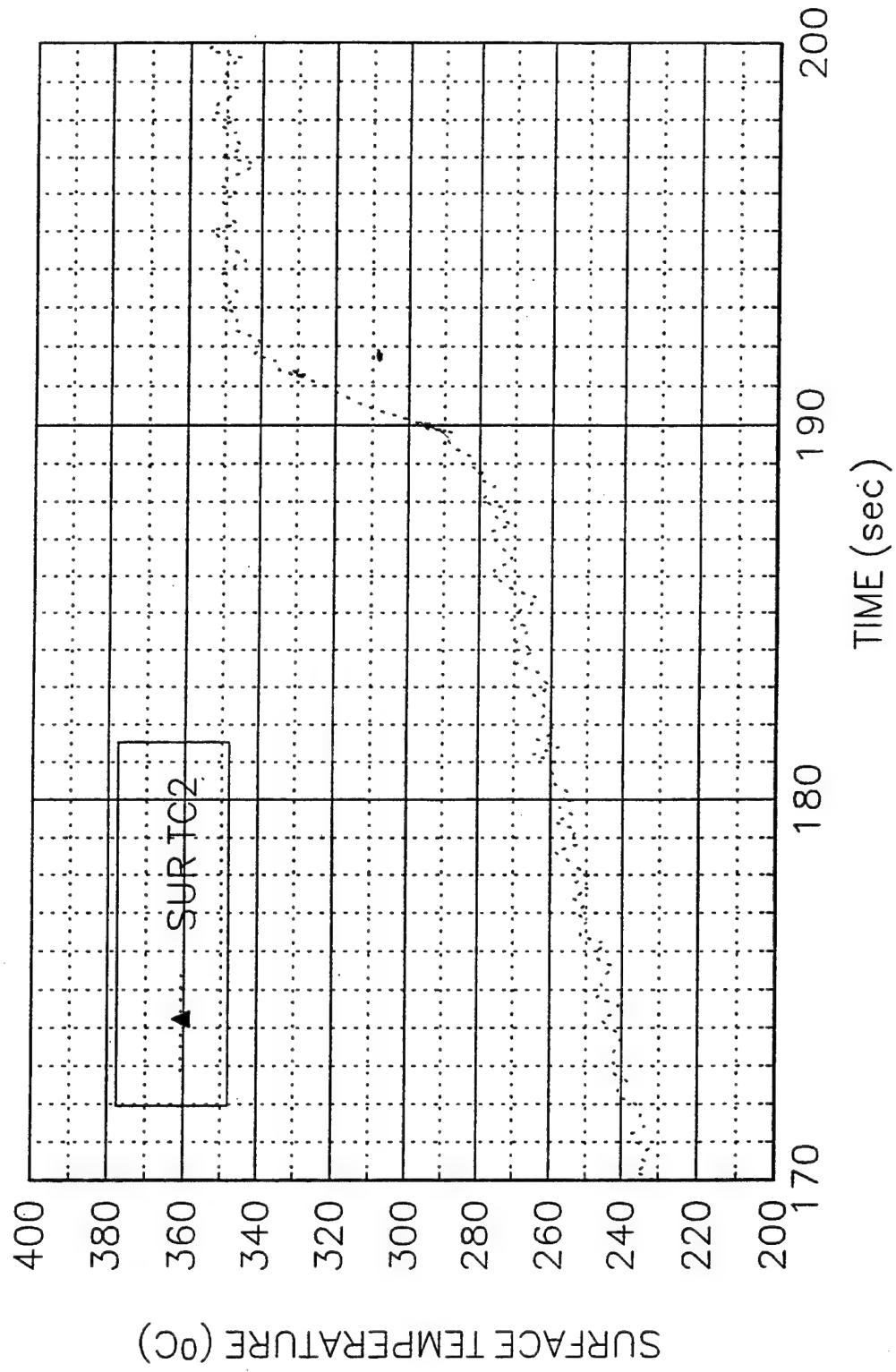
P30K823

1/4" PMMA Sheet, V=1.90 mm/s



P30K823

1/4" PMMA Sheet, V=1.90 mm/s



**Data Sheet**  
**Constant Horizontal Flame Spread Experiment**

Experimental No.: 36

Date: 8/09/94 Tu

Time: 3:30 pm

**Pre-Experiment**

Heat Flux at 425 mm Location (Planned) (kW/m<sup>2</sup>): 10

Slider Speed (mm/s): 0.5 mm/s

**Burning Sample Data**

Material: 3/4" PMMA Sheet

Dimension(LxWxH, mm): 600x152x6.35

**Instrumentation**

Number of Thermocouples: 5

Number of Heat Flux Gauges: 2

Station	Sensor	x (mm)	z (mm)	File Column	Note
1	TC	174	1.30	B	GAS TC1
1	TC	174	0	C	SURFACE TC1
2	TC	351	1.43	D	GAS TC2
2	TC	351	0	E	SURFACE TC2
2	HG	351	0	G	SERIAL 86862
3	TC	576	0	F	SURFACE TC3
3	HG	576	0	H	SERIAL 525842

**Experiment**

Flux Gauge Reading @ 425 mm (Serial No. 27844, mV): 2.90-10 kW/m<sup>2</sup>

Preheating Time without Pilot Flame (seconds): 240

Time to Sample Ignition After Applying the Pilot Flame (seconds): 130

Speed Used (SIM"Steps"): 79

Number of Steps (IIM"Steps"): 80629

File Names (.PRN): M10K809

Set-up File Name:

Sampling Rate (Hz): 5      Duration of Sampling (sec): 2500

Time to Start Moving the Sample (sec): 582.8

Ignition Heat Flux (Calculated, kW/m<sup>2</sup>):

**Ambient Conditions**

Temperature (°C): 23.

**Observations** Burning area 8.5 cm, taking some data when marinite board cover is on. Small flux gage is recessed at the beginning. Slide moves too fast, stops sometime. There is a lag in front of the small flux gage. Taking data when cover-on for about 82.4 seconds

Personnel V.M., Y.C.

Processing of Data: SUR TC1:  $1/\tau=0.18$ ,  $T_p=370^\circ\text{C}$ ,  $T_{\text{ext}}=234.3^\circ\text{C}$ ,  
 $k\rho c=0.2798 \times 1200 \times 2200=738672$ ,

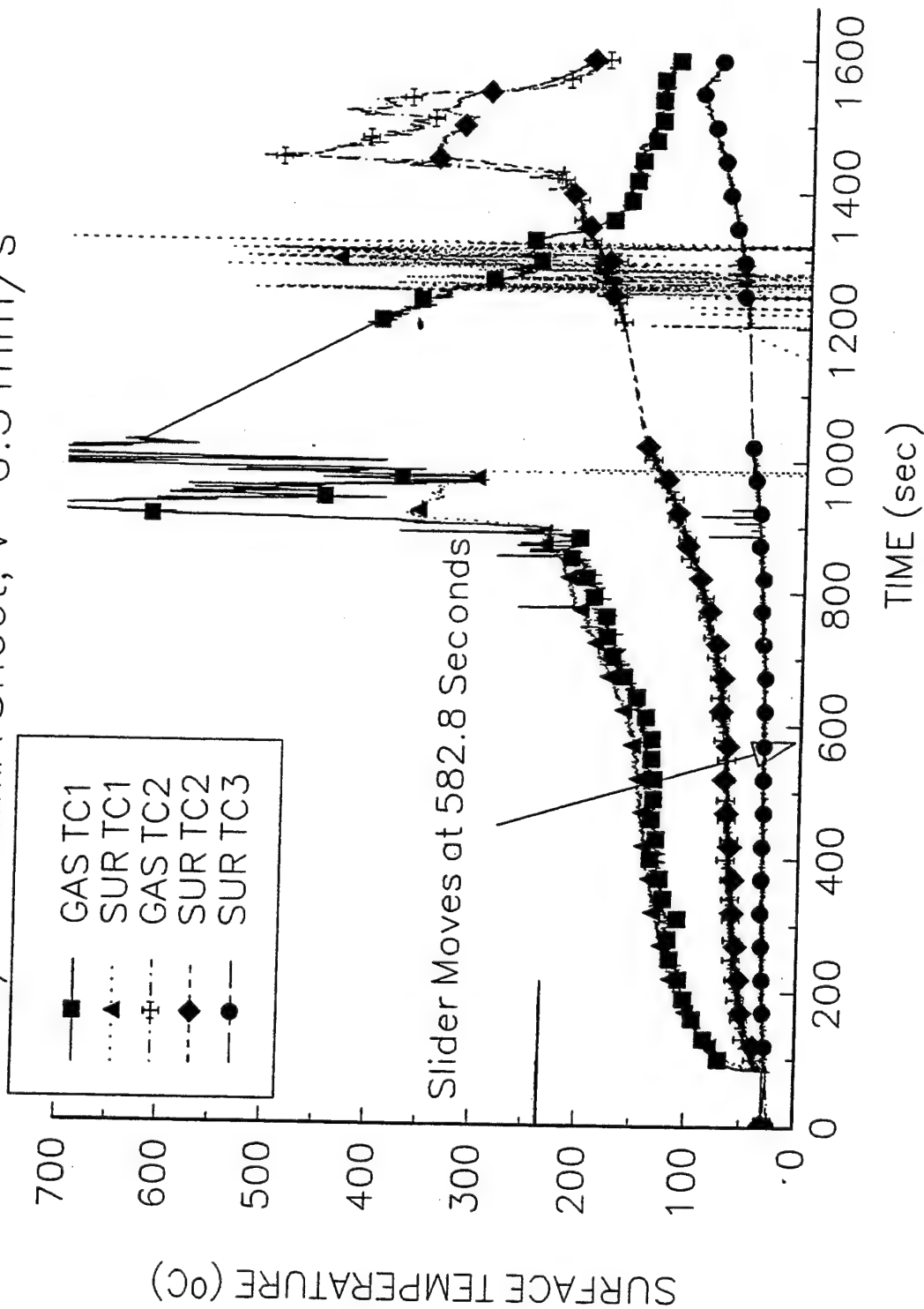
$\dot{q}_0^*=(\pi k\rho c)^{1/2}(T_p-T_{\text{ext}})(V/\delta)^{1/2}=(738672)^{1/2} \times (370.-234.3)(0.18)^{1/2}=49.73 \text{ kW/m}^2$

SUR TC2:  $1/\tau=0.11$ ,  $T_p=370^\circ\text{C}$ ,  $T_{\text{ext}}=234.3^\circ\text{C}$ ,

$\dot{q}_0^*=(\pi k\rho c)^{1/2}(T_p-T_{\text{ext}})(V/\delta)^{1/2}=(738672)^{1/2} \times (370-234.3)(0.)^{1/2}=39.32 \text{ kW/m}^2$

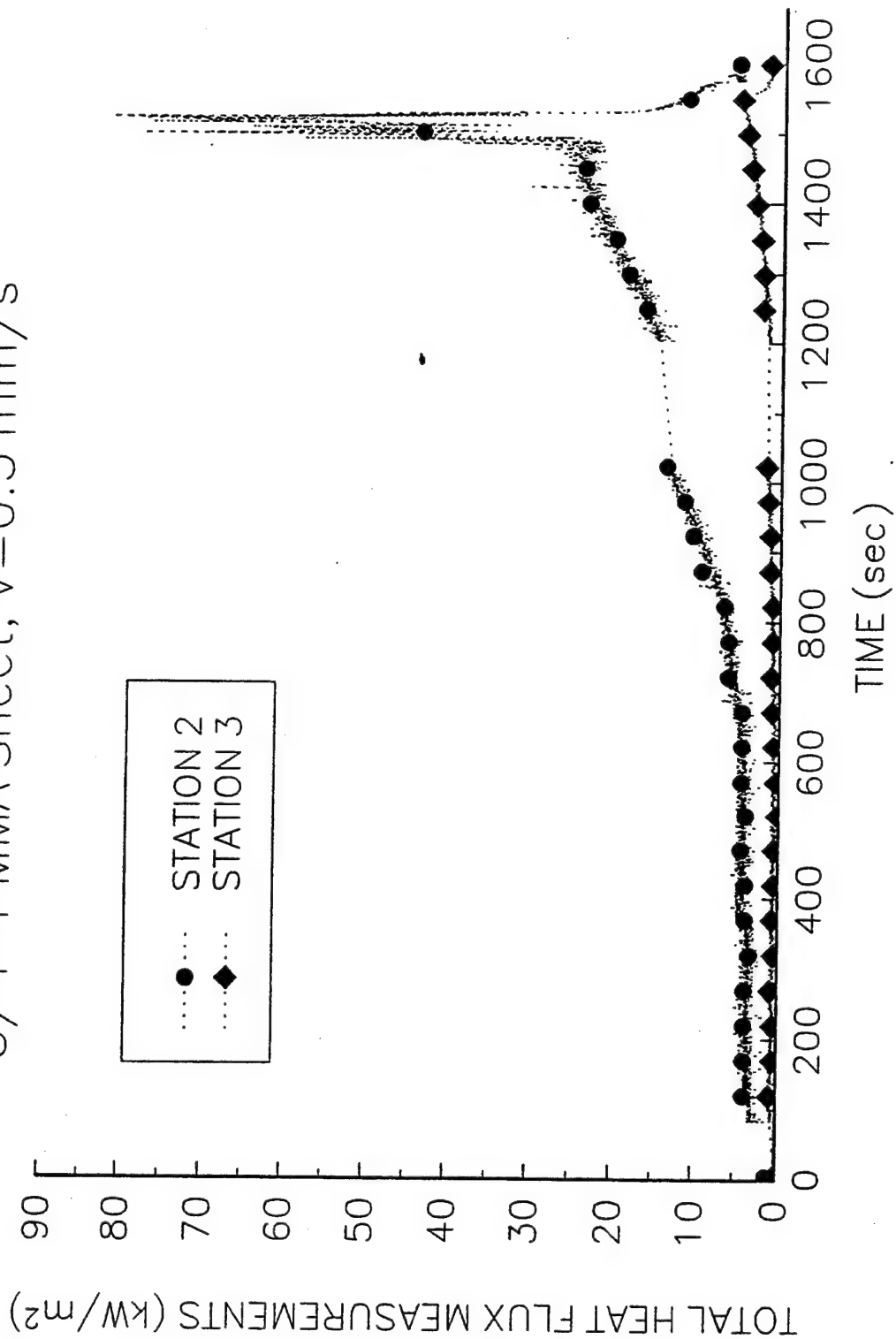
M10K809

3/4" PMMA Sheet, V=0.5 mm/s



M10K809

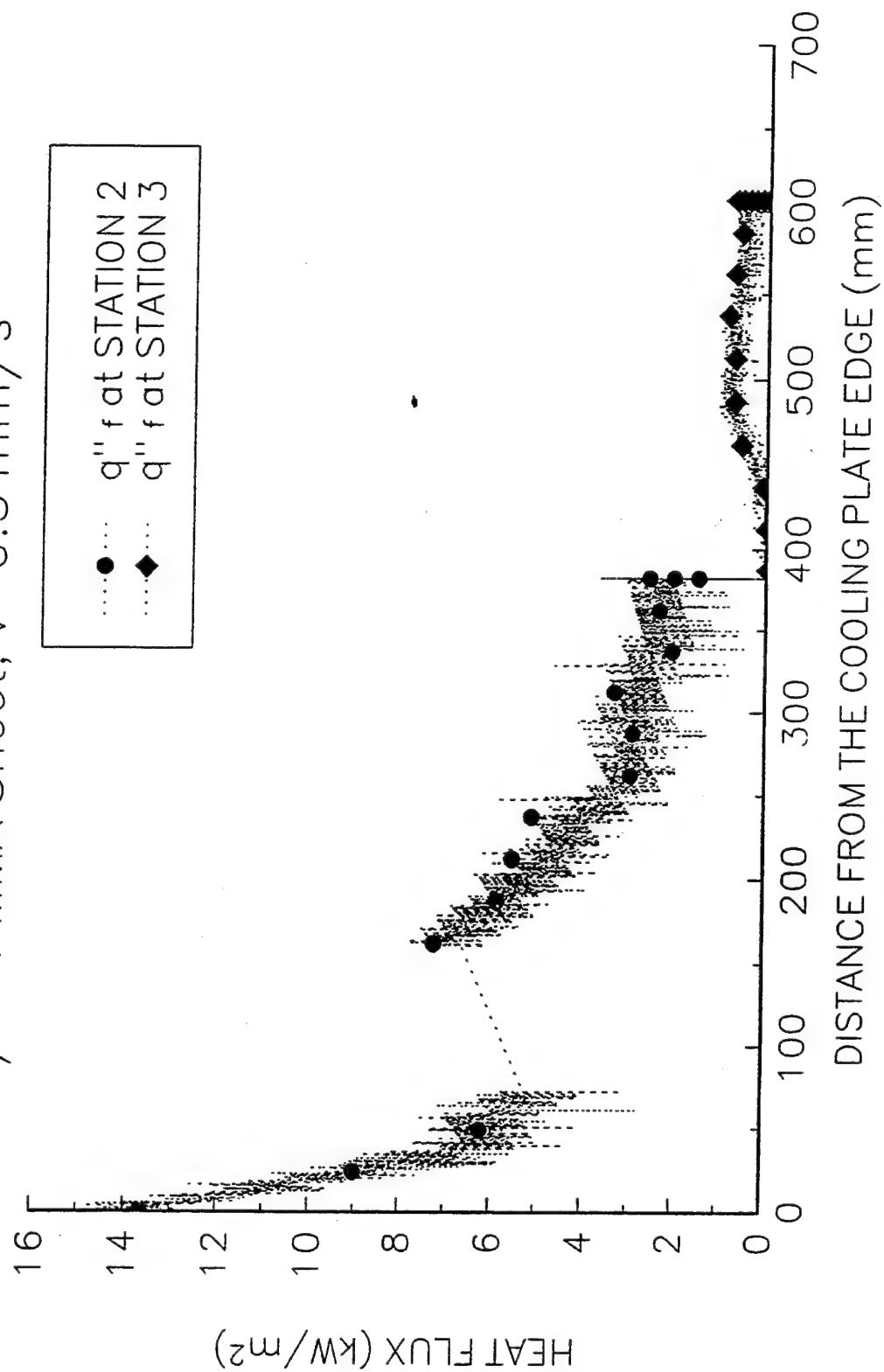
3/4" PMMA Sheet,  $V=0.5 \text{ mm/s}$





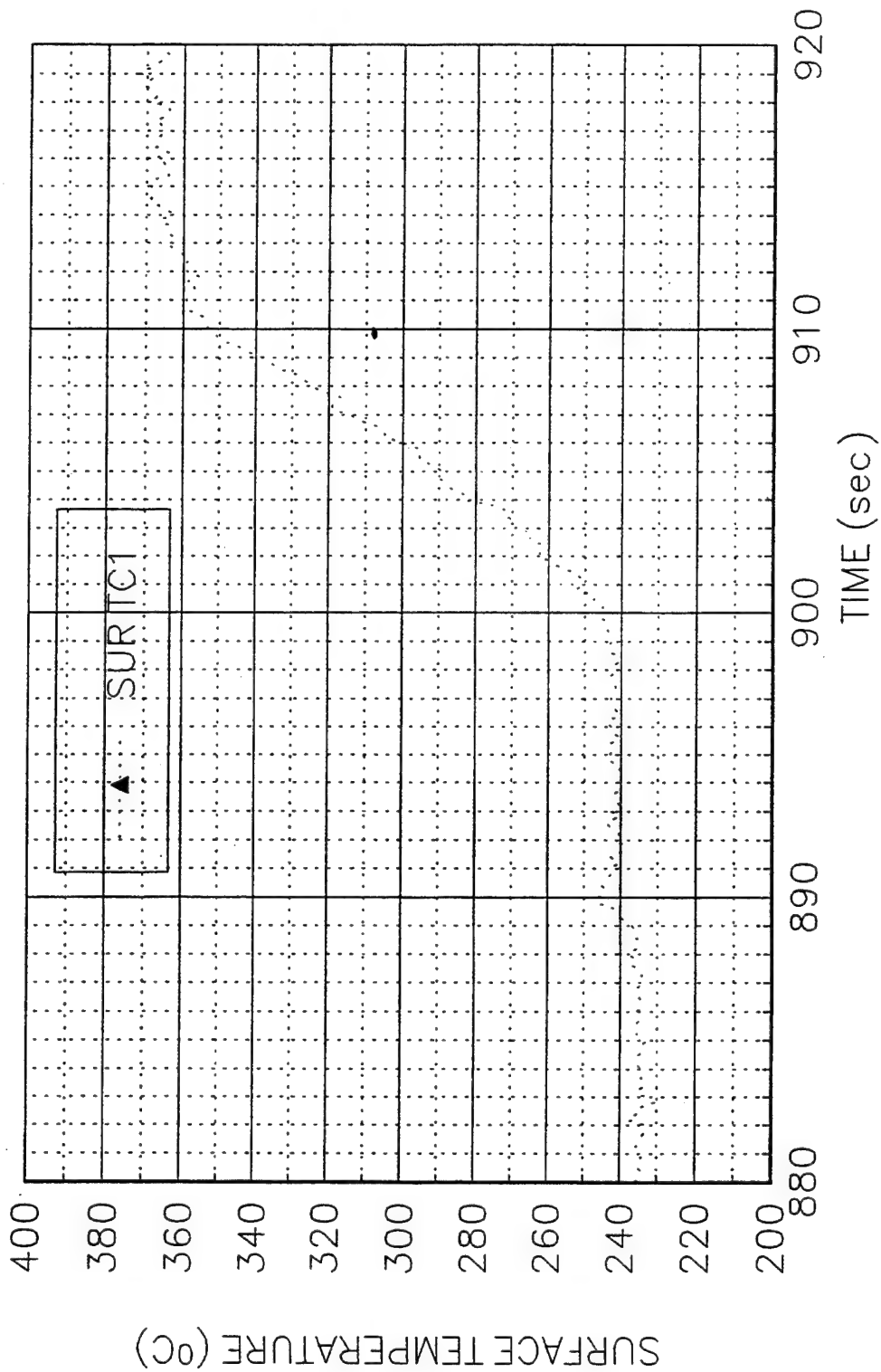
M10K809

1/4" PMMA Sheet,  $V=0.5 \text{ mm/s}$



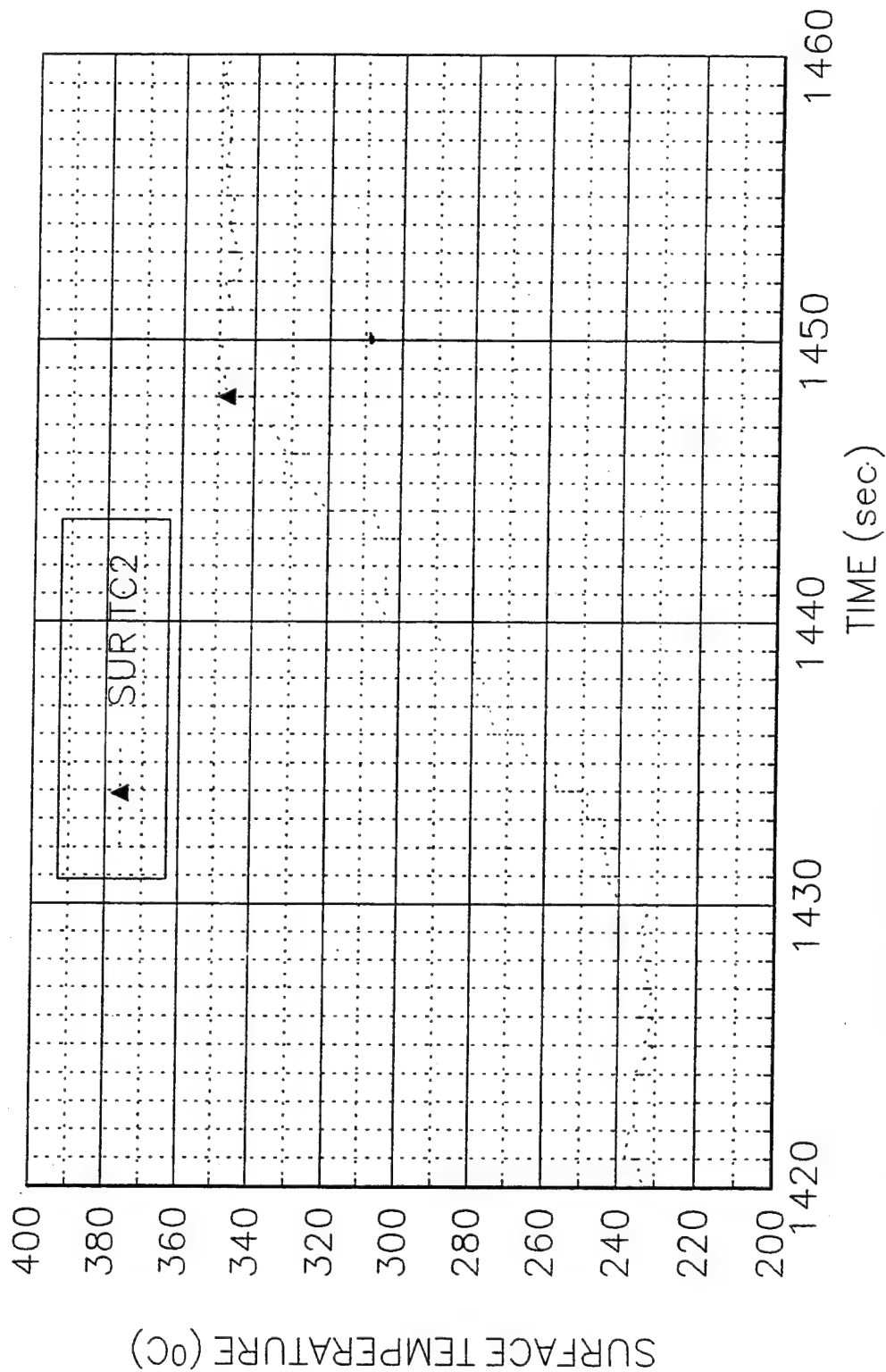
M10K809

3/4" PMMA Sheet, V=0.5 mm/s



M10K809

3/4" PMMA Sheet, V=0.5 mm/s



**Data Sheet**  
**Constant Horizontal Flame Spread Experiment**

Experimental No.: 37

Date: 8/10/94 Tu

Time: 10:00 pm

**Pre-Experiment**

Heat Flux at 425 mm Location (Planned) (kW/m<sup>2</sup>): 10

Slider Speed (mm/s): 0.2 mm/s

**Burning Sample Data**

Material: 3/4" PMMA Sheet

Dimension(LxWxH, mm): 600x152x6.35

**Instrumentation**

Number of Thermocouples: 5

Number of Heat Flux Gauges: 2

Station	Sensor	x (mm)	z (mm)	File Column	Note
1	TC	177	0.58	B	GAS TC1
1	TC	177	0	C	SURFACE TC1
2	TC	351	0.78	D	GAS TC2
2	TC	351	0	E	SURFACE TC2
2	HG	351	0	G	SERIAL 86862
3	TC	576	0	F	SURFACE TC3
3	HG	576	0	H	SERIAL 525842

**Experiment**

Flux Gauge Reading @ 425 mm (Serial No. 27844, mV): 2.90-10 kW/m<sup>2</sup>

Preheating Time without Pilot Flame (seconds): 240

Time to Sample Ignition After Applying the Pilot Flame (seconds): 120

Speed Used (S1M"Steps"): 32

Number of Steps (I1M"Steps"): 80629

File Names (.PRN): M10K810, M10K81a

Set-up File Name:

Sampling Rate (Hz): 5      Duration of Sampling (sec): 2500

Time to Start Moving the Sample (sec): 486.2

Ignition Heat Flux (Calculated, kW/m<sup>2</sup>): 20.1 kW/m<sup>2</sup>

**Ambient Conditions**

Temperature (°C): 23.

**Observations** Burning area 10 cm, good ignition, growing to ~ 12.5 c, size little bit too large. Data acquisition terminates about 100 seconds. ~ 20 cm when flame front @45 cm location

Personnel Yijun Hu, Y.C.

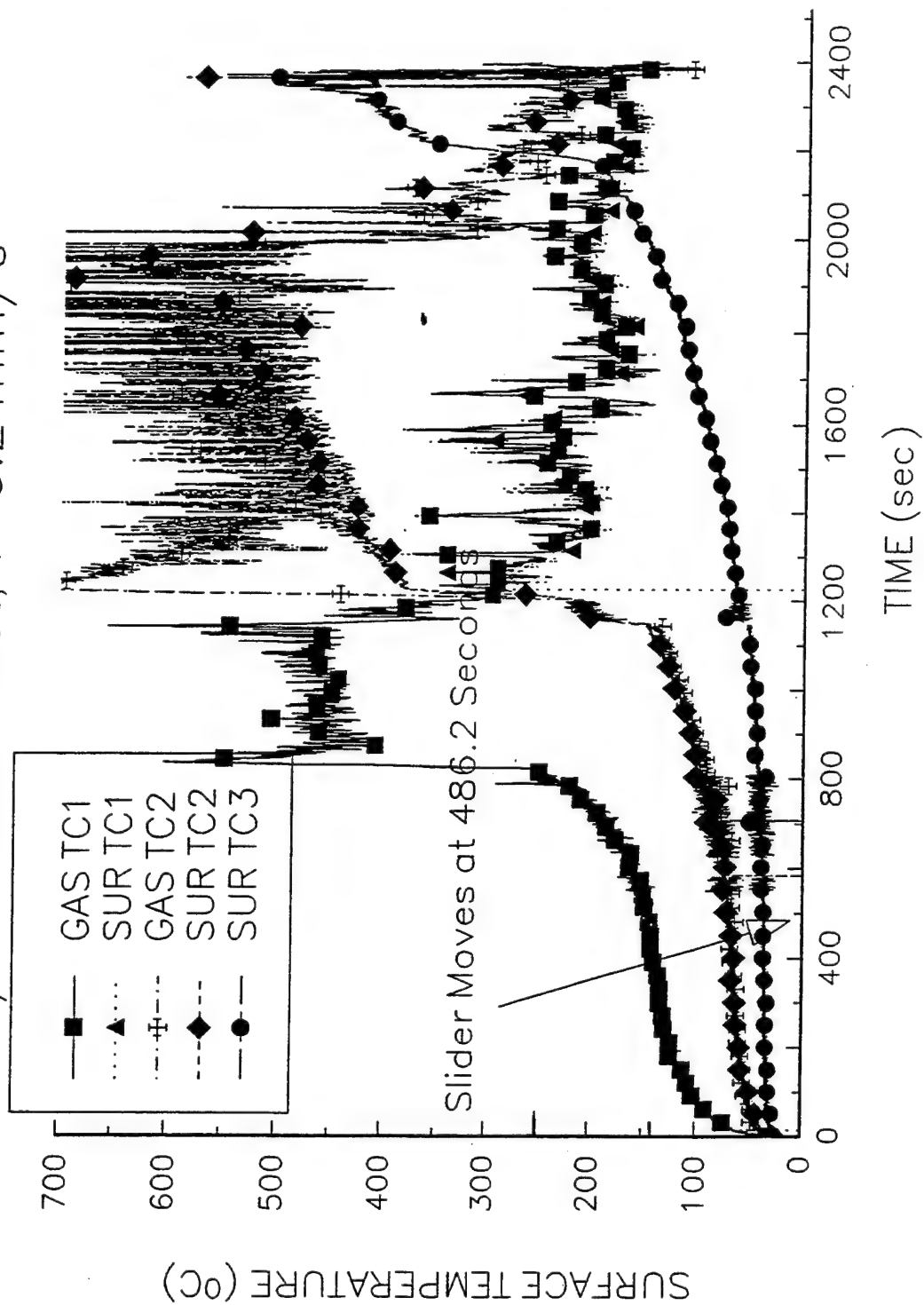
Processing of Data:  $k\rho c = 0.2798 \times 1200 \times 2200 = 738672$

SUR TC2:  $1/\tau = 0.14$ ,  $T_p = 370^\circ\text{C}$ ,  $T_{\text{ext}} = 230.4^\circ\text{C}$ ,

$$\dot{q}_0'' = (\pi k\rho c)^{1/2} (T_p - T_{\text{ext}}) (V/\delta)^{1/2} = (738672)^{1/2} \times (370 - 230.4) (0.14)^{1/2} = 44.61 \text{ kW/m}^2$$

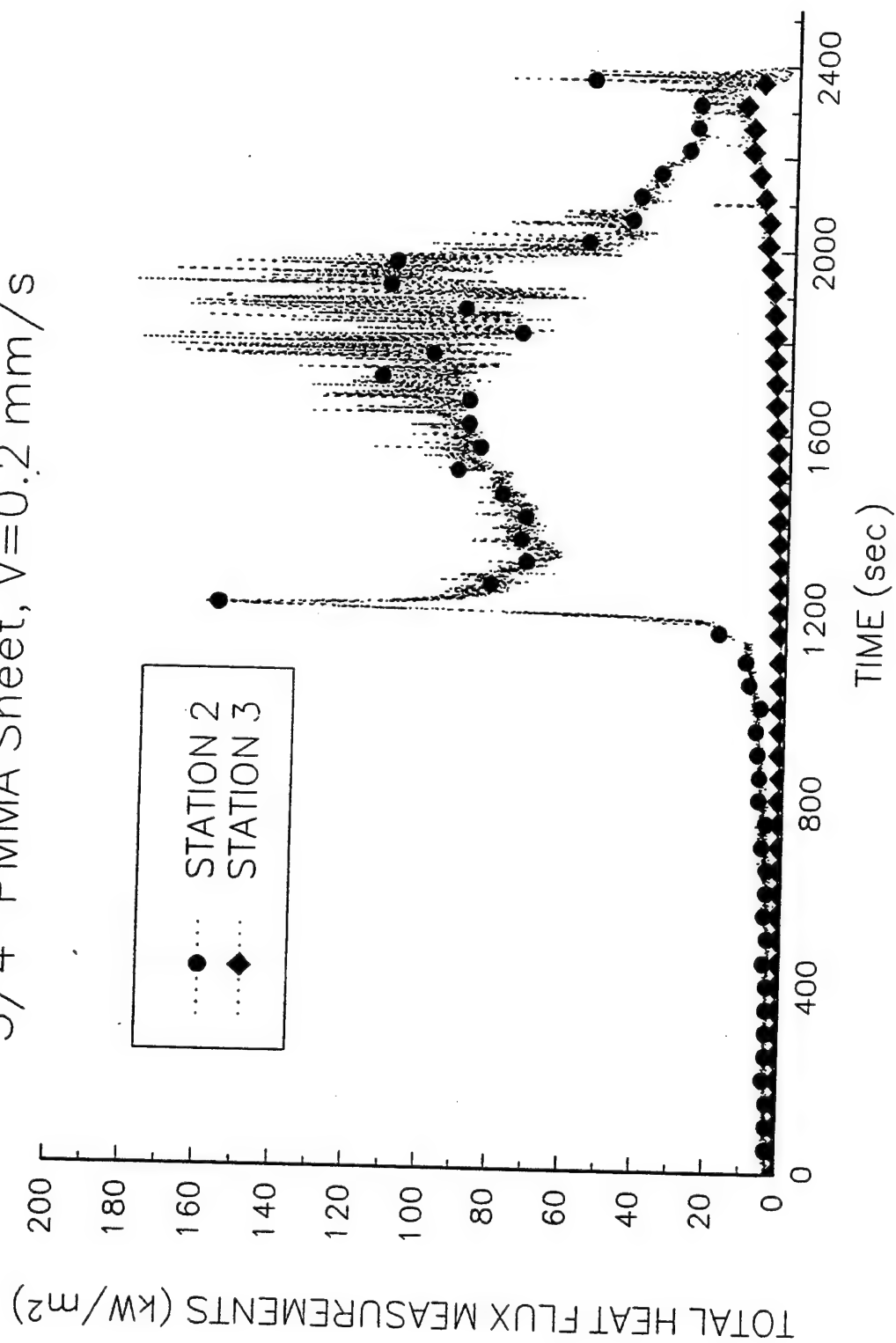
M10K810

3/4" PMMA Sheet,  $V=0.2 \text{ mm/s}$



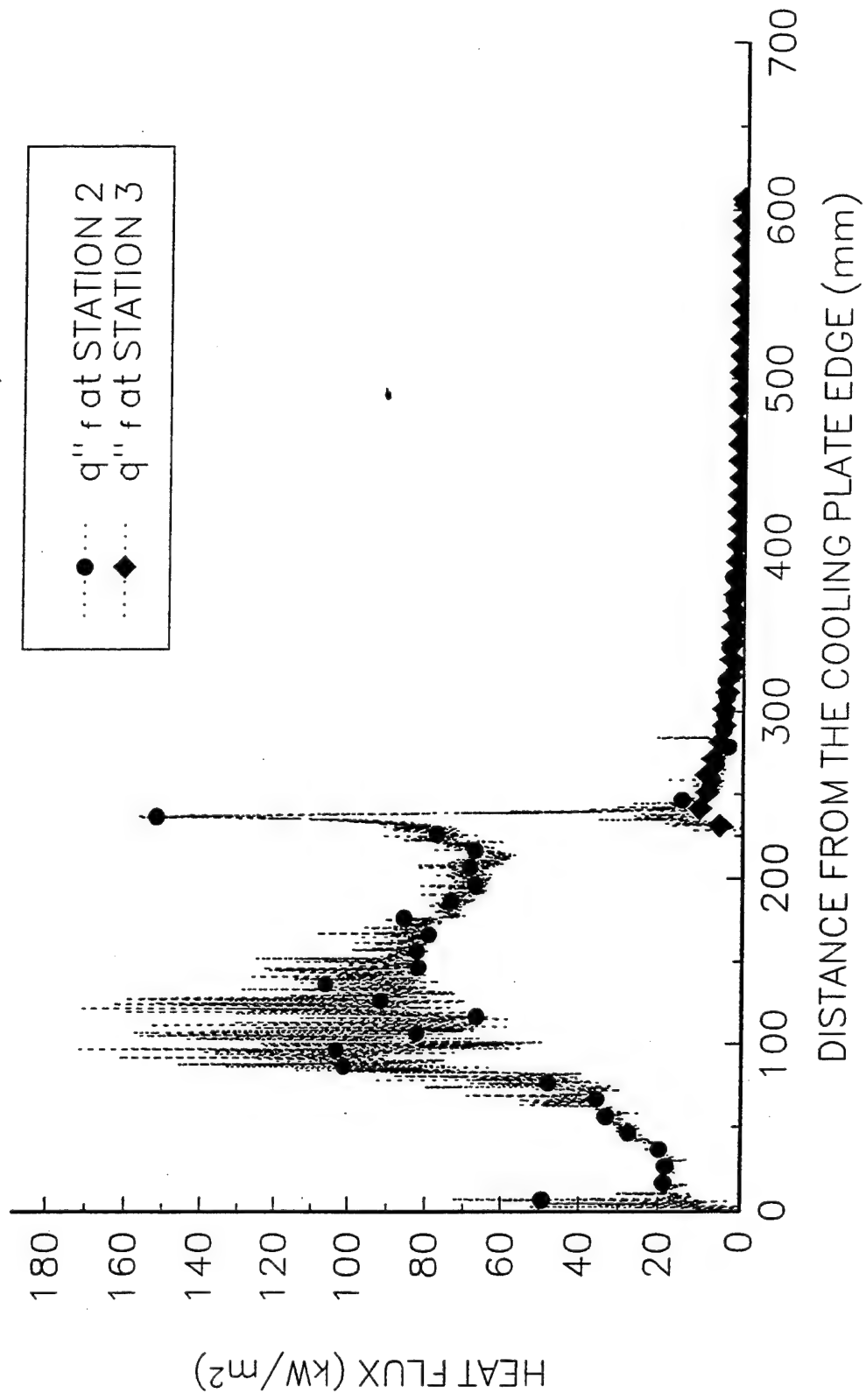
M10K810

3/4" PMMA Sheet,  $V=0.2$  mm/s



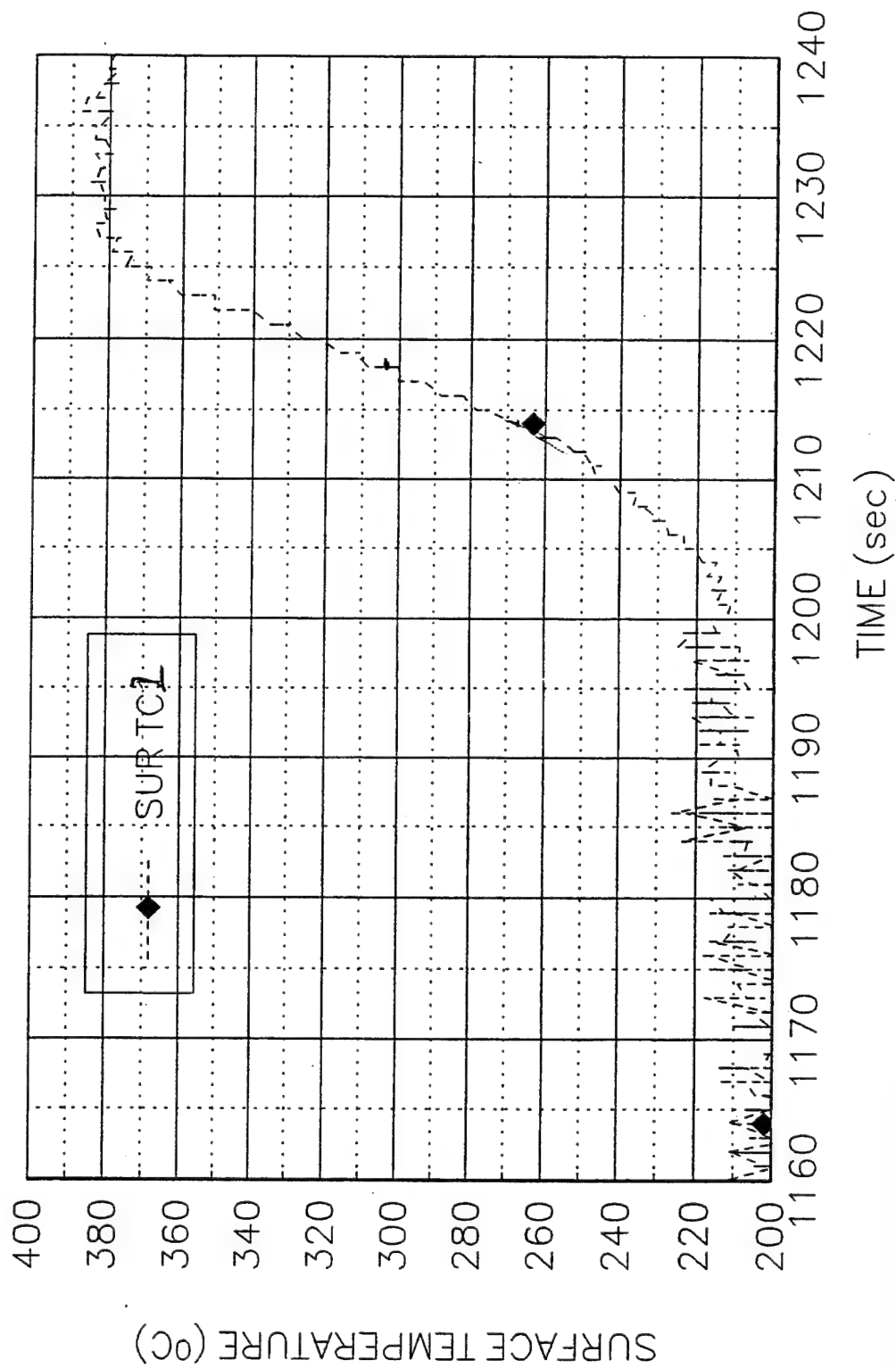
M10K810

3/4" PMMA Sheet,  $V=0.2 \text{ mm/s}$



M10K810

3/4" PMMA Sheet, V=0.2 mm/s





**Data Sheet**  
**Constant Horizontal Flame Spread Experiment**

Experimental No.: 38

Date: 8/12/94 Fri

Time: 11.00 am

**Pre-Experiment**

Heat Flux at 425 mm Location (Planned) (kW/m<sup>2</sup>): 10

Slider Speed (mm/s): 0.35 mm/s

**Burning Sample Data**

Material: 3/4" PMMA Sheet

Dimension(LxWxH, mm): 600x152x6.35

**Instrumentation**

Number of Thermocouples: 5

Number of Heat Flux Gauges: 2

Station	Sensor	x (mm)	z (mm)	File Column	Note
1	TC	178	1.38	B	GAS TC1
1	TC	178	0	C	SURFACE TC1
2	TC	353	1.43	D	GAS TC2
2	TC	353	0	E	SURFACE TC2
2	HG	353	0	G	SERIAL 86862
3	TC	578	0	F	SURFACE TC3
3	HG	578	0	H	SERIAL 525842

**Experiment**

Flux Gauge Reading @ 425 mm (Serial No. 27844, mV): 3.0-10.3448kW/m<sup>2</sup>

Preheating Time without Pilot Flame (seconds): 240

Time to Sample Ignition After Applying the Pilot Flame (seconds): 105

Speed Used (S1M"Steps"): 55

Number of Steps (I1M"Steps"): 80629

File Names (.PRN): M10K812

Set-up File Name:

Sampling Rate (Hz): 5      Duration of Sampling (sec): 2500

Time to Start Moving the Sample (sec): 452.8

Ignition Heat Flux (Calculated, kW/m<sup>2</sup>): 23.5

Ambient Conditions 25.5

Temperature (°C): 22.

Observations Burning area 12.5 cm, constant

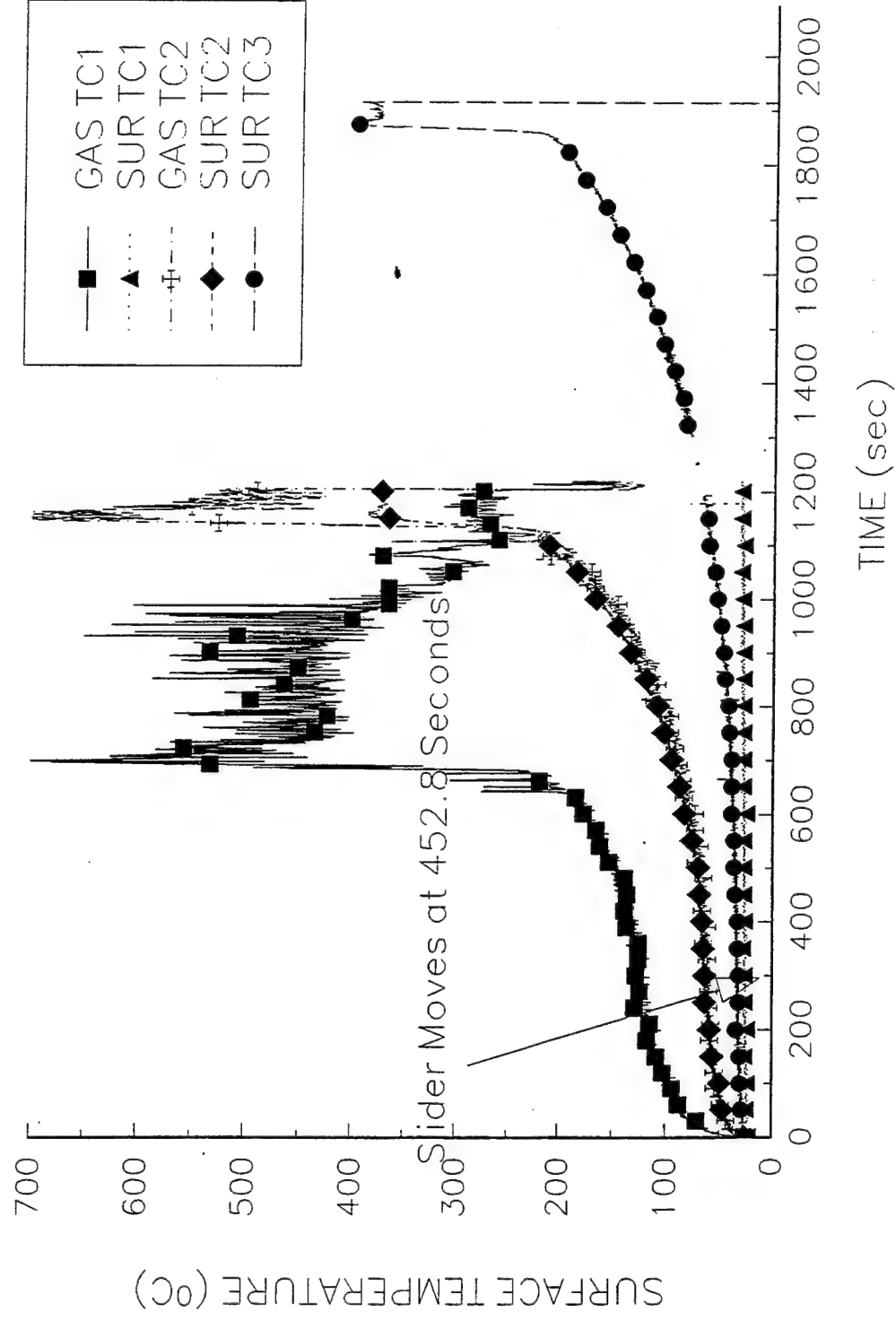
Personnel Rich Kashian, Y.C.

Processing of Data: SUR TC2,  $1/\tau=0.14$ ,  $T_p=370^\circ\text{C}$ ,  $T_{ext}=227.8^\circ\text{C}$ ,  
 $k\rho c=0.2798 \times 1200 \times 2200=738672$

$$\dot{q}_0'' = (\pi k \rho c)^{1/2} (T_p - T_{ext}) (V/\delta)^{1/2} = (738672)^{1/2} \times (370 - 227.8) (0.14)^{1/2} = 46.53 \text{ kW/m}^2$$

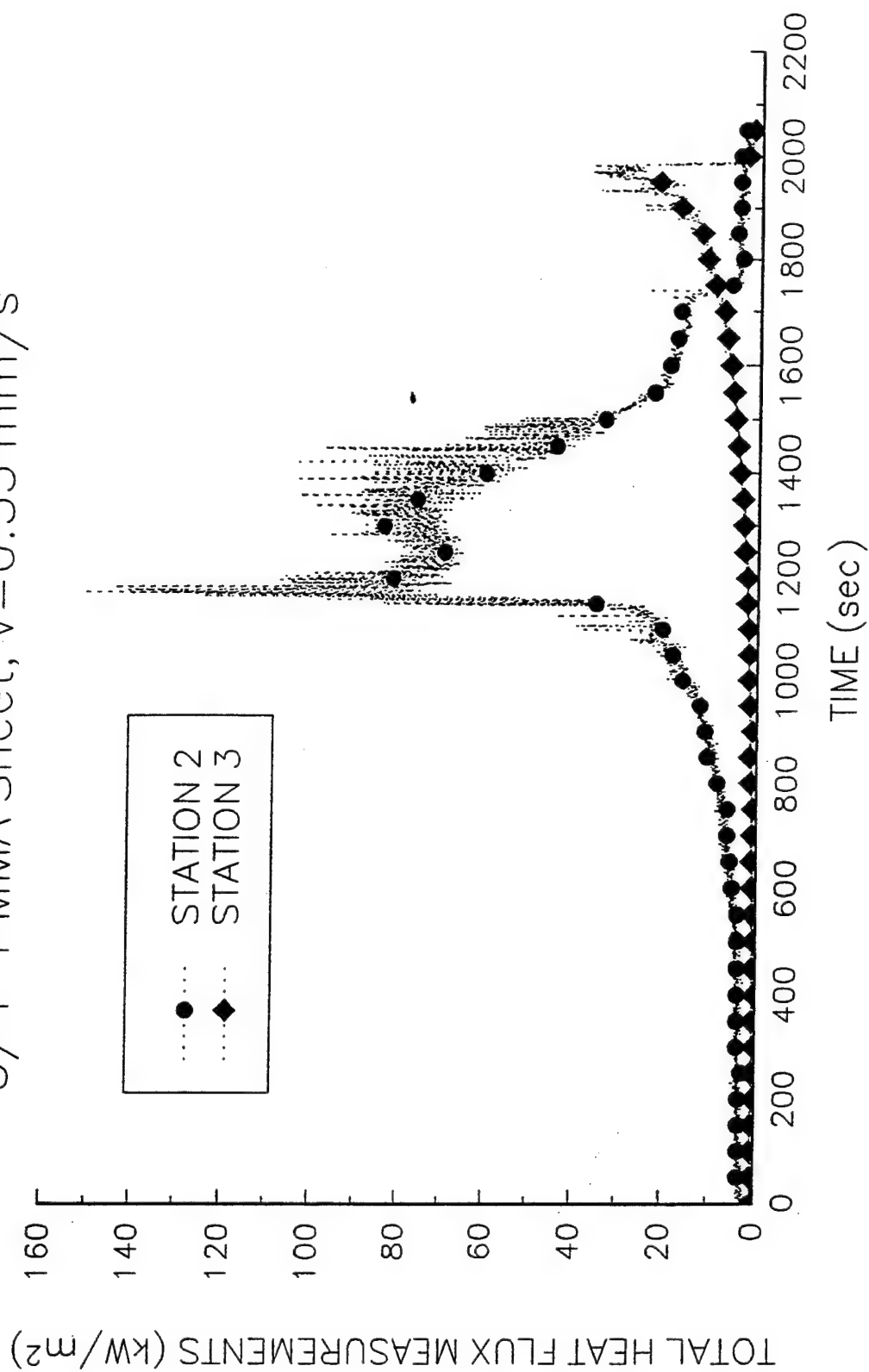
M10K812

3/4" PMMA Sheet,  $V=0.35$  mm/s



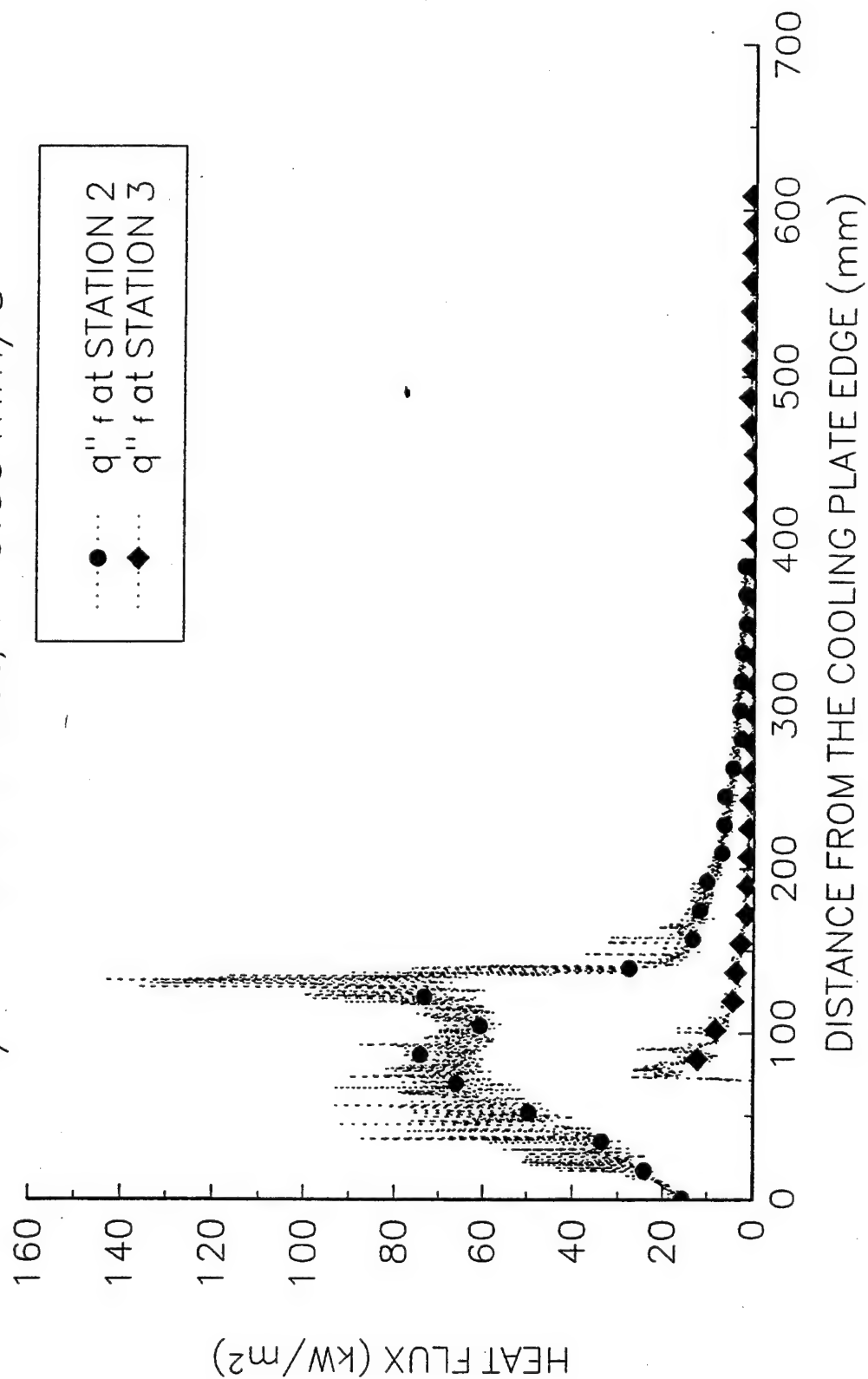
M10K812

3/4" PMMA Sheet,  $V=0.35$  mm/s



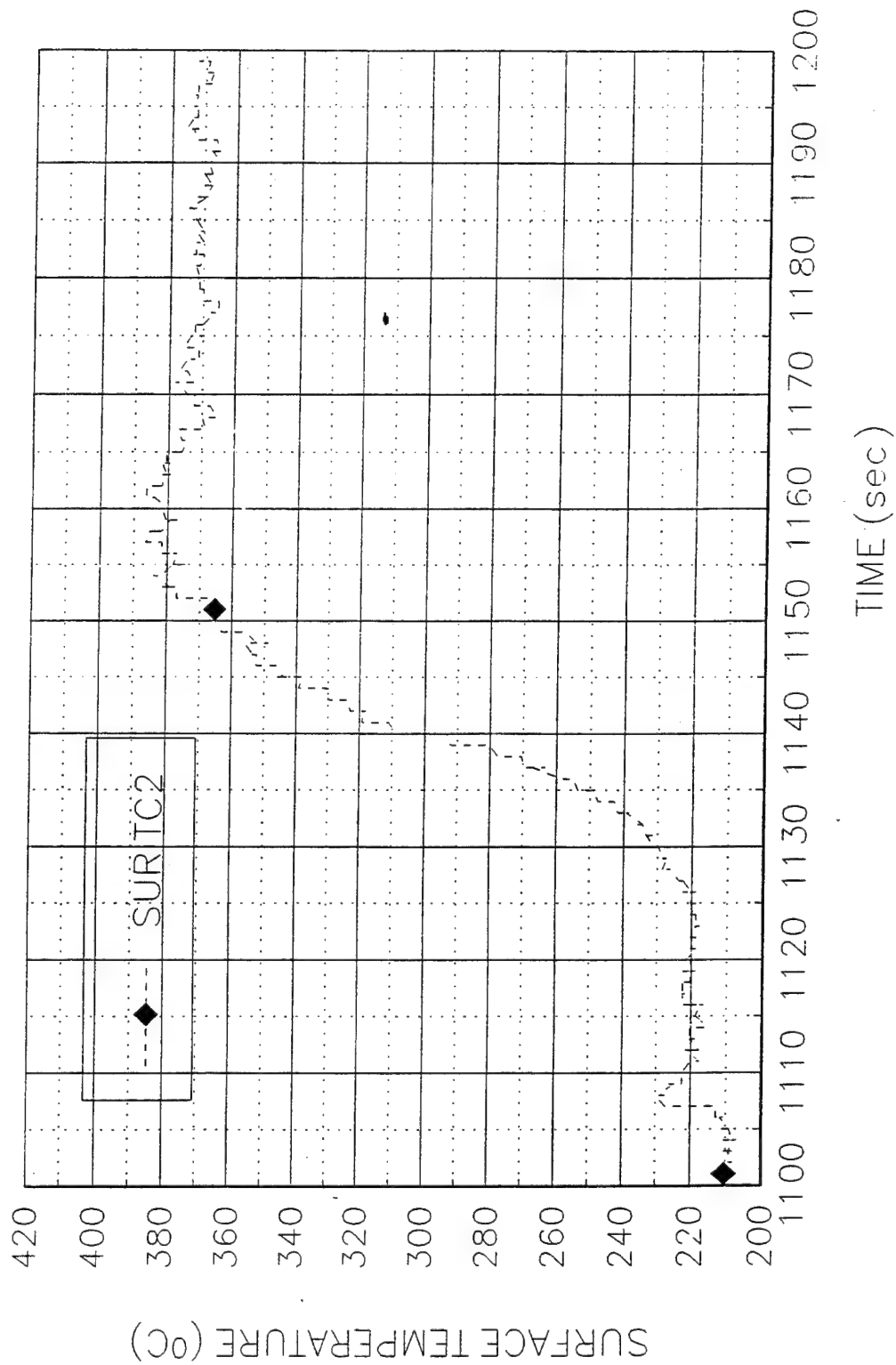
M10K812

3/4" PMMA Sheet,  $V=0.35$  mm/s



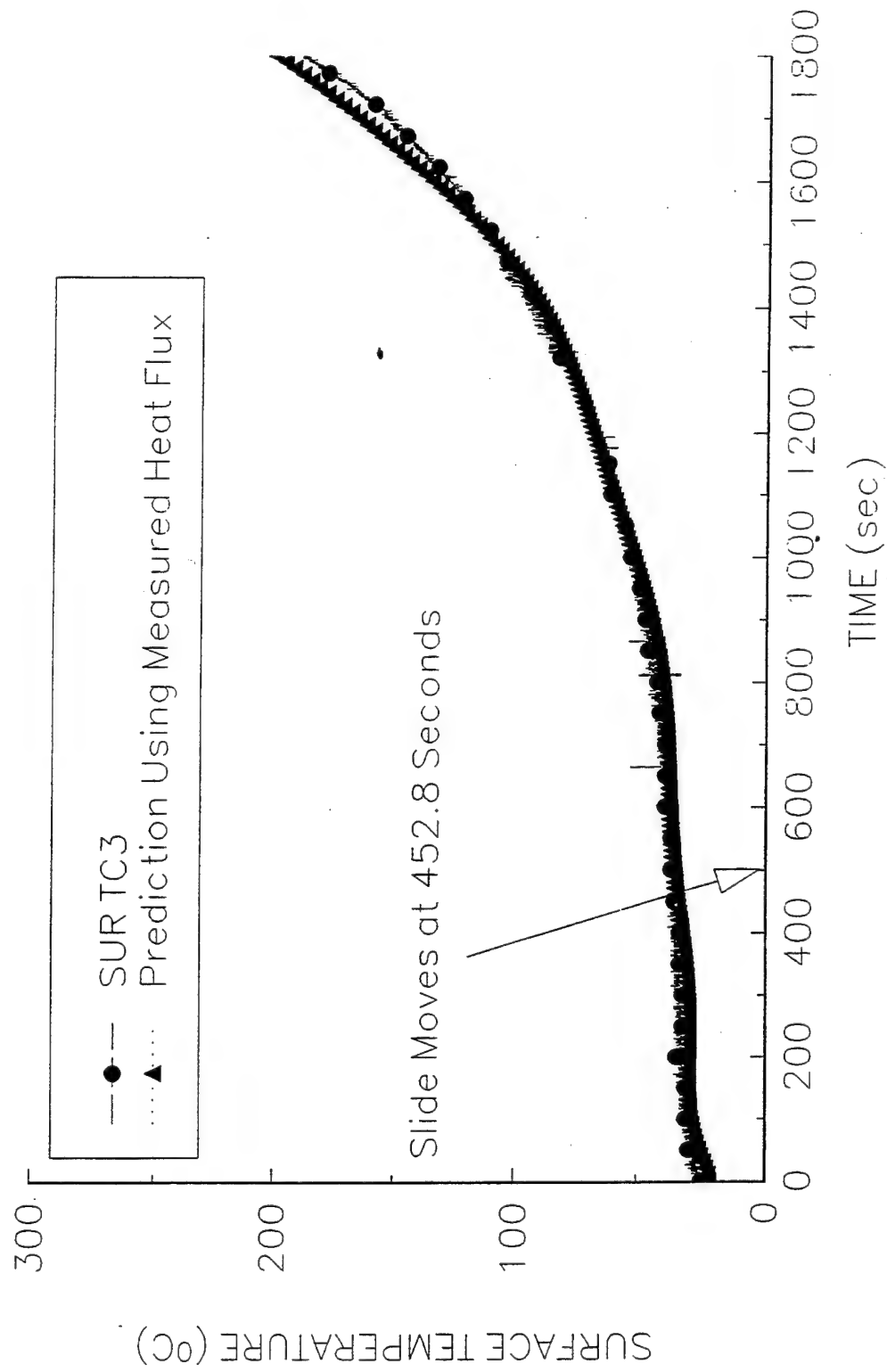
M10K812

3/4" PMMA Sheet, V=0.35 mm/s



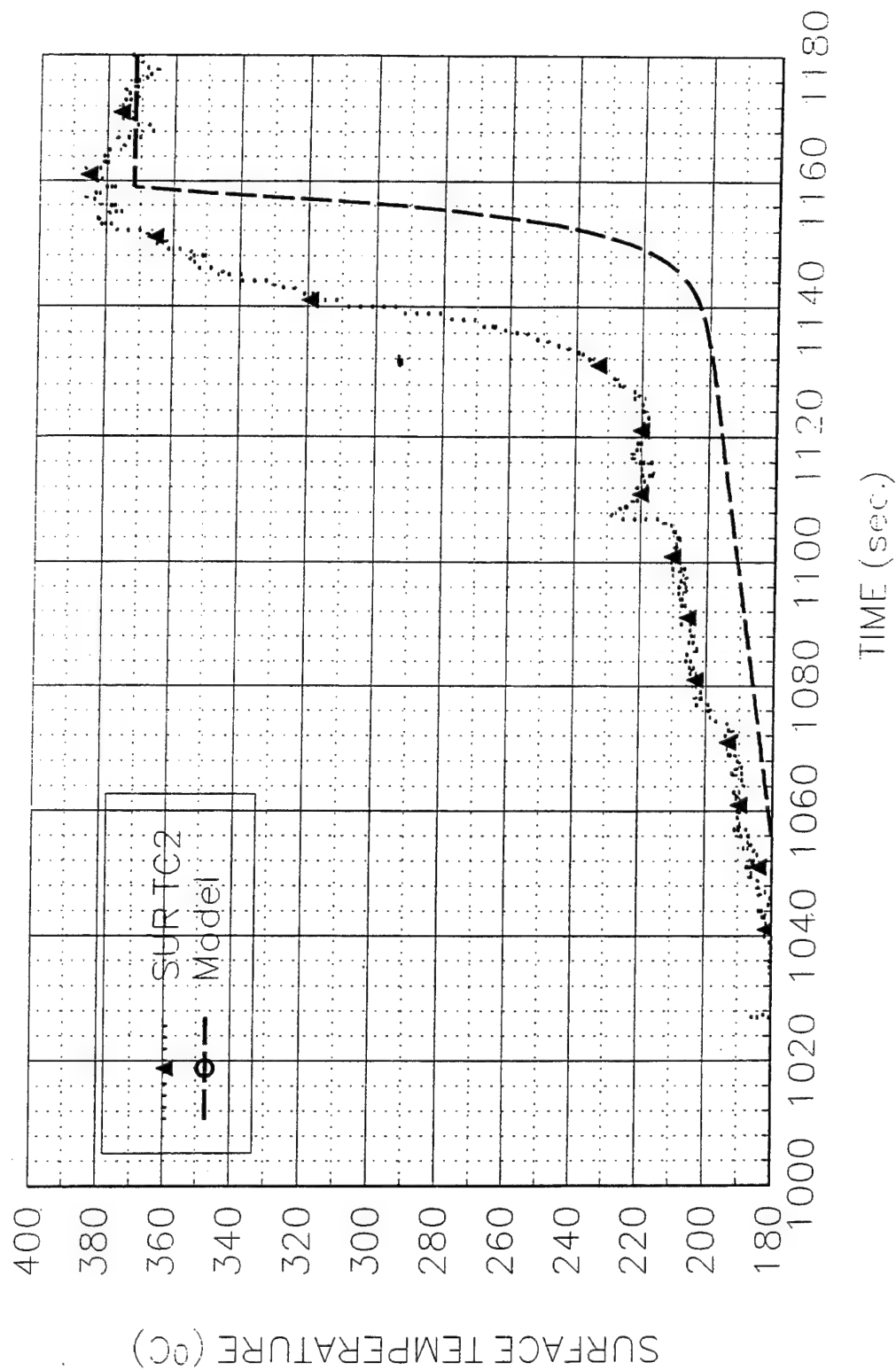
MI 01-812

3/4" PMMA Sheet,  $V=0.35$  mm/s



M101812

3/4" PMMA Sheet,  $V=0.35$  mm/s



**Data Sheet**  
**Constant Horizontal Flame Spread Experiment**

Experimental No.: 32

Date: 7/8/94 Tu

Time: 11.30 am

**Pre-Experiment**

Heat Flux at 425 mm Location (Planned) (kW/m<sup>2</sup>): 20

Slider Speed (mm/s): 1.27 mm/s

**Burning Sample Data**

Material: 3/4" PMMA Sheet

Dimension(LxWxH, mm): 600x152x6.35

**Instrumentation**

Number of Thermocouples: 3

Number of Heat Flux Gauges: 2

Station	Sensor	x (mm)	z (mm)	File Column	Note
1	TC			N/A	GAS TC1
1	TC	175	0	B	SURFACE TC1
2	TC			N/A	GAS TC2
2	TC	338	0	C	SURFACE TC2
2	HG			N/A	SERIAL 86862
3	TC	572	0	D	SURFACE TC3
3	HG	572	0	E	SERIAL 525842

**Experiment**

Flux Gauge Reading @ 425 mm (Serial No. 27844, mV): 5.90-20.5156 kW/m<sup>2</sup>

Preheating Time without Pilot Flame (seconds): 90

Time to Sample Ignition After Applying the Pilot Flame (seconds): 10

Speed Used (S1M"Steps"): 200

Number of Steps (I1M"Steps"): 100000

File Names (.PRN): M20K708

Set-up File Name:

Sampling Rate (Hz): 5      Duration of Sampling (sec): 1500

Time to Start Moving the Sample (sec): 143.6

Ignition Heat Flux (Calculated, kW/m<sup>2</sup>):

**Ambient Conditions**

Temperature (°C): 25

Observations Burning width ~7.5 cm

Personnel V.M., Y.C

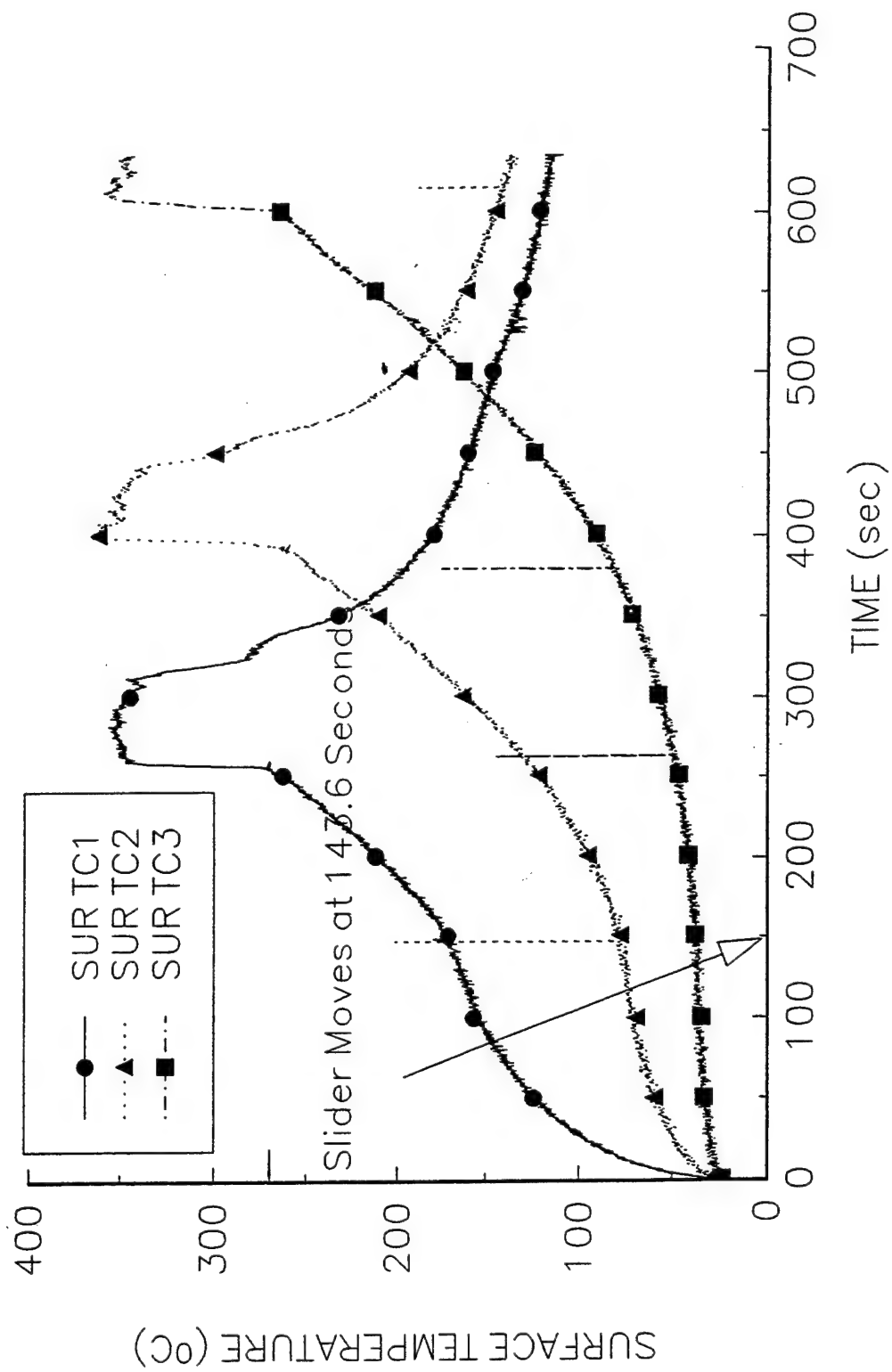
Processing of Data: Surface TC1:  $1/\tau = 0.65, T_p = 370^\circ\text{C}, T_{\text{ext}} = 269.6^\circ\text{C},$   
 $k\rho c = 0.2798 \times 1200 \times 2200 = 738672,$   $\dot{q}_0'' = (k\rho c)^{1/2} (T_p - T_{\text{ext}}) (1/\tau)^{1/2} = (738672)^{1/2} \times (370 - 269.6) (0.65)^{1/2} = 69.44 \text{ kW/m}^2$

Surface TC2:  $1/\tau = 0.73, T_p = 370^\circ\text{C}, T_{\text{ext}} = 269.6^\circ\text{C},$   $\dot{q}_0'' = (k\rho c)^{1/2} (T_p - T_{\text{ext}}) (1/\tau)^{1/2} = (738672)^{1/2} \times (370 - 269.6) (0.73)^{1/2} = 73.72 \text{ kW/m}^2$



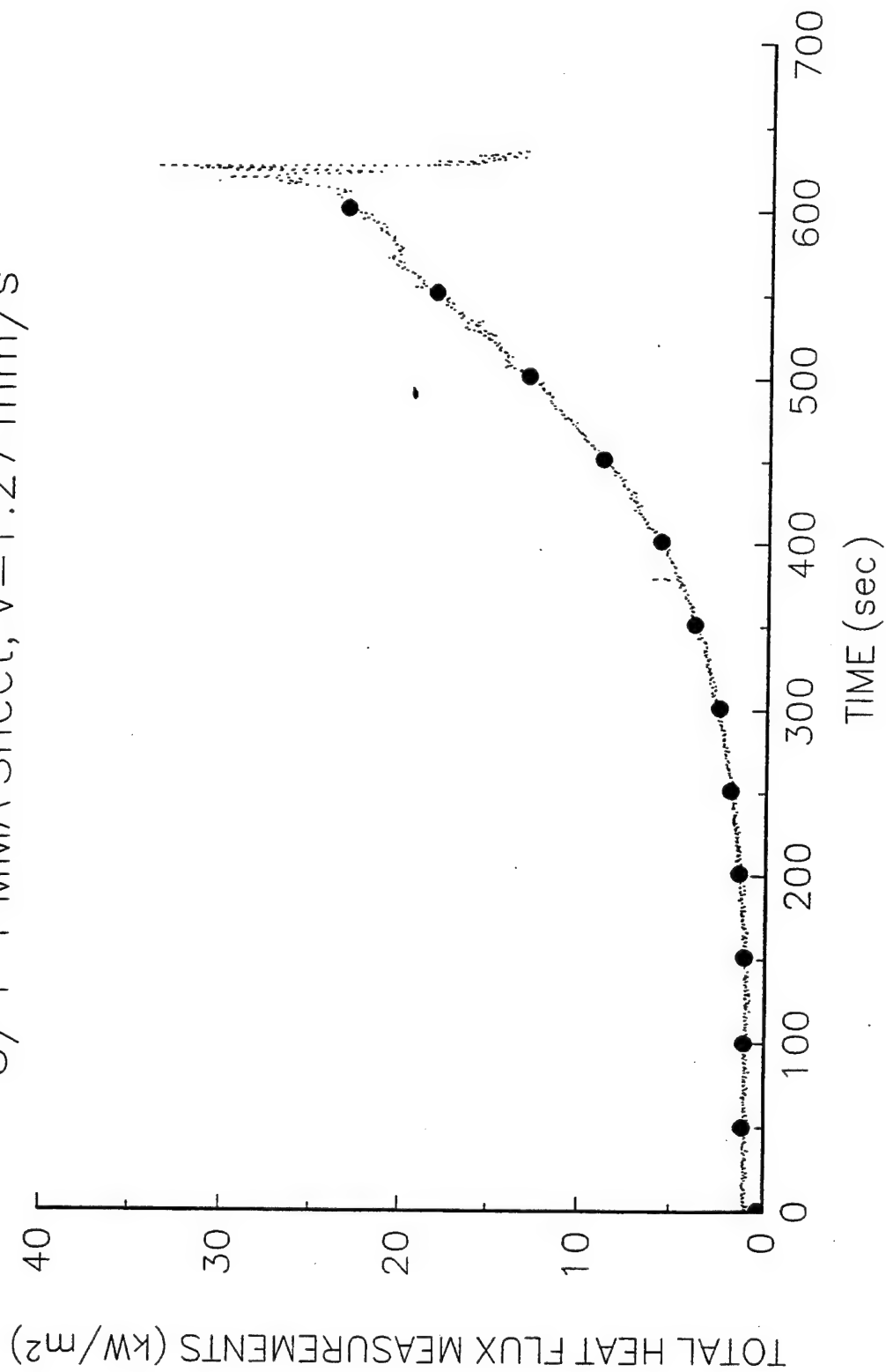
M20K708

3/4" PMMA Sheet,  $V=1.27 \text{ mm/s}$



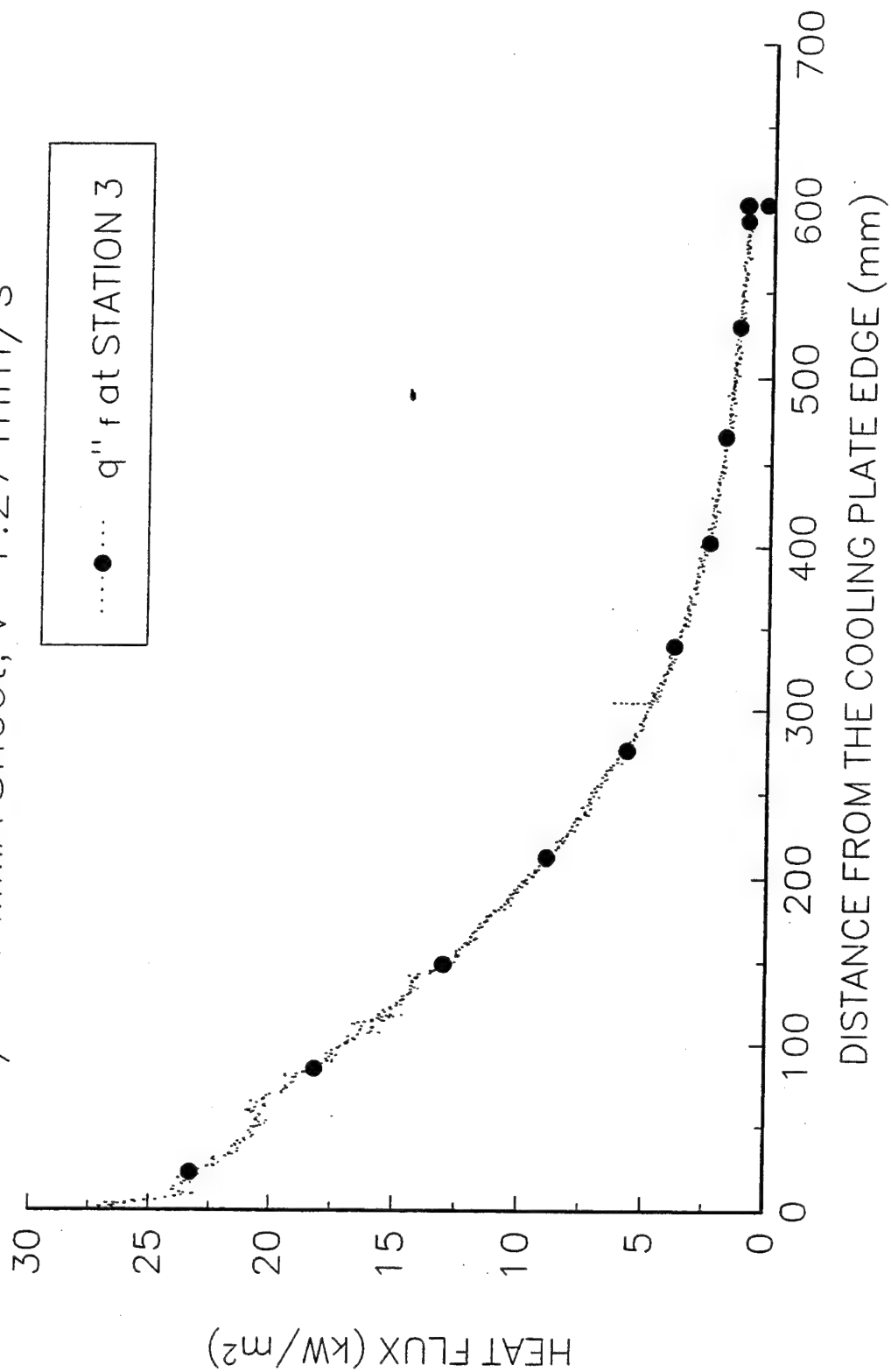
M20K708

3/4" PMMA Sheet,  $V=1.27$  mm/s



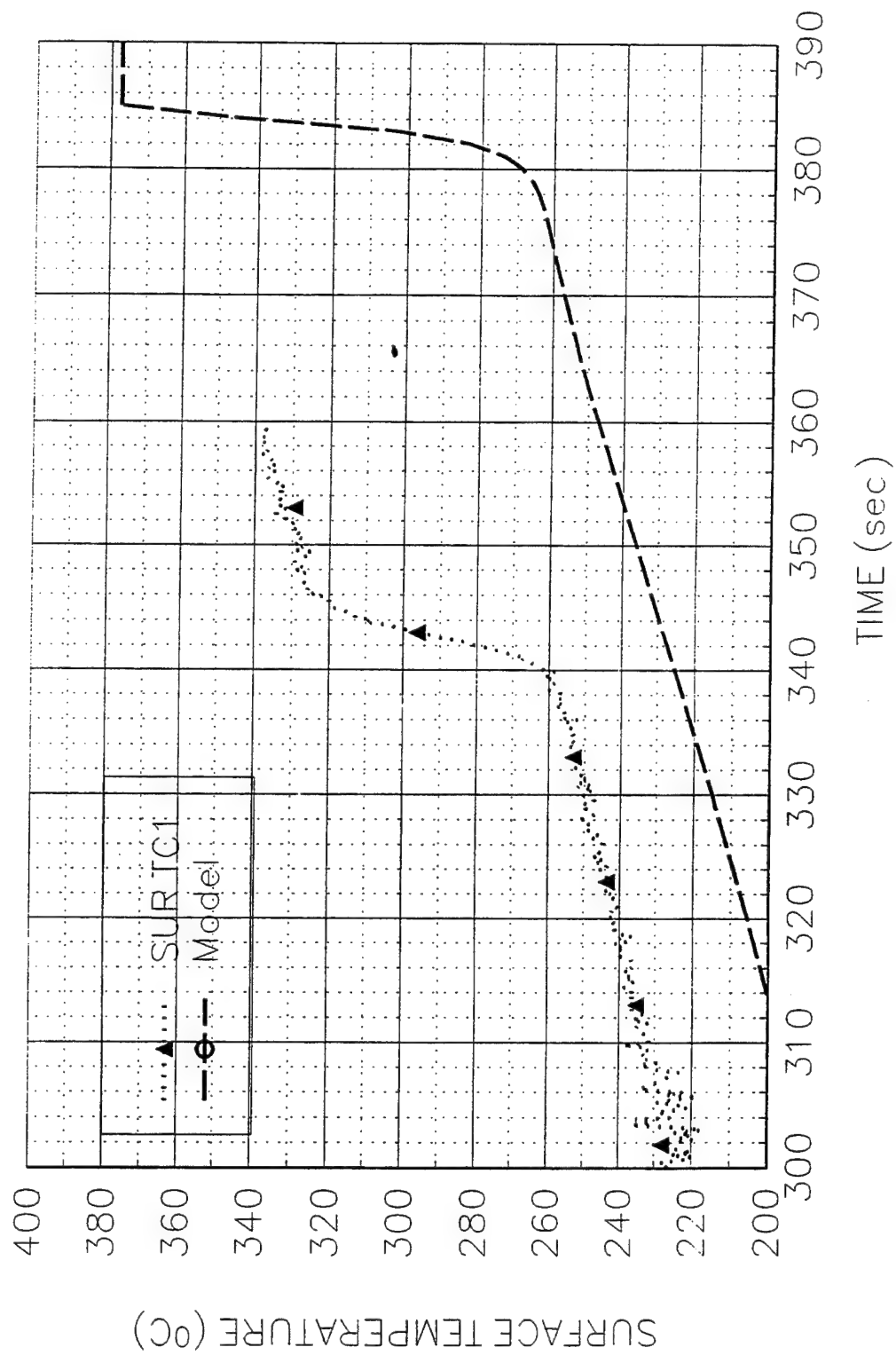
M20K708

3/4" PMMA Sheet,  $V=1.27$  mm/s



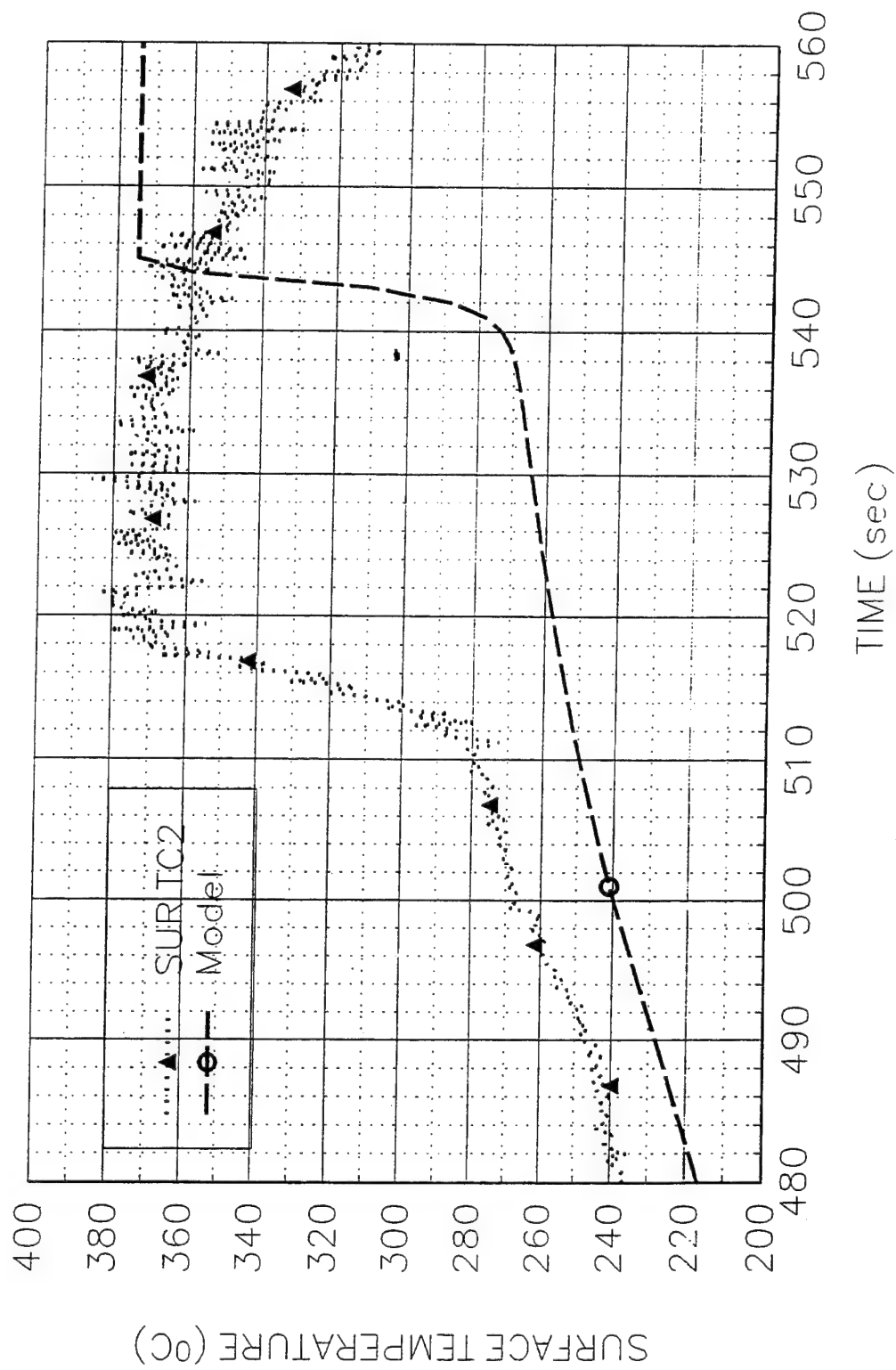
M201809

3/4" PMMA Sheet,  $V=1.27$  mm/s



M201-809

3/4" PMMA Sheet,  $V=1.27$  mm/s



**Data Sheet**  
**Constant Horizontal Flame Spread Experiment**

Experimental No.: 39

Date: 8/12/94 Fri

Time: 6.30 pm

**Pre-Experiment**

Heat Flux at 425 mm Location (Planned) (kW/m<sup>2</sup>): 30

Slider Speed (mm/s): 1.90 mm/s

**Burning Sample Data**

Material: 3/4" PMMA Sheet

Dimension(LxWxH, mm): 600x152x6.35

**Instrumentation**

Number of Thermocouples: 5

Number of Heat Flux Gauges: 2

Station	Sensor	x (mm)	z (mm)	File Column	Note
1	TC	176	1.38	B	GAS TC1
1	TC	176	0	C	SURFACE TC1
2	TC	350	1.43	D	GAS TC2
2	TC	350	0	E	SURFACE TC2
2	HG	350	0	G	SERIAL 86862
3	TC	573	0	F	SURFACE TC3
3	HG	573	0	H	SERIAL 525842

**Experiment**

Flux Gauge Reading @ 425 mm (Serial No. 27844, mV): 8.7-29.9976 kW/m<sup>2</sup>

Preheating Time without Pilot Flame (seconds): 60

Time to Sample Ignition After Applying the Pilot Flame (seconds): 0

Speed Used (S1M"Steps"): 300

Number of Steps (I1M"Steps"): 80629

File Names (.PRN): M30K812

Set-up File Name:

Sampling Rate (Hz): 5      Duration of Sampling (sec): 2500

Time to Start Moving the Sample (sec): 121.4

Ignition Heat Flux (Calculated, kW/m<sup>2</sup>): 40.1

**Ambient Conditions**

Temperature (°C): 23.5

**Observations** Burning area 11 cm, constant

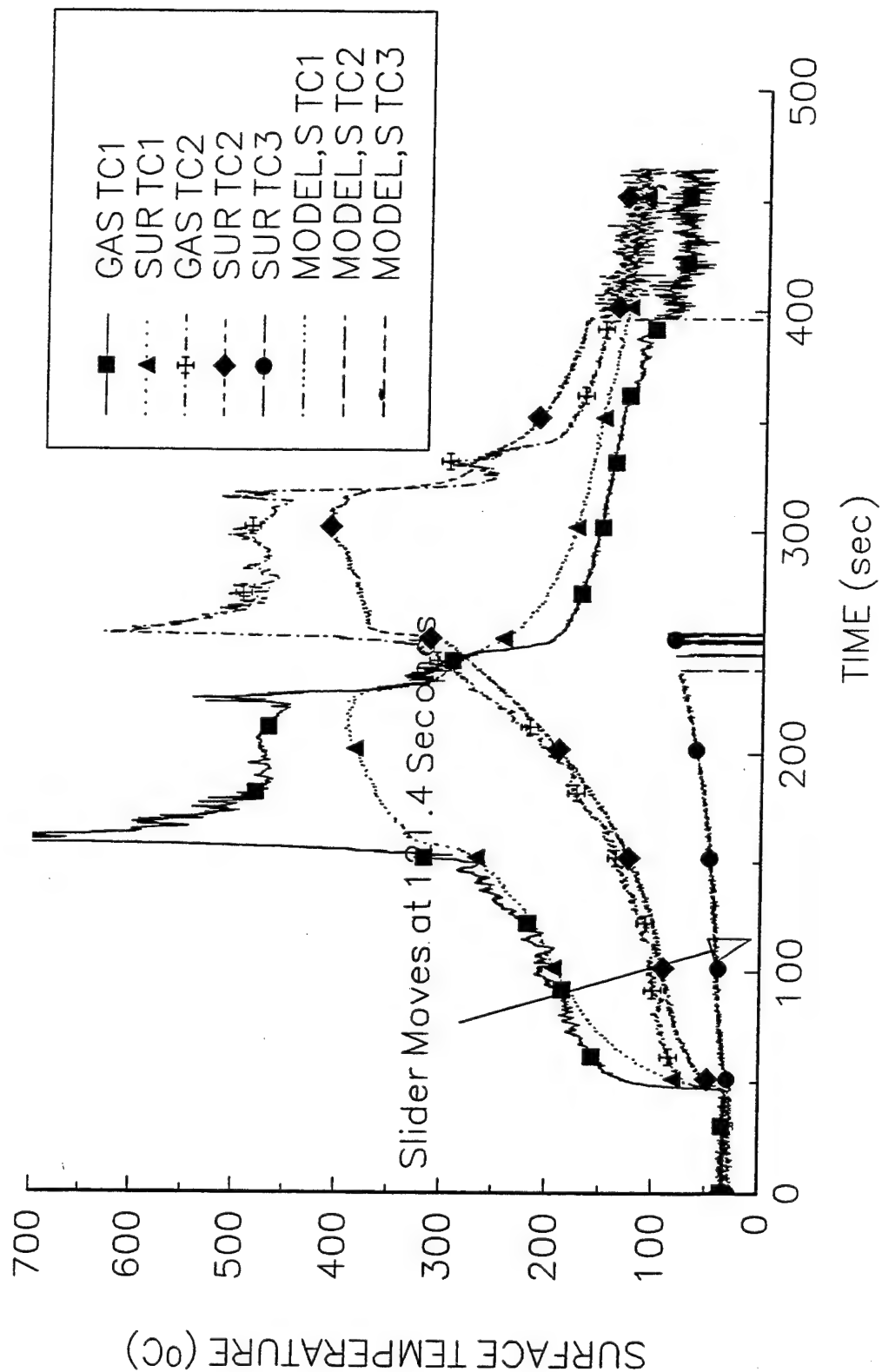
Personnel Rich Kashian, Y.C.

Processing of Data: SUR TC1,  $1/\tau=0.26$ ,  $T_p=370^\circ\text{C}$ ,  $T_{ext}=269.2^\circ\text{C}$ ,  
 $k\rho c=0.2798 \times 1200 \times 2200=738672$ ,  $\dot{q}_0''=(k\rho c)^{1/2}(T_p-T_{ext})(V/\delta)^{1/2}=(738672)^{1/2} \times (370-269.2)(0.26)^{1/2}=43.41 \text{ kW/m}^2$

SUR TC2,  $1/\tau=0.83$ ,  $T_p=370^\circ\text{C}$ ,  $T_{ext}=306.3^\circ\text{C}$ ,  $\dot{q}_0''=(k\rho c)^{1/2}(T_p-T_{ext})(V/\delta)^{1/2}=(738672)^{1/2} \times (370-306.3)(0.83)^{1/2}=52.00 \text{ kW/m}^2$

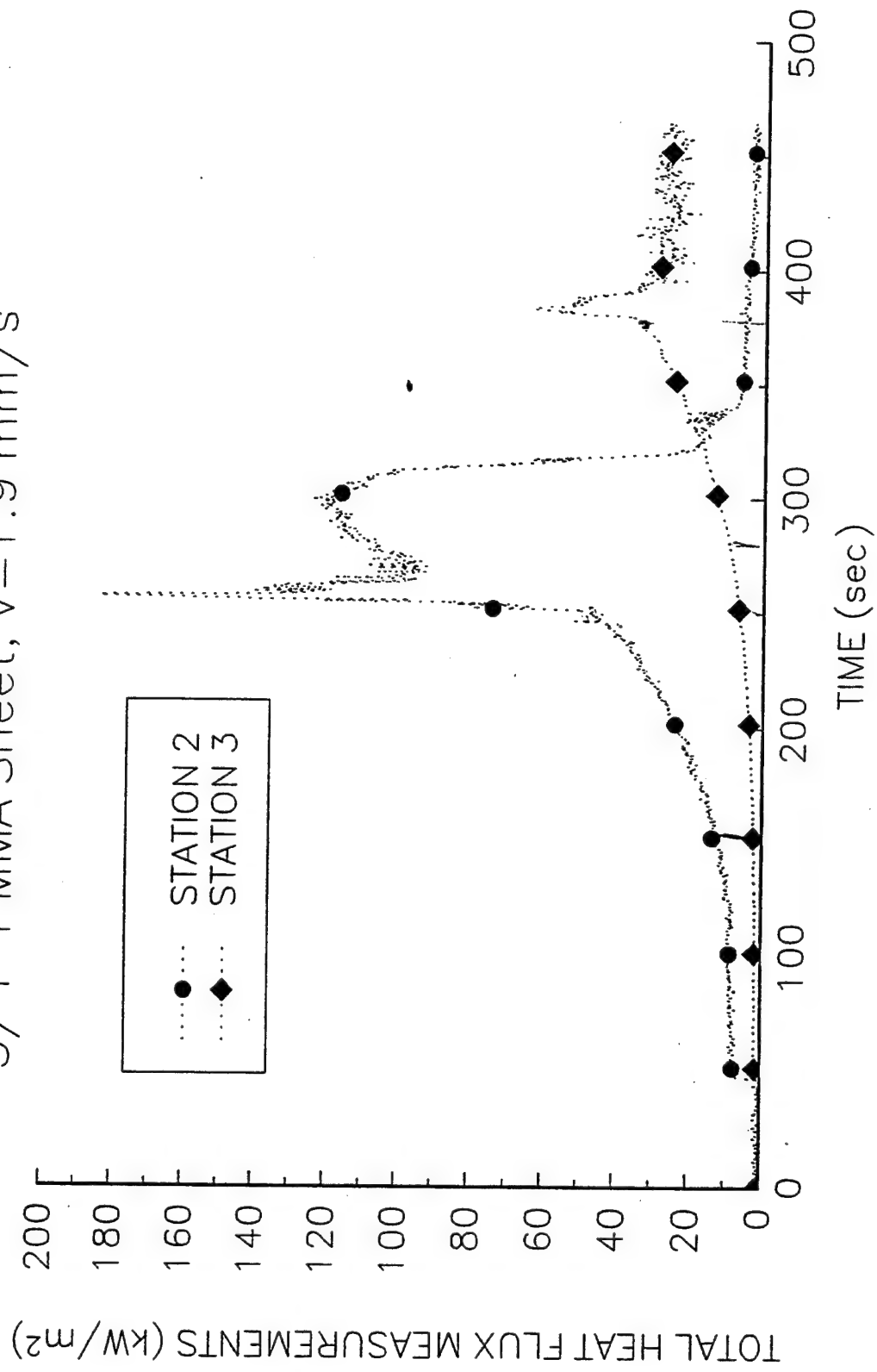
M30K812

3/4" PMMA Sheet,  $V=1.9 \text{ mm/s}$



M30K812

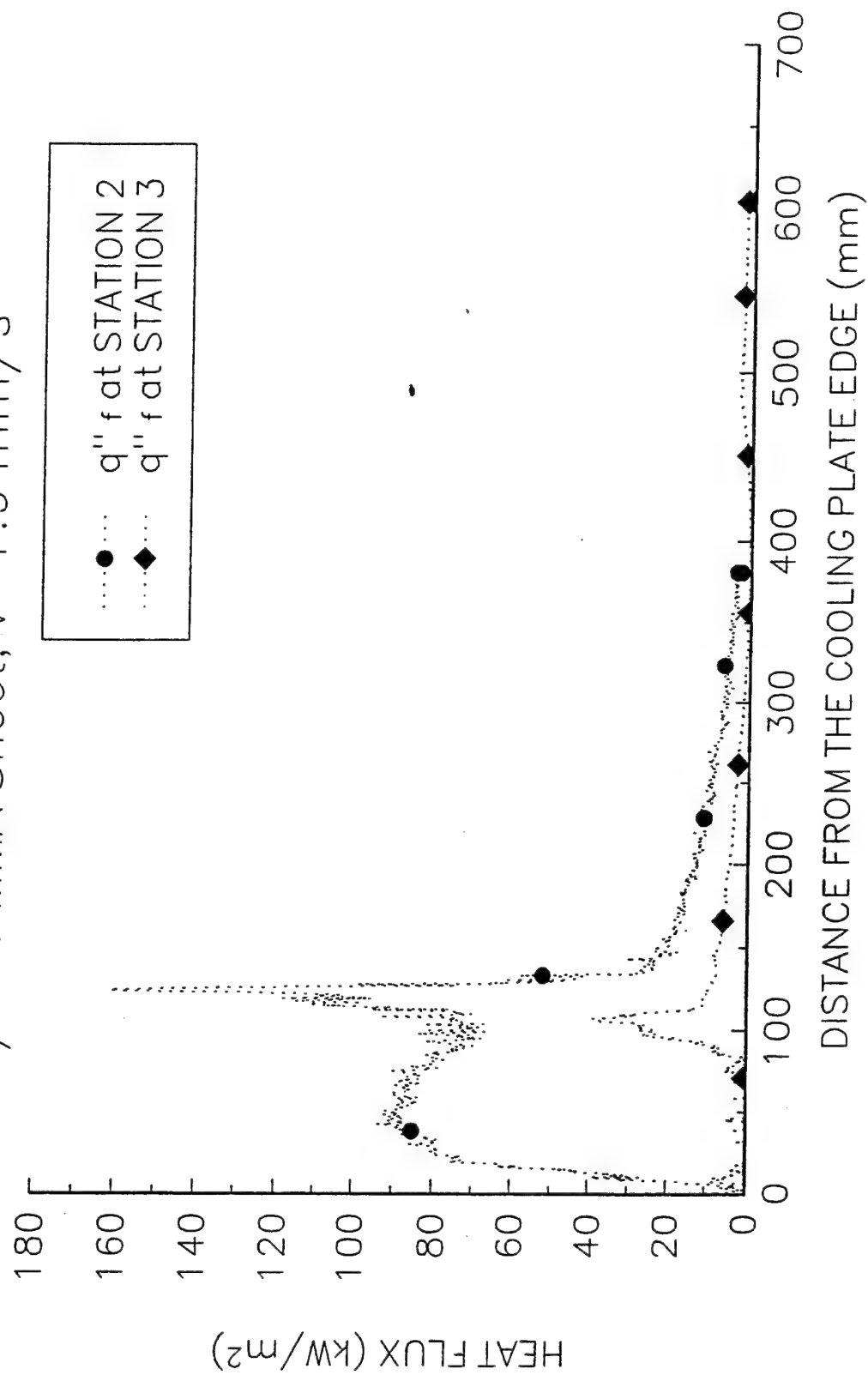
3/4" PMMA Sheet,  $V=1.9 \text{ mm/s}$





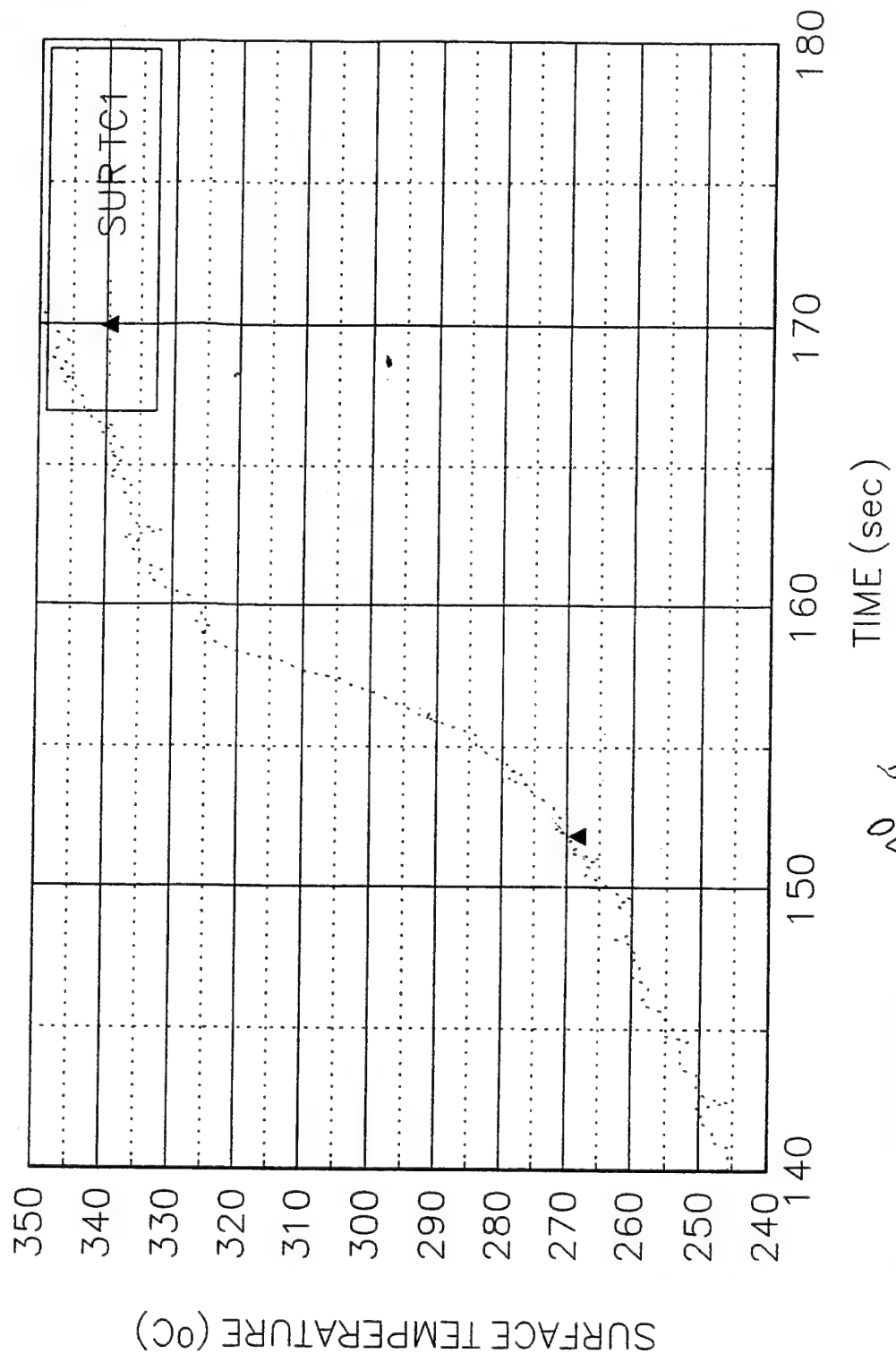
M30K812

3/4" PMMA Sheet,  $V=1.9 \text{ mm/s}$



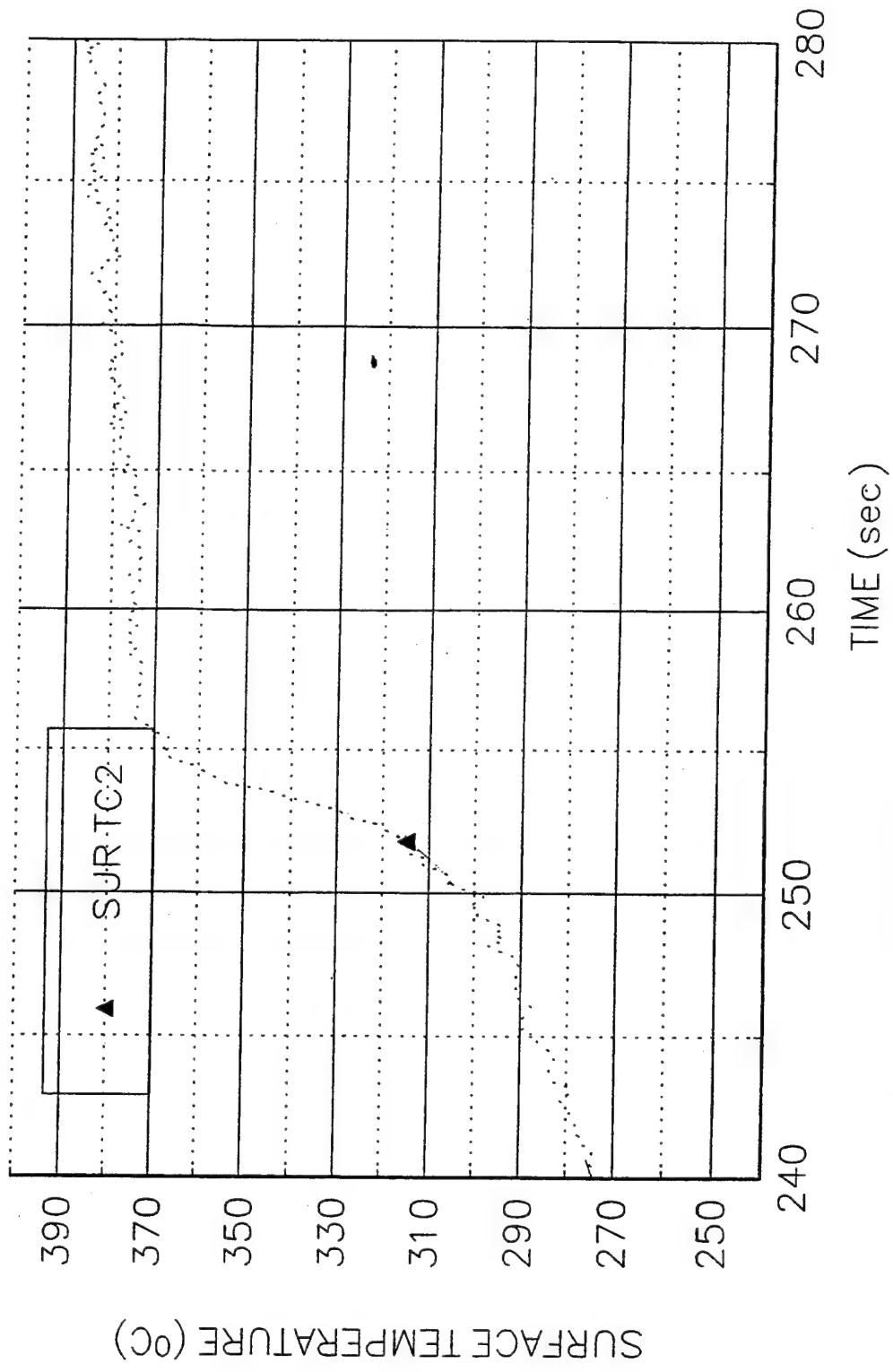
M30K812

3/4" PMMA Sheet, V=1.9 mm/s



M30K812

3/4" PMMA Sheet, V=1.9 mm/s



**Data Sheet**  
**Constant Horizontal Flame Spread Experiment**

Experimental No.: 40

Date: 8/16/94 Tu

Time: 10:30 am

**Pre-Experiment**

Heat Flux at 425 mm Location (Planned) (kW/m<sup>2</sup>): 30

Slider Speed (mm/s): 1.90 mm/s

**Burning Sample Data**

Material: 3/4" PMMA Sheet

Dimension(LxWxH, mm): 600x152x6.35

**Instrumentation**

Number of Thermocouples: 5

Number of Heat Flux Gauges: 2

Station	Sensor	x (mm)	z (mm)	File Column	Note
1	TC	176	1.38	B	GAS TC1
1	TC	176	0	C	SURFACE TC1
2	TC	350	1.43	D	GAS TC2
2	TC	350	0	E	SURFACE TC2
2	HG	350	0	G	SERIAL 86862
3	TC	573	0	F	SURFACE TC3
3	HG	573	0	H	SERIAL 525842

**Experiment**

Flux Gauge Reading @ 425 mm (Serial No. 27844, mV): 8.7-29.9976 kW/m<sup>2</sup>

Preheating Time without Pilot Flame (seconds): 60

Time to Sample Ignition After Applying the Pilot Flame (seconds): 0

Speed Used (S1M"Steps"): 300

Number of Steps (I1M"Steps"): 80629

File Names (.PRN): M30K816

Set-up File Name:

Sampling Rate (Hz): 5      Duration of Sampling (sec): 2500

Time to Start Moving the Sample (sec): ~~121.4~~ 74.7

Ignition Heat Flux (Calculated, kW/m<sup>2</sup>): ~~40.1~~ 43.3

**Ambient Conditions**

Temperature (°C): 20.

**Observations** Burning area 15 cm, original leading edge is 35.5 mm (?) ahead of ignition burner.  
Ignition burner is 403 mm from the panel lower edge

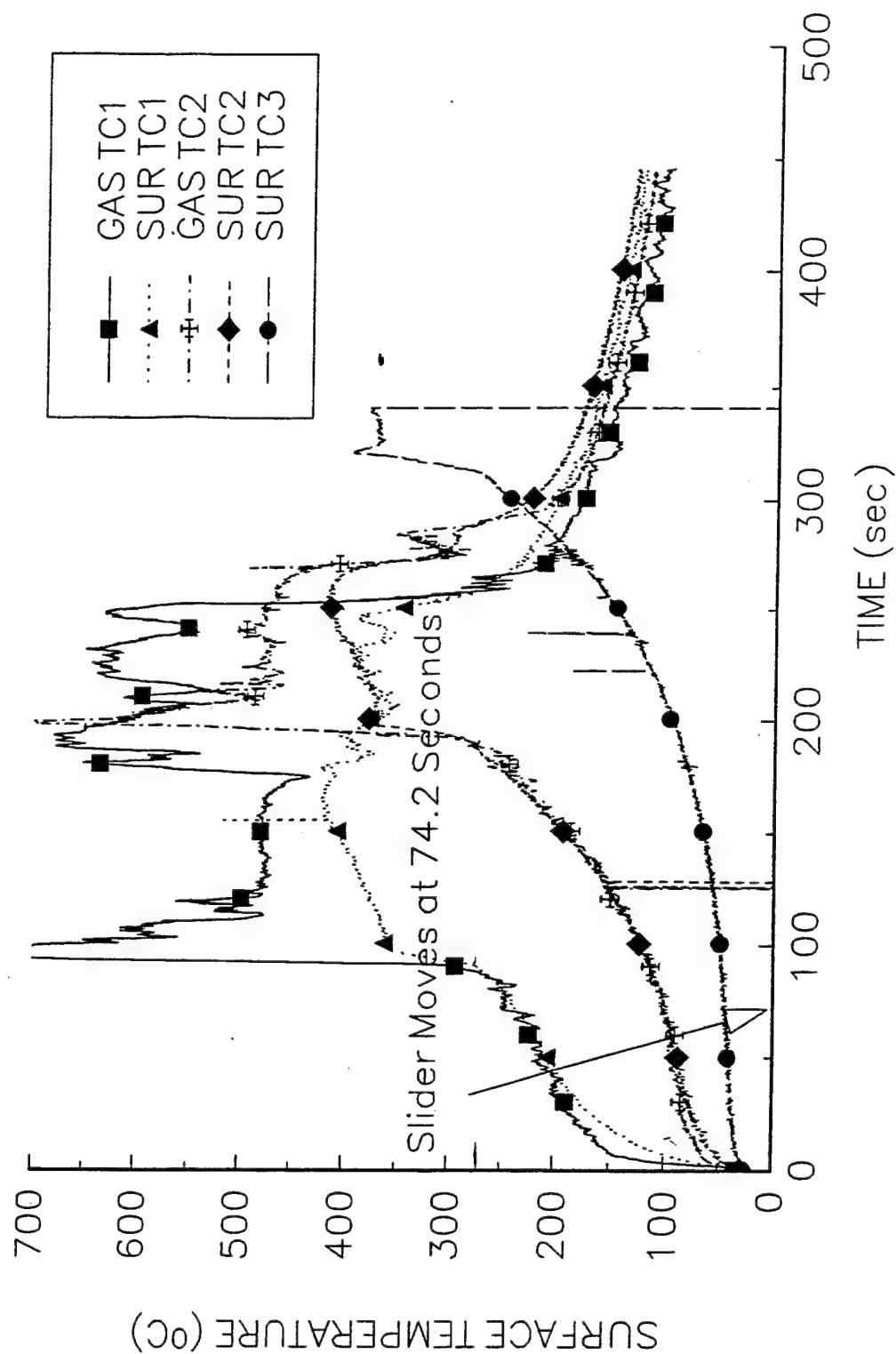
Personnel V.M., Y.C.

Processing of Data: SUR TC1,  $1/\tau=0.35$ ,  $T_p=370^\circ\text{C}$ ,  $T_{ext}=270.9^\circ\text{C}$ ,  
 $k\rho c=0.2798 \times 1200 \times 2200=738672$ ,  $\dot{q}_0''=(k\rho c)^{1/2}(T_p-T_{ext})(V/\delta)^{1/2}=(738672)^{1/2} \times (370-270.9)(0.35)^{1/2}=50.45 \text{ kW/m}^2$

SUR TC2,  $1/\tau=0.34$ ,  $T_p=370^\circ\text{C}$ ,  $T_{ext}=270.9^\circ\text{C}$ ,  $\dot{q}_0''=(k\rho c)^{1/2}(T_p-T_{ext})(V/\delta)^{1/2}=(738672)^{1/2} \times (370-270.9)(0.34)^{1/2}=49.94 \text{ kW/m}^2$

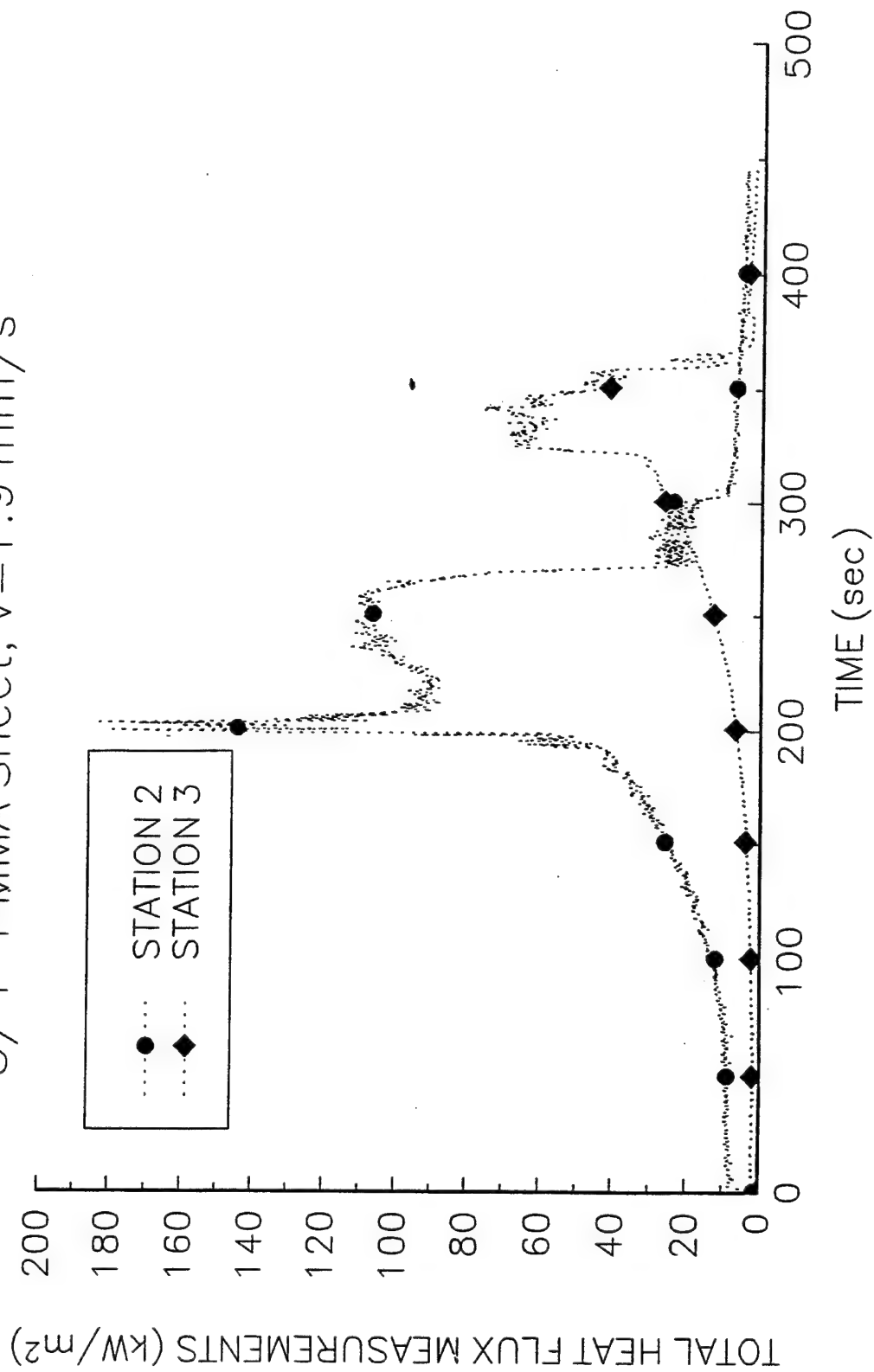
M30K816

3/4" PMMA Sheet,  $V=1.9 \text{ mm/s}$



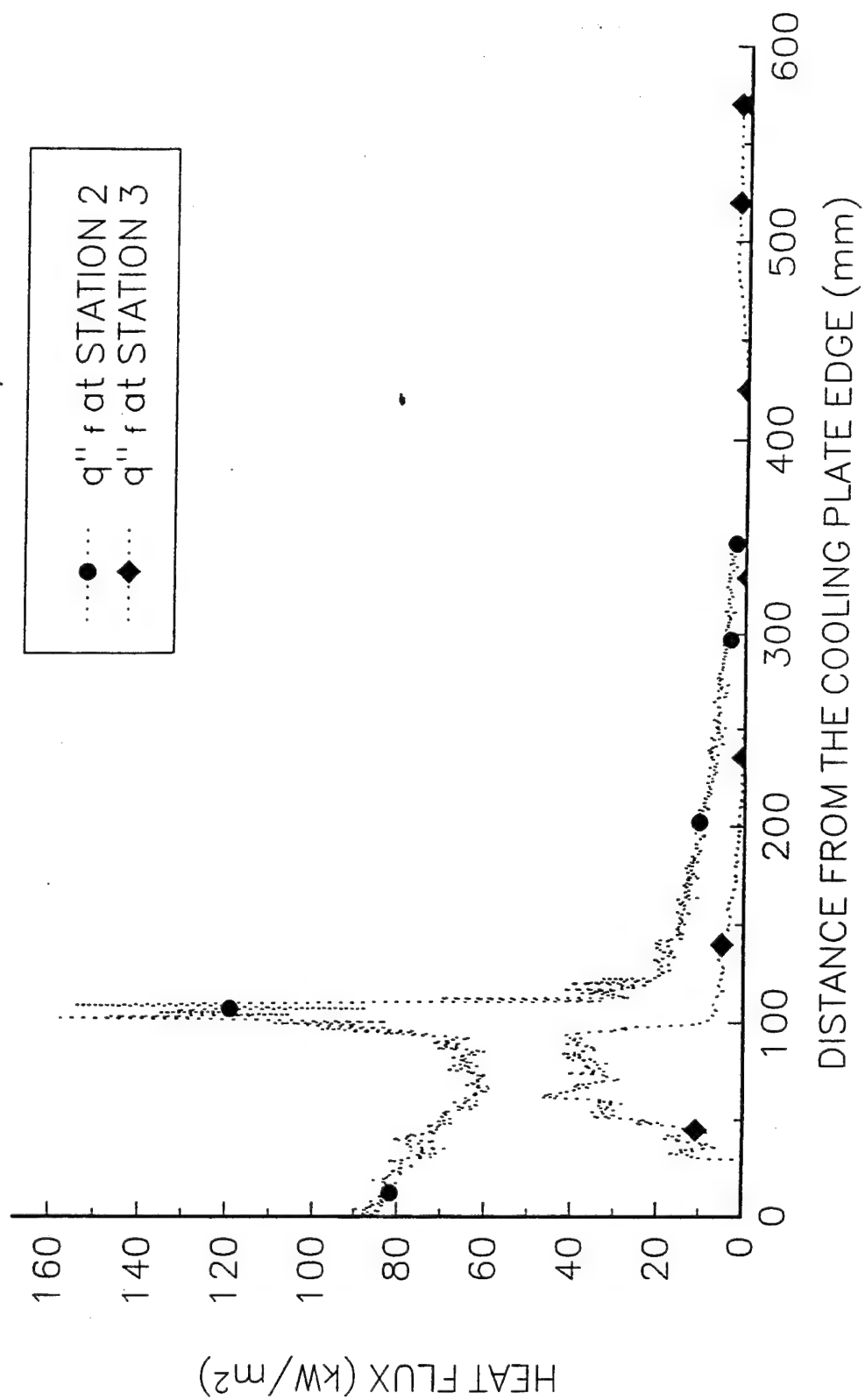
M30K816

3/4" PMMA Sheet,  $V=1.9 \text{ mm/s}$



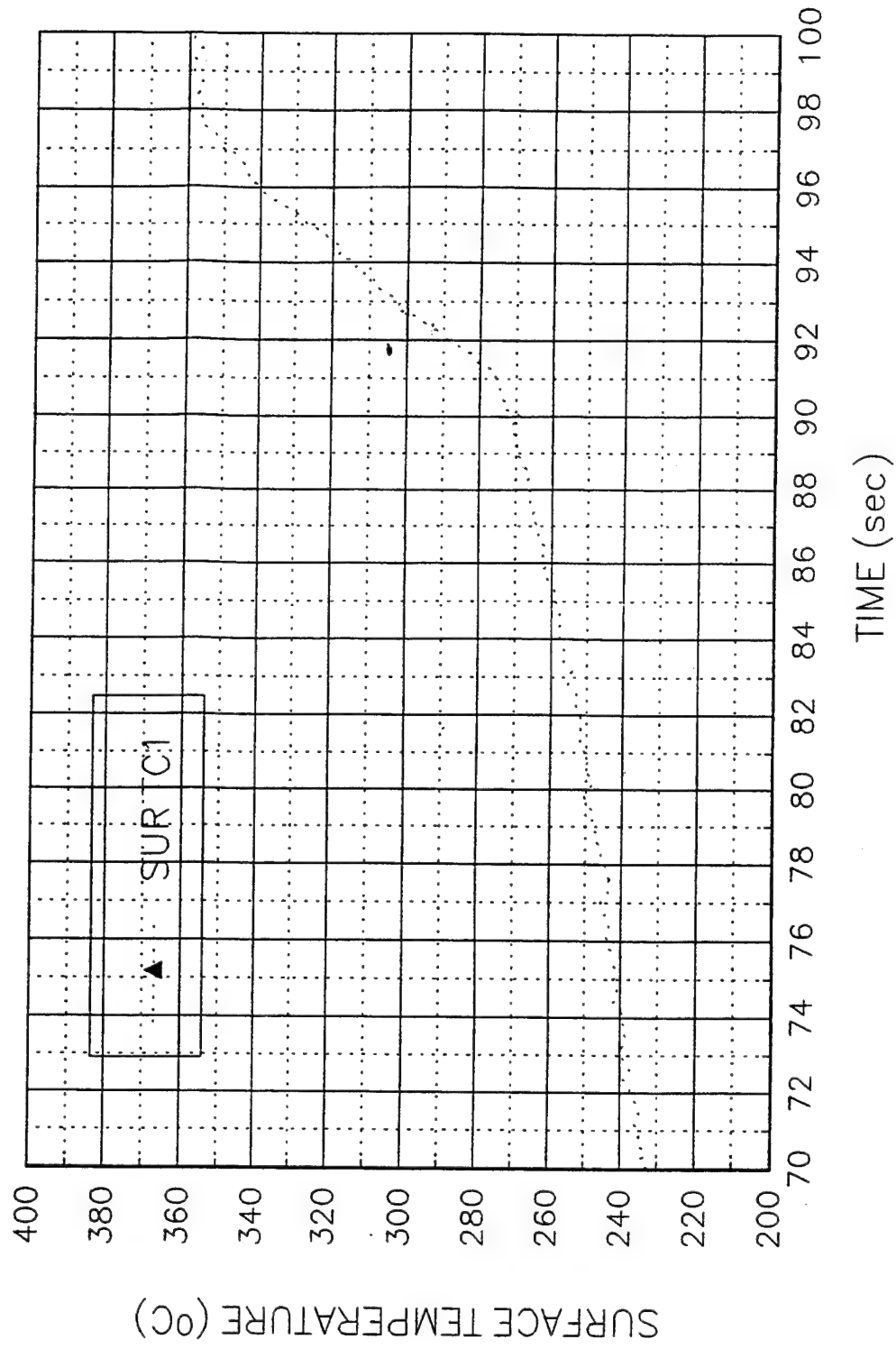
M30K816

3/4" PMMA Sheet,  $V=1.9 \text{ mm/s}$



M30K816

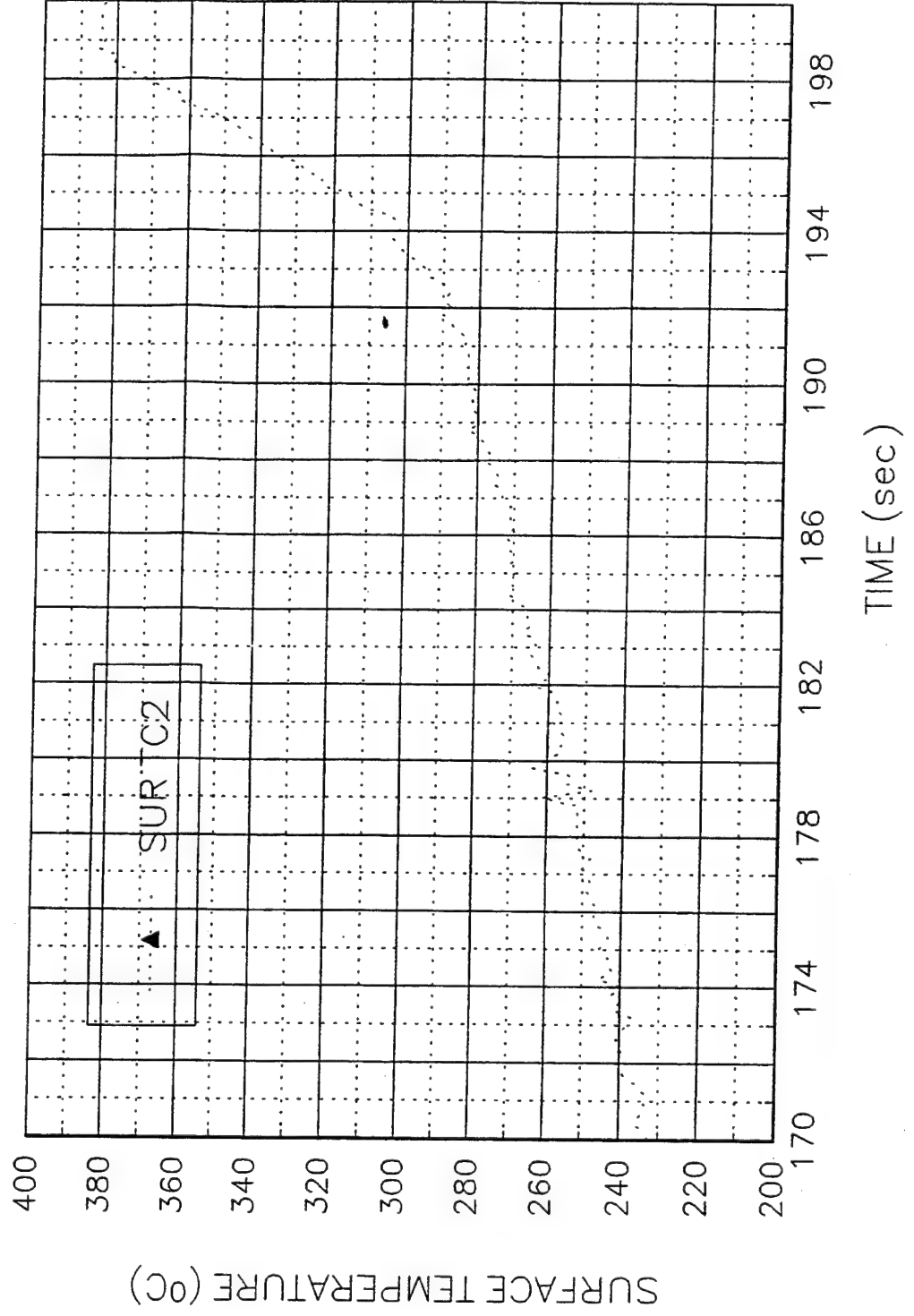
3/4" PMMA Sheet, V=1.9 mm/s





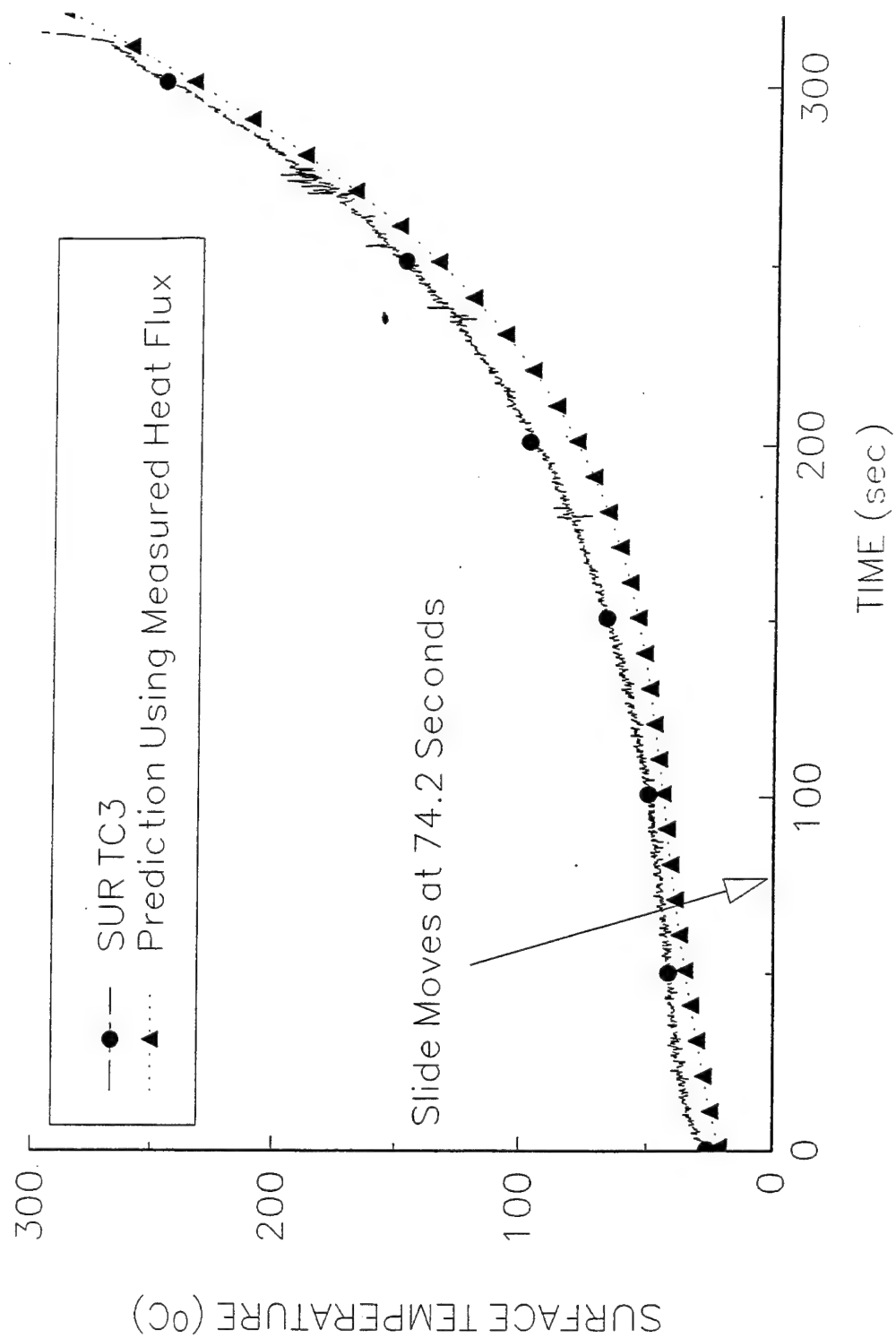
M30K816

3/4" PMMA Sheet, V=1.9 mm/s



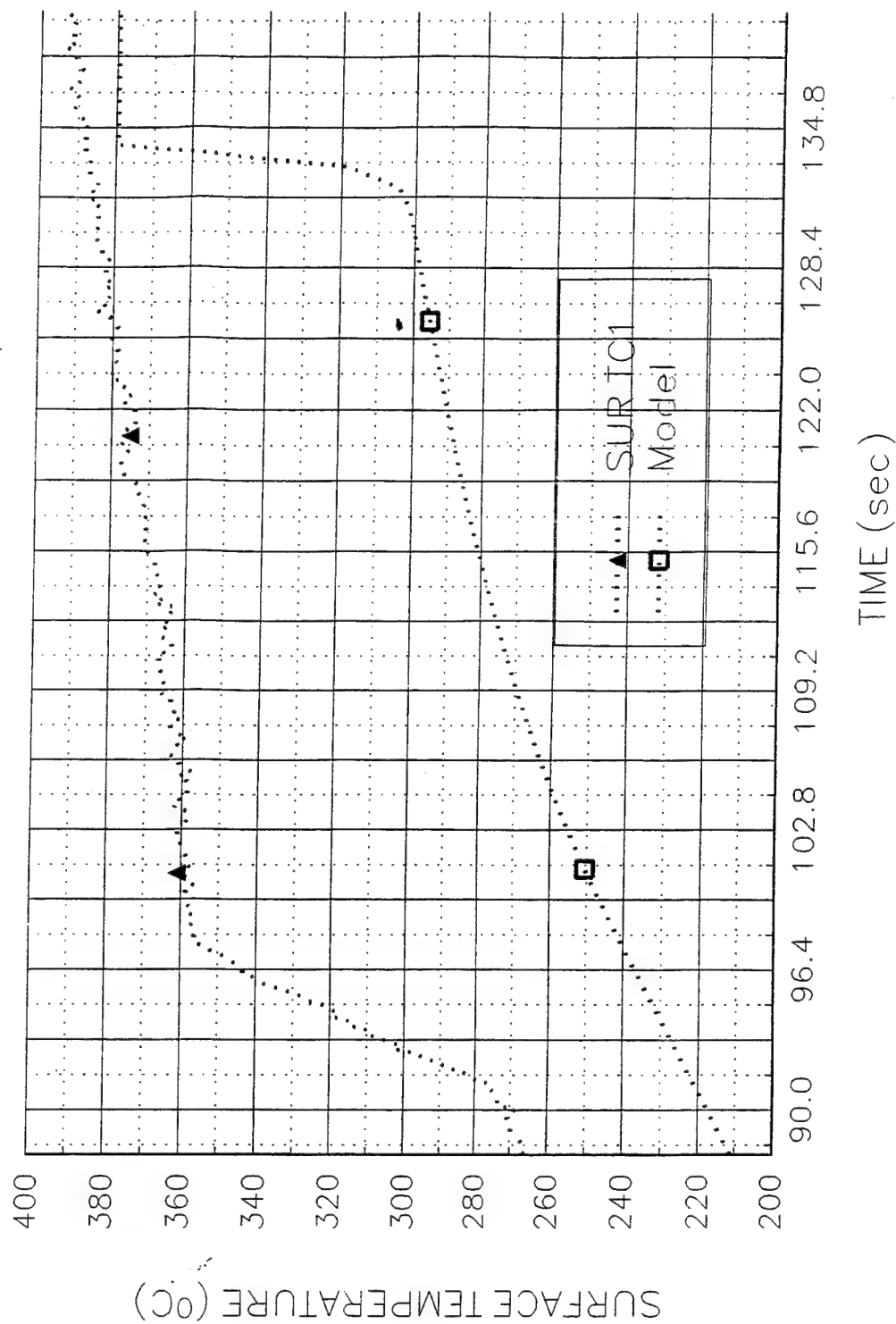
M30K816

3/4" PMMA Sheet,  $V=1.90 \text{ mm/s}$



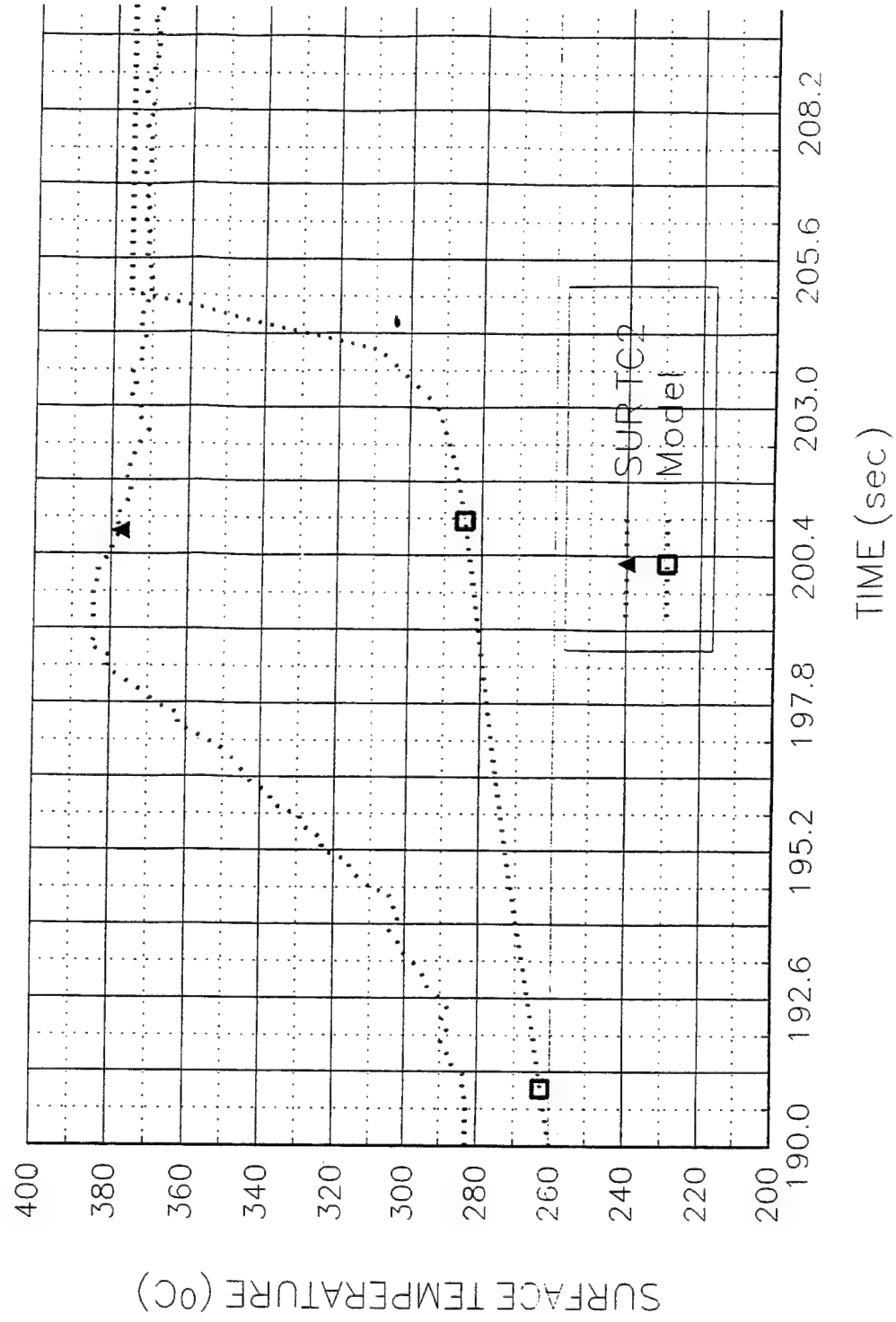
M30K816

3/4" PMMA Sheet, V=1.9 mm/s



M301-816

3/4" PMMA Sheet, V=1.9 mm/s



## Appendix M Tables of Char Depth Measurements

This Appendix contains the measurement of char depth along the particle board samples for all 3 external fluxes and 3 tests at each level. Measurements were made at every 5 cm along the length. At each of these locations, the center left and right measurements refer to the center of the specimen along the width, right and left were at mid points between the edge and the center. The specimen total thickness was also measured. Both measurements were averaged.

The test numbering system is as follows:

Letter

T: Particle board

P: PMMA sheet (6.35 mm thick - 1/4")

M: PMMA Sheet (19 mm thick - 3/4")

10k, 20k, 30k refer to the nominal external flux level in kW/m<sup>2</sup>.

Last 3 to four digits are the month and day of the test.

# Char depth raw data for Particle Board

Left, Middle and Right refer to approximate positions along the width of the test specimen

## Board A : TEST 26 30kW

Section (cm)	Board Thickness (in)			Char Thickness (in)			Board Averag	Char Averag
	Left	Middle	Right	Left	Middle	Right		
10	0.767	0.766	0.772	0.06	0.0545	0.0522	0.7683	0.05557
15	0.769	0.77	0.769	0.0601	0.0633	0.0544	0.7693	0.05927
20	0.768	0.767	0.77	0.0629	0.0495	0.0645	0.7683	0.05897
25	0.768	0.765	0.766	0.0543	0.04	0.0457	0.7663	0.04667
30	0.767	0.766	0.77	0.0546	0.0547	0.0531	0.7677	0.05413
40	0.764	0.761	0.773	0.0508	0.0542	0.0355	0.7660	0.04683
50	0.768	0.769	0.771	0.0549	0.0502	0.0495	0.7693	0.05153

## Board B : T20K621.PRN

Section (cm)	Board Thickness (in)			Char Thickness (in)			Board Averag	Char Averag
	Left	Middle	Right	Left	Middle	Right		
10	0.775	0.771	0.77	0.0601	0.0619	0.0695	0.5337	0.06383
15	0.774	0.77	0.763	0.0869	0.0879	0.0903	0.5400	0.08837
20	0.774	0.771	0.764	0.096	0.097	0.0822	0.5437	0.09173
25	0.772	0.767	0.762	0.0927	0.0931	0.1009	0.5406	0.09557
30	0.771	0.764	0.759	0.1068	0.1065	0.0921	0.5433	0.10180
40	0.771	0.772	0.776	0.0879	0.1045	0.108	0.5453	0.10013
50	0.781	0.783	0.784	0.0824	0.0864	0.0922	0.5498	0.08700

# Board C : T20K622.PRN

Section (cm)	Board Thickness (in)			Char Thickness (in)			Board Averag	Char Averag
	Left	Middle	Right	Left	Middle	Right		
10	0.761	0.755	0.76	0.1028	0.09	0.089	0.5393	0.09393
15	0.762	0.762	0.756	0.09	0.0851	0.0848	0.5360	0.08663
20	0.763	0.764	0.763	0.079	0.0845	0.0821	0.5353	0.08187
25	0.759	0.763	0.767	0.0792	0.07	0.0825	0.5364	0.07723
30	0.763	0.763	0.769	0.0787	0.0675	0.0944	0.5369	0.08020
40	0.763	0.765	0.767	0.0724	0.081	0.0673	0.5348	0.07357
50	0.769	0.765	0.773	0.0879	0.096	0.0769	0.5420	0.08693

# Board D : T30K623.PRN

Section (cm)	Board Thickness (in)			Char Thickness (in)			Board Averag	Char Averag
	Left	Middle	Right	Left	Middle	Right		
10	0.771	0.766	0.764	0.0571	0.0645	0.0605	0.5290	0.06070
15	0.769	0.768	0.767	0.0542	0.0581	0.0565	0.5297	0.05627
20	0.768	0.767	0.765	0.0589	0.0491	0.0549	0.5303	0.05430
25	0.769	0.768	0.767	0.0526	0.0571	0.0539	0.5292	0.05453
30	0.767	0.763	0.764	0.0613	0.0639	0.0611	0.5294	0.06210
40	0.771	0.768	0.764	0.053	0.0665	0.0485	0.5283	0.05600
50	0.774	0.77	0.771	0.0459	0.048	0.0552	0.5290	0.04970

Board E : T30K624.PRN

Section (cm)	Board Thickness (in)			Char Thickness (in)			Board Averag	Char Averag
	Left	Middle	Right	Left	Middle	Right		
10	0.772	0.772	0.774	0.0632	0.055	0.0518	0.5364	0.05667
15	0.772	0.775	0.775	0.0504	0.054	0.0531	0.5335	0.05250
20	0.768	0.772	0.774	0.0557	0.0558	0.048	0.5339	0.05317
25	0.765	0.771	0.771	0.0479	0.0458	0.0578	0.5300	0.05050
30	0.767	0.772	0.772	0.0451	0.0442	0.0474	0.5297	0.04557
40	0.771	0.772	0.772	0.0485	0.0571	0.0513	0.5308	0.05230
50	0.769	0.771	0.772	0.0462	0.0482	0.0439	0.5297	0.04610

Board F : T10K620.PRN

Section (cm)	Board Thickness (in)			Char Thickness (in)			Board Averag	Char Averag
	Left	Middle	Right	Left	Middle	Right		
10	0.761	0.762	0.765	0.1819	0.1626	0.1773	0.5696	0.17393
15	0.775	0.752	0.759	0.1952	0.2064	0.179	0.5687	0.19353
20	0.743	0.753	0.757	0.2208	0.202	0.2122	0.5769	0.21167
25	0.752	0.742	0.757	0.2081	0.193	0.2072	0.5690	0.20277
30	0.737	0.743	0.759	0.2319	0.205	0.225	0.5780	0.22063
40	0.745	0.749	0.746	0.225	0.1989	0.1951	0.5733	0.20633
50	0.746	0.76	0.755	0.1928	0.1888	0.16	0.5693	0.18053



# Board G : T10K617.PRN

Section (cm)	Board Thickness (in)			Char Thickness (in)			Board Averag	Char Averag
	Left	Middle	Right	Left	Middle	Right		
10	0.751	0.759	0.755	0.1532	0.1793	0.1619	0.5557	0.16480
15	0.749	0.757	0.76	0.1777	0.1576	0.1605	0.5649	0.16527
20	0.748	0.757	0.754	0.1841	0.1589	0.1553	0.5650	0.16610
25	0.748	0.758	0.753	0.1703	0.1651	0.172	0.5604	0.16913
30	0.742	0.752	0.756	0.1833	0.167	0.1661	0.5638	0.17213
40	0.741	0.751	0.749	0.163	0.1569	0.1569	0.5543	0.15893
50	0.758	0.751	0.754	0.1531	0.1459	0.1627	0.5527	0.15390

# Board H : T10K621.PRN

Section (cm)	Board Thickness (in)			Char Thickness (in)			Board Averag	Char Averag
	Left	Middle	Right	Left	Middle	Right		
10	0.759	0.756	0.761	0.187	0.1762	0.1723	0.5680	0.17850
15	0.755	0.75	0.752	0.1769	0.2085	0.1731	0.5596	0.18617
20	0.748	0.748	0.743	0.195	0.1666	0.1789	0.5620	0.18017
25	0.757	0.756	0.751	0.195	0.1831	0.1781	0.5673	0.18540
30	0.754	0.742	0.753	0.2069	0.198	0.1912	0.5673	0.19870
40	0.743	0.757	0.756	0.197	0.21	0.2042	0.5700	0.20373
50	0.761	0.765	0.771	0.1541	0.1515	0.1375	0.5634	0.14770

REPORT DOCUMENTATION PAGE			Form Approved OMB No. 0704-0188	
Public reporting burden for this collection of information is estimated to average 1 hour per response, including the time for reviewing instructions, searching existing data sources, gathering and maintaining the data needed, and completing and reviewing the collection of information. Send comments regarding this burden estimate or any other aspect of this collection of information, including suggestions for reducing this burden, to Washington Headquarters Services, Directorate for Information Operations and Reports, 1215 Jefferson Davis Highway, Suite 1204, Arlington, VA 22202-4302, and to the Office of Management and Budget, Paperwork Reduction Project (0704-0188), Washington, DC 20503.				
1. AGENCY USE ONLY (Leave blank)	2. REPORT DATE 30 Dec., 1995	3. REPORT TYPE AND DATES COVERED Final Technical: 9-5-91 to 6-5-95		
4. TITLE AND SUBTITLE  HORIZONTAL FLAME SPREAD ON SHIP COMPARTMENT SURFACES		5. FUNDING NUMBERS  Grant No: N00014-91-J-202-3		
6. AUTHOR(S)  Yonggang Chen and Vahid Motevalli (1) Michael Delichatsios (2)				
7. PERFORMING ORGANIZATION NAME(S) AND ADDRESS(ES) (1) Worcester Polytechnic Institute 100 Institute Rd. Worcester, MA 01609 (2) Factory Mutual Research Corp. 1151 Boston-Providence Tpk. Norwood, MA 02062		8. PERFORMING ORGANIZATION REPORT NUMBER		
9. SPONSORING/MONITORING AGENCY NAME(S) AND ADDRESS(ES) Department of the Navy Naval Research Laboratory 4555 Overlook Ave., S.E. Washington, D.C. 20375-5001		10. SPONSORING/MONITORING AGENCY REPORT NUMBER		
11. SUPPLEMENTARY NOTES Computer program supplied on a magnetic medium to the scientific officer.				
12a. DISTRIBUTION/AVAILABILITY STATEMENT  NO RESTRICTION ON AVAILABILITY		12b. DISTRIBUTION CODE		
13. ABSTRACT (Maximum 200 words)  This research resulted in the development of a computer model for prediction of Horizontal Flame Spread on Compartment Surfaces (HFSCS) complemented by a Combustion Model. The HFSCS was developed to predict flame spread on <u>real material</u> (whose properties are not always known or well-defined). The intent of the work was to provide the Navy with a validated and practical numerical model that can be used either as an stand alone for material flame spread characterization or ideally be incorporated into a compartment fire model, such as C-FAST developed by NIST. The horizontal flame spread code has been assembled including burning and radiation from the spreading fire. The numerical model was validated by comparison predicted flame spread rates and surface temperatures with measurements from several experiments which included effects of external and flame radiative heat fluxes. Good agreements between the numerical predictions and the experimental data were obtained.  The theoretical details of the models, subroutines and analysis are contained in Appendixes A-F. The computer code for the HFSCS and the combustion model are provided on magnetic disk. A listing of the HFSCS and the combustion model along with their input and description of the input are included in Appendix (G-J). Extensive presentation of the data and results are included in the Appendixes L and M.				
14. SUBJECT TERMS  Flame Spread, Combustion, Pyrolysis, Charring, Radiation, integral pyrolysis model		15. NUMBER OF PAGES 468		
		16. PRICE CODE		
17. SECURITY CLASSIFICATION OF REPORT  UNCLASSIFIED	18. SECURITY CLASSIFICATION OF THIS PAGE  UNCLASSIFIED	19. SECURITY CLASSIFICATION OF ABSTRACT  UNCLASSIFIED	20. LIMITATION OF ABSTRACT	

## GENERAL INSTRUCTIONS FOR COMPLETING SF 298

The Report Documentation Page (RDP) is used in announcing and cataloging reports. It is important that this information be consistent with the rest of the report, particularly the cover and title page. Instructions for filling in each block of the form follow. It is important to *stay within the lines* to meet optical scanning requirements.

**Block 1. Agency Use Only (Leave blank).**

**Block 2. Report Date.** Full publication date including day, month, and year, if available (e.g. 1 Jan 88). Must cite at least the year.

**Block 3. Type of Report and Dates Covered.** State whether report is interim, final, etc. If applicable, enter inclusive report dates (e.g. 10 Jun 87 - 30 Jun 88).

**Block 4. Title and Subtitle.** A title is taken from the part of the report that provides the most meaningful and complete information. When a report is prepared in more than one volume, repeat the primary title, add volume number, and include subtitle for the specific volume. On classified documents enter the title classification in parentheses.

**Block 5. Funding Numbers.** To include contract and grant numbers; may include program element number(s), project number(s), task number(s), and work unit number(s). Use the following labels:

C - Contract	PR - Project
G - Grant	TA - Task
PE - Program Element	WU - Work Unit Accession No.

**Block 6. Author(s).** Name(s) of person(s) responsible for writing the report, performing the research, or credited with the content of the report. If editor or compiler, this should follow the name(s).

**Block 7. Performing Organization Name(s) and Address(es).** Self-explanatory.

**Block 8. Performing Organization Report Number.** Enter the unique alphanumeric report number(s) assigned by the organization performing the report.

**Block 9. Sponsoring/Monitoring Agency Name(s) and Address(es).** Self-explanatory.

**Block 10. Sponsoring/Monitoring Agency Report Number.** (If known)

**Block 11. Supplementary Notes.** Enter information not included elsewhere such as: Prepared in cooperation with...; Trans. of...; To be published in.... When a report is revised, include a statement whether the new report supersedes or supplements the older report.

**Block 12a. Distribution/Availability Statement.** Denotes public availability or limitations. Cite any availability to the public. Enter additional limitations or special markings in all capitals (e.g. NOFORN, REL, ITAR).

DOD - See DoDD 5230.24, "Distribution Statements on Technical Documents."

DOE - See authorities.

NASA - See Handbook NHB 2200.2.

NTIS - Leave blank.

**Block 12b. Distribution Code.**

DOD - Leave blank.

DOE - Enter DOE distribution categories from the Standard Distribution for Unclassified Scientific and Technical Reports.

NASA - Leave blank.

NTIS - Leave blank.

**Block 13. Abstract.** Include a brief (*Maximum 200 words*) factual summary of the most significant information contained in the report.

**Block 14. Subject Terms.** Keywords or phrases identifying major subjects in the report.

**Block 15. Number of Pages.** Enter the total number of pages.

**Block 16. Price Code.** Enter appropriate price code (*NTIS only*).

**Blocks 17. - 19. Security Classifications.** Self-explanatory. Enter U.S. Security Classification in accordance with U.S. Security Regulations (i.e., UNCLASSIFIED). If form contains classified information, stamp classification on the top and bottom of the page.

**Block 20. Limitation of Abstract.** This block must be completed to assign a limitation to the abstract. Enter either UL (unlimited) or SAR (same as report). An entry in this block is necessary if the abstract is to be limited. If blank, the abstract is assumed to be unlimited.